MLIV 22

Philips Research Reports

Volume 3

1948

All rights reserved by N. V. Philips' Gloeilampenfabrieken, Eindhoven, Netherlands.
Articles or illustrations reproduced, in whole or in part, must be accompanied by full acknowledgement of the source: Philips Research Reports.

CHRONOLOGICAL INDEX

PHILIPS RESEARCH REPORTS, VOL. 3

			Page
R 66	K. F. Niessen	Indication of landing courses independent of weather conditions, part I	1-12
R 67	A. van der Ziel and A. Versnel	Induced grid noise and total-emission noise	13-23
R 68	B. D. H. Tellegen	The determination of the integration constants when calculating transient phenomena	24-36
R 69	H. J. Lindenhovius and J. C. van der Breggen	The measurement of permeability and magnetic losses of non-conducting ferromagnetic material at high frequencies	37-45
R 70	F. A. Kröger, J. M. Stevels and Th. P. J. Botden	The fluorescence of hexavalent uranium in glass	46-48
R 71	W. J. Oosterkamp	The heat dissipation in the anode of an X-ray tube. I. Introduction; loads of short duration applied to stationary anodes	49-59
R 72	J. F. Klinkhamer	Empirical determination of wave-filter transfer functions with specified properties, part I	60-80
R 73	B. D. H. Tellegen	The gyrator, a new electric network element	81-101
R 74	H. Bremmer	On the theory of spherically symmetric inhomogeneous wave guides, in connection with tropospheric radio propagation and under-water acoustic propagation	102-120
R 75	A. van der Ziel and A. Versnel	Measurements of noise factors of penthodes at 7·25-m wavelength	121-129
R 76	K. F. Niessen	Indication of landing courses independent of weather conditions, part II	130-139
R 77	J. M. van Hofweegen and K. S. Knol	A universal adjustable transformer for u.h.f. work	140-145
R 78	W. J. Oosterkamp	The heat dissipation in the anode of an X-ray tube. II. Loads of short duration applied to rotating anodes	161-173
R 79	Balth. van der Pol	Mathematics and radio problems	174-190

			Page
R 80	A. van Weel	Developments in radio-receiver circuits for the ultra-short-wave range	191-212
R 81	C. J. Bouwkamp	On the theory of coupled antennae	213-226
R 82	W. W. Boelens	Valve characteristic giving linear modulation when a feedback resistor is inserted in the cathode lead	227-234
R 83	J. M. Stevels	Some investigations in the system Na_2O-PbO-TiO_2-SiO_2	235-238
R 84	F. L. H. M. Stumpers	Noise in a pulse-frequency-modulation system	241-254
R 85	A. van der Ziel and A. Versnel	The noise factor of grounded-grid valves	255-270
R 86	J. D. Fast	The equilibrium between liquid silica and liquid iron	271-280
R 87	J. L. Meijering	Retrograde solubility curves, especially in alloy solid solutions	281-302
R 88	W. J. Oosterkamp	The heat dissipation in the anode of an X-ray tube. III. Continuous loads	303-317
R 89	B. D. H. Tellegen	The synthesis of passive, resistanceless four-poles that may violate the reciprocity relation	321-337
R 90	W. Elenbaas	Dissipation of heat by free convection, part I	338-360
R 91	A. van Weel	A new principle for transceivers	361-370
R 92	J. H. van Santen and G. H. Jonker	The temperature dependency of the index of refraction of heteropolar solids	371-377
R 93	J. F. Klinkhamer	Empirical determination of wave-filter transfer functions with specified properties, part II	378-400
R 94	J. A. Haringx	On highly compressible helical springs and rubber rods, and their application for vibration-free mountings, part I	401-449
R 95	W. Elenbaas	Dissipation of heat by free convection, part II	450-465
R 96	C. Zwikker	Anticaustics — A cord construction and a general formula	466-473
	Abstracts of papers	156-160, 239-240, 318-320,	474-475
	Subject index		476-477
	Author index		478-479
	Index according to the universal decimal classification system		480

VOL. 3 NR 1 FEBRUARY 1948

Philips Research Reports

EDITED BY THE RESEARCH LABORATORY
OF N.V. PHILIPS' GLOEILAMPENFABRIEKEN, EINDHOVEN, NETHERLANDS

R 66 *Philips Res. Rep.* **3**, *1-12, 1948*

INDICATION OF LANDING COURSES INDEPENDENT OF WEATHER CONDITIONS

by K. F. NIESSEN

621.396.933.23

Summary

Straight landing courses with a small angle of elevation and independent of changes in the electric constants of the ground (as produced, for instance, by rain and snow fall) are indicated. In the first part we consider only infinite dipoles at unequal heights.

Résumé

Traité de trajectoires d'atterrissage rectilignes à faible angle d'élévation et indépendantes de variations des propriétés électriques du sol (par exemple, des variations dues à la chute de pluie ou de neige). Dans la première partie on considère des dipôles hertziens situés à des hauteurs differentes.

Introduction

A straight line in space can be indicated, for instance, by means of two planes. Therefore, a straight landing course could be determined by the intersection of a vertical plane F_1 and a second plane F_2 perpendicular to F_1. The first plane, F_1, may be fixed in a well-known manner by means of two vertical emitters A_1 and A_2 (fig. 1) identical in power, wavelength and form, and at the same height above the ground. If these emitters radiate in counter-phase, then the medium plane perpendicular to A_1A_2, which may serve as F_1, can be found experimentally by the condition of vanishing field strength as a consequence of the interference of the two emitters.

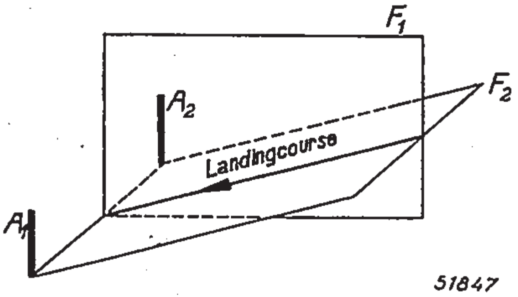

Fig. 1. Indication of a landing course by means of two planes F_1 and F_2, of which the vertical one is determined by two emitters A_1 and A_2.

If the emitters A_1 and A_2 are modulated differently and received separately, this plane F_1 can be found as one of equal field strengths.

In both cases the plane given by the experiment is the medium plane of A_1A_2, and therefore determined independently of the physical conditions of the soil.

The remaining problem therefore will be to find a second plane, also located independently of conditions of soil and weather, in order to indicate the landing course in an invariable manner.

In free space (i.e. if the earth were absent) an indication of such a second plane could be given by two parallel horizontal antennae B_1 and B_2 of the same strength and form (fig. 2), whose medium plane would be a plane of vanishing field strength (if B_1 and B_2 were coherent and driven in opposite phase), or a plane of equal field strengths (if B_1 and B_2 were modulated differently). But on account of the presence of the earth, points of vanishing or equal field strengths do no longer lie in the medium plane of B_1B_2. In the case of an ideal earth of infinite conductance, for instance, points of vanishing field strength are only to be found on the surface of the earth, the images of the horizontal dipoles being in counter-phase with, and of the same strength as, the original dipoles (fig. 3).

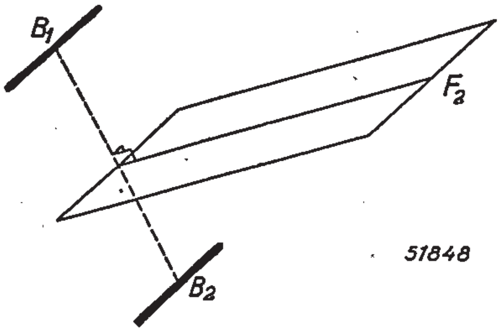

Fig. 2. Determination of the second plane (F_2) by two horizontal antennae, neglecting the influence of the earth.

We therefore have to find out quite another method for the determination of the second plane. In what follows this second plane will not be a flat surface but the surface of a cone, whose axis lies in F_1. The straight lines common to F_1 and this conical surface are the wanted landing courses.

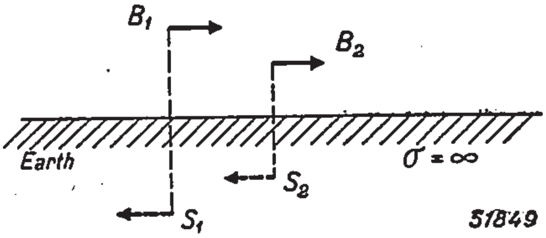

Fig. 3. Influence of an infinitely conducting earth on the location of F_2 in the case of fig. 2.

PART I. EMITTERS AT UNEQUAL HEIGHTS

We consider two vertical dipoles C_1 and C_2 of infinitesimal length on the same vertical line and situated at heights h_1 and h_2, respectively, above the earth (fig. 4). The moments of these dipoles are supposed to be equal ($m_1 = m_2 = m$), but the dipoles themselves are modulated differently so that their radiation is received separately.

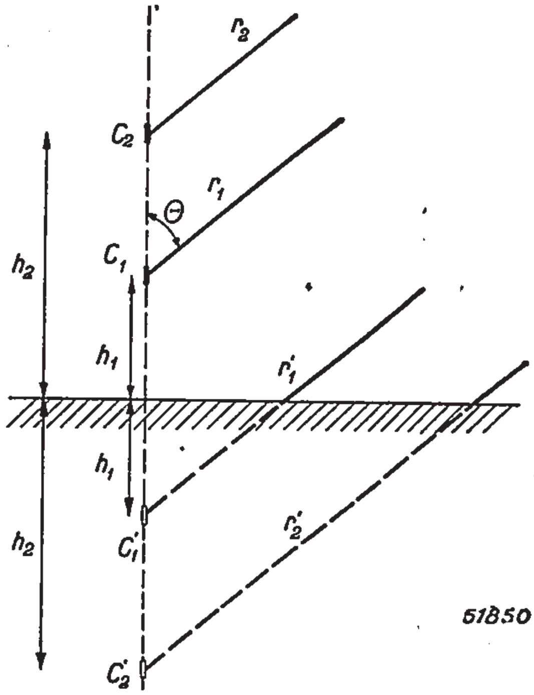

Fig. 4. Two vertical mathematical dipoles of the same moment and frequency but modulated differently, situated at different heights above the earth.

Since the distance between the aeroplane and the emitters is very large with respect to λ and to h_1 and h_2, the field strength of the radiation from C_1 may be calculated by means of the well-known reflection formula, and will thus be proportional to

$$m \cos^2 \alpha \left| \frac{e^{jk_1r_1}}{r_1} + K \frac{e^{jk_1r_1'}}{r_1'} \right|, \tag{1}$$

where α is the angle of elevation of the line of sight above the horizon, r_1 and r_1' the distances from the aeroplane to C_1, respectively, the image of C_1, with respect to the surface of the earth, and $k_1 = 2\pi/\lambda$. The factor $\cos^2\alpha$ appears from the application of well-known formulae valid for distances from the emitter great compared with the wavelength. Its appearance instead of $\cos \alpha$ may be understood if we consider for a moment a *free* vertical dipole. One factor $\cos \alpha$, then, is based upon the radiation of a dipole being maximal in the equatorial plane, and a second factor cos α is related to the projection of the electric force (being perpendicular to the line of sight) onto the antenna of the aeroplane (being vertical).

Further, K is the complex reflection coefficient for plane waves with the electric vector in the plane of incidence and falling at an angle of incidence $\Theta = \pi/2 - \alpha$ upon the surface of the earth.

The formula (1) is called the reflection formula, and for the region where it holds we refer to a former paper [1]. We suppose the aeroplane to be in that region.

K is a function of λ, Θ, the dielectric constant ε, and the conductance σ of the earth; K is complex since during the reflection the incident wave undergoes a change in intensity as well as in phase. We have

$$K = Re^{j\Delta}.$$

R and Δ are real and do not depend on h_1 and h_2, this reflection coefficient K being defined for plane waves. In the denominators of (1) we may take $r_1 = r_1'$, but not in the exponential factors. There we have to substitute

$$r_1' - r_1 = 2h_1 \cos \Theta.$$

Thus we obtain for small angles α:

$$\left.\begin{array}{l}\text{field strength}\\ \text{originating}\\ \text{from } C_1\end{array}\right\} \sim \frac{m_1}{r_1}\left|1 + R \exp j\left(\frac{4\pi\, h_1 \cos\Theta}{\lambda} + \Delta\right)\right| =$$

$$= \frac{m_1}{r_1}\sqrt{1 + R^2 + 2R\cos\left(\frac{4\pi\, h_1 \cos\Theta}{\lambda} + \Delta\right)}. \quad (2)$$

In receiving the radiation from C_2 we have to do with the same values of R and Δ as when receiving C_1 since on account of the large distance of the aeroplane we have $\Theta_1 = \Theta_2$. Therefore,

$$\left.\begin{array}{l}\text{field strength}\\ \text{originating}\\ \text{from } C_2\end{array}\right\} \sim \frac{m_2}{r_2}\sqrt{1 + R^2 + 2R\cos\left(\frac{4\pi\, h_2 \cos\Theta}{\lambda} + \Delta\right)}. \quad (3)$$

According to (2) and (3), and with the approximation $r_1 = r_2$, the two emitters will be received with equal intensity in those directions Θ which obey the equation

$$\cos\left(\frac{4\pi\, h_1 \cos\Theta}{\lambda} + \Delta\right) = \cos\left(\frac{4\pi\, h_2 \cos\Theta}{\lambda} + \Delta\right),$$

i.e., in the directions obeying

$$\frac{4\pi\, h_2 \cos\Theta}{\lambda} = \frac{4\pi\, h_1 \cos\Theta}{\lambda} + 2p\pi \quad (p = 0, \pm 1, \pm 2, \ldots)$$

as well as in those obeying

$$\frac{4\pi\, h_2 \cos \Theta}{\lambda} + \Delta = 2\pi - \frac{4\pi\, h_1 \cos \Theta}{\lambda} - \Delta + 2q\pi. \quad (q = 0, \pm 1, \pm 2, \ldots)$$

These conditions may be written in the form

$$(h_2 - h_1) \cos \Theta = \frac{\lambda}{2} p \qquad (A) \qquad (4)$$

$$(h_2 + h_1) \cos \Theta = \frac{\lambda}{2}\left(q + 1 - \frac{\Delta}{\pi}\right) \qquad (B) \qquad (5)$$

Treating in this first part emitters at unequal heights, we suppose in the first group of directions $p > 0$, i.e., $h_2 > h_1$ (a matter of definition!), and in order to keep $h_2 - h_1$ as small as possible we take $p = 1$. Now, the required elevation of the landing course is given. Let it be α_0 (for example, $\alpha_0 = 3°$). To establish that course by means of a beacon based on condition (A) we have to take

$$h_2 - h_1 = \frac{\lambda}{2 \cos \Theta_0}, \qquad (6)$$

where

$$\Theta_0 = \frac{\pi}{2} - \alpha_0.$$

Thanks to this difference in height the two dipoles are equally strong received on the surface of a cone whose half-opening equals Θ_0. But there are still other cones on whose surface the two field strengths appear to be equal when for $h_2 - h_1$ the value (6) is chosen, namely those cones whose half-opening Θ fulfils the relation

$$(h_2 - h_1) \cos \Theta = \frac{\lambda}{2} p. \quad (p = 2, 3, 4, \ldots)$$

Substitution of (6) gives

$$\cos \Theta = p \cos \Theta_0. \quad (p = 2, 3, 4, \ldots) \qquad (7)$$

An illustration of the corresponding cones is given in fig. 5.

Their location in space is independent of the physical constitution of the soil since the constants ε and σ do not appear in (6) and (7). The intersection of such a cone with the plane F_1 mentioned in the beginning, gives straight lines of invariable direction in space, independent of possible changes in the constants of the soil, due, for example, to rain or snow fall. Of these lines we can only use that with $\Theta = \Theta_0$ as a landing course, the elevation of the other ones (corresponding to $p = 2, 3, 4, \ldots$) being too large for a landing.

We now consider the second group of directions of equal field strengths, that is, those contained in

$$(h_2 + h_1)\cos\Theta' = \frac{\lambda}{2}\left(q+1-\frac{\Delta}{\pi}\right). \quad (q=0, \pm1, \pm2, \ldots) \qquad (8)$$

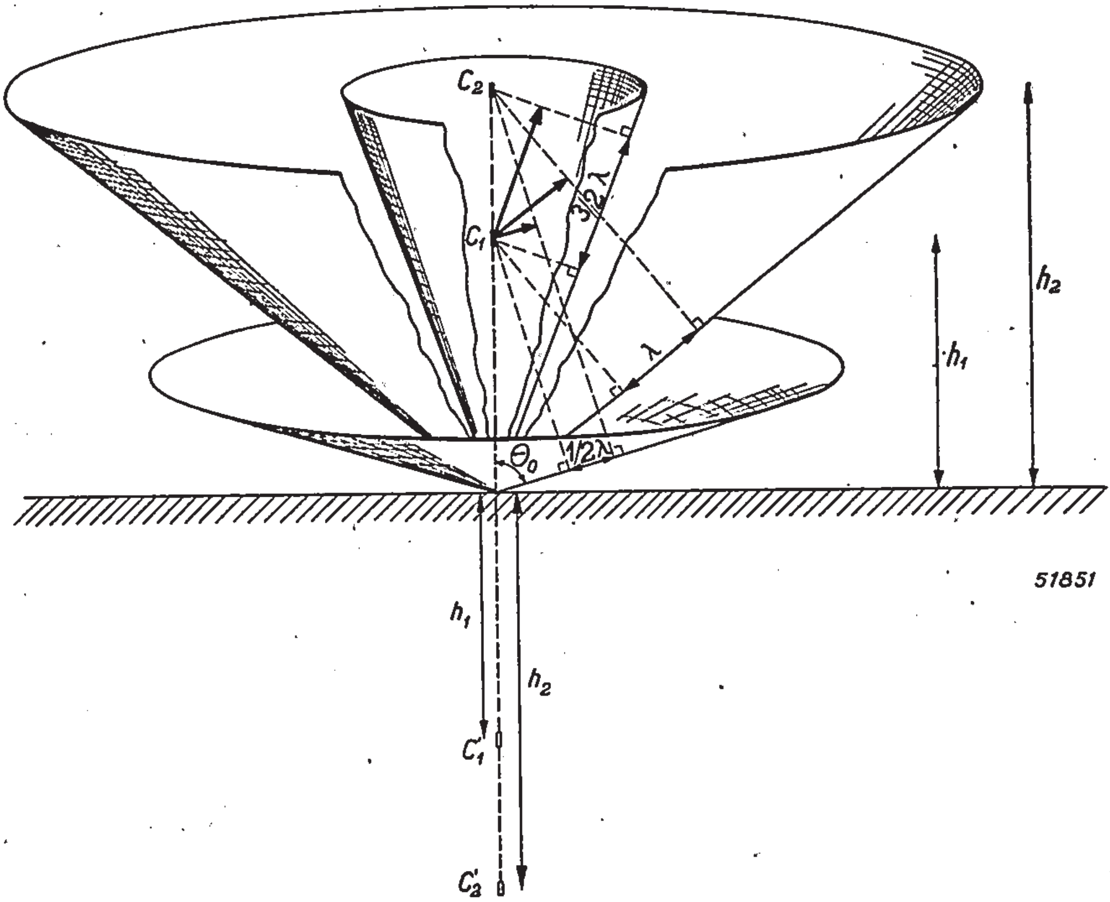

Fig. 5. Conical surfaces on which the vertical dipoles C_1 and C_2 of fig. 4 are received with equal intensities.

In the condition (*B*) a quantity (namely Δ) appears that depends on ε and σ, so that the corresponding directions will vary with the physical constitution of the ground. *In principle* we therefore should not use such cones as a second surface F_2, but *in practice* we may do it sometimes as will be seen later on.

The condition (*B*) can be used for two different purposes: We may ask how to choose the heights h_1 and h_2 so that the corresponding value Θ' equals the desired value Θ_0 of the landing course. It is advisable, then, to take $q = 0$, in order to avoid large heights. But we may also ask what values Θ', i.e., what other cones of equal field strength, are to be expected still if we have prescribed the values of h_1 and h_2; and it is this last way we now will go.

Choosing $h_2 - h_1 = \lambda/2 \cos \Theta_0$ we obtain a fixed cone Θ_0 and some other fixed ones with Θ obeying $\cos \Theta = p \cos \Theta_0$ ($p = 2, 3, \ldots$), and we now ask for the variable cones Θ' which still come into play on account of (8), using this same value of $h_2 - h_1$. Thus far nothing has been said about $h_2 + h_1$, necessary for (8). So we have to choose h_1 and h_2 separately. We take for a moment

$$h_1 = 0, \quad h_2 = \frac{\lambda}{2 \cos \Theta_0}.$$

Then the condition to be fulfilled by Θ' reads as follows:

$$\frac{\cos \Theta'}{\cos \Theta_0} = q + 1 - \frac{\Delta}{\pi}. \quad (q = 0, \pm 1, \pm 2, \ldots)$$

Δ, in its region $\Theta < \Delta < \pi$, as well as the real reflection coefficient R, follows from

$$Re^{j\Delta} = \frac{\nu_2 - \nu_1}{\nu_2 + \nu_1},$$

where

$$\nu_1 = \sqrt{1 - \frac{k_1^2}{k_2^2} \sin^2 \Theta'},$$

$$\nu_2 = \frac{k_2}{k_1} \cos \Theta',$$

$$\frac{k_2^2}{k_1^2} = \varepsilon + j2c\sigma\lambda$$

(c = velocity of light; roots with positive real parts!).

Considering only values of Θ' lying near to $\pi/2$, that is, assuming

$$\cos \Theta' \ll 1,$$

we have for the usual values of k_2/k_1 to do with

$$\nu_2 \ll 1,$$

and therefore

$$Re^{j\Delta} = -1 + 2\frac{\nu_2}{\nu_1} = -1 + 2 \cos \Theta' \frac{k_2/k_1}{\sqrt{1 - (k_1^2/k_2^2)}}.$$

Introducing n and χ by means of

$$\frac{k_2^2}{k_1^2} = n^2 e^{j\chi}, \qquad \left(0 < \chi < \frac{\pi}{2}\right)$$

a straight-forward calculation gives:

$$R = 1 - \delta_1 ,$$
$$\varDelta = \pi - \delta_2 ,$$

with

$$\frac{\delta_1}{\delta_2} = \frac{2n^2 \genfrac{}{}{0pt}{}{\cos}{\sin}\left(\chi - \frac{A}{2}\right)}{\sqrt[4]{n^4 - 2n^2 \cos \chi + 1}} \cos \Theta', \tag{9}$$

where

$$A = \arctan \frac{n^2 \sin \chi}{n^2 \cos \chi - 1} \cdot \quad \left(0 < |A| < \frac{\pi}{2}\right)$$

In the region $\cos \Theta' \ll 1$ the values of Θ' therefore are determined by

$$\frac{\cos \Theta'}{\cos \Theta_0} = q + \frac{\delta_2}{\pi}, \quad (q = 0, 1, 2, 3, \ldots)$$

with the expression (9) for δ_2, this being a very small quantity.

For $q = 0$ we find $\cos \Theta' = 0$, this being, however, meaningless for our purpose. Moreover we cannot take $\cos \Theta'$ too small, since we accepted the reflection formula to be valid.

For $q = 1, 2, \ldots$ we find (since $\delta_2 \ll \pi$)

$$\cos \Theta' = q \cos \Theta_0 .$$

Since we assumed $\cos \Theta' \ll 1$ we may only use here:

$$q = 1, 2, 3, \ldots \ll \frac{1}{\cos \Theta_0} .$$

For an actual landing course $1/\cos \Theta_0$ is about 20, so that $q = 1, 2, 3$ are permitted.

The new cones Θ' clearly fall together with some already found in the invariable group, and their dependence on the constants of the soil (essential for solution (B)) may be neglected.

We recall how this coincidence was based upon $\delta_2 \ll \pi$ or $\varDelta \approx \pi$, which followed from $\nu_2 \ll 1$, which on its turn was a consequence of $\cos \Theta' \ll 1$ and the finiteness of k_2/k_1. Contrarily to a perfectly conducting earth (where $|k_2^2|/k_1^2 = \infty$) we would have $\nu_2 = 1$ and $\varDelta = 0$. So we see how the above coincidence is a typical consequence of the fact that we have to take into account also the dielectric current when using frequencies belonging to the usual region for aeroplanes.

The configuration we arrived at consisted of two vertical dipoles C_1 and C_2 of different modulation, one on the surface of the earth ($h_1 = 0$), the other at the height $h_2 = \lambda/2 \cos \Theta_0$. This pair is to be added to the antennae A_1 and A_2 used for the determination of the plane F_1.

But the assumption $h_1 = 0$ is not so favourable for the reflection formula to be valid for small angles of elevation (see reference above). We better take (fig. 6)

$$h_1 \approx \lambda, \quad h_2 = h_1 + \frac{\lambda}{2 \cos \Theta_0},$$

to which again belong the invariable cones

$$\cos \Theta = p \cos \Theta_0, \ (p = 1, 2, 3, \ldots)$$

based upon condition (A), and those based upon (B), of which also the widest ones are practically invariable. Substitution of the value of h_2 in (B) gives for these widest cones of (B):

$$\cos \Theta' = \frac{q \cos \Theta_0}{1 + \dfrac{4h_1 \cos \Theta_0}{\lambda}},$$

with $q = 1, 2, \ldots \ll \dfrac{1}{\cos \Theta_0}$. They thus no longer fall exactly together with

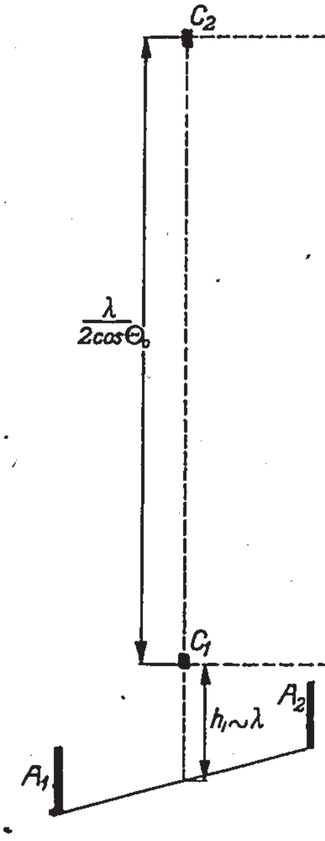

Fig. 6

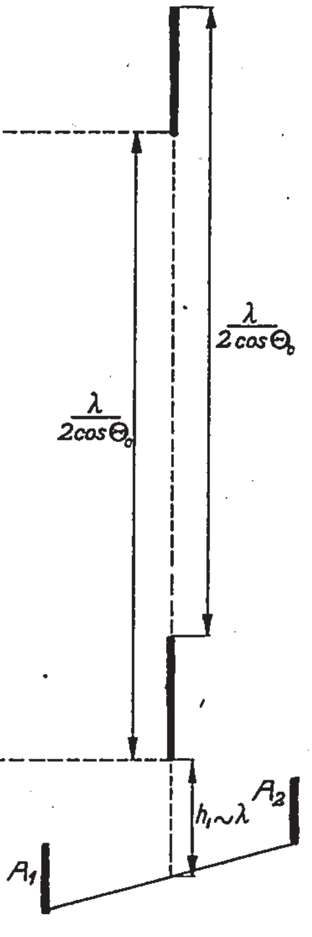
$\frac{\lambda}{2\cos\Theta_0}$
$\frac{\lambda}{2\cos\Theta_0}$
$h_1 \sim \lambda$
A_2
A_1

Fig. 6a

51852

Fig. 6. A configuration of infinitesimal dipoles according to condition (A).
Fig. 6a. A configuration of finite antennae according to condition (A).

the widest ones of (*A*). This coincidence took place only for $h_1 = 0$, but the slight difference occurring for $h_1 \approx \lambda$ may be neglected since $4h_1/\lambda \cos \Theta_0 \ll 1$.

The whole configuration, indicated in fig. 6, is called "configuration *A*" since its construction was based on condition (*A*).

In the above a method was developed for an indication of the landing course (with an invariable elevation α_0), based on the condition (*A*), $h_2 - h_1$ being taken in accordance with (6) and $h_1 \approx \lambda$; and it was shown that the additional cones following from (*B*) and inherent to the chosen values h_2 and h_1 did not give any trouble.

We shall now construct a configuration that is entirely based upon condition (*B*).

By choosing

$$h_2 - h_1 \leqq \frac{\lambda}{2},$$

we make it quite impossible to fulfil condition (*A*), so that the required value Θ_0 of the landing course has to be given by condition (*B*) (with $\Theta' = \Theta_0$).

A reasoning as above teaches that, for $\cos \Theta \ll 1$, $1 - \Delta/\pi$ is practically zero, and condition (*B*) may be written:

$$h_1 + h_2 = q \frac{\lambda}{2 \cos \Theta}. \quad \left(q = 1, 2, \ldots \ll \frac{1}{\cos \Theta}\right)$$

In order to keep h_1 and h_2 as low as possible we choose $q = 1$ and wish to base the indication of Θ_0 on

$$h_1 + h_2 = \frac{\lambda}{2 \cos \Theta_0}. \tag{10}$$

Taking further

$$h_2 - h_1 = \frac{\lambda}{2},$$

in order to avoid cones based on (*A*), we arrive at:

$$\left.\begin{aligned} h_2 &= \frac{\lambda}{4}\left(\frac{1}{\cos \Theta_0} + 1\right), \\ h_1 &= \frac{\lambda}{4}\left(\frac{1}{\cos \Theta_0} - 1\right). \end{aligned}\right\} \tag{11}$$

This configuration of vertical dipoles C_1 and C_2 in addition to the antennae A_1 and A_2 for the determination of F_1 is very useful if we wish to diminish the total height of the beacon. This height was in configuration (*A*) at least

$$\frac{\lambda}{2\cos\Theta_0}$$

and is now reduced to about half its value.

Substituting the chosen heights (11) in (10) we find the other cones Θ' of equal field strength (at least the widest ones) from

$$\cos\Theta' = q\cos\Theta_0. \quad \left(q = 2,\ldots \ll \frac{1}{\cos\Theta_0}\right)$$

The corresponding elevations are all much larger than α_0 $(=3°)$ and will not disturb that (α_0) we found with $q = 1$.

In the configuration above a cone of equal intensity based upon condition (A) was made impossible, but it would not give any trouble if at the same time such a cone of equal field strength was possible, say, with $\Theta = 80°$, an angle of elevation of 10° being much too large for a landing course.

This would occur if we would choose

$$h_2 - h_1 = \frac{\lambda}{2\cos 80°} = \text{about } 3\lambda\,.$$

This, together with (10), would then lead to:

$$h_2 = \frac{\lambda}{4\cos\Theta_0} + 3\,\frac{\lambda}{2},$$

$$h_1 = \frac{\lambda}{4\cos\Theta_0} \div 3\,\frac{\lambda}{2},$$

a configuration giving the same cones $\cos\Theta' = q\cos\Theta_0$ as above (since

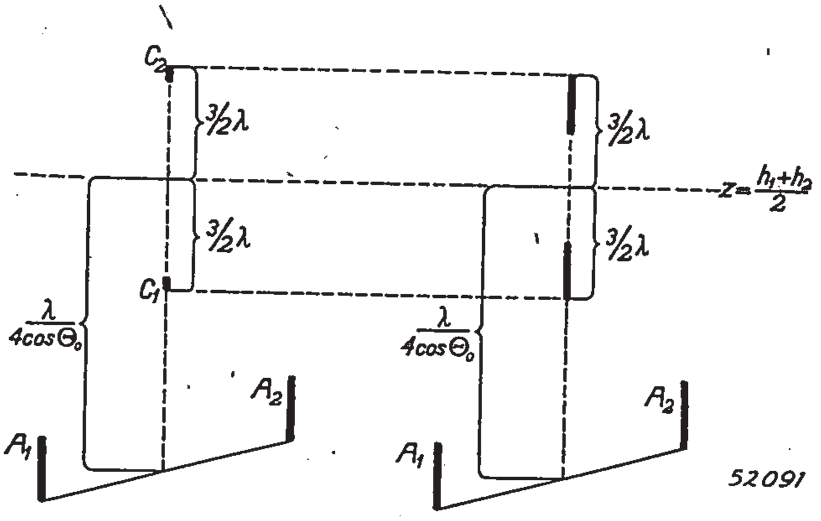

Fig. 7 Fig. 7a

Fig. 7. A configuration of infinitesimal dipoles according to condition (B).
Fig. 7a. A configuration of finite antennae according to condition (B).

$h_2 + h_1$ remained constant) and giving further under condition (A) some additional cones with $\Theta \leqq 80°$ which neither interest nor trouble us. This configuration (containing also the emitters A_1 and A_2, and indicated in fig. 7) will be called "configuration B" since its construction was based on condition (B).

The total height in (B) is somewhat larger than in (11), yet (B) is to be preferred to (11) since the two polar diagrams of (B) (one originating from the dipole C_2 at h_2, the other from C_1 at h_1) will be more different in shape than those of (11) where h_2—h_1 is rather small. In the case $h_2 - h_1 = 0$, for instance, the polar diagrams would have been identical.

The more different these diagrams are, the easier it will be for the pilot to find exactly places of equal intensities.

Eindhoven, September 1947

(To be continued)

REFERENCE

¹) K. F. Niessen, Philips Res. Rep. 1, 51-62, 1946.

R 67 *Philips Res. Rep.* **3**, *13-23, 1948*

INDUCED GRID NOISE AND TOTAL-EMISSION NOISE

by A. van der ZIEL and A. VERSNEL

621.385.3:621.396.822

Summary

In space-charge-limited triodes the fluctuations in the number of electrons that have sufficient energy to pass the potential minimum give rise, by electric induction, to a noise current flowing to the grid; the fluctuations in the number of the electrons returning in front of the potential minimum give rise, by electric induction, to a noise current flowing from cathode to grid. The first noise current is generally called "induced grid noise" and the latter "total-emission noise". Measurements are given of the noise resonance curve of the input circuit of pentodes at 7·25 m wavelength. It is shown that the asymmetry of the noise resonance curve of the input circuit of pentodes at u.h.f. is due to the phase relation between the induced grid noise and the normal shot-effect noise.

Further, it is shown that for diodes in the cut-off region at 7·25 m wavelength the total-emission noise may be described by assuming that the equivalent noise temperature of the "total-emission conductance" is equal to the cathode temperature.

Résumé

Dans les triodes limités par charge spatiale, les fluctuations dans le nombre d'électrons possédant suffisamment d'énergie pour passer le potentiel minimum, donnent lieu, par induction électrique, à un courant de soufflement vers la grille, alors que les fluctuations dans le nombre d'électrons retournant en face de ce potentiel minimum, provoquent, par induction électrique, un courant de soufflement de la cathode à la grille. Le premier courant est appelé „soufflement induit de grille" et le second „soufflement d'émission totale".

L'article donne des mesures de la courbe de résonance du bruit de fond du circuit d'entrée de pentodes pour une longueur d'onde de 7,25 m et établit que l'asymétrie de cette courbe en U.H.F. est due au déphasage entre le soufflement induit de grille et l'effet de grenaille normal.

On montre ensuite que, pour des diodes dans la région du cut-off, sur 7,25 m de longueur d'onde, le soufflement d'émission totale peut être décrit en admettant que la température équivalente de soufflement de la „conductance d'émission totale" est égale à la température de la cathode.

1. Introduction

In a space-charge-limited triode some of the electrons have sufficient energy to pass the potential minimum in front of the cathode, and these give rise to the anode current I_a. The great majority (e.g. 99%) of the electrons, however, return in front of the potential minimum to the cathode.

Supposing the input and the output of the valve short-circuited we can distinguish between the following kinds of noise currents.

The fluctuations in the number of the electrons that pass the grid and arrive at the anode give rise to a noise current in the anode circuit, which is called "shot-effect noise". By electric induction these fluctuations also give rise to a noise current flowing into the grid circuit, which is called "induced grid noise".

The fluctuations in the number of the electrons that return in front of the potential minimum give rise, by electric induction, to a noise current flowing from the cathode to the grid; this noise current is called "total-emission noise", because the total emission of the cathode contributes to this noise current. These electrons also give rise to an additional input conductance, which is called "total-emission conductance" [1]).

Induced grid noise and total-emission noise are both transit-time effects, and occur at v.h.f. and u.h.f. only. It is very difficult to distinguish between these two noise currents. Under normal conditions induced grid noise is the most important effect. For valves in the cut-off region, in which hardly any electrons arrive at the anode, however, induced grid noise is absent whereas total-emission noise is still an important effect, in particular on the shortest wavelengths. Total-emission noise also occurs in diodes; the best way to measure this effect is to use a diode in the cut-off region (total-emission noise is one of the chief causes of the poor signal-to-noise ratio of diode frequency changers for microwaves).

Total-emission noise was first mentioned by Smyth [1]), whilst measurements have been carried out by the authors [2]). It is practically uncorrelated to shot-effect noise and induced grid noise.

Induced grid noise was discovered by Bakker [3]) and independently by North and Ferris [4]). Strutt and Van der Ziel [5]) pointed out the importance of the correlation between induced grid noise and shot-effect noise. As induced grid noise is 90 degrees out of phase with respect to shot-effect noise, a suitable detuning of the input circuit might give rise to a noise voltage between grid and cathode such that the shot-effect noise in the output circuit would be partly suppressed. This was experimentally verified by Kleen [6]).

It is the object of this paper to give additional evidence for the phase relation between shot-effect noise and induced grid noise, and to give measurements of total-emission noise.

Some time ago we built a linear noise amplifier with thermo-couple detector at 7·25 m wavelength for the measurement of signal-to-noise ratios. The tuned impedance of the input circuit had to be obtained from the "noise resonance curve", in which the output of the thermo-couple was plotted against the calibrated capacity C of the tuning condenser of the input circuit. We found asymmetric noise resonance curves at 7·25 m wavelength. This asymmetry, too, is caused by the correlation between induced grid noise and shot-effect noise. Since shot-effect noise in the output circuit of the first amplifier stage might be partly suppressed by a suitable detuning of the input circuit, it is obvious that the shot-effect noise in the output circuit will be enhanced by a detuning in the opposite direction, because the noise voltage across the input circuit will then attain opposite phase. We were able to show that the asymmetry was really due to induced grid noise and not to other causes; for by allowing a large saturated-diode noise current to flow into the input circuit the noise resonance curve of the input circuit became perfectly symmetric, as was to be expected.

We shall show here that the observed asymmetry of the noise resonance curve may be *quantitatively* explained by the above phase relation between induced grid noise and shot-effect noise. We finally succeeded in designing the first stage of the amplifier in such a way that the asymmetry disappeared. We were then able to measure total-emission noise of large diodes at 7·25 m wavelength.

2. Phase relation between induced grid noise and shot-effect noise

In the first stage of our amplifier we used a pentode. For a better understanding of the measurements we shall first give a short summary of the u.h.f. valve theory [5]) [8]).

When in a pentode a signal voltage V_g is applied to the grid it will give rise to a current $S_0 V_g$ flowing from cathode to grid, a current $S_1 V_g$ flowing from grid to screen grid, a current flowing from screen grid to suppressor grid, and a current $S_a V_g$ flowing from suppressor grid to anode. Owing to the transit time of the electrons these currents will be delayed in phase with respect to V_g; $S_1 V_g$ is more delayed than $S_0 V_g$, and $S_a V_g$ still more.

The noise in pentodes consists of three independent parts.

(a) *Total-emission noise*; this noise current is flowing from cathode to grid. As the input circuit is inserted between cathode and grid, the thermal noise of the input circuit and the total-emission noise can be treated in the same way.

(b) *Shot-effect noise*; this gives rise to a noise current i_0 flowing from cathode to grid, a noise current i_1 flowing from grid to screen grid, a noise current flowing from screen grid to suppressor grid, and a noise current i_a flowing from suppressor grid to anode. Owing to the transit time of the electrons, i_1 is delayed in phase with respect to i_0, and i_a is still more delayed. As a consequence of the Fourier analysis of shot effect the noise currents will be distributed between the various electrodes in practically the same way as the signal currents of the same frequency. Hence, we have in good approximation:

$$\frac{i_1}{S_1} = \frac{i_a}{S_a}. \tag{1}$$

The phase relation between i_0, i_1, and i_a is shown in fig. 1. Owing to the phase difference between i_0 and i_1, a noise current (i_0-i_1) is flowing to the grid. This is the induced-grid-noise current, which is about 90 degrees advanced in phase with respect to i_0, as already mentioned.

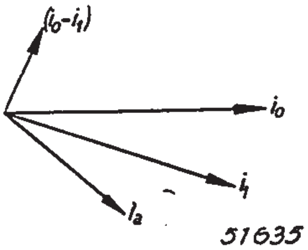

Fig. 1. Phase relation between shot-effect currents i_0, i_1, and i_a flowing, respectively, from cathode to grid, from grid to screen grid, and from suppressor grid to anode. Owing to the phase difference between i_0 and i_1, a noise current i_0-i_1 is flowing to the grid (induced grid noise).

(c) *Partition-current fluctuations* i_p, caused by the irregular distribution of the individual electrons between screen grid and anode (these fluctuations flow from screen grid to anode and do not occur in the cathode lead). The fact that i_a and i_p are independent means that the two noise currents have to be added quadratically.

We now turn to the equivalent input circuit of the first amplifier stage (fig. 2). Let R denote the total tuned input impedance (circuit + valve input) and C the detuning of the input circuit ($C = 0$ means that the input circuit is tuned). The noise output of the amplifier is directly proportional to the mean-square value $\overline{i^2}$ of the total noise current in the lead short-circuiting the output of the first stage. $\overline{i^2}$ consists of three parts.

(a) A part due to the partition-noise current i_p. This part is $\overline{i_p^2}$.

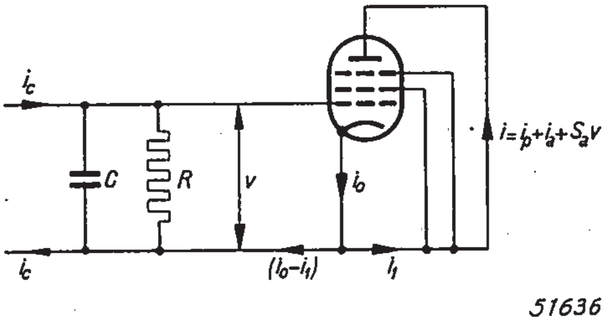

Fig. 2. Equivalent circuit of the first amplifier stage; the output is short-circuited. i_0, i_1, and i_a have the same meaning as in fig. 1, i_p denotes the partition-noise current, i_c describes the thermal noise of the input circuit, R denotes the total tuned impedance of the input circuit (circuit + valve input), and C denotes the detuning of the input circuit. The noise current i_0-i_1 flowing to the grid gives rise to a noise voltage v across the input circuit and hence to a noise current $S_a v$ in the anode lead.

(b) A part due to the thermal noise of the input circuit and the total-emission noise. Let these noises be denoted by the noise current i_c flowing into the input circuit; then we have for this part:

$$\overline{i_c^2}\,\frac{R^2\,|S_a|^2}{1+\omega^2C^2R^2}. \tag{2}$$

(c) A part due to the shot-effect current i_a and the induced-grid-noise current (i_0-i_1). The latter gives rise to a noise voltage between grid and cathode

$$v = -\,(i_0-i_1)\,\frac{R}{1+j\omega CR}, \tag{3}$$

and hence to an output noise current

$$-\,(i_0-i_1)\,\frac{R\,S_a}{1+j\omega CR}, \tag{3a}$$

which has to be added to the shot-effect current i_a. Hence we obtain for the third part:

$$\overline{\left|i_a-\frac{(i_0-i_1)R\,S_a}{1+j\omega CR}\right|^2}=\overline{i_a^2}\left|1-\frac{jae^{j\varphi}}{1+j\omega CR}\right|^2=$$

$$=\overline{i_a^2}+\frac{\overline{i_a^2}\,(a^2+2a\sin\varphi)-\overline{i_a^2}\,.\,\omega CR\,.\,2a\cos\varphi}{(1+\omega^2C^2R^2)}, \tag{4}$$

in which (compare (1))

$$jae^{j\varphi}=\frac{(i_0-i_1)\,R\,S_a}{i_a}=\frac{(i_0-i_1)\,R\,S_1}{i_1};\ a^2=\frac{\overline{(i_0-i_1)^2}\,R^2\,|S_1|^2}{\overline{i_1^2}}. \tag{4a}$$

The total mean-square noise current becomes:

$$\overline{i^2}=\overline{i_p^2}+\overline{i_a^2}+\frac{\overline{i_c^2}\,R^2\,|S_a|^2+\overline{i_a^2}\,(a^2+2a\sin\varphi)-\overline{i_a^2}\,.\,\omega CR\,.\,2a\cos\varphi}{1+\omega^2C^2R^2} \tag{5}$$

Hence the output of the amplifier is of the general form

$$A_1+\frac{A_2-A_3\omega CR}{1+\omega^2C^2R^2}, \tag{6}$$

in which A_1, A_2, and A_3 are independent of C.

We shall now turn to our measurements and show that our asymmetric resonance curves are of the general form (6).

Fig. 3 shows the noise resonance curve obtained with an EF 50 pentode. The measured points are denoted by crosses; the full-drawn curve is the best fitting theoretical curve (6), which is obtained by suitably chosen values of A_1, A_2, and A_3. An arrow shows the value of the tuning capacity for which $\omega CR = 0$ (input circuit tuned). This value and the tuned impedance R were obtained with an external noise signal from a saturated diode. According to fig. 3 the measured noise resonance curve is, within the experimental error, represented by an equation of the type (6). This must be considered as a definite proof that the assumed phase relation between induced grid noise and shot-effect noise really exists.

Fig. 3 also show the dashed curve

$$\frac{A_1 + A_2}{1 + \omega^2 C^2 R^2}, \tag{6a}$$

in which A_1 and A_2 are those of the full-drawn curve. It gives the resonance curve for an external signal when noise is ignored. By dividing equation (6) by (6a) we obtain the noise-to-signal ratio of the amplifier in relative units:

$$\frac{A_1 + A_2 + A_1\,\omega^2 C^2 R^2 - A_3\,\omega CR}{(A_1 + A_2)}. \tag{6b}$$

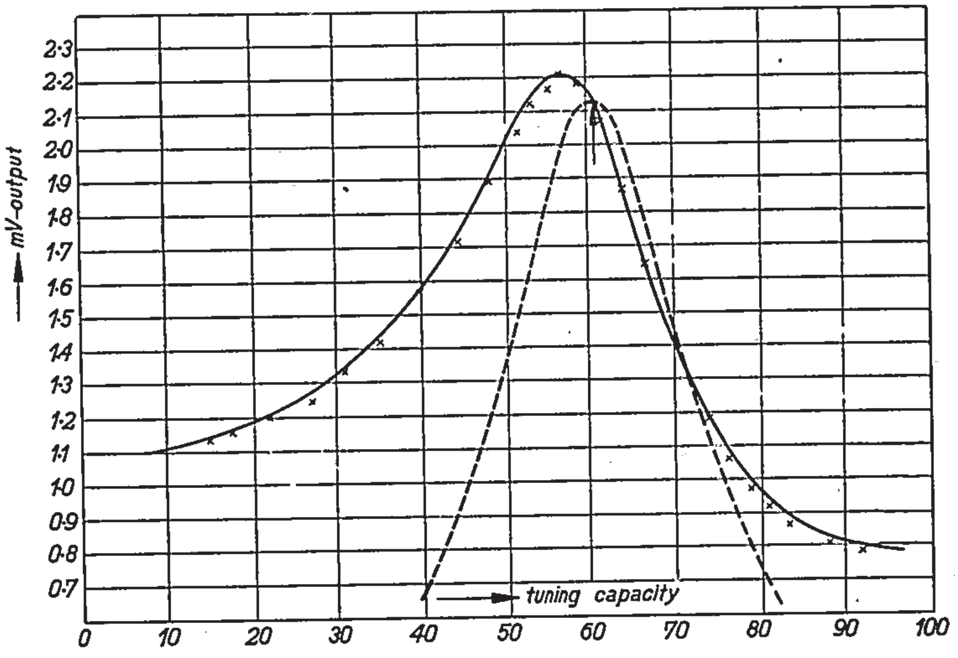

Fig. 3. Noise resonance curve for an EF 50 pentode at 7·25 m wavelength (mV output versus tuning capacity; one scale division of the abscissa corresponds to 0·171 pF). Measured points are denoted by crosses, the full-drawn curve is the best fitting theoretical curve (6), which is obtained by choosing

$$A_1 = 0{\cdot}845,\ A_2 = 1{\cdot}285,\ A_3 = 0{\cdot}685.$$

The deviation between the curve and the measured points at both ends of the scale is due to the non-linearity of the tuning condenser there (compare also fig. 4).
An arrow shows that value of the tuning capacity for which the input circuit is tuned ($\omega CR = 0$). The dashed curve (equation (6a)) represents the input signal as a function of the tuning capacity of the input circuit in relative units; it was measured with an external noise signal. From the full-drawn curve and the dashed curve the noise-to-signal ratio of the amplifier may be obtained in relative units.

Hence it follows from equation (6b) that, if the noise-to-signal ratio is measured as a function of the tuning capacity, we obtain a minimum value when $\omega CR = \frac{1}{2}A_3/A_1$. Introducing the measured values of A_1 and A_3 of fig. 3, we obtain a maximum decrease of 6% with respect to the value for $C = 0$. For a larger value of the induced-grid-noise current a much larger decrease in noise-to-signal ratio might have been obtained.

Equation (6b), which is obtained without making any specified assumption about shot-effect noise and induced grid noise, is valid for a very wide frequency range. It shows that the noise-to-signal ratio is a quadratic function of the tuning capacity. An experimental noise-to-signal-ratio curve at 1 m wavelength was published by Kleen 6). It shows a deviation from the quadratic law (6b), which is most probably due to small experimental errors.

A very important improvement in symmetry was obtained by using a push-pull pentode EFF 50, with the two systems connected in parallel, instead of an EF 50 pentode. According to fig. 4 the noise resonance curve is practically symmetric. This is to be expected theoretically, because most terms in (5) are proportional to the square of the transconductance. For the EFF 50 in parallel connection the transconductance is about three times as large as for the EF 50. Hence the constant A_2 is increased by about a factor 9 and the constant A_3 only by a factor 3, so that the last

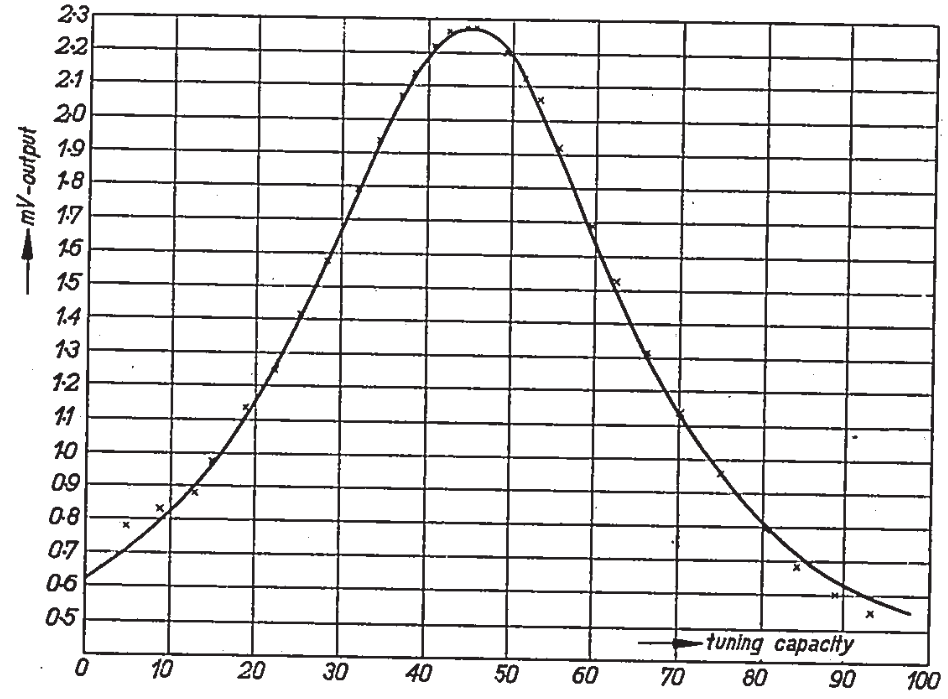

Fig. 4. Noise resonance curve for an EFF 50 pentode with the two systems connected in parallel. The resonance curve is practically symmetric. Crosses measured; the full-drawn line is the symmetric theoretical curve.

term of (6) becomes relatively unimportant. The tuned impedance of the input circuit may then be obtained in the normal way. A small asymmetry does not greatly affect the half-value width of the resonance curve.

3. Total-emission noise

Total-emission noise was measured for large diodes. These measurements were made in two parts.

(a) Measurement of the input conductance $1/R$ of the diode (total-emission conductance).

(b) Measurement of the equivalent saturated current I_e, which is defined such that the noise current of the diode is equal to the noise current of a saturated diode having an anode current I_e. The method of measurement has already been described in a previous paper [7]).

Denoting normal room temperature by T, Boltzmann's constant by k, and the noise ratio of the diode by a, we have [7]):

$$a = \frac{e}{2kT} I_e R = 20 I_e R = T_e/T. \tag{7}$$

(I_e in A, R in Ω). As a is a noise ratio, it may be written as a ratio of two equivalent noise temperatures T_e and T, T_e being the noise temperature of the diode and T again normal room temperature.

Measurements were carried out at 7·25 m wavelength on a diode [2]) having an emitting cathode area of 10 cm² and an anode-cathode distance of 0·1 cm. The results are shown in figs 5 and 6. In fig. 5 $1/R$ is plotted against the anode voltage V_a, in fig. 6 I_e is plotted against V_a for a heater voltage $V_f = 12$ V as well as for $V_f = 8$ V. According to fig. 6 the equivalent current I_e is much larger than the anode current I_a. The relation

$$I_e = I_a$$

would be expected for diodes in the cut-off region at long wavelengths; the increase in I_e at 7·25 m is due to total-emission noise.

The saturation currents for $V_f = 12$ V and $V_f = 8$ V differed by a factor 50, whereas, for the same value of V_a, I_e and $1/R$ only differ by a factor 3. Hence, $1/R$ and I_e are only slightly dependent upon the saturation current.

$1/R$ and I_e are approximately proportional to V_a^{-2}. This is shown by the dashed curves $C\,V_a^{-2}$ in figs 5 and 6 in which the values of the constant C are chosen such that each dashed curve coincides with the corresponding full-drawn curve at $V_a = -1{\cdot}0$ V (the curves of figs 5 and 6 are not corrected for contact potentials).

Fig. 6 also shows the noise ratio $a = T_e/T$. As $T = 290$ °K we have approximately, according to fig. 6:

$$V_f = 12 \text{ V}, \quad T_e = 1200\ ^\circ\text{K};$$
$$V_f = 8 \text{ V}, \quad T_e = 900\ ^\circ\text{K}.$$

This almost coincides with the actual cathode temperature, so that the total-emission noise may be described by assuming that the equivalent noise temperature T_e of the total-emission conductance $1/R$ is equal to the actual cathode temperature.

This relation certainly holds for the cut-off region if the influence of space-charge upon the potential distribution between cathode and anode (or between cathode and grid in a triode) is negligible, as will be shown in a subsequent paper.

The following theoretical argument may be put forward for its general validity.

It is well known that at long wavelengths (no total-emission noise) the equivalent noise temperature of a diode in the exponential part of its characteristic is equal to $\frac{1}{2}\,T_c$, if T_c denotes the cathode temperature. The reason

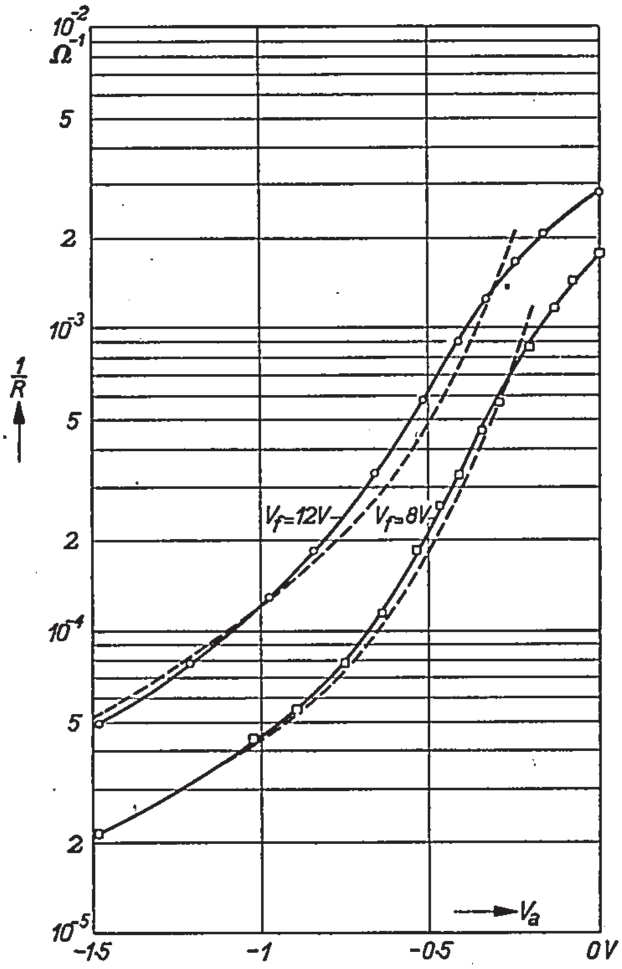

51639

Fig. 5. $1/R$ as a function of V_a for heater voltages V_f of 12 V and 8 V.

why the equivalent noise temperature of the diode is not equal to the cathode temperature T_c, is that — owing to the existence of the anode current I_a — the diode is not a resistance R in the normal sense. It would behave as an ordinary resistance R if not only a current I_a arrived at the anode, but also a saturated current I_a were emitted by the anode in the opposite direction (as long as this does not cause a potential minimum between cathode and anode, the internal resistance R will not be changed). The mean-square value of the current fluctuations is then doubled, because both currents give rise to independent current fluctuations of the same mean-square value, and hence the equivalent noise temperature of the new diode is equal to T_c. The total current being zero, the diode behaves in every respect as a resistance at cathode temperature T_c. From a thermodynamical point of view we should also expect the equivalent noise temperature of this diode to be equal to the cathode temperature T_c [9]).

The above reasoning should also hold for higher frequencies. Of course,

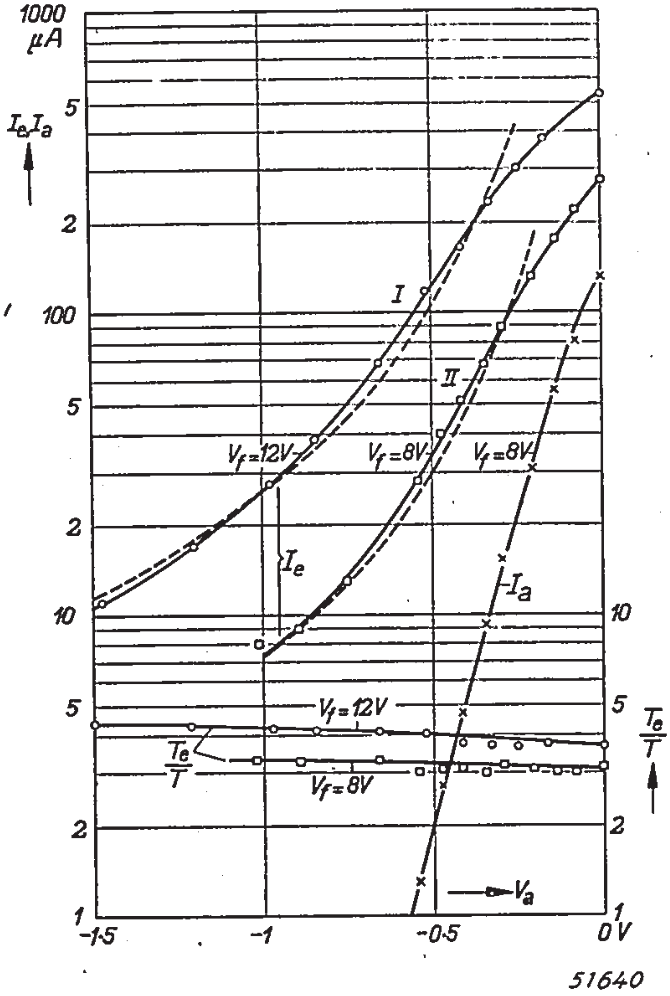

Fig. 6. I_e, I_a and T_e/T as a function of V_a for heater voltages V_f of 12 V and 8 V.

the internal resistance of this diode may be changed (owing to total-emission conductance [1])) and its equivalent diode current I_e' may be changed too (due to total-emission noise), but there is no reason whatever why the equivalent noise temperature of this diode should differ from the cathode temperature (except perhaps at very high frequencies, for which the transit time of the electrons is great in comparison with the period of the oscillations).

Turning again to a normal diode, having an anode current I_a and not showing anode emission, we find that the equivalent diode current becomes $I_e = I_e' - I_a$ instead of I_e', because the equivalent diode current of the anode emission was equal to I_a. Since the internal resistance of the diode is practically independent of the anode emission, we should expect an equivalent noise temperature of

$$T_e = \frac{I_e' - I_a}{I_e'} \cdot T_c = \frac{I_e}{I_e + I_a} \cdot T_c \,. \qquad (8)$$

If $I_e \gg I_a$ this is practically equal to the cathode temperature T_c.

Eindhoven, June 1947

REFERENCES

[1]) C. N. Smyth, Nature **157**, 841, 1946.
[2]) A. van der Ziel and A. Versnel, Nature **159**, 640, 1947.
[3]) C. J. Bakker, Physica, 's-Grav. **8**, 23-43, 1941.
[4]) D. O. North and W. R. Ferris, Proc. Inst. Radio Engrs **29**, 49-50, 1941.
[5]) M. J. O. Strutt and A. van der Ziel, Physica, 's-Grav. **8**, 1-22, 1941.
[6]) W. Kleen, Telefunkenröhre **23**, 274, 1941.
[7]) A. van der Ziel, Philips Res. Rep. **2**, 321-330, 1947.
[8]) A. van der Ziel, Philips Res. Rep. **1**, 381-399, 1946.
[9]) D. O. North, RCA Rev. **4**, 441-472, 1939; **5**, 106-124, 1940.

R 68 Philips Res. Rep. 3, 24-36, 1948

THE DETERMINATION OF THE INTEGRATION CONSTANTS WHEN CALCULATING TRANSIENT PHENOMENA *)

by B. D. H. TELLEGEN

621.392.1:537.311.5:517.941

Summary

A network is considered containing a voltage source v under the influence of which a current i flows in a certain branch. A method is given for calculating from the differential equation connecting i and v the discontinuities in i and its derivatives resulting from discontinuities in v and its derivatives. The method is applied to the calculation of periodic phenomena caused by periodic sources containing discontinuities.

Résumé

On considère un circuit contenant une source de tension v poussant un courant i dans une certaine branche et on donne une méthode pour calculer, à partir de l'équation différentielle relative à i et v, les discontinuités dans i et ses dérivées, résultant des discontinuités dans v et ses dérivées. La méthode est appliquée au calcul de phénomènes périodiques provoqués par des sources périodiques présentant des discontinuités.

1. The problem

If a voltage source v, when acting upon a network composed of linear, constant elements, produces a current i in a certain branch of this network, the connection between i and v will be expressed by an ordinary linear differential equation with constant coefficients of the type

$$(a_0\mathrm{D}^n + a_1\mathrm{D}^{n-1} + \dots + a_n)\, i = (b_0\mathrm{D}^n + b_1\mathrm{D}^{n-1} + \dots + b_n)\, v\,. \tag{1}$$

Here D is the differential operator d/dt, and the a's and b's are determined by the numerical magnitude of the elements composing the network; some of the a's and b's may be zero.

If v is of sinusoidal wave form with angular frequency ω, there will exist a sinusoidal solution for i with the same angular frequency ω. This solution is obtained by replacing D in (1) by $j\omega$, and i and v by their complex values I and V; this gives

$$I = \frac{b_0(j\omega)^n + b_1(j\omega)^{n-1} + \dots + b_n}{a_0(j\omega)^n + a_1(j\omega)^{n-1} + \dots + a_n}\, V. \tag{2}$$

Conversely, if (2) is known we may deduce the differential equation from it by multiplying by the denominator and replacing $j\omega$ by D, and I and V

---

*) Published in Dutch in Tijdschr. Ned. Radiogenootschap 11, 173, 1946.

by their instantaneous values i and v; frequently this is a simpler way to deduce the differential equation than its direct derivation from the network diagram.

If v and, with it, the right-hand side of equation (1) are prescribed functions of the time, i will have to satisfy a non-homogeneous differential equation with constant coefficients. According to common theory, the general solution of such an equation is obtained by adding the general solution of the corresponding homogeneous equation to a particular solution of the non-homogeneous equation, so that i will in general be

$$i = \sum_{k=1}^{n} A_k e^{p_k t} + \text{particular solution}, \tag{3}$$

where the p_k's are the roots of

$$a_0 p^n + a_1 p^{n-1} + \ldots + a_n = 0\,, \tag{4}$$

and the A_k's are a set of n integration constants. How to determine these integration constants, will be the problem discussed in this paper.

If from a certain instant, $t = 0$, onwards v is a given function of time, the currents and voltages in the network will be determined, provided the energy distribution in the network at $t = 0$ is known, or, what comes to the same thing, provided we know the initial direction and magnitude of the voltages across the condensers and of the currents through the coils. These are the initial conditions, and the number of integration constants will consequently be equal to the number of independent data necessary to determine the energy distribution at the initial point $t = 0$. This number will never exceed the sum of the number of condensers and the number of coils in the network, but it may be smaller; for instance, if the network comprises three condensers in delta connection or three coils in star connection, two independent data will suffice to determine the energy distribution in each of these three-element sets.

Instead of computing the current in a certain branch we may be asked to compute the voltage on a certain branch, and instead of a voltage source the network may contain a current source. The differential equations needed for these purposes are analogous to (2) so that all arguments will also apply to them.

2. First method

A first method for determining the integration constants consists in expressing the voltages across the condensers and the currents through the coils in the current sought, i, in the prescribed voltage, v, and in their derivatives. As a rule this can be carried out from the network diagram without having to perform integrations. Substituting for i in the expressions obtained its value according to (3), and then putting $t = 0$, we shall be led to n independent linear equations from which the integration constants may be computed.

Let us illustrate this method by a simple example: we are asked to find the current i produced by the voltage source v in the network of fig. 1. The A.C. calculus easily yields

$$I = \frac{j\omega CR_2 + 1}{j\omega CR_1R_2 + R_1 + R_2}\,V, \tag{5}$$

so that the corresponding differential equation will be

$$(CR_1R_2\,\mathrm{D} + R_1 + R_2)\,i = (CR_2\,\mathrm{D} + 1)\,v\,. \tag{6}$$

The general solution of this equation is

$$i = Ae^{-at} + f(t)\,, \tag{7}$$

where $a = (R_1 + R_2)/CR_1R_2$ and $f(t)$ is a particular solution.

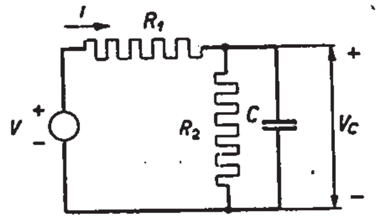

Fig. 1. Simple network diagram.

To find A we have now to express the voltage across the condenser, v_C, in i and v and substitute for i its value according to (7). From fig. 1 we thus obtain

$$v_C = v - R_1 i = v - AR_1 e^{-at} - R_1 f(t)\,,$$

which for $t = 0$ reduces to

$$v_{C0} = v_0 - AR_1 - R_1 f(0)\,,$$

where v_{C0} and v_0 represent the voltages v_C and v at time $t = 0$. For A we thus have

$$A = \frac{v_0 - v_{C0}}{R_1} - f(0)\,. \tag{8}$$

3. A second method

A second method of determining the integration constants consists in expressing i and its first n—1 derivatives in terms of the voltages across the condensers, the currents through the coils, v and derivatives of v. Again these calculations can in general be carried out from the network diagram without additional integrations. By substituting the resultant expressions in (3) and in the equations obtained from (3) by differentiating $(n-1)$ times with respect to t, and by then putting $t=0$, we arrive, as before, at a set of n independent linear equations from which the integration constants may be computed.

Applying this method to the example discussed above we have at once from fig. 1

$$i=\frac{v-v_C}{R_1}.$$

If this is substituted in (7) and t is put equal to zero we obtain

$$\frac{v_0-v_{C0}}{R_1}=A+f(0),$$

which is the same equation as (8).

There will be a more pronounced difference between the first method and the second when they are applied to networks leading to differential equations of higher order.

4. A third method

In both the methods outlined above we have to compute n quantities from the network diagram, and this may be a laborious procedure. We shall now show that in many cases the differential equation contains all the data necessary for computing the integration constants from the initial conditions, and on this principle we shall base a third method for computing these constants. In following this practice we need no longer consider the network diagram once the differential equation has been obtained, and consequently we are led to the desired end by a shorter path.

Let us first consider the case where the initial energy in the network is zero. To show that under these conditions the differential equation completely determines the current i as a function of the time, we suppose that v has also been prescribed previous to $t=0$, and in particular that in this interval v is constantly zero; likewise we suppose that previous to $t=0$ the energy in the network and, with it, the current i were both zero. If now, at $t=0$, v suddenly jumps to a value v_0, then (except in a particular case, to which we shall return in section 4·3) the energy immediately after this jump will still be zero, so that, for computing the current i in the interval following $t=0$, we have again to solve our original problem. The current i will now have to satisfy the differential equation both for $t<0$ and for $t>0$; but at $t=0$ there are discontinuities so that it cannot be stated that i satisfies the differential equation at this point. But if, instead of assuming a jump in v, we conceive v as changing gradually in a short interval, which will be designated as the transition interval, i will also have to satisfy the differential equation during this transition interval; consequently, i will now satisfy one differential equation for every value of t. The initial conditionswill be that $i = 0$ for $t < 0$. The differential equation must now suffice to compute i for $t > 0$ without any further reference to the network diagram. By finally reducing the transition interval to zero we arrive at the solution of our actual problem.

If in the initial state the network does possess energy, and this energy is determined by the voltages across the condensers and the currents through the coils, we shall have to use the network diagram for computing the integration constants, as indicated in sections 2 and 3. Often, however, the problems actually to be solved are of a different nature: a voltage v, acting on a network and producing in a certain branch of this network an already known current i, makes a jump at $t = 0$, and we wish to calculate the future course of the current i. For instance, the closing of a switch will lead to such a jump, for a switch may be considered as a voltage source equal to the voltage across the switch, which suddenly drops to zero upon the switch being closed (the opening of a switch may better be considered as equivalent to a jump in a current source, for a switch may also be considered as a current source equal to the current through the switch, which suddenly drops to zero upon the switch being opened). If we assume the change in v to be a gradual one, taking place in a short interval, i will again have to satisfy a single differential equation, the initial conditions now being that for $t < 0$ i must be a known function of the time. As before, it must now be possible to evaluate the integration constants without referring to the network diagram.

In a more general way these results may be stated as follows. If i and v are connected by a differential equation of the nth order in i, and if the prescribed value of v includes a jump at $t = 0$, the general expression for i will include n integration constants both for $t < 0$ and for $t > 0$. But if the jump in v is replaced by a gradual change within a short transition interval, the general expression for i will include only one set of n integration constants. Hence, there will necessarily exist n relations between the integration constants valid for $t < 0$ and those valid for $t > 0$. We shall now put the problem of deducing these relations for the case when the transition interval is reduced to zero.

4·1. Requirements of continuity

When the transition interval is reduced to zero, in v a jump will arise at $t = 0$ and v will thus become discontinuous at this point; $\int v dt$, however, which for the sake of brevity will sometimes be designated as $D^{-1}v$, will remain continuous, and the same will hold true for $D^{-2}v$, $D^{-3}v$, and so on.

If we now first integrate (1) $(n+1)$ times with respect to the time for a finite transition interval and then reduce this interval to zero we obtain

$$(a_0 D^n + a_1 D^{n-1} + \dots + a_n)\, D^{-n-1} i = (b_0 D^{-1} + b_1 D^{-2} + \dots + b_n D^{-n-1})\, v. \quad (9)$$

From the above arguments it follows that the right-hand side of this equation is a continuous function of the time. On the left-hand side we may consider $D^{-n-1} i$ as a new independent variable. From the theory of differential equations we then know that if $a_0 \neq 0$ there will exist solutions of (9) that are continuous and possess n continuous derivatives, so that $D^{-n-1} i$ and its n derivatives will all be continuous functions of t.

If we now write (1) in the form

$$D^n(a_0 i - b_0 v) + D^{n-1}(a_1 i - b_1 v) + \dots + (a_n i - b_n v) = 0, \quad (10)$$

integrate n times with respect to t for a finite transition interval, and then reduce this interval to zero, we have

$$(a_0 i - b_0 v) + D^{-1}(a_1 i - b_1 v) + \dots + D^{-n}(a_n i - b_n v) = 0.$$

Since in this equation we know all the terms except the first to be continuous, the first term will be continuous too, so that

$$(a_0 i - b_0 v) \text{ will be continuous at } t = 0. \quad (11)$$

Therefore, if at $t = 0$ v makes a jump, e.g. increases by an amount Δv, i will also make a jump at $t = 0$ and will increase by an amount Δi which may be computed from $a_0 \Delta i - b_0 \Delta v = 0$.

Likewise, integrating (10) $(n-1)$ times we obtain

$$D(a_0 i - b_0 v) + (a_1 i - b_1 v) + \dots + D^{-n+1}(a_n i - b_n v) = 0.$$

Since in this equation we know all terms, except the first two, to be continuous, the sum of the first two terms will be continuous too, so that

$$D(a_0 i - b_0 v) + (a_1 i - b_1 v) \text{ will be continuous at } t = 0. \quad (12)$$

By integrating (10) respectively n, $(n-1)$, $(n-2)$, ..., 1 times, and applying the same arguments to each of the resultant expressions, we thus obtain n relations of which the last one will be that

$$D^{n-1}(a_0 i - b_0 v) + D^{n-2}(a_1 i - b_1 v) + \dots + (a_{n-1} i - b_{n-1} v)$$
$$\text{will be continuous at } t = 0. \quad (13)$$

These are the n relations that we have been seeking. They will still remain valid when v is continuous and Dv discontinuous, or when v and Dv are both continuous but $D^2 v$ discontinuous, and so on. This result may be summarized as follows.

Let v *and* i *be two functions of* t *that are connected by a linear differential equation of the form*

$$(a_0\mathrm{D}^n + a_1\mathrm{D}^{n-1} + \dots + a_n)\, i = (b_0\mathrm{D}^n + b_1\mathrm{D}^{n-1} + \dots + b_n)\, v\,.$$

If v *and* i *both pass through an infinite sequence of functions that tend to a limit function, the* n *quantities*

$$(a_0i-b_0v),\ \mathrm{D}(a_0i-b_0v) + (a_1i-b_1v),\ \dots \\ \dots,\ \mathrm{D}^{n-1}(a_0i-b_0v) + \mathrm{D}^{n-2}(a_1i-b_1v) + \dots + (a_{n-1}i-b_{n-1}v)$$

computed for this limit will all be continuous, provided $a_0 \neq 0$ *and* $\int v\mathrm{d}t$ *remains continuous in the limit.*

If at $t = 0$ v or a derivative of v makes a jump, the corresponding discontinuity in i will be computable from the condition that "a_0i-b_0v is continuous"; next, from the condition that "$\mathrm{D}(a_0i-b_0v) + a_1i-b_1v$ is continuous", the discontinuity in Di may be computed, and so on. If i is known for $t < 0$, the values of i and its first $n-1$ derivatives immediately after $t = 0$ may all be computed in this manner. In the particular case of a voltage source connected at $t = 0$ to a network that contains no energy, the quantities a_0i-b_0v, $\mathrm{D}(a_0i-b_0v) + a_1i-b_1v$, etc. will be zero immediately after $t = 0$. By substituting the resulting values of i and its $n-1$ derivatives for $t = 0$ in equation (3) and in the $n-1$ equations deduced from (3) by differentiation, and by making $t = 0$, we are again led to n independent linear equations for the integration constants.

By applying this method to the circuit of fig. 1, for which according to (6) $a_0 = CR_1R_2$ and $b_0 = CR_2$, we find that $CR_1R_2i-CR_2v$ will be continuous for $t = 0$, so that $\Delta i = \Delta v/R_1$, a result that may also directly be read from fig. 1.

4·2. Discontinuities of different order

The significance of the differential equation for the transition interval may also be investigated in the following way.

If in the transition interval v increases monotonically, Dv will show a sharp maximum, D^2v a sharp maximum followed by a zero and a sharp minimum, and so on (fig. 2). If the transition interval approaches zero these different curves will tend to discontinuities of different type: in v there will arise a jump; in Dv the maximum will become infinite whereas the area under the curve will remain finite, or, in other words, in the limit Dv will show a pulse; in D^2v the discontinuity will be of a still more complicated type, which we shall designate as a discontinuity of the second order. Likewise, a pulse will be called a discontinuity of the first order and a jump a discontinuity of order zero. Similar changes will take place in the current i: there will be a jump in i, a pulse in Di, and so on.

It will now be clear that in the differential equation written in the form (10) the highest-order discontinuities will be contained only in the first term. As these cannot be compensated by discontinuities of lower order, this term, a_0i-b_0v, will have to be continuous, for in that case $D^n(a_0i-b_0v)$ will possess a discontinuity of an order not higher than the $(n-1)$th. The highest discontinuities then remaining are those of the $(n-1)$th order, and these can only be due to the first two terms, which may be written as

$$D^{n-1}\{D(a_0i-b_0v) + (a_1i-b_1v)\}.$$

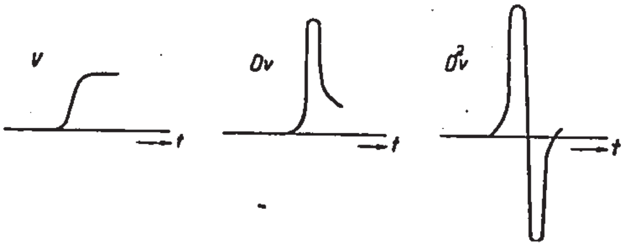

Fig. 2. Discontinuities of increasing order.

Since these discontinuities of order $(n-1)$ will have to cancel out, $D(a_0i-b_0v) + (a_1i-b_1v)$ will be continuous, and so on. We are thus led to the same conditions as were deduced above, and these may be interpreted as the conditions requiring that the discontinuities of order n, $(n-1)$, ... shall successively cancel out.

4·3. The case $a_0 = 0$

If $a_0 = 0$ but $b_0 \neq 0$, we put $i = Dq$, q thus being the electric charge that has passed through the particular branch under consideration. The differential equation then becomes:

$$(a_1D^n + a_2D^{n-1} + \dots + a_nD)\,q = (b_0D^n + b_1D^{n-1} + \dots + b_n)\,v. \quad (14)$$

For $a_1 \neq 0$ all the arguments given above still apply; we conclude that

$$(a_1q-b_0v) \text{ will be continuous, etc.} \quad (15)$$

A jump in v will produce a jump in q and a pulse in $i = Dq$.

This will apply, for instance, to a network in which a voltage source v forms part of a mesh composed solely of condensers; a jump in v will cause jumps in the voltages across the condensers and pulses in the currents through the condensers. If the energy in the network was originally zero it will no longer be zero immediately after the jump in v.

A simple example will be obtained by making $R_1 = 0$ in the network drawn in fig. 1. Putting $i = Dq$, (6) becomes:

$$R_2\,Dq = (CR_2\,D + 1)\,v\,, \quad (16)$$

from which in virtue of (15) it follows that $R_2q - CR_2v$ must be continuous at $t = 0$; hence $\Delta q = C\Delta v$, a result that may also directly be deduced from fig. 1.

Analogous conditions will prevail if a current source forms part of a network such that every mesh containing the current source also contains a coil. An example is provided by the network of fig. 3, which will be discussed in detail in section 5; a jump in the current source necessitates jumps in the currents through the coils and pulses in the voltages across the coils. If the energy in the network is at first zero, it will no longer be zero immediately after the jump in the current source.

The case $a_0 = 0$, $a_1 = 0$, $a_2 \neq 0$, $b_0 \neq 0$ may be treated by putting $i = \mathrm{D}^2 s$.

4·4. A discontinuity in $\int v\mathrm{d}t$

In case the discontinuity in v is not a jump but a pulse, also $\int v\mathrm{d}t$ will be discontinuous. Putting $v = \mathrm{D}\varphi$, φ will make a jump and $\int \varphi\mathrm{d}t$ will be continuous; by substituting $v = \mathrm{D}\varphi$ in the differential equation we are led back to cases that have already been investigated above.

Discontinuities of the second order in v may similarly be treated by putting $v = \mathrm{D}^2\psi$, $\int \psi\mathrm{d}t$ now being continuous.

5. Periodic voltage sources with discontinuities

The methods adopted above may be used for computing the periodic currents in a network produced by a periodic voltage source comprising discontinuities. As an example we shall compute the current through one of two coils connected in parallel in the anode circuit of an amplifier tube having a saw-tooth voltage impressed upon its grid. The tube will be supposed to possess a transconductance S and a high internal resistance. After replacing the tube by a current source Sv we are faced with the circuit of fig. 3; L_1 and R_1 are the inductance and the resistance of the coil carrying the current to be computed and L_2 and R_2 are the corresponding quantities for the second coil.

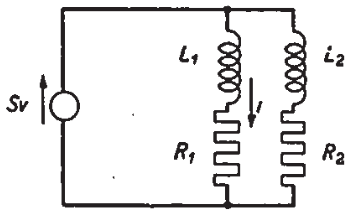

Fig. 3. A current source in parallel to two coils.

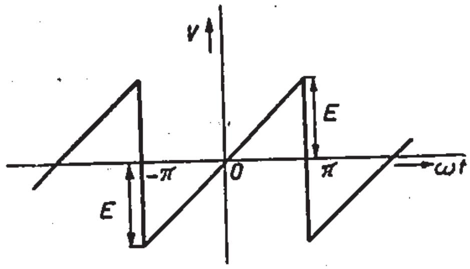

Fig. 4. Saw-tooth voltage.

From the diagram we have

$$I = \frac{j\omega L_2 + R_2}{j\omega\,(L_1 + L_2) + R_1 + R_2}\,SV,$$

so that the differential equation reads

$$\{(L_1 + L_2)\mathrm{D} + R_1 + R_2\}\, i = (L_2 S\,\mathrm{D} + R_2 S)\, v. \tag{17}$$

If the saw-tooth voltage varies as indicated in fig. 4, we have $v = E\omega t/\pi$ when $-\pi < \omega t < \pi$, and the general solution of the differential equation will be

$$i = Ae^{-\frac{R_1+R_2}{L_1+L_2}t} + \frac{R_2}{R_1 + R_2}\cdot\frac{SE}{\pi}\omega t + \frac{L_2R_1 - L_1R_2}{(R_1 + R_2)^2}\cdot\frac{SE}{\pi}\,\omega, \tag{18}$$

as may be readily verified; A is the integration constant.

There is a jump in v at $\omega t = \pi$, so that applying the theory developed above we conclude that $(L_1 + L_2)i - L_2Sv$ will be continuous at this point. As we require a periodic solution for i, the value of i directly after the jump in v at $\omega t = \pi$ will be the same as the value of i at $\omega t = -\pi$; we are thus led to

$$\{(L_1 + L_2)\, i - L_2\, Sv\}_{\omega t=\pi} = \{(L_1 + L_2)\, i - L_2\, Sv\}_{\omega t=-\pi}, \tag{19}$$

whence

$$(L_1 + L_2)\left\{Ae^{-\frac{R_1+R_2}{L_1+L_2}\cdot\frac{\pi}{\omega}} + \frac{R_2}{R_1 + R_2}\cdot SE + \frac{L_2R_1 - L_1R_2}{(R_1 + R_2)^2}\cdot\frac{SE}{\pi}\omega\right\} - L_2SE =$$

$$= (L_1 + L_2)\left\{Ae^{\frac{R_1+R_2}{L_1+L_2}\cdot\frac{\pi}{\omega}} - \frac{R_2}{R_1 + R_2}\cdot SE + \frac{L_2R_1 - L_1R_2}{(R_1 + R_2)^2}\cdot\frac{SE}{\pi}\omega\right\} + L_2\,SE.$$

The integration constant will consequently be given by

$$A = \frac{L_1R_2 - L_2R_1}{(R_1 + R_2)\,(L_1 + L_2)}\cdot\frac{SE}{\sinh\left(\frac{R_1 + R_2}{L_1 + L_2}\cdot\frac{\pi}{\omega}\right)}. \tag{20}$$

6. The periodic opening and closing of a switch

We now proceed to apply our theory to the calculation of the periodic currents and voltages in a network comprising switches that are periodically opened and closed. This will be illustrated by a simple example for which the physical interpretation of the conditions for the integration constants can at once be understood from the network diagram.

In fig. 5 the D.C. source E is connected to a circuit consisting of R, L, and C in series; C is shunted by a switch that is operated periodically. We suppose that the switch is closed at $t = 0$, $t = T$, $t = 2T$, etc., and opened at $t = aT$, $(1 + a)T$, $(2 + a)T$, etc. $(0 < a < 1)$, and we shall seek to compute the current through and the voltage across the switch.

The differential equation connecting i and v is easily derived as being

$$(CL\,\mathrm{D}^2 + CR\,\mathrm{D} + 1)\,v + (L\,\mathrm{D} + R)\,i = E. \tag{21}$$

In the interval $0 < t < aT$ the switch is closed; thus $v = 0$ and the differential equation is solved by

$$i = Ae^{pt} + E/R, \tag{22}$$

A being the integration constant and $p = -R/L$.
When $aT < t < T$ the switch is open; thus $i = 0$ and the differential equation is solved by

$$v = B_1 e^{q_1 t} + B_2 e^{q_2 t} + E, \tag{23}$$

B_1 and B_2 being the two integration constants, and q_1 and q_2 being the roots of $CLq^2 + CRq + 1 = 0$.

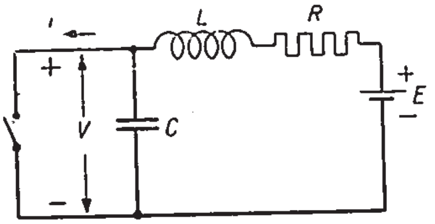

Fig. 5. Network comprising a periodically opening and closing switch.

At $t = aT$ the switch opens and thus i makes a jump. Since the right-hand side of the differential equation is continuous, in investigating the discontinuities we have only to consider the left-hand side. From it we deduce that CLv and $CL\mathrm{D}v + CRv + Li$ must both be continuous at $t = aT$.

The first of these conditions gives

$$v_{aT+0} = v_{aT-0} = 0, \tag{24}$$

where the index $aT + 0$ indicates the moment immediately following and $aT - 0$ the moment immediately preceding the opening of the switch. Combining this result with the second condition we obtain

$$(C\mathrm{D}v + i)_{aT+0} = (C\mathrm{D}v + i)_{aT-0},$$

from which

$$C\mathrm{D}v_{aT+0} = i_{aT-0}. \tag{25}$$

The expressions (24) and (25) allow a straight-forward physical interpretation; (24) expresses that the voltage across the condenser does not change when the switch opens and (25) expresses that the current through the coil does not change either, for this current will be i when the switch is closed and CDv when the switch is open. Combining (24) and (25) with (22) and (23) we obtain

$$B_1 e^{q_1 aT} + B_2 e^{q_2 aT} + E = 0 \tag{26}$$

and

$$C(q_1 B_1 e^{q_1 aT} + q_2 B_2 e^{q_2 aT}) = A e^{paT} + E/R. \tag{27}$$

At $t = T$ the switch closes, so that v makes a jump. From the differential equation it follows that i will acquire a pulse, so that we put $i = \mathrm{D}q$. It may then be deduced that $CLv + Lq$ and $CL\mathrm{D}v + CRv + L\mathrm{D}q + Rq$ are both continuous at $t = T$. By multiplying the first of these expressions by R/L and subtracting it from the second one, q is eliminated, and we find that $CL\mathrm{D}v + L\mathrm{D}q$, or $C\mathrm{D}v + i$, must be continuous at $t = T$. Hence

$$i_{T+0} = C\mathrm{D}v_{T-0}. \tag{28}$$

Analogous to (25) this equation expresses that the current through the coil does not change upon the closing of the switch. In order that the phenomena shall be periodic, i directly after $t = T$ must be equal to i directly after $t = 0$. It then follows from (28), (22), and (23) that

$$A + E/R = C(q_1 B_1 e^{q_1 T} + q_2 B_2 e^{q_2 T}). \tag{29}$$

From (26), (27), and (29) the integration constants may now be computed.

If the switch is a gas-filled triode in which a periodic grid voltage produces periodic discharges, the interval during which the tube passes current is as a rule only a small fraction of the total period. To compute the voltage across the condenser under these circumstances, in the equations for the integration constants a must be made to approach zero; at the same time, A may be eliminated. Thereby we obtain

$$B_1 + B_2 + E = 0 \tag{30}$$

and

$$q_1 B_1 + q_2 B_2 = q_1 B_1 e^{q_1 T} + q_2 B_2 e^{q_2 T}. \tag{31}$$

Equation (30) states that the voltage will be zero immediately after the discharge, that is, immediately after $t = 0$. Equation (31) may be deduced directly by observing that, under the conditions considered here, i acquires pulses at $t = 0$, $t = T$, etc., but is otherwise zero. We therefore substitute $i = \mathrm{D}q$ in (21) and, just as above, deduce from this equation that $C\mathrm{D}v + i$ must be continuous at the moment of the discharge. As i is zero both before and after this point, $\mathrm{D}v$ must be continuous. In physical terms this signifies that the current through the condenser, and hence the current through the coil, just before the discharge is equal to that just after the discharge. If the voltage is to be periodic, $\mathrm{D}v$ must have the same value just after $t = 0$ and just before $t = T$; this leads to (31).

7. Final remarks

All theories concerning the influence of discontinuities in voltage or current sources are only approximations of reality; this should always be borne in mind. Discontinuities in the sense of mathematics are excluded in actual phenomena; the transitions will always take place in finite intervals, and it will depend on the nature of the problems under investigation whether it is permissible to approximate these transitions by mathematical discontinuities.

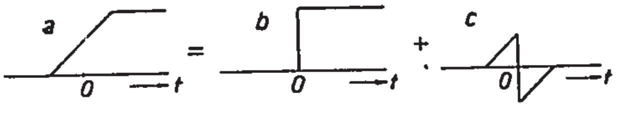

Fig. 6. Approximation of a transition by a jump.

For instance, when our voltage source varies as in fig. 6*a* we may try an approximation according to fig. 6*b*, and in so doing we disregard the difference between the two, represented in fig. 6*c*. If this is not allowed, the voltage of fig. 6*c* may be approximated by a discontinuity of the second order, which may be added to the jump of fig. 6*b*.

If the voltage source varies as in fig. 7, then in reducing the transition interval to zero we may either keep the peak voltage constant, so that $\int v\,dt$ will be continuous in the limit, or we may keep the area under the curve constant, so that in the limit $\int v\,dt$ will show a jump. It will depend on the nature of the problem which of these approximations is the more suitable, a jump or a jump and a pulse. This raises the problem to what extent an arbitrary transition may be approximated by the sum of a set of discontinuities of increasing order.

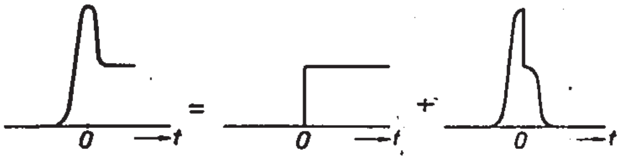

Fig. 7. Approximation of another transition.

The method developed in the paper is also applicable to differential equations whose coefficients are no longer constant but are continuous functions of the time. In the neighbourhood of a discontinuity these coefficients can be regarded as constant. The deduction of the differential equation from the complex expressions by replaing $j\omega$ by D is, of course, no longer possible in this case.

If the coefficients of the differential equation vary discontinuously, at switching processes in the network, the method may be applied by regarding, as mentioned in section 4, the closing of a switch as a jump in a voltage source, and the opening of a switch as the jump in a current source.

Eindhoven, March 1946

R 69 *Philips Res. Rep.* **3**, *37-45, 1948*

THE MEASUREMENT OF PERMEABILITY AND MAGNETIC LOSSES OF NON-CONDUCTING FERROMAGNETIC MATERIAL AT HIGH FREQUENCIES

by H. J. LINDENHOVIUS and J. C. van der BREGGEN

621.317.41:621.317.43:538.221

Summary

A method is described for a rapid and accurate determination of the permeability and the magnetic losses of non-conducting ferromagnetic material.
For frequencies between 30 and 300 Mc/s this method makes use of a coaxial cavity resonator with end-capacitance, accurately tuned to the frequency of an oscillator to which it is coupled. We measure the changes in the resonance frequency of this cavity resonator after successively inserting, concentrically with the inner conductor, a ring made of the ferromagnetic material to be tested and a ring of the same size made of a well-conducting metal. The susceptibility ($\chi = \mu - 1$) of the ferromagnetic material equals the ratio of these two frequency changes.
The magnetic losses can easily be computed from the bandwidths of the cavity resonator with and without the ferromagnetic ring.
For frequencies above 300 Mc/s we have used a coaxial Lecher system instead of the cavity resonator. A minor complication of a dielectric nature then arising is eliminated in a simple way. The equations are the same as for the cavity resonator.
Some data obtained with compressed iron powder and with ferroxcube are given.

Résumé

L'article décrit une méthode de détermination rapide et exacte de la perméabilité et des pertes magnétiques de matériaux ferromagnétiques nonconducteurs.
Pour les fréquences comprises entre 30 et 300 Mc/s cette méthode fait usage d'une cavité résonante coaxiale à capacité terminale, accordée exactement sur la fréquence d'un oscillateur avec lequel elle est couplée. On mesure successivement les changements de la fréquence de résonance de cette cavité résultant de l'insertion, concentriquement au conducteur intérieur, d'un anneau de matériel ferromagnétique à examiner et ensuite d'un anneau de forme identique mais en métal bon-conducteur. La susceptibilité ($\chi = \mu - 1$) du matériel ferromagnétique est égale au rapport de ces deux changements de fréquence.
Les pertes magnétiques peuvent être facilement déduites de largeurs de bande de la cavité de résonance avec et sans anneau ferromagnétique.
Pour les fréquences supérieures à 300 Mc/s on utilise un système de Lecher au lieu d'une cavité de résonance. Une légère complication de nature diélectrique inhérente à l'emploi de ce système est éliminée de manière simple. Les équations sont les mêmes que pour la cavité de résonance.
L'article mentionne quelques chiffres obtenus avec du fer en forme de poudre comprimée et avec le ferroxcube.

1. Introduction

The permeability of non-conducting ferromagnetic material is usually determined by providing a ring of this material with a winding and then measuring its self-inductance in a bridge or a resonance circuit. The permeability relative to vacuum will then be given by

$$\mu = \frac{10^9\, Ll}{4\pi\, N^2 O}, \tag{1}$$

where L is the self-inductance in henries, N the number of turns of the winding, and l and O the length and the cross-section of the magnetic circuit expressed in cm and cm^2, respectively.

Likewise, the losses may be determined by measuring the resistance of the coil, again in a bridge or a resonance circuit. They will of course include the copper losses in the winding and the dielectric losses in the core, but these can be determined by separate experiments and then eliminated by subtraction. We shall not here describe these methods in detail.

The measurements outlined above can be performed from the lowest frequencies up to about 30 Mc/s, provided the number of turns of the winding is, particularly at higher frequencies, kept so low that the resonance frequency of the coil itself, as determined by its self-inductance and its distributed capacitance, lies far above the measuring frequency; otherwise the interpretation of the observations becomes too involved.

There is, however, a limit below which the number of turns cannot be reduced, because the loose magnetic coupling between the turns would render equation (1) invalid; moreover, as by a decrease of the number of turns the self-inductance will be diminished, the disturbing influence of the self-inductance of the leads will increase in a corresponding degree.

These considerations have induced us to look for some other method, not subject to the disadvantages referred to. It soon became evident that coaxial cavity resonators are very suitable for this purpose. In the range from 30 to 300 Mc/s we have used a coaxial cavity resonator with end-capacitance and at still higher frequencies one without end-capacitance. The former will briefly be called a cavity resonator and the latter a Lecher system.

2. The measuring method for frequencies between 30 and 300 Mc/s

A. *Permeability*

It will be remembered that the cavity resonator can be regarded as a shortened, coaxial Lecher system with a lumped capacitance at the end; the self-inductance can be envisaged as being concentrated in the space between the inner and the outer conductor, and the capacitance as located between the two condenser plates. The magnetic lines of force are circles concentric with the inner conductor, and the strength of the magnetic field decreases in inverse proportion to the radius. If now, while keeping the current constant, we place the ferromagnetic ring inside the resonator and concentrically with the inner conductor (fig. 1), nothing will change in the magnetic field of force, not even in the interior of the ring, since eddy currents which would tend to alter the magnetic field within the ring are precluded by the non-conductivity of the ferromagnetic material. But the induction inside the ring will of course be μ times as large as before and hence the self-inductance of the circuit will increase. If the space occupied by the ring initially contributed an amount L_0 to the self-inductance, its contribution after insertion of the ring will be μL_0 and consequently the self-inductance will have increased by $(\mu-1)L_0$.

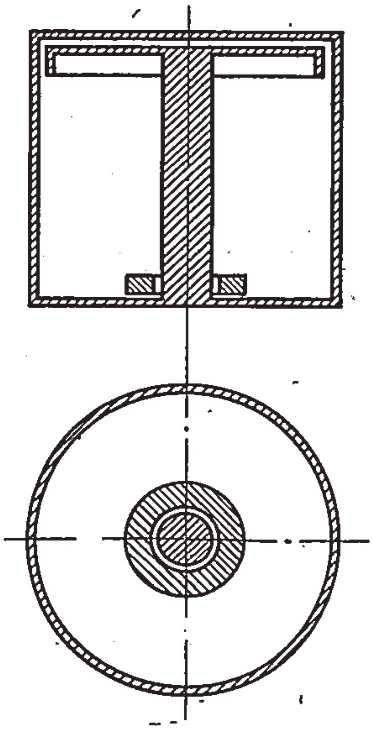

Fig. 1. Vertical and horizontal cross-sections through a coaxial cavity resonator with, on the bottom, the ferromagnetic ring whose permeability and losses have to be determined.

Next we replace the non-conducting magnetic ring by a highly conducting metallic ring of the same dimensions. Again, the magnetic field will be unchanged except, however, inside the ring, where it will be completely nullified by eddy currents at the surface of the ring; hence this space will no longer contribute to the self-inductance of the circuit, which consequently decreases by the amount L_0.

Thus we see that the ratio of the increase in self-inductance produced by the ferromagnetic ring to the decrease produced by the metallic ring equals $\mu-1$. These changes in self-inductance can simply and accurately be measured by determining the resonance frequency of the circuit, which can be done very simply by exciting the circuit by means of an oscillator and observing the frequency for which the voltage across the circuit reaches a maximum; or, alternatively, we may use the circuit as an oscillator and determine the frequency of its oscillations.

Recalling that the change in frequency corresponding to a certain change in self-inductence is given by

$$2\frac{\mathrm{d}\omega}{\omega} = -\frac{\mathrm{d}L}{L}\,{}^{*)} \tag{2}$$

we may write

$$\mu - 1 = -\frac{\mathrm{d}\omega_F}{\mathrm{d}\omega_c} = -\frac{\mathrm{d}f_F}{\mathrm{d}f_c}, \tag{3}$$

where $\mathrm{d}f_F$ and $\mathrm{d}f_c$ represent the frequency changes produced by inserting the ferromagnetic and the metallic ring, respectively. From this it follows that, in performing the measurements indicated above, we do not need to know either the frequency of the circuit, or its self-inductance or capacitance; we only require to know the frequency changes, and even these only in relative measure.

B. *Losses*

Upon inserting the ferromagnetic ring, not only the self-inductance has undergone a change; the resistance is changed as well. Since the copper losses remain unchanged upon the insertion of the ring, because the current distribution is not modified, the increase in resistance must be attributed to losses in the ferromagnetic material.

Denoting by R_c and L_c the original resistance and self-inductance of the resonator and by R_F and L_F the contributions to resistance and self-inductance produced by the ring, we have

$$\frac{R}{L} = \frac{R_c + R_F}{L_c + \frac{\mu-1}{\mu} L_F}, \tag{4 **)}$$

or, rearranged,

$$\frac{R_F}{L_F} = \frac{\mu-1}{\mu}\frac{R}{L} + \frac{L_c}{L_F}\left(\frac{R}{L} - \frac{R_c}{L_c}\right). \tag{5}$$

---

*) Neglecting the influence of losses, which is generally small.

**) In the denominator we have written $(\mu-1)/\mu$ as the space occupied by the ring contributes the amount L_F/μ to the self-inductance before the ring is introduced; the increase in self-inductance due to the insertion of the ring will then be

$$L_F - \frac{L_F}{\mu} = \frac{\mu-1}{\mu} L_F.$$

Thus we see that

$$\tan\delta_F = \frac{\mu-1}{\mu}\tan\delta + \frac{L_c}{L_F}(\tan\delta - \tan\delta_c), \tag{6}$$

where

$$\tan\delta = \frac{R}{\omega L}, \text{ etc.}$$

The ratio L_c/L_F can be deduced from the amount of detuning of the circuit by the ring; since the increase in the self-inductance is $\varDelta L = \frac{\mu-1}{\mu} L_F$, we have by (2)

$$2\frac{\varDelta\omega_F}{\omega} = -\frac{\mu-1}{\mu}\frac{L_F}{L_c}, \tag{7}$$

and consequently

$$\frac{L_c}{L_F} = \frac{\mu-1}{\mu}\frac{\omega}{-2\varDelta\omega_F}. \tag{8}$$

Furthermore, remembering that for an arbitrary circuit $\tan\delta = \overline{\varDelta}\omega/\omega$, where $\overline{\varDelta}\omega$ designates the $\sqrt{2}$-bandwidth, which can easily be determined by the resonance method, we may write

$$\tan\delta_F = \frac{\mu-1}{\mu}\frac{\overline{\varDelta}\omega_{\text{tot}}}{\omega} + \frac{\mu-1}{\mu}\frac{\omega}{-2\varDelta\omega_F}\left(\frac{\overline{\varDelta}\omega_{\text{tot}} - \overline{\varDelta}\omega_c}{\omega}\right), \tag{9}$$

or

$$\tan\delta_F = \frac{\mu-1}{\mu}\left\{\frac{\overline{\varDelta}\omega_{\text{tot}}}{\omega} + \frac{\overline{\varDelta}\omega_{\text{tot}} - \overline{\varDelta}\omega_c}{-2\varDelta\omega_F}\right\}. \tag{10}$$

Once again we see that frequency measurements are all that is required, and that we need not know any of the specific constants of the circuit.

In the majority of cases the first term within the braces of (10) may be ignored in comparison with the second, so that this equation simplifies to

$$\tan\delta_F = \frac{\mu-1}{\mu}\frac{\overline{\varDelta}\omega_{\text{tot}} - \overline{\varDelta}\omega_c}{-2\varDelta\omega_F}, \tag{11}$$

which, when $\mu \gg 1$, further simplifies to

$$\tan\delta_F = \frac{\overline{\varDelta}\omega_{\text{tot}} - \overline{\varDelta}\omega_c}{-2\varDelta\omega_F}. \tag{12}$$

In these cases three frequency measurements will suffice.

3. The measuring method for frequencies higher than 300 Mc/s

At frequencies above 300 Mc/s the cavity resonator can no longer be applied because its size becomes too small; in this region we have used Lecher systems of one quarter wavelength and short-circuited at one end. In this case, too, a ferromagnetic ring is placed concentrically around the inner conductor (fig. 2), and the observations are carried out in precisely the same way as with the cavity resonator.

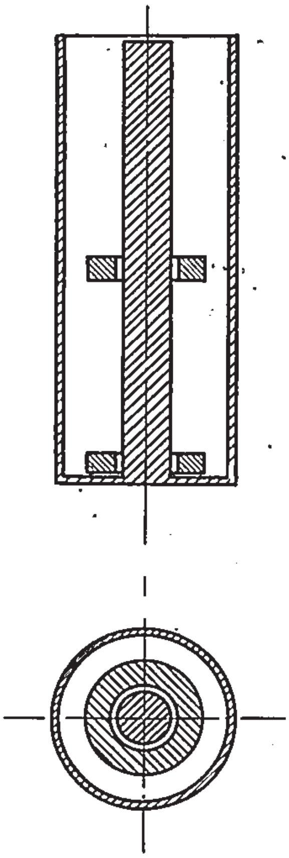

Fig. 2: Vertical and horizontal cross-sections through a $\lambda/4$ Lecher system with the ferromagnetic ring to be measured. Instead of on the bottom the ring can also be placed at some distance from the bottom, in order to diminish the damping of the circuit by the losses in the ring.

One point of difference, however, should be noted: in the Lecher system the strength of the magnetic field decreases with increasing distance from the bottom of the system, which is not the case in the cavity resonator; hence the magnetic coupling between the ring and the circuit may be loosened by placing the ring at a greater distance from the bottom. In the present instance this is a feature of practical importance because, when the ring rests on the bottom and the coupling is therefore at its maximum, the total resistance may become so high as to render the resonance method inapplicable.

The placing of the ring at some distance from the bottom introduces, however, a further complication, since the electric field in the Lecher system increases as we move away from the bottom. Hence, the decrease in magnetic coupling will be accompanied by an increase in electric coupling, and the detuning of the circuit by the insertion of the ring will be the result of simultaneous changes in self-inductance and capacitance, the ferromagnetic material having a dielectric constant differing from unity. Besides, dielectric losses in the ferromagnetic material will add their quota to the increase in the resistance produced by the ring.

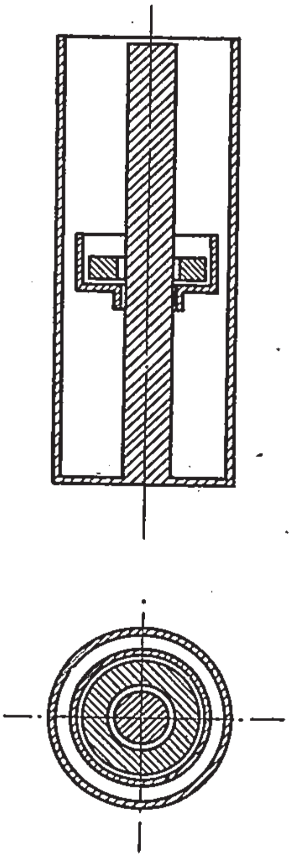

Fig. 3. To avoid disturbing dielectric influences the ring is placed in an open, cylindrical, screening box.

These sources of error can be avoided by placing the ring inside a metallic shield in the shape of an open cylindrical box and forming part of the inner conductor, as indicated in fig. 3. For, inside this shield the electric field will be practically zero whereas the magnetic field will be unchanged. Hence, the observations can be made in exactly the same way as with the cavity resonator: we observe in succession the resonance frequency of the system without a ring, with a ferromagnetic ring, and with a metallic ring inside the shield.

The conditions of the experiment are now essentially the same as those for the cavity resonator, and it can easily be shown *) that the formulae deduced for this case remain valid in the present instance.

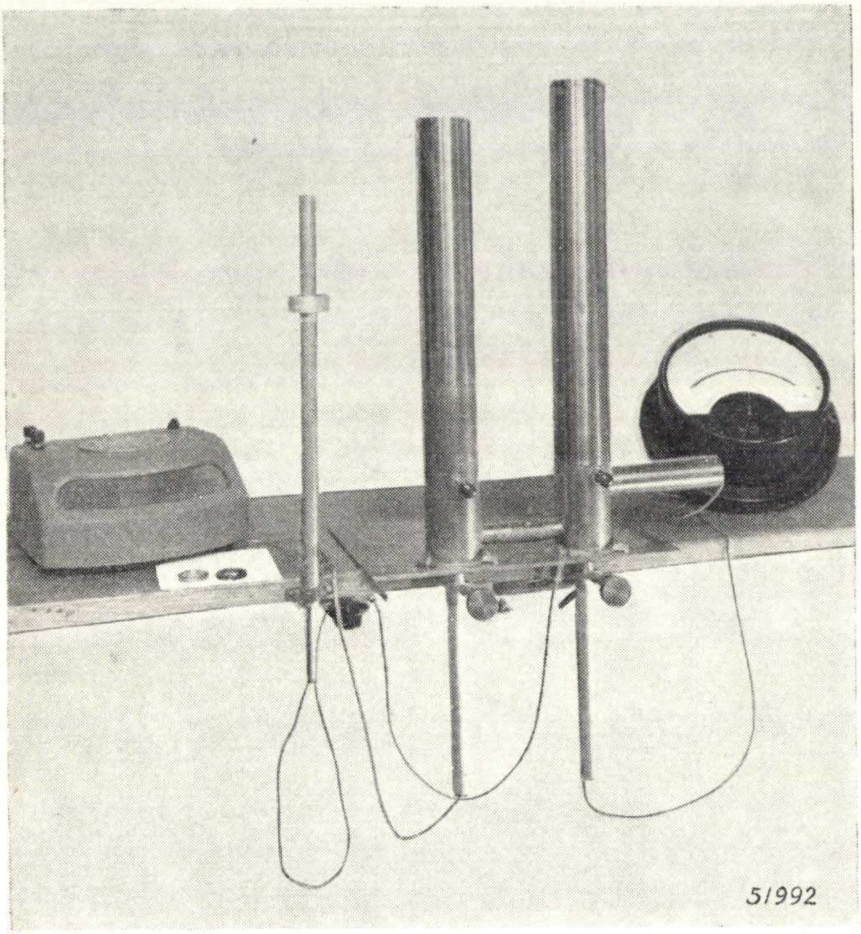

Fig. 4. The arrangement of measurement. The cylindrical tube in the middle is the $\lambda/4$ Lecher system mentioned in the text; the inner conductor with the screening box is separately shown to the left. The circuit voltage is measured by means of a crystal detector placed at the top of the inner conductor; it is read on the left meter. In front of this meter lie a ferromagnetic and a brass ring. The cylindrical tube to the right is the oscillator, also a $\lambda/4$ Lecher system; the oscillator voltage is read on the right meter. The frequency meter, which is of the heterodyne type, is not shown.

---

*) The formulae applying to the Lecher system are almost identical with those deduced for the cavity resonator. Whereas in the cavity resonator the current is constant over the entire length of the inner conductor, this is not so for the Lecher system, and all resistances and self-inductances must be referred to the current at some fixed point, for which we ordinarily choose the bottom of the system.
If the ring has been placed at a point where the current is a times the current at the bottom, its contributions to the resistance and the self-inductance will no longer be R_F and L_F but a^2R_F and a^2L_F instead. Under these circumstances equations (4) to (8) will still hold, provided we replace R_F and L_F by a^2R_F and a^2L_F, respectively. It will be found, however, that by this substitution the final equations (9) to (12) are not altered at all; these equations are valid both for the cavity resonator and for the Lecher system. It hardly needs stating that this also holds for equation (3) used in determining the permeability.

It will also be understood that we may use $\frac{3}{4}\lambda$ or $\frac{5}{4}\lambda$ instead of $\frac{1}{4}\lambda$ Lecher systems if this should be preferable for one reason or another; the same set of equations will still be applicable.

4. Some observations

While bringing these principles into practice we have experienced that this method for measuring the permeability or the losses at high frequencies requires less time than the same set of observations at low frequencies, whereas the observations are equally reliable. Besides, the apparatus needed is extremely simple.

In the table some observations at 300 Mc/s and at 1 Mc/s have been compared:

	300 Mc/s	1 Mc/s	300 Mc/s	1 Mc/s
	μ		tan δ	
Compressed iron powder	12·6	13·2	0·244	0·0011
'Ferroxcube I'	11·0	66	1·51	0·0109

For iron powder the permeability slightly decreases with increasing frequency, whereas tan δ strongly increases, though not quite in proportion to the frequency.

'Ferroxcube I' shows a marked decrease in permeability and an increase in tan δ, which is less pronounced than for iron powder.

Eindhoven, November 1947

R 70 *Philips Res. Rep.* **3**, *46-48, 1948*

THE FLUORESCENCE OF HEXAVALENT URANIUM IN GLASS

by F. A. KRÖGER, J. M. STEVELS and Th. P. J. BOTDEN

535.371:546.791.6:666.113.791.6

Summary

In glasses hexavalent uranium may be present as uranyl groups or as uranate groups. The uranyl groups give rise to fluorescence at room temperature, but both uranyl and uranate groups show fluorescence at low temperatures. It is shown that there is a direct relation between the emission bands and the absorption bands.

Résumé

Dans les verres il peut y avoir de l'uranium hexavalent sous forme de groupes d'uranite ou d'uranate. Les groupes d'uranite provoquent la fluorescence à la température ambiante. Les deux groupes d'uranite et d'uranate présentent une fluorescence aux basses températures. On montre qu'il y a une relation entre les bandes d'émission et les bandes d'absorption.

In uranium glasses prepared under oxidizing conditions the uranium is present in the hexavalent state. Dependent on the composition of the glass, the uranium predominantly acts as a network-former or as a network-modifier, in such a way that excess of basic oxides favours the first, excess of acid oxides the second situation; furthermore, uranium present in high concentrations seems to prefer the network-former positions, while low concentrations favour the modifier positions. Uranium as a network-former may be considered to form uranate groups, while as a modifier it forms uranyl groups 1) 2). According to Weyl c.s. only the uranyl groups cause luminescence. In the present investigation we have found this to be true at room temperature, but at low temperatures the uranate groups also give rise to luminescence.

Table I shows the composition of an acid and a basic glass with low resp. high UO_3 concentration, prepared by fusing Na_2CO_3, SiO_2 and UO_3 in air at about 1300 °C. The acid glass is yellow, the basic glass orange. Fig. 1 shows the absorption spectrum of the two glasses at room temperature, together with the spectral distribution of the fluorescence at —180 °C.

TABLE I

Glass	UO_3 concentration	
	weight %	mole/l
1) $Na_2O . 2\,SiO_2$	1·5	0·126
2) 1·5 $Na_2O . 2\,SiO_2$	12	1·0

In agreement with the result of Colbert and Kreidl [2]), for uranate glass the absorption extends towards longer wavelengths than for uranyl glass. Both absorption spectra show indications of a fine-strucure. The uranyl shows bands with maxima at 4150 Å, 4700 Å (?), 4900 Å and 5200 Å; the uranate shows increasing absorption beyond 4700 Å and bands at 4900 Å, 5400 Å and 6400 Å. The fluorescence of the uranyl glass takes place in a band between 5000 and 6500 Å; the band shows a fine-structure, indicating that it consists of some equidistant sub-bands as is normal for uranyl fluorescence. The emission spectrum is practically independent of the wavelength of the exciting radiation ($\lambda < 5300$ Å), small differences being due to self-absorption. The emission for excitation by $\lambda \doteq 3650$ Å is shown in figure 1, curve I. The basic glass shows different fluorescence dependent on the wavelength of the exciting radiation. Excitation by $\lambda < 5300$ Å in the region in which the absorption bands of uranate and uranyl overlap gives rise to a broad emission which is a superposition of bands due to uranyl groups present in this glass (emission between 5000-5500 Å) and two new bands which are probably due to uranate groups.

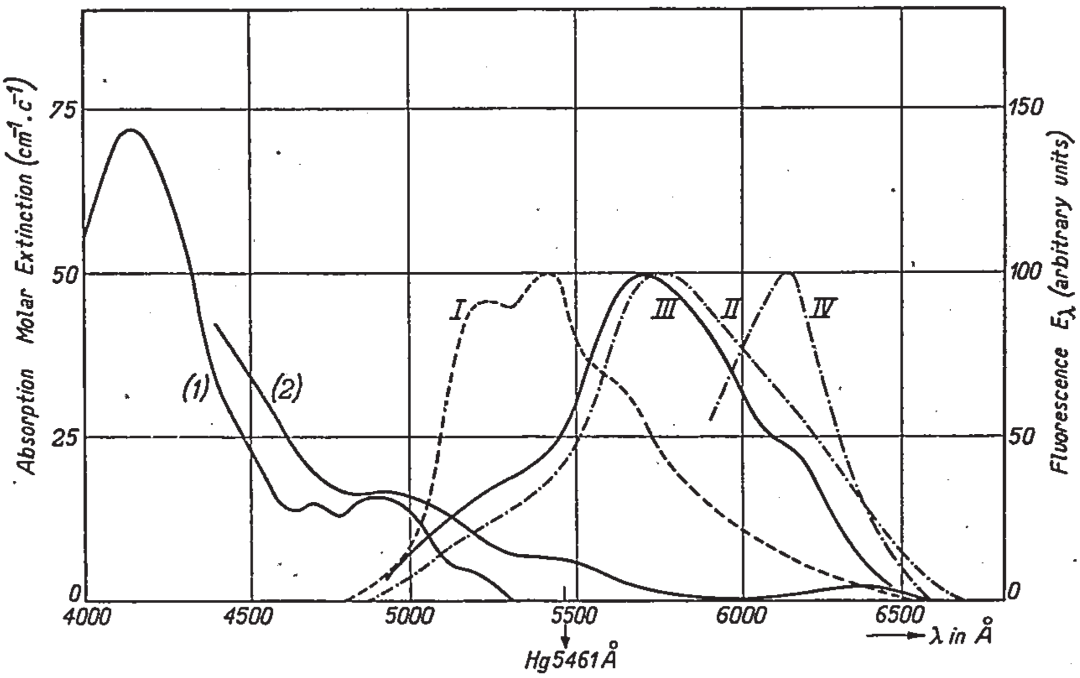

Fig. 1. Absorption at 25 °C: (1) for a uranyl glass and (2) for a uranate glass. Fluorescence at —180 °C: (I) for the uranyl glass, excited by $\lambda = 3650$ Å; (II) for the uranate glass, excited by $\lambda = 3650$ Å; (III) for the uranate glass, excited by $\lambda = 4047 + 4358$ Å; and (IV) for the uranate glass, excited by $\lambda = 5461$ Å.

The absorption is expressed in the usual way in the molar extinction; the fluorescence is expressed in arbitrary units, so normalized that the maxima of the spectral energy distributions are represented by the same figure (100).

For excitation by $\lambda = 3650$ Å the latter two bands are not resolved (curve II). The emission excited by Hg $\lambda = 4047 + 4359$ Å, however, shows maxima at 5700 Å and 6150 Å (curve III).

Excitation by $\lambda = 5461$ Å in the long-wave uranate absorption band (curve IV) produces the long-wave emission band alone. Hence there seems to be a direct relation between the various absorption and emission bands of the uranate, which is such that the absorption band at 5400 Å and the emission at 6150 Å are based on the same electronic transition, while the absorption at 4900 Å and the emission at 5700 Å correspond in a similar way. The displacement of the emission towards the long-wave side with respect to the absorption can be accounted for on the basis of the Franck-Condon principle.

Similar uranate emission bands have been observed with the tungstates of cadmium, magnesium and zinc, activated with uranium ^{3}).

Eindhoven, July 1947

REFERENCES

^{1}) W. Weyl, J. Soc. Glass Tech. **30**, 90-172, 1946.
W. Weyl and E. Thümen, Sprechsaal **67**, 95, 1934.
C. Kühl, H. Rüdow and W. Weyl, Sprechsaal **71**, 91, 104, 117, 1938.

^{2}) W. Colbert and N. J. Kreidl, J. Opt. Soc. Am. **35**, 731-735, 1945.

^{3}) Brit. Pat. Spec. 528.873;
F. A. Kröger, Some Aspects of the Luminescence in Solids, Amsterdam 1947, in the press, chapter IV.

R 71 *Philips Res. Rep.* 3, 49-59, 1948

THE HEAT DISSIPATION IN THE ANODE OF AN X-RAY TUBE*)

by W. J. OOSTERKAMP

621.386.1.032.22:536.212.1

I. INTRODUCTION; LOADS OF SHORT DURATION APPLIED TO STATIONARY ANODES

Summary

The life of an X-ray tube is often determined by the rate of evaporation of the target, and hence by the maximum temperature occurring during an exposure. For a given inflow of heat through the focus the temperature of the target may be computed from the equations of heat conduction. The requisite general equations are developed and are then applied to the problem of loads of short duration in tubes with stationary anodes. The problems connected with rotating anodes and with continuous loads will be treated in two further papers shortly to be published in this journal.

Résumé

La vie d'un tube à rayons X dépend d'ordinaire de la rapidité avec laquelle l'anticathode s'épuise et, par suite, du maximum de température atteint pendant son exposition au faisceau cathodique. Pour un apport donné de chaleur par le foyer, la température de l'anticathode peut être déduite de l'équation de la conduction calorifique. Les équations générales nécessaires sont développées et appliquées ensuite au problème de charges brèves dans des tubes à anode fixe. Les problèmes relatifs aux anodes tournantes et aux charges continues seront traités dans deux articles qui paraîtront d'ici peu de temps.

1. Introduction

The anode of an X-ray tube is shown diagrammatically in fig. 1; a tungsten target slightly larger than the focal spot is embedded in the front face of a copper anode, the cooling of which is effected by means of a large radiating body appended to it. The copper anode is also fitted with a ring for sealing to the glass envelope of the tube.

When a load is applied a beam of high-velocity electrons will strike the target, but only a small fraction of the total energy contained in this beam will be emitted as X-rays, the remainder being almost entirely converted into heat. The ensuing temperature increase limits the rating capacity, that is, the highest load at which the tube has an acceptable life.

As soon as its temperature rises above 2000 °K the target will be able to emit electrons in a measurable quantity, and when the tube is operated on

---

*) Slightly abridged and modified translation of Chapter II of the author's thesis originally published in 1939 [1]).

A.C. an electronic current will be drawn from the anode to the cathode in the inverse phase. The consequent electron bombardment causes an increase in the temperature, and hence in the emission, of the cathode filament, which in turn leads to a further increase in the temperature of the target, and so on. This unstable condition, known as "inverse emission", rapidly ends in the burning out of the filament. The temperature of the target in an A.C.-driven X-ray tube should therefore never rise above 2000 °K during the inverse phase.

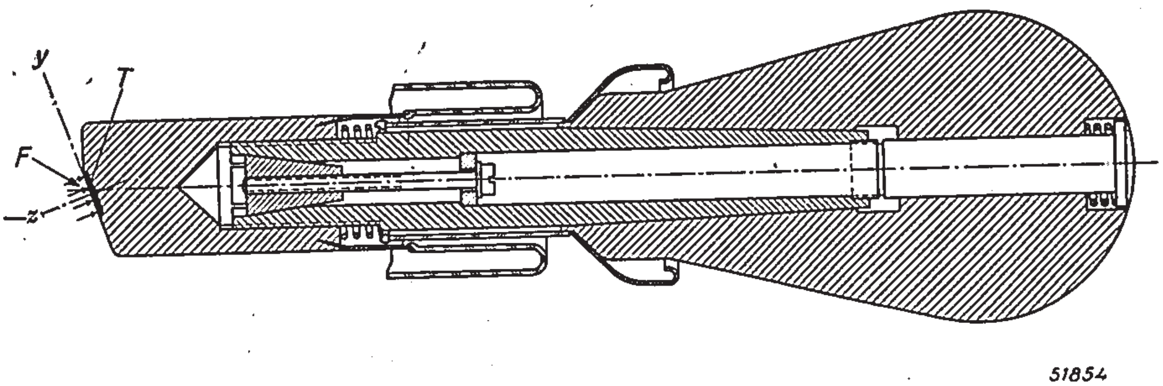

Fig. 1. Sectional view of an anode, with coordinate system; F = focus, T = tungsten target.

However, most tubes are operated on D.C., and higher temperatures can then be permitted, until evaporation of the tungsten becomes appreciable. Owing to different orientations of the tungsten crystals and local differences in temperature, the rate of evaporation will not be uniform and the surface of the target will gradually become roughened. This causes absorption of part of the emitted X-rays in the anode itself, and hence a decrease in output.

In practice a total amount of evaporation of about 100 mg per cm^2, corresponding to a layer of 0·05 mm, can be permitted, and on this basis the life of an X-ray tube is represented in fig. 2 as a function of the target temperature. If we require a life-time of, say, 10 000 exposures of 0·1 sec each, the total time of exposure is not more than 16 minutes and the temperature may run up to 3200 °K; for 10 000 exposures of 10 sec the total time of exposure is 100 times as long and the maximum temperature lies in the neighbourhood of 2800 °K. For continuous loads, where a life of 1000 hours is usually demanded, the maximum temperature should not exceed 2600 °K.

Too high temperatures may limit the life of a tube in other ways; for instance, by causing gas eruptions, or by melting of the tungsten target or the copper behind it; these are accidents, however, that, with tubes of proper design, only occur as a result of faulty operation. Also, a heavy load may give rise to such pronounced temperature gradients that the target or the copper backing gets cracked by the resultant stresses; by the use of suitable technological measures this can usually be avoided, and as a rule it is only observed in special types of tubes designed to withstand exceptionally heavy loads.

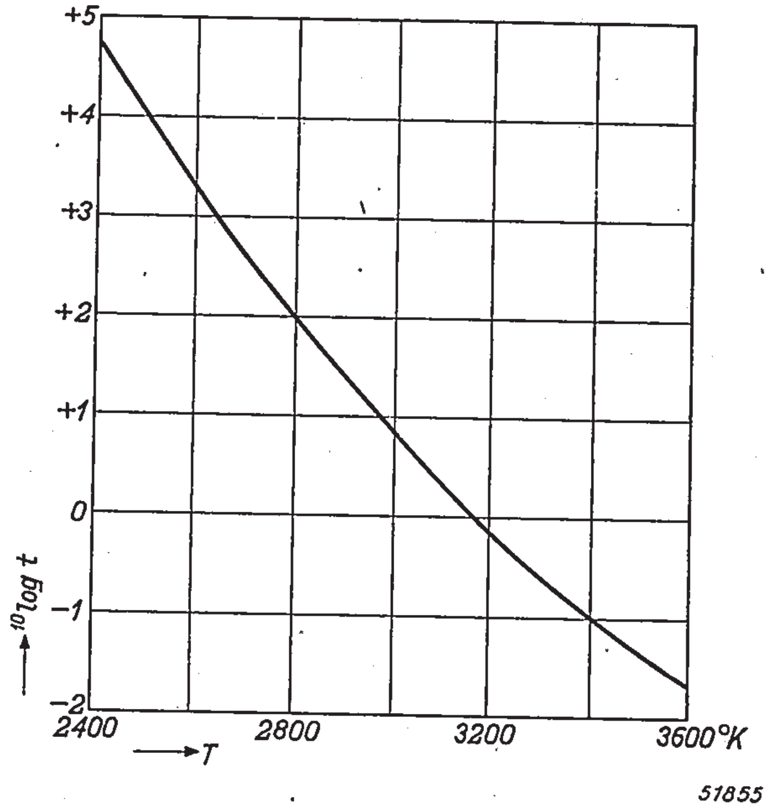

Fig. 2. Life-time of a tungsten target as a function of the temperature in °K for a total evaporation of 100 mg cm^{-2}.

In all the common types of tube the useful life as far as this is affected by temperature effects, is determined either by inverse emission or by the rate of evaporation, and we shall direct our attention mainly to the temperature limits set by these phenomena.

2. The equation of heat conduction

The temperature distribution in the anode during an exposure will be described by the equation of Fourier:

$$a^2 \Delta T - \frac{\partial T}{\partial t} + \frac{a^2 q}{k} = 0 , \qquad (1)$$

in combination with the appropriate boundary conditions, where:

T = temperature,
t = time,
a^2 = k/c = thermometric conductivity,
k = thermal conductivity,

c = thermal capacity per unit volume,
q = internal heat gained or lost per unit volume in unit time,
Δ = Laplace's operator $= \frac{\partial^2}{\partial x^2} + \frac{\partial^2}{\partial y^2} + \frac{\partial^2}{\partial z^2}$.

As heat is not generated within the anode but only dissipated at the boundary, the last term on the left-hand side is zero and the equation reduces to

$$a^2 \Delta T - \frac{\partial T}{\partial t} = 0. \tag{2}$$

In solving this equation we shall make two essential assumptions, viz:

(a) That the inflow of heat into the anode takes place only through the focal spot. This is not quite correct since the greater part of the secondary electrons dislodged in the focus returns to the anode outside the focal area, carrying with them an energy that, according to Seeman and Schotzky [2]), may amount to 20% of the primary energy; the actual temperatures will then be lower than the calculated temperatures so that we err on the safe side in making this assumption.

(b) That the thermal properties of the anode materials are independent of temperature. This assumption may give errors of about 10% in the results of our calculations.

We shall discuss solutions of equation (2) in two particular cases, viz:

Loads of short duration, such that all the heat generated in the focus during one exposure is stored up in the anode, practically no heat being dissipated. This condition holds in medical radiography.

Continuous loads, leading to a state of equilibrium between the heat supplied and the heat dissipated. This is a condition that nearly always holds in therapeutical and technical X-ray applications.

Intermediate conditions, where energy is partly stored in the anode and partly dissipated at its boundary, are encountered in medical fluoroscopy and in some technical applications. Under these circumstances the solution of (2) grows too complex for simple treatment, but insight into the temperature distribution can be obtained from the solutions for the two cases mentioned above.

It may incidentally be noted that the dissipation of heat by the anode can be brought about in various ways. For small loads this is generally effected by using a cooling body, as shown in fig. 1, mounted in air or immersed in oil; for heavy loads it is, however, necessary to cool the anode by a forced stream of air or by a flow of liquid (water or oil). In addition to this, cooling by radiation is applied in medical tubes with rotating anodes and occasionally in other tubes too.

In the remainder of the present article we shall discuss the problems arising when loads of short duration are applied to stationary anodes. A considerable increase in output can be achieved by using rotating anodes, as the inflow of heat is then spread out over a larger area; the problems of short loads applied to a rotating anode will be treated in a second article, whilst in a third paper we shall discuss continuous loads in combination with stationary and with rotating anodes.

3. Loads of short duration applied to stationary anodes

A. *General solution of equation* (2)

As the dimensions of the focal spot are considerably smaller than the diameter of the anode, we may safely assume that the latter extends to infinity in both the x- and the y-direction *).

Moreover, our definition of "loads of short duration" implies that during one exposure no heat is conducted away at the boundary of the anode or the cooling body appended to it. Consequently the temperature of the anode at a certain distance from the focal spot remains substantially constant, so that in the z-direction, too, the anode can be assumed to extend to infinity.

The load W may be inhomogeneously distributed over the focal area and may vary with time; hence we shall suppose that the specific load W, which will be expressed in watts/cm², is a function of x, y and t. We shall also suppose that at time $t = 0$ the anode has a temperature $T = 0$.

Since the amount of energy lost as thermal radiation or in the form of X-rays may be ignored in comparison with the energy supplied, the appropriate boundary conditions will be as follows:

$$z = 0: \begin{cases} \dfrac{\partial T}{\partial z} = -\dfrac{W}{k} \text{ in the focus,} \\[2ex] \dfrac{\partial T}{\partial z} = 0 \text{ outside the focus,} \end{cases} \tag{3}$$

and $$t = 0: \quad T = 0.$$

Let us first solve equation (2) for a homogeneous isotropic anode. This may be done by a consistent application of the superposition principle, which holds in virtue of the linearity of the differential equation: the temperature field under the influence of any number of sources of energy is equal to the sum of the temperature fields brought about by each source separately. From this it follows at once that the temperature at any point and at any time will be proportional to the load W. In solving (2) two different cases will be considered.

---

*) This does not hold for a line focus but in that case only a negligible amount of heat will be conveyed in the y-direction. Hence T will be independent of y, and the problem reduces from three to two dimensions.

a) The focal spot has finite dimensions both in the x- and in the y-direction.

If at time $t = 0$ an amount of energy $\mathrm{d}E$ is supplied to a point inside a homogeneous and isotropic body the consequent temperature rise at time τ and at distance r is known to be [3])

$$\mathrm{d}T = \frac{\mathrm{d}E}{8ka\pi^{3/2}\tau^{3/2}}\, e^{-\frac{r^2}{4a^2\tau}}. \tag{4}$$

The temperature distribution will be symmetrical with respect to a plane through the point source, and there will be no heat transport through such a plane. Hence it is possible to apply expression (4) to our present problem; to that purpose we have only to repace $\mathrm{d}E$ by $2W\,\mathrm{d}F\,\mathrm{d}\tau$, where $\mathrm{d}F$ is a surface element of the focus, and to integrate over the focal area and over the interval during which the load is applied. This yields

$$T = \frac{1}{4\pi^{3/2}ka} \int_0^t \int_F \frac{W}{\tau^{3/2}}\, e^{-\frac{r^2}{4a^2\tau}}\, \mathrm{d}\tau \mathrm{d}F, \tag{5}$$

where r is now the distance between the point for which the temperature is computed and the focus element $\mathrm{d}F$. This expression gives the temperature for any point in the anode and after any time of exposure.

b) The focus extends to infinity in the y-direction and has a width of 2δ in the x-direction; we shall call this a line focus of width 2δ.

The temperature will now be independent of x, and the solution of (2) may be derived from the two-dimensional analogue of (4), viz:

$$\mathrm{d}T = \frac{\mathrm{d}E}{4\pi k\tau}\, e^{-\frac{r^2}{4a^2\tau}}. \tag{6}$$

This equation expresses the relation between the energy $\mathrm{d}E$ supplied to a line focus per unit length at time $t = 0$, and the rise in temperature thereby produced in a point at a distance r and the time τ.

Substituting $2W\,\mathrm{d}x\,\mathrm{d}\tau$ for $\mathrm{d}E$ as before, and integrating over the focal width and the time of exposure, we obtain

$$T = \frac{1}{2\pi k} \int_0^t \int_{-\delta}^{+\delta} \frac{W}{\tau}\, e^{-\frac{r^2}{4a^2\tau}}\, \mathrm{d}\tau \mathrm{d}x, \tag{7}$$

which gives the temperature in any point of the anode at the end of an exposure. This equation may also be deduced from (5) by a single integration.

We now proceed to calculate the temperature field from equations (5) and (7) in a few practical cases. The temperature will of course be highest at the centre of the focal spot, and to this point we shall mainly direct our attention.

B. *A circular focus of radius R and homogeneously distributed load*

From the general equation (5) we find for the temperature T_m at the centre of the focus

$$T_m = \frac{W}{2ka\sqrt{\pi}} \int_0^t \frac{d\tau}{\tau^{3/2}} \int_0^R e^{-\frac{r^2}{4a^2\tau}}\, r\, dr\,,$$

or

$$T_m = \frac{2W}{\sqrt{kc\pi}} \sqrt{t}\, [1 - e^{-\alpha^2} + \alpha\sqrt{\pi}\,\}1 - \Phi(\alpha)\{]\,,$$

where

$$\alpha = \frac{R}{2a\sqrt{t}}$$

and Φ denotes the error integral *) which may be taken from tables [3]). Putting

$$\Psi(\alpha) = 1 - e^{-\alpha^2} + \alpha\sqrt{\pi}\,\}1 - \Phi(\alpha)\{,$$

this equation becomes

$$T_m = \frac{WR}{k} \frac{1}{\alpha\sqrt{\pi}} \Psi(\alpha)\,. \tag{8}$$

Two particular cases may be distinguished:
1) Exposures of such short duration that

$$\alpha = \frac{R}{2a\sqrt{t}} > 1{\cdot}5\,.$$

Then $\Psi(\alpha) = 1$, and consequently

$$T_m = 2W\sqrt{\frac{t}{\pi kc}}\,, \tag{9}$$

from which we see that the temperature at the centre of the focal spot is proportional to the square root of the time of exposure and independent of the diameter of the focus.

---

*) $$\Phi(\alpha) = \frac{2}{\sqrt{\pi}} \int_0^\alpha e^{-\beta^2}\, d\beta.$$

If we assume that the focal spot extends to infinity both in the x- and in the y-direction, heat conduction will take place solely in the z-direction, and equation (7) transforms into

$$T = \frac{1}{\sqrt{\pi k c}} \int_0^t \frac{W}{\sqrt{\tau}} e^{-\frac{z^2}{4a^2\tau}} \mathrm{d}\tau, \tag{10}$$

which for $z = 0$ yields

$$T = \frac{W}{\sqrt{\pi k c}} \int_0^t \frac{1}{\sqrt{\tau}} \mathrm{d}\tau = \frac{2W}{\sqrt{\pi k c}} \sqrt{t}, \tag{11}$$

an expression identical with (9). It may be noted that equation (9) applies to focal spots of any shape provided $f/4a\sqrt{t} > 1{\cdot}5$, where f is the smallest dimension of the focus; under these conditions an appreciable transfer of heat takes place in the z-direction only, as during one exposure no heat penetrates into the anode to a depth of the same order of magnitude as the dimensions of the focus, so that lateral dissipation of heat does not yet play a part.

Such conditions prevail in tubes with a homogeneous copper or tungsten anode when the exposures last 0·005 sec or less. With a bimetallic anode this holds for even longer exposures, up to 0·05 sec, if the thermal conductivity of the target material (f.i. tungsten) is considerably lower than that of the basis metal (copper), as will be explained more fully in part D of this section.

2) Long exposures for which

$$\frac{R}{2a\sqrt{t}} < 0{\cdot}5;$$

then $\Psi(\alpha) = \alpha\sqrt{\pi}$, and we obtain:

$$T_m = \frac{WR}{k}. \tag{12}$$

Thus we see that for these long exposures the maximum temperature in the focus decreases — and consequently the specific rating capacity per mm^2 increases — with decreasing focal dimensions; this results from the influence of lateral heat dissipation. This equation will be deduced in a different and very simple way in our third paper, where we shall deal with continuous loads.

It should be noted that the long exposures we are here considering still belong to the class of loads of short duration as defined in section 2. Equation (12) shows that under these conditions the maximum temperature is independent of the time of exposure.

For a copper anode and a circular focus of 6 mm diameter the quantity kT_m/W computed from equations (12) and (9) has been plotted in fig. 3 against the time of exposure, curves I and II respectively. By comparing these curves it becomes apparent at what time of exposure the lateral heat dissipation begins to take effect.

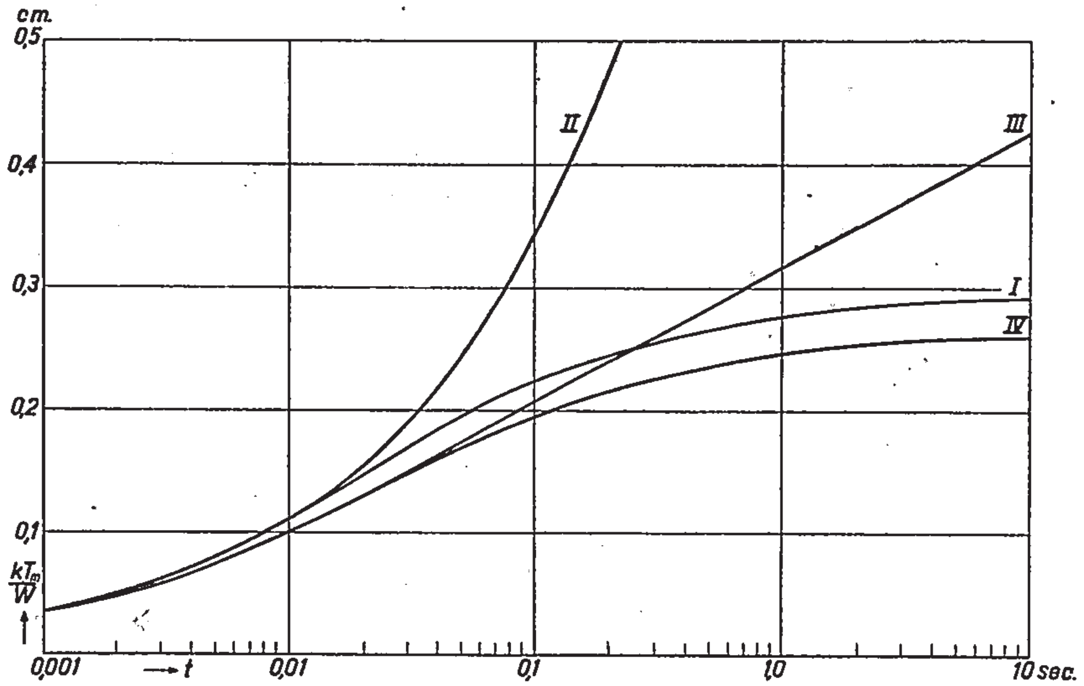

Fig. 3. kT_m/W as a function of the time of exposure for an isotropic copper anode and a homogeneous distribution of the load over the focal spot.
Curve I: a circular focus of 6 mm diameter.
Curve II: a focus of arbitrary shape if the time of exposure is very short (equation (9)).
Curve III: an infinite line focus of a width of 3 mm.
Curve IV: a finite line focus of 3×9 mm².

C. *A homogeneously loaded line focus of width 2δ*

In this case equation (7) yields for the maximum temperature at the centre of the focus:

$$T_m = \frac{W\delta}{k\sqrt{\pi}} \int_{\frac{\delta}{2a\sqrt{t}}}^{\infty} \frac{1}{\alpha^2}\, \Phi(\alpha)\mathrm{d}\alpha\,, \qquad (13)$$

where $\Phi(\alpha)$ is the error integral as before; kT_m/W computed from this expression for a copper anode and 3 mm focal width is represented by curve III of fig. 3.

For a finite line focus of 3×9 mm², having about the same area as the circular focus of 6 mm diameter, the maximum temperature at the centre has been computed in an analogous manner and is represented in fig. 3, curve IV. For long exposures the difference in rating capacity is approximately 10% in favour of the line focus, but this is only a secondary advantage. As is well known, the major advantage is that a focus of 3×9 mm^2 when projected at an angle of 19° into a square of 3×3 mm^2 gives a brightness about three times that in a perpendicular direction, owing to the fact that the X-rays are emitted with uniform intensity in all directions.

D. *Discussion of practical data*

We have seen above that the permissible maximum specific load is proportional to $T\sqrt{kc}$ and to Tk for short and for long exposures respectively, where T is the permissible maximum temperature of the target material. The ratio of the energy radiated as X-rays to the heat dissipated in the anode is proportional to the atomic number Z, and consequently the maximum X-ray output obtainable per unit area will be determined by the product $ZT\sqrt{kc}$ for short and ZTk for long exposures. For the metals generally used as target materials the data determining the maximum output have been collected in table I.

TABLE I

Thermal data for various target metals

	Z	k	c	Melting point °C	$T\sqrt{kc}$	$ZT\sqrt{kc}$	Tk	ZTk
Cu	29	3·9	3·5	1080	$4{\cdot}0 \times 10^3$	$1{\cdot}2 \times 10^5$	$4{\cdot}2 \times 10^3$	$1{\cdot}2 \times 10^5$
Ag	47	4·2	2·5	960	$3{\cdot}1 \times 10^3$	$1{\cdot}5 \times 10^5$	$4{\cdot}0 \times 10^3$	$1{\cdot}9 \times 10^5$
Ta	73	0·53	2·4	3000	$3{\cdot}4 \times 10^3$	$2{\cdot}5 \times 10^5$	$1{\cdot}6 \times 10^3$	$1{\cdot}2 \times 10^5$
W	74	1·60	2·7	3350	$7{\cdot}0 \times 10^3$	$5{\cdot}2 \times 10^5$	$5{\cdot}4 \times 10^3$	$4{\cdot}0 \times 10^5$
Pt	78	0·70	2·8	1770	$2{\cdot}5 \times 10^3$	$1{\cdot}9 \times 10^5$	$1{\cdot}2 \times 10^3$	$0{\cdot}9 \times 10^5$
Au	79	2·96	2·5	1060	$2{\cdot}9 \times 10^3$	$2{\cdot}3 \times 10^5$	$3{\cdot}1 \times 10^3$	$2{\cdot}4 \times 10^5$

k = thermal conductivity in watts cm^{-1} °C^{-1};
c = heat capacity per unit volume in watts sec cm^{-3} °C^{-1};
$T\sqrt{kc}$ is expressed in watts sec$^{1/2}$ cm^{-2};
Tk is expressed in watts cm^{-1}.

Since the vapour pressures of these metals are not known with sufficient accuracy, the melting points have been used to indicate the maximum temperatures that can be permitted; the temperature limit set by evaporation lies as a rule from 20 to 30% below the melting point; this suffices since in drawing conclusions from these data a high accuracy will not be required.

Tungsten is by far the best target metal owing to its high atomic number, its high maximum temperature, and its comparatively good thermal conductivity. As the thermal conductivity of copper is far higher still, a considerable improvement can be effected by embedding a thin tungsten target in a solid copper anode. The optimum thickness of the tungsten will then be that thickness for which the tungsten and the copper simultaneously reach their permissible maximum temperatures.

For short exposures and a fixed maximum temperature the specific load is inversely proportional to the square root of the time of exposure, and the temperature gradient in the z-direction will vary in the same way, whereas the depth of thermal penetration will be directly proportional to the square root of the time of exposure. For long exposures the rate of decrease of the specific load with time will be slower owing to the lateral dissipation of heat. It will be evident that the optimum thickness of the tungsten target will vary with the time of exposure in a similar way. For exposures of 1 sec — an average value in medical diagnostics — the optimum thickness for stationary anodes is 2 mm according to Bouwers [4]).

The temperature distribution in such a bimetallic anode can be computed in much the same way as for a homogeneous anode. Since the lines of flow of heat will be refracted from the normal in the ratio of the thermal conductivities, the divergence in the tungsten will be less than in a homogeneous copper anode. Hence the rating capacity remains independent of the focal dimensions up to higher values of the time of exposure than in the case of a homogeneous copper anode.

Eindhoven, January 1948

REFERENCES

1) W. J. Oosterkamp, Problemen bij de constructie van technische röntgenbuizen, Thesis, Delft, 1939.
2) H. Seemann and K. F. Schotzky, Z. Phys. **71**, 1-25, 1937.
3) Jahnke-Emde, Funktionentafeln, Teubner, Leipzig, 1928, pp. 48, 97.
4) A. Bouwers, Z. tech. Phys. **8**, 272-277, 1927.

R 72 *Philips Res. Rep.* *3*, *60-80, 1948.*

EMPIRICAL DETERMINATION OF WAVE-FILTER TRANSFER FUNCTIONS WITH SPECIFIED PROPERTIES

by J. F. KLINKHAMER

621.392.52:621.317.729.1

PART I

Summary of part I and part II

A method is described for determining wave-filter transfer functions $z(\lambda) = e_u/e_i$ with specified properties by means of measurements in an electrolytic tank, e_u being the output voltage, e_i the input voltage, and λ the complex frequency parameter. At the same time other functions are discussed which are equally useful in calculating the filter-network performance (the "characteristic functions" of Piloty). The position of the transmission bands, the permissible variation of the attenuation within these bands, and the position and the minimum attenuation of the attenuation bands are supposed to be given. As the method is applicable to filters with several transmission and attenuation bands not necessarily equal in attenuation qualities, the new method is more general than that of Cauer, though it bears a close relation to the latter. In the case of one transmission band and one attenuation band, and in the case of several transmission and attenuation bands with equal attenuation qualities, the results of the two methods are identical. The paper concludes with a list of manipulations to be carried out for the actual determination of a transfer function.

Résumé

L'article décrit une méthode de détermination des fonctions de transfert $z(\lambda) = e_u/e_i$, à propriétés déterminées, d'un filtre d'ondes, au moyen de mesures effectuées dans une cuve électrolytique; e_u est la tension de sortie, e_i la tension d'entrée et λ le paramètre complexe de fréquence. D'autres fonctions, également utilisables pour le calcul des propriétés d'un circuit filtrant („fonctions caractéristiques" de Piloty) sont également examinées. La position des bandes de transmission, la variation d'atténuation admissible dans ces bandes, et la position des bandes d'atténuation et leur atténuation minimum sont supposées être données. La nouvelle méthode étant applicable à des filtres à plusieurs bandes de transmission et d'atténuation, mais n'ayant pas nécessairement les mêmes qualités d'atténuation, elle est plus générale que celle de Cauer, quoiqu'elle soit en relation très étroite avec cette dernière. Dans le cas d'une seule bande de transmission et d'une seule bande d'atténuation, et dans le cas de plusieurs bandes de transmission et d'atténuation ayant les mêmes qualités d'atténuation, les résultats des deux méthodes sont identiques. L'article se termine sur une liste des opérations à effectuer pour déterminer une fonction de transfert.

CONTENTS OF PART I

1. Introduction
1·1. Solution of a simple problem by Cauer's method
1·2. Solution of the same problem by the method developed in the present paper

1·3. Field equations of the electrolytic tank
1·4. The differential equation of Laplace
1·5. Singularities
1·6. Representation of the imaginary part of $z(\lambda)$ in the tank in which the real part is represented by the potential

2. **Determination of the transfer function**

2·1. Statement of the problem
2·2. Deduction, from the transfer function f/g, of a function h/f the poles and zeros of which lie on the ω-axis
2·3. Deduction of the requirements for h/f from those for g/f
2·4. Non-rational auxiliary function F_1
2·5. Approximation of F_1 by a rational function A: the function F
2·6. Finding the singularities of $\ln|A|$
2·7. Preventing the appearance of zeros of A in the attenuation bands or of poles of A in the transmission bands

1. Introduction

A practical problem, repeatedly presenting itself in communication engineering, is how to construct a filter that transmits one or more given frequency bands and attenuates other bands, each to a given extent.

This problem may be attacked by Zobel's well-known method leading to a network consisting of a series of sections with matched image impedances. This manner of approach, however, is not the most economical one, the price of a filter in mass production being roughly proportional to the number of coils involved.

A more general way of attack, which leads to the minimum number of coils, may be found immediately by remembering that the transfer functions of a finite network consisting of lumped impedances can only be rational functions of λ with real coefficients, where λ denotes the frequency parameter $\varkappa + j\omega$; $\varkappa =$ damping constant, $\omega =$ frequency *).

The problem may then be split into two parts:

(1) How to find a rational function of λ with real coefficients, and with a modulus meeting the conditions:
  (a) The minimum attenuation in all "transmission bands" D_1, $D_2, \ldots, D_\nu, \ldots$ is the same; the attenuation in the transmission band D_ν does not depart from the minimum value by more than a given maximum value $2\Delta a_\nu$.
  (b) The attenuation in the "attenuation bands" $G_1, G_2, \ldots, G_\mu, \ldots$ is greater than the minimum attenuation in the transmission bands plus a given attenuation $a_1, a_2, \ldots, a_\mu, \ldots$ (in our case a different a_μ for each band G_μ may be given).

---

*) An alternating current with frequency parameter $\lambda = \varkappa + j\omega$ is represented by the function $i(t) = i_0 \exp(\varkappa t + j\omega t)$. A real-valued alternating current of frequency ω with an amplitude increasing as $|i| = |i_0| \exp(\varkappa t)$ therefore consists of a component $\frac{1}{2}|i_0| \exp(\varkappa t + j\omega t)$ and a component $\frac{1}{2}|i_0| \exp(\varkappa t - j\omega t)$.

(2) How to construct a four-pole with a transfer function that is equal to the rational function given by (1).

In this paper we shall consider only the first part of the problem. The second part is dealt with by Bader [1]) and others; we intend to return to it in another paper. The method we shall discuss for the solution of the first part was derived from a method given by Cauer *). Yet, it is more general than Cauer's method and, as we believe, more adapted to practice. In fact, it reduces the determination of the rational function to the determination of its poles and zeros, which are found as the points of intersection of two sets of equipotentials in an electrolytic tank.

By way of introduction, we shall discuss the solution of a simple problem, first by Cauer's method, then by that described in the present paper (sections 1·1 and 1·2).

The second part of our introduction deals with the analogy between the potential distribution in a flat electrolytic tank and the real part of an analytic function in the complex plane (sections 1·3 to 1·6).

1·1. Solution of a simple problem by Cauer's method

We put the following conditions **):

(1) The attenuation of the filter between the frequencies 0 and 1 (the transmission band) shall lie between 0 and 0·097 neper.

This means that the modulus of the rational function of λ representing the ratio e_i/e_u of the input to the output voltage has to lie between the values 1 and 1·1 for $\lambda = j\omega$ $(0 < \omega < +1)$.

(2) The rational function shall have no poles except the multiple one at $\lambda = \infty$.

This means that our rational function reduces to a polynomial. (The reason for putting this condition is that it makes the calculation as simple as possible.)

(3) The filter shall consist of a third-order network. This implies that the polynomial mentioned under (2) is of the third degree.

Condition (3) limits the number of extrema of the attenuation curve, $\ln|e_i/e_u| = f(\omega)$ where $\lambda = j\omega$, to five. From (2) and (3) it follows in fact that the polynomial

$$e_i/e_u = a_3\,\lambda^3 + a_2\,\lambda^2 + a_1\,\lambda + a_0 = P$$

has (for $\lambda = j\omega$) the modulus

$$\sqrt{(-a_3\,\omega^3 + a_1\,\omega)^2 + (-a_2\,\omega^2 + a_0)^2}\,,$$

whose derivative is given by

---

*) Reference [2]), pp. 258-263, 410-428.

**) As an illustration of conditions (1) - (7), see fig. 1.

$$\frac{2\,(-a_3\,\omega^3 + a_1\,\omega)\,(-3\,a_3\,\omega^2 + a_1) + 2\,(-a_2\,\omega^2 + a_0)\,(-2a_2\,\omega)}{2\,\sqrt{(-a_3\,\omega^3 + a_1\,\omega)^2 + (-a_2\,\omega^2 + a_0)^2}},$$

which is zero at no more than five real values of ω.

Not every rational function of λ is realizable by a passive network. Conditions for the possibility of realization are:

(4) The coefficients of the polynomials in the numerator and denominator of the function must be real.

The function will thus have conjugate-complex values for conjugate-complex λ's. Therefore the band $0 < \omega < +1$ in which (1) is valid can be extended to $-1 < \omega < +1$.

(5) The numerator polynomial of e_i/e_u must be a Hurwitz polynomial. This means that the real part of any of its zeros must be negative *).

Now, Cauer puts two additional conditions:

(6) The attenuation curve shall contain the maximum possible number of extrema, all extrema lying in the transmission band.

(7) The minima shall all be equal (for example, attenuation is zero); the maxima shall all be equal, and equal to the attenuation at $\omega = 1$ (in our case the attenuation is 0·097 neper).

Cauer showed that this is possible in one way only, and that at the same time this way gives the maximum possible attenuation outside the transmission band **).

The method of Cauer for obtaining the required function now follows.

The function $|e_i/e_u|$ must oscillate between two extremum values, 1 and 1·1, in the band $-1 < \omega < +1$. Now $|e_i/e_u|$ is the square root of an even sixth-degree polynomial in ω, as follows from condition (3). This polynomial, therefore, must oscillate between 1^2 and $1{\cdot}1^2$.

We know an even polynomial of the sixth degree that oscillates between the values ± 1 for $-1 < \omega < +1$; namely, the Chebyshev polynomial

$$A = \cos\,(6 \arcsin \omega) = 1-2 \sin^2 (3 \arcsin \omega) = 1-2\omega^2\,(3-4\omega^2)^2.$$

The function $(1-A)/2$ varies between 0 and 1 for $-1 < \omega < +1$, and it increases to $+\infty$ for values of ω outside this band. We can construct a polynomial that meets our requirements, by multiplying $(1-A)/2$ by $1{\cdot}1^2-1$ and adding 1 to it. It becomes

$$B \approx 1 + 0{\cdot}2\,\omega^2(3-4\omega^2)^2.$$

We now have found a suitable expression for $|e_i/e_u|^2$ but not yet for

---

*) The zeros of the numerator polynomial of e_i/e_u represent the free oscillations of the network, i.e., if P has a zero $\varkappa + j\omega$ the network has a free oscillation $e_u = e_{u0} \exp\,(\varkappa t) \cos \omega t$. A positive $\varkappa$ means a free oscillation of increasing amplitude, which is impossible in a passive network.

**) Reference [2]), pp. 371-402.

$e_i/e_u = P$. The latter may be found as follows. As ω is by definition a real quantity, the function B has only a meaning along the ω-axis. We can easily derive from it a function $\bar{B}$ that has a definite value at each point of the complex λ-plane by substituting $-j\lambda$ for ω:

$$\bar{B} = 1 + 0{\cdot}2(-j\lambda)^2\,[3-4(-j\lambda)^2]^2.$$

Along the ω-axis B and $\bar{B}$ are identical since along this axis $\lambda = j\omega$.

As B coincides with

$$|e_i/e_u|^2 = (-a_3\,\omega^2 + a_1)^2\,\omega^2 + (-a_2\,\omega^2 + a_0)^2,$$

$\bar{B}$ must coincide with

$$-\,(a_3\,\lambda^2 + a_1)^2\,\lambda^2 + (a_2\,\lambda^2 + a_0)^2 =$$
$$= [a_2\,\lambda^2 + a_0 + \lambda(a_3\,\lambda^2 + a_1)]\,.\,[a_2\,\lambda^2 + a_0 - \lambda(a_3\,\lambda^2 + a_1)] = P(\lambda)\;P(-\lambda)\,.$$

To derive from the known function $\bar{B} = P(\lambda)\;P(-\lambda)$ the unknown $P(\lambda)$, we split $P(\lambda)$ into factors $(\lambda-\lambda_1)\;(\lambda-\lambda_2)\;(\lambda-\lambda_3)$ in which λ_1, λ_2, λ_3 are the roots of the equation $P(\lambda) = 0$.

As $P(-\lambda)$ follows from $P(\lambda)$ by substituting $-\lambda$ for λ, the zeros of $P(-\lambda)$ are $-\lambda_1$, $-\lambda_2$, $-\lambda_3$, and therefore $\bar{B}$ may be written as follows:

$$\bar{B} = (\lambda-\lambda_1)\;(\lambda+\lambda_1)\;(\lambda-\lambda_2)\;(\lambda+\lambda_2)\;(\lambda-\lambda_3)\;(\lambda+\lambda_3)\,.$$

The way to evaluate $P(\lambda)$ is clear now: by solving the sixth-degree equation $\bar{B} = 0$, we find six roots λ_1, $-\lambda_1$, λ_2, $-\lambda_2$, λ_3, $-\lambda_3$.

As P has to fulfil the condition (5), the real part of any of its roots has to be negative.

From each of the three pairs of roots $\pm\,\lambda_1$, $\pm\,\lambda_2$, $\pm\,\lambda_3$ we have therefore to select the one with the negative real part to construct the polynomial

$$P(\lambda) = (\lambda-\lambda_1)\;(\lambda-\lambda_2)\;(\lambda-\lambda_3)\,.$$

In our numerical example the roots of $\bar{B}$ are those of the equation

$$5 - 9\lambda^2 - 24\,\lambda^4 - 16\,\lambda^6 = 0\,,$$

or $\lambda_1 = \pm\,0{\cdot}538$, $\lambda_2 = \pm\,(0{\cdot}268 - 0{\cdot}983j)$, $\lambda_3 = \pm\,(0{\cdot}268 + 0{\cdot}983j)$.

Therefore P becomes

$$(\lambda + 0{\cdot}538)\;(\lambda + 0{\cdot}268 + 0{\cdot}983j)\;(\lambda + 0{\cdot}268 - 0{\cdot}983j)\,.$$

The attenuation curve in decibels, $20 \log |P|$, is given in fig. 1.

1·2. Solution of the same problem by the method developed in the present paper

The procedure according to the method to be described in this paper is as follows.

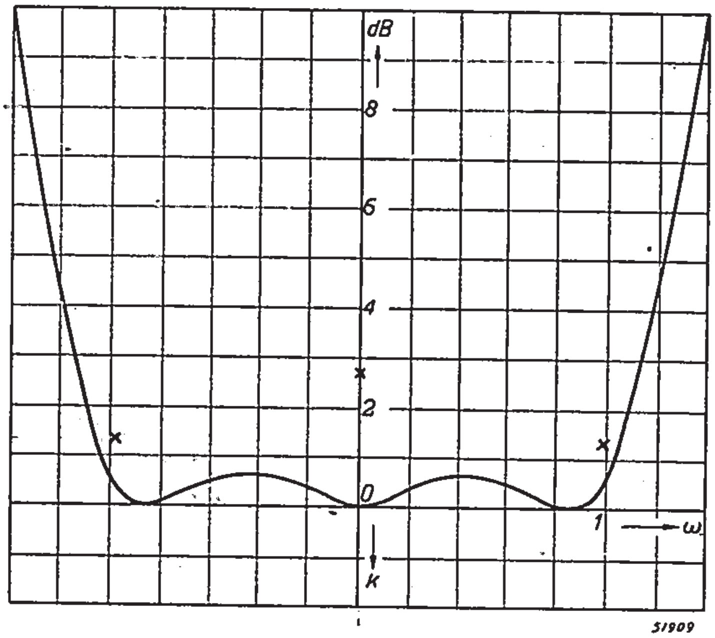

Fig. 1. Attenuation curve satisfying conditions (1) - (7). The frequency ω is plotted along the horizontal axis. Along the vertical axis are plotted the damping constant $\varkappa$ as well as the attenuation in db. The three crosses represent the zeros of e_i/e_u in the complex plane of $\lambda = \varkappa + j\omega$.

A flat electrolytic tank gives a representation of the complex λ-plane. A band-shaped electrode A is inserted lying along the ω-axis between $-1 < \omega < +1$. Another band-shaped electrode B, running in a large circle around the point $\lambda = 0$, represents the point $\lambda = \infty$. The potential of A is made zero; B is fed with a current of three units (the unit current is a constant of the apparatus). That equipotential β (fig. 2) is traced where the potential is equal to $V = -\frac{1}{2} \ln (0{\cdot}097/2)$ potential units *). The potential unit must be so chosen as to yield a potential at each point of the tank equal to the natural logarithm of the modulus of the function that is represented. Electrodes A and B are then removed, and two electrodes C and D are inserted along the ω-axis: C from $\omega = -\infty$ to $\omega = -1$ and D from $\omega = +1$ to $\omega = +\infty$.

C is put at zero potential and D at potential V_0. Those points λ_1, λ_2,

---

*) A first-order pole of a function is represented in the tank by a needle-shaped electrode that feeds a unit current into the electrolyte. A first-order zero is represented by a needle-shaped electrode taking a unit current from the electrolyte.
Thus we may determine the potential unit, for example, by putting two needle-shaped electrodes into the tank at the points $\lambda = \pm 1$; the one fed with a positive, the other with a negative current unit. The potential difference between the points $\pm {}^1/_2$, measured in potential units, then must be

$$\ln\frac{\frac{1}{2}+1}{1-\frac{1}{2}} - \ln\frac{-\frac{1}{2}+1}{1+\frac{1}{2}} = 2 \ln 3.$$

λ_3, λ_4, λ_5, λ_6 of β where the potential is equal to $V_0/6$, $V_0/2$ and $5V_0/6$ are traced. The three points λ_1, λ_2, λ_3 lying in the negative half-plane represent the zeros of the polynomial that gives the required transfer function.

In this simple case the functions that are used in constructing the transfer function are trigonometric (in the Chebyshev function). Cauer, in the more general case of one transmission and one attenuation condition, needs elliptic functions.

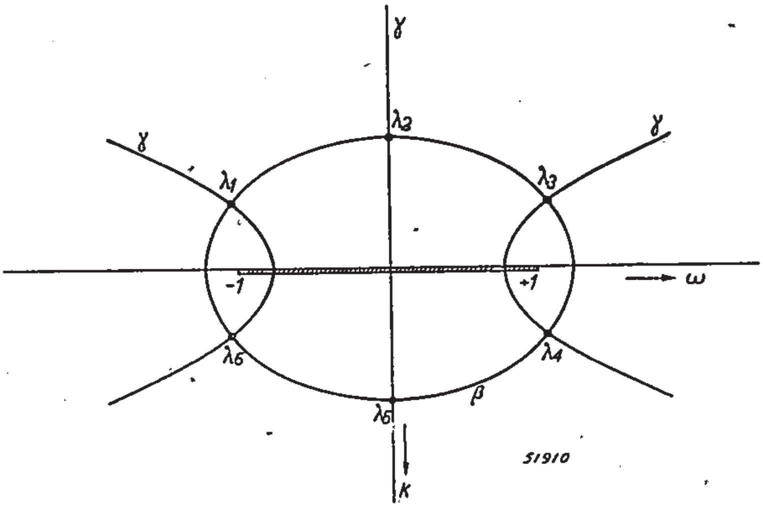

Fig. 2. Equipotentials in the electrolytic tank. The electrode is inserted along the heavy line from $\omega = -1$ to $\omega = +1$ and gives an equipotential β bearing the potential $-\frac{1}{2}\ln(0{\cdot}097/2)$. Then the electrode is replaced by two electrodes from $\omega = -\infty$ to $\omega = -1$ and from $\omega = +1$ to $\omega = +\infty$, producing the equipotentials γ. The points of intersection of β and γ give the roots $\lambda_1, \ldots, \lambda_6$.

If we put several different attenuation conditions we come to hyperelliptic functions for the construction of the transfer function. In these complicated cases the use of the electrolytic tank continues to give a relatively simple way of determining the transfer functions.

1·3. Field equations of the electrolytic tank

As our method is mainly based on the correspondence between the real (or the imaginary) component of an analytic function and the potential field in a flat electrolytic tank, it may be useful to give a brief review of that correspondence (sections 1·3 to 1·6) before going into the main problem.

We shall first recall the field equation of the electrolytic tank. Let us consider a volume element of the electrolyte (fig. 3). If no electrode is present, the sum of the currents passing through the sides of the element must, in the stationary state, be zero; therefore

$$\frac{\partial i_\xi}{\partial \xi} + \frac{\partial i_\eta}{\partial \eta} + \frac{\partial i_\zeta}{\partial \zeta} = \operatorname{div} \mathbf{i} = 0 \qquad \text{(1a)}$$

where **i** denotes the current-density vector, and ξ, η, ζ rectangular cartesian coordinates.

In the proximity of an infinitesimal electrode, feeding a finite current I into the electrolyte, the left side of equation (1a) becomes meaningless. (1a) may be replaced in this case by

$$\int_S \mathbf{i} \cdot d\mathbf{S} = I \tag{1b}$$

The left-hand side of (1b) is a surface integral of **i** over a closed surface surrounding the electrode.

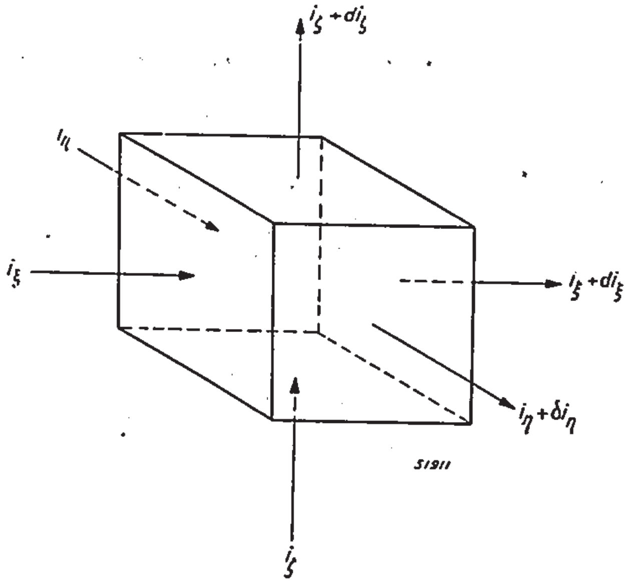

Fig. 3. Volume element of the electrolyte.

The electric field strength **F** in the stationary state will have the same direction as the current-density vector, and will be given by

$$\mathbf{F} = \varrho\, \mathbf{i}\,, \tag{2}$$

where ϱ is the specific resistance of the electrolyte.

The electrostatic potential V is defined by

$$\left.\begin{aligned} \frac{\partial V}{\partial \xi} &= -F_\xi \\ \frac{\partial V}{\partial \eta} &= -F_\eta \\ \frac{\partial V}{\partial \zeta} &= -F_\zeta \end{aligned}\right\} \text{ or } \operatorname{grad} V = -\mathbf{F}. \tag{3}$$

Combining (1a) or (1b), (2), and (3), we get (ϱ being constant)

$$\frac{\partial^2 V}{\partial \xi^2} + \frac{\partial^2 V}{\partial \eta^2} + \frac{\partial^2 V}{\partial \zeta^2} = 0 \text{ if no electrode is present,} \tag{4a}$$

$$(1/\varrho) \int \text{grad } V.\, \mathrm{dS} = -I \text{ if an electrode is present carrying the current } I. \tag{4b}$$

The correspondence between these equations and the electrostatic and hydrodynamic field equations has led to the use of the electrolytic tank in many experiments.

1·4. The differential equation of Laplace

We shall now consider the analytic function

$$z(\lambda) = x(\lambda) + jy(\lambda) = x(\varkappa, \omega) + jy(\varkappa, \omega)\,. \tag{5}$$

The independent variable is designated by $\lambda = \varkappa + j\omega$ and the dependent variable by $z = x + jy$. In the case of networks, λ represents the frequency parameter, ω the frequency, $\varkappa$ the damping constant, and z the ratio of either two currents, or two voltages, or a voltage and a current.

From the condition that the differential quotient at any point shall be independent of the direction of $d\lambda$, the two differential equations of Cauchy-Riemann follow, viz.

$$\frac{\partial x}{\partial \varkappa} = \frac{\partial y}{\partial \omega}, \tag{6a}$$

$$\frac{\partial x}{\partial \omega} = -\frac{\partial y}{\partial \varkappa}, \tag{6b}$$

which, after differentiation, give the well-known Laplace equation

$$\frac{\partial^2 x}{\partial \varkappa^2} + \frac{\partial^2 x}{\partial \omega^2} = \frac{\partial^2 y}{\partial \varkappa^2} + \frac{\partial^2 y}{\partial \omega^2} = 0\,, \tag{7}$$

which must be valid in all except the singular points of the λ-plane.

As (7) corresponds to the two-dimensional case of (4a), it is possible, by satisfying the boundary conditions, to represent one of the components x or y in a part of the λ-plane by the potential V in a flat electrolytic tank with vertical cylindrical electrodes.

The correspondence between a component of an analytic function and the hydrodynamic potential of a two-dimensional fluid motion has often been used. Klein ³) applied the electric current in closed surface layers of conducting material as an illustration for considerations regarding the theory of functions. Kleynen ⁴) used the analogy between the electrostatic potential in the two-dimensional case and the height of a rubber membrane (which also approximately satisfies the Laplace equation) for the determination of potentials and electron paths in electronic devices. Schouten and Klute [5]) used the analogy between a rubber or soap membrane and a component of an analytic function for considerations regarding the influence of internal losses on the characteristic of a wave filter.

1·5. Singularities

So far we have considered only those domains in which the function $z(\lambda)$ is analytic. We shall now discuss the singular points. As our aim is to construct a transfer function that can be realized by a finite network of lumped impedances, and as this transfer function is a rational function of the frequency parameter λ, we are interested in rational functions only.

Now it is always possible to write a rational function $z(\lambda)$ in the following way

$$z(\lambda) = A\,\frac{(\lambda-\lambda_{T_1})\,(\lambda-\lambda_{T_2})\dots(\lambda-\lambda_{T_n})}{(\lambda-\lambda_{N_1})\,(\lambda-\lambda_{N_2})\dots(\lambda-\lambda_{N_m})}, \tag{8}$$

$\lambda_{T_1}, \dots, \lambda_{T_n}$ being the zeros of the numerator, and $\lambda_{N_1}, \dots, \lambda_{N_m}$ those of the denominator.

For our purpose it is convenient to consider the logarithm of this function which may be written as the sum of a series of terms:

$$\ln z = \ln A + \ln(\lambda-\lambda_{T_1}) + \dots + \ln(\lambda-\lambda_{T_n}) - \ln(\lambda-\lambda_{N_1}) - \dots - \ln(\lambda-\lambda_{N_m})\,. \tag{9}$$

This equation can be separated into

$$\ln|z| = \ln|A| + \ln|\lambda-\lambda_{T_1}| + \dots + \ln|\lambda-\lambda_{T_n}| - \ln|\lambda-\lambda_{N_1}| - \dots - \ln|\lambda-\lambda_{N_m}|, \tag{10a}$$

$$\arg z = \arg A + \arg(\lambda-\lambda_{T_1}) + \dots + \arg(\lambda-\lambda_{T_n}) - \arg(\lambda-\lambda_{N_1}) - \dots \\ - \arg(\lambda-\lambda_{N_m}), \tag{10b}$$

$|z|$ being the absolute value of z, arg z the argument, arctan (y/x), of z, etc.

Consider one of the terms $\ln|\lambda-\lambda_{T_\nu}|$; it represents the logarithm of the distance $|\lambda-\lambda_{T_\nu}|$ from the point λ to the zero λ_{T_ν} in the λ-plane. Upon representing the λ-plane by the flat electrolytic tank we can obtain a potential proportional to the logarithm of the distance between the point under consideration λ and a fixed point λ_{T_ν} by putting a needle-shaped electrode at the point λ_{T_ν} giving a current I to the electrolyte, and placing another electrode at $\lambda = \infty$ taking a current I from the electrolyte.

In the vicinity of λ_{T_ν}, the equipotentials are small circles around this point; therefore we may use a small electrode of circular cross-section (radius δ) and of finite potential instead of an infinitesimally thin one with potential ∞, without essentially deforming the potential field (except, of course, in the area covered by the cross-section of the finite electrode). The electrode at $\lambda = \infty$ may in our case be represented by a band-shaped electrode running in a large circle of radius $1/\delta$ around the point $\lambda = 0$.

If $|\lambda_{T_\nu}| \ll 1/\delta$ the deformation of the field by this approximation will be small.

From (4b) we further see that, if the current I in the electrode is changed into μI, the potential $V(\lambda)$ at any point λ will increase by a factor μ. From (4) there also follows the well-known law of additivity of the potential field, which says that the field caused by a combination of two or more infinitesimal electrodes equals the sum of the fields caused by the single electrodes, provided each of them carries the same current as in the combined case.

Therefore, if we put electrodes carrying currents $-2\pi/\varrho$ at $\lambda = \lambda_{T_1}$, λ_{T_2}, ... and others carrying currents $+2\pi/\varrho$ at $\lambda = \lambda_{N_1}$, λ_{N_2}, ... (while an electrode at $\lambda = \infty$ absorbs the difference) we get a potential field described by

$$V = \ln|\lambda - \lambda_{T_1}| + \dots + \ln|\lambda - \lambda_{T_n}| - \ln|\lambda - \lambda_{N_1}| - \dots - \ln|\lambda - \lambda_{N_m}| \quad (11)$$

or

$$V = \ln \left| \frac{(\lambda - \lambda_{T_1}) \dots (\lambda - \lambda_{T_n})}{(\lambda - \lambda_{N_1}) \dots (\lambda - \lambda_{N_m})} \right| , \quad (12)$$

which gives the required representation of the logarithm of the modulus of a rational function in the tank. This reasoning is correct only if we take infinitesimal electrodes and a surrounding circle of infinite radius, but it holds fairly well approximately if we take finite electrodes of small radius δ and a surrounding circle of large radius $1/\delta$ *).

1·6. Representation of the imaginary part of $z(\lambda)$ in the tank in which the real part is represented by the potential

If the potential in the electrolytic tank represents the real part x of an analytic function $z(\lambda)$, the imaginary part y may be represented in the tank in the following way. The field strength F at the point λ represents the variation of x per unit of length in the direction perpendicular to the equipotential. According to Cauchy-Riemann this is equal to the variation of y per unit of length along the equipotential, and according to (2) it is

---

*) Generalizing this to an infinite number of infinitesimal electrodes carrying positive or negative infinitesimal currents of the same absolute value, we get

$$V(\lambda_0) = \int m(\lambda) \ln|\lambda_0 - \lambda| \, \mathrm{d}S , \quad (13)$$

$m(\lambda)$ being the number of electrodes carrying a positive current per unit area of the tank minus the number of electrodes carrying a negative current in the same unit area, and $\mathrm{d}S$ being the surface element.

This is the analogue of the electrostatic equation

$$V(\mathbf{r}_1) = \int \frac{\varrho(\mathbf{r})}{|\mathbf{r}_1 - \mathbf{r}|} \, \mathrm{d}v$$

in three dimensions, where $\varrho(\mathbf{r})$ is the charge density and $\mathrm{d}v$ the volume element.

equal to ϱi, that is, ϱ times the current per unit of length of the equipotential. The difference $y(\lambda_1) - y(\lambda_2)$ for two points on the same equipotential (fig. 4) is therefore equal to the integral of ϱi along the intermediate part of the equipotential, that is, ϱ times the current passing between these two points.

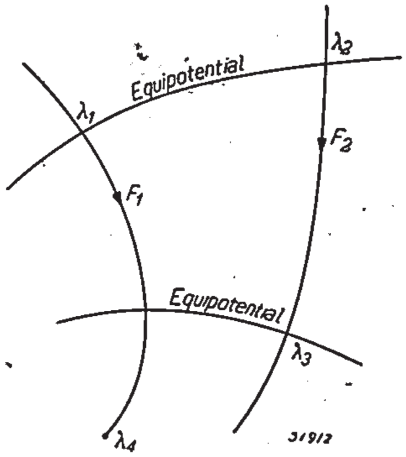

Fig. 4. Equipotentials and gradient curves in the electrolyte.

If we pass from λ_2 to λ_3 along a gradient curve, the imaginary part does not change. Therefore, the difference between y_3 and y_4 at two random points λ_3 and λ_4 is represented by the current flowing through the Faraday tube whose two boundaries pass through λ_3 and λ_4.

2. Determination of the transfer function

2·1. Statement of the problem

We shall now proceed to our main problem, the determination of the transfer function.

Let it be required to construct a filter with a number of transmission bands $D_1, D_2, \ldots, D_n$ along the frequency axis in which the attenuation is allowed to vary between the minimum α_0 and $\alpha_0 + 2\Delta\alpha_1, \alpha_0 + 2\Delta\alpha_2, \ldots, \alpha_0 + 2\Delta\alpha_n$ ($\Delta\alpha_1, \Delta\alpha_2, \ldots, \Delta\alpha_n$ being given quantities smaller than, say, 1 db). Further it is supposed that we want a number of attenuation bands $G_1, G_2, \ldots, G_m$ where the attenuation is allowed to vary between $\alpha_0 + \alpha_1, \alpha_0 + \alpha_2, \ldots, \alpha_0 + \alpha_m$ and $\alpha_0 + \alpha_1 + 2\overline{\Delta}\alpha_1, \alpha_0 + \alpha_2 + 2\overline{\Delta}\alpha_2, \ldots, \alpha_0 + \alpha_m + 2\overline{\Delta}\alpha_m$ ($\alpha_1, \alpha_2, \ldots, \alpha_m$ being given quantities $>$ 15 db and $\overline{\Delta}\alpha_1, \overline{\Delta}\alpha_2, \ldots, \overline{\Delta}\alpha_m$ given variations of attenuation, ranging from 0 to ∞). The problem is to find a rational function of which the poles and zeros lie in the negative half of the λ-plane, and of which the logarithm of the modulus represents on the ω-axis a curve corresponding to the requirements given above (see fig. 5) *).

Though it is possible to realize transfer functions with zeros in the positive half-plane, we have included the condition that the zeros shall lie in the negative half-plane, as this leads to less complicated networks.

The method may be extended without difficulty to the case where also the minimum attenuations in the different transmission bands are different. This, however, seems to be of no practical importance.

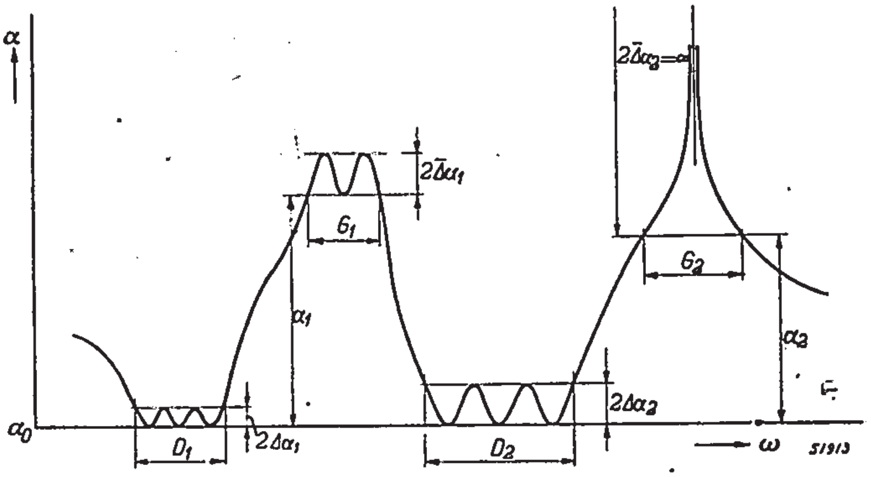

Fig. 5. Filter curve satisfying the conditions of section 2·1.

To solve this problem we shall discuss in section 2·4 an electrode configuration for the electrolytic tank that furnishes a potential distribution $\ln|F_1|$ with the property that on the ω-axis $\sqrt{\varepsilon^{2\alpha_0} + |F_1|^2}$ answers to the requirements for the modulus of the reciprocal of the transfer function.

The function F_1, however, is equivalent, mathematically, to a non-rational complex function. Therefore, in section 2·5 we shall derive a rational function that is a close approximation to the function F_1.

This rational function we call h/f, h and f being polynomials in λ with real coefficients. The difference between h/f and the original function F_1 is made sufficiently small to warrant that also $\sqrt{\varepsilon^{2\alpha_0} + |h/f|^2}$ answers the requirements for the modulus of the reciprocal transfer function.

h/f will turn out to have poles and zeros on the ω-axis only. The function $\varepsilon^{2\alpha_0} + |h/f|^2$ appears to be rational and real-valued on the ω-axis. Its zeros are lying symmetrically to the ω-axis. From this function there can be derived a rational function g/f, the zeros of g being the zeros of $\varepsilon^{2\alpha_0} + |h/f|^2$ that are to the left of the ω-axis. Then g/f answers the requirements mentioned above, and g/f can be realized as the transfer function of a four-pole.

---

*) In fig. 5, at all maxima and minima of the attenuation curve in each of the bands, the attenuation reaches one of the limits α_0, $\alpha_0 + 2\Delta\alpha_\nu$ or $\alpha_0 + \alpha_\mu$, $\alpha_0 + \alpha_\mu + 2\bar{\Delta}\alpha_\mu$ which it may not surpass in virtue of the mentioned conditions.
In section 4·7 it will be made plausible that this leads to the minimum numbers of coils.

As the evaluation of g/f from h/f amounts to solving an algebraic equation of high degree (which may be done, for instance, by Graeffe's method [6])) we may then consider our problem as solved in principle.

More efficient methods are discussed in sections 3·6, 3·7, and 3·8. As only the requirements of $|g/f|$ are given we shall follow the above reasoning in the opposite direction by deriving from g/f the requirements for h/f (sections 2·2 and 2·3) and F_1.

2·2. Deduction, from the transfer function g/f, of a function h/f the poles and zeros of which lie on the ω-axis

We denote the transfer function by f/g, in which f and g are polynomials in λ with real coefficients, having the zeros $f_1, f_2, \ldots, f_\mu, \ldots,$ and $g_1, g_2, \ldots, g_\mu, \ldots$ *).

Now, instead of by f/g, the filter may be characterized by a function of f/g.

From the conditions for the transfer function we now want to deduce those for a rational function h/f, the poles and zeros of which all lie on the ω-axis.

We shall follow here a reasoning of Piloty **). $|g/f|^2 - \varepsilon^{2a_0}$ will tend to zero in the transmission band. Now $|g/f|^2 = (g/f)_R^2 + (g/f)_I^2$, if $(g/f)_R$ denotes the real and $(g/f)_I$ the imaginary part of g/f. Along the ω-axis the real part coincides with the even part, and the imaginary part with $-j$ times the odd part.

Therefore, on the ω-axis we can write

$$|g/f|^2 = (g/f)_E^2 - (g/f)_O^2 = [(g/f)_E + (g/f)_O]\cdot[(g/f)_E - (g/f)_O] = \frac{g(\lambda)g(-\lambda)}{f(\lambda)f(-\lambda)}. \quad (14)$$

(This result also is evident from the fact that $g(\lambda)/f(\lambda)$ and $g(-\lambda)/f(-\lambda)$ are conjugate complex if λ is imaginary.)

To every pole or zero $\lambda = \lambda_a$ of $g(\lambda)/f(\lambda)$ there belongs a pole or zero $\lambda = -\lambda_a$ of $g(-\lambda)/f(-\lambda)$. Therefore $g(\lambda)g(-\lambda)$ and $f(\lambda)f(-\lambda)$ may be written as a product of factors

$$(\lambda - \lambda_a)(\lambda + \lambda_a) = \lambda^2 - \lambda_a^2; \quad (15)$$

so, $g(\lambda)g(-\lambda)/f(\lambda)f(-\lambda)$ is a rational function of λ^2.

---

*) If f and g are polynomials of different degrees ν_1 and ν_2, the quotient f/g will tend to $\lambda^{\nu_1-\nu_2}$ as λ tends to ∞, and therefore the point $\lambda = \infty$ is a zero of degree $\nu_1 - \nu_2$ or a pole of degree $\nu_2 - \nu_1$ of the quotient. As all other zeros of the quotient are zeros of f and all other poles are zeros of g, the total number of zeros of f/g is equal to its total number of poles (a zero (pole) of degree n may be understood as the limit case of n zeros (poles) at intermediate distances that tend to 0). For simplicity we will speak of these zeros or poles at $\lambda = \infty$ as additional zeros of f or g respectively. In this way of expression f and g have an equal number ν_1 or ν_2 of zeros.

**) Reference [2]), pp. 389-402.

Therefore we can write

$$\frac{g(\lambda)\,g(-\lambda)}{f(\lambda)\,f(-\lambda)} - \varepsilon^{2a_0} = R, \tag{16}$$

in which R is a rational function of λ^2 that may be written as

$$R = A^2\,\frac{(\lambda^2-\lambda_{T_1}{}^2)\,(\lambda^2-\lambda_{T_2}{}^2)\cdots}{(\lambda^2-\lambda_{N_1}{}^2)\,(\lambda^2-\lambda_{N_2}{}^2)\cdots} =$$

$$= A\,\frac{(\lambda-\lambda_{T_1})\,(\lambda-\lambda_{T_2})\cdots}{(\lambda-\lambda_{N_1})\,(\lambda-\lambda_{N_2})\cdots}\,.\,A\,\frac{(\lambda+\lambda_{T_1})\,(\lambda+\lambda_{T_2})\cdots}{(\lambda+\lambda_{N_1})\,(\lambda+\lambda_{N_2})\cdots} = S(\lambda)\,S(-\lambda). \tag{17}$$

In general, different functions $S(\lambda)$ are possible.

In the actual construction of the network, the function $h(\lambda)/f(\lambda) = S(\lambda)$ (see below) turns up, and there it is necessary to use an $h(\lambda)$ with real coefficients. This means that to every zero λ_{T_ν} of h there should be a conjugate-complex root $\lambda^*_{T_\nu}$.

There remains, however, freedom to choose out of pairs of zeros $\pm\,\lambda_{T_\nu}$ an arbitrary one for $h(\lambda)$, the other then being a root of $h(-\lambda)$. If $h(\lambda)$ has to have n_1 complex zeros and n_2 real ones, there are therefore $2^{n_2+n_1/2}$ different $h(\lambda)$'s possible. If the zeros of $h(\lambda)$ are all lying on the ω-axis this arbitrariness disappears. Any zero λ_{T_ν} of $h(\lambda)$ then coincides with a zero $-\lambda^*_{T_\nu}$ of $h(-\lambda)$, and, of course, its conjugate $\lambda^*_{T_\nu}$ coincides with $-\lambda_{T_\nu}$ of $h(-\lambda)$.

On the ω-axis R is equal to $|g/f|^2-\varepsilon^{2a_0}$. The poles of S are those of g/f; therefore S may be written as h/f, in which h and f are polynomials, and our equation ultimately becomes

$$\frac{g(\lambda)\,g(-\lambda)}{f(\lambda)\,f(-\lambda)} - \varepsilon^{2a_0} = \frac{h(\lambda)\,h(-\lambda)}{f(\lambda)\,f(-\lambda)}. \tag{18}$$

We will assume for the moment that the zeros of f are already situated on the ω-axis (this means that the attenuation in the attenuation bands oscillates between the minimum attenuation of the band and ∞). Later on, in section 3·9, we shall discuss the cases in which the zeros of f are not on the ω-axis.

The zeros of h on the ω-axis are the points in which $|g/f| = \varepsilon^{a_0}$, and therefore, according to the conditions of section 2·1, the points where g/f reaches its minimum.

Making allowance for the conditions of section 2·1, we may give $|g/f|$ such shape as to bring all zeros of h on the ω-axis by giving it a number of minima, $|g/f| = \varepsilon^{+a_0}$, in the transmission bands equal to the number of zeros of g, and therefore it is possible to use h/f as a function characterizing the filter, with poles and zeros on the ω-axis *). In agreement with Cauer and Piloty we shall call h/f the characteristic function.

2·3. Deduction of the requirements for h/f from those for g/f

The requirements for the attenuation curve given in section 2·1 may be transformed into those which the function h/f has to satisfy if some small approximations are allowed.

If we assume the minimum attenuation in the attenuation bands to be always more than 15 db, we find in these bands

$$\varepsilon^{-a_0}\,|g/f| > \sqrt[4]{1000}, \quad \text{so} \quad \varepsilon^{-2a_0}\,|g/f|^2 > 30\,.$$

Therefore, according to (18),

$$\frac{|g/f|^2 - |h/f|^2}{|h/f|^2} < \tfrac{1}{29}\,.$$

Thus, if we put

$$|h/f|^2 \approx |g/f|^2,$$

the relative error in $|h/f|^2$ will be smaller than $\frac{1}{29}$, which corresponds to 0·17 neper = 0·15 db.

In the transmission band D_ν

$$\varepsilon^{-a_0}\,|g/f| = \varepsilon^{\delta},$$

δ here being a small number varying between the values 0 and $2\Delta a_\nu$ (Δa_ν is the attenuation variation mentioned in section 2·1, measured in nepers).

The value of $\varepsilon^{-2a_0}\,|g/f|^2$ then is approximately equal to $1 + 2\delta$, and thus, according to (18), the value of $\varepsilon^{-2a_0}\,|h/f|^2$ varies between 0 and $4\Delta a_\nu$; so $\ln|h/f| - a_0$ varies between $-\infty$ and $\ln 2 + \frac{1}{2}\ln\Delta a_\nu$. If we assume Δa_ν to be always smaller than 0·1 neper, the error in $\varepsilon^{-2a_0}|g/f|^2$ is less than 0·09; so the relative error in the maximum value of $|h/f|\varepsilon^{-a_0}$ is less than $\frac{1}{2}\cdot 0{\cdot}09/0{\cdot}4 = 11{\cdot}2$ %, corresponding to 0·15 neper = 1 db.

We find that, apart from the approximations we have introduced, the requirements of 2·1 are transformed into the following requirements for h/f:

in the transmission band D_ν, $\ln|h/f| - a_0$ must be $\leqq \ln 2 + \frac{1}{2}\ln\Delta a_\nu$, (19)

in the attenuation band G_μ, $\ln|h/f| - a_0$ must be $\geqq a_\mu$, (20)

---

*) In the case of a purely reactive network, if $a_0 = 0$, the function $\ln(g/h)$ is identical with the reflection function defined by Cauer and Piloty (reference ²), p. 397), and the equation (18) then can be written as $1 = \dfrac{f(\lambda)\,f(-\lambda)}{g(\lambda)\,g(-\lambda)} + \dfrac{h(\lambda)\,h(-\lambda)}{g(\lambda)\,g(-\lambda)}$, which means that transmitted power + reflected power = inflected power.

2·4. Non-rational auxiliary function F_1

In the preceding section we found the conditions that must be fulfilled by h/f in order that g/f may fulfil the conditions of section 2·1. We have yet to find a function h/f that actually fulfils these conditions. To this end we first discuss an auxiliary function, F_1, which is non-rational and fulfils the requirements (19) and (20), using the correspondence between the real part of an analytic function and the potential in a flat electrolytic tank as described in sections 1·3-1·6.

A non-rational function F_1 satisfying to (19) and (20) is easily found. At every point of the transmission band D_ν we make $\ln|F_1| = \ln 2 + \frac{1}{2}\ln \Delta a_\nu$, and everywhere in the attenuation band G_μ we make $\ln|F_1| = a_\mu$ *).

We may now find the values of the function $\ln|F_1|$ at other points by putting in a tank, representing the λ-plane, a number of band-shaped electrodes along the transmission and attenuation bands on the ω-axis, having potentials proportional to the attenuation constants mentioned. If the point at infinity is not included in the transmission or attenuation bands, no special measures have to be taken for that point. If it is, it might be taken into account by giving to a large circular electrode around the origin the potential of the transmission or attenuation band that is passing through infinity. A special tank, in which the point at infinity is transformed into a definite point in the electrolyte, will be described later.

The potential at an arbitrary point of the λ-plane will then be proportional to $\ln|F_1|$ at that point; so we may, if it should be desired, find experimentally the value of $\ln|F_1|$ at every point of the λ-plane.

2·5. Approximation of F_1 by a rational function A; the function F

Using the electrode configuration discussed in the preceding section we may express the potential at an arbitrary point λ_p by equation (13) (footnote). Here we can replace the surface integral by a linear integral along the electrodes, as only along these electrodes current is flowing into or out of the electrolyte.

We find therefore

$$V = \frac{2\pi}{\varrho} \int i(\lambda) \ln|\lambda_p - \lambda| \, \mathrm{d}\lambda \,, \tag{21}$$

where $i(\lambda)$ means the current per unit of length of each band electrode flowing out of the electrolyte (where the current is flowing in the opposite direction we use the — sign).

We may divide each band electrode by a number of points a, b, c, ... (fig. 6) so chosen that the currents flowing from the electrode into the electrolyte between any pair of adjoining points are equal, while the first and the last of the points coincide with the two edges of the electrode. The integral (21) may be written as

---

*) We have dropped here the constant a_0 as being quite unimportant for the calculation; it may always be introduced again at the end.

$$\int_a^b i(\lambda) \ln |\lambda_p - \lambda| \, \mathrm{d}\lambda + \int_b^c i(\lambda) \ln |\lambda_p - \lambda| \, \mathrm{d}\lambda + \ldots .$$

Now, if the distance ab is small compared with $|\lambda_p - \lambda|$, the variation of $|\lambda_p - \lambda|$ along the traject ab will be small, and we obtain a good approximation if we replace the integral

$$\int_a^b i(\lambda) \ln |\lambda_p - \lambda| \, \mathrm{d}\lambda \quad \text{by} \quad \ln |\lambda_p - \lambda_A| \int_a^b i(\lambda) \, \mathrm{d}\lambda ,$$

where A is so chosen that the current entering aA is equal to that entering Ab (fig. 6).

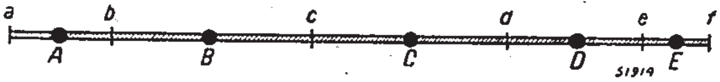

Fig. 6. The heavy line represents a band electrode. In the region *ab* the same amount of current is fed into the electrolyte as in *bc*, *cd*, *de*, *ef*. The band electrode is replaced by needle electrodes at *A*, *B*, *C*, *D*, *E*. The potential distribution remains, to a fair degree of approximation, the same at points not too close to *af*.

This particular subdivision leads to a transfer function in which the extrema of the attenuation of each kind in each band all are equal, as will be shown in section 3·4. In section 4·7 it will be seen to be the most economic transfer function (maximum attenuation a_μ and minimum variation of attenuation Δa_ν with a given number of coils).

We may extend this procedure to all trajects ab, bc, ... The modified formula (21) is

$$V = \frac{2\pi}{\varrho} \ln |\lambda_p - \lambda_A| \int_a^b i(\lambda) \, \mathrm{d}\lambda + \frac{2\pi}{\varrho} \ln |\lambda_p - \lambda_B| \int_b^c i(\lambda) \, \mathrm{d}\lambda + \ldots , \tag{22}$$

which gives us the potential distribution that would be caused by a number of needle-shaped electrodes at the points A, B, . . . , each carrying a current $\int_b^a i(\lambda) \, \mathrm{d}\lambda$.

According to (12), this electrode configuration corresponds to a rational function

$$A = \frac{(\lambda_p - \lambda_A) \, (\lambda_p - \lambda_B) \cdots}{(\qquad) \, (\qquad) \cdots}$$

or to any power of it. (A constant factor in A amounts to a constant additional term in V. As this term is of no importance to the procedure, it will be omitted.) Here the factors in the numerator correspond to the needle electrodes taking current from the electrode; those in the denominator to the ones that give current. We can now alter the number of points a, b, c, d, etc., until the current that is to be fed to the needle electrodes replacing the band electrodes in order to acquire the desired potential distribution, is plus or minus a unit of current (the relation between the unit of current and the unit of potential is given in section 1·1). Provided the number of needle electrodes needed in each band is an integral number, the new function becomes a purely rational function. This function is a good approximation of F_1 at all points of the λ-plane except at those where the distances to two adjoining needle electrodes are about equal to, or less than, the distance between those two electrodes. In practice this means that in the vicinity of the transmission and attenuation bands the difference between $\ln|A|$ and $\ln|F_1|$ becomes perceptible.

Along the transmission or attenuation bands in which the needles are situated, the mean potential is equal to the potential of the band-shaped electrode. Now, the potentials of the needles will tend to infinity as their cross-sections are reduced to zero. At the needles of small cross-section the potentials are higher than the potential of the band-shaped electrode, and, therefore, at the minima between the needles the potential will be lower. As will be discussed in section 3·4 the difference between the minimum and the mean potential amounts to ln 2. Therefore, in actual determination of h/f we have to use a function F given by $\ln|F| = \ln|F_1| - \ln 2$ in the transmission bands and $\ln|F| = \ln|F_1| + \ln 2$ in the attenuation bands.

2·6. Finding the singularities of $\ln|A|$

Except for the difference between A and h/f mentioned at the end of the preceding section, our problem now is reduced to finding a distribution of needle-shaped electrodes along the different attenuation and transmission bands in which every electrode will feed or take an equal amount of current, and which produces a mean potential distribution approximating that of the band-shaped electrodes mentioned in section 2·4.

We can find such a distribution if we start by putting band-shaped electrodes into the tank along the different bands and on the desired potentials, then measuring the distribution of current along these electrodes. If afterwards we replace every band electrode by a series of identical needle-shaped electrodes, making everywhere the number of needles per cm proportional to the measured current per cm, we can feed each needle with the same amount of current. At some distance from the electrodes the current distribution will then be approximately equal to the one that was generated by the original band-shaped electrode, and therefore the potentials in both cases will also be the same.

In principle we may find the distribution of current along the band-shaped electrodes by tracing an equipotential curve running very close to the electrode. The distance between an arbitrary point of this curve and the electrode is then proportional to the current per cm at that point.

However, in section 3 a method will be discussed for finding the positions of the needle electrodes, based on the same principles but allowing a more accurate formulation and a more accurate result.

2·7. Preventing the appearance of zeros of A in the attenuation bands or of poles of A in the transmission bands

In those parts of the band-shaped electrodes which feed current into the electrolyte, the function A will have poles, while in parts of the electrodes that take current, the function has zeros.

Now it may happen that the attenuation requirements lead to a configuration in which current is taken at some parts of the attenuation bands. In the more general situation where there are several transmission bands, all with different attenuations and/or attenuation variations, the reverse case, i.e., when current is given in the transmission bands, may also occur. This means that the function A will then have zeros in the attenuation bands or poles in the transmission bands.

Now, if we remove a zero from A the value of A in the vicinity of that zero will increase, which means, according to section 2·3, that the attenuation of the filter will increase. Therefore, by removing a zero from an attenuation band we are improving the filter. So, if there are in the attenuation bands band electrodes entirely or partially taking current, we may remove them, or shorten them, until the remaining part is giving current over the whole of its length. In the transmission bands the same goes for electrodes partially or entirely giving current.

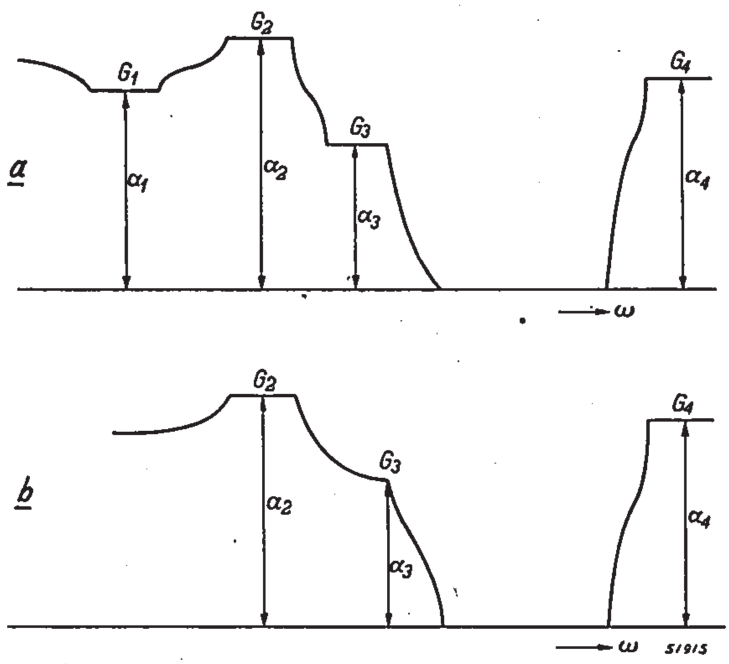

Fig. 7. The system of fig. 7*b* satisfies the same attenuation conditions as that of fig. 7*a*, but leads to a transfer function with a smaller number of poles and zeros.

In fig. 7 we have given an example of what will happen to the attenuation characteristics if one removes the electrodes taking current from the attenuation bands. In the ranges G_1, G_2, G_3, G_4 the required attenuations are a_1, a_2, a_3, a_4. When the auxiliary function $\ln |F_1|$ is made constant in these ranges, the shape of the attenuation characteristic is approximately as shown in fig. 7*a*. The attenuation in the proximity of G_1 here turns out to be higher than at G_1 itself. If, therefore, we leave the function undefined at G_1 and only fix it by means of the remaining electrodes, the attenuation at G_1 will be higher, and the characteristic will be better. The electrode in G_3 may be shortened until at the left-hand extremity the current taken per cm is zero Then, the gradient of the potential there must also be zero; the potential function, therefore, must match smoothely with the horizontal part. The modified curve is given in fig 7*b*.

As will become evident in section 3·4, the same reasoning holds if we read $\ln|F|$ for $\ln|F_1|$ and h/f for A.

REFERENCES

1) W. Bader, Tel. Ferns. Tech. 31, 177-189, 1942.

2) W. Cauer, Theorie der linearen Wechselstromschaltungen, Akad. Verl. Ges., Leipzig, 1941.

3) F. Klein, Gesammelte Werke III, Julius Springer, Berlin, 1923.

4) P. H. J. A. Kleynen, Philips tech. Rev. 2, 338-346, 1937.

5) J. F. Schouten and J. W. Klute, Philips tech. Rev. 7, 138-147, 1942.

6) Enz. Math. Wiss. I, p. 440.

VOL. 3 NR 2 APRIL 1948

Philips Research Reports

EDITED BY THE RESEARCH LABORATORY
OF N. V. PHILIPS' GLOEILAMPENFABRIEKEN, EINDHOVEN, NETHERLANDS

R 73 *Philips Res. Rep. 3, 81-101, 1948*

THE GYRATOR, A NEW ELECTRIC NETWORK ELEMENT

by B. D. H. TELLEGEN

538.55:621.392

Summary

Besides the capacitor, the resistor, the inductor, and the ideal transformer a fifth, linear, constant, passive network element is conceivable which violates the reciprocity relation and which is defined by (10). We have denoted it by the name of "ideal gyrator". By its introduction the system of network elements is completed and network synthesis is much simplified. The gyrator can be realized by means of a medium consisting of particles carrying both permanent electric and permanent magnetic dipoles or by means of a gyromagnetic effect of a ferromagnetic medium.

Résumé

A côté de la capacité, de la résistance, de l'inductance et du transformateur idéal on peut concevoir un cinquième élément de circuit, linéaire, constant et passif, qui transgresse la relation de réciprocité et qui est défini par (10). Nous l'avons appelé „gyrateur idéal". En l'introduisant, le système d'éléments de circuit est complété et la synthèse de circuits s'en trouve très simplifiée. Le gyrateur peut être réalisé à l'aide d'un milieu composé de particles portant à la fois des dipôles électriques permanents et des dipôles magnétiques permanents ou au moyen d'un effet gyromagnétique d'un milieu ferromagnétique.

1. Introduction

The physical investigation of electric phenomena led to the creation of several devices which afterwards were used in engineering for the construction of electric networks.

From electrostatics resulted the *capacitor*, whose properties are described by

$$i = C\frac{\mathrm{d}v}{\mathrm{d}t}, \tag{1}$$

where i is the current and v the voltage. The coefficient C is called the *capacitance* and is always positive.

From the investigation of currents in conductors resulted the *resistor*, described by

$$v = Ri\,. \tag{2}$$

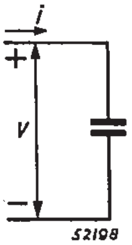

Fig. 1. Capacitor.

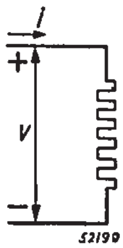

Fig. 2. Resistor.

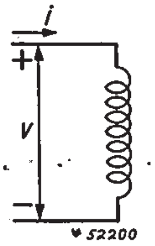

Fig. 3. Coil.

The coefficient R is called the *resistance* and is always positive.

From electromagnetism resulted the *inductor* or *coil*, described by

$$v = L \frac{di}{dt}. \tag{3}$$

The coefficient L is called the *self-inductance* and is always positive.

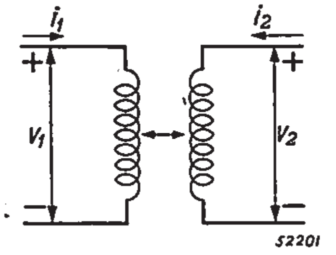

Fig. 4. Two coupled coils.

Two *coupled coils* are described by a set of two equations

$$\left.\begin{aligned} v_1 &= L_1 \frac{di_1}{dt} + M \frac{di_2}{dt}, \\ v_2 &= M \frac{di_1}{dt} + L_2 \frac{di_2}{dt}. \end{aligned}\right\} \tag{4}$$

The coefficient M is called the *mutual inductance* and is restricted by $M^2 \leqq L_1 L_2$.

Further development of physics has not resulted in the creation of other similar devices and coefficients. Engineering has taken these devices into use as network elements, and we shall begin by recalling broadly what has been done with them.

1·1. The network elements

As to the *network elements* themselves, many types of capacitor, resistor and inductor are constructed for different purposes, with different values, for different currents and voltages, fixed and variable. It was soon discovered that elements whose properties are given by (1), (2), and (3) must be considered as *ideal elements*, which in practice can only be approximated; every capacitor, for instance, has some losses and some inductance, and similar remarks hold for resistors and inductors.

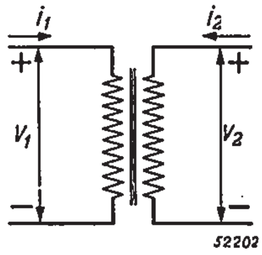

Fig. 5.
Ideal transformer.

From the system of two coupled coils a more radical development started. By making the coupling coefficient M^2/L_1L_2 as nearly as possible equal to 1, the transformer was created, whose properties in the ideal state are described by

$$\left.\begin{aligned} i_1 &= -u i_2, \\ v_2 &= u v_1. \end{aligned}\right\} \tag{5}$$

The coefficient u is called the *transformation ratio.*

For general considerations on networks we can better regard this *ideal transformer* as being the fourth network element rather than the general system of two coupled coils.

As to energy relations: an ideal capacitor and an ideal inductor can only store energy; an ideal resistor can only dissipate energy; an ideal transformer, however, can neither store nor dissipate energy but can only transfer energy, for, by (5), the absorbed power is always zero:

$$i_1 v_1 + i_2 v_2 = 0 . \tag{6}$$

1·2. The networks

By connecting the four types of network element together, *networks* can be constructed which give rise to several problems. In the first place, when given voltage or current sources are connected to a given network one may ask for the voltages and currents of the various branches of the network. These problems are denoted by the name of network *analysis* and may be considered generally solved.

For engineering purposes networks are often not given, but it may be asked to construct networks with specified properties. The problems arising therefrom are denoted by the name of network *synthesis*, and we shall go into them in some detail.

To solve these problems the networks are classified in several ways. In the first place the networks are classified by the number of terminals, which we shall suppose always to be combined in pairs such that the current entering the network by one terminal of a pair is always equal to the current leaving the network by the other terminal of the same pair. Thus we distinguish between two-poles, four-poles, six-poles, . . . , $2n$-poles when a network has 1, 2, 3, . . . , n terminal pairs, respectively. In the second place the networks are classified as resistanceless networks and as networks with resistance. In the third place the networks are classified, according to the order of the differential equation to which they give rise, as networks of zeroth order, first order, second order, and so on.

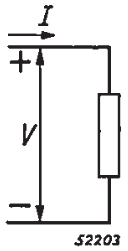

Fig. 6. Two-pole.

A two-pole is characterized by a relation between the voltage and the current of the terminals, which may be written in complex form, for instance, as

$$V = ZI . \tag{7}$$

The two-pole parameter Z is the impedance of the two-pole and is a function of frequency.

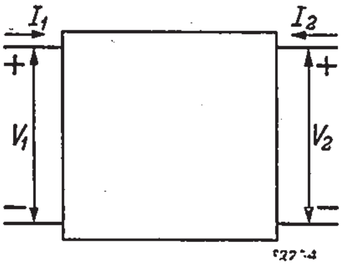

Fig. 7. Four-pole.

A four-pole is characterized by two relations between the voltages and the currents of the terminals, which may be written in complex form, for instance, as

$$\left.\begin{aligned} V_1 &= Z_{11} I_1 + Z_{12} I_2 , \\ V_2 &= Z_{21} I_1 + Z_{22} I_2 . \end{aligned}\right\} \tag{8}$$

The four-pole parameters Z_{11}, Z_{12}, Z_{21}, Z_{22} are functions of frequency.

A $2n$-pole is thus characterized by n similar relations between the voltages and the currents of the terminals. The corresponding parameters of two $2n$-poles with different networks may be equal functions of frequency. Such $2n$-poles are said to be *equivalent*.

The problem of network synthesis may be stated as the problem of finding the necessary and sufficient conditions for a system of functions of frequency in order that these may represent the parameters of a $2n$-pole composed of the above-mentioned four types of network element; and further as the problem of indicating for each such set of parameters at least one way to construct a corresponding network. However, when it is required to construct a $2n$-pole with specified properties, as a rule its parameters cannot be considered as given but must first be found. Now, in general, the more complicated we are prepared to make the network, the better we shall be able to satisfy given requirements. As the classification of networks by their order is essentially a classification by their complexity, the problem of network synthesis may also be stated as the problem of finding the parameters of the most general $2n$-poles of a certain order that are realizable with the help of the four types of network element, and of indicating for each such set of parameters at least one way to construct a corresponding network [1]).

The synthesis problem is solved in both senses for resistanceless two-poles, for resistanceless four-poles, and for two-poles with resistance. For four-poles with resistance it is only solved in the first sense.

The synthesis of resistanceless two-poles was accomplished by Foster [2]). The result, for the zeroth to the fourth order, is given by fig. 8. For every order there are two types of two-pole. Fig. 8 contains all those two-pole networks of these orders composed of L's and C's for which the sum of the numbers of L's and C's is equal to the order of the two-pole. For the third order both types of two-pole can be realized by two such equivalent networks, for the fourth order by four.

The synthesis of resistanceless four-poles of a certain order was accomplished by the author [1]). Apart from order zero there are four types of four-pole of odd order and five types of even order.

The synthesis of two-poles with resistance was accomplished by Brune [3]). For the 0th, 1st, 2nd, 3rd, and 4th orders there are, respectively, 1, 2, 5, 12, and 29 types of two-pole.

The synthesis of four-poles with resistance was studied by Gewertz [4]), who succeeded in finding necessary and sufficient conditions for the four-pole parameters. He did not, however, tackle the problem of finding all four-pole parameters of a certain order; so we might try to solve this problem and to construct the simplest corresponding networks. This problem is not an academic one, as four-poles are most extensively used in engineering. However, we have seen above that the synthesis both of resistanceless four-poles and of two-poles with resistance is more complicated than that of resistanceless two-poles, and we must therefore expect the synthesis of four-poles with resistance to be still more complicated.

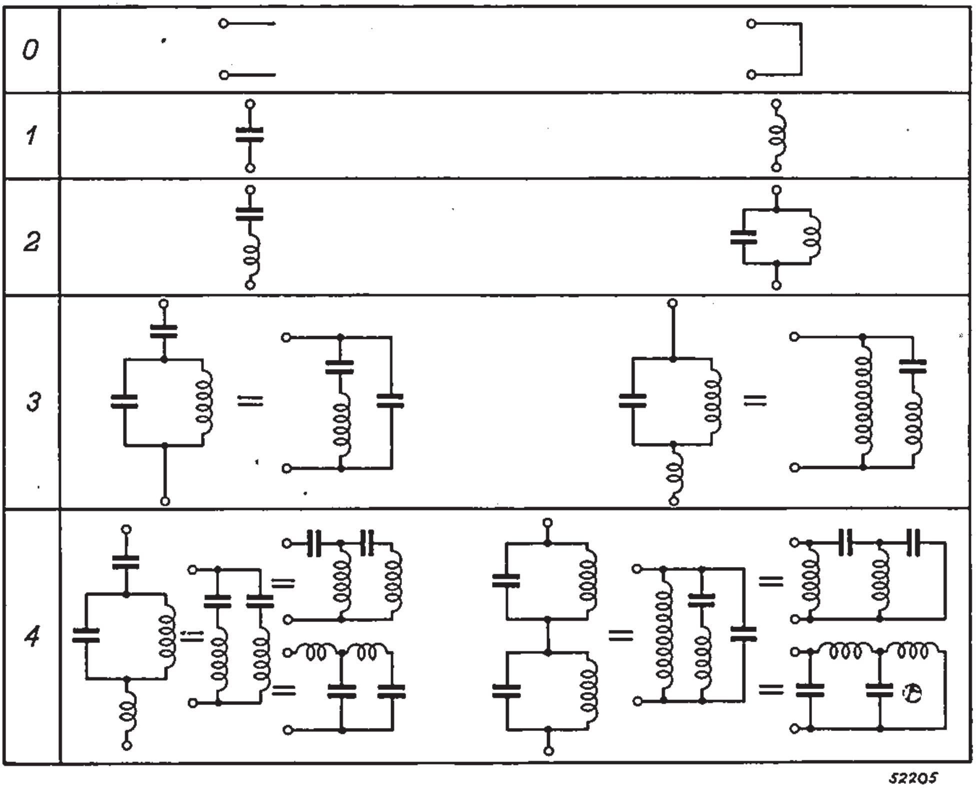

Fig. 8. Synthesis of resistanceless two-poles from the zeroth to the fourth order.

2. Statement of the problem — the ideal gyrator

For these reasons, before starting to try solving this problem, let us stop for a moment and look backwards. What are we doing as a matter of fact? Our four network elements have their origin in physics, and engineering has taken them for granted. It is worth while asking whether the system of four network elements is complete. The physicist has no reason to raise this question. He studies the phenomena of nature as they present themselves to him. For the technician, who wants to create useful systems, this question is of the utmost importance, and so we ask: *"Besides the four known network elements are other, similar elements conceivable?"*

At first this question seems rather vague: what is similar? — what is conceivable? However, the question appears to be a very definite one if we pay attention to the methods and results of network synthesis.

These are based upon the finding, first, of a number of general properties of $2n$-poles composed of the four known network elements, and then trying to construct any $2n$-pole possessing these properties by means of these elements. These properties are:

(a) the relation between the voltages and the currents of the terminals is formed by a system of ordinary *linear* differential equations, with

(b) *constant* coefficients;

(c) the $2n$-pole is *passive*, i.e., it can deliver no energy;

(d) the *reciprocity* relation.

This last property is expressed by the equality of those coefficients of the four-pole equations that lie symmetrically with respect to the principal diagonal if these equations express both voltages in both currents, or vice versa — the voltages and currents being taken positive according to fig. 7. Thus in (8) $Z_{21} = Z_{12}$, and also (4) shows an example of this form of the reciprocity relation. If, however, the current of one pair of terminals and the voltage of the other pair are expressed in the voltage of the first pair and the current of the second pair, the reciprocity relation is expressed by the opposite equality of the corresponding coefficients; for from (8) it follows that

$$\left.\begin{aligned} I_1 &= (1/Z_{11})\ V_1 - (Z_{12}/Z_{11})\ I_2\,, \\ V_2 &= (Z_{21}/Z_{11})\ V_1 + (Z_{22} - Z_{21}Z_{12}/Z_{11})\ I_2\,. \end{aligned}\right\} \qquad (9)$$

Equations (5) exhibit an example of this form of the reciprocity relation.

The above-mentioned investigations on network synthesis show that any two-pole and four-pole possessing these four properties can be realized by a network composed of the four elements. It seems very unlikely that this will be otherwise for $2n$-poles with $n > 2$. Therefore, if we restrict ourselves to $2n$-poles possessing the four mentioned properties the answer to our principal question is in the negative: no other similar network elements are conceivable. If we want to extend the possibilities we must drop one or more of the four properties.

If we drop the first property, the linearity, the principle of superposition will no longer hold and the systems will become much more complicated. Consequently, we want to keep this property.

If we drop the second property, the coefficients may become functions of the time, for instance periodic functions. Frequency conversion may then arise and this also complicates the system considerably, so that we want to keep the second property too.

If we drop the third property, the system must contain some source of energy. Amplifier valves, for instance, whose properties when dealing with small alternating voltages and currents are described by linear equations with constant coefficients, need D.C. sources of energy and thus constitute elements more complicated than those passive elements considered so far. Consequently, we want to keep also the third property.

As to the fourth property, the reciprocity, however, compared with the former three properties this is of much less importance. A $2n$-pole possessing the first three properties but lacking the fourth may very well be termed similar to the $2n$-poles composed of the four normal network elements. Therefore it seems worth while to investigate what it will lead to if we maintain the first three properties but drop the fourth.

We shall need some new type of network element to realize these $2n$-poles, in particular an element violating the reciprocity relation. This requirement has no significance for a two-pole element, such as C, R and L, so we must look for a new four-pole element. The simplest types of four-pole are the resistanceless ones of order zero. These are types for which $i_1 v_1 + i_2 v_2 = 0$, as this expresses that energy can neither be dissipated nor stored in the four-pole. The ideal transformer, whose equations are given by (5):

$$\left.\begin{aligned} i_1 &= -u\, i_2\,, \\ v_2 &= u\, v_1\,, \end{aligned}\right\} \tag{5}$$

is an example of such a four-pole satisfying the reciprocity relation. Another such four-pole, but violating the reciprocity relation, is described by

$$\left.\begin{aligned} v_1 &= -s\, i_2\,, \\ v_2 &= s\, i_1\,. \end{aligned}\right\} \tag{10}$$

In fact, from (10) it follows that $i_1 v_1 + i_2 v_2 = 0$ whereas the coefficients in (10) are not equal, as the reciprocity relation requires, but oppositely equal.

For reasons given below we shall denote such a four-pole by the name of *ideal gyrator*. We shall consider the ideal gyrator as a fifth network element.

3. Properties of the ideal gyrator

The ideal gyrator has the property that it "gyrates" a current into a voltage, and vice versa. The coefficient s, which has the dimension of a resistance, we shall call the *gyration resistance*, whilst $1/s$ we shall call the *gyration conductance*. In circuit diagrams we shall represent the ideal gyrator by the symbol of fig. 9.

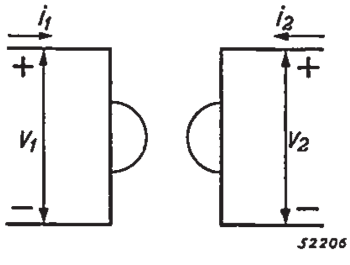

Fig. 9. Proposed symbol for the ideal gyrator.

The following properties of the ideal gyrator are easily derived from (10).

If we leave the secondary terminals open, $i_2 = 0$, the primary terminals are short-circuited, $v_1 = 0$, and vice versa. If we connect the secondary terminals by an inductance L, between the primary terminals we find a capacitance $C = L/s^2$. Conversely, if we connect the secondary terminals by a capacitance C, between the primary terminals we find an inductance $L = s^2C$. Generally, if we connect the secondary terminals by an impedance Z we find between the primary terminals an impedance s^2/Z. An impedance Z in series with or in parallel to the secondary terminals is equivalent to an impedance s^2/Z in parallel to respectively in series with the primary terminals, and vice versa (fig. 10).

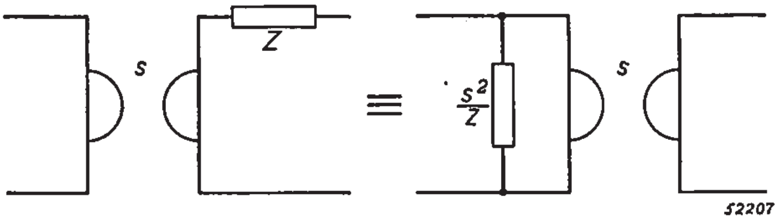

Fig. 10. An impedance in series with one pair of terminals of an ideal gyrator is equivalent to another impedance in parallel to the other pair of terminals.

Two ideal gyrators in cascade constitute an ideal transformer; an ideal gyrator and an ideal transformer in cascade constitute another ideal gyrator.

4. Networks with ideal gyrators

If ideal gyrators were available we could investigate anew all network problems arising in engineering, and since the extension of the system of four network elements to five is a relatively large one, we may expect considerably improved solutions to be possible for most network problems. As an example we may mention the system of two equal, critically coupled, tuned circuits such as are commonly used in the intermediate-frequency stages of superheterodyne radio receivers. If the circuits are coupled in an appropriate way by a gyrator and a resistance, the amplification per stage, compared with that obtained with inductively or capacitively coupled circuits under similar conditions, can be made larger by a factor $1 + \sqrt{2}$. Further details will be given in a subsequent paper.

Before investigating how an ideal gyrator might be realized or approximated, we shall first devote attention to the theory of networks that may contain ideal gyrators. As the reciprocity relation is of only subordinate importance in the methods of network analysis, this part of network theory is not much influenced by the introduction of the gyrator. Network synthesis, however, is influenced by it to a great extent and proves to be much simplified.

The synthesis of resistanceless two-poles does not change by the introduction of the gyrator. We may add that, by connecting them to an ideal gyrator, the two types of two-pole of a certain order are transformed one into the other, as mentioned above for the two-poles of the first order, the L and the C.

The synthesis of resistanceless four-poles is much simplified by the introduction of the gyrator. For every order there are two types, which can be transformed one into the other by connecting an ideal gyrator to any one of their terminal pairs.

As to the synthesis of two-poles with resistance, the addition of the gyrator does not create new possibilities, for the properties of a two-pole do not depend upon the reciprocity relation. However, the number of networks necessary for the realization of the most general two-pole of a certain order can be reduced to one by the use of ideal gyrators. We can construct this general type of two-pole of a certain order by taking any one of the two types of resistanceless four-pole of the same order and connecting any one of its two pairs of terminals by a resistance, whereby the four-pole changes into a two-pole.

The same simplicity is expected to hold for $2n$-poles. For every order of a resistanceless $2n$-pole there are probably two types, which can be transformed one into the other by connecting a gyrator to any one of their terminal pairs. For every order of a $2(n-1)$-pole with resistance there is probably one type, which can be constructed by taking any one of the two types of resistanceless $2n$-pole of the same order and connecting any one of its n pairs of terminals by a resistance.

These results of network synthesis will be fully dealt with in subsequent papers. They show how much network synthesis is simplified by the introduction of the ideal gyrator, and demonstrate that it is only by adding the ideal gyrator to the four known network elements that a complete set of elements arises.

5. Related problems in mechanics and electromechanics

Before turning to the problem of realizing the gyrator we shall give a short survey of related problems in mechanics and electromechanics.

Systems whose properties are described by a set of ordinary linear differential equations with constant coefficients were first studied in mechanics under the theory of small vibrations. A full account of these studies is given by Thomson and Tait in their "Treatise on natural philosophy". In these equations special terms may occur, called by those authors "gyroscopic" or "gyrostatic" terms, "because they occur when fly-wheels each given in a state of rapid rotation form part of the system by being mounted on frictionless bearings connected through framework with other parts of the system; and because they occur when the motion considered is motion of the given system relatively to a rigid body revolving with a constrainedly constant angular velocity round a fixed axis" [5]).

As an example let us consider a system described by

$$\left.\begin{aligned} a_1 \frac{\mathrm{d}^2\psi_1}{\mathrm{d}t^2} + c_1\psi_1 - b\frac{\mathrm{d}\psi_2}{\mathrm{d}t} &= \Psi_1, \\ a_2 \frac{\mathrm{d}^2\psi_2}{\mathrm{d}t^2} + c_2\psi_2 + b\frac{\mathrm{d}\psi_1}{\mathrm{d}t} &= \Psi_2. \end{aligned}\right\} \tag{11}$$

In these equations ψ_1 and ψ_2 denote two general coordinates of the system, Ψ_1 and Ψ_2 the corresponding general forces; a_1 and a_2 are the general masses, c_1 and c_2 the general stiffnesses. The terms $-b\,\mathrm{d}\psi_2/\mathrm{d}t$ and $b\,\mathrm{d}\psi_1/\mathrm{d}t$, whose coefficients are oppositely equal, are called gyrostatic terms.

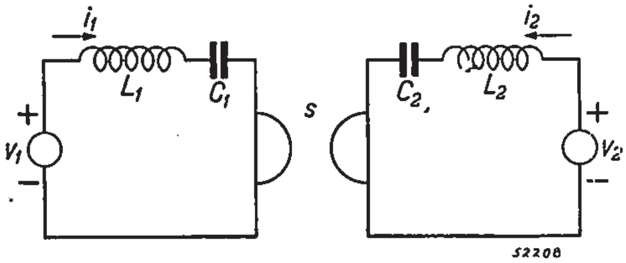

Fig. 11. Two circuits coupled by an ideal gyrator.

Let us compare with such a mechanical system the electrical system of fig. 11 in which two tuned circuits, L_1-C_1 and L_2-C_2, incorporating e.m.f.'s v_1 and v_2, respectively, are coupled by an ideal gyrator with gyration resistance s. The equations of this system are

$$\left.\begin{aligned} L_1 \frac{\mathrm{d}i_1}{\mathrm{d}t} + \frac{1}{C_1}\int i_1\mathrm{d}t - s\,i_2 &= v_1, \\ L_2 \frac{\mathrm{d}i_2}{\mathrm{d}t} + \frac{1}{C_2}\int i_2\mathrm{d}t + s\,i_1 &= v_2. \end{aligned}\right\} \tag{12}$$

If we put $i_1 = \mathrm{d}Q_1/\mathrm{d}t$ and $i_2 = \mathrm{d}Q_2/\mathrm{d}t$, we come to

$$\left.\begin{aligned} L_1 \frac{\mathrm{d}^2Q_1}{\mathrm{d}t^2} + \frac{1}{C_1}Q_1 - s\frac{\mathrm{d}Q_2}{\mathrm{d}t} &= v_1, \\ L_2 \frac{\mathrm{d}^2Q_2}{\mathrm{d}t^2} + \frac{1}{C_2}Q_2 + s\frac{\mathrm{d}Q_1}{\mathrm{d}t} &= v_2, \end{aligned}\right\} \tag{13}$$

which is of quite the same form as (11). The gyrostatic terms of (11) correspond to the terms of (13) arising from the gyrator, and it is because of this correspondence that we have chosen the name of gyrator for the new network element. Recently Bloch [6]) devised an ideal gyroscopic coupler which is the exact mechanical equivalent of our gyrator.

Another field where gyrostatic terms arise is in the theory of electromechanical transducers. Poincaré, in his theory of the telephone receiver 7) 8), deduced equations that in complex notation are of the form

$$\left.\begin{aligned} V &= Z_e I - A W , \\ F &= A I + Z_m W . \end{aligned}\right\} \tag{14}$$

V, F, I, W are, respectively, the (complex) voltage, force, current, velocity; Z_e is the (complex) electrical and Z_m the (complex) mechanical impedance; $-AW$ and AI are the coupling terms, in which A is real.

We can derive from (14) the equations of a corresponding mechanical system by replacing the voltage by a force and the current by a velocity. The coupling terms then become a pair of gyrostatic terms, and so in equation (14) they are also often called gyrostatic terms.

Equations of the form (14) occur in the theory of magnetic or moving-coil transducers. In the theory of electrostatic or piezo-electric transducers the coefficients of the coupling terms have equal signs 8). Thus, if a magnetic and an electrostatic transducer are connected in cascade, so that by the former electrical oscillations are transduced into mechanical oscillations and by the latter the mechanical oscillations are again transduced into electrical oscillations, the resultant four-pole will violate the reciprocity relation of ordinary networks. This was explicitly stated by Jefferson 9) and by Mc. Millan 10).

So we could try to approximate the ideal gyrator by some special electromechanical apparatus. However, if we want to develop a gyrator that can also be used in high-frequency networks we must remember that high-frequency oscillations in electromechanical systems are only possible by the use of resonance (such as in piezo-quartz oscillators), and so we could at most arrive at a gyrator for a very narrow frequency range, contrary to the ideal gyrator, which has an unlimited frequency range. Our object must therefore be to approximate the ideal gyrator by other than electromechanical means.

6. The origin of the reciprocity relation

As the gyrator violates the reciprocity relation of ordinary networks we begin by recalling the origin of this relation, in the expectation that this will show us how to dispense with it *).

Let us first consider two insulated conductors 1 and 2 with potentials v_1 and v_2 and charges Q_1 and Q_2. The charges are linear functions of the potentials of the form

$$\left.\begin{aligned} Q_1 &= C_{11} v_1 + C_{12} v_2 , \\ Q_2 &= C_{21} v_1 + C_{22} v_2 . \end{aligned}\right\} \tag{15}$$

---

*) As the ideal gyrator has no dissipation we restrict our investigation to systems without dissipation. The reciprocity relation of systems with dissipation has been studied by Onsager 11).

To change the charges by amounts $\mathrm{d}Q_1$ and $\mathrm{d}Q_2$ there must be supplied an energy

$$v_1\,\mathrm{d}Q_1 + v_2\,\mathrm{d}Q_2 = (C_{11}\,v_1 + C_{21}\,v_2)\,\mathrm{d}v_1 + (C_{12}\,v_1 + C_{22}\,v_2)\,\mathrm{d}v_2\,. \tag{16}$$

As this must be a total differential $\mathrm{d}U$,

$$\left.\begin{aligned} C_{11}\,v_1 + C_{21}\,v_2 &= \partial U/\partial v_1\,,\\ C_{12}\,v_1 + C_{22}\,v_2 &= \partial U/\partial v_2\,,\end{aligned}\right\} \tag{17}$$

from which we arrive at

$$C_{21} = \frac{\partial^2 U}{\partial v_1 \partial v_2} = \frac{\partial^2 U}{\partial v_2 \partial v_1} = C_{12}\,, \tag{18}$$

the reciprocity relation of electrostatics.

We may generalize this result (Ehrenfest [12]).

There are many more pairs of quantities in physics, such as Q and v, whose product is an energy; e.g., magnetic flux Φ and current i, mechanical displacement s and force K, turning angle φ and moment M, entropy S and temperature T. If a pair of such quantities characterizing the state of a system are slightly changed, the energy supplied to the system is equal to one of these quantities multiplied by the increment of the other quantity:

$$v\mathrm{d}Q,\ i\mathrm{d}\Phi,\ K\mathrm{d}s,\ M\mathrm{d}\varphi,\ T\mathrm{d}S.$$

The quantities are thereby divided into two classes: v, i, K, M, T belong to one class of quantities and Q, Φ, s, φ, S belong to the other class.

Suppose now, we have a system whose state is characterized by two pairs of such quantities, denoted by x_1, y_1 and x_2, y_2, and let a linear relationship exist between them such as

$$\left.\begin{aligned} y_1 &= a_{11}\,x_1 + a_{12}\,x_2\,,\\ y_2 &= a_{21}\,x_1 + a_{22}\,x_2\,.\end{aligned}\right\} \tag{19}$$

Then, if x_1 and x_2 belong to one class of quantities and therefore y_1 and y_2 to the other class, by a reasoning similar to that in the electrostatic case we may deduce $a_{12} = a_{21}$. On the other hand, if x_1 and x_2 belong to different classes of quantities we arrive at $a_{12} = -a_{21}$.

7. The violation of the reciprocity relation

The network equations, such as (8), are usually written with voltages and currents as variables. Now, these do not form a pair of quantities such as those mentioned above, for their product is not an energy but a power. We can change from the former to the latter pairs of quantities by differentiation with respect to the time. From the electrostatic equations (15) we thus come to

$$\left.\begin{aligned} i_1 &= C_{11}\frac{\mathrm{d}v_1}{\mathrm{d}t} + C_{12}\frac{\mathrm{d}v_2}{\mathrm{d}t}, \\ i_2 &= C_{21}\frac{\mathrm{d}v_1}{\mathrm{d}t} + C_{22}\frac{\mathrm{d}v_2}{\mathrm{d}t}. \end{aligned}\right\} \tag{20}$$

By comparing this with what has been written in section 2 we see that $C_{12} = C_{21}$ corresponds to the reciprocity relation of networks.

If we start from the equations of two coupled coils

$$\left.\begin{aligned} \Phi_1 &= L_{11}\, i_1 + L_{12}\, i_2, \\ \Phi_2 &= L_{21}\, i_1 + L_{22}\, i_2, \end{aligned}\right\} \tag{21}$$

where the i's are the currents and the Φ's are the fluxes through the coils, we arrive at $L_{12} = L_{21}$. By differentiation we come to

$$\left.\begin{aligned} v_1 &= L_{11}\frac{\mathrm{d}i_1}{\mathrm{d}t} + L_{12}\frac{\mathrm{d}i_2}{\mathrm{d}t}, \\ v_2 &= L_{21}\frac{\mathrm{d}i_1}{\mathrm{d}t} + L_{22}\frac{\mathrm{d}i_2}{\mathrm{d}t}. \end{aligned}\right\} \tag{22}$$

Here, too, the relation $L_{12} = L_{21}$ corresponds to the reciprocity relation of networks.

To come to a violation of the reciprocity relation of networks we must start from a system characterized by a pair of quantities Q_1, v_1 and a pair of quantities Φ_2, i_2. The equations will then take the form

$$\left.\begin{aligned} Q_1 &= C\, v_1 + A\, i_2, \\ \Phi_2 &= A\, v_1 + L\, i_2, \end{aligned}\right\} \tag{23}$$

where the two coefficients A will be equal. By differentiation we now arrive at

$$\left.\begin{aligned} i_1 &= C\,\frac{\mathrm{d}v_1}{\mathrm{d}t} + A\,\frac{di_2}{\mathrm{d}t}, \\ v_2 &= A\,\frac{\mathrm{d}v_1}{\mathrm{d}t} + L\,\frac{\mathrm{d}i_2}{\mathrm{d}t}, \end{aligned}\right\} \tag{24}$$

which, according to section 2, violates the reciprocity relation of networks if $A \neq 0$.

The equations (24) bear much resemblance to the equations (4). The energy of the system is equal to

$$U = \int i_1 v_1\, \mathrm{d}t + \int i_2 v_2\, \mathrm{d}t = \tfrac{1}{2}\, C\, v_1^2 + A\, v_1 i_2 + \tfrac{1}{2}\, L\, i_2^2, \tag{25}$$

if we take this energy as zero when $v_1 = 0$ and $i_2 = 0$. As this energy can never become negative in a passive system, C and L must be positive and A is restricted by $A^2 \leqq CL$.

In the same way as we can approximate the ideal transformer from the system described by (4), we can approximate the ideal gyrator from a system described by (24) by making the "coupling coefficient" A^2/CL as nearly as possible equal to 1.

8. The realization of the gyrator

Our object, therefore, is to devise a system described by (23) with a coupling coefficient as nearly as possible equal to 1. To investigate how this can be done we first show how such a system could be constructed if a medium were available characterized by relations between the field vectors of the type

$$\left.\begin{aligned} \mathbf{D} &= \varepsilon\,\mathbf{E} + \gamma\,\mathbf{H}\,, \\ \mathbf{B} &= \gamma\,\mathbf{E} + \mu\,\mathbf{H}\,, \end{aligned}\right\} \qquad (26)$$

and with $\gamma^2/\varepsilon\mu$ nearly equal to 1.

Let us consider the system of fig.12. This consists of two flat parallel electrodes the space between which is filled with a medium described by (26). Besides, there is a yoke of magnetic material, having a very large permeability, on which a coil is wound. The electrodes constitute the terminals 1 of the system and the coil terminals constitute the terminals 2.

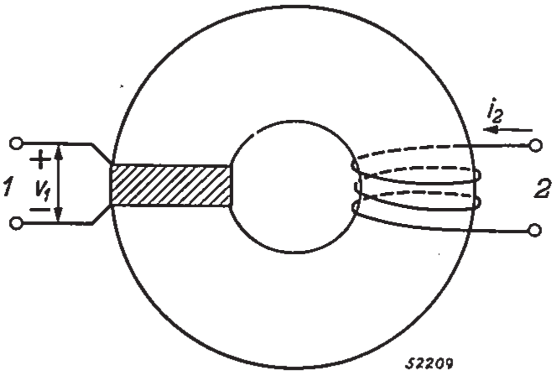

Fig. 12. A construction of the gyrator.

Let the area of the electrodes and of the cross-section of the yoke be S, then the charge Q_1 on the electrodes will be *)

$$Q_1 = S\,D = \varepsilon S\,E + \gamma S\,H \qquad (27)$$

and the flux Φ_2 through the coil will be

$$\Phi_2 = nS\,B = \gamma nS\,E + \mu nS\,H\,, \qquad (28)$$

where n is the number of turns of the coil.

The field vectors in the medium will all be perpendicular to the electrodes.

Let the distance between the electrodes be l, then the voltage v_1 between the electrodes will be

$$v_1 = lE \qquad (29)$$

and the current i_2 through the coil will be

$$i_2 = H\,l/n\,. \qquad (30)$$

---

*) We use the rationalized Giorgi system of units.

Putting (29) and (30) in (27) and (28) we get

$$\left.\begin{aligned} Q_1 &= \frac{\varepsilon S}{l} \cdot v_1 + \frac{\gamma n S}{l} \cdot i_2 \,, \\ \Phi_2 &= \frac{\gamma n S}{l} \cdot v_1 + \frac{\mu n^2 S}{l} \cdot i_2 \,. \end{aligned}\right\} \tag{31}$$

This corresponds to (23) and shows that $A^2/CL = \gamma^2/\varepsilon\mu$. Therefore, if $\gamma^2/\varepsilon\mu$ is nearly equal to·1, the same holds for A^2/CL.

8·1. The medium

To investigate media as described by (26) we first introduce the electric polarization **P** and the magnetic polarization **J** by putting

$$\mathbf{D} = \varepsilon_0 \mathbf{E} + \mathbf{P} \quad \text{and} \quad \mathbf{B} = \mu_0 \mathbf{H} + \mathbf{J}$$

and further putting $\varepsilon - \varepsilon_0 = \varkappa$ and $\mu - \mu_0 = \chi$.
By substituting this in (26) we get

$$\left.\begin{aligned} \mathbf{P} &= \varkappa \mathbf{E} + \gamma \mathbf{H} \,, \\ \mathbf{J} &= \gamma \mathbf{E} + \chi \mathbf{H} \,. \end{aligned}\right\} \tag{32}$$

Now, what does this represent? The coefficients $\varkappa$ and χ are ordinary electric and magnetic susceptibilities, the coefficient γ is something new. The term γ**E** expresses that when the medium is exposed to an electric field it will become magnetically polarized; the term γ**H** expresses that when the medium is exposed to a magnetic field it will become electrically polarized.

How can we get a medium with such properties? When a material medium is placed in a field, polarization of the medium may result from two different causes. Firstly, the elements of the medium, e.g. the molecules or the atoms, can acquire a dipole moment by the action of the field, i.e., they are polarizable; and, secondly, the elements of the medium can be permanently polarized and are oriented by the action of the field.

It is difficult to imagine how magnetic and electric polarizations due to the first cause can be coupled to each other in such a way that a medium with a coefficient γ results. When we consider polarization due to the second cause, however, we see immediately that our purpose can be attained if the elements of the medium bear both permanent electric and permanent magnetic dipoles, and if in all elements these dipoles are parallel or are anti-parallel. If we place such a medium in an electric field the electric dipoles will be oriented and thus the magnetic dipoles will be oriented at the same time, and the same will take place if the medium is placed in a magnetic field. The magnetic and the electric polarizations will then be proportional to each other. This means that **P/J** will be independent of **E** and **H**, from which we deduce by (23) that $\varkappa/\gamma = \gamma/\chi$ or $\gamma^2/\varkappa\chi = 1$. If, besides bearing permanent dipoles, the elements of the medium have some polarizability, $\varkappa$ and χ will in general become larger, so that $\gamma^2/\varkappa\chi \leqq 1$.

As mentioned above, $\gamma^2/\varepsilon\mu$ should be nearly equal to 1. Now

$$\frac{\gamma^2}{\varepsilon\mu} = \frac{\gamma^2}{(\varepsilon_0 + \varkappa)\,(\mu_0 + \chi)} \leqq \frac{\gamma^2}{\varkappa\chi} \leqq 1.$$

So we see that to reach this end we must make $\varkappa \gg \varepsilon_0$ and $\chi \gg \mu_0$, whilst these large susceptibilities must exclusively result from the orientation of permanent dipoles.

Media with large permanent, orientable, electric dipoles exist in abundance, e.g. water, which maintains its great electric susceptibility up to very high frequencies.

Media with permanent, orientable, magnetic dipoles are the paramagnetic media, whose magnetic susceptibility, however, is small compared with μ_0 and thus does not comply with the requirements just mentioned. In ferromagnetic media the susceptibility is due to the orientation of the electron spins, but it is hard to imagine how these could be directly coupled to a permanent electric dipole. We can, however, imagine a medium consisting of small ferromagnetic particles with permanent moments, small permanent magnets, suspended in some appropriate liquid.

We made some preliminary experiments in this direction by grinding some magnet steel and sifting out the smallest particles, which under a microscope were found to have dimensions of about one micron. From this a stable suspension was made which was put into a test-tube carrying a coil, and the self-inductance of the coil was measured. Then the suspension was magnetized by pouring it between the poles of a permanent magnet, after which it was again put into the test-tube. The self-inductance was increased by a factor 1·3. However, it is rather difficult to achieve a suspension that is stable during a long time, and one calls for very small magnetized particles.

9. Another realization of the gyrator

As experiments in this direction seem to be rather difficult it was considered worth while first to investigate whether there are conceivable fundamentally different possibilities of realizing the gyrator. Since the ideal transformer shows some analogy to the ideal gyrator we may include this in these investigations.

From the point of view of network theory the ideal transformer and the ideal gyrator are network elements defined by the equations (5) and (10), irrespective of any method of realizing them physically. To investigate how this could be done we first turn our attention to the terminals. Any terminal pair consists of two terminals situated closely together, so that even at very high frequencies we can speak of the voltage between the terminals. From such a terminal pair there start two wires of well-conducting material connecting the terminals with the element proper. Within the element these wires may be separated or connected. If the wires are separated we can deform the ends of them into two parallel electrodes. If we supply a voltage to the terminals, an electric charge Q will flow to the electrodes, and thus a current $i = \mathrm{d}Q/\mathrm{d}t$ will arise. If the wires are connected we can deform them into a coil. If we supply a current to the terminals, a magnetic flux Φ will flow through the coil, and thus a voltage $v = \mathrm{d}\Phi/\mathrm{d}t$ will arise. Therefore, we shall refer to the first type of terminal pair as the electric type and to the second as the magnetic type. According to the types of terminal pair of a four-pole element we shall refer to it as a double-electric, a double-magnetic, or an electromagnetic type. We could try to realize the transformer and the gyrator by means of each of these three types.

9·1. The general medium

Between the electrodes of an electric pair of terminals and within the coil of a magnetic pair of terminals we may now introduce some material medium. The type of four-pole that then results will depend to a large extent upon the properties of the medium. Therefore we ask what are the most general, linear relations by which the electric and magnetic properties of a medium can be phenomenologically described. These relations will consist of relations between the electric and magnetic polarizations **P** and **J** and the electric and magnetic field strengths **E** and **H** through which these polarizations may arise.

An example of relations of this kind is presented by the equations (32), but these do not constitute the most general form these relations can take. In the first place the medium may be anisotropic. For such a medium the equations must take a form wherein the three components of **P** and the three components of **J** along the directions of some rectangular system of coordinates are expressed in the three components of **E** and the three components of **H** along the same directions. In the second place we can suppose all components to vary sinusoidally with time with the same angular frequency ω. Then the components can be represented by complex quantities whereby the amplitude and the phase of each component can be expressed. We thus arrive at a system of six linear, homogeneous equations between twelve complex quantities and with complex coefficients.

As the ideal transformer and the ideal gyrator have no dissipation, we shall confine our conderations to media without dissipation. For such a medium some properties of the above-mentioned coefficients are deduced in the appendix. The equations for a medium without dissipation may thus be written in full as:

$$\begin{aligned}
P_x &= \varkappa_{xx}E_x+(\varkappa_{xy}+j\lambda_{xy})E_y+(\varkappa_{zx}+j\lambda_{zx})E_z+(\gamma_{xx}+j\delta_{xx})H_x+(\gamma_{xy}+j\delta_{xy})H_y+(\gamma_{xz}+j\delta_{xz})H\\
P_y &= (\varkappa_{xy}-j\lambda_{xy})E_x+\varkappa_{yy}E_y+(\varkappa_{yz}+j\lambda_{yz})E_z+(\gamma_{yx}+j\delta_{yx})H_x+(\gamma_{yy}+j\delta_{yy})H_y+(\gamma_{yz}+j\delta_{yz})H\\
P_z &= (\varkappa_{zx}-j\lambda_{zx})E_x+(\varkappa_{yz}-j\lambda_{yz})E_y+\varkappa_{zz}E_z+(\gamma_{zx}+j\delta_{zx})H_x+(\gamma_{zy}+j\delta_{zy})H_y+(\gamma_{zz}+j\delta_{zz})H\\
J_x &= (\gamma_{xx}-j\delta_{xx})E_x+(\gamma_{yx}-j\delta_{yx})E_y+(\gamma_{zx}-j\delta_{zx})E_z+\chi_{xx}H_x+(\chi_{xy}+j\zeta_{xy})H_y+(\chi_{zx}+j\zeta_{zx})H\\
J_y &= (\gamma_{xy}-j\delta_{xy})E_x+(\gamma_{yy}-j\delta_{yy})E_y+(\gamma_{zy}-j\delta_{zy})E_z+(\chi_{xy}-j\zeta_{xy})H_x+\chi_{yy}H_y+(\chi_{yz}+j\zeta_{yz})H\\
J_z &= (\gamma_{xz}-j\delta_{xz})E_x+(\gamma_{yz}-j\delta_{yz})E_y+(\gamma_{zz}-j\delta_{zz})E_z+(\chi_{zx}-j\zeta_{zx})H_x+(\chi_{yz}-j\zeta_{yz})H_y+\chi_{zz}H
\end{aligned}$$

(3

The coefficients in the principal diagonal are real; the coefficients lying symmetrically with respect to this diagonal are conjugate complex.

The coefficients consist of six groups of quantities, denoted by $\varkappa$, λ, γ, δ, χ, ζ, representing six different properties of the medium. If the terminal pairs of a four-pole are coupled to each other by means of one of these properties of the medium constituting the four-pole, this four-pole will be of a certain type.

In the first place this four-pole will or will not satisfy the reciprocity relation. To investigate this we differentiate the equations (33) with respect to t. The left-hand sides will then become $\mathrm{d}P_x/\mathrm{d}t$, etc. and $\mathrm{d}J_x/\mathrm{d}t$, etc., and the right-hand sides we may multiply by $j\omega$. Now $\mathrm{d}P/\mathrm{d}t$ is a part of a current, $\mathrm{d}J/\mathrm{d}t$ is a part of a voltage, E is a part of a voltage, and H is a part of a current. So, bearing in mind what has been said in section 2 about the way the reciprocity relation is expressed by equality or opposite equality of certain four-pole coefficients, we see that those four-poles of which the terminal pairs are coupled to each other by means of the property of the medium represented by $\varkappa$, δ, or χ, respectively by λ, γ, or ζ, will, respectively will not, satisfy the reciprocity relation of networks.

Furthermore, P and E are related to electric pairs of terminals and J and H to magnetic pairs. Therefore, if a transformer or a gyrator could be realized by coupling two terminal pairs by means of one of the above-mentioned six properties of a medium, coupling by
$\varkappa$ could lead only to a double-electric transformer,
λ to a double-electric gyrator,
γ to an electromagnetic gyrator,
δ to an electromagnetic transformer,
χ to a double-magnetic transformer,
ζ to a double-magnetic gyrator.

Thus we see that both for the transformer and for the gyrator there are three fundamentally different ways in which we could try to realize them.

Let us examine the properties of the medium more closely. The $\varkappa$'s represent the electric susceptibility, which in the general, anisotropic case has the form of a symmetric tensor, characterized by six components. Likewise, the χ's represent the magnetic susceptibility. The γ's are the generalizations of the coefficient γ discussed in section 8·1, where we pointed out the experimental difficulties to be overcome in realizing a medium with γ'-properties. The λ's and ζ's show two other ways of realizing the gyrator.

As previously mentioned, the λ's can only lead to a double-electric gyrator. Double-electric elements depend on the properties of the electric field. Now the electric field, because of curl $\mathbf{E} = 0$, has limited possibilities: a voltage step-up is impossible in a dielectric. As a consequence the only ideal transformer realizable by means of a dielectric is a transformer with a one-to-one ratio, which hardly deserves the name of transformer. As similar limitations may be expected when trying to realize an ideal gyrator by means of a dielectric with a λ-property, we shall not go into the questions what this λ-property represents and how a medium with such a property could be achieved.

Thus we are left with the problem of investigating the ζ-property of a medium and the realization of a gyrator by means of it. To investigate the ζ-property we suppose the medium to be characterized by χ's and ζ's only, the $\varkappa$'s, λ's, γ's, and δ's being zero. The equations (33) then reduce to three, expressing the components of $\mathbf{J}$ in the components of $\mathbf{H}$. Instead of studying these equations it is simpler to study the inverse equations by which the components of $\mathbf{H}$ are expressed in the components of $\mathbf{J}$. If in these equations we replace j by $(1/\omega)\mathrm{d}/\mathrm{d}t$ we arrive at equations of the form

$$\left.\begin{aligned} H_x &= \xi_{xx} J_x + (\xi_{xy} - \eta_z\,\mathrm{d}/\mathrm{d}t)\,J_y + (\xi_{zx} + \eta_y\,\mathrm{d}/\mathrm{d}t)\,J_z\,, \\ H_y &= (\xi_{xy} + \eta_z\,\mathrm{d}/\mathrm{d}t)\,J_x + \xi_{yy} J_y + (\xi_{yz} - \eta_x\,\mathrm{d}/\mathrm{d}t)\,J_z\,, \\ H_z &= (\xi_{zx} - \eta_y\,\mathrm{d}/\mathrm{d}t)\,J_x + (\xi_{yz} + \eta_x\,\mathrm{d}/\mathrm{d}t)\,J_y + \xi_{zz} J_z\,. \end{aligned}\right\} \quad (34)$$

The ξ's constitute an inverse susceptibility. It is the terms with η in which we are particularly interested. The equations show that these terms give a contribution to the field that may be written in vector notation as

$$\mathbf{H}' = \vec{\eta} \times \frac{\mathrm{d}\mathbf{J}}{\mathrm{d}t}, \quad (35)$$

where × denotes the vector product and the components of $\vec{\eta}$ are η_x, η_y, η_z.

This shows that the η's describe some transverse effect in the medium: a rate of change of the magnetic polarization of the medium, $\mathrm{d}\mathbf{J}/\mathrm{d}t$, has to give rise to a component of the magnetic field, $\mathbf{H}'$, at right angles to it. Such an effect can be expected in a ferromagnetic medium when this is magnetized to saturation in a certain direction, e.g. by placing it in a sufficiently strong constant magnetic field. The spins of the electrons contributing to the ferromagnetism will then all be parallel to one another. When the magnetization changes in a direction perpendicular to the direction of saturation the spins will turn. As the electrons carry not only a magnetic moment but also an angular momentum, there is a tendency for the spins to deviate in a transverse direction, perpendicular to the direction of the saturation and the direction in which we want them to turn. This tendency is equivalent to the action of a magnetic-field component in that direction and can thus be balanced by a component in the opposite direction. This effect is related to the various known types of gyromagnetic effect. In a subsequent paper we shall show how this effect enables us to realize the gyrator.

10. Appendix

The mean dissipated energy in a medium per unit of time and per unit of volume is equal to the real part of

$$\left(\mathbf{E}^* \,.\, \frac{\mathrm{d}\mathbf{D}}{\mathrm{d}t} + \mathbf{H}^* \,.\, \frac{\mathrm{d}\mathbf{B}}{\mathrm{d}t}\right),$$

where the asterisk denotes the conjugate complex value and the dot the scalar product. For a medium without dissipation this energy must be zero, so we come to

$$\mathrm{Re}\,(\mathbf{E}^* \,.\, j\omega\,\mathbf{D} + \mathbf{H}^* \,.\, j\omega\mathbf{B}) = 0.$$

Substituting $\mathbf{D} = \varepsilon_0\mathbf{E} + \mathbf{P}$ and $\mathbf{B} = \mu_0\mathbf{H} + \mathbf{J}$, we get

$$\mathrm{Im}\,(\mathbf{E}^* \,.\, \mathbf{P} + \mathbf{H}^* \,.\, \mathbf{J}) = 0. \tag{36}$$

Let us suppose first that $\mathbf{H} = 0$ and that $\mathbf{E}$ has only a component E_x. Then (36) becomes

$$\mathrm{Im}\,(E_x^*\, P_x) = 0. \tag{37}$$

In this case the equation for P_x reduces to an equation of the form

$$P_x = (\varkappa_{xx} + j\lambda_{xx})\, E_x\,. \tag{38}$$

Substituting this in (37) we arrive at $\lambda_{xx} = 0$. Thus the coefficient of E_x in the equation for P_x is real. By similar reasoning we may show that also the coefficient of E_y in the equation for P_y, etc., and the coefficient of H_x in the equation for J_x, etc., are real.

Let us now suppose that $\mathbf{H} = 0$ and that $\mathbf{E}$ has only components E_x and E_y. Then (36) becomes

$$\mathrm{Im}\,(E_x{}^*\,P_x + E_y{}^*\,P_y) = 0\,. \tag{39}$$

In this case the equations for P_x and P_y reduce to equations of the form

$$\left.\begin{aligned} P_x &= \varkappa_{xx}\,E_x + (\varkappa_{xy} + j\lambda_{xy})\,E_y\,, \\ P_y &= (\varkappa_{yx} + j\lambda_{yx})\,E_x + x_{yy}\,E_y\,, \end{aligned}\right\} \tag{40}$$

the coefficient of E_x in the first equation and the coefficient of E_y in the second equation being real on account of what has just been proved. Substituting this in (39) we get

$$\mathrm{Im}\,\}(\varkappa_{xy} + j\lambda_{xy})\,E_x{}^*\,E_y + (\varkappa_{yx} + j\lambda_{yx})\,E_x\,E_y{}^*\{ = 0\,.$$

As $\mathrm{Re}(E_xE_y{}^*) = \mathrm{Re}(E_x{}^*E_y)$ and $\mathrm{Im}(E_xE_y{}^*) = -\,\mathrm{Im}(E_x{}^*E_y)$, we get

$$(\varkappa_{xy} - \varkappa_{yx})\,\mathrm{Im}(E_x{}^*E_y) + j(\lambda_{xy} + \lambda_{yx})\,\mathrm{Re}(E_x{}^*E_y) = 0.$$

As this must be true for every value of $E_x{}^*E_y$, we finally get

$$\varkappa_{yx} = \varkappa_{xy} \quad \text{and} \quad \lambda_{yx} = -\,\lambda_{xy}\,.$$

Thus the coefficient of E_y in the equation for P_x and the coefficient of E_x in the equation for P_y are conjugate complex. By similar reasoning we may show that many other analogous pairs of coefficients are conjugate complex.

Eindhoven, September 1947

REFERENCES

(1) B. D. H. Tellegen, Network synthesis, especially the synthesis of resistanceless four-terminal networks, Philips Res. Rep. **1**, 169-184, 1946.

(2) R. M. Foster, A reactance theorem, Bell Syst. tech. J. **3**, 259-267, 1924.

(3) O. Brune, Synthesis of a finite two-terminal network whose driving-point impedance is a prescribed function of frequency, J. Math. Phys. **10**, 191-236, 1931.

(4) C. Gewertz, Synthesis of a finite four-terminal network from its prescribed driving-point functions and transfer function, J. Math. Phys. **12**, 1-257, 1933.

(5) W. Thomson and P. G. Tait, Treatise on natural philosophy, Part I, section 345VI.

(6) A. Bloch, A new approach to the dynamics of systems with gyroscopic coupling terms, Phil. Mag. **35**, 315-334, 1944.

(7) H. Poincaré, Etude du récepteur téléphonique, Eclair. élect. **50**, 221-234, 1907.

(8) Ph. le Corbeiller, Origine des termes gyroscopiques dans les équations des appareils électromécaniques, Ann. P.T.T. **18**, 1-22, 1929.

(9) H. Jefferson, Gyroscopic coupling terms, Phil. Mag. **36**, 223-224, 1945.

(10) E. M. Mc. Millan, Violation of the reciprocity theorem in linear passive electromechanical systems, J. Acous. Soc. Am. **18**, 344-347, 1946.

(11) See, for example, H. B. G. Casimir, On Onsager's principle of microscopic reversibility, Philips Res. Rep. **1**, 185-196, 1946.

(12) P. Ehrenfest, Das Prinzip von Le Chatelier-Braun und die Reziprozitätssätze der Thermodynamik, Z. phys. Chem. **77**, 227-244, 1911.

R 74 *Philips Res. Rep.* *3, 102-120, 1948*

ON THE THEORY OF SPHERICALLY SYMMETRIC INHOMOGENEOUS WAVE GUIDES, IN CONNECTION WITH TROPOSPHERIC RADIO PROPAGATION AND UNDER-WATER ACOUSTIC PROPAGATION

by H. BREMMER 538.566.5:534.221.1:621.392

Summary

The conception of the atmosphere as a curved wave guide consisting of an inhomogeneous medium through which radio waves and acoustic waves can be propagated, is worked out. The guiding effect is compared with that occurring in the propagation of acoustic waves through oceans. The properties of these two types of spherical wave guide are in many respects interrelated, but there are some essential differences which are brought to the fore. These differences are due to the fact that the product $r\mu$ ($r =$ distance to the centre of the earth, $\mu(r) =$ index of refraction) shows at least one minimum in the case of atmospheric propagation and one maximum in the case of oceanic propagation. As a consequence there is a difference, for instance, in the distribution of the times of arrival of consecutive rays originating from a point source: in the first case the intervals between these times are smallest for the rays coming latest, in the second case they are smallest for the rays arriving earliest.

Some general remarks are made with respect to arbitrary spherically symmetric wave guides. For example, the concept of cut-off frequency is discussed from the point of view of the modes as well as from that of geometric optics.

Résumé

On considère ici l'atmosphère comme un guide d'ondes courbé, formé par une couche non-homogène, dans laquelle se propagent des ondes électromagnétiques et acoustiques. D'une manière analogue on traite le problème de la propagation des ondes acoustiques dans un océan. Ces deux types de guides d'ondes montrent, d'autre part, des différences essentielles dues à l'existence d'un minimum de $r\mu(r)$ dans le premier cas, et d'un maximum de la même fonction dans le second cas ($r =$ distance au centre de la terre, $\mu(r) =$ indice de réfraction). Par exemple, la répartition des temps d'arrivé des rayons successifs provenant d'une source ponctuelle: dans le premier cas le nombre de rayons arrivant par unité de temps devient de plus en plus grand, dans le second cas ce nombre devient de plus en plus petit.

Le problème résumé mène à quelques remarques générales concernant les guides d'ondes à symétrie sphérique. Par exemple, on étudie la longueur d'onde de coupure du point de vue des fonctions propres que de celui de l'optique géometrique.

1. Introduction

The theory of ordinary wave guides consisting of a homogeneous medium enclosed by sharply defined walls has been investigated in detail. Next, the guided transmission of radio waves through the atmosphere, enabling these waves to overcome the curvature of the earth's surface, led to the concept of a wave guide consisting of an inhomogeneous infinite medium.

This wave guide has a sharply defined boundary at one side only, namely at the earth's surface. In connection with the guiding effect, particularly the ionized layers of the atmosphere (ionosphere) and the inhomogeneous region immediately above the earth (troposphere) are active, though only the latter is predominant for micro-waves (tropospheric super-refraction). For sound waves the role of the ionosphere is taken over by the high-temperature region near the upper boundary of the stratosphere.

In all these cases we have to do with spherically curved inhomogeneous wave guides possessing only a *single* sharply defined boundary. They may therefore be contrasted, e.g., with the propagation of sound waves over great distances through the ocean, indicated by the abbreviation 'Sofar' (sound fixing and ranging). Here we have an inhomogeneous spherical wave guide where propagation takes place between *two* sharply defined boundaries (the surface and the bottom of the ocean). In what follows we shall investigate in detail the general character of such spherical inhomogeneous wave guides; they are wholly determined by their refractive index μ as a function of the distance r to the centre of the earth if we neglect local inhomogeneities in the horizontal direction. In particular we shall consider the cases of tropospheric super-refraction and Sofar; these constitute illustrative examples of properties that are opposite in many respects. Moreover, these two examples are relatively simple since (a) the influence of dispersion is negligible, (b) the function μ may be approximated by a parabolic one throughout the *whole* space (the same is not applicable when considering the guiding effect of the ionosphere, whose layers are separated from the earth by a nearly homogeneous space).

2. General geometric-optical considerations

In a geometric-optical *) treatment the course of the rays within a spherically symmetric inhomogeneous medium is determined by Snellius's law, which may be written in the form:

$$r\mu \sin \tau = \text{constant} = C, \tag{1}$$

τ being the angle between the tangent of the ray and the vertical.

The effect of the curvature is clear from the occurrence of the product $r\mu$ rather than μ. Special attention should be paid to the sign of the slope of $r\mu$. As a matter of fact, a ray horizontally directed ($\mathrm{d}r/\mathrm{d}\vartheta = 0$) at some point P, will have its *lowest* point at P if P lies in a region for which $\mathrm{d}(r\mu)/\mathrm{d}r > 0$, and a *highest* point at P if $\mathrm{d}(r\mu)/\mathrm{d}r < 0$.

As regards the function $r\mu$ a fundamental difference exists between trophospheric radio propagation (referred to further on by T) and sound propagation through the ocean (abbreviated by O). In the first case, owing to exceptional meteorologic condictions, the refractive index μ of the air decreases so rapidly with height that also the product $r\mu$ does decrease notwithstanding the increasing factor r. At greater heights, however, the influence of μ, being very near to 1, becomes so small that $r\mu$ increases almost proportionally to r. As a consequence a transition level $r = r_0$ exists, where $r\mu$ has a *minimum*; under normal weather conditions the increase of this quantity starts right at the earth's surface ($r = a$). In the case O, however, the acoustical index of refraction μ of the sea-water first increases with increasing depth below the surface, owing to a decrease of the temperature of the water; finally, when a nearly constant temperature of 4 °C has been attained, a decrease of μ is caused by the still increasing pressure. Therefore μ will now pass through a *maximum* value; the same then holds, at some level $r = r_0$, for $r\mu$, since the influence of the factor r is relatively small in this case.

---

*) We shall use this term for acoustic problems also.

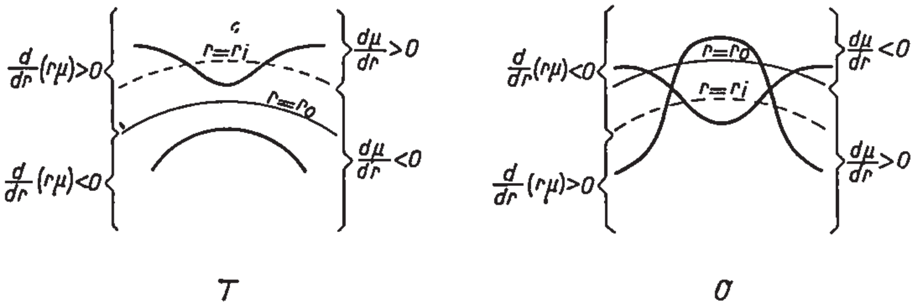

Fig. 1. Survey of the signs of the slopes of μ and $r\mu$, for T and O.

The immediate consequences of the minimum for $r\mu$ in T and of the maximum in O are illustrated by fig. 1. In the first case $\mathrm{d}(r\mu)/\mathrm{d}r$ is positive above $r = r_0$ and negative below it, so that rays horizontal at some point will, in the vicinity of that point, always be deflected in a direction *away* from the r_0-level; in the second case the opposite holds, so that rays being horizontal somewhere are deflected *towards* the r_0-level in neighbouring points and will cross the r_0-level at a distant point. Moreover there exists, for both T and O, a level $r = r_i$ at which $\mathrm{d}\mu/\mathrm{d}r = 0$ and where each ray crossing that level will have an inflection point; this level is situated above $r = r_0$ for T and below it for O. A point of conformity between T and O is the fact that a ray starting horizontally at some point of the transition level $r = r_0$ will never deviate from that level and consequently will follow the curvature of the earth.

Another consequence of the described difference in behaviour of $r\mu$ is that the guiding effect can be maintained by the inhomogeneous medium itself in the case O, whereas in the case T the presence of a sharply defined inner boundary is essential. In fact, in O the rays starting with an elevation (with respect to the horizon) that is not too great, will be compelled by the inhomogeneity of the medium to oscillate around the r_0-level. In *T*, however, the rays can be prevented from being deflected too far away from the r_0-level only by the presence of a sharply defined reflecting surface or, occasionally, by the existence of a maximum of $r\mu$ beside the minimum. Thus, in T, the earth's surface is mostly essential for rays to be guided within the space $a < r < r_0$. In O, on the contrary, the boundaries formed by the surface and the bottom of the sea constitute adverse conditions for the propagation since they cause reflection losses for those rays that cannot be gradually reflected within the inhomogeneous medium itself, the initial elevation being too great (compare section 8).

3. The beam of rays originating in a point source

For the sake of simplicity we assume a source Q at the earth's surface in the case T, and one at the r_0-level in the case O (the latter situation is approximately realized in Sofar-practice). The energy radiated by the source is transmitted along the geometric-optical rays radiating from Q, while each ray can be marked by its elevation angle τ_a or τ_0 respectively (see fig. 2). In both cases T and O there are important limiting values for these angles. First, in T, we have to do with the angle τ_l, which is determined by

$$\sin \tau_l = \frac{r_0\, \mu(r_0)}{a\, \mu(a)},$$

the corresponding ray approaching the r_0-level asymptotically. The latter ray separates the rays $\tau_a > \tau_l$, which are gradually reflected downwards within the space $a < r < r_0$ (the 'duct'), from the rays $\tau_a < \tau_l$ which escape into space ($r > r_0$). Similarly, in O there exists a limiting ray, determined by

$$\sin \tau_l = \frac{a\, \mu(a)}{r_0\, \mu(r_0)},$$

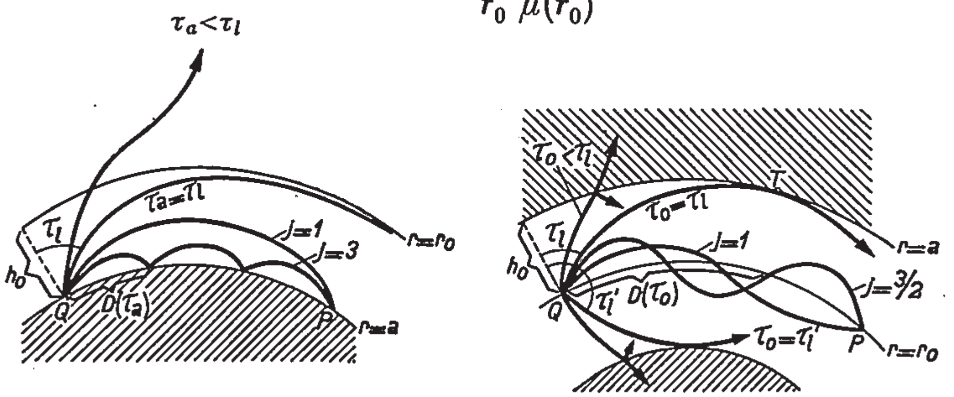

T O

Fig. 2. The courses of the rays radiating from a point sourse, for T and O.

just touching the surface of the sea at some point T at a finite distance. Here this limiting ray separates the rays with $\tau_0 > \tau_l$, which are gradually reflected downwards, from the group of rays with $\tau_0 < \tau_l$ which are reflected abruptly at the surface of the sea at $r = a$. Moreover, a second limiting angle τ_l' ($> \pi/2$) characterizes the ray that, while sent downwards from Q, just touches the bottom of the sea.

We now consider a receiver P at the same level as the source, thus at $r = a$ or $r = r_0$ respectively. This receiver can be reached by a large number of rays each of which may be labelled by the number of times (j) it has gone up and down before arriving. The definition of j requires integral values of this parameter for T (see the examples of $j = 1$ and 3, fig. 2T), whereas it may be also half an integer for O (see $j = 1$ and $\frac{3}{2}$, fig. 2O).

Of course, the total number of hops j by which a ray with a special value of τ_a or τ_0 may reach P, depends on the distance $D(\tau_a)$ or $D(\tau_0)$ covered in one single hop. In order to get an idea of the latter distances we assume the most simple dependence of $r\mu$ on r that produces a maximum for T and a minimum for O at the level $r = r_0$. The dependence in question is obtained by a quadratic formula for $r^2\mu^2$; accordingly we take:

$$r^2\mu^2 = r_0^2\mu_0^2 \left\{1 + \frac{(r-r_0)^2}{r_1^2}\right\}, \tag{2, T}$$

$$r^2\mu^2 = r_0^2\mu_0^2 \left\{1 - \frac{(r-r_0)^2}{r_1^2}\right\}. \tag{2, O}$$

The limiting angles τ_l are then determined by

$$\cot \tau_l = \frac{h_0}{r_1}, \qquad (h_0 = r_0 - a) \tag{3, T}$$

$$\cos \tau_l = \frac{h_0}{r_1}, \qquad (h_0 = a - r_0) \tag{3, O}$$

respectively. Further, the distance $|r_0 - r_i|$ between the r_0-level and the level of the inflection points will in both cases be r_1^2/r_0; owing to the slight curvature of the earth's surface, in practice this distance is very small (of the order of a few metres).

With the aid of formula (1), applied to the μ-functions (2), we are able to compute the whole course of the rays determined by τ_a or τ_0, and particularly their single-hop ranges $D(\tau_a)$ and $D(\tau_0)$. The following formulae are valid when assuming for O that the r_0-level is situated half-way between the surface and the bottom of the sea ($\tau_l' = \pi - \tau_l$):

$$D(\tau_a) = 2a^2\mu(a)\sin\tau_a \int_a^{r_0 - r_1\left(\frac{\sin^2\tau_a}{\sin^2\tau_l}-1\right)^{1/2}} \frac{\mathrm{d}r}{r\,\}r^2\mu^2(r) - a^2\mu^2(a)\sin^2\tau_a\{^{1/2}} \approx$$

$$\approx r_1 \sin\tau_a \ln\left(\frac{\cos\tau_l + \cos\tau_a}{\cos\tau_l - \cos\tau_a}\right), \quad (4,\mathrm{T})$$

$$D(\tau_0) = \begin{cases} 2\mu_0 r_0^2 \sin\tau_0 \displaystyle\int_{r_0 - r_1\cos\tau_0}^{r_0 + r_1\cos\tau_0} \frac{\mathrm{d}r}{r\,\}r^2\mu^2(r) - r_0^2\mu_0^2\sin^2\tau_0\{^{1/2}} \approx 2\pi r_1 \sin\tau_0 \,(\tau_0 > \tau_l) \\ 4\mu_0 r_0^2 \sin\tau_0 \displaystyle\int_{r_0}^{a} \frac{\mathrm{d}r}{r\,\}r^2\mu^2(r) - r_0^2\mu_0^2\sin^2\tau_0\{^{1/2}} \approx \end{cases}$$

$$\approx 4r_1 \sin\tau_0 \arcsin\left(\frac{\cos\tau_l}{\cos\tau_0}\right) (\tau_0 < \tau_l). \quad (4,\mathrm{O})$$

The integrals here given are also valid for other functions μ if the limits of integration (apart from a and r_0) are replaced by the r-values of the levels at which the radical vanishes for the μ-function considered; these latter levels indicate the heights of gradual reflections. The first formula of (4, O) corresponds to rays reflected gradually within the sea, the second one to rays reflected abruptly at the surface or the bottom of the sea.

Here, once more, an essential difference between T- and O-propagation presents itself. In T-propagation $D(\tau_a)$ may assume any value, which signifies that the receiver P may be reached always by a single-hop transmission ($j = 1$). In O-propagation, on the other hand, $D(\tau_0)$ has a maximum value of $D_0 = 2\pi r_1$, so that a receiver at great distances can only be reached, apart from the ray following the level $r = r_0$, by rays going up and down a number of times at least equal to D/D_0. Further numerical consequences of this effect are dealt with in section 8.

4. The focussing of the rays

Characteristic for wave guides is their property of keeping together rays that, in the case of an empty space, would diverge to all directions. A measure for this effect is given by the divergence coefficient α which can be defined as follows. A narrow pencil of rays starting from a point source Q will have at some point P a cross-section $\mathrm{d}O$ which may be compared with the cross-section $\mathrm{d}O'$ existing in the case of propagation over the same distance along straight lines through a homogeneous space. By taking

$$\alpha = \sqrt{\frac{\mathrm{d}O'}{\mathrm{d}O}}, \quad (5)$$

we introduce a parameter that is smaller than 1 if the inhomogeneity has a diverging effect and greater than 1 if its influence is a converging one.

We next explain the physical importance of a. In an inhomogeneous isotropic medium the flow of energy is propagated everywhere in the same direction as the rays, while its magnitude is proportional to the square, A^2, of the amplitude of the field. Therefore, the energy radiated at Q within a narrow pencil does not escape from this pencil, and it will cause a flow of energy proportional to $A^2\,\mathrm{d}O$. Since this flow of energy has to be constant throughout the whole pencil, the field will change proportionally to $1/\sqrt{\mathrm{d}O}$. In a homogeneous space, the field decreases proportionally to $1/\sqrt{\mathrm{d}O'}$; in this case, O' being proportional to D^2, we obtain the well-known law of inverse distance. Thereupon $a = \sqrt{\mathrm{d}O'/\mathrm{d}O}$ represents the ratio of the actual field to the field corresponding to the same distance in the case of propagation through a homogeneous space.

When computing (5) for our radially symmetric media, we obtain the following value for a at some point P situated on the same r-level as the source Q and having an angular distance ϑ from it:

$$a = \frac{\widehat{D}}{r}\sqrt{\frac{\tan\tau\left|\dfrac{\mathrm{d}\tau}{\mathrm{d}\vartheta}\right|}{\sin\vartheta}}. \tag{6}$$

In this formula $\widehat{D}$ is the length of the curved path QP, while τ represents the angle $\tau_a(\vartheta)$ or $\tau_0(\vartheta)$ which the ray in question, connecting Q and P, makes with the vertical at its end points (see fig. 3). In the cases we are considering, Q and P being given, we have to do with several rays, whilst each ray is labelled by the number of times j it is going up and down between Q and P. Of course, each ray has its own value a_j. We shall determine a when the source and the receiver are situated on the level $r = a$ in T and $r = r_0$ in O, so that:

$$a\vartheta = jD(\tau_a), \tag{T}$$
$$r_0\vartheta = jD(\tau_0). \tag{O}$$

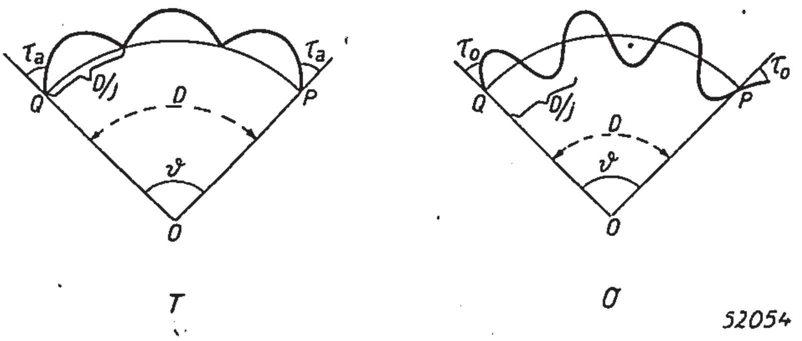

Fig. 3. Multi-hop transmission, for T and O.

On the basis of the special assumption (2) we find by using the approximation formulae of (4) for the determination of $d\tau/d\vartheta$ and for the elimination of τ:

$$a_j \approx \frac{D}{\sqrt{r_1\, a \sin(D/a)}}\, \frac{1}{\sqrt{j \sinh(D/jr_1)}}, \qquad (7,\mathrm{T})$$

$$\begin{cases} a_0 \approx \left\{\dfrac{2\pi\, D/D_0}{\sin(2\pi\, D/D_0)}\right\}^{1/2}, \\[2ex] a_j \approx \dfrac{D^{3/2}}{\sqrt{r_0 \sin(D/r_0)}\,\sqrt{j^2 D_0^2 - D^2}}. \qquad \left(j > \dfrac{D}{D_0};\ \tau_0 > \tau_l\right) \end{cases} \qquad (7,\mathrm{O})$$

In both derivations we have approximated $\widehat{D}$ by D; moreover, in (7, T) $\cos\tau_l \ll 1$ is assumed. In (7, O) a_0 corresponds to the ray $j = 0$ that follows the circle $r = r_0$.

The expression (7, T) refers to trophospheric propagation of radio waves for a transmitter and a receiver at the earth's surface. Here we note the increase of a_j with j, whilst the following limiting value is found for $j \to \infty$:

$$a_\infty \approx \sqrt{\frac{D}{a \sin(D/a)}} = \sqrt{\frac{\vartheta}{\sin\vartheta}}.$$

This quantity is slightly greater than 1. Thus not only does the duct prevent the rays from escaping away from the earth, but it even makes them slightly more convergent than rays propagated rectilinearly. This convergence effect is still more pronounced for elevated transmitters and receivers.

As regards O, we should bear in mind that, apart from the exceptional value $j = 0$, j has to be greater than D/D_0. Apparently a_j is now decreasing with increasing j, while it may become very great for the lowest possible values of j (which are the smallest half integers above D/D_0). The latter values correspond to rays running very near to the r_0-level (this well-marked focussing of rays departing with small elevation angles from $r = r_0$ is not observed in T, since there the rays in question can be deflected backwards to the r_0-level only by reflection against the earth's surface, and not by the inhomogeneity of the medium near to $r = r_0$). The focussing is particularly clear from the fact that a_0 becomes infinite at the points $D = (k/2)D_0$ (k integer). These latter points are foci in the true sense of the word; they constitute cusps of the caustic corresponding to the rays radiating from Q.

5. Geometric-optical derivation of the wave-guide condition

The divergence coefficient just described is insufficient for an explanation of the wave-guide properties of the inhomogeneous media here considered since it does not account for the possibility of interference of different rays. For a clear comprehension it is necessary to know the phases $\varphi(D, j)$ of the various j-rays upon their arrival at the receiving point P. These phases consist of a contribution determined by the changes along the curved path of the ray and a contribution due to the intermediate reflections (which are either gradual or abrupt). We shall discuss these contributions separately.

The first contribution can be represented, in the case of a monochromatic wave of wavelength λ (measured at a level for which $\mu = 1$), by $(2\pi/\lambda)\, \overline{D}(D, j)$. $\overline{D}/c$ equals the time needed for covering the path QP (c = velocity of propagation for $\mu = 1$). Owing to our ignoring dispersion, $\overline{D}$ does not depend on λ. With the aid of (1) we find in the case of T, again assuming both the source and the receiver at the earth's surface,

$$\overline{D} = \int_{Q}^{P} \mu \, \mathrm{d}s = \int_{Q}^{P} \frac{r\mu^2}{\}r^2\mu^2(r) - a^2\mu^2(a)\sin^2\tau_a\{^{1/2}}\, \mathrm{d}r =$$

$$= 2j \int_{a}^{r_0 - r_1 \left(\frac{\sin^2\tau_a}{\sin^2\tau_l} - 1\right)^{2/2}} \}r^2\mu^2(r) - a^2\mu^2(a)\sin^2\tau_a\{^{1/2} \frac{\mathrm{d}r}{r} + \mu(a)\sin\tau_a D = jf\left(\frac{D}{j}\right). \qquad (8)$$

Here $f(D/j)$ is the variation in phase during one single hop, which variation is wholly determined by the corresponding horizontal distance D/j or by the elevation angle τ_a leading to this one-hop distance (see fig. 3 with $j = 3$). The last form of (8) suggests an extension of the definition of $\overline{D}$ for non-integral values of j, given D; the ray $j = 11/8$, e.g., will cover in one hop a horizontal distance $(8/11)D$ and therefore has the same elevation angle τ_a as the ray covering the distance $8D$ in 11 hops. We can now derive the differential quotient of (8) with respect to j, D being constant; it then should be remarked that $\overline{D}$ does depend also implicitly on j by means of τ_a. By doing the same in the case of O (source and receiver being at the level $r = r_0$) we find in both cases the important, simple formula:

$$\frac{\partial \overline{D}}{\partial j} = L(D) = \frac{\overline{D} - \mu(a)\sin\tau_a D}{j}, \qquad (9)$$

in which:

$$L = 2 \int_{a}^{r_0 - r_1 \left(\frac{\sin^2\tau_a}{\sin^2\tau_l} - 1\right)^{1/2}} \frac{\mathrm{d}r}{r} \}r^2\mu^2(r) - a^2\mu^2(a)\sin^2\tau_a\{^{1/2}, \qquad (10,\ \mathrm{T})$$

$$L = 2 \int_{r_0 - r_1 \cos \tau_0}^{r_0 + r_1 \cos \tau_0} \frac{\mathrm{d}r}{r} \left\{ r^2 \mu^2(r) - r_0^2 \mu_0^2 \sin^2 \tau_0 \right\}^{1/2}. \quad (\tau_0 > \tau_l) \qquad (10,\ \mathrm{O})$$

These formulae are also valid for functions $\mu(r)$ other than (2) if the limits of integration (except a) are replaced by the r-values for which the radical vanishes (i.e. the levels of gradual reflections).

We now consider the variations in phase due to reflections. In T, we have to do in the first place with the reflections at the earth's surface. Since, in practice, τ_l is very near to $\pi/2$, the incidence of the rays to be considered is almost grazing, so that the reflection coefficient can be approximated by -1 and the change in phase at each reflection by π. Moreover, a second change in phase of $-\pi/2$ is related to the passing of each of the highest points H of the ray; such a change in phase is characteristic for gradual reflections in inhomogeneous media, as may be derived theoretically from the W.K.B. approximation of the solution of the wave equation that corresponds to the ray in question. Thus we find in T, the number of intermediate gradual reflections and of intermediate reflections against the earth's surface being j and $j-1$ respectively, as resulting pression for the phase of the jth ray at P:

$$\varphi(D, j) = \frac{2\pi}{\lambda} \bar{D}(D, j) - j \frac{\pi}{2} + (j-1)\,\pi. \qquad (11,\ \mathrm{T})$$

In the case O, however, when restricting ourselves to the rays with $\tau_0 > \tau_l$, we have to do only with intermediate gradual reflections, which are $2j$ in number now. To each of these reflections there will correspond, once more, a change in phase of $-\pi/2$, so that instead of (11, T) we obtain:

$$\varphi(D, j) = \frac{2\pi}{\lambda} \bar{D}(D, j) - 2j \frac{\pi}{2}. \qquad (11,\ \mathrm{O})$$

From these considerations it will be clear that, if λ is so great that the increase of the first term of (11) for an increase of j by 1 is small compared with 2π, the rays with consecutive values of j will cancel each other to a great extent by interference. This is only true insofar as the amplitudes of two consecutive rays are of the same order of magnitude; in general this happens to be true since the divergence coefficient a_j does change only slowly with j. Therefore a necessary condition for favourable propagation is that there shall exist at least one group of consecutive rays arriving with phase differences of the order of 2π. We thus arrive at the wave-guide condition

$$\max \left\{ \varphi(D, j+1) - \varphi(D, j) \right\} > 2\pi,$$

in which the maximum is meant with respect to j, D being given. In practice we can replace this unequality by the more convenient one

$$\max \frac{\partial \varphi}{\partial j} > 2\pi \,, \tag{12}$$

which will be worked out in the next section.

6. The cut-off wavelength λ_0

The differential quotient $\partial\varphi/\partial j$ of (12) depends on D and j; nevertheless, the resulting wave-guide condition proves to be independent of D, as will now be demonstrated. To this end we transform (12), with the aid of (11) and (9), into:

$$\lambda < \lambda_0 = \tfrac{4}{3} \max L \,, \tag{13, T}$$

$$\lambda < \lambda_0 = \tfrac{2}{3} \max L \,. \tag{13, O}$$

Here the maximum still refers to j, which parameter occurs implicitly in L, τ_a or τ_0 being a function of j for given D. Now, the maximum value of L corresponds to the minimum value of τ_a or τ_0 yielding a real L. This may be verified from the relations

$$\frac{\mathrm{d}L}{\mathrm{d}\sin\tau_a} = -\mu(a)\, D(\tau_a) \;\;, \;\; \frac{\mathrm{d}L}{\mathrm{d}\sin\tau_0} = -\mu_0\, D(\tau_0) \,, \tag{14}$$

which, again, are valid for every μ-function. In T this minimum value of τ_a equals τ_l since the rays $\tau_a < \tau_l$ escape into the space $r > r_0$ above the duct. In O we can similarly take as minimum value of τ_0 the angle τ_l; it is true that also $\tau_0 < \tau_l$ leads to real values of L, but the corresponding rays are to be excluded since their amplitudes do not change slowly with j, a condition necessary for the derivation of (12). In fact, the amplitudes of the rays with $\tau_0 < \tau_l$ diminish rapidly as a consequence of the large attenuation caused by the reflections of these rays against the surface and the bottom of the sea, these reflections not being 'total' as are the gradual reflections occurring for $\tau_0 > \tau_l$. Thus, deriving the maximum value of L by substituting τ_l for τ_a in T and τ_l for τ_0 in O, we obtain from (13):

$$\lambda_0 = \tfrac{8}{3} \int\limits_{a}^{r_0} \frac{\mathrm{d}r}{r} \,\}r^2\mu^2(r) - a^2\mu^2(a)\sin^2\tau_l\{^{1/2}, \tag{15, T}$$

$$\lambda_0 = \tfrac{4}{3} \int\limits_{r_0-h_0}^{r_0+h_0} \frac{\mathrm{d}r}{r} \,\}r^2\mu^2(r) - r_0^2\mu_0^2\sin^2\tau_l\{^{1/2}. \tag{15, O}$$

Not only are these expressions independent of our assumptions regarding the μ-function but they are equally independent of the distance, and they thus determine an upper wavelength limit (cut-off wavelength) under very general conditions. By using the formula (2) for μ we find, by replacing once more the factor r in the integrand of (15) by a constant value,

$$\lambda_0 = \tfrac{4}{3}\,\mu(a)\,\frac{h_0^2}{r_1} = \tfrac{4}{3}\mu(a)\,h_0 \cot \tau_l \approx \tfrac{4}{3}\,h_0 \cos \tau_l\,, \tag{16, T}$$

$$\lambda_0 = \tfrac{8}{3}\,\pi\mu_0\,h_0 \cos \tau_l\,. \tag{16, O}$$

These strikingly simple formulae, though dependent on the assumption of a parabolic function for $r^2\mu^2$, give in any case a qualitative idea of the conditions met in practice. In T, the small value of $\cos \tau_l$ causes a very small value of λ_0 so that guided tropospheric propagation is observable only for micro-waves; thus, for instance, from the values $h_0 = 15$ m and $\cos \tau_l = 0{\cdot}004$ (whose orders of magnitude are in agreement with observations at Antiqua [1]), we derive $\lambda_0 = 8$ cm. We now make a comparison with the guiding effect of the ionosphere. Here, downward gradual reflections are possible for nearly all values of τ (though the situation is very complicated owing to dispersion effects); therefore we can substitute for the limiting angle in (15, T) $\tau_l = 0$ while, approximately, μ is equal to 1 in nearly the whole interval of integration which extends mainly over the homogeneous space below the ionosphere. We thus find $\lambda_0 \approx \frac{8}{3}\,h_0$ (h_0 = height of the ionosphere above the earth), from which the guiding property of the space between the earth and the ionosphere is evident for the whole radio spectrum used in practice.

In the case of oceanic acoustic propagation, the quantities $h_0 = 1$ km and $\tau_l = 78°$ are of the right orders of magnitude; the corresponding value of the cut-off frequency, i.e. $f_0 = c/\lambda_0$, leads to $f_0 = 3{\cdot}4$ hertz, by which the guiding effect is explained for all ordinary acoustic frequencies.

7. The phase-integral equation

In general the properties of wave guides are not derived by the geometric-optical method developed above. Particularly this method is often unsuitable for the computation of the field of a point source. The geometric-optical determination of such a field amounts to a summation of the contributions of the individual j-rays, a summation leading in many cases to a very slowly convergent series. Therefore these fields are usually derived from a linear combination of the characteristic solutions or 'modes' corresponding to the problem in question. Incidentally it can be demonstrated that the geometric-optical series is transformable into the series of modes by the so-called transformation formula of Poisson.

In many cases the modes occur as the residues of a contour integral representing rigorously the field, so that their amplitudes are known at the same time. However, the form of the modes is independent of any special conditions like those referring to the presence of a point source, and, therefore, can be derived straight-forwardly. Thus in our case of radial symmetry of μ the modes not dependent on the azimuth angle φ correspond to those solutions of the wave equation that consist of a product of a function of r and a function of ϑ. The latter function amounts to a spherical harmonic P_ν (cos ϑ) so that each individual mode can be characterized by its special value ν_s for the order ν.

The r-function of the modes in question can be found with the aid of the well-known W.K.B. approximation method, where the requirement of one-valuedness and finiteness everywhere in space leads to the following equation, the wave number $k_1 = 2\pi/\lambda$ being given,

$$2k_1 \int_{r_{1,s}}^{r_{2,s}} \frac{\mathrm{d}r}{r} \left\{ r^2\mu^2(r) - \frac{\nu_s^2}{k_1^2} \right\}^{1/2} - i \ln \left\{ R_1(\nu_s)\, R_2(\nu_s) \right\} = 2\pi s. \quad (s \text{ integer}, i = \sqrt{-1}). \tag{17}$$

Here the limits of integration are either the r-values of sharply defined boundaries of the space considered, or levels for which the radical vanishes. In the former case we have to do with abrupt reflections, in the latter with gradual reflections, while, in each case, R_1 and R_2 denote reflection coefficients for the r_1-level and r_2-level respectively. For abrupt reflections R_1 and R_2 depend on the angles of incidence $\tau_{s,1}$ and $\tau_{s,2}$ to be derived from

$$\frac{\nu_s}{k_1} = r_1\mu(r_1) \sin \tau_{s,1} = r_2\mu(r_2) \sin \tau_{s,2}. \tag{18}$$

For gradual reflections R_1 and R_2 are invariably equal to $-i$ as stated before. By working out (17) for T and O we find, when approximating once more the reflection coefficient at the earth's surface by -1,

$$2 \int_{a}^{r_0 - r_1 \left(\frac{\sin^2\tau_{a,s}}{\sin^2\tau_l} - 1 \right)^{1/2}} \frac{\mathrm{d}r}{r} \left\{ r^2\mu^2(r) - \frac{\nu_s^2}{k_1^2} \right\}^{1/2} = \lambda(s - \tfrac{1}{4}), \tag{19, T}$$

$$2 \int_{r_0 - r_1 \cos \tau_{0,s}}^{r_0 + r_1 \cos \tau_{0,s}} \frac{\mathrm{d}r}{r} \left\{ r^2\mu^2(r) - \frac{\nu_s^2}{k_1^2} \right\}^{1/2} = \lambda(s + \tfrac{1}{2}). \qquad (\tau_{0,s} > \tau_l) \tag{19, O}$$

The formulae (18) suggest for real ν_s a connection of the sth mode with *rays* going up and down that have either angles of incidence $\tau_{s,1}$ and $\tau_{s,2}$ at sharply defined boundaries or a common level of gradual reflection at

$r = r_{1,s}$ or $r = r_{2,s}$ (some possible situations are sketched in fig. 4). All the rays corresponding to a special mode are congruent, and are transformed into each other by simple rotation; an occasional common level of reflection can be considered as their caustic.

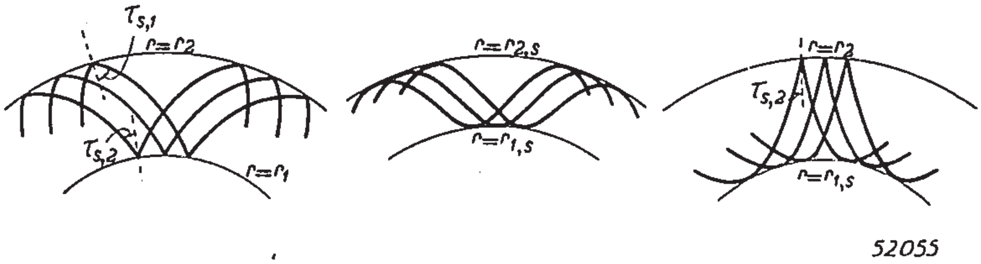

Fig. 4. Courses of the rays corresponding to a real mode.

This geometric-optical interpretation of the sth mode is confirmed as follows. According to our previous nomenclature we call $\varphi_s(D, j)$ the difference in phase at two points Q and P situated on a ray of the sth mode in such a way that between these points the ray is going up and down j times. Thereupon we can split φ_s into a contribution due to the change in phase along the curved path and a contribution due to the reflections. In the most general case the multiplication of the intensity by R_1 or R_2, as occurring at each reflection, may be considered as a change in phase of $-i \ln R_1$ or $-i \ln R_2$ respectively. We then find, similar to (11):

$$\varphi_s(D, j) = k_1 \bar{D}_s(D, j) - ij \ln R_1 - i\,(j-1) \ln R_2 .$$

Just as in section 5, we differentiate this relation with respect to j for constant D. Now, for gradual reflections, R_1 and R_2 are independent of the angle of incidence, and consequently of j; the same holds approximately for abrupt reflections (as may be seen from our approximation -1 for the reflection coefficient of the earth's surface). Thus, with the aid of (9), we find the following very simple form for the so-called phase-integral equation (17):

$$\frac{\partial \varphi_s}{\partial j} = 2\pi s . \tag{20}$$

The differential quotient may be replaced by the difference quotient $\varphi_s(j + 1) - \varphi_s(j)$ just as was done when deriving the wave-guide condition geometric-optically. It then appears that the modes with real ν_s can be characterized as follows: their corresponding rays, when arriving at some point P after making j hops since the departure from a point Q on the same r-level as P, are in resonance with the ray covering the same distance in $j + 1$ hops.

We are now able to construct the wave-guide condition (12) also from the point of view of the modes. In fact, the factor $P_{\nu_s}(\cos\vartheta)$ of the latter corresponds to a change in intensity which is approximately proportional to $\exp(i\nu_s\vartheta)$; consequently, a non-attenuated propagation in the ϑ-direction is to be expected only if (20) is satisfied by at least one real root ν_s. Moreover, for the possibility of such a root it is necessary that the maximum value of $\partial\varphi/\partial j$ for real rays does exceed 2π, since otherwise (20) cannot be satisfied for any integer s (apart from the trivial value $s = 0$). Thus we are again led to the condition (12) and to a corresponding cut-off wavelength λ_0. When $\lambda < \lambda_0$ the number of real modes will be the greater the shorter the wavelength is.

From the foregoing it is evident that the field of a point source may be considered as a combination of modes (characterized by the integers s) but equally well as a combination of contributions due to geometric-optical rays (characterized by the integer j). The latter conception is clearer inasmuch it is *always* connected with real rays, whereas the same holds for the modes only if ν_s is real. For numerical computations the method of modes is particularly useful if the consideration of a small number of modes suffices, i.e. when λ_0/λ is not very large, as in the practical cases of super-refraction. In other cases, as in Sofar-practice, λ_0/λ is very large for ordinary wavelengths, so that a great number of real modes has to be considered; the number of important geometric-optical rays, however, is small there (see below), so that the geometric-optical method is very suitable. Thus the two methods appear as being mutually complementary.

In Booker's theory of super-refraction the modes with real ν_s are called 'trapped modes' in contrast to the name 'leaking modes', applied when ν is complex. This nomenclature clearly indicates that for the former the energy cannot escape through the boundaries of the guide; for the latter, however, a leaking of energy through the boundaries is possible by means of a (gradual or abrupt) refraction. Finally we remark that the modes of an inhomogeneous wave guide, enclosed between two homogeneous spaces, are transformed into surface waves when the thickness of the guide becomes infinitely small.

8. The consecutive arrival of the geometric-optical rays

The geometric-optical representation is particularly suitable when considering a point source operating during an infinitely short time at $t = 0$. If the surrounding space is considered as homogeneous with propagation velocity c the field of such a source will be proportional to

$$\delta\left(t-\frac{D}{c}\right),$$

where δ is Dirac's impulse function. In an inhomogeneous space (assumed once more spherically symmetric; source and receiving point at the same r-level) this function has to be multiplied by the divergence coefficient a and, occasionally, also by the reflection coefficients. Moreover the propagation time D/c then has to be replaced by the term $\overline{D}/c$ which accounts for the local values c/μ of the propagation velocity. Accordingly the field due to a ray making j intermediate hops will be proportional to

$$a_j\,\delta\left\{t-\frac{1}{c}\,\overline{D}(D,j)\right\}, \tag{21}$$

a_j being the corresponding divergence coefficient. The distribution of the times of arrival, $t_j = \overline{D}_j/c$, of the different j-rays shows a remarkable difference for T and O, as will next be discussed.

For a consideration of t_j as a function of j, given D, we write (9) as $\partial t_j/\partial j = L/c$. The positive value of the differential quotient informs us that the rays arrive in a sequence corresponding to their number of hops j, those with greatest j arriving latest. Moreover we conclude from (14) that L decreases with increasing τ_a or τ_0. Hence the same holds for the time difference $t_{j+1}—t_j \approx \partial t_j/\partial j$ between the arrival of two consecutive rays. Here the geometrical differences between T- and O-propagations present themselves once more since, in T, increasing τ_a corresponds to a decreasing distance $D(\tau_a)$ covered in one hop and consequently to increasing j, whereas, in O, increasing τ_0 corresponds to increasing $D(\tau_0)$ and to decreasing j (compare fig. 2 and the formulae (4)). Thus, since $\partial t_j/\partial j$ decreases in any case for increasing τ, this decrease refers to increasing j in T but to decreasing j in O. It means that for T-propagation the rays finally arrive in a more and more rapid succession, whereas for O-propagation they arrive at increasing intervals.

The differences in behaviour described depends only on whether the extremum of $r\mu$ is a minimum or a maximum. It may again be illustrated in more detail by the specialization (2) for μ. We then find (restricting ourselves for O to the rays with $\tau_0 > \tau_l$ and for T to the rays for which $\cos\tau_a \ll \cos\tau_l$):

$$t_j \approx t_\infty - \frac{(t_\infty - t_1)}{j^2}, \tag{22, T}$$

$$t_j = \frac{t_{\min}}{2}\left(\frac{j}{j_{\min}} + \frac{j_{\min}}{j}\right). \qquad (j \neq 0) \tag{22, O}$$

In the first expression,

$$t_1 = \mu(a)\,\frac{D}{c}\left(1-\frac{\cos^4\tau_l}{24\,h_0^2}\,D^2\right)$$

signifies the time of arrival of the first ray (if also for this ray $\cos\tau_a \ll \cos\tau_l$), and $t_\infty = \mu(a)\,D/c$ the time of abrupt termination of arrival of the rays. In the second expression, $t_{\min} = \mu(r_0)\,D/c$ is the time of arrival of the first ray, i.e. the ray $j = 0$ that follows the level $r = r_0$; further the quantity $j_{\min} = D/D_0$ marks a lower limit for the possible number of hops for the rays with $j \neq 0$.

Whereas in T the process terminates *rigorously* at the time t_∞, in O it terminates only *practically* at the time

$$t_l = \frac{t_{\min}}{2}\left(\sin\tau_l + \frac{1}{\sin\tau_l}\right)$$

at which a ray just touching the surface or the bottom of the sea may arrive; of course this ray actually arrives only if D is equal to a multiple of the distance $\frac{1}{2}\,D_l = \pi\, r_1 \sin\tau_l$ covered by this ray by going once up and down between the r_0-level and the surface, or between the r_0-level and the bottom of the sea (the latter two were assumed at equal distances from the r_0-level). Theoretically the process still goes on for $t > t_l$, but the rays then arriving are highly attenuated by their numerous reflections against the surface and the bottom of the sea.

We shall now estimate the decay in intensity of the rays arriving after $t = t_l$ in Sofar-practice. For those few rays which are of numerical importance the incidence at the sea surface is almost grazing (angle of incidence $\tau_a \approx \pi/2$) so that the reflection coefficient may be approximated by

$$R(\tau_a) \approx -1 + \frac{2}{(m^2-1)^{1/2}}\cos\tau_a\,, \tag{23}$$

$m = 4{\cdot}35$ being the refraction index for the transition from water to air. The angle of incidence itself follows from

$$\sin\tau_a = \frac{\sin\tau_0}{\sin\tau_l} \approx \frac{1}{\sin\tau_l}\left\{1 - \frac{\cos^2\tau_l}{\sin^2(\pi j_l/2j)}\right\}^{1/2} \approx 1 - \frac{\pi^2}{8}\cot^2\tau_l\left(\frac{j}{j_l} - 1\right)^2.$$

Hence we derive from (23):

$$R(\tau_a) \approx -1 + \frac{\pi}{(m^2-1)^{1/2}}\cot\tau_l\left(\frac{j}{j_l} - 1\right),$$

so that the attenuation factor for the rays with j-values near to or greater than j_l proves to be:

$$|R(\tau_a)|^j \approx |R(\tau_a)|^{j_l} \approx \exp\left(-\frac{\pi\cot\tau_l}{(m^2-1)^{1/2}}(j - j_l)\right) \approx \exp\left(-\frac{c(t-t_l)}{(m^2-1)^{1/2}\,h_0\sin\tau_l}\right).$$

When taking $\tau_l = 78°$, $h_0 = 1$ km, $c = 1{\cdot}48$ km/sec (velocity of sound in sea-water), we find

$$|R(\tau_a)|^j \approx e^{-0{\cdot}158(j-j_l)} \approx e^{-0{\cdot}357(t-t_l)_{\text{sec}}}.$$

Thus the rapid decrease of the intensity of the rays arriving at $t > t_l$ is demonstrated if $j_l \gg 1$, a condition fulfilled in any case for $D \gg D_0 = 2\pi h_0/\cos \tau_l = 30{\cdot}2$ km.

In view of this example we may mention the smallness of the number of non-attenuated geometric-optical rays; indeed this number is of the order or $j_l - j_{\min} + 1 = (D/D_0)\,(\operatorname{cosec} \tau_l - 1) + 1$, i.e. here $0{\cdot}00074\, D_{\mathrm{km}} + 1$. For an experiment in which a pulse signal is transmitted through the ocean over a distance of say 4000 km, this would mean that at the receiving point only four separate pulses are observed that are not attenuated by abrupt reflections. These pulses are followed by others, the amplitude of which is reduced owing to reflections at the surface of the ocean. The first four of these suffer amplitude losses under 50%. The 8 pulses here considered arrive within an interval of 2·6 sec.

We mention yet another difference in T- and O-propagations. Since for the former the rays with high j-values arrive with the smallest differences in time, these rays will have the smallest differences in phase in the case of sinusoidal excitation. They will to a great extent cancel one another since these differences in phase approach to the limiting value of $-\pi/2 + \pi = \pi/2$ for two consecutive rays (see section 5), whereas their intensities are nearly equal according to the limiting value of the divergence coefficient (see section 4). Thus the wave-guide effect is due to the rays with low j-values since, only for the latter, the differences in phase may exceed 2π. Also in O the lower j-rays are the more important ones, but for quite another reason, namely as a consequence of their focussing effect (great value of a_j according to (7, O)).

9. Final remarks

In the foregoing, our discussion on spherical inhomogeneous wave guides has been restricted to two special cases characterized by one single extremum of $r\mu$. Since essential differences have been established according as this extremum is a maximum or a minimum, the behaviour of more general wave guides with several extrema will depend to a great extent on the distribution of the maxima and minima of $r\mu$. However, the most essential properties described, e.g. the focussing of rays near a maximum, the geometric-optical explanation on the wave-guide character according to (12), and the physical interpretation of the phase-integral equation with the aid of (20), are applicable to all inhomogeneous wave guides having spherical symmetry.

In the following an enumeration of some examples showing several extrema of $r\mu$ is given:

1) Radio waves: the space reaching from the earth to the upper boundary of the ionosphere. Each layer of the ionosphere shows a minimum of $r\mu$

(depending on the frequency) near its middle, and two maxima near its upper and lower boundaries;

2) Acoustic waves: the space formed by the troposphere and stratosphere. Here $r\mu$ starts by increasing with the height owing to the fall of the temperature (at least under normal weather conditions); at stratospheric heights $r\mu$ passes through a maximum and decreases later on as a consequence of the rising temperature; at still greater heights (above the ozonosphere) a new fall of the temperature produces once more an increase of $r\mu$ after a minimum has been passed;

3) H.f.radio and acoustic waves: the complex conditions depending on the occasional presence in the troposphere of several temperature inversions may lead to a corresponding number of extrema of $r\mu$ for both kinds of waves.

We may conclude by remembering the well-known analogy between mechanical problems with a potential function V and optical problems with an index of refraction $\mu = \sqrt{1-V/E}$, where E is the energy of the mechanical particle. Extrema of $r\mu$ correspond to extrema of the function $r\sqrt{1-V(r)/E}$ in the equivalent mechanical problems. Thus the circular rays in optics along the levels for which $\mathrm{d}(r\mu)/\mathrm{d}r = 0$ correspond in mechanics to circular orbits determined by the relation

$$E-V(r) = \frac{r}{2}\frac{\mathrm{d}V}{\mathrm{d}r}.$$

The Schrödinger wave equation is based on the optic-mechanical analogy mentioned; the W.K.B.method for the determination of the characteristic values corresponds to the phase-integral equation treated above. It is just the success of this approximation method in the theory of Schrödinger's equation which led Eckersley [3]) to the application of the phase-integral equation to radio-propagation problems.

Eindhoven, December 1947

REFERENCES

1) C. L. Pekeris, Proc. Inst. Radio Engrs **35**, 453-462, 1947.
2) T. L. Eckersley, Proc. roy. Soc. London (A) **136**, 499-527, 1932.
T. L. Eckersley and G. Millington, Phil. Trans. roy. Soc. (A) **237**, 273-309, 1938.

R 75 *Philips Res. Rep.* **3**, *121-129, 1948*

MEASUREMENTS OF NOISE FACTORS OF PENTODES AT 7·25-M WAVELENGTH

by A. van der ZIEL and A. VERSNEL

621.396.822:621.385.5

Summary

Measurements are given of noise factors of pentodes at 7·25-m wavelength as a function of the transformed antenna resistance, and the results are compared with theory. Theoretically, induced grid noise might be partly suppressed by inserting a small resistance of, e.g., 30 Ω in the cathode lead. This should reduce the noise factor, but in practice other effects cancel this reduction. It is shown that in many cases the self-inductance of the cathode lead increases the noise factor, but this may be counteracted by inserting a condenser in the cathode lead, so that series resonance is obtained. Finally, the influence of internal feed-back is investigated, and it is shown that it may give rise to an increase of the noise factor.

Résumé

Les auteurs renseignent des mesures de nombres de soufflement de pentodes, à 7,25 m de longueur d'onde, en fonction de la résistance transformée d'antenne et ils confrontent les résultats avec la théorie. Théoriquement le soufflement induit de grille peut être supprimé en partie par l'insertion d'une petite résistance d'environ 30 Ω dans la cathode. Elle réduira le nombre de soufflement, mais en pratique d'autres effets annulent cette réduction. Les auteurs montrent que dans beaucoup de cas l'inductance du conducteur de cathode augmente le nombre de soufflement, mais on peut y remédier en insérant dans la cathode un condensateur de façon à obtenir la résonance série. Enfin les auteurs examinent l'influence de la réaction interne et montrent qu'elle peut donner lieu à un accroissement du nombre de soufflement.

1. Introduction

Recently several papers [1]) have been published about the noise factor of pentodes at v.h.f. We, too, have carried out many measurements on the same subject, covering several questions that have not yet been treated elsewhere. The measurements were carried out with a linear amplifier feeding a thermo-couple detector. The method of measurement has already been described previously [2]).

The signal-to-noise ratio of receivers or receiver stages is generally determined by the noise factor F defined as:

$$F = \frac{\text{noise output power of receiver}}{\text{noise output power due to antenna noise}};$$

the noise temperature of the antenna is assumed to be equal to normal room temperature.

This definition means that $F = 1$ for the antenna itself, so that the part $(F-1)$ is a good measure for the noise contribution of the receiver itself or of an individual receiver stage. For this reason we give in our measured curves the factor $(F-1)$ instead of the factor F.

2. Noise factor as a function of the transformed antenna resistance R_1'

The measurements were carried out with the input circuit tuned to the desired frequency. As induced grid noise has a phase difference of 90 degrees with respect to shot-effect noise [8]), the output power of the receiver due to them is obtained by quadratic addition of the two effects. Hence, the induced grid noise may be taken into account by assuming a suitable noise temperature of the input parallel resistance of the valve. Moreover, total-emission noise [9]) and input-circuit noise have to be taken into account.

Let R_1 denote the parallel resistance of the tuned input circuit of the first stage (tuned circuit + valve) and let a_1 denote its noise ratio. This means that the noise due to the spontaneous fluctuations of the input circuit may be described by assuming a noise generator e_1 in series with R_1 such that

$$\overline{e_1^2} = a_1 \,.\, 4kTR_1 \,\Delta\nu\,, \tag{1}$$

in which a_1 is practically independent of frequency; k denotes Boltzmann's constant, T absolute room temperature and $\Delta\nu$ a small frequency interval. The shot-effect noise and the partition-current fluctuations are described by the equivalent noise voltage e_n (cf. fig. 1) or by the equivalent noise resistance R_n of the valve:

$$\overline{e_n^2} = 4kTR_n \,\Delta\nu\,.$$

Denoting the transformed antenna resistance by R_1', we have for the mean-square value of the equivalent noise voltage between grid and cathode due to both effects:

$$a_1 \,.\, 4kTR_1 \,\Delta\nu \left(\frac{R_1'}{R_1' + R_1}\right)^2 + 4kTR_n \,\Delta\nu. \tag{2}$$

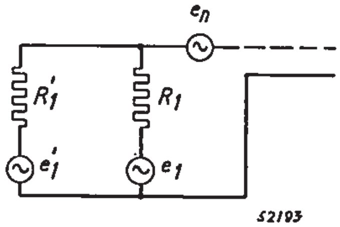

Fig. 1. Equivalent input circuit of a receiver stage.
R_1 input resistance of valve + circuit.
R_1' transformed antenna resistance.
e_1', e_1, and e_n noise generators.
$\overline{e_1^2} = a_1 \,.\, 4kTR_1 \,\Delta\nu$; $\overline{e_1'^2} = 4kTR_1' \,\Delta\nu$; $\overline{e_n^2} = 4kTR_n \,\Delta\nu$.

The antenna noise gives rise to a mean-square noise voltage

$$4kTR_1'\,\Delta\nu\left(\frac{R_1}{R_1'+R_1}\right)^2. \tag{2a}$$

$(F—1)$ is obtained by dividing (2) by (2a):

$$(F—1)=a_1\frac{R_1'}{R_1}+\frac{R_n}{R_1}\,\frac{(R_1+R_1')^2}{R_1\,R_1'}=\left(a_1+\frac{R_n}{R_1}\right)\frac{R_1'}{R_1}+\frac{R_n}{R_1'}+2\frac{R_n}{R_1}. \tag{3}$$

As a function of R_1' (3) has a minimum value

$$(F_{\min}—1)=2\frac{R_n}{R_1}+2\sqrt{\left(a_1+\frac{R_n}{R_1}\right)\frac{R_n}{R_1}}, \tag{3a}$$

if

$$R_1'=\sqrt{\frac{R_n\,R_1}{a_1+R_n/R_1}}. \tag{3b}$$

a_1 may be measured in the following way. After taking $R_1'=\infty$ (no transformed antenna resistance across the input circuit) the filament current of a noise diode across the input circuit is turned up until the output power of the receiver is doubled. Let I_0 denote the anode current of the noise diode in this case, then the mean-square value of the noise voltage across the input circuit is

$$2eI_0\,\Delta\nu\,.\,R_1^2. \tag{4a}$$

As the noise of the second stage of the receiver is generally negligible for pentodes (otherwise corrections have to be made), the equivalent noise voltage across the input, due to input circuit and valve, becomes

$$a_1\,.\,4kTR_1\,\Delta\nu+4kTR_n\,\Delta\nu\,. \tag{4b}$$

Equating (4a) and (4b) yields

$$\frac{e}{2kT}I_0R_1=20I_0R_1=a_1+\frac{R_n}{R_1}\qquad (I_0 \text{ in A, } R_1 \text{ in } \Omega)\,. \tag{4c}$$

We measured $(F—1)$ as a function of R_1' for a pentode EF50 at 7·25-m wavelength. The input resistance R_1 was found to be equal to 15000 Ω; this large value was obtained by tuning the cathode lead of the valve to series resonance by connecting a condenser of 400 pF parallel to the bias resistor in the cathode lead. From the measurement of I_0, R_1, and $(F—1)_{\min}$ we were able to deduce values for a_1 and R_n/R_1 with the help of (3a) and (4c). We obtained:

$$a_1=5{\cdot}3\;;\;2R_n/R_1=0{\cdot}21 \text{ or } R_n=1600\,\Omega\,.$$

Introducing these values into (3) we obtain the theoretical curve for (F—1) as a function of R_1'. Fig. 2 shows this theoretical curve (lower curve) and also the experimental results. The agreement between theory and experiment is very good. Moreover, the value for R_n agrees with the long-wave value.

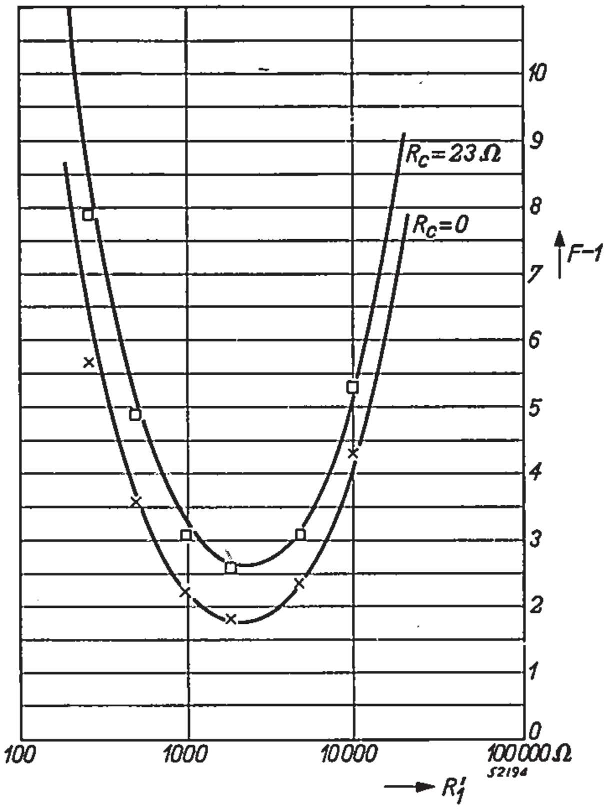

Fig. 2. (F—1) as a function of the transformed antenna resistance R_1' at 7·25-m wavelength of an EF 50. The self-inductance is tuned to series resonance by a condenser of 400 pF. The lower curve is obtained for R_1 = 15000 Ω, a_1 = 5·3, $2R_n/R_1$ = 0·21; crosses denote measured values.
The upper curve is obtained for R_1 = 5000 Ω, a_1 = 2·8, $2R_n/R_1$ = 0·80, corresponding to an unbypassed resistance of 23 Ω inserted in the cathode lead; squares denote measured values.

According to fig. 2, (F—1) has at 7·25-m wavelength a minimum value for R_1' = 2000 Ω, and hence (because R_1 is inversely proportional to ω^2) at higher frequencies for lower values of R_1' (cf. (3b)). If the required bandwidth were such that lower values of R_1' would be necessary, then it might be advantageous to use valves having a higher value of the transconductance as this would give rise to lower values of R_n and R_1 (cf. also (3a) and (3b)).

We may also draw another conclusion from (3a). If a valve had no partition-current fluctuations (e.g. a triode), then the value of R_n would be for instance 3 or 4 times smaller, and hence (F_{min}—1) would be much smaller too. Taking R_n = 400 Ω, R_1 = 15000 Ω, and a_1 = 5·3 we would obtain $(F_{\min}-1) = 0{\cdot}8$ (instead of 1·8 for the EF 50) for $R_1' = 1000\ \Omega$ (instead of 2000 Ω for the EF 50). This result may be achieved by using a neutralized triode of high transconductance instead of a pentode [1]).

3. Unbypassed resistance in the cathode lead

Strutt and Van der Ziel [3]) pointed out that a reduction *) in induced grid noise might be expected if a small unbypassed resistance R_c were inserted in the cathode lead (fig. 3). We carried out measurements on various types of valve with $R_c = 23\ \Omega$ and found that the expected noise reduction was completely masked by spurious effects.

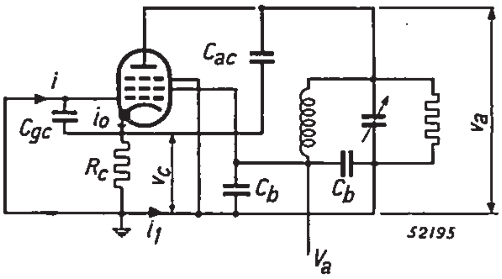

Fig. 3. An unbypassed resistance R_c is inserted in the cathode lead, the input circuit being short-circuited for the sake of simplicity. A noise current i_0 is flowing from cathode to grid and a noise current i_1 (delayed in phase with respect to i_0) from grid to screen grid, thus giving rise to the induced-grid-noise current (i_0-i_1), which has a phase advance of 90° with respect to i_0. C_b denote bypass condensers.

(a) It was found that a feed-back from the output circuit due to the direct capacity $C_{a:}$ between anode and cathode was the chief cause for an increase in induced grid noise. Even with a comparatively small capacity (as e.g. in the case of an EF50) the amplified noise voltage across the output circuit (fig. 3) gives rise to an appreciable noise current flowing to the grid **).

(b) The resistance R_c, which is connected in series with the valve capacity C_{gc}, constitutes an appreciable additional input resistance R_2:

$$1/R_2 = \omega^2\, C_{gc}^2\, R_c\,. \tag{5}$$

With $R_c = 23\ \Omega$ equation (5) yields a value of about 10000 Ω for R_2 for reasonable values of the capacity C_{gc} (8 pF).

---

*) That this reduction should be possible may be seen from fig. 3. The noise current i_0 gives rise to a noise voltage $i_0 R_c$ across R_c and to a noise current $i = -i_0 R_c j\omega C_{gc}$ to the grid. This noise current has a phase delay of 90° with respect to i_0, whereas the induced-grid-noise current (i_0-i_1) has a phase advance of 90° with respect to i_0. Hence, by a proper choice of R_c a suppression of induced grid noise should be possible.

**) This also follows from fig. 3. The amplified noise voltage v_a gives rise to a noise voltage $v_c = v_a\,.\,j\omega C_{ac} R_c$ across R_c and to a noise current $i = -v_c j\omega C_{gc}$ to the grid, thus causing an increase in induced grid noise.

(c) The resistance R_c in the cathode lead constitutes a negative feed-back, such that the transconductance of the valve is reduced by a factor $(1 + S_0R_c)$, where S_0 *) denotes the transconductance of the cathode lead [4]). The shot-effect noise is reduced by the same factor, but the partition-current fluctuations are not flowing through the resistance R_c, and hence they will not be reduced. Putting for $R_c = 0$

$$R_n = R_{nc} + R_{np} \tag{6a}$$

(R_{nc} is the contribution of the shot-effect noise to the noise resistance R_n, and R_{np} is the contribution of the partition-current fluctuations), we have to expect for $R_c \neq 0$ (as a direct consequence of the proper definition of the noise resistance R_n) a noise resistance R'_n:

$$R'_n = R_{nc} + R_{np}\,(1 + S_0R_c)^2. \tag{6b}$$

For an EF 50 we have: $R_n = 1600\ \Omega$, $R_{nc} = 500\ \Omega$, $R_{np} = 1100\ \Omega$, $S_0 = 8{\cdot}5$ mA/V, $(1 + S_0R_c)^2 = 1{\cdot}4$, and hence R'_n is about 2000 Ω.

We found that $(F—1)$ could be represented by an equation of the type (3). We measured also I_0 in equation (4c); moreover we found $R_1 \doteq 5000\ \Omega$. From the measured value of $(F_{\text{min}}—1)$ we deduced with the help of (3a) and (4c) values for a_1 and R'_n/R_1:

$$a_1 = 2{\cdot}8,\ 2R'_n/R_1 = 0{\cdot}80 \text{ or } R'_n = 2000\ \Omega.$$

As may be seen from fig. 2, the agreement between theory and experiment is very good.

As we have $R_1 = 15000\ \Omega$ for $R_c = 0$ and $R_1 = 5000\ \Omega$ for $R_c = 23\ \Omega$, the additional input resistance $R_2 = 7500\ \Omega$ is in reasonable agreement with the expected value. Moreover, the noise resistance R'_n agrees with the value to be expected according to (6b).

We may finally draw conclusions from the measured values of a_1 for $R_c = 0$ and $R_c = 23\ \Omega$.

R_1 consists of a parallel connection of a resistance of 15000 Ω having a noise ratio a, and a resistance of 7500 Ω having a noise ratio 1. As the parallel connection of the two resistances has a noise ratio of 2·8, we find $a = 6{\cdot}4$ for $R_c = 23\ \Omega$, whereas we found $a = a_1 = 5{\cdot}3$ for $R_c = 0$. This shows that even in this case the resistance R_c caused an increase in induced grid noise. This is most probably due to the feed-back through the capacity C_{ac}.

Hence, the final result is that the proposed method of reduction of induced grid noise does not work.

---

*) At the frequencies under consideration S_0 is practically a real quantity.

4. Influence of internal feed-back

We now turn to some measurements on experimental valves having a transconductance which was about 30% higher than for an EF 50. Hence it was expected that an improvement in noise factor would be obtained by applying these valves. We found, however, that this was true for very low values of the transformed antenna resistance R_1' only; for large values of R_1', however, the noise factor was higher than for an EF 50.

We found that the tuning of the output circuit was strongly dependent upon R_1' for the experimental valves. Moreover, the tuned input impedance depended upon the tuning of the output circuit. This showed that an appreciable feed-back was present, presumably due to the capacity C_{ag}. The large value of C_{ag} was probably due to lead effects; these effects are less important for EF 50 valves. For EF 50 valves the tuning of the output circuit was independent of R_1', so that internal feed-back was negligible for these valves.

We now prove that internal feed-back may give rise to an increase in noise factor. It is generally known that the signal-to-noise ratio of an amplifier is not altered by applying a feed-back from the output of an amplifier to its input [5]). Hence at first sight it might be expected that the noise factor would not change by applying feed-back.

That this is not true in our case is due to the fact that the feed-back gives rise to a detuning of the input circuit. If the input circuit is not retuned, the noise factor remains unaltered when applying feed-back. If, however, the input circuit is retuned, the noise factor increases.

In order to make this point clearer we mention another theorem [6]) which may easily be proved: the output signal-to-noise *voltage*-ratio of an amplifier (e.g. incorporating feed-back) is equal to the output signal-to-noise *current*-ratio obtained by short-circuiting the output of the amplifier.

Now let us suppose that we have an amplifier stage incorporating internal feed-back due to the capacity C_{ag}, and that input and output circuits are tuned to maximum signal. Let the dashed curve of fig. 4 denote

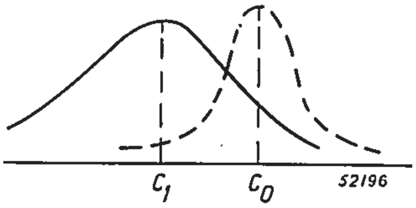

Fig. 4. Input and output circuits of an amplifier incorporating internal feed-back are tuned to maximum signal. The dashed curve is the resonance curve of the input circuit as a function of the tuning capacitance C (resonance for $C = C_0$); the tuning of the output circuit is fixed. The full-drawn curve is the resonance curve of the input circuit for a short-circuited output (resonance for $C = C_1$).

the resonance curve of the input circuit as a function of the tuning capacity C, and let it have a maximum value for $C = C_0$. If the output of the stage is short-circuited the influence of internal feed-back is negligible. The resonance curve of the input circuit is now denoted by the full-drawn curve of fig. 4, which has a maximum for $C = C_1$ (the shift between the two curves is due to the fact that the feed-back gives rise to a detuning of the input circuit). Now, according to the above theorem the signal-to-noise ratio for $C = C_0$ is equal in both cases (compare fig. 4). However, if feed-back is negligible (full-drawn curve) the signal-to-noise ratio attains a maximum value (and hence the noise factor a minimum value) when the input circuit is tuned, that is, for $C = C_1$, and becomes worse when the input circuit is detuned, that is, e.g., for $C = C_0$. This effect is appreciable, especially if the input resonance curve is a relatively narrow one, which is the case for large values of the transformed antenna resistance R_1'. Hence, this effect will be unimportant for low values of R_1' and important for high values of R_1'. This also follows from fig. 5, which shows the factor $(F-1)$ of one of the experimental valves as a function of the transformed

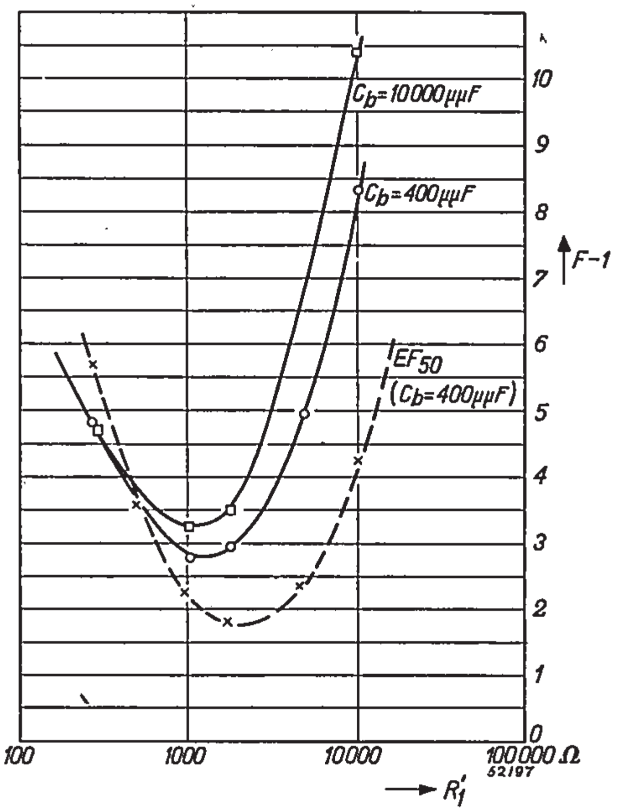

Fig. 5. *Lower full-drawn curve.*
$(F-1)$ as a function of R_1' for an experimental pentode having a large internal feed-back due to the capaity C_{ag}. The self-inductance of the cathode lead is tuned to series resonance. For comparison a similar curve is shown for the EF 50 (dashed curve).
Upper full-drawn curve.
$(F-1)$ as a function of R_1' for the same valve, but with the self-inductance of the cathode lead not tuned to series resonance.

antenna resistance in comparison with the same factor for the EF 50 valve of fig. 2.

5.Influence of the self-inductance of the cathode lead

Up till now, all measurements have been carried out by using a bypass condenser C_b of 400 pF across the cathode bias resistor. This resulted in a tuning to series resonance of the self-inductance of the cathode lead. We also carried out measurements on the already-mentioned experimental valves with $C_b = 10\,000$ pF in order to investigate the influence of the self-inductance of the cathode lead. This results in an input conductance 7):

$$1/R = \omega^2 S_0 L_c C_{cg}, \tag{7}$$

in which L_c denotes the self-inductance of the cathode lead and C_{cg} the capacitance between cathode and grid. We found an increase in noise factor especially for large values of the transformed antenna resistance R_1'.

This is to be expected from a theoretical point of view. Due to the input conductance $1/R$ of equation (7) the voltage between grid and cathode is decreased by a factor

$$\frac{R}{R + R_1 R_1'/(R_1 + R_1')}, \tag{8}$$

while it may be shown that the shot noise is decreased by the same factor 4). As the partition-current fluctuations remain unaltered, their influence becomes relatively more important, resulting in an increase in noise factor. According to (8) this increase is negligible for low values of R_1' ($R_1' \ll R$) and becomes more important for large values of R_1'. This is also shown experimentally in fig. 5.

Eindhoven, June 1947

REFERENCES

1) L. A. Moxon, Wireless World **53**, 171-176, 1947.
2) A. van der Ziel, Philips Res. Rep. **2**, 321-330, 1947.
3) M. J. O. Strutt and A. van der Ziel, Physica, 's-Grav. **8**, 1-22, 1941.
4) M. J. O. Strutt and A. van der Ziel, Elekt. Nach. Tech. **13**, 260-268, 1936.
5) M. J. O. Strutt and A. van der Ziel, Physica, 's-Grav. **9**, 513-527,1942.
6) A. van der Ziel, Philips Res. Rep. **1**, 381-399, 1946.
7) M. J. O. Strutt and A. van der Ziel, Proc. Inst. Radio Engrs **26**, 1011-1032, 1938.
8) A. van der Ziel and A. Versnel, Philips Res. Rep. **3**, 13-23, 1948.
9) A. van der Ziel and A. Versnel, Nature **159**, 640, 1947.

R 76 *Philips Res. Rep.* **3**, *130-139, 1948*

INDICATION OF LANDING COURSES INDEPENDENT OF WEATHER CONDITIONS

by K. F. NIESSEN

621.396.933.23

Summary

Straight landing courses with a small angle of elevation are indicated in a way independent of changes of the electric constants of the ground. In a definite vertical plane, given by two antennae of finite length, the landing course is indicated by a second pair of emitters, also of finite length, and placed either at different heights or at the same height above the ground.

Résumé

Des axes d'atterrissage droits à faible angle d'élévation peuvent être indiqués indépendamment de fluctuations des constantes électriques du sol. Dans un plan vertical défini par deux antennes de longueur finie, l'axe d'atterrissage est indiqué par une seconde paire d'émetteurs, également de longueur finie, et placés à des hauteurs différentes ou à la même hauteur au-dessus du sol.

PART II

Extension of dipoles to antennae of finite length

So far¹) it has been assumed that we have to do with dipoles C_1 and C_2 of infinitesimal length (only the antennae A_1 and A_2 were of finite length). Now we shall investigate in how far these infinitesimal dipoles may be extended to antennae of finite length (of course of the same length, form and power).

First we consider fig. 8, where to the vertical dipole C_1 at h_1 (of moment m_1) a second one has been added, namely, a vertical dipole of moment

$$\overline{m}_1 = m_1 \varkappa e^{j\tau} \text{ at } \overline{h}_1 = h_1 + a\,,$$

coherent with the first one and modulated in the same way.

In a similar way we add to the vertical dipole C_2 at h_2 (of moment m_2) a second vertical dipole of moment

$$\overline{m}_2 = m_2\, \alpha e^{j\tau} \text{ at } \overline{h}_2 = h_2 + a\,,$$

coherent with m_2 and modulated in the same way, the modulation being different from that of $(m_1, \overline{m}_1)$.

An observer in the direction Θ is at distances

$$\overline{r}_1 = r_1 - a \cos \Theta\,,$$
$$\overline{r}_2 = r_2 - a \cos \Theta$$

from these new dipoles, and thanks to the different modulation he receives the first pair of dipoles separately from the second pair.

For the first pair the hertzian function (on account of the influence of the earth) is

$$\frac{m_1 e^{jk_1 r_1}}{r}\left[1+R\exp j\left(\Delta+\frac{4\pi h_1}{\lambda}\cos\Theta\right)\right]+$$

$$+\frac{\varkappa e^{j\tau} m_1 e^{jk_1 \bar{r}_1}}{r}\left[1+R\exp j\left(\Delta+\frac{4\pi \bar{h}_1\cos\Theta}{\lambda}\right)\right]=$$

$$=\frac{m_1 e^{jk_1 r_1}}{r}\left[1+Re^{ju_1}+\varkappa e^{jv}+\varkappa R e^{jw_1}\right]$$

with:

$$\left.\begin{aligned} u_1 &= \Delta+\frac{4\pi h_1\cos\Theta}{\lambda} \\ v &= \tau-\frac{2\pi a\cos\Theta}{\lambda} \\ w_1 &= \tau+\Delta+\frac{4\pi h_1\cos\Theta}{\lambda}+\frac{2\pi a\cos\Theta}{\lambda} \end{aligned}\right\} \tag{13}$$

(The values of both $\bar{r}_1$ and $\bar{h}_1$ were substituted.)
Apparently we have

$$w_1 = u_1+\tau+\frac{2\pi a\cos\Theta}{\lambda}.$$

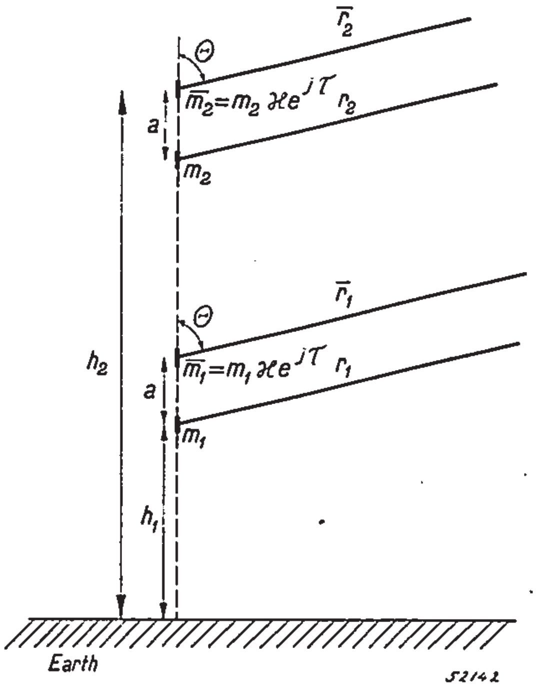

Fig. 8. Two pairs of dipoles of different modulation, each pair replacing one of the dipoles in a configuration A.

The field strength of the system $(m_1, \overline{m}_1)$ at a point with $\cos\Theta \ll 1$ is therefore given (f being a factor of proportionality) by

$$f\frac{m_1}{r}[(1+R\cos u_1+\varkappa\cos v+\varkappa R\cos w_1)^2+(R\sin u_1+\varkappa\sin v+\varkappa R\sin w_1)^2]^{1/2}=$$

$$=f\frac{m_1}{r}[1+R^2+\varkappa^2+\varkappa^2R^2+2R\cos u_1+2\varkappa\cos v+2\varkappa R\cos w_1+$$

$$+2\varkappa R\cos(u_1-v)+2\varkappa R^2\cos(u_1-w_1)+2\varkappa^2R\cos(w_1-v)]^{1/2},$$

and that of $(m_2, \overline{m}_2)$ is given similarly by the same expression with the only difference that the subscript 1 has been replaced by the subscript 2, and where

$$\left.\begin{aligned} u_2 &= \Delta+\frac{4\pi h_2\cos\Theta}{\lambda} \\ w_2 &= \tau+\Delta+\frac{4\pi h_2\cos\Theta}{\lambda}+\frac{2\pi a\cos\Theta}{\lambda}. \end{aligned}\right\} \tag{13a}$$

We see from (13) and (13a) that

$$u_2-w_2=u_1-w_1.$$

Equal intensity for the two radiations will be found in a direction Θ for which

$$2R\cos u_1+2\varkappa R\cos w_1+2\varkappa R\cos(u_1-v)+2\varkappa R^2\cos(u_1-w_1)+2\varkappa^2R\cos(w_1-v)=$$
$$=2R\cos u_2+2\varkappa R\cos w_2+2\varkappa R\cos(u_2-v)+2\varkappa R^2\cos(u_2-w_2)+2\varkappa^2R\cos(w_2-v),$$

since we have already assumed $m_1=m_2$. If this direction has to be independent of the constitution of the soil, the above equation must be fulfilled for every value of R and Δ.

Any dependence on R will be eliminated if it is possible to fulfil at the same time:

$$\left.\begin{aligned} \cos u_2 &= \cos u_1 \\ \cos w_2 &= \cos w_1 \\ \cos(u_2-v) &= \cos(u_1-v) \\ \cos(w_2-v) &= \cos(w_1-v) \end{aligned}\right\} \tag{14}$$

The first condition is the same as previously encountered when treating the case of one dipole m_1 at h_1 and one dipole m_2 at h_2, modulated differently, which was solved by one of the two possibilities (A) and (B), which we can now write in the form

$$u_2=u_1+2p\pi \tag{A}$$
$$u_2=2\pi-u_1+2q\pi\,. \tag{B}$$

From the definition of v, w_1 and w_2 it will be clear that using (A) we satisfy at the same time also the other conditions of (14). This is not the case if we use the solution (B), since the appearance of the function v then makes it impossible to fulfil at the same time:

$$\begin{aligned} u_2 &= 2\pi - u_1 + 2q\pi \\ u_2 - v &= 2\pi - (u_1 - v) + 2q\pi. \end{aligned}$$

Thus we see that, if in the simple case of two dipoles C_1 and C_2 the difference of height $h_2 - h_1$ has been chosen in accordance with the solution (A) (see part I), *it is permitted to extend these dipoles to antennae of finite length, provided this extension is made in the same direction* (for we used $\overline{h}_1 = h_1 + a$ and $\overline{h}_2 = h_2 + a$) *and the currents in both antennae are identical* (for we chose $\overline{m}_1 = \overline{m}_2 = m\,\varkappa e^{j\tau}$) (see fig. 6a).

It remains to investigate what kind of extension to finite antennae is possible in the simple case of two dipoles C_1 and C_2 if the sum $h_1 + h_2$ has been chosen in accordance with condition (B). In this case we shall try an extension in two opposite directions.

Therefore we take as the first system two dipoles

$$\left\{ \begin{array}{l} m_1 \text{ at } h_1 \\ n_1 = \varkappa e^{j\tau} m_1 \text{ at } h_1 + a \end{array} \right.$$

and as the second system two dipoles

$$\left\{ \begin{array}{l} m_2 \text{ at } h_2 \\ n_2 = \varkappa e^{-j\tau} m_2 \text{ at } h_2 - a, \end{array} \right.$$

the latter pair being modulated in a manner different from the former pair (fig. 9).

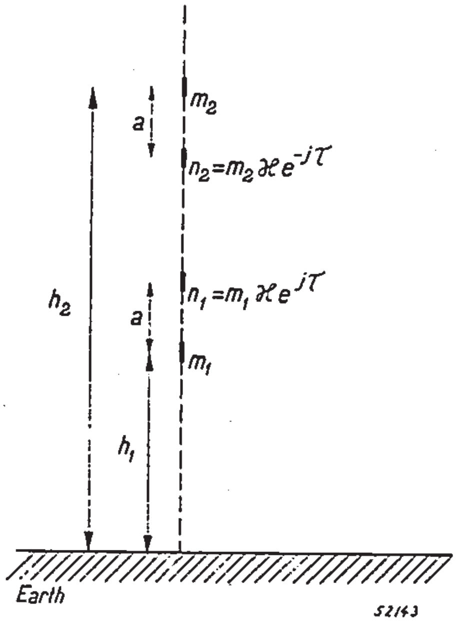
m_2
a
$n_2 = m_2 \varkappa e^{-j\tau}$
h_2
a
$n_1 = m_1 \varkappa e^{j\tau}$
m_1
h_1
Earth
52143

Fig. 9. The same as in fig. 8 but for configuration *B*.

The pair m_1, n_1 is identical with m_1, $\overline{m}_1$ as used above, and the pair m_2, n_2 differs from the former m_2, $\overline{m}_2$ in two respects: the phase factor in n_2 is $e^{-j\tau}$ instead of $e^{+j\tau}$ in $\overline{m}_2$, and the location of the new dipoles is indicated by $h_2—a$ instead of $h_2 + a$ for $\overline{m}_2$.

The expression for the intensity with which the system (m_2, n_2) will be received therefore contains other quantities than those found in the expression for the intensity of $(m_2, \overline{m}_2)$. We now need to consider:

$$u_2{}' = \Delta + \frac{4\pi h_2 \cos\Theta}{\lambda} \qquad (= u_2)$$

$$v' = -\tau + \frac{2\pi a \cos\Theta}{\lambda} \qquad (= -v)$$

$$w_2{}' = -\tau + \Delta + \frac{4\pi h_2 \cos\Theta}{\lambda} - \frac{2\pi a \cos\Theta}{\lambda} \neq w_2\,.$$

From our previous considerations it will be clear that both pairs of dipoles will now be received with equal intensity as soon as

$$\begin{aligned}
&m_2 = m_1\\
&\cos u_2{}' = \cos u_1\\
&\cos w_2{}' = \cos w_1\\
&\cos v' = \cos v\\
&\cos(u_2{}'-v') = \cos(u_1-v)\\
&\cos(u_2{}'-w_2{}') = \cos(u_1-w_1)\,.
\end{aligned}$$

We chose already $h_1 + h_2$ in accordance with condition (B) for $\Theta = \Theta_0$, so that we have for $\Theta = \Theta_0$:

$$\begin{aligned}
&u_1 + u_2{}' = (q+1)\,2\pi\\
&w_1 + w_2{}' = (q+1)\,2\pi\\
&(u_2{}'-v') + (u_1-v) = (u_2{}' + u_1) - (v + v') = (q+1)\,2\pi,\\
&(u_2{}'-w_2{}') + (u_1-w_1) = (q+1)\,2\pi,
\end{aligned}$$

so that all conditions for equal reception are fulfilled.

The landing course $\Theta = \Theta_0$, indicated by the dipoles m_1 and m_2 (based upon condition B), therefore remains unchanged if both dipoles are extended in opposite directions (i.e., to one another or from one another) and in such a way that we get two antennae, one of which is the image of the other, with respect to the horizontal plane that lies at a height $(h_1 + h_2)/2$ above the earth. Phase differences in one antenna have to be opposite to the corresponding phase differences in the other antenna. If there is, for instance, a wave travelling upwards through one antenna, we should make a wave travelling downwards in the other — in general there must be symmetry also in this respect with regard to the horizontal plane at $(h_1 + h_2)/2$ (see fig. 7a).

PART III

Emitters at equal heights

Now we shall occupy ourselves with two systems of emitters both at the height $h_1 = h_2$. An indication of a landing course by means of the condition of equal reception can — in principle — only be realized if the polar diagrams of the two systems are very much unlike! In the former case of unequal heights, $h_2 \neq h_1$, we chose emitters of identical form and strength, and the difference in the diagrams mentioned above was brought about by the difference in height above the ground, and now, in the case of $h_2 = h_1$, the necessary difference in the polar diagrams will be realized by differences in number, strength and internal phase differences of the components constituting the systems.

Therefore we now consider in fig. 10 a group G_1 of coherent vertical (mathematical) dipoles, all situated at the same height h above the ground and at distances of the order of λ from one another. At a point of observation P ($r = PG_1 \gg \lambda$) situated in a direction Θ in the vertical plane F_1 (indicated by two other emitters A_1 and A_2 as before) the modulus of the hertzian-vector function amounts to:

$$\left|1+R(\Theta)\exp j\left\{\Delta(\Theta)+\frac{4\pi h\cos\Theta}{\lambda}\right\}\right|\cdot\left|\frac{m_1}{r}+e^{ja'}\frac{m_1'}{r}+e^{ja''}\frac{m_1''}{r}+\dots\right| \qquad (15)$$

where m_1, m_1', m_1'' are the moments of the separate dipoles. These dipoles of G_1 being coherent, their contributions to the hertzian function have to be added vectorially. These contributions show phase differences a', a'', a''' *), which are caused partly by path differences, partly by specific phase differences of the dipoles themselves. Adding each time the contribution of a dipole and that of its image with respect to the surface of the

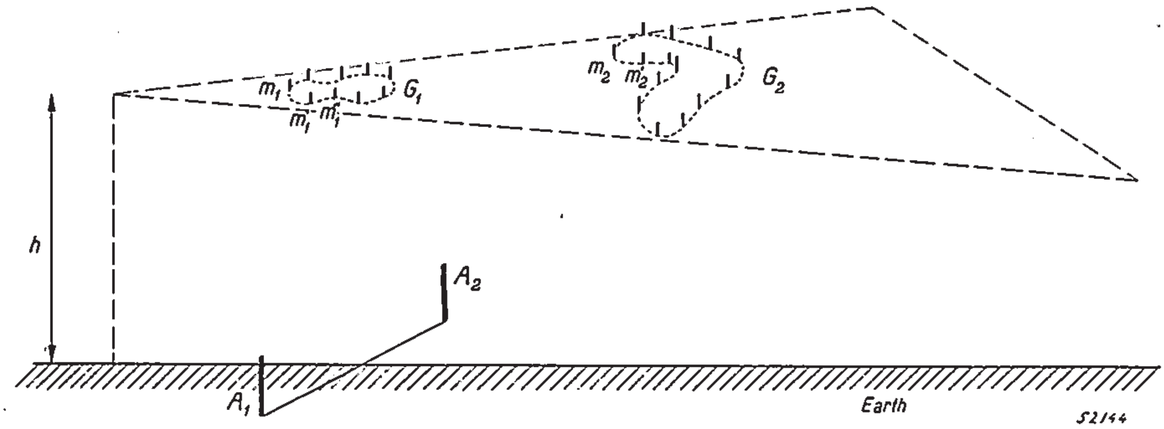

Fig. 10. Two groups G_1 and G_2 of vertical mathematical dipoles at equal heights and modulated differently, showing two polar diagrams of different forms.

---

*) This notation (used for a moment only) is not to be confused with a for the angle of elevation of the line of sight.

earth and summing those sums for all dipoles, we obtain a common factor

$$1 + R(\Theta) \exp j \left\{ \Delta(\Theta) + j \frac{4\pi h \cos \Theta}{\lambda} \right\},$$

since all dipoles have been assumed to be situated at the same height and all lines connecting the emitters with the observer had the same direction Θ.

The field strength at P, being proportional to (15) for small values of $\alpha = \pi/2 - \Theta$, may be written as:

$$f \left\{ 1 + R^2(\Theta) + 2R(\Theta) \cos \left(\Delta(\Theta) + \frac{4\pi h \cos \Theta}{\lambda} \right) \right\}^{1/2} \cdot \frac{K_1(\Theta)}{r}$$

with

$$K_1(\Theta) = |m_1 + e^{j\alpha'} m_1' + e^{j\alpha''} m_1'' + \ldots| .$$

K_1 is a function of Θ since the quantities α', α'', α''', ... contained not only internal phase differences but also path differences; f is a factor of proportionality which would contain $\cos^2 \alpha$ for larger values of the angle of elevation $\alpha = \pi/2 - \Theta$.

In an analogous way another group G_2 of vertical coherent dipoles, also situated at the heigth h but modulated differently from G_1, will give in P the field strength

$$f \left\{ 1 + R^2(\Theta) + 2R(\Theta) \cos \left(\Delta(\Theta) + \frac{4\pi h \cos \Theta}{\lambda} \right) \right\}^{1/2} \cdot \frac{K_2(\Theta)}{r}$$

if the distance between G_1 and G_2 is of the order of λ, so that practically the same distance r appears in this formula.

Here we have:

$$K_2(\Theta) = |m_2 + e^{j\beta'} m_2' + e^{j\beta''} m_2'' + \ldots| . \tag{16}$$

What α', α'', ... are in (15) with respect to the dipole m_1, β', β'', ... in (16) are with respect to the dipole m_2.

The β's are other functions of Θ than the α's. Moreover G_2 may contain more or fewer dipoles than G_1, whose specific internal phase differences (independent of path differences) may also be quite different from those of the dipoles in G_1. Also the moments m_2, m_2', m_2'', ... are in general different from m_1, m_1', ...

Therefore we have in general

$$K_1(\Theta) \neq K_2(\Theta) .$$

But it is possible to choose the moments m, m', ..., m_2, m_2', m_2'', ..., and the specific phase differences and the location of the dipoles such that just for an angle $\Theta = \Theta_0$ (for example the polar angle of the landing course wanted) we have:

$$K_1(\Theta_0) = K_2(\Theta_0)\,, \tag{17}$$

but then for other values $\Theta \neq \Theta_0$ of course:

$$K_1(\Theta) \neq K_2(\Theta) \quad (\Theta \neq \Theta_0)\,. \tag{18}$$

Now a change in the physical constitution of the soil is perceived only in $R(\Theta)$ and $\Delta(\Theta)$ which contain ε and σ, and it will thus affect both the field strength originating from G_1 and that from G_2, but both only by means of the common factor

$$\left\{1 + R^2(\Theta) + 2R(\Theta)\cos\left(\Delta(\Theta) + \frac{4\pi h \cos\Theta}{\lambda}\right)\right\}^{1/2}.$$

The relative increase or decrease of field strength will thus be a function of Θ but the same function for both G_1 and G_2, so that a direction Θ_0 in which formerly $K_1(\Theta_0) = K_2(\Theta_0)$ held is again characterized by an equality, now of the new functions:

$$K_1'(\Theta_0) = K_2'(\Theta_0)\,.$$

Where formerly $K_1(\Theta) \neq K_2(\Theta)$ held, there now holds:

$$K_1'(\Theta) \neq K_2'(\Theta) \quad (\Theta \neq \Theta_0)\,.$$

This means that our indication of the landing course by means of the prescription of equal reception of G_1 and G_2 is "weatherproof".

It is easily proved, in a manner used already on another occasion, that the above conclusion remains valid if the dipoles are extended to antennae of finite length, unless the upper and lower ends lie at the same height H and H' respectively (fig. 11) and all antennae are built in the same way and carry currents of the same strength and form.

Instead of two groups G_1 and G_2 of vertical dipoles we could have used also two groups of horizontal ones, all at the same height h above the ground and all being parallel to one another (perpendicular to the plane

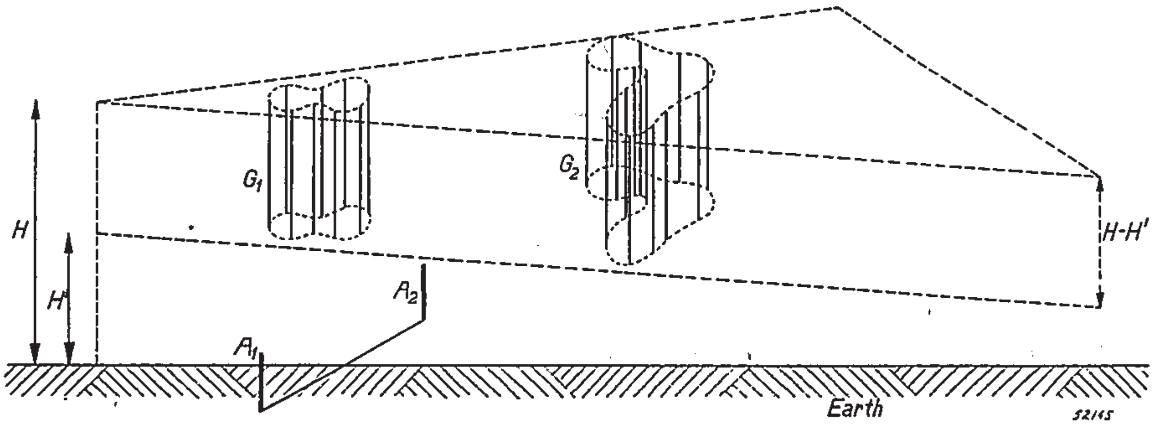

Fig. 11. The same as in fig. 10 but for antennae of finite length.

F_1). Of course we should then have to use another kind of reflection coefficient, but the form of all formulae would remain the same. The horizontal dipoles may also be added simply to horizontal antennae of finite length, all lying at the height h (see fig. 12).

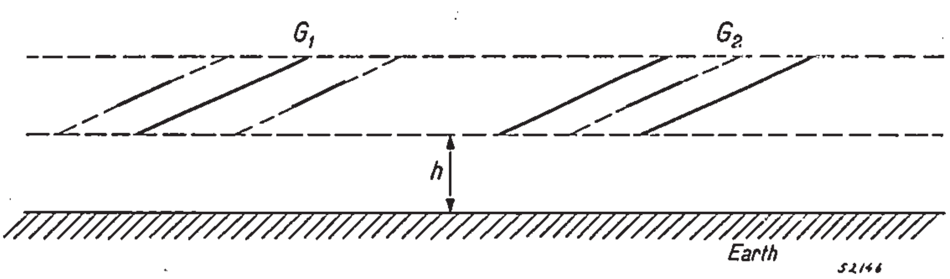

Fig. 12. Two differently modulated systems of parallel horizontal antennae at equal heights but showing polar diagrams of different forms.

The number and kind of antennae in both groups G_1 and G_2 must again be chosen such that (17) and (18) hold for $\Theta = \Theta_0$ and $\Theta \neq \Theta_0$ respectively.

A simple example is realized if we take for the first system one horizontal antenna D_1 and for the second system two horizontal antennae $D_2{}^l$ and $D_2{}^r$, these two being in phase with each other and further parallel to and at the same height as the antenna D_1 (fig. 13). We choose the mutual distance d of $D_2{}^l$ and $D_2{}^r$ in such a way that the polar diagram of the second system will differ very much in shape from that of D_1 (the first system). For that purpose we choose some angle $\bar{\alpha}$ different from α_0 ($\alpha_0 = \pi/2 - \Theta_0$ being the elevation of the landing course wanted) and construct the distance d as indicated in fig. 13, by means of the known value of $\lambda/2$. That is, we take

$$d = \frac{\lambda}{2 \sin \bar{\alpha}} \cdot$$

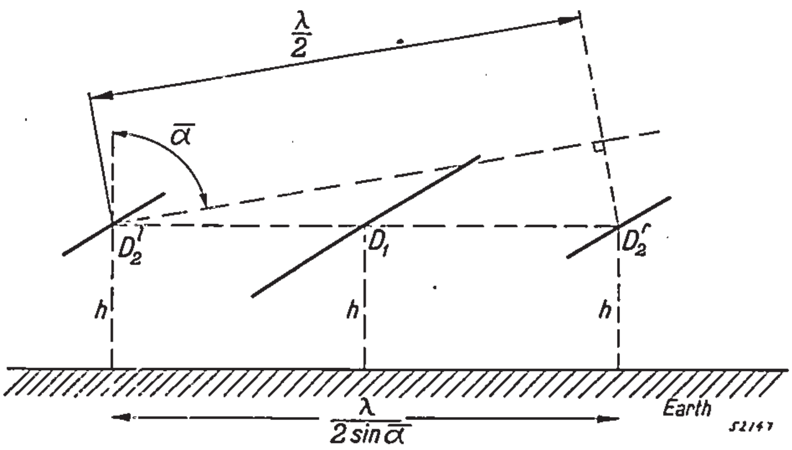

Fig. 13. A simple example of the case of fig. 12. One system consists only of the antenna D_1, the other of the two antennae $D_2{}^l$ and $D_2{}^r$.

If for a moment we could ignore the influence of the earth, the polar diagram of the first system (taken in the plane F_1 perpendicular to all horizontal antennae) would be a circle and that of the second system a more complicated figure with a zero point (radius vector $= 0$) in the direction $\overline{\Theta} = \pi/2 - \overline{\alpha}$. But owing to the influence of the earth both polar diagrams are changed very much, though they still remain of very different form. The second diagram will keep its vanishing radius vector in the direction $\overline{\Theta} = \pi/2 - \overline{\alpha}$, but since we chose $\overline{\alpha} \neq \alpha_0$ there might still be a considerable radiation in the desired direction $\Theta_0 = \pi/2 - \alpha_0$.

The power of the systems (modulated differently) may be chosen such that (17) and (18) hold for $\Theta = \Theta_0$ and $\Theta \neq \Theta_0$ respectively. Then both polar diagrams intersect on the radius with

$$\Theta = \Theta_0 ,$$

the polar angle of the landing course wanted.

During changes in the weather conditions and soil constants this point of intersection will move on the radius $\Theta = \Theta_0$, always remaining on it, so that a pilot receiving both systems with equal intensity can be sure to be on the cone $\Theta = \Theta_0$. The landing course found as intersection of this course and the medium plane F_1 given by the emitters A_1 and A_2 is therefore "weatherproof".

I am very much obliged to Ir K. Posthumus, who, being told of the contents of the first and second parts, drew my attention to the possibilities mentioned in the third part of the paper.

Eindhoven, September 1947

REFERENCE

[1]) K. F. Niessen, Philips Res. Rep. 3, 1-12, 1948.

R 77 *Philips Res. Rep.* **3**, *140-155, 1948*

A UNIVERSAL ADJUSTABLE TRANSFORMER FOR U. H. F. WORK

by J. M. van HOFWEEGEN and K. S. KNOL

621.392.43.029.6

Summary

A matching device for u.h.f. work is described with which any impedance can be matched to any other impedance by properly adjusting two shorting bridges. It consists of a screened two-wire Lecher system asymmetrically loaded with respect to the screen. The device can also be used for coarse impedance measurements. Based on the same principle, a universal adjustable transformer using wave guides can also be made.

Résumé

Les auteurs décrivent un dispositif à l'aide duquel il est possible, dans le domaine des ondes ultra-courtes, d'adapter deux impédances arbitraires, en fixant d'une manière appropriée la position de deux ponts de shuntage. Ce dispositif consiste en un système de Lecher blindé à deux conducteurs parallèles, qui est chargé asymétriquement par rapport au blindage. Le dispositif peut aussi être utilisé à des mesures approchées d'impédances. En partant du même principe, on peut aussi construire un transformateur universel à guides d'ondes.

1. Introduction

In u.h.f. engineering impedance matching is very often necessary. Several matching circuits are well known and commonly used, e.g., for matching antennae or power sources to transmission lines. The circuits mostly used are quarter-wavelength transmission lines and matching circuits using one or two stubs. In the designing of transmitters and receivers these circuits give satisfactory results, as the matching problem usually has to be solved only for certain fixed and well-known impedances and at a fixed frequency or in a certain frequency band. For several measurements and investigations in the u.h.f. range it is useful, however, to dispose of a device that can transform any impedance into any other desired impedance, the transforming circuit thus being continuously variable. These transformers are particularly suitable when the impedances to be matched or the frequency is variable or not exactly known. Several circuits having this feature are not applicable in practice for purely practical reasons. Transmission lines with variable length, for instance, mostly lead to unfavourable and unpractical constructions, particularly when the transmission lines used are screened. The use of slidable stubs should also be avoided, because of the difficulties arising when they are used with screened transmission lines.

In the following pages a device will be described that has proved to be very practical for the purpose mentioned above. It consists of a short two-wire transmission line (Lecher system) surrounded by a screen and carrying two shorting bridges. The impedances between which it is to be used as a matching transformer are not connected between the two wires in the usual way, but each of them is connected between one of the two wires and the screen. Thus the Lecher system is asymmetrically loaded, the currents and voltages in the wires are unbalanced, and the inner side of the screen is an essential part of the circuit. Of the two shorting bridges one is placed between the two wires and has no conducting contact with the screen; the other is a short-circuit between the two wires and the screen.

2. The universal adjustable transformer

The properties of this device can best be approached by starting with the four-terminal network of fig. 1, consisting of three reactances, which will be considered as free of loss. This is a symmetrical π-network. When an impedance $Z_e = R_e + jX_e$ is connected between one of the terminal pairs, the impedance between the other terminal pair is

$$Z_0 = R_0 + jX_0 = jX_1 \frac{j(X_1 + X_2)\, Z_e - X_1X_2}{j(2X_1 + X_2)\, Z_e - X_1X_2 - X_1^2}. \qquad (1)$$

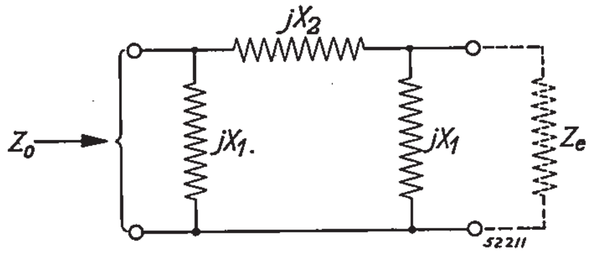

Fig. 1. Symmetrical π-network. By a suitable choice of X_1 and X_2 one can transform any impedance Z_e into any desired impedance Z_0.

From this equation it can be shown by simple computation that one can transform any impedance Z_e into any desired impedance Z_0 by a suitable choice of X_1 and X_2.

In u.h.f. engineering, instead of the lumped reactances shown in fig. 1 one will of course use short sections of transmission lines (Lecher systems) carrying slidable shorting bridges (fig. 2). By moving these bridges over half a wavelength, the reactances X_1 and X_2 can be varied between $-\infty$ and $+\infty$, so that, when the Lecher systems are sufficiently long (longer than half a wavelength), this circuit has the universal transforming properties mentioned.

Up till now it has been assumed that there is no inductive coupling between the three Lecher systems, for only in this case are the reactances building the π-circuit independent of one another. If an inductive coupling between the several parts could be allowed, a very simple construction would be possible. This construction is obtained by bending the Lecher system e-f down until the wire e coincides with b and f coincides with d and by moving a and c towards each other until these wires coincide too.

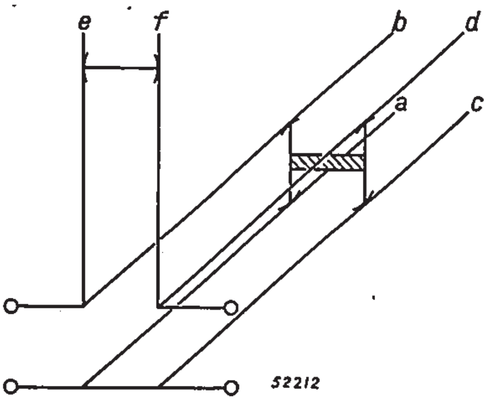

Fig. 2. Symmetrical four-terminal network consisting of three Lecher systems and having the same properties as the network of fig. 1.

We then obtain a system consisting of three wires 1, 2, 3 (fig. 3), originating respectively from the coincidence of b and e, d and f, a and c. The two shorting bridges on the Lecher systems a-b and c-d are now joined into one bridge K_1, short-circuiting all three wires, while the bridge on the Lecher system e-f is now slidable on the wires 1 and 2 (K_2). Because of the inductive coupling existing between the pairs of wires 1-2, 2-3 and 3-1 it is not obvious that by moving the two bridges K_1 and K_2 the same universal transforming properties as mentioned above also exist for the device of fig. 3. The proof that this is actually the case will be given below.

It is not necessary that the three conductors 1, 2, and 3 of fig. 3 all have the same cross-sectional shape. As it is only necessary that 3 should

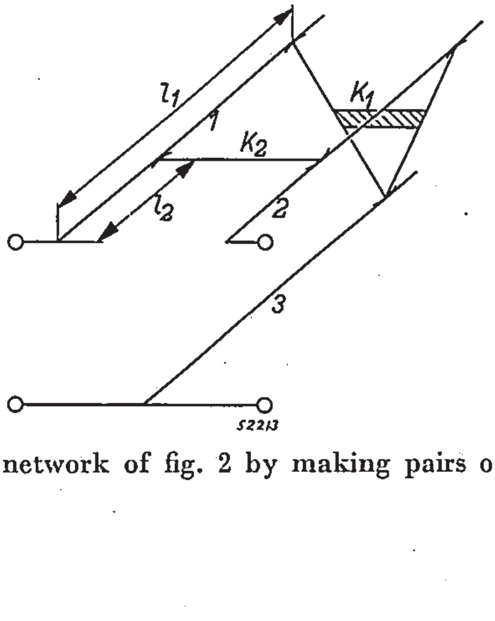

Fig. 3. Simplification of the network of fig. 2 by making pairs of wires of the several Lecher systems coincide.

be in a symmetrical position with respect to 1 and 2, it is admissible that 3 has a different shape. It may consist, for instance, of a cylindrical screen surrounding the conductors 1 and 2, from which the construction of fig. 4 results *). The shorting bridge K_1 now gets the shape of a plug and K_2 that of a bar, short-circuiting only the two wires, without making contact with the screen. The impedance to be transformed, Z_e, is connected between one of the inner conductors and the outer conductor (screen), while the transformed impedance, Z_0, is obtained between the other inner conductor and the outer conductor. Thus we have a screened Lecher system that is asymmetrically loaded with respect to the screen, and the voltages and currents in the wires will in general be out of balance with respect to the screen.

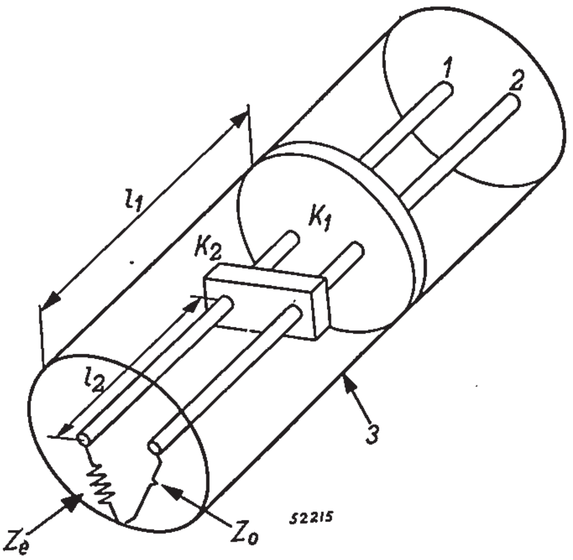

Fig. 4. Screened, asymmetrically loaded two-wire Lecher system having the same properties as the network of fig. 3.

3. Proof of the universal adjustibility

Nearly all the literature about transmission lines and Lecher systems deals only with a two-wire system (screened or unscreened) with balanced voltages and currents or with lines of the coaxial type. The equations concerning these systems are well known. In our case, where the Lecher system is asymmetrically loaded, these equations are not immediately applicable. We can, however, use the normal transmission-line equations by resolving the voltages and currents into balanced and unbalanced components and applying the equations to both of them.

In order to get simpler figures we shall not draw the third conductor as a screen surrounding the other two, but as a third wire, as already done in fig. 3.

---

*) The dimensions of the screen are restricted by the condition that the circumference must be small with respect to a quarter wavelength.

In fig. 5 the three wires are again labelled 1, 2, and 3. We now introduce the following notations for the complex voltages and currents:

V_1 = the voltage between 3 and 1,
V_2 = the voltage between 3 and 2,
I_1 = the current in 1,
I_2 = the current in 2,
I_3 = the current in 3.

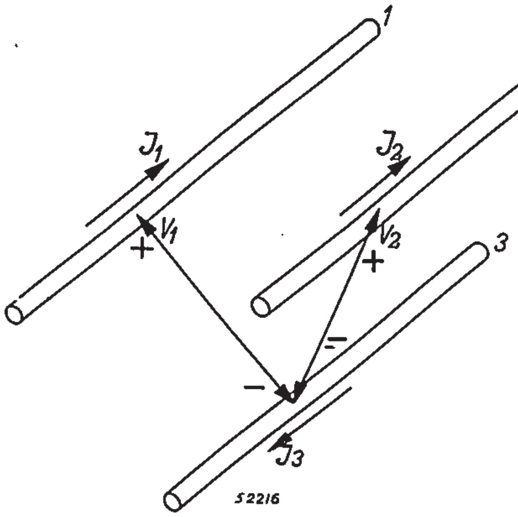

Fig. 5. Indication of the voltages and currents in the three-wire Lecher system.

The voltages and currents are considered as positive in the directions indicated in fig. 5. As no other conductors are present, the currents on all corresponding places on the three-wire system are related by the equation

$$I_1 + I_2 = I_3 . \tag{2}$$

The voltages and currents can now be resolved into balanced and unbalanced components V_b and V_p, respectively I_b and I_p, as is shown in fig. 6.

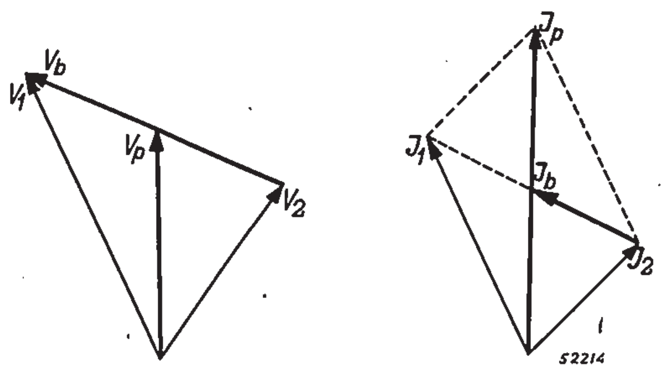

Fig. 6. Resolution of the voltages and currents into balanced and unbalanced components.

$$\left.\begin{aligned} V_1 &= V_p + \tfrac{1}{2} V_b, \\ V_2 &= V_p - \tfrac{1}{2} V_b, \\ I_1 &= \tfrac{1}{2} I_p + I_b, \\ I_2 &= \tfrac{1}{2} I_p - I_b. \end{aligned}\right\}{}^{*)} \tag{3}$$

First of all we shall consider these components separately.

As the unbalanced components V_p of the voltages V_1 and V_2 are equal in all corresponding points of the wires 1 and 2, with respect to these components we can consider these wires as being in parallel. The system consisting of 1 and 2 in parallel as one wire and 3 as the other wire will have a certain surge impedance, which we shall indicate by ζ_p. In consequence of the equality of V_p for the wires 1 and 2, we can, with respect to the unbalanced components of voltages and currents, ignore the presence of the shorting bridge K_2. As the bridge K_1 short-circuits the unbalanced system we can write the ratio of V_{p0} and I_{p0} (unbalanced components of voltages and currents at the beginning of the wires) as

$$\frac{V_{p0}}{I_{p0}} = j\zeta_p \tan \beta l_1, \tag{4}$$

where $\beta = 2\pi/\lambda$ and $l_1 =$ the distance from the beginning of the wires to the shorting plug K_1 (see figs 3 and 4).

Considering now the balanced components V_b and I_b, we can ignore the presence of the wire 3. Since the bridge K_2 acts as a short-circuit for these components, we can write the ratio of V_{b0} and I_{b0} (balanced components of voltages and currents at the beginning of the wires) as

$$\frac{V_{b0}}{I_{b0}} = j\zeta_b \tan \beta l_2, \tag{5}$$

where $\zeta_b =$ the surge impedance of the wires 1 and 2, used in a balanced circuit, and $l_2 =$ the distance from the beginning of the wires to the shorting bar K_2.

When the impedance Z_e is connected between the wires 1 and 3, then, taking into account the positive directions of voltage and current as shown in fig. 5, we can write down the ratio of V_1 and I_1 at the beginning of the wires as:

$$\frac{V_{10}}{I_{10}} = -Z_e. \tag{6}$$

---

*) The factor ½ has been put before V_b and I_p for the sake of agreement with the normal meaning of the terms 'balanced voltage' and 'unbalanced current' on two conductors, as these terms normally indicate the total voltage between the conductors and the total current in both conductors together.

As Z_0 is measured between the wires 2 and 3, we have furthermore the equation:

$$\frac{V_{20}}{I_{20}} = Z_0 . \tag{7}$$

From (3), (4), (5), (6), and (7) we can compute the following relation between Z_0 and Z_e:

$$Z_0 = \frac{jZ_e\,(\zeta_p \tan \beta l_1 + \frac{1}{4}\,\zeta_b \tan \beta l_2) - \zeta_p \zeta_b \tan \beta l_1 \tan \beta l_2}{Z_e + j\,(\zeta_p \tan \beta l_1 + \frac{1}{4}\,\zeta_b \tan \beta l_2)} . \tag{8}$$

If we again write $Z_0 = R_0 + jX_0$ and $Z_e = R_e + jX_e$, from the equality of the real and imaginary parts of (8) we can find expressions for $\tan \beta l_1$ and $\tan \beta l_2$:

$$\left.\begin{aligned} 2\zeta_p \tan \beta l_1 &= \frac{R_e X_0 + R_0 X_e}{R_e - R_0} \pm \frac{\sqrt{R_0 R_e \{(X_e + X_0)^2 + (R_e - R_0)^2\}}}{R_e - R_0} \\ \tfrac{1}{2}\,\zeta_b \tan \beta l_2 &= \frac{R_e X_0 + R_0 X_e}{R_e - R_0} \mp \frac{\sqrt{R_0 R_e \{(X_e + X_0)^2 + (R_e - R_0)^2\}}}{R_e - R_0} \end{aligned}\right\} \tag{9}$$

Since R_0 and R_e are always positive, $\tan \beta l_1$ and $\tan \beta l_2$ are always real. Hence we see that it is possible to transform any impedance Z_e into any desired value Z_0 by properly adjusting l_1 and l_2. As $\tan \beta l_1$ and $\tan \beta l_2$ must be variable between $-\infty$ and $+\infty$, the distance over which the two shorting bridges must be slidable is at least half a wavelength.

4. Examples of application

The matching transformer described above has already found many applications in laboratory u.h.f. work. In fig. 7 a practical model is shown. The two shorting bridges are slidable by means of rack-and-pinion drives. The bridge K_2 is moved by a rod of insulating material between the wires 1 and 2 and leading through a hole in the shorting plug K_1.

Fig. 8 shows the use of the transformer for matching a wave-guide probe to a crystal detector. The wavelength being only 10 cm, the total length over which the shorting bridges must be slidable is only 5 cm.

As an example of its application for measuring purposes we mention the comparison of the sensitivity of several types of power meter (bolometers, thermo-couples, crystal detectors). By matching these power meters to an u.h.f. power source one can ensure that the same power is delivered to the different types in spite of the different impedances, so that their sensitivity can be compared.

Another application of the adjustable matching transformer is the measurement of the power gain of an amplifier or converter stage.

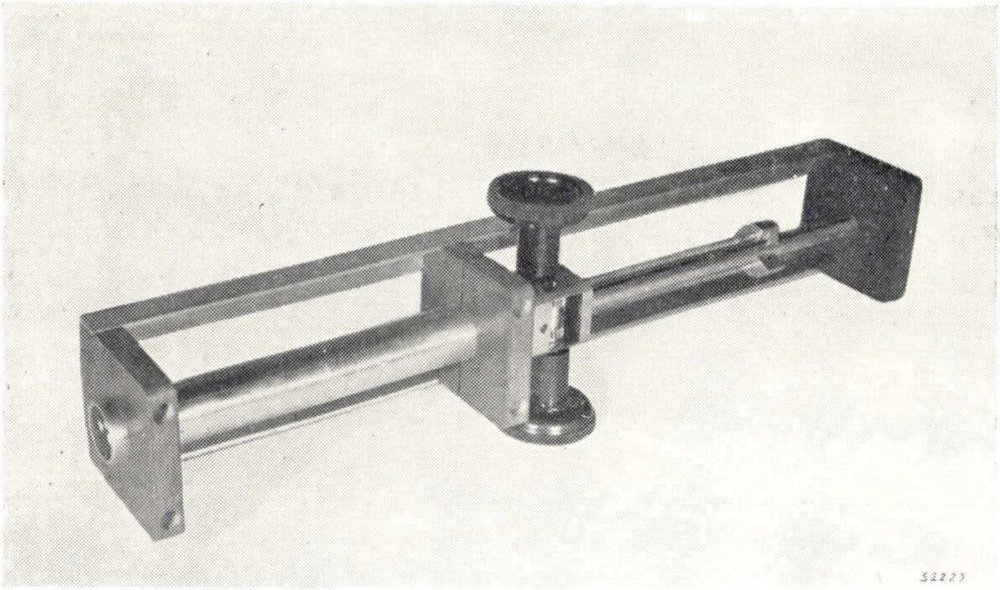

Fig. 7. Practical model of a universal adjustable transformer, for wavelengths below 50 cm.

In this case the input terminals of this stage are connected to a power source via the matching transformer. Thus the input impedance is matched to the power source. Furthermore, the output impedance of the amplifier is matched to some type of power meter. The two transformers are adjusted to maximum power transfer. When this power is compared with the power obtainable when the power meter is matched directly to the

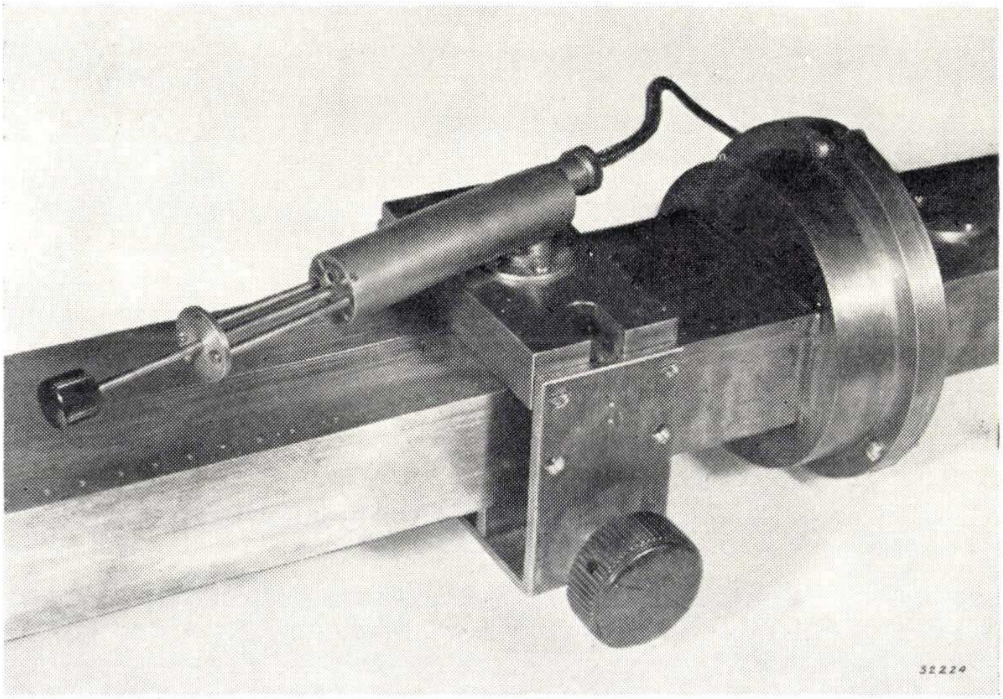

Fig. 8. Use of the transformer for matching a crystal detector to a wave-guide probe.

power source, the power gain of the amplifier stage is found under the most favourable conditions (matched input and output).

Particularly with tubes of the disc-seal type the measuring assembly becomes very simple, as is shown in fig. 9.

Attention must be paid to the fact that the matching conditions (equations (9)) depend on the frequency; the use of a matching transformer in the input and output leads of an amplifier stage will therefore restrict the bandwidth. When making measurements on wide-band amplifiers this must be taken into account. If the conductors are long enough, the correct matching can be obtained with several positions of the shorting bridges K_1 and K_2 (an increase of both l_1 and l_2 by half a wavelength gives the same values of tan βl_1 and tan βl_2). As is the case with every tuned Lecher system, the bandwidth decreases with increasing length; therefore, when investigating wide-band amplifiers it is recommended to use the smallest possible values of l_1 and l_2. If necessary, when designing the transformer, this requirement may be taken into account by providing for the shorting bridges to approach as nearly as possible to the beginning of the conductors. As an increase of the surge impedances ζ_b and ζ_p has also an increasing effect on the bandwidth, one can occasionally make these surge impedances as large as possible.

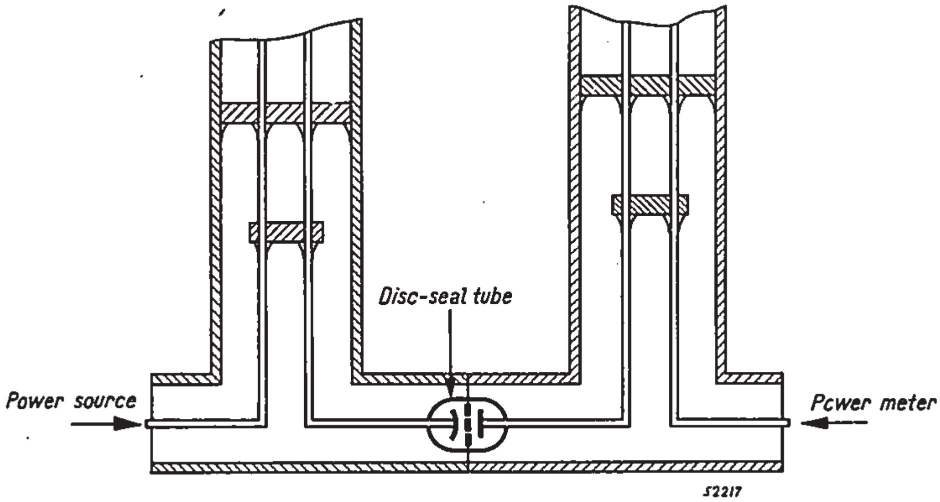

Fig. 9. Use of two impedance transformers for measuring the power gain of a disc-seal tube.

Of course, if desired, the power gain can also be investigated under mismatch conditions by adjusting one or both of the transformers to a certain mismatch.

5. Use of the adjustable transformer for impedance measurements

When R_0 and X_0 are known it is possible to calculate R_e and X_e from tan βl_1 and tan βl_2. In this way the adjustable transformer can be used under special conditions as an impedance-measuring device. When, for instance, one side of the transformer is connected to a power source with a known output impedance and the other side to a power meter, and the transformer is adjusted to maximum power transfer to the meter, the impedance of the power meter is transformed into the conjugate-complex value of the output impedance of the source. Hence, from the position of the two shorting bridges the input impedance of the power meter can be computed. One must not, however, expect great accuracy from this method of measuring. Actually, for an accurate calculation several corrections must be applied to the lengths l_1 and l_2. These corrections, which are discussed in more detail below, have a great influence on the results, and in general they are not known very exactly *).

When solving the equations (9) for R_e and X_e we find:

$$\left.\begin{aligned} \frac{R_e}{R_0} &= \frac{(a-b)^2}{R_0^2 + (a+b-X_0)^2}, \\ X_e &= \frac{R_e}{R_0}(a+b-X_0) - (a+b), \end{aligned}\right\} \tag{10}$$

where $a = \zeta_p \tan \beta l_1$ and $b = \frac{1}{4}\zeta_b \tan \beta l_2$.

Frequent computations of R_e and X_e may be simplified by introducing:

$$\frac{a-b}{\sqrt{R_0 R_e}} = \xi, \quad \frac{a+b-X_0}{R_0} = \eta.$$

The first of the equations (10) may then be written:

$$\xi^2 - \eta^2 = 1. \tag{11}$$

When a, b, R_0, and X_0 are known we can calculate η. Equation (11) then gives ξ, from which R_e results. Finally X_e is found as:

$$X_e = \eta R_e - (a+b). \tag{12}$$

If required, the hyperbola given by (11) may be drawn for quickly finding ξ from η.

6. Corrections of the lengths l_1 and l_2

When constructing an adjustable transformer according to the principle of fig. 4, it will in general be necessary to support the ends of the wires 1 and 2 by a disc of some insulating material. The mutual capacitances between the wires and the screen caused by this insulator are indicated in

---

*) They have, however, no influence on the universal adjustability of the transformer.

fig. 10 by C_{12}, C_{23}, and C_{13}. The latter two capacitances are in parallel with Z_0 and Z_e, so it is very simple to take them into account.

The shorting bridge K_2 has a certain self-inductance L_2 and a certain capacitance C_2 against the screen. Also the plug K_1 will not be a pure short-circuit, but it may be represented by small self-inductances L_{12}, L_{23}, and L_{13} *).

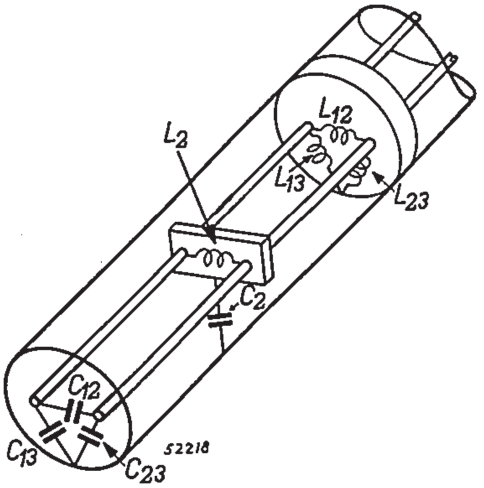

Fig. 10. Indication of capacitances and self-inductances making several corrections necessary in the calculated results when using the transformer for impedance measurements.

C_{12}, L_2, and L_{12} have only influence on the balanced components of voltage and current. Since there are no balanced components behind K_2, the presence of L_{12} may be ignored. The influence of C_{12} and L_2 can be taken into account by introducing a length l_2' instead of l_2 that is given by

$$j\zeta_b \tan \beta l_2' = \zeta_b \frac{j\omega L_2 \cos \beta l_2 + j\zeta_b \sin \beta l_2}{\zeta_b \cos \beta l_2 - \omega L_2 \sin \beta l_2} \,//\, \frac{1}{j\omega C_{12}}. \tag{13}$$

C_2, L_{13}, and L_{23} only influence the unbalanced components. They may be dealt with by introducing a length $(l_1-l_2)'$ instead of (l_1-l_2) that is given by the equation:

$$j\zeta_p \tan \beta(l_1-l_2)' = \zeta_p \frac{j\omega L_3 \cos \beta(l_1-l_2) + j\zeta_p \sin \beta(l_1-l_2)}{\zeta_p \cos \beta(l_1-l_2) - \omega L_3 \sin \beta(l_1-l_2)} \,//\, \frac{1}{j\omega C_2}, \tag{14}$$

where L_3 represents L_{13} and L_{23} in parallel.

The correction caused by the very small self-inductance L_3 may usually be ignored, so (14) may be simplified to

$$j\zeta_p \tan \beta(l_1-l_2)' = j\zeta_p \tan \beta(l_1-l_2) \,//\, \frac{1}{j\omega C_2} = \frac{j\zeta_p \tan \beta(l_1-l_2)}{1-\omega C_2 \zeta_p \tan \beta(l_1-l_2)}. \tag{15}$$

---

*) In practice, the self-inductances L_2, L_{12}, L_{13}, and L_{23} are for the greater part due to contact springs between K_1, K_2, and the conductors 1 and 2.

L_2 and C_2, however, cannot be ignored. When the dimensions of the bridge K_2 are so much reduced that C_2 becomes very small, L_2 increases, and vice versa. Therefore, when using the transformer as an impedance-measuring device, corrections must be applied for both of them. The influence of C_{12} may only be ignored when the insulating support has a very small capacity. In general, however, a correction of l_2 by C_{12} will also be necessary.

7. Formulae for ζ_b and ζ_p

When using the adjustable transformer for matching purposes it is not necessary to know the surge impedances ζ_b and ζ_p. When, however, one wishes to compute R_e and X_e from the positions of the shorting bridges K_1 and K_2, it is necessary to know the values of ζ_b and ζ_p. For this reason we give here the formulae for calculating these surge impedances from the dimensions of the device as indicated in fig. 11:

$$\zeta_b = 120 \ln \left(p + \sqrt{p^2-1}\right) \text{ ohms}, \tag{16}$$

where $p = \dfrac{a}{d} \cdot \dfrac{D^2 - (a^2-d^2)}{D^2 + (a^2-d^2)}$;

$$\zeta_p = 30 \ln \left(q + \sqrt{q^2-1}\right) \text{ ohms}, \tag{17}$$

where $q = \dfrac{D^4 - (a^2-d^2)^2}{4adD^2}$.

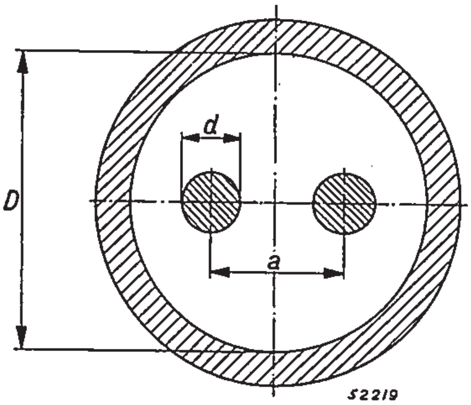

Fig. 11. Indication of the dimensions of a two-wire, screened Lecher system.

8. Balanced input and output circuits

A transformer according to fig. 4 is of course only applicable when the input and output circuits are unbalanced. It is, however, easy to deduce from the principles outlined above a device for matching two *balanced* circuits. In this case we use a four-wire system with three shorting bridges, two of which are slidable together, so that the number of variable elements is again only two (fig. 12).

Of course, it is preferable to provide the four-wire system with a screen; but in this case the screen is not an essential part of the circuit.

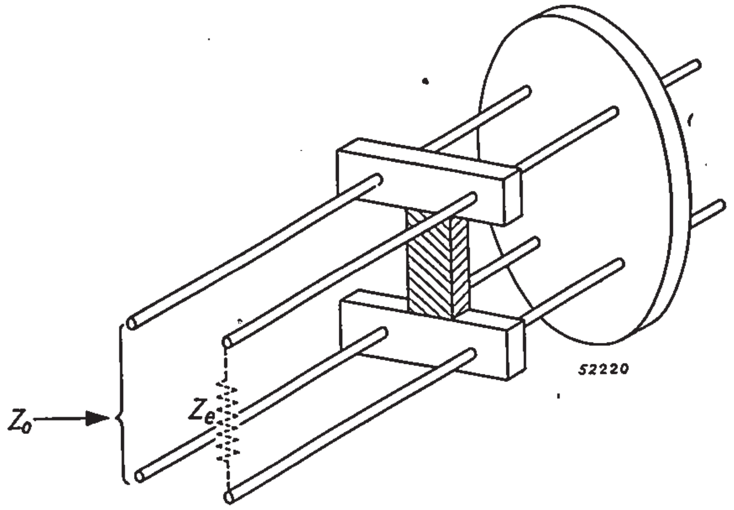

Fig. 12. Four-wire Lecher system applicable for matching two balanced circuits.

9. An adjustable transformer for wave guides

The matching of wave guides to loads or power sources is also a problem that often arises in micro-wave work. The well-known matching means (inductive or capacitive windows, series or shunt tee sections, tuning screws) can only be used in certain pre-determined impedance ranges and at certain frequencies. The universal adjustability of these matching devices always involves very unfavourable constructions. A tee section with a slidable branching point, for instance, is very difficult to realize; but if a tee section is to be of use for matching any load to a wave guide, the branching point should be variable.

Along the same principles as outlined above for a Lecher system it has appeared to be possible to construct a transformer for wave guides, and on account of its universal adjustability it has proved to be very useful in experimental micro-wave work. A fundamental constructional sketch of this wave-guide transformer is given in fig. 13. It consists of a wave guide provided with a slidable shorting plug, *K*, and a septum, *p*, also slidable. Thus the length of the wave guide, *l*, and the width of the aperture, *a*, are both adjustable. It can be shown that any desired impedance transformation between the parts I and II of the wave guide can be adjusted by varying the place of the plug and the width of the aperture. In this way any desired load (e.g., a radiating horn) connected to part I can be matched to a wave-guide transmission system connected to part II.

In the design of fig. 13 the connection of the parts to be matched to the adjustable transformer is effected by inserting corners provided with slanting planes for eliminating reflections, as is common practice in wave guides.

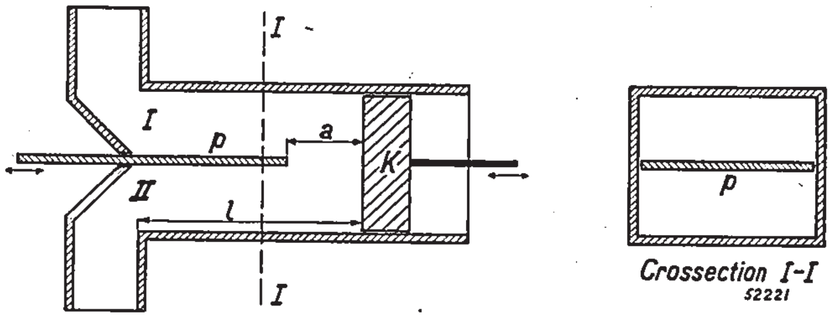

Fig. 13. Universal adjustable matching transformer for wave guides.

As is well known, two kinds of waves can occur in wave guides, transverse electric (TE) and transverse magnetic (TM) waves. We shall first consider the TE waves. In the parts I and II these waves will in general be of a different size and phase, but the electric and magnetic field intensities (E and H) may be resolved into phase and counterphase components in the following way:

$$\left.\begin{aligned} E_I &= E_{ph} + E_c\,, \\ E_{II} &= E_{ph} - E_c\,, \\ H_I &= H_{ph} + H_c\,, \\ H_{II} &= H_{ph} - H_c\,, \end{aligned}\right\} \tag{18}$$

where the subscripts ph and c indicate, respectively, the phase and counterphase components. Assuming the directions indicated in fig. 14 as positive, when considering the counterphase components we can ignore the presence of the septum p. Thus these counterphase components are reflected at the shorting plug K, and the ratio of the transverse components of E_c and H_c at the entrance of the wave guide (plane A-A) is given by the formula:

$$\frac{E_c}{H_c} = j\,120\pi\,\frac{\lambda_g}{\lambda}\tan\beta l\,, \tag{19}$$

where E_c is measured in volts/metre and H_c in amps/metre, so E_c/H_c in ohms, and furthermore:

λ_g = the wavelength in the wave guide,
λ = the free-space wavelength,
$\beta = 2\pi/\lambda_g$ = the phase constant.

According to a well-known formula, the relation between λ_g and λ is given by

$$\lambda_g = \frac{\lambda}{\sqrt{1-\left(\frac{\lambda}{\lambda_c}\right)^2}}, \tag{20}$$

where $\lambda_c =$ the wavelength at cut-off.

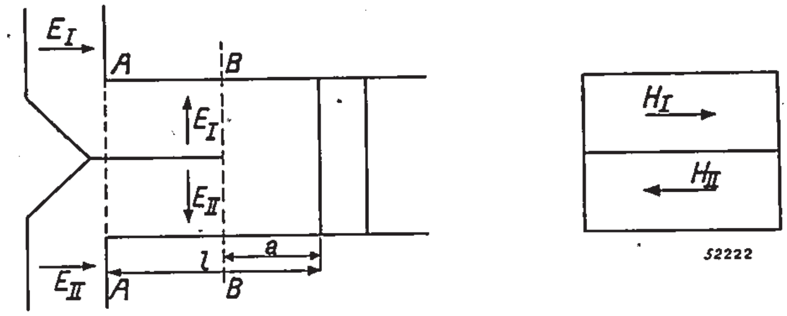

Fig. 14. Assumption of positive directions for the transverse components of the electric and magnetic field intensities.

The phase components, however, cancel in the part of the wave guide to the right of the plane *B-B*, which means a total reflection at the open ends of the parts I and II in this plane. Therefore, the ratio of the transverse components of E_{ph} and H_{ph} at the entrance of the guide is given by

$$\frac{E_{ph}}{H_{ph}} = -j\,120\pi\,\frac{\lambda_g}{\lambda}\cot\beta(l-a)\,. \tag{21}$$

From (15), (16), and (18) we can compute the following relation between E_I/H_I and E_{II}/H_{II}:

$$\frac{E_I}{H_I} = \frac{j\,60\pi\,\frac{\lambda_g}{\lambda}\frac{E_{II}}{H_{II}}\,\}\tan\beta l - \cot\beta(l-a)\{ - \left(120\pi\,\frac{\lambda_g}{\lambda}\right)^2 \tan\beta l\cot\beta(l-a)}{\frac{E_{II}}{H_{II}} - j\,60\pi\,\frac{\lambda_g}{\lambda}\,\}\tan\beta l - \cot\beta(l-a)\{}\,. \tag{22}$$

If we write $E_I/H_I = p + jq$ and $E_{II}/H_{II} = r + js$, from the equality of the real and imaginary parts of (22) we can find expressions for $\tan\beta l$ and $\cot\beta(l-a)$:

$$\left.\begin{aligned} -120\pi\,\frac{\lambda_g}{\lambda}\cot\beta(l-a) &= \frac{qr+ps}{p+r} \pm \frac{\sqrt{-pr\,\}(q-s)^2+(p+r)^2\{}}{p+r}, \\ 120\pi\,\frac{\lambda_g}{\lambda}\tan\beta l &= \frac{qr+ps}{p+r} \mp \frac{\sqrt{-pr\,\}(q-s)^2+(p+r)^2\{}}{p+r}. \end{aligned}\right\} \tag{23}$$

As p and r have always the opposite sign (the contrary would mean a constant flow of energy into or out of the transformer), cot $\beta(l-a)$ and tan βl are always real. Hence we see that it is possible to transform any value E_{II}/H_{II} into any desired value of E_I/H_I by properly adjusting l and a.

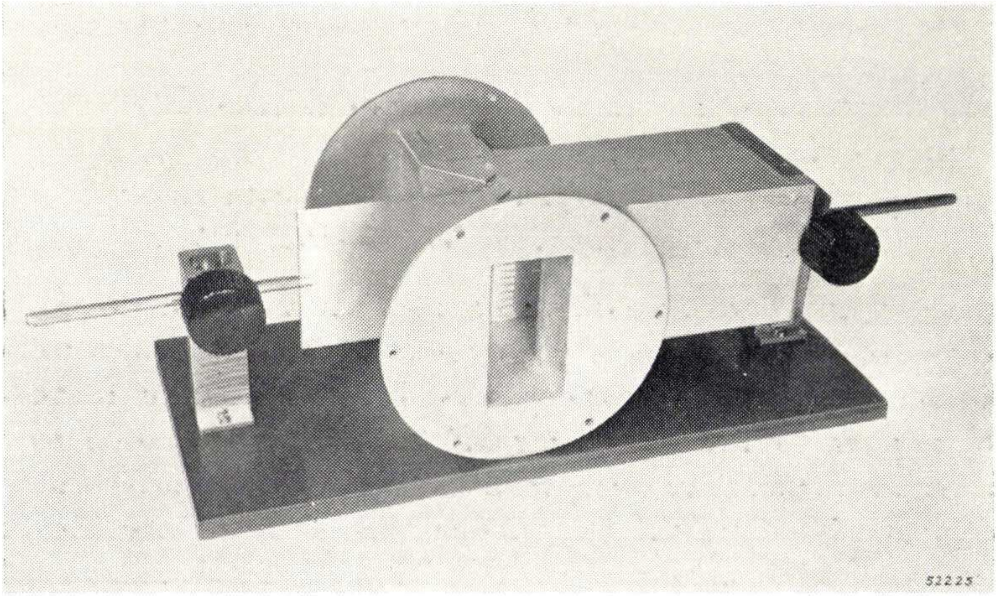

Fig. 15. Practical model of an adjustable transformer for wave guides.

Considering the TM waves, a computation very similar to the one given above can be carried out. The results are the same, except for the factor λ_g/λ in the equations (16), (18), (19), and (20), which for TM waves must be replaced by λ/λ_g. Therefore, also when the mode of transmission is a TM wave, any desired transformation can be obtained by adjustment of l and a.

In fig. 15 a practical model is shown of a wave-guide transformer based on the principle outlined above. The shorting plug and the septum are slidable by means of rack-and-pinion drives.

Eindhoven, September 1947

ABSTRACTS OF RECENT SCIENTIFIC PUBLICATIONS OF THE N.V. PHILIPS' GLOEILAMPENFABRIEKEN

Reprints of the majority of these papers can be obtained on application to the Administration of the Research Laboratory, Kastanjelaan, Eindhoven, Netherlands. Those papers of which no reprints are available in sufficient number are marked with an asterisk (*).

1717: J. M. Stevels: The physical properties of glasses. *)
III. The density of borate glasses.
IV. The density of phosphate and germanate glasses.
(J. Soc. Glass Technology **30**, 173-197, 1946).

The theory given in an earlier communication **) on the density of silicate glasses (as a function of their composition) is extended to borate, boro-silicate and boro-aluminate glasses. It is shown that in the three cases there is an "accumulation region" (where the O^{2-} ions form tetrahedral instead of triangular configurations round the B^{3+} ions) and a "destruction region" (where the O^{2-} ions are taken up by the breaking of linkages between the network formers). For the boro-aluminates a "crystalline region" (where al least two phases are formed, of which at least one is crystalline) occurs as well. Methods are given for calculating the density. The values so derived are in satisfactory agreement with those obtained by experiment. The theory given is found to hold also for phosphate and germanate glasses.

1718: J. M. Stevels: The physical properties of glasses.
V. A peculiar phenomenon in the vitreous system Na_2O-B_2O_3.
VI. The relationship between the volume and the number of glass-forming ions in silicate glasses.
VII. The molecular refraction of glasses.
(J. Soc. Glass Technology **30**, 303-317, 1946.)

V. The density-concentration curve of sodium-borate glasses is determined and the S-shaped curve found is discussed. At a concentration of 4 per cent Na_2O a widening of the oxygen network is found which is, however, not connected essentially with the sudden increase of the electric conductivity at this composition.

VI. It is shown that, at least in silicate glasses, there is no perceptible difference between the volumes of bridging and non-bridging oxygen ions. The volume of the interstices in the

---

*) Correction to same abstract published in Philips Res. Rep. **2**, 441, 1947.
) J. M. Stevels, Rec. Trav. chim. Pays-Bas **60, 85, 1941; **62**, 19, 1942.

oxygen network is proportional to $R^{3/2}$ (R being the ratio of the number of oxygen ions to the number of glass-forming ions) as is decuded from a simple model of the glass structure. Using these two results the volume of a block of glass containing one gram-atom of oxygen is calculated as a function of R. The values obtained are identical, within the limits of error, with those derived from a formula obtained previously.

VII. It is shown that the molecular refraction of abnormal glasses can be calculated in an additive way, with the aid of atomic (ionic) refractions, provided that distinction is made between bridging and non-bridging oxygen ions. This additivity is not expected for normal glasses. These expectations are found to be realized for a large number of pure silicate glasses containing Na^+, K^+, and Ca^{++} ions only. The deviations between experimental and calculated molecular refractions for the abnormal glasses are less than 0·3 per cent. Glasses containing isolated oxygen tetrahedra are not examined.

1729*: J. L. Snoek: New developments in ferromagnetic materials; Elsevier Publishing Company, Inc., New York, Amsterdam, 1947, 136 pp., 52 figs.

This book is not a textbook on the subject, but it gives a collection of publications on research work carried out during 1940-1945. It is divided into three chapters dealing with the "statics" and "dynamics" of ferromagnetism and the development of magnetic materials respectively. The first chapter includes such topics as the general theory of hysteresis, hysteresis at low values of the induction, crystal anisotropy and magnetostriction in ternary systems, permeability and coercive force of cubic ferromagnetic oxides, effect of cold-rolling on the alloys of Ni and Fe. The second chapter chiefly deals with the magnetic after-effect and disaccomodation in alpha-iron as well as in ferromagnetic non-metals. Other topics are: eddy-current problems, magnetic skin-effect, large Barkhausen discontinuities. The third chapter gives extensive information on new magnetic ferrites developed by the author and co-workers ("ferroxcube" 1,2,3,4), and gives some information on magnet steels.

1730: E. J. W. Verwey: Theory of the stability of lyophobic colloids (J. phys. Colloid Chem. **51**, 631-636, 1947).

The theory of the interaction of the double layers surrounding colloidal particles in suspension in the presence of an electrolyte is reviewed in relation to the stability of lyophobic colloids. It is concluded that the interaction of the double layers must be associated with an increase of free energy, leading to a repulsion between the particles. The calculated repulsive potential for special cases is combined with the Van der Waals-London attractive potential calculated by Hamaker, to obtain curves of potential against distance. Predictions based on these curves appear to agree well with various experimental data. For example, the influence of electrolytic concentration and of the valencies of the ions on flocculation is satisfactorily explained in terms of the theory, although many complicated phenomena remain to be correlated with it.

1731: Th. P. J. Botden and F. A. Kröger: Fluorescence of cadmium borates activated by manganese (Physica, s'-Grav. **13**, 216-224, 1947).

In the system CdO. B_2O_3 four compounds exist, each of which shows fluorescence when activated by manganese. $Cd_2B_2O_5$-Mn is excited by $\lambda < 3200$ Å and cathode rays, and then shows an orange luminescence, whereas CdB_2O_4, $Cd_2B_6O_{11}$ and $Cd_3B_2O_6$ show a green cathode-luminescence only.

The luminescence of the $Cd_2B_2O_5$-$Mn_2B_2O_5$ phase is studied quantitatively both as a function of the manganese content and as a function of the exciting radiation and temperature. It is shown that an ultra-violet emission appearing at low temperatures in some of the products cannot be responsible for the anomalous decrease of the red luminescence towards low temperatures.

1732: F. A. Kröger: Fluorescence of tungstates and molybdates (Nature, London, **159**, 674, 1947).

Certain molybdates and tungstates that are non-luminescent at ordinary temperatures prove to show luminescence at low temperatures. The temperature-quenching of the luminescence of a number of tungstates and molybdates in the interval —200 to +200 °C is given in a graph.

1733: F. A. Kröger: Tetravalent manganese as an activator in luminescence (Nature, London, **159**, 705, 1947).

In a number of systems, such as zinc aluminate, magnesium aluminate, α- and β-aluminium oxide, magnesium titanate, all activated with manganese, the luminescence is markedly different according as the products are prepared under oxidizing or reducing conditions. The reduced products (except the titanate) show a green cathode-luminescence, which is due to divalent manganese. The oxidized products show a deep-red luminescence upon excitation by cathode rays or ultra-violet (3650 Å). The valency of Mn in magnesium titanate is found by titration to lie between 3 and 4. Analogy between the emission spectra of Mg_2TiO_4-Cr^{3+} and Mg_2TiO_4-Mn shows that Mn is present in the form of Mn^{4+}.

1734: E. J. W. Verwey: Nieuwe onderzoekingen over de atoomrangschikking in spinellen in verband met hun physische eigenschappen (Chem. Weekblad, Amsterdam, **43**, 229-232, 1947) (New investigations on the atomic arrangement in spinels in relation to their physical properties; in Dutch).

For the contents of this paper the reader is referred to Philips tech. Rev. **9**, 186-191, 239-248, 1947.

1735: A. van der Ziel and A. Versnel: Total-emission noise in diodes (Nature, London, **159**, 640, 1947).

Measurements of the input damping $1/R$ and the equivalent saturated diode current I_e are carried out at 7.25-m wavelength on a diode (cathode area 10 cm², anode-cathode distance 0.1 cm). Both quantities are approximately proportional to V_a^{-2}. The total emission may be described by assuming the "equivalent noise temperature" T_e of the conductance $1/R$ to be equal to the cathode temperature. It is expected that this result holds for a very wide frequency range, because $1/R$ and I_e are both proportional to the square of the frequency.

1736: A. van der Ziel: Total-emission damping in diodes (Nature, London, **159**, 675, 1947).

Measurements of the "total-emission damping", which is a transit-time effect due to space charge and occurring at ultra-high frequencies, are carried out at 5.8-m wavelength on a diode (cathode area 10 cm², cathode-anode distance 0.1 cm). The conductive part $1/R$ and the reactive part $\omega\Delta C$ are plotted against V_a (heater voltage 6, 8, 10 and 12 V). It is proved that $\omega\Delta C$ and $1/R$ are proportional to V_a^{-1} and V_a^{-2} respectively. It is to be expected that ΔC does scarcely depend on the frequency and that $1/R$ is proportional to ω^2, except for the highest frequencies.

1737: J. L. Snoek: Gyromagnetic resonance in ferrites (Nature, London, **160**, 90, 1947).

In polycrystalline magnetic ferrites of great homogeneity prepared by the author, the tangent of the loss angle between B and H is found to rise at about 10 Mc/s from values less than 0.01 to values exceeding 1.

At the same time the permeability goes down to very low values. The results are compared with the Landau and Lifshitz theory of gyromagnetic resonance expected to occur in a ferromagnetic dielectric if the frequency of the applied field equals the frequency of precession of the spins around the direction of the internal field. (In Landau's model the specimen is assumed to be a single crystal and the applied field is at right angles to the crystal field). According to Landau

$$\frac{\chi_t \cdot f_h}{I_{\max}} = \frac{\sqrt{2}}{2\pi}\,\frac{e}{mc} = 4 \times 10^6 \text{ cycles/Oe.sec,}$$

(χ_t = transverse susceptibility, f_h = frequency for which the real part of the susceptibility is halved, $I_{\max}$ = saturation magnetisation) whereas for the polycrystalline sample this expression equals $1{\cdot}75.10^6$ cycles/Oe.sec.

The approximate agreement between theory and experiment warrants the conclusion that the rapid decrease of the permeability in ferrites at high frequencies is probably due to gyromagnetic resonance around directions prescribed by the internal field.

1738: E. J. W. Verwey and E. L. Heilmann: Physical properties and cation arrangement of oxides with spinel structures. I. Cation arrangement in spinels (J. Chem. Phys. **15**, 174-180, 1947).

By means of a detailed X-ray study of a large number of oxides having a spinel structure, it has been established whether they crystallize in the "normal" spinel-type structure, XY_2O_4, or in the "inversed" type of structure, $Y(XY)O_4$, discovered by Barth and Posnjak. Certain rules can be derived which are also applicable to more complicated spinels or to solid solutions of different spinel oxides. Madelung constants have been calculated for different spinel types in order to investigate their stability on the basis of an ionic concept of the chemical bond (Born's lattice theory). The experimental results are only partially explainable on this basis. All exceptions to the electrostatic principles can be understood by assuming that Fe^{3+}, Ga^{3+}, In^{3+}, Zn^{2+}, and Cd^{2+} favour a configuration having the coordination number 4, because of a considerable covalent contribution to the chemical bond for that configuration.

For the contents of this paper see also the article by E. J. W. Verwey, P. W. Haayman and E. L. Heilmann, Philips tech. Rev. **9**, 186-191, 1947.

VOL. 3 NR 3 JUNE 1948

Philips Research Reports

EDITED BY THE RESEARCH LABORATORY
OF N.V. PHILIPS' GLOEILAMPENFABRIEKEN, EINDHOVEN, NETHERLANDS

R 78 *Philips Res. Rep. 3, 161-173, 1948*

THE HEAT DISSIPATION IN THE ANODE OF AN X-RAY TUBE

by W. J. OOSTERKAMP

621.386.1.032.22:536.212.1

II. LOADS OF SHORT DURATION APPLIED TO ROTATING ANODES

Summary

The maximum temperatures occurring in the target of an X-ray tube, or in the copper backing behind it, are computed on the same principles as adopted in the first part of the paper, but this time for a rotating anode. It is shown that for short exposures the lateral dissipation of heat may be disregarded. Exposures lasting less than one revolution and lasting several revolutions are separately dealt with. From the resulting formulae the rating capacity is computed as a function of the time of exposure and is found closely to agree with life-test experiments.

Résumé

Les températures maxima apparaissant dans l'anticathode d'un tube à rayons X ou dans le support en cuivre qui y fait suite sont calculées sur les mêmes principes que ceux adoptés dans la première partie de l'article, mais cette fois pour une anode tournante. L'auteur montre que pour des expositions de courte durée, la dissipation latérale de chaleur peut être négligée. Les expositions de moins d'une révolution et celles de plusieurs révolutions sont traitées séparément. Les formules trouvées permettent de déduire la limite de charge en fonction de la durée d'exposition. Elles concordent avec les expériences relatives à la durée des tubes.

4. Loads of short duration applied to rotating anodes

As stated in the first paper of this series ¹), a considerable increase in the rating capacity of an X-ray tube can be achieved by the use of a rotating anode. The construction of this type of tube is shown in fig. 4; it is mainly applied for medical purposes.

Two types of anode are in common use, the one consisting of a tungsten disk several millimetres thick, the other of a thin disk of tungsten backed by a solid body of copper. The theory developed below may be applied to both cases, but in working out a practical example we shall treat only the more complicated bimetallic type of anode.

In one of the regular types of tube the central ray of the X-ray beam leaves the target at an angle of 15°, so that, for the apparent focus to be a square, the actual focus must be a line focus four times as long as wide. Focus widths varying from 0·8 to 2·0 mm are in general use, and for obvious reasons the line focus is placed in a radial direction. The average diameter of the focal path is 38 mm, the number of revolutions 50 per sec, so that the speed of the anode in the focal spot is approximately 600 cm/sec; consequently, a fixed point on the anode is hit by the electron beam during not more than a few ten-thousandths of a second in each revolution. The thickness of the tungsten target in the bimetallic anode is usually 0·5 mm.

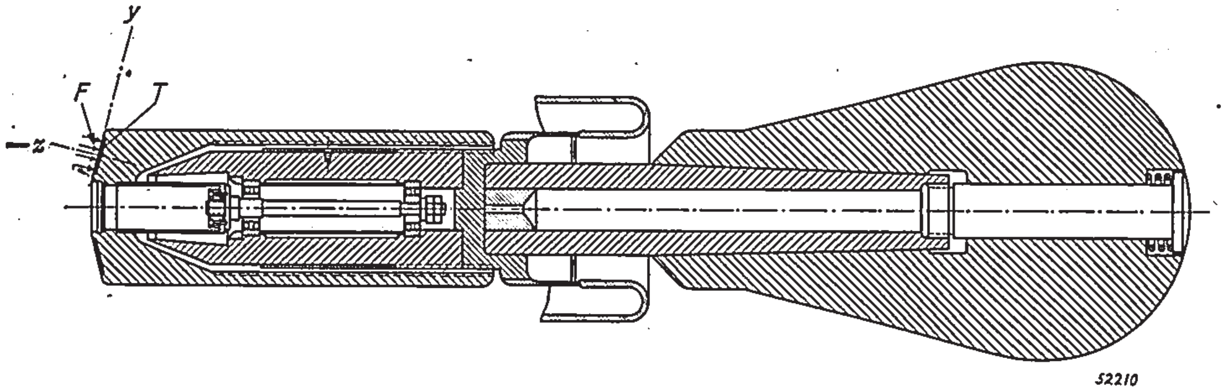

Fig. 4. Sectional view of the rotating anode of a "Rotalix" tube; F = focus, T = tungsten target; z and y indicate the system of coordinates used, the x-axis being perpendicular to the y- and z-axes.

In computing the temperature we shall follow the same methods as in our first paper, again assuming that the energy is homogeneously distributed over the focal area.

A. *Exposures lasting less than one revolution*

For this case the rating capacity has been computed by Bouwers [2]), whose results will briefly be repeated here for the sake of completeness.

To simplify matters we suppose that the anode, instead of rotating, exhibits a translational motion in the x-direction with the speed $v = \pi \nu D$, ν being the number of revolutions per second and D the diameter of the focal path. If 2δ designates the width of the focus, a point on the surface of the target will be hit by the beam during a time interval

$$\Delta t = \frac{2\delta}{v} \tag{14}$$

per revolution.

For stationary anodes, and for exposures less than a few thousandths of a second, we found that the lateral heat dissipation can be ignored.

For the rotating anode this will still hold in the y-direction, the length of the focus being large enough to be regarded as practically infinite. In the x-direction, however, the distribution of temperature is essentially different from that prevailing in a stationary anode; that the lateral heat dissipation may be disregarded here also, requires a separate proof which will be given under heading D of this section.

If the lateral dissipation may be ignored, we obtain the maximum temperature simply from formula (9) by substituting for the time of exposure, t, the time of passage of the beam, Δt, as given by (14); this yields

$$T_m = 2\,W \sqrt{\frac{\Delta t}{\pi k c}} = 2\,W \sqrt{\frac{2\delta}{v \pi k c}} = \frac{2\,W}{\sqrt{\pi k c}} \sqrt{\frac{2\delta}{v \pi D}}. \tag{15}$$

According to this expression the permissible maximum load for less than one revolution is independent of the time of exposure *). If the maximum temperature remains the same, the improvement p in the specific rating capacity relative to a stationary anode, and for an exposure lasting just one revolution, is

$$p = \sqrt{\frac{\pi D}{2\delta}}; \tag{16}$$

or, in words, it is equal to the square root of the ratio of the circumference of the focal path to the width of the focal spot.

B. *The cooling of the focus during one revolution*

Before discussing the problem of exposures lasting several revolutions, we have to study the rate of cooling of the focus during one revolution. We shall first assume that the anode is homogeneous and investigate the temperature distribution in the z-direction.

For any point on the focal path the load is W watts.cm^{-2} from $t = 0$ to $t = \Delta t = 2\delta/v$, and afterwards zero. This load can be regarded as the superposition of a load

W watts.cm^{-2} from 0 to t and
$-W$ watts.cm^{-2} from Δt to t.

Since the heat transfer is in the direction of z only (see under D) the temperature at a distance z from the surface and at the time t may be deduced from equation (10):

---

*) Except of course in the trivial case that the time of exposure is smaller than the time $2\delta/v$, required for the passage of the beam; the anode may then be considered as not moving at all.

$$T_{z,t} = \frac{W}{\sqrt{\pi k c}} \int\limits_{t-\Delta t}^{t} \frac{e^{-\frac{z^2}{4a^2\tau}}}{\sqrt{\tau}}\, d\tau\,. \tag{17}$$

If $t \gg \Delta t$ the integrand may be considered as constant, so that

$$T_{z,t} = \frac{W}{\sqrt{\pi k c t}}\, e^{-\frac{z^2}{4a^2 t}}\, \Delta t\,, \tag{18}$$

or by (15)

$$T_{z,t} = \frac{T_m}{2} \sqrt{\frac{\Delta t}{t}}\, e^{-\frac{z^2}{4a^2 t}}. \tag{19}$$

Consequently, the temperature of a point on the focal path ($z = 0$) and at the end of one revolution ($\Delta t = 2\delta/v$, $t = \pi D/v$) is

$$T_{0,t} = \frac{T_m}{2} \sqrt{\frac{2\delta}{\pi D}} = \frac{T_m}{2p}\,, \tag{20}$$

where p is the relative improvement in rating capacity as given by (16), which depends only on the geometrical dimensions and not on the physical properties of the anode material.

We infer from this equation that the ratio of the highest temperature (just after passage of the beam) to the lowest temperature (at the end of one revolution) is independent of the anode material and the speed of rotation. This may seem surprising, for it might be expected that, when raised to the same maximum temperature, a copper anode would cool down more rapidly than a tungsten anode. But it must be remembered that to raise the copper to the same temperature it is necessary to apply a heavier load; consequently a greater amount of heat penetrates into the copper anode during the passage of the beam, and thereby the rate of cooling is reduced to just the same extent as it is increased by the higher conductivity.

A point on the surface will reach its maximum temperature at the end of the passage of the beam, but a point inside the anode will reach its maximum temperature a little later. For a point a distance z away from the surface we find the time of occurrence of the maximum temperature by equating to zero the derivative of (19) with respect to time. This gives

$$t_{z,m} = \frac{z^2}{2a^2}\,, \tag{21}$$

which, inserted in (19), yields for the maximum temperature itself:

$$T_{z,m} = \frac{T_m a e^{-1/2} \sqrt{\Delta t}}{z\sqrt{2}}\,. \tag{22}$$

For a focal width of 2 mm, fig. 5 shows the temperature-distribution curves computed from (19) at different moments together with their envelope as given by (22). This envelope indicates the maximum temperature that will occur at any depth z behind the anode surface. We see from this figure that 75% of the heat entering during the passage of the beam has, after one revolution, penetrated into the anode to a depth greater than 0·5 mm; that is, to a depth greater than the thickness of the tungsten target. This enables us to estimate the rate of cooling in a bimetallic anode.

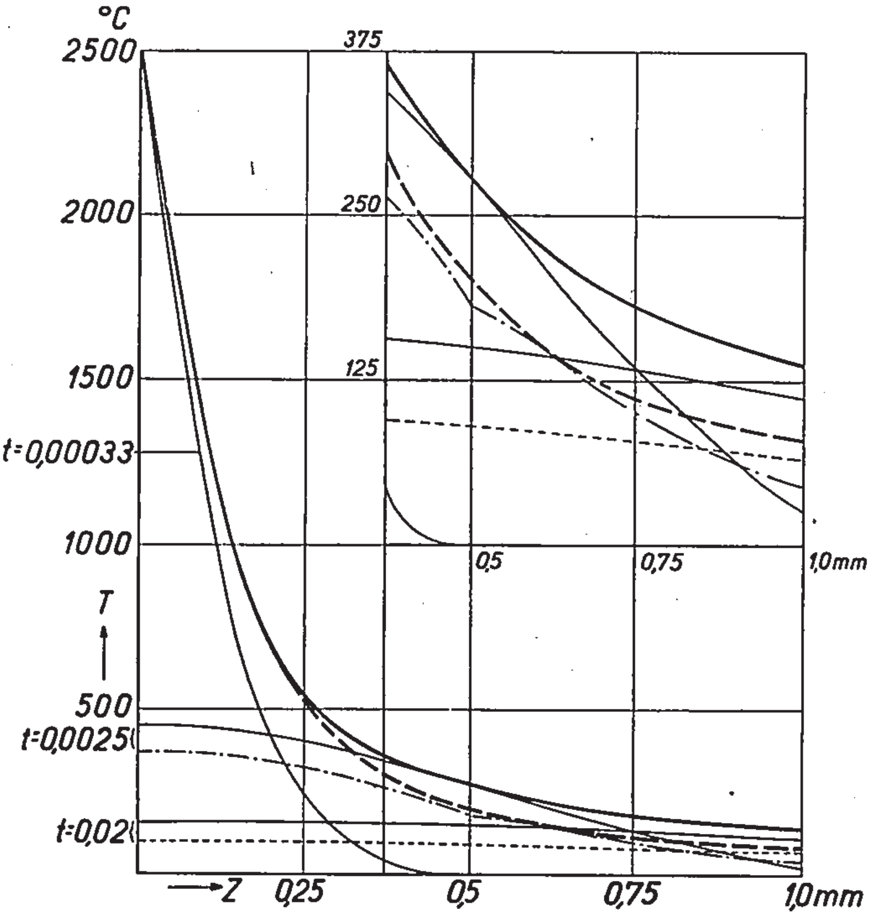

Fig. 5. Temperature distribution in the anode of a "Rotalix" tube, immediately after the passage of the beam, and during the cooling period, the time of exposure being less than one revolution. For $z > 0{\cdot}375$ the curves have been drawn on an enlarged scale in the inset. The solid curves refer to a solid tungsten anode, the dashed curves to a copper anode with a 0·5-mm tungsten target in front. The curves were computed for a focus width of 2 mm and for a load of 40 kW.

During the passage of the beam, the heat will not yet reach the copper backing, and the maximum temperature will practically be the same as with a massive tungsten anode; but at the end of one revolution a major proportion of the heat has passed into the copper, and the temperatures will therefore be approximately those which would prevail in a massive copper anode. Now, for the same power input, all temperatures are by (15) and

(19) lower in copper than in tungsten in the ratio $(\sqrt{kc})_W/(\sqrt{kc})_{Cu}$; hence if T_m is the maximum temperature in tungsten, the surface temperature of the bimetallic anode at the end of one revolution will approximately be

$$\frac{T_m}{2p}\,\frac{(\sqrt{kc})_W}{(\sqrt{kc})_{Cu}} = 0{\cdot}6\;T_m/2p\;{}^{*)}.$$

Thus the copper backing is seen to produce a considerable improvement.

C. *Several revolutions*

So far we have considered the rate of cooling during a single revolution. It follows from the same arguments that, after an exposure lasting less than one revolution and producing a maximum temperature T_m, the temperature after n revolutions will have dropped to

$$T_n = \frac{T_m}{2p}\,\frac{(\sqrt{kc})_W}{(\sqrt{kc})_{Cu}}\,\frac{1}{\sqrt{n}}. \tag{23}$$

Moreover, by considering an exposure lasting several revolutions as a superposition of successive energy pulses, the maximum temperature just before the $(n+1)$th passage of the beam is by addition found to be

$$T = \sum_1^n T_n = \frac{T_m}{2p}\,\frac{(\sqrt{kc})_W}{(\sqrt{kc})_{Cu}}\left\{1 + \frac{1}{\sqrt{2}} + \frac{1}{\sqrt{3}} + \ldots + \frac{1}{\sqrt{n}}\right\}, \tag{24}$$

while at the end of the $(n+1)$th passage of the beam the temperature will be

$$T = T_m\left[1 + \frac{1}{2p}\,\frac{(\sqrt{kc})_W}{(\sqrt{kc})_{Cu}}\left\{1 + \frac{1}{\sqrt{2}} + \frac{1}{\sqrt{3}} + \ldots + \frac{1}{\sqrt{n}}\right\}\right]. \tag{25}$$

For sufficiently large values of n the sum in these equations may be replaced by an integral plus a correction for the first few terms; this gives

$$\sum_1^n \frac{1}{\sqrt{m}} = 2\sqrt{n} - 1{\cdot}4, \tag{26}$$

and for large values of n the constant term on the right may even be neglected without serious error. The maximum temperature of the tungsten target at the end of the $(n+1)$th passage of the beam then is approximately given by

$$T = \frac{2W}{\sqrt{\pi (kc)_W}}\cdot\frac{1}{p\sqrt{v}}\left\{1 + \frac{\sqrt{n}}{p}\,\frac{(\sqrt{kc})_W}{(\sqrt{kc})_{Cu}}\right\}, \tag{27}$$

---

*) Compare the data of table I of the first paper.

and likewise just before the $(n+1)$th passage of the beam we have

$$T = \frac{2W}{\sqrt{\pi (kc)_{Cu}}} \cdot \frac{1}{p^2} \sqrt{\frac{n}{\nu}}, \tag{28}$$

where use has been made of equation (15) expressing T_m in terms of the load W.

These equations refer to the surface temperatures in the tungsten target. For longer exposures the melting temperature of the copper is the limiting factor, and we must now pay closer attention to the temperatures occurring at the tungsten-copper interface.

The maximum temperature in the copper will be reached some time after the electron beam has passed over the corresponding spot on the surface of the target, and during this interval the peak of the temperature pulse is greatly reduced. This is clearly demonstrated in fig. 5; if the tungsten target is 0·5 mm thick, the maximum temperature at the interface will occur about 0·0025 sec (one-eighth of a revolution) after the passage of the beam, and the height of the temperature pulse has decreased from 2500 °C at the target surface to about 200 °C at the interface. After reaching this maximum the copper will cool down to a minimum temperature given by (24); for we see from fig. 5 that at the end of one revolution ($t = 0{\cdot}02$ sec) the heat pulse has been completely smoothed out, so that the temperatures at the surface and the interface are practically the same. Then follows a second pulse with a maximum about 200 °C above this minimum, and so on. Thus the actual temperature at the interface will be fluctuating with an amplitude of 200 °C about a steadily increasing level.

Fig. 5 holds for a load of 40 kW, which raises the target temperature to its permitted maximum in one revolution. For exposures lasting several revolutions the load must be lower and the amplitude of the temperature fluctuations will diminish in proportion; for instance, with a load of 22 kW the amplitude will be 110 °C. For this case the actual temperature at the interface has been plotted in fig. 6 as a function of the time. Curve II in this figure represents the minimum temperatures computed from (24), whereas curve III gives the temperatures as calculated from (28). Since, in deducing (28) from (24), the term 1·4 in (26) has been neglected, the temperatures computed from (28) are too high, as may be seen from the figure. They lie even closer to the maximum than to the minimum temperatures. Hence (28) can be used as a rough approximation of the maximum temperatures occurring in the copper backing. This approximation will be the better, the longer the exposures, for then the permissible load will be lower and the amplitude of the fluctuations correspondingly smaller.

In medical fluoroscopy, rotating-anode tubes are used under a small continuous load on which short heavy pulses are super-imposed when making instantaneous photographs. The energy supplied by the continuous load is dissipated by radiation towards the stationary parts of the anode, and the normal conditions are such that the target and the copper backing may reach an average temperature of about 450 °C. Under these circumstances the permissible maximum rise in temperature during a heavy pulse is 550 °C for the copper backing and 2500 °C for the tungsten target. As for stationary anodes, the rating capacity is limited by the rate of evaporation of tungsten (and hence by (27)) for short exposures, and by the melting of the copper (and hence by (28)) for longer exposures.

From fig. 6 we see, for instance, that the temperature in the copper backing rises 550 °C in about 0·5 sec when the load is 22 kW; for such a load 0·5 sec is the longest exposure that can be safely used.

Curve I in fig. 7 represents the permissible load as a function of the time

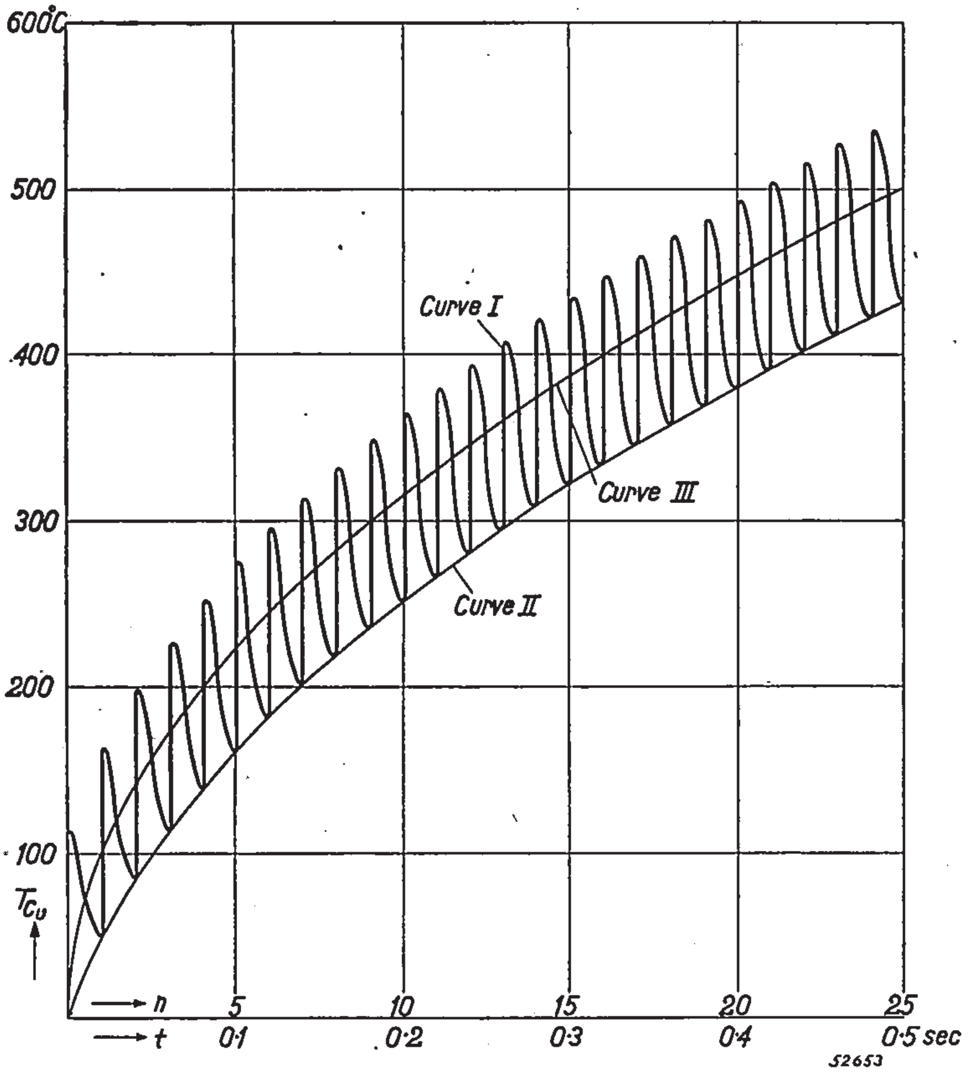

Fig. 6. The temperature at the tungsten-copper interface as a function of time for a load of 22 kW (curve I).
The rise in temperature has reached its permissible maximum of 550 °C after about 0·5 sec.
Curve II: minimum temperatures according to (24).
Curve III: approximate temperatures computed from (28).

of exposure for a focus of 2×8 mm^2 as computed from equations (27) and (28); in performing the computations corrections were applied for the term 1·4 in (26), and for the fact that the copper reaches its maximum temperatures not during the passage of the beam but, according to (21), 0·0025 sec later. Curve II in the same figure gives the permissible load as determined from life tests; the agreement between theory and practice is very satisfactory, though, as we shall see later, the close coincidence between these two curves is too flattering; some corrections, yet to be made, will make the agreement somewhat less favourable.

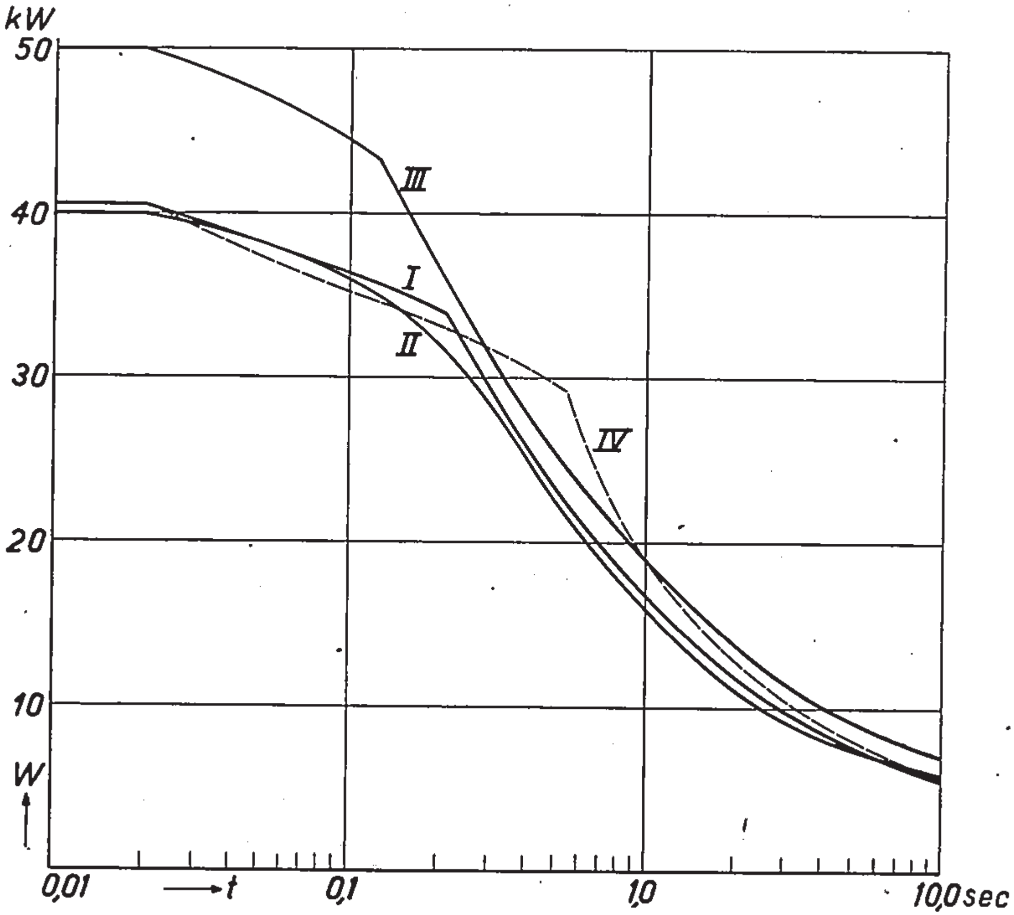

Fig. 7. The rating capacity of a "Rotalix" tube with a focus width of 2 mm, as a function of the time of exposure.
Curve I: computed for a target of 0·5 mm without corrections;
Curve II: deduced from life-test experiments;
Curve III: as curve I but corrected for secondary emission and lateral dissipation;
Curve IV: uncorrected curve computed for a target 2 mm thick.

D. *The influence of lateral dissipation of heat*

If we neglect the lateral heat dissipation, it is easy to compute the temperature distribution along the surface of the anode. Let, at a given moment, the front line of the focal spot be at $x = 0$ and the rear at

$x = -2\delta$. Any point between $x = 0$ and $x = -2\delta$ will have been exposed to the beam during an interval $-x/v$, and its temperature will be given by equation (9) if in it we substitute this value for the time of exposure t; thus we have

$$T = 2W\sqrt{\frac{-x}{v\pi kc}} = T_m\sqrt{\frac{-x}{2\delta}} \quad \text{for} \quad -2\delta \leqq x \leqq 0, \tag{29}$$

in virtue of (15).

In the region $x < -2\delta$ the anode is cooling and for such points we find the temperature by integrating (17) for $z = 0$ and then substituting $2\delta/v$ for Δt and $-x/v$ for t. This gives

$$T = \frac{2W}{\sqrt{\pi kc}}\left\{\sqrt{\frac{-x}{v}} - \sqrt{\frac{-x-2\delta}{v}}\right\} = T_m\left\{\sqrt{\frac{-x}{2\delta}} - \sqrt{\frac{-x-2\delta}{2\delta}}\right\} \quad \text{for} \quad x \leqq -2\delta. \tag{30}$$

As illustrated in fig. 8, equations (29) and (30) yield a temperature distribution with very pronounced temperature gradients at the front and the back of the focal spot, so that it is open to question whether the lateral dissipation of heat can be ignored, as we did so far. To settle this point we have to compute the actual temperature and then to compare it with that computed under the simplifying assumption.

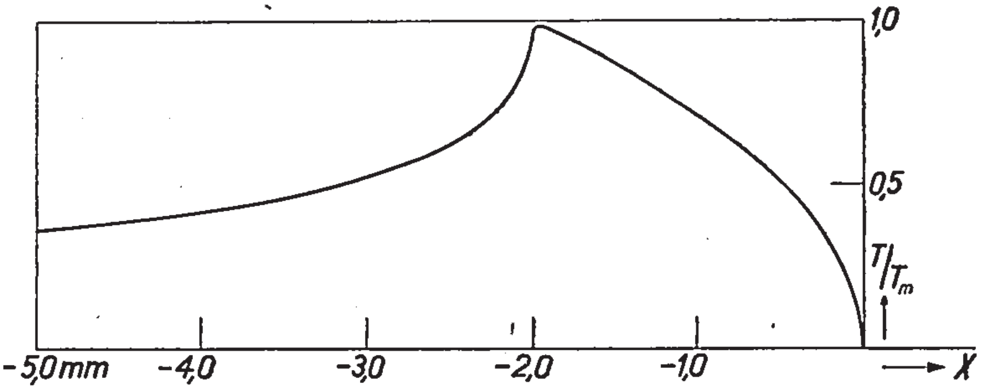

Fig. 8. Temperature distribution over the surface of the target of a rotating-anode tube in the direction of focus width; focus width 2 mm.

When a line focus of infinitesimal width dx inside a homogeneous body is exposed to a load of specific density $2W$ watts per cm² during a short time $\Delta\tau$, the temperature field thereby produced after an interval τ is according to equation (6)

$$dT = \frac{2W\,dx}{4\pi k\tau}\, e^{-\frac{x^2}{4a^2\tau}}\, d\tau, \tag{31}$$

and this expression we shall now have to use. If we consider a moving focus, it is evidently the same whether we compute the temperature distribution at a given instant, or whether we calculate the temperature at a certain point as a function of the time while the beam sweeps over it. Let us therefore consider a moving focus the front line of which passes the point $x = 0$, at time $t = 0$, and let us compute the temperature at $x = 0$ as a function of the time. At the time t the line focus will be located between vt and $(vt - 2\delta)$, and an interval τ earlier than this the focus was between $v(t-\tau)$ and $\}v(t-\tau)-2\delta\{$. If we consider the focus as stationary in this position for an interval $\Delta\tau$ the corresponding contribution to the temperature at time t and at the point $x = 0$ will by (31) be

$$dT = \frac{W}{2\pi k}\,\frac{d\tau}{\tau}\int\limits_{v(t-\tau)-2\delta}^{v(t-\tau)} e^{-\frac{x^2}{4a^2\tau}}\,dx\,. \tag{32}$$

The actual temperature at $x = 0$ is obtained by integrating this expression with respect to τ from $\tau = 0$ to $\tau = \infty$, which yields

$$T = \frac{W}{2\pi k}\int\limits_0^\infty \frac{d\tau}{\tau}\int\limits_{v(t-\tau)-2\delta}^{v(t-\tau)} e^{-\frac{x^2}{4a^2\tau}}\,dx\,. \tag{33}$$

Numerical evaluation of this integral is simplified by the substitutions

$$\frac{x^2}{4a^2\tau} = \xi^2 \text{ and } 4a^2\tau = \sigma,$$

which lead to

$$T = \frac{W}{2\pi k}\int\limits_0^\infty \frac{d\sigma}{\sqrt{\sigma}}\int\limits_{\frac{\left(t-\frac{\sigma}{4a^2}\right)v-2\delta}{\sqrt{\sigma}}}^{\frac{\left(t-\frac{\sigma}{4a^2}\right)v}{\sqrt{\sigma}}} e^{-\xi^2}\,d\xi$$

or

$$T = \frac{W}{2\pi k}\int\limits_0^\infty \frac{d\sigma}{\sqrt{\sigma}}\left[\Phi\left\{\frac{\left(t-\frac{\sigma}{4a^2}\right)v}{\sqrt{\sigma}}\right\} - \Phi\left\{\frac{\left(t-\frac{\sigma}{4a^2}\right)v-2\delta}{\sqrt{\sigma}}\right\}\right]. \tag{34}$$

This expresses the temperature at $x = 0$ at time t when the line focus lies between vt and $(vt - 2\delta)$. As explicit integration of (34) is not possible, a graphical integration has been carried out in a few cases of particular interest. For a focus of 2 mm width the temperature was computed at time $t = 2\delta/v$, that is, just when the entire focus has passed; this temperature was only 3% lower than the maximum temperature calculated from the simpler equation (15). Actually the maximum temperature will occur somewhat earlier, because as we approach the rear boundary of the line focus a certain amount of cooling will take place owing to lateral dissipation. A second evaluation of (34) was therefore carried out for $t = (2\delta/v - 5\cdot10^{-6})$ sec and the resulting temperature was now only 1% lower than the maximum computed without regard to lateral dissipation. This demonstrates that lateral dissipation of heat can, indeed, be ignored.

The explanation is that, owing to the very steep temperature gradient in the z-direction, the effective cross-section of the flow of heat in a lateral direction is so small that hardly any heat passes through it despite the high lateral temperature gradients.

E. *Discussion*

Two important factors have not yet been taken into account.

Firstly the actual area traversed by the focus is 9·6 cm², whereas the cross-section of the anode farther away is 14 cm²; hence there exists a certain divergence in the flow of heat which will play a part especially in long exposures (of the order of 0·5 sec and longer); consequently the actual rating capacity will be higher than that computed from equation (15).

And secondly, as mentioned in section 2, a fraction of the energy in the electron beam — which may amount to 20% — is carried away by the secondary electrons to parts of the anode surface outside the focal area. The rise in the surface temperature during the passage of the beam will consequently be lower than computed, but deeper inside the anode the temperature will mainly be determined by the total influx of heat independent of the actual place of entrance; this factor will therefore mainly be effective in short exposures ($<$ 0·2 sec).

After correcting for these two factors, the rating capacity as a function of the time of exposure will be roughly as shown by curve III in fig. 7. This curve lies up to 20% above the curve obtained from experimental life tests, but since in determining the latter a fairly large safety factor has been adopted, the agreement between theory and practice is in fact rather satisfactory; since, as explained in Part I, the temperature dependence of the thermal properties of the anode materials has been neglected, a closer coincidence between theory and practice can hardly be expected.

With a rotating anode the actual time at maximum temperature is about 50 times smaller than with a stationary anode, and, as a result of this, the permissible maximum temperature may be fixed at a higher value. The limit is no longer set by the rate of evaporation but by the vapour pressure, so that temperatures up to 3250 °K can be used, against not more then 3000 °K with a stationary anode.

Owing to the heavier loads the temperature gradients in the anode, and the strain resulting therefrom, will also be higher, bringing with them more stringent mechanical requirements; these, however, have been found possible being satisfied in practice.

The question as to the optimum thickness of the tungsten target may be settled by the following arguments. It follows from fig. 5 that, when the permissible rise in the temperature of the copper is 550 °C (see under C), the thickness of the tungsten target should not be less than 0·25 mm. And we see from fig. 5 and equation (21) that for this thickness not more than about 5% of the heat generated at the surface penetrates as far as the copper backing, during the passage of the beam. Consequently the copper backing will have no perceptible influence on the maximum temperature, even if the target is as thin as can be tolerated with regard to the temperature in the copper.

At the end of one revolution the heat has, on the other hand, penetrated to such depths that the thickness of the tungsten target will have only a minor influence on the temperature just before the second passage of the beam. This is illustrated by curve IV in fig. 7 giving the rating capacity as a function of the time of exposure, also for a target thickness of 2 mm; at short exposures the rating capacity decreases somewhat more rapidly with the time of exposure than for a target of 0·5 mm; but the downward bend *) in the curve lies at a higher value of t, so that for an exposure of 0·5 sec the thicker target will take a load about 15% heavier than the thinner target. The optimum thickness is not a very critical factor for a stationary anode. The high load applicable to rotating anodes renders them especially suitable for taking photographs of rapidly moving objects, which requires exposures of not more than a few tenths of a second; for this reason a target thickness of 0·5 mm is mainly used in practical tubes.

---

*) This bend occurs at the point where the critical region, limiting the rating capacity, changes from the surface of the tungsten target to the interface tungsten-copper.

Eindhoven, January 1948

REFERENCES

[1]) W. J. Oosterkamp, Philips Res. Rep. **3**, 49-59, 1948.
[2]) A. Bouwers, Physica, 's-Grav. **10**, 125-134, 1930.

R 79 *Philips Res. Rep. 3, 174-190, 1948*

MATHEMATICS AND RADIO PROBLEMS *)

by Balth. van der POL

51:621.396

Summary

Lecture given before the Dutch Mathematical Centre. The author discusses the lack of mutual understanding between technicians, physicists and mathematicians. Other topics dealt with are: the relation between Dirac's delta function and Stieltjes integrals; Hurwitz's determinants characterizing the stability of linear systems; wave equation; diffraction around a sphere (propagation of radio waves); continued fractions applied to filter circuits; non-linear differential equations as related to valve oscillators; modern electrical calculating machines.

Résumé

Sommaire d'une causerie faite au „Mathematisch Centrum" à Amsterdam. L'auteur parle du manque de compréhension mutuelle entre techniciens, physiciens et mathématiciens qui parlent chacun une „langue" qui leur est propre. Y furent traités la fonction δ de Dirac et les intégrales de Stieltjes, le symbole O de Landau, les déterminants de Hurwitz et la stabilité de systèmes linéaires, l'équation d'onde (diffraction de rayons lumineux autour d'une sphère, d'ondes radioélectriques autour de la terre), fractions continues se rapportant à des filtres électriques, équations différentielles non-linéaires de circuits oscillants, machines à calculer modernes.

1. We all know what *Mathematics* is, but *Radio* needs defining. Radio may be regarded as a branch of *Electrotechnics*, which in turn is a branch of *Technology*.

Now technology may be regarded as *Applied Physics* (including *Chemistry*), and we shall therefore consider to-day the relations:

$$\text{Mathematics} \leftrightarrow \text{Physics} \leftrightarrow \text{Technology}.$$

In my thirty years experience of research work I have been struck time and time again by the fact that the mathematician speaks a language different from that of the physicist, and the latter employs a language at variance with that of the technician. This difference in languages seems to me to be one of the obstacles standing in the way of mutual understanding and appreciation.

There is a hiatus between mathematics and physics on the one hand, and between physics and technology on the other, and since technology bears no other relation to mathematics than via physics there are two gaps between mathematics and technology.

---

*) Lecture given before the Dutch Mathematical Centre at Amsterdam on March 15th, 1947. Originally published in Dutch, Simon Stevin, Groningen, 25, 179-198, 1947.

A consequence of this is illustrated by a saying from among mathematical circles (ascribed to Cailey): *"Bessel functions are beautiful functions in spite of their many applications"*, and in Landau's "Vorlesungen über Zahlentheorie" (volume I, page 21) we read: *"Die Zahlentheorie is nützlich, weil man nämlich mit ihr promovieren kann"* (The theory of numbers is useful in that one can master a degree by it.) Moreover, in Hardy's otherwise engaging book "A mathematician's apology", one finds an underestimation of the value of applied mathematics in technology.

On the other hand, from purely technical sources too I have often come across expressions that bear witness of a lack of appreciation of mathematics. Arguments usually culminate in the question: *"What use is it?"*

The difficulty in all this lies in the fact that an interpreter is needed between mathematics and physics and a second between physics and technology. But it is well known that to be an interpreter one must be acquainted more or less with the subject-matter to be interpreted. Unfortunately these two kinds of interpreters are seldom met with.

To give a striking example of the different language used by these groups I would quote something I heard recently in radio-technical quarters: "I have connected a small C across the valve to cut out the whistling from back to front", by which was meant in the language of mathematics that coefficients describing the electrical behaviour of a certain amplifying system gave rise to instability, due to an unintentional coupling term, and that this instability could be neutralized by a certain change in the coefficients corresponding to the application of a capacitor as extra circuit element.

Also the language of the mathematician is occasionally not understandable to the physicist, and ad fortiorem to the technician, as may be illustrated by an example I recently came across in Grave's "Theory of functions of real variables" (New York 1946), in which, on page 168, the author deals from a purely mathematical point of view with the equation

$$\ddot{y} = -g \sin y.$$

He observes that this equation is representative of the movement of a pendulum of unit length, and from his mathematical considerations he deduces the following rule:

$$M>0 \,.\, \varepsilon>0 : \supset : \exists\, \delta>0 \ni : |\eta'| < \delta \,.\, |x| < M \,.\, \supset \,.\, |y\,(x, 0, \pi, \eta') - \pi| < \varepsilon .$$

But as a further explanation (perhaps somewhat reluctantly) he adds: *"This means that the pendulum will remain within an angular distance ε of the vertically upward position for M units of time, provided its initial velocity is sufficiently small"*, a conclusion that the physicist and even the technician could give at once in simple language and without mathematics.

Another recent and striking example of the difference in language between the physicist and the mathematician, which is also expressed in the notation, is found in the employment in physics of the delta function of Dirac:

$$\delta(x).$$

The physicist says: "This is a function having the characteristic of being everywhere zero except at the point $x = 0$, where it becomes so infinite that its area is equal to unity". The integral property

$$\int_{-\infty}^{\infty} f(x - \xi)\, \delta(\xi)\, d\xi = f(x),$$

whereby this function $\delta(x)$ extracts, as it were, from this integral the value of the function $f(x)$ at a sharply determined point of the integration interval (here $\xi = 0$), led the physicist to name the function $\delta(x)$ a *pincette function*. The (strict) mathematician, however, argues, and quite rightly, that in his concept of functions there is no place for this delta function, thereby denying its existence. But the mathematician has no qualms about writing down the following Stieltjes integral:

$$\int_{-\infty}^{\infty} f(x - \xi)\, dU(\xi) = f(x),$$

in which

$$U(x) = \begin{cases} 1, & x < 0, \\ \frac{1}{2}, & x = 0, \\ 0, & x > 0, \end{cases}$$

thus a function showing a discontinuity at $x = 0$.

To my mind this is nothing else than writing the same thing in two different ways, to which I add that, when the impulse function is first carefully defined, for instance as

$$\delta(x) = \lim_{\varepsilon \to +0} \frac{1}{\pi} \frac{\varepsilon}{x^2 + \varepsilon^2},$$

and then one takes into account the right order in which the limit transition $\varepsilon \to +0$ and the integration have to be performed, all reasonable requirements of rigour are fully satisfied.

Generally speaking, as a consequence of using different languages, the one scientist has little knowledge of the domain of the other. For instance, the technician thinks that the mathematician works in absolutely unnecessary abstractions, whilst on the other hand some mathematicians have the impression that technology is represented by very high transformers which one does not approach too closely for fear of being struck dead, or, where they are in oil, for fear of dirtying one's fingers.

2. Just as his language, the mathematician's way of thinking differs greatly from that of the physicist or the technician. Naturally the physicist (or technician) thinks in more concrete terms, whilst the mathematician is more abstract. The latter will always tend to generalize his concepts and hypotheses further and further, regardless of whether his symbols or concepts have also concrete applications in physics or technology. It is in this sense that one must understand the words of the mathematician-philosopher Bertrand Russell, who said something like this: "*A mathematician is never so happy as when he does not know what he is talking about*".

On the other hand there is an expression used by Lord Rutherford, who, himself not mathematically minded, jokingly remarked when faced with a mathematical problem: "*We must give this problem to a tame mathematician in a cage*".

As a consequence of the more concrete manner of thinking of the physicist compared with the mathematician, the former is more graphically minded than the latter, of which fact I will give some typical examples. Watson's famous classical work "Bessel functions" contains 804 pages. In the compilation of that book (I quite well remember that he was working on it in Cambridge 30 years ago) he dared to avail himself of mechanical calculating machines for working out numerical values of Bessel functions, which are given in 90 pages of tables at the end of the book. But not a single graphical representation of even one Bessel function is to be found in the whole book. The only illustrations contained in it concern contour integrations.

Hobson goes still further, for in his book of 500 pages on "Spherical and Ellipsoidal Harmonics", there is not a single numerical table, let alone graph, of his functions.

Finally, an example of this is to be found in the seven heavy volumes "Arithmetik, Algebra und Analysis" of the "Enzyklopaedie der Mathematischen Wissenschaften", which in all comprise 5000 pages. Except for two articles on numerical methods and calculating machines, we find on the other 4500 pages only 25 illustrations, which amounts to one illustration per 180 pages.

Sharply contrasted with this is the book of Jahnke & Emde, "Funktionentafeln", which is intended more for the physicist and technician. In the latest edition one finds not only functions commonly applied in physics and technology but also, for instance, Riemann's zeta function. Of all these functions two-dimensional graphs are given, or, where three variables are concerned, the two-dimensional projections of three-dimensional bodies. The mathematician will argue that a two-dimensional graph of a function can only be given, for instance, for the real values of the argument, but in Jahnke & Emde's work several graphs are to be found in which the modulus of the function of a complex argument is represented by means of contours. Such representations undeniably say much more to the physicist than to the mathematician, although not infrequently the latter (maybe without fully admitting it) appreciates a graphical representation for its great heuristic value; instances are to be found in Felix Klein and, more recently, in the number-theorist Viggo Brun.

I should now like to say something about the O and o symbols introduced by Landau. It is known that $f(x) = O(x^{1/2})$ for $x \to \infty$ means:

$$\overline{\lim_{x \to \infty}} \left| \frac{f(x)}{x^{1/2}} \right| < A,$$

in which A is a constant. And on the other hand it is known that $f(x) = o(x^{1/2})$ is a short way of writing for

$$\overline{\lim_{x \to \infty}} \left| \frac{f(x)}{x^{1/2}} \right| = 0.$$

Particularly Titchmarsh, for instance where he deals with Riemann's zeta function, employs these symbols extensively. This zeta function is defined as:

$$\zeta(s) = \frac{1}{1^s} + \frac{1}{2^s} + \frac{1}{3^s} + \ldots,$$

which Dirichlet series is convergent only for $\mathrm{Re}\, s > 1$, so that this series represents the function in the shaded part of fig. 1.

The zeta function, however, can analytically be continued over the whole complex plane and it can thereby be demonstrated that it has a pole at $s = 1$ and zeros at $s = -2, -4, -6, \ldots$, but in 1857 Riemann conjectured

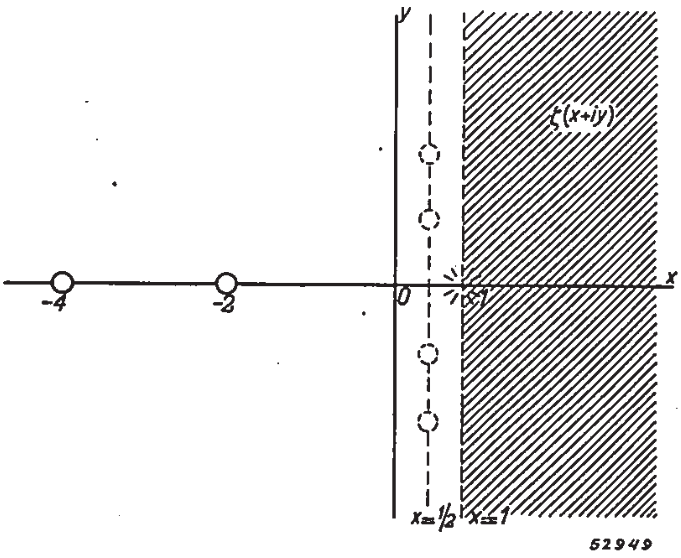

Fig. 1

that *all* other (so-called non-trivial) zeros are situated on the line Re $s = \frac{1}{2}$ (see fig. 1), which famous conjecture has up to the present day neither been proved nor disproved.

Shortly before the war Titchmarsh condescended to attempt to calculate by simple numerical means as many zeros as possible. He did actually find all these to lie on the line Re $s = \frac{1}{2}$. Upon re-reading his articles one is struck by the fact that although he started with Landau's O and o notations he soon had to drop them for the sake of the numerical calculation. This is probably one of the reasons why the physicist is not by any means so familiar with these Landau symbols as is the mathematician.

3. Although in recent times mathematics, physics and technology have mostly followed their own ways, it is interesting to note how in the course of time these sciences have stimulated and fructified each other. Sometimes one sees how theory leads to experiment and often also how experiment leads to the formulation of new theories. Without any attempt at completeness I would like to quote a few typical cases.

One will remember how Faraday, working entirely alone in the Royal Institute in Albemarle Street in London, developed the fundamentals of the science of electricity, his researches being crowned with the famous law of induction. It is most remarkable that he set to work absolutely experimentally and that all his results, visualized in three-dimensional space, were represented without any formulae. Then Maxwell arrived on the scene and translated Faraday's ideas into the language of mathematics; at first, however, without employing the vector notation, which was not introduced into the field of electricity until some time later, by Heaviside and Lorentz.

I may not say, therefore, that Faraday represented his results for the electric and magnetic forces in the free ether in the mathematical form:

$$\operatorname{curl} \mathbf{E} = -\frac{1}{c}\dot{\mathbf{H}},$$

$$\operatorname{curl} \mathbf{H} = \frac{1}{c}\dot{\mathbf{E}},$$

$$(\operatorname{div} \mathbf{E} = \operatorname{div} \mathbf{H} = 0)$$

but I do believe that Faraday adjudged aright the relations expressed by each of these equations and was able to interpret them in words. But it was not until Maxwell had written the deeper views of Faraday in terms of mathematical language that it was possible by purely mathematical means to eliminate one of the variables **E** or **H**, when it was suddenly discovered that both the vector **E** and the vector **H** satisfy the wave equation

$$\Delta u = \frac{1}{c^2}\ddot{u} \qquad \left(\Delta = \frac{\partial^2}{\partial x^2} + \frac{\partial^2}{\partial y^2} + \frac{\partial^2}{\partial z^2}\right).$$

It is undoubtedly beyond human power to realize this process of elimination without mathematical symbols, though in principle it should be possible.

Thus Maxwell was able to arrive at the conclusion that electromagnetic waves exist; to achieve this result without mathematical symbols would have been beyond human possibility.

In this connection it is interesting to note the following citation from a letter written by Faraday to Maxwell in 1857: "*There is one thing I would be glad to ask you. When a mathematician engaged in investigating physical actions and results has arrived at his conclusions, may they not be expressed in common language as fully, clearly, and definitely as in mathematical formulae? If so, would it not be a great boon to such as I to express them so? — translating them out of their hieroglyphics, that we also might work upon them by experiment. I think it must be so, because I have always found that you could convey to me a perfectly clear idea of your conclusions, which, though they may give me no full understanding of the steps of your process, give me the results neither above nor below the truth, and so clear in character that I can think and work for them. If this be possible, would it not be a good thing if mathematicians, working on these subjects, were to give us the results in this popular, useful, working state, as well as in that which is their own and proper to them?*" *).

The thoughts expressed in the above passage hold good just as much to-day as they did in 1857.

It was not until 1886 that Heinrich Hertz, stimulated partly by a problem set by Von Hemholtz based on the Maxwell theory, demonstrated the existence of electromagnetic waves in the laboratory. As everyone knows, this gave birth to wireless telegraphy and telephony, but what is perhaps less well-known is the fact that only a few weeks before he found electromagnetic waves Hertz had discovered the photo-electric effect forming the basis of present-day television.

Another instance where physics (or astronomy) has led mathematics to bear fruit is to be found in a treatise by Laplace (1789) on the rings of Saturnus, where for the first time we come across the potential equation $\Delta u = 0$. This equation, when necessary extended to more dimensions and written in other than rectangular coordinates, gives rise to the study of all kinds of mathematical functions with very interesting properties. When in this equation, extended to more dimensions, u is taken periodic in one of the independent variables, it leads to the wave equation

$$(\Delta + k^2)\, u = 0\,,$$

from which an extensive collection of functions has arisen. It seems to me, therefore, more desirable not to study, say, the Bessel functions or the spherical harmonics one for one, but to evolve them together from the wave equation, upon which the mutual relation — which in essence comes to the same thing as a Fourier transform — presents itself in all clarity.

---

*) Maxwell's answer to this letter is not known to me.

Another example in which experiment and theory go closely hand in hand is to be found in the discovery of the Zeeman effect, for which Lorentz immediately found a theoretical interpretation, with the consequence that the Nobel prize was awarded to these two Dutchmen jointly.

On the other hand it is interesting to note that Riemann's non-Euclidean geometry in abstracto was already complete when Albert Einstein, following up Lorentz's special relativity theory, formulated his general theory of relativity, so that the materials for his structure were all ready to hand. Equally fortunate was Schrödinger, whose considerations on wave-mechanics were crystallized in the equation named after him, though he found all the preparatory work as regards the theory of the characteristic functions and values in boundary-value problems worked out by Courant and his school.

Finally in this connection I would draw attention to a technical problem which has led to a purely algebraic theorem. The turbine engineer Stodola had encountered difficulties in his experiments from unexpected instabilities causing vibrations, whereupon he put to the mathematician Hurwitz the question (formulated in mathematical terms): what conditions must the coefficients in the nth-degree equation

$$a_0 z^n + a_1 z^{n-1} + \ldots + a_n = 0$$

satisfy in order that the real part of all roots shall be negative?

Hurwitz's answer *) to this technical question was that all determinants D_k had to be positive ($k = 1, 2, \ldots, n$), where

$$D_1 = a_1, \qquad D_2 = \begin{vmatrix} a_1 & a_0 \\ a_3 & a_2 \end{vmatrix}, \qquad D_3 = \begin{vmatrix} a_1 & a_0 & 0 \\ a_3 & a_2 & a_1 \\ a_5 & a_4 & a_3 \end{vmatrix},$$

$$D_n = \begin{vmatrix} a_1 & a_0 & 0 & 0 & \ldots & 0 \\ a_3 & a_2 & a_1 & a_0 & \ldots & 0 \\ a_5 & a_4 & a_3 & a_2 & \ldots & 0 \\ \cdot & & & & & \\ \cdot & & & & & \\ \cdot & & & & & \\ a_{2n-1} & a_{2n-2} & & & \ldots & a_n \end{vmatrix} \qquad (a_s = 0 \text{ when } s > n).$$

---

*) Math. Ann. 46, 273 (1895). Routh, in a treatise on the stability of motion had already, treated this problem (1877), but he did not give his results in the elegant form of determinants that is due to Hurwitz.

This criterion for stability is not infrequently applied in modern radiotechnics.

4. I would now claim your attention for a moment to speak of the application of mathematics in industry. Under industry we have to distinguish: (a) the factory, which has to turn out the products to be sold; behind that is (b) the works laboratory, where the products are developed from ideas, which ideas are first developed by (c) the research laboratory. I am, therefore, entirely in agreement with what I once heard in a lecture at Sydney: "*The output of a research laboratory should be thoughts rather than things*".

The applications of mathematics in the factory, the works laboratory and the research laboratory differ widely. Its application by the production engineer is usually confined to adding, subtracting, multiplying and dividing (being on his guard against dividing by zero). The development engineer makes a wider use of mathematics, often in the form of ready formulae — for instance for the self-inductance of a coil — taking care to use the right units in his practical working out of the formulae (for he, too, has to be careful). But he may run past himself in another respect, since the formulae he uses are often ready-made in a form that enables him to work with a slide-rule — these formulae should not contain, for instance, mathematical functions like elliptic integrals, because usually he has neither the time nor the inclination to study such abstract matters. Now it so happens, unfortunately, that with the approximative formulae he frequently employs, the conditions under which the approximations have been derived are not indicated, so that he runs the danger of going beyond the range for which his formulae are valid, with the result that the whole matter may become hopelessly confused.

I once came across a typical example of how a development engineer regards mathematics. The engineer in question told me that he had on his desk a wooden ruler with two marks on it. When one of his subordinates came to him with a theoretical result he always measured the formula placed before him to see that it did not extend beyond the marks on his ruler. If it did, then he sent the man back to simplify his formula.

A recent example of the use of mathematical theory, taken from the latest development of radio technique, is to be found in the new broadcasting system termed frequency modulation, in contrast to the old system of amplitude modulation.

In the old system the amplitude of the electromagnetic wave transmitted is made a linear function of the momentary sound pressure in front of the microphone, whilst everything is done to avoid the zero passages being affected. With frequency modulation it is just the other way round. With this system the amplitude of the waves transmitted is kept strictly constant, while the density of the zeros taken as an average over a certain time is varied linearly with the sound pressure on the microphone. Now unfortunately most of the formulae learnt by the engineer or physicist in the Technical College or University for tackling ordinary alternating-current problems suddenly lose all their practical utility with the innovation of frequency modulation. They include all those problems with a purely periodic second member (represented by $e^{i\omega t}$) in his linear differential equations with constant coefficients, and with which he had mastered the concepts of complex impedance and admittance only after a great deal of trouble. The engineer or physicist therefore has to start all over again, not just where his studies left off but right where they began. That is to say, the whole theory has to be built up anew from the original differential equations, and all theoretical rules plus many of the practical rules that served him so well for amplitude modulation (never thinking of writing down the differential equation again) have become superfluous [1]). If nowhere else, then the wise words of Boltzmann certainly apply here: "*Es gibt nichts Praktischeres als eine gute Theorie*" (There is nothing more practical than a good theory).

Another recent radio development, which played such a great part in the war, is Radar. For one millionth part of a second, radio waves are transmitted on a wavelength of a few centimetres, antennae being used that beam the rays sharply, much like a searchlight. The radio beam is directed, for instance, upon an invisible enemy aircraft flying above the clouds and this aircraft sends back a radio echo of the waves to the transmitter, the direction of maximum reflection indicating the direction of the aircraft; the time interval between transmission and reception of the echo gives a direct measure of the distance, thereby determining the position of the aircraft in space.

The technique of radar had to be developed during the war in the shortest possible time. A Radiation Laboratory was established for the purpose at Cambridge (Mass.) where a thousand and more mathematicians, physicists and technicians were set to work. I was told that the proportion of theorists to experimentalists was originally 1 : 25, but the director, Dr Rabi, said that if he had to undertake such work again he would choose a proportion of 1:4, thus indicating how the war has contributed towards a much greater appreciation of the work of the theorist (also in government and other services).

Working at the same place was Prof. Van Vleck, who on theoretical grounds had predicted that for electromagnetic waves, water vapour in the atmosphere would cause selective absorption for waves of $\lambda = 1{\cdot}3$ cm, and that the oxygen would show such an absorption band at $\lambda = 0{\cdot}5$ cm, which subsequently was fully confirmed experimentally. In order to detect low-incoming aircraft at the greatest possible distance, the radar wavelength was reduced more and more, but, so Prof. Van Vleck told me, in the enemy camp they wrongly expected a resonant frequency for $\lambda \approx 10$ cm, an error that was fatal for radar development in Germany.

Many theorists were also engaged in the research work on the atomic bomb under the theorist Oppenheimer, and in the leading circles, as I was given to understand, the proportion of theorists to experimentalists was 1 : 1.

5. I would now like to say something about the application of specific parts of mathematics in technology in general and in radio technique in particular.

When a physical problem has to be worked out, the first data sometimes come from the experimentalist, who gives the results of his findings in physical terms (first stage). In the second stage the physical results have to be translated into mathematical language, and this is something that the mathematician is not usually capable of doing owing to his inadequate physical knowledge, but the physicist that is somewhat theoretically minded succeeds in doing so. The third stage is the solution of the mathematical problem, and this is something that usually neither of them can do because the mathematical problem in its generality is too difficult. Then (fourth stage) an attempt has to be made to cast out as many of the variables contained in the problem as can be ignored without losing the essence of the effect sought. This calls for a fine power of discernment, such as is so often needed in science as well as in technology. When the mathematical problem with all non-essential elements eliminated, has been reduced to its simplest form, then there is some chance of its solution representing something of value.

In this modus operandi a mathematical question arises to which hitherto, so far as we can ascertain, in its generality not much mathematical attention has been paid, namely the consequence of ignoring terms or parameters of differential equations, particularly in regard to the solution for large values of the independent variable, the whole being regarded as an initial-value problem.

Another not infrequently neglected gift that the mathematician presents to the physicist concerns the second root of a quadratic equation, whilst the physicist is used to basing his arguments on one root. There is of course no doubt that a proper introduction of a second root gives a deeper and a sharper insight into a problem both mathematically and physically.

Further, the mathematician regards it as a matter of course that, when a mathematical expression for physical phenomena shows poles, the first question occurring to the physicist should be what these poles physically mean, a question that, as we know from experience, is sometimes disregarded in physical circles.

Particularly in regard to radio technique it may be said that, apart from ordinary three-dimensional considerations, there are times when also n-dimensional problems and higher geometry play a part. For instance one sometimes comes up against topological questions in connection with the general network theory [2]).

It also sometimes occurs in this theory (particularly in regard to four-poles) that a non-Euclidean treatment provides some simplification [3]).

Finally, the propagation of waves through the ionosphere, having regard to the earth's magnetic field, could be interpreted with the aid of non-Euclidean geometry.

As already stated, physicists and technicians often show more interest in the properties of special functions than mathematicians do. Whether this is the reason why that excellent book on "Modern Analysis" by Whittaker and Watson is better known, in this country, in physical and technical circles than among mathematicians, I dare not say, but it is a fact beyond doubt.

Further, the work of serious radio researchers necessarily involves problems concerning the theory of complex functions, both in connection with linear networks and in respect to the theory of potentials, and also in other fields. Moreover, in his work the radio researcher often employs Bessel functions and spherical harmonics, but Mathieu functions (and Lamé functions) also occur. The whole of the modern theory of frequency modulation, which I have already mentioned, is in fact closely related to the theory of Mathieu functions.

It may not be suspected, although it is true, that in some radio problems of the present day (and technical developments thereof) certain decidedly not superficial ideas of the theory of numbers present themselves (in spite of the statement by Landau already quoted).

The fact that the theta functions of Jacobi can be used to advantage in problems concerning crystal structures will not surprise the initiated.

It goes without saying that the wave equation

$$(\Delta + k^2)\, u = 0$$

is fundamental for all matters concerning the propagation of periodic electromagnetic waves. This branch of mathematics, which connects as it were the radio transmitter to the radio receiver, is much more fundamental for radio technique than is often suspected even in radio-technical circles. Quite recently an attempt was made to draw up a new plan of broadcasting wavelengths for long and medium waves for the whole of Europe to improve the chaotic conditions brought about by the war, extensive use being made of the following mathematical problem: it was required to solve the wave equation for the propagation of waves around a sphere (the earth) of a given dielectric constant ε and conductivity σ, such as to satisfy the known Maxwell boundary conditions on the surface of that sphere. Further, the solution had to possess a singularity behaving as $1/r$ at a point outside the sphere at a height h (position of the transmitter). When this problem has been solved generally, one is able to calculate the field of a transmitter at any other point at an angular distance ϑ and height h_2 above the earth's surface. In this problem the atmosphere may be taken to be homogeneous or not. The simple case of a homogeneous atmosphere already leads to an infinite series of spherical harmonics, in each term of which a coefficient occurs that, properly counted, contains eight Bessel functions [4]):

$$\Pi_{\text{tot}} = \frac{e^{ik_1R_1}}{ik_1R_1} + \sum_{n=0}^{\infty} (2n+1)\, R_n \frac{\psi_n(k_1a)}{\zeta_n^{(1)}(k_1a)}\, \zeta_n^{(1)}(k_1b)\, \zeta_n^{(1)}(k_1r)\, P_n(\cos\vartheta), \quad (r > a)$$

in which

$$\zeta_n^{(1)}(x) = \sqrt{\frac{\pi}{2x}}\, H^{(1)}_{n+1/2}(x),$$

$$\zeta_n^{(2)}(x) = \sqrt{\frac{\pi}{2x}}\, H^{(2)}_{n+1/2}(x),$$

$$\psi_n(x) = \sqrt{\frac{\pi}{2x}}\, J_{n+1/2}(x),$$

$$R_n = \frac{-\left[\dfrac{1}{x}\dfrac{\mathrm{d}}{\mathrm{d}x} \ln \{x\psi_n(x)\}\right]_{x=k_1a} + \left[\dfrac{1}{x}\dfrac{\mathrm{d}}{\mathrm{d}x} \ln \{x\psi_n(x)\}\right]_{x=k_2a}}{\left[\dfrac{1}{x}\dfrac{\mathrm{d}}{\mathrm{d}x} \ln \{x\zeta_n^{(1)}(x)\}\right]_{x=k_1a} - \left[\dfrac{1}{x}\dfrac{\mathrm{d}}{\mathrm{d}x} \ln \{x\psi_n(x)\}\right]_{x=k_2a}},$$

r and ϑ coordinates of the sphere, a = radius of the earth,

$$k_1{}^2 = \frac{\omega^2}{c^2}, \quad k_2{}^2 = \frac{\varepsilon_2\omega^2 + i\sigma_2\omega}{c^2},$$

$H^{(1,2)}_{n+1/2}$ = Hankel functions, $J_{n+1/2}$ = Bessel functions, P_n = Legendre polynomials, $b - a = h_1$, $r - a = h_2$.

The foregoing series appears to oscillate, so that the successive terms approximately compensate each other. The greatest contribution lies in the terms whose order is equal to the ratio of the circumference of the sphere to the wavelength used, which ratio is for all practical radio problems a very large number.

One succeeded in mastering this series numerically to a sufficient degree of approximation for practical use, so that for this particular technical problem graphs could be made which were used as basis for the European broadcasting scheme.

It is interesting to note that while this theoretical problem was being worked out a new theory of the rainbow was incidentally discovered, from the similarity of electromagnetic waves (sun light) falling on small spheres (rain drops), the circumference of these drops likewise being large relative to the wavelength. Some new polarization phenomena of the rainbow which this theory produced were verified experimentally by optical means.

It frequently occurs that, once a link has been found between a certain part of mathematics and physics or technology, already existing abstract mathematical work can directly be translated into physical or technical terms. I came across an example of this — not in itself of importance — some time ago in Perron's "Kettenbrüche", where the author deals with linear transformations of the elements of a continued fraction that leave the value of the fraction invariable. When the continued fraction is interpreted as a "filter" (a one-dimensional continuous series of electrical networks) these transformations are directly translatable as the known star-delta transformation of the electro-technician.

An important application of mathematics occurring almost daily in deeper radio research is the Laplace transformation, which, for instance in the form given to it by Heaviside for all transient phenomena in linear networks, leads to by far the simplest method of calculation. In the course of time these transient phenomena have become more and more important in electrotechnics, especially so with the advent of television and culminating in the modern theory of radar technique.

But it is not only the *differential* equations which the ratio investigator comes up against, for also *difference* equations and *integral* equations frequently occur. For instance, the problem of the radiation from a simple cylindrical wire (the simplest form of antenna) was reduced by Hallén to an integral equation; although a great deal of work has recently been done in various quarters in an attempt to solve this problem (i.e. to calculate the radiation of a cylindrical antenne) [5]), it cannot yet be said that this fundamental radio question has been absolutely mastered.

As in many other techniques, arithmetical methods are much used also in radio technique, considerably facilitated by mechanical calculating machines. The modern electrical calculating machines as developed during the war (for instance the ENIAC) promise to be of great assistance in the future. It is important to note that in the course of discussions on methods of building these machines so as to minimize the number of operations to reach a given mathematical result, the question has again arisen whether the decimal system so keenly advocated by Simon Stevin is really the most suitable. Voices are raised in favour of a return to the binary system.

Leibniz seems to have employed this system already for the multiplication of two large numbers because it makes it simple to write down the partial products owing to the occurrence of only the digits 1 and 0.

Finally I would draw your attention to the mathematical method of dealing with another radio problem: how does a retroactive triode cause a simple electric circuit to oscillate?

In 1920 I was able, by ignoring all secondary phenomena, to crystallize this perhaps most fundamental of all modern radio problems into the following, non-linear differential equation [6]:

$$\ddot{v} - \varepsilon\,(1 - v^2)\,\dot{v} + v = 0,$$

in which the constant $\varepsilon > 0$, and the dots signify differentiation with respect to time, whilst v is the voltage across the oscillator circuit.

This apparently so simple equation has since been the subject of at least one hundred papers and books. Particularly from Russian and French quarters, and more recently also from America, important contributions have been made both from technical-physical and from mathematical circles, including the case in which the equation is not homogeneous but contains a periodic second member. So far no one has succeeded in transforming the solution into known functions [7]). The properties of the solutions are so interesting, as proved partly theoretically and partly experimentally, that the investigations have indeed been worth while.

A certain phase of this subject was concluded a few months ago by highly important investigations carried out by Miss Cartwright and Littlewood [8]).

If may be of historical importance to note that this equation was originally worked out for the technical problem mentioned, where ε was assumed to be small. But in 1926, purely as a matter of mathematical interest, we asked ourselves whether this equation also led to interesting results in cases where ε is large, and this disclosed the theory of *relaxation oscillations*, where the period of the periodic phenomenon is no longer given by $\sqrt{LC}$ (L = self-inductance, C = capacitance) but by a typical relaxation time such as RC (R = resistance). As fig. 2 shows, in the latter case the solution is far from sinusoidal, having sharp assents and sharp descents.

It would lead me too far into details, to go further into the consequences of this theory. Suffice it to say that from it there has crystallized a new theory of the rhythm of the human heart, with applications to hitherto still unknown irregularities, whilst all sorts of vibration phenomena could be predicted both theoretically and experimentally, phenomena that upon the arrival of television could be immediately applied thereto.

This problem has landed us in the domain of non-linear differential equations, a domain in which, from the purely mathematical aspect, exceptional difficulties are often involved. This is the very reason why, in my opinion, there are still undisclosed in this domain a number of effects that are difficult to prophesy just because the theory is so difficult. The said equation was one of the first to be graphically integrated with Bush's Differential Analyzer (which perhaps might better be named "integrating synthesizer"), and I was gratified to learn that in Philadelphia they have now become so familiar with it in practice that it is being used, inversely, as a standard test for verifying the Bush machine.

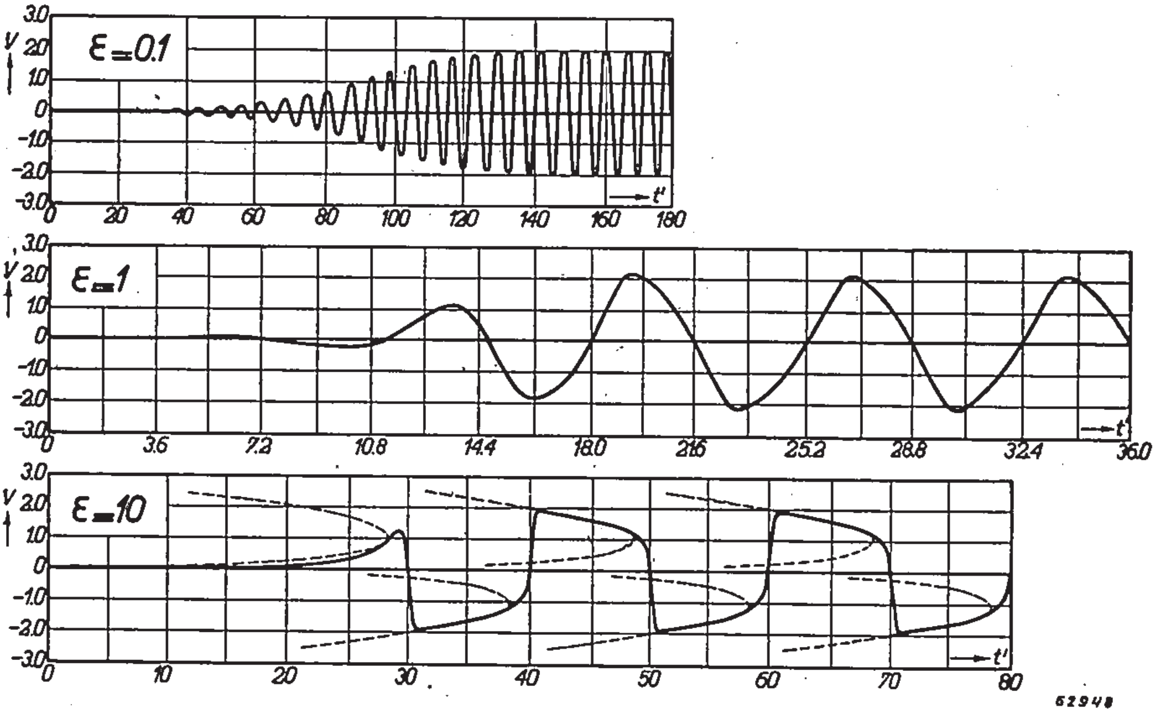

Fig. 2

I have now given you a brief and in many respects incomplete exposé of my views on the relations between mathematics and physics, technology and radio.

As repeatedly pointed out, the fact that the mathematician, the physicist and the radio expert use different languages is partly the reason for the lack of mutual appreciation between these three groups.

It seems to me, therefore, most fortunate that the Centre for Mathematics has been established, in Amsterdam, an institution concerned not only with mathematics pure but also with its applications, so that as such it can undertake the role of interpreter.

It will afford me great pleasure if my lecture may have contributed towards giving mathematicians an insight into the theoretical problems arising in radio, a field still pregnant with fine problems awaiting solution and in which, as I hope to have demonstrated, so many branches of mathematics can lend a helping hand.

In conclusion, the technical problems may well provide fresh stimulants, as they have often done before, for that beautiful science of ours, Mathematics, the pure aesthetical side of which is often insufficiently appreciated.

Eindhoven, March 1947

REFERENCES

1) F. L. H. M. Stumpers, Some investigation of oscillations with frequency modulation, Thesis, Delft, 1946; in Dutch.

2) Cf. B. D. H. Tellegen, Geometrical configurations and duality of electrical networks, Tijdschr. Ned. Radiogenootschap, **9**, 37-40, 1941; in Dutch.

3) J. van Slooten, Geometrical considerations regarding the theory of electrical fourpoles, Thesis, Delft, 1946; in Dutch.

4) Balth. van der Pol and H. Bremmer, Phil. Mag. **24**, 141-176, 1937.

5) Cf. C. J. Bouwkamp, Physica, 's-Grav. **9**, 609-631, 1942.

6) Balth. van der Pol, Tijdschr. Ned. Radiogenootschap **1**, 1-31, 1920.

7) Cf. N. G. de Bruijn, Philips Res. Rep. **1**, 401-406, 1946.

8) Miss Cartwright and J. E. Littlewood, J. London Math. Soc. **20**, 180-189, 1945.

R 80 *Philips Res. Rep.* **3**, *191-212, 1948*

DEVELOPMENTS IN RADIO-RECEIVER CIRCUITS FOR THE ULTRA-SHORT-WAVE RANGE

by A. van WEEL **621.396.621.54.029.6**

Summary

Push-pull converter stages are described in which the antenna signal is used in push-pull whereas the local-oscillator voltage is supplied in parallel. The input circuit of the mixing valve is tuned to both frequencies at the same time. Special measures to prevent the local-oscillator voltage from penetrating into the antenna are described. Diode and triode mixing stages are dealt with in detail. It proves to be possible to design self-oscillating triode converter stages, as a consequence of which a separate local-oscillator valve is made superfluous and the noise that might be induced by this valve is eliminated.

Résumé

L'auteur décrit des étages changeurs de fréquence en push-pull dans lesquels le signal d'antenne est utilisé en push-pull tandis que la tension de l'oscillateur local est fournie en parallèle. Le circuit d'entrée du tube changeur de fréquence est accordé sur les deux fréquences en même temps. Des mesures spéciales sont prises pour éviter que la tension de l'oscillateur local n'arrive à l'antenne. Des étages changeurs de fréquence à diode et triode sont décrits en détail. Il paraît être possible de créer des étages changeurs de fréquence à triode auto-oscillante; en conséquence un tube oscillateur local devient superflu et le soufflement induit par ce tube est éliminé.

CONTENTS

1. Introduction
2. Diode mixing stages
3. Blocking the antenna for the local-oscillator voltage
4. Coupling the local-oscillator circuit to the mixing stage
5. Influence of asymmetry of the push-pull circuit; choice of the intermediate frequency
6. Complete circuit diagram for a diode mixing stage
7. Triode mixing stages
8. Blocking the antenna for the local-oscillator voltage in triode mixing stages
9. Complete circuit diagrams of self-oscillating triode mixing stages
10. Low noise level of self-oscillating mixing stages

Appendices I, II and III.

1. Introduction

All the circuits described in this article are based on one principle: the possibility of connecting the corresponding pairs of electrodes of two valves to two tuned circuits, to one of which the valves are connected in push-pull and to the other in parallel. This principle can best be understood from fig. 1, giving for an example the anode circuit of two diodes. The push-pull circuit consists of the inductance L_2 and capacity C_2, while the asymmetric circuit, to which both diodes are connected in parallel, consists of L_1 and C_1 and the leakage inductance of L_2 if the windings of the latter inductance are not fully coupled. The push-pull or symmetric circuit can be tuned by varying C_2, while the asymmetric circuit can be tuned with the aid of C_1. If symmetry is fully maintained these tunings do not affect each other.

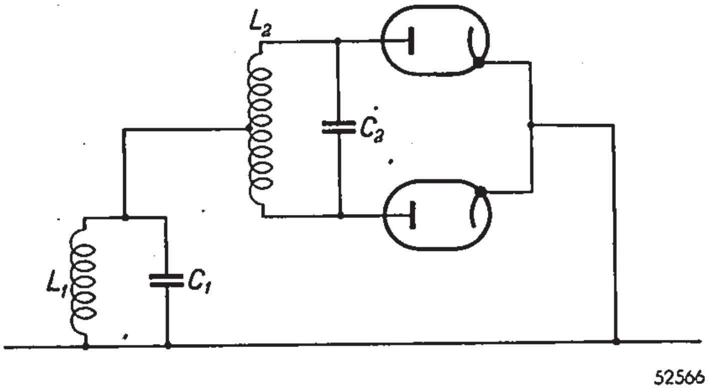

Fig. 1. Two diodes, connected to both an asymmetric circuit (L_1-C_1) and a push-pull circuit (L_2-C_2).

This principle is of special importance for mixing stages at very high frequencies ($\nu > 100$ Mc/s, $\lambda < 3$ m), independent of the use of either diodes or triodes as converter valves. At these wavelengths there are several reasons for using push-pull valves, such as smaller input capacity, higher input resistance due to short inter-electrode leads, and simple coupling with a symmetric antenna.

There is a general theorem regarding the three frequencies playing a part in a mixing stage (signal frequency, local-oscillator frequency, and intermediate frequency), which states that for push-pull mixing stages two of these frequencies should be in push-pull while the third should be asymmetric. For the performance of the mixing stage it is immaterial which of the three frequencies is the asymmetric one.

In conventional mixing stages at longer wavelengths ($\lambda > 3$ m) the signal and local-oscillator frequencies are usually fed to separate electrodes. With the diode or triode converter valves used at short wavelengths the signal and oscillator frequencies are fed to the same pair of electrodes. At longer wavelengths these frequencies normally differ a great deal, owing to the intermediate frequency not being very small compared with the signal frequency. At short wavelengths the intermediate frequency is usually very small compared with the signal frequency; as a consequence the difference between the signal and the oscillator frequencies is comparatively small.

For a good efficiency of mixing stages for short waves it is necessary that there should be a high local-oscillator voltage between the input electrodes. As the impedance of the valve capacities is small, due to the high frequency, it is advisable to tune the input to the local-oscillator frequency. On the other hand it is necessary to tune the input to the signal frequency. As a consequence of the small relative difference between signal frequency and local-oscillator frequency these two conditions are hard to fulfil in conventional circuits (unless the intermediate frequency is *very* low indeed, with no image rejection at all as an unpleasant consequence).

However, by applying the principle outlined above this condition can quite easily be satisfied if the signal voltage is used in push-pull and the local-oscillator stage asymmetric, or vice versa. As the antenna voltage is usually given in push-pull, the first possibility is the most important and will be considered in detail. The second possibility, however, may be as useful in special circumstances.

In view of the fact that these circuits are particularly important for the ultra-short-wave range, in the following diagrams parallel-wire systems (or "Lecher systems") will often be used as input circuits.

2. Diode mixing stages *)

In a diode mixing stage not less than three circuits tuned to three different frequencies have to be connected to the same electrodes, because the intermediate-frequency current must also be taken from the only pair of electrodes (in our case in push-pull, according to the rule given above). The intermediate frequency being substantially different from the signal frequency, it is not difficult to separate the two tuned circuits with the aid of small condensers and high-frequency chokes.

In section 6 we shall give a complete circuit diagram of a diode mixing stage, from which it can be seen how the intermediate-frequency circuit should be connected to the diodes. Since the intermediate frequency does not influence the signal-frequency circuit we shall omit this part of the diagram in the following figures, which therefore show only the signal circuit and the local-oscillator circuit.

In fig. 2 a circuit diagram is drawn in which a parallel-wire system is connected to the anodes of two diodes, the cathodes of which are supposed to be directly connected. The parallel-wire system is tuned to the signal frequency with the aid of a movable short-circuiting bar *AA'*, while the antenna is conveniently tapped on the two wires. The asymmetric circuit consists of the parallel connection of both wires between the fixed short-circuiting bar *BB'* and the diodes, the diode impedances connected in parallel, and an impedance *Z*, which may be either a lumped impedance or a part of an asymmetric Lecher system.

---

*) The same principles hold, of course, for crystal mixing stages.

By varying *Z*, the asymmetric circuit can be tuned to the local-oscillator frequency. Voltage of this frequency may be induced in the circuit by coupling it to the local-oscillator circuit, to which subject we shall return in section 4.

The circuit drawn in fig. 2 gives only one possibility for tuning the asymmetric circuit; other possibilities are given in Appendix I.

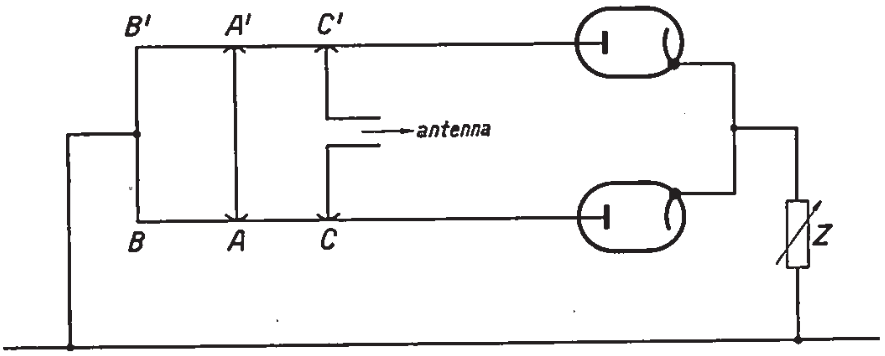

Fig. 2. Push-pull diode converter circuit with asymmetric oscillator voltage.

The circuit of fig. 2 quite easily answers the requirements as regards the tuning of the two circuits, but remains unsatisfactory in one other aspect. Between the points *CC'*, where the antenna (feeder) is connected to the wires, and "earth" a considerable asymmetric voltage of the local-oscillator frequency may be measured. This has two main disadvantages: firstly, the antenna could radiate this frequency, and secondly, since there is local-oscillator voltage between the antenna and earth, the antenna forms a part of the local-oscillator circuit and any change in the (asymmetric) antenna impedance may alter the local-oscillator voltage or frequency, while particularly the possibility of frequency variation is very undesirable. We must therefore find means of preventing the local-oscillator frequency from penetrating into the antenna.

3. Blocking the antenna for the local-oscillator voltage

The simplest way of achieving this is to couple the antenna inductively to the balanced input circuit (fig. 3). If the symmetry is sufficiently maintained no asymmetric voltage will be measured between antenna and earth.

However, this principle cannot always be put into practice. The following three principles give other possibilities for suppressing the asymmetric frequency, the last two of which are particularly suited in the case of preceding H.F. amplification.

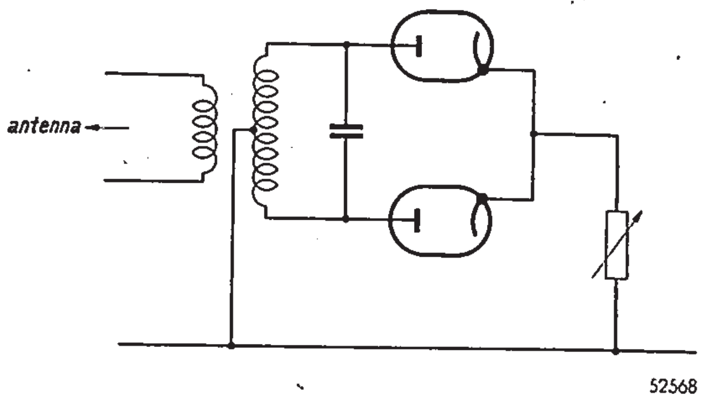

Fig. 3. Push-pull diode converter circuit with inductive antenna coupling.

The first way is to insert between receiver and antenna a filter, which, while blocking the asymmetric frequency, does not influence the push-pull frequency. This can be accomplished by using a filter as shown in fig. 4. First, let us consider this filter as a blocking filter for the asymmetric voltage, i.e., with both wires connected directly in parallel (fig. 5). The lattice then forms a tuned parallel circuit, which should be tuned to the local-oscillator frequency:

$$\omega_{\mathrm{osc}} = \frac{1}{\sqrt{{}^1/_2 L_1 \,.\, 2C_1}} = \frac{1}{\sqrt{L_1 C_1}}. \tag{1}$$

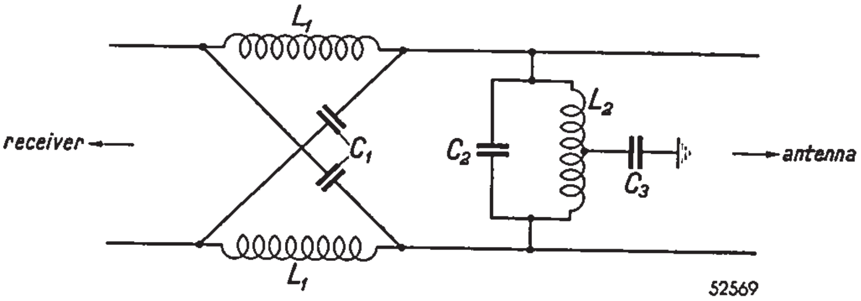

Fig. 4. Antenna-feeder filter, blocking the asymmetric oscillator voltage.

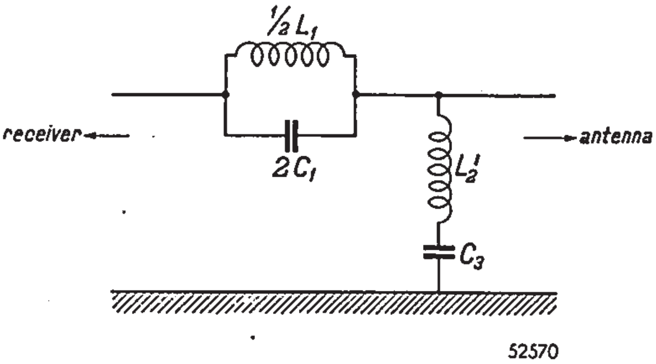

Fig. 5. Equivalent circuit of fig. 4 for the asymmetric voltage.

There is no asymmetric voltage between the terminals of the condenser C_2; so we need not consider this condenser at the moment. But the inductance L_2 should be taken into account because the centre of it is connected to earth via the condenser C_3. As the windings of L_2 are never fully coupled to one another, there remains a certain leakage inductance L_2' to be considered. By tuning this inductance with C_3 to ω_{osc}, an effective blocking filter for the local-oscillator frequency is formed.

The second requirement was that the filter should not influence the transfer of the symmetric voltage. To satisfy this requirement we use the well-known property of a lattice network that, if it is matched at one end with the resistance

$$Z_0 = \sqrt{L_1/C_1},$$

the same resistance is measured between the other terminals. Therefore, if we make Z_0 equal to the antenna resistance Z_{ant},

$$Z_{\text{ant}} = \sqrt{\frac{L_1}{C_1}}, \tag{2}$$

this part of the filter does not influence the signal frequency. From equations (1) and (2) the values for L_1 and C_1 can be calculated.

The impedance of L_2 should be large compared with the antenna resistance, i.e., it should act as a choke. By tuning it with a parallel condenser C_2 this can be reached, even for small values of the inductance L_2.

To give an idea of the numerical values for L_1 and C_1 we have calculated them for an antenna resistance of 100 Ω and a frequency of 300 Mc/s ($\lambda = 100$ cm). The results are:

$$L_1 = 50.10^{-9}\ \text{H}, \qquad C_1 = 5\ \text{pF}.$$

When the antenna is not directly connected to the receiver, but over a feeder, part of this feeder may be used to replace the lattice structure. The circuit is shown in fig. 6, and fig. 7 gives the equivalent circuit for the asymmetric voltage. Taking into account that L'-C_3 are tuned to ω_{osc},

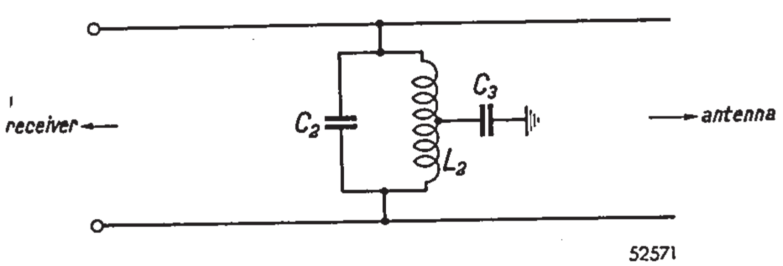

Fig. 6. Part of the antenna feeder used as blocking filter for the asymmetric voltage.

it can be seen that a $^1/_4\lambda$-system is built with a virtual short-circuiting between the points AA'. Any voltage between BB' is transformed down to almost nothing between the points AA' (depending on the losses of L'-C_3). If necessary the filter may be repeated so as to reduce the coupling between antenna and receiver still further.

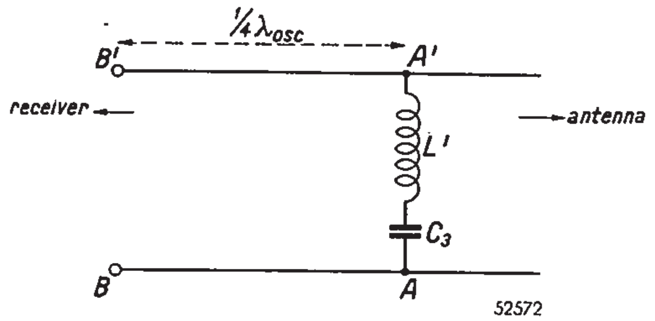

Fig. 7. Equivalent circuit of fig. 6 for the asymmetric voltage.

A second means of preventing penetration of the local-oscillator frequency into the antenna is to connect the antenna to points of the input circuit that carry no local-oscillator-frequency voltage to earth. Fig. 8 gives the complete diagram, while fig. 9 shows the equivalent circuit for the asymmetric voltage.

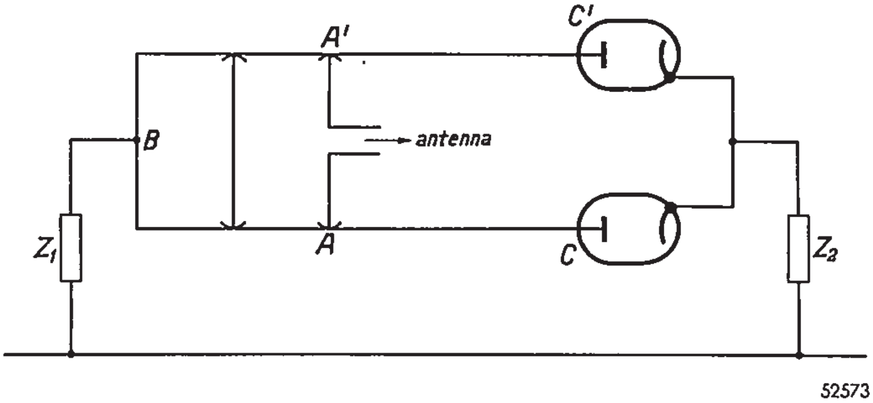

Fig. 8. Blocking the antenna for the asymmetric oscillator voltage by connecting the antenna feeder to points with minimum asymmetric voltage.

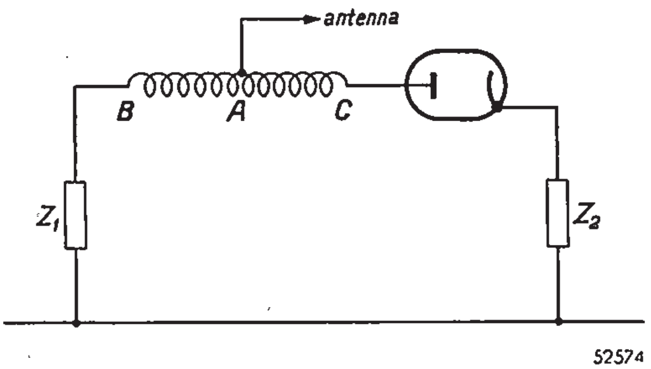

Fig. 9. Equivalent circuit of fig. 8 for the asymmetric voltage.

We have presumed that the asymmetric impedance of the parallel-wire system could be represented by an inductance; as the parallel-wire system is usually shorter than a quarter of a wavelength, this assumption is justified in most cases.

The requirement mentioned above (no local-oscillator voltage between A and earth) can be satisfied by choosing the impedance Z_1 in such a way that, looking from the point A to the left, series resonance for the local-oscillator frequency is measured. *In the circuit of fig. 9, Z_1 should therefore be capacitive.*

But the condition that the whole asymmetric circuit should be tuned to the local-oscillator frequency still remains to be fulfilled. This may be achieved by inserting the second impedance Z_2 in the circuit; Z_2 should be chosen so as to tune the whole asymmetric circuit. This means that looking from A to the right, one should again measure series resonance. It depends on the value of the inductance AC and of the diode capacity what kind of impedance Z_2 (inductive or capacitive) must be used.

As the elements of the circuit are not ideal inductances or capacities, but always carry some losses, the impedance between A and earth is never absolutely zero, as a consequence of which some asymmetric voltage remains between A and earth. However, this voltage is very small and receivers constructed on this principle usually do not show any influence of the antenna on the local-oscillator circuit.

Other means of obtaining a voltage minimum for the local-oscillator frequency at the antenna connections are described in Appendix II.

The third possibility to keep the antenna free from local-oscillator voltage is to design the circuit in such a way that no voltage of this frequency occurs between the input electrodes of the converter valve and earth. This principle may be illustrated by the circuit shown in fig. 10 and its equivalent circuit for the asymmetric voltage drawn in fig. 11. If the ratio C_1/C_d (C_d = diode capacity) equals the ratio L_2/L_1, no voltage will be measured between the anodes of the diodes and the point connecting L_1, L_2 and earth.

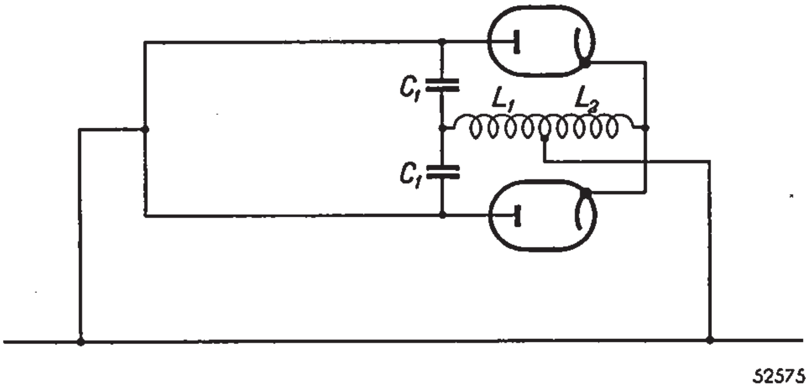

Fig. 10. Converter circuit with input Lecher wires free from asymmetric voltage.

This only holds exactly for circuits without losses, or for circuits in which L_1 and L_2 are fully coupled. In practical circuits, however, a certain voltage remains between the anodes and earth, but as this voltage is only very small the circuit satisfies the requirement for all practical purposes.

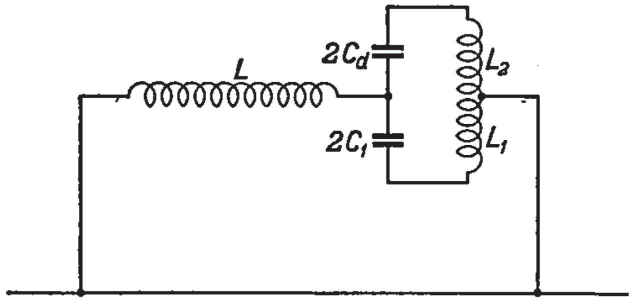

Fig. 11. Equivalent circuit of fig. 10 for the asymmetric voltage.

The sign or the value of the impedance of the parallel-wire system for the asymmetric voltage does not influence the tuned circuit L_1, L_2-$2C_1$, $2C_2$, provided this impedance is not very small. If by mischance this impedance should show series resonance for the local-oscillator frequency, an extra impedance should be inserted between the short-circuiting bar and earth so as to form a sufficiently high impedance.

Recapitulating the results it may be stated that to prevent the local-oscillator frequency from penetrating into the antenna one can

(1) couple the antenna inductively to the symmetric input circuit,
(2) insert a filter for the asymmetric voltage between receiver and antenna,
(3) connect the antenna to a point of the input circuit carrying minimum asymmetric voltage to earth, and
(4) make the whole input circuit free from local-oscillator voltage by making the input electrodes of the converter valves free from this voltage.

The first method is often the simplest; it uncouples the antenna from the local oscillator for all frequencies.

The second method makes it possible to design the whole input and mixing circuit without the need of paying attention to the unwanted coupling of the antenna with the local-oscillator circuit.

The third method may be realized with fewer elements but puts certain demands on the input circuit.

In the last method the input circuit can be designed independently of the local-oscillator circuit (apart from the condensers C_1 in fig. 10), but special demands have to be met by this local-oscillator circuit. However, if these demands are satisfied, the input circuit is free from asymmetric voltage, independently of the frequency.

4. Coupling the local-oscillator circuit to the mixing stage

In diode mixing stages the local-oscillator frequency is usually generated in a separate oscillator circuit. Voltage of this frequency must be induced in the asymmetric input circuit. When this circuit is tuned to the local-oscillator frequency only a small amount of power is needed and a very loose coupling between input and local-oscillator circuits is sufficient; this coupling may be either inductive or capacitive.

Inductive coupling may be achieved by coupling the coil of the oscillator circuit with an inductance of the asymmetric input circuit. This system has the disadvantage that it is often difficult to prevent coupling between the symmetric input circuit and the oscillator circuit, which coupling would result in symmetric local-oscillator-frequency voltage being developed across the diodes; reduced efficiency of the mixing stage would be the consequence.

By using capacitive coupling it is comparatively simple to screen the whole oscillator circuit from the input system. Apart from this it is much simpler to adjust this coupling to its optimum value. In fig. 12 the principle is illustrated for the coupling of a Hartley oscillator circuit with an input system consisting of a parallel-wire system. The asymmetric input system is tuned to the local-oscillator frequency by means of the variable condenser C_3; as capacitive coupling is "voltage coupling", the coupling condenser C_2 should be connected between two points showing considerable impedance to earth. In fig. 12 this condenser is connected between the upper end of the oscillator circuit and the upper end of C_3.

However, as mentioned above, the amount of coupling needed between the two circuits is usually only very small, i.e., condenser C_2 must have a very small capacity. To make a variable condenser of, say, 1 pF maximum

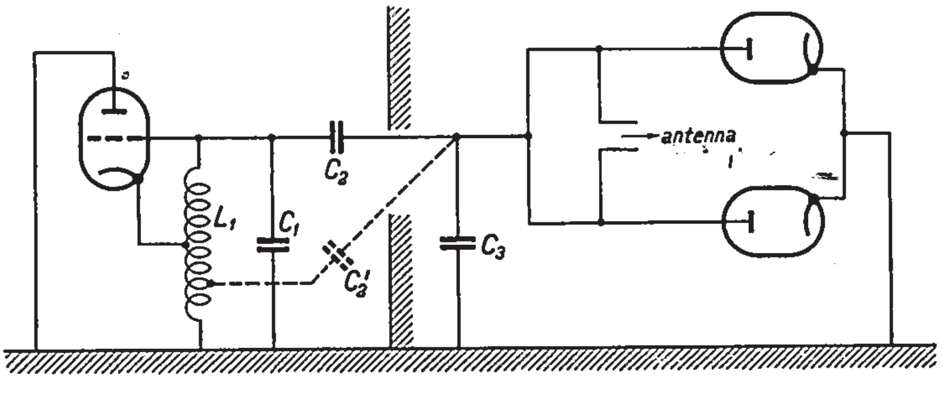

Fig. 12. Coupling the local oscillator to the converter circuit; direct (C_2) or tapped (C_2').

capacity is not easy; therefore it is much simpler to connect C_2 to a lower tap of the oscillator circuit (indicated by the dashed condenser C_2' in fig. 12). A much larger value for C_2' may then be used.

In fig. 12 the screening of the local-oscillator circuit from the input circuit is also indicated. Only a small hole in this screen is necessary to pass through the wire connecting the two circuits.

5. Influence of asymmetry of the push-pull; circuit choice of the intermediate frequency

Up till now we have supposed the push-pull circuit to be fully symmetric, which means that no coupling exists between the push-pull circuit and the asymmetric circuit. However, in practical circumstances this symmetry can never be maintained sufficiently to preclude any coupling between these two tuned circuits. This remaining coupling, being usually small, is not important if both circuits are tuned to two frequencies quite distinct from each other. This is the case if the intermediate frequency is not too small (or if mixing takes place with a harmonic of the local-oscillator frequency).

To estimate the difference necessary between the two frequencies we must go into details about the consequences of asymmetry. As already mentioned, asymmetry means that push-pull circuit and asymmetric circuit are coupled together. Current induced in the asymmetric circuit will therefore cause not only asymmetric voltage across the diodes but also push-pull voltage. The latter voltage will be larger when the asymmetric frequency differs less from the resonance frequency of the push-pull circuit.

The resulting voltages across both diodes depend on the phases of the two voltages. Fig. 13 shows an arbitrary phase relation between the push-

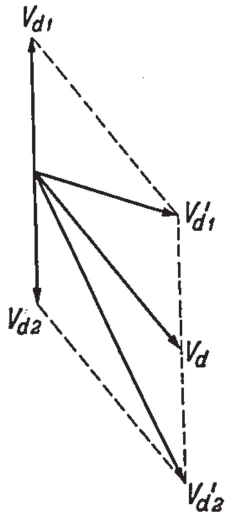

Fig. 13. Vector diagram, showing the push-pull voltages on both diodes, V_{d1} and V_{d2}, and the asymmetric voltage, V_d, with arbitrary mutual phase relation.

pull voltages, V_{d_1} and V_{d_2}, and the asymmetric voltages, V_d (which are of course the same for both diodes). The resulting diode voltages, V_{d_1}' and V_{d_2}', show an appreciable difference in amplitude as well as in phase.

In fig. 14 the resulting voltage amplitudes are plotted against the frequency for the case where the asymmetry is due to a slight difference between the diode capacities.

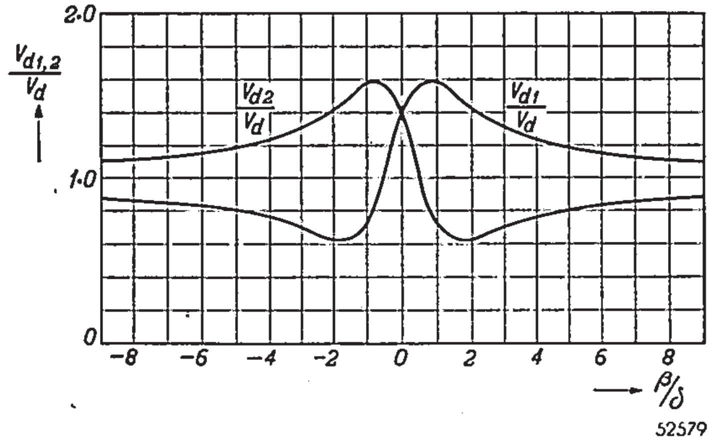

Fig. 14. Local-oscillator voltages on both diodes as a function of the tuning of the push-pull input circuit (theoretical).

These curves are calculated in Appendix III for one special case, for which we chose the relative capacity difference, $(C_1—C_2)/C_1$, being equal to twice the reciprocal value of the circuit quality $(1/Q = r/\omega L)$.

Fig. 15 shows an experimental curve measured in a diode mixing stage tuned to a signal wavelength of 130 cm. The resemblance is obvious.

The necessary difference between the two frequencies depends on the quality of the circuits and the degree of asymmetry. A frequency difference of 1/20 of the signal frequency is enough in most cases.

To avoid these phenomena the intermediate frequency should therefore not be less than 1/20 of the signal frequency.

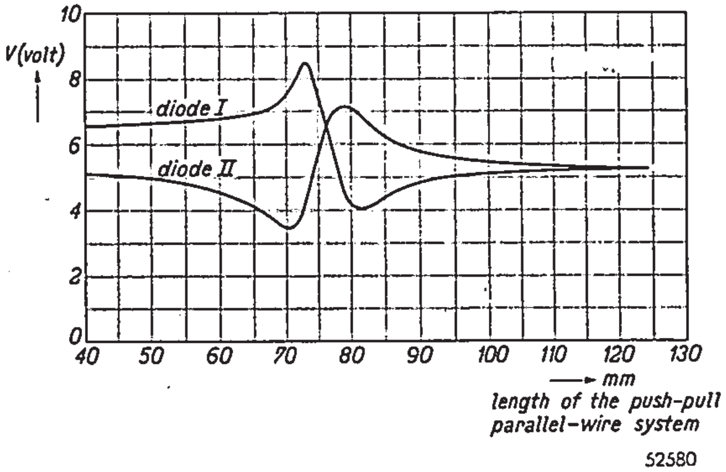

Fig. 15. The same curves as those from fig. 14, as measured in an actual circuit.

6. Complete circuit diagram for a diode mixing stage

The circuit diagram (fig. 16) shows a parallel-wire system connected to the mixing diodes via the condensers C_6 and C_7, which act as blocking condensers for the intermediate frequency but should pass the high-frequency current freely. The antenna is inductively coupled to the input circuit.

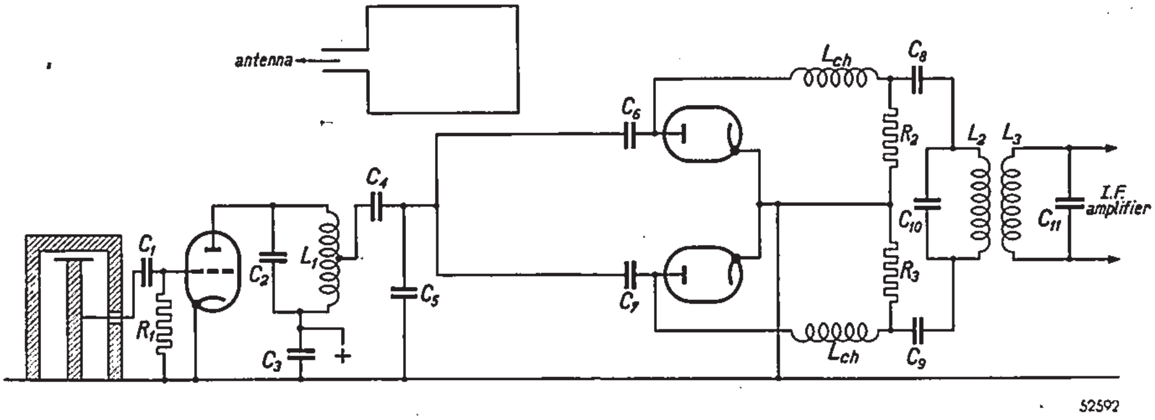

Fig. 16. Complete circuit diagram for a diode converter stage.

The I.F. current is led over two chokes L_{ch}, which should block the H.F. current to the I.F. circuit L_2-C_{10}. The condensers C_8 and C_9 are blocking condensers for D.C., so as to give each diode its own D.C. voltage. The I.F. circuit L_2-C_{10} is coupled to a second I.F. circuit L_3-C_{11}, which is assumed to be connected to the I.F. amplifier.

The asymmetric circuit is tuned to the oscillator frequency by means of C_5 and coupled to an oscillator circuit over the condenser C_4. The frequency of the oscillator circuit is stabilized by using a cavity resonator as grid impedance; the anode impedance is a conventional tuned circuit.

7. Triode mixing stages

For the input circuit of triode converters the same considerations hold as given for the diode converters. However, there are some interesting possibilities worth mentioning here. In the following circuit diagrams the I.F. circuits are again omitted, except in the complete diagram given at the end.

As shown in an earlier publication *), the signal-to-noise ratio in the I.F. current of a triode converter can be increased by using positive feedback for the signal frequency. At H.F. this may be achieved by inserting an inductance in the anode circuit. The principle is shown in fig. 17, where the inductance is connected between the anodes. The amount of feedback must, of course, be kept below the level where oscillation starts. The feedback for the push-pull input circuit shown in fig. 17 does not affect the asymmetric circuit.

---

*) A. van Weel, Thesis, Delft 1943.

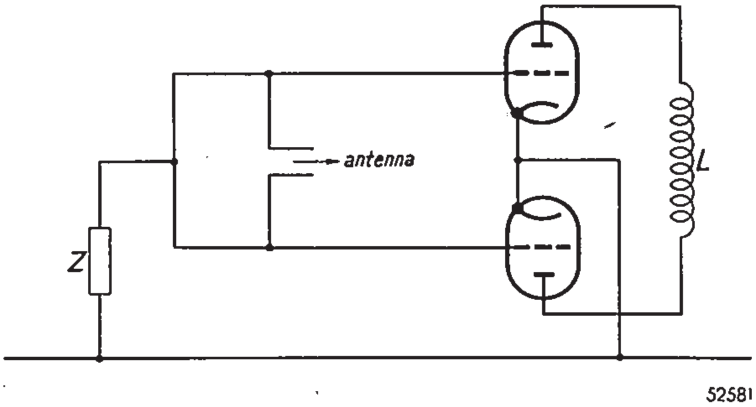

Fig. 17. Triode converter circuit with feedback for the push-pull input circuit.

However, it is also quite possible to design a feedback that affects only the asymmetric circuit, and if this feedback is made strong enough the asymmetric circuit will start oscillations. *This means that no separate oscillator is needed; the mixing stage is self-oscillating.*

This principle is illustrated in fig. 18. The asymmetric and push-pull input circuits are the same as in fig. 17. Positive feedback for the asymmetric circuit is realized by connecting the impedance Z_2 between the middle of L_1 and earth.

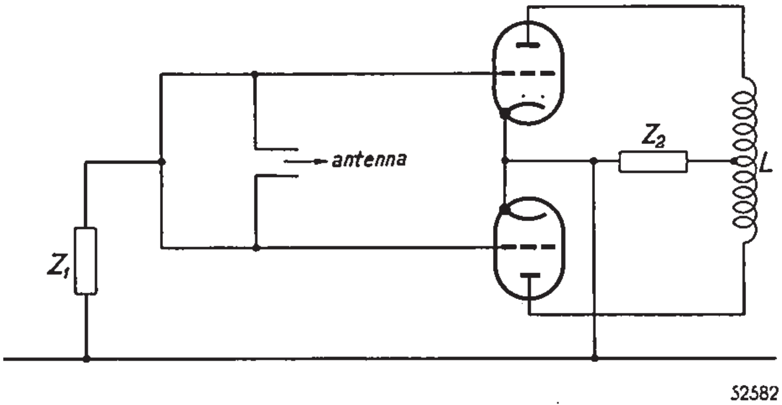

Fig. 18. Triode converter circuit with feedback for the push-pull as well as for the asymmetric input circuit.

The equivalent circuit for the asymmetric voltage is shown in fig. 19. Taking into account the internal valve capacities, it can be seen that this oscillator is of the tuned-anode tuned-grid type.

For tuning this oscillator, both the anode and the grid circuits should be tunable, and as the push-pull circuit should not be influenced by the tuning of the oscillator the only possibility is to make Z_1 and Z_2 variable.

The frequency of the oscillator can be stabilized by using a cavity resonator either for Z_1 or for Z_2.

Circuits based on the same principle may also be used with balanced triodes of the grounded-grid type.

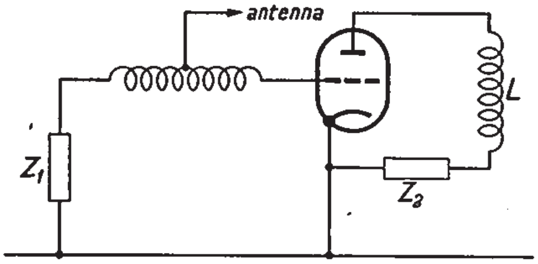

Fig. 19. Equivalent circuit of fig. 18 for the asymmetric voltage.

8. Blocking the antenna for the local-oscillator voltage in triode mixing stages

The same four principles as given for diode converters apply to triodes. However, the last principle (connecting the mixing stages in such a way that no asymmetric voltage occurs between input electrodes and earth) is realized in a somewhat different way for triodes, as these valves have three electrodes compared with the two electrodes of a diode. We shall therefore only go into the details of this last principle.

As this method is much simpler to realize for the grounded-grid type of push-pull valves than for the grounded-cathode type, we shall consider the grounded-grid type now.

In fig. 20 a conventional oscillator circuit for ultra-high frequencies is drawn, consisting of a tuned circuit connected between anode and grid, while the D.C. voltage to all three electrodes is supplied over impedances that are high for the oscillator frequency (either chokes, L_{ch}, or high resistances, R_g). None of the electrodes is directly "earthed" for the oscillator frequency. The circuit is a "Colpitts" oscillator; the internal valve capacities (dashed in the diagram) act as the capacitive potentiometer.

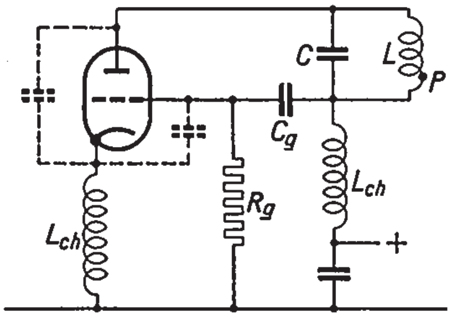

Fig. 20. Oscillator circuit for ultra-high frequencies.

As a consequence, the cathode is tapped on the anode-grid voltage. On each branch of the tuned parallel circuit L-C we could find a point that is in the same way tapped on this voltage, say the point P on the inductance. If we connect this point directly to earth, the cathode will automatically take earth potential, because no potential difference exists between the cathode and the point P.

We could, of course, also divide the capacity C into two parts in such a way that the connecting point of the two parts has the same potential as the cathode.

A third possibility is to use, for the blocking impedances between grid and earth and between anode and earth, impedances of the same kind, while the ratio of their magnitudes equals the ratio of the impedances of the grid-cathode capacity and the anode-cathode capacity.

Fig. 22 shows the complete diagram of a mixing stage based on the last-mentioned principle.

With push-pull converter triodes of the grounded-cathode type it is not so easy to put this principle into practice. Since in this case the input electrodes are formed by the grids, the anode-cathode impedance in the asymmetric oscillator circuit should be divided in the same ratio as that between the anode-grid impedance and the cathode-grid impedance of the oscillator circuit. In an oscillator circuit these impedances are always opposite in sign, i.e., if one is capacitive the other is inductive, and vice versa. As a consequence it is not so simple to apply this principle with a grounded-cathode circuit.

9. Complete circuit diagrams of self-oscillating triode mixing stages

In fig. 21 the circuit diagram is shown for a grounded-cathode circuit. The antenna is inductively coupled to the input circuit. The asymmetric input circuit is tuned to the oscillator frequency with the aid of C_1, to which the grid-leak resistance R_1 is connected in parallel.

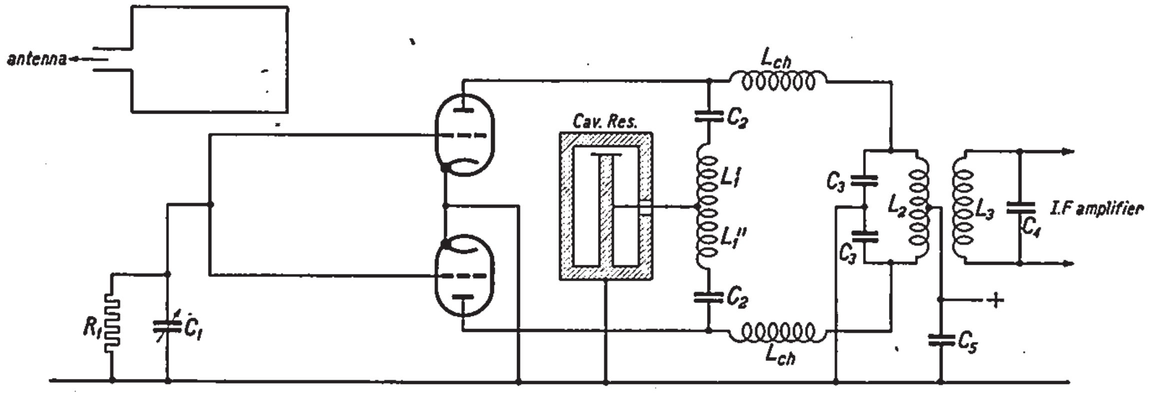

Fig. 21. Complete circuit diagram for a grounded-cathode triode converter stage.

The H.F. anode circuit consists of the capacities C_2 (blocking the intermediate frequency) and the inductance L_1, which provides for the amount of feedback needed for the push-pull input circuit. The middle of L_1 is connected to the cavity resonator stabilizing the oscillator frequency.

The intermediate-frequency current passes the high-frequency chokes L_{ch} and is fed to the circuit L_2-C_3, which is tuned to the intermediate frequency and coupled to a second circuit L_3-C_4 connected to the I.F. amplifier. The capacity C_3 is split into two parts, so as to offer a low impedance to earth for the high frequencies.

A grounded-grid mixing stage is drawn in fig. 22. The antenna being directly connected to the input circuit, it is necessary to design the oscillator circuit in such a way that no asymmetric voltage occurs between the input electrodes (the cathodes) and earth. This is realized by choosing the impedances of the high-frequency chokes L_{ch}' and L_{ch}'' of such values that their ratio equals the ratio $C_{ak}/2C_{gk}$.

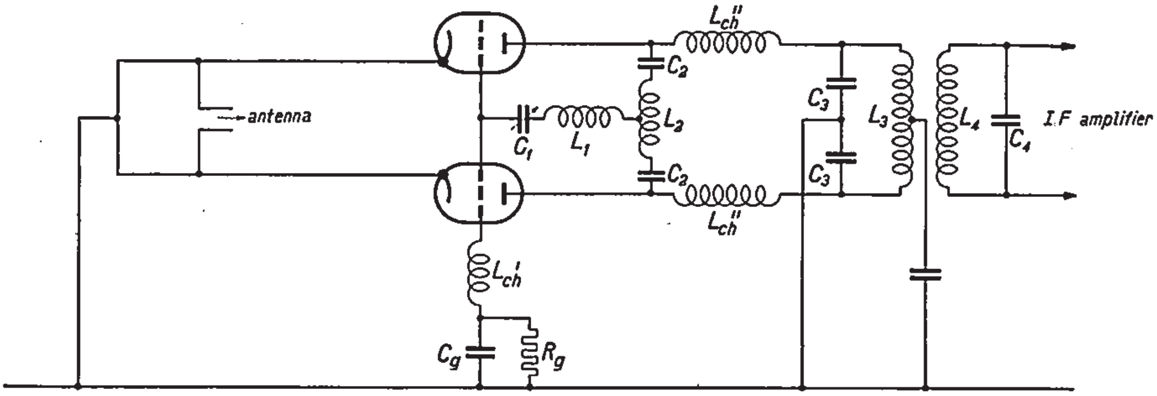

Fig. 22. Complete circuit diagram for a grounded-grid triode converter stage.

The condensers C_2 act as blocking condensers for the intermediate frequency. The inductance L_2 provides for the push-pull feedback, while the asymmetric anode-grid circuit is closed by L_1 and the variable condenser C_1, which enables this circuit to be tuned.

The intermediate frequency circuits are the same as in fig. 21.

10. Low noise level of self-oscillating mixing stages

As shown in an earlier publication *), the local-oscillator valve may cause an appreciable increase of the noise level of a converter stage. In the oscillator valve the normal sources of noise are present, and across the oscillator circuit, apart from the large oscillator voltage, a certain noise voltage will be measured, comprising in theory all frequencies but in

---

*) A. van Weel, loc. cit.

particular those in the neighbourhood of the oscillator frequency, since the circuit is tuned to this frequency. This noise voltage will be pressed on the mixing valve together with the oscillator voltage, and the components in the signal-frequency band, image-frequency band, and intermediate-frequency band will increase the noise level in the I.F. current. The effect will be more pronounced when the signal and oscillator frequencies are closer to each other. This effect is not only of theoretical interest, as can be judged from the fact that we first measured it experimentally as an unexplained high noise level, for which this explanation was subsequently found.

In the self-oscillating triode mixing stages described in this article there is no separate oscillator and therefore the source of this "oscillator noise" does not exist. Apart from any practical consideration, these mixing stages therefore have the advantage of better noise properties.

Appendix I

In the following circuit diagrams various systems are given for tuning a push-pull circuit to an asymmetric voltage.

Figs 23 and 24 need no explanation. In fig. 25 the impedance Z_1 is

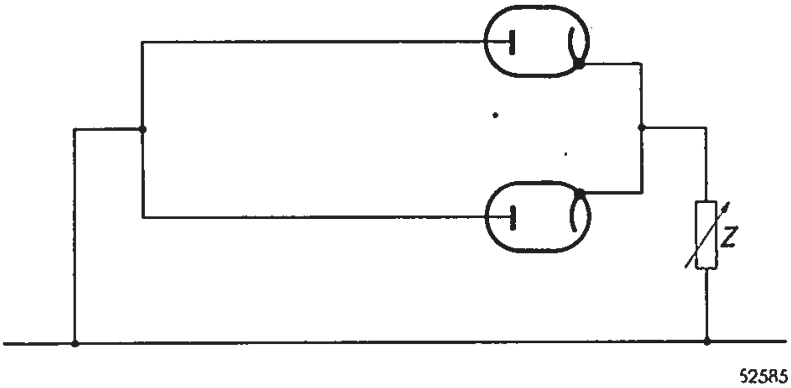

Fig. 23. Tuning the asymmetric circuit to the local-oscillator voltage by means of an impedance Z in series with the cathodes.

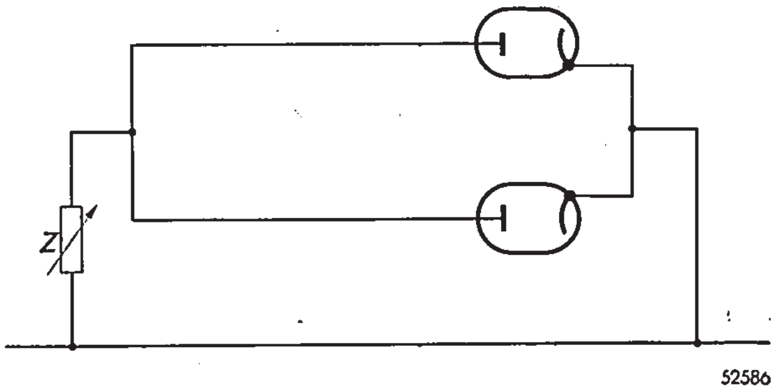

Fig. 24. Tuning the asymmetric circuit to the local-oscillator voltage by means of an impedance in series with the input circuit.

supposed to be so high as not to appreciably influence the push-pull circuit. Tuning for the asymmetric voltage is accomplished by varying Z_2.

In these circuits a given length of push-pull system was presumed, and the asymmetric circuit was tuned by inserting a special impedance carrying only the asymmetric current. But the tuning of the whole system to two different frequencies could also be accomplished the other way round, i.e., assuming a certain length of the wire system, which is itself tuned to the asymmetric frequency, and tuning the push-pull system either by shifting a second short-circuiting bar or by varying an impedance, carrying only the symmetric current. Both possibilities are shown in fig. 26.

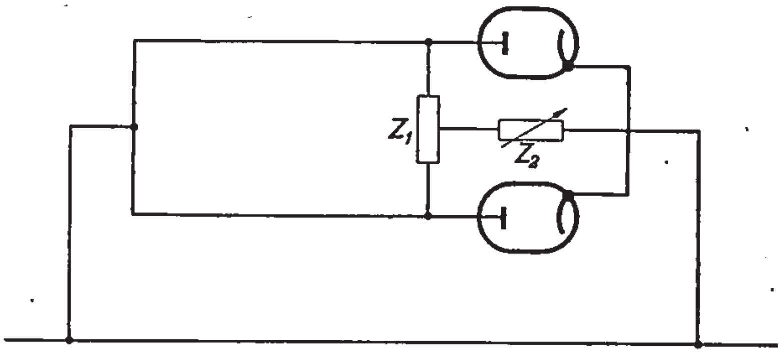

52587

Fig. 25. Tuning the asymmetric circuit to the local-oscillator voltage by means of a parallel circuit, Z_1-Z_2.

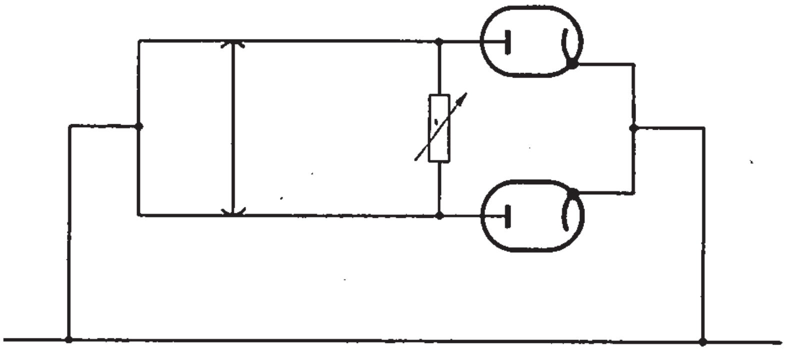

52588

Fig. 26. Tuning the push-pull input circuit to the signal frequency.

Combinations of the principles underlying any of these four circuits are, or course, also possible, while there are still other possibilities into which for shortness's sake we cannot enter here.

Appendix II

A minimum for the asymmetric voltage at the points where the antenna is connected to the input circuit can be realized in two different ways, as shown in figs 27 and 28. Fig. 27 is the same as fig. 8 and needs no explanation.

To understand fig. 28 it should be noted that the asymmetric equivalent of the star formed by the two parts of the inductance L and the capacity C is an inductance L', depending on the amount of leakage inductance of L, in series with C. By correctly tuning C, series resonance can be achieved.

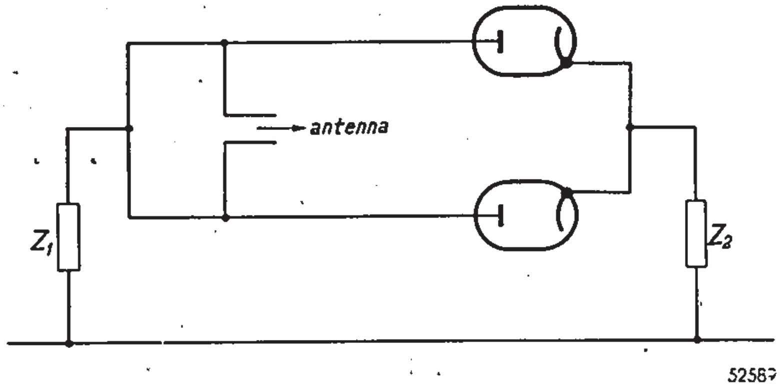

Fig. 27. Blocking the antenna for the asymmetric oscillator voltage by connecting the antenna feeder to points with minimum asymmetric voltage.

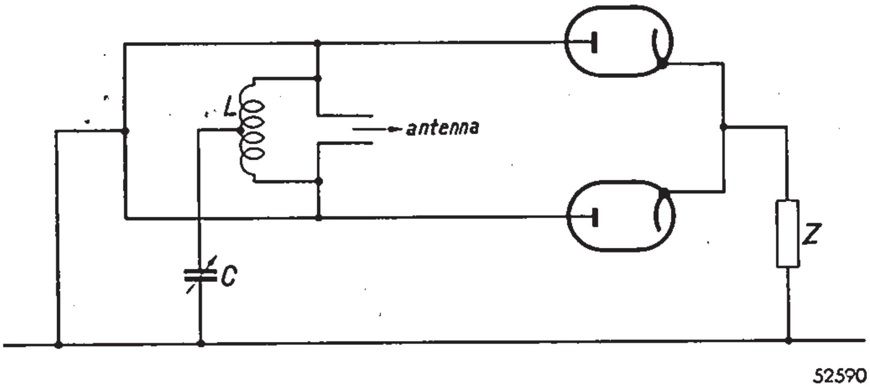

Fig. 28. Blocking the antenna for the asymmetric local-oscillator voltage by means of a "series" circuit L-C, tuned to the local-oscillator frequency.

The star formed by the two parts of the inductance L and the capacity C may be replaced by a star of two capacities between the antenna connection points and one inductance to earth, which, however, is not so easy to tune in practice.

For tuning the right half of these circuits to the asymmetric frequency any one of the circuits given in appendix I could be used instead of the series impedance Z.

Appendix III

To calculate the influence of asymmetry on the performance of a push-pull converter stage with asymmetric oscillator voltage we use the circuit of fig. 29, where the push-pull circuit is drawn and an asymmetric current is fed to the two points A and B.

The inductances are assumed to be exactly equal, whereas the (diode) capacities show a slight difference, given by the value of ε.

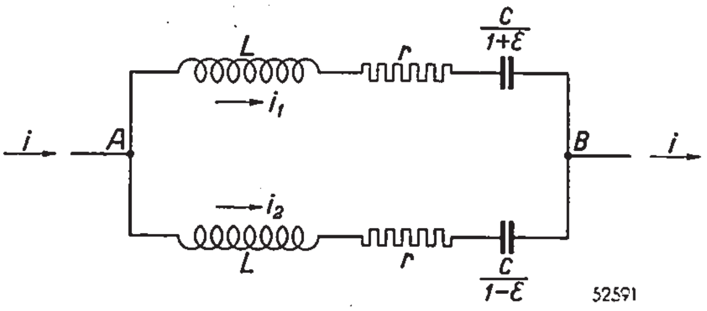

Fig. 29. Equivalent circuit for a push-pull diode converter stage with slightly asymmetric diode capacities.

From Kirchhoff's laws we derive the following equations:

$$i = i_1 + i_2, \tag{3}$$

$$i_1\left(j\omega L + r + \frac{1+\varepsilon}{j\omega C}\right) = i_2\left(j\omega L + r + \frac{1-\varepsilon}{j\omega C}\right). \tag{4}$$

Dividing both sides of equation (4) by $j\omega_0 L$ ($\omega_0 = 1/\sqrt{LC}$) and substituting $\beta = \frac{\omega}{\omega_0} - \frac{\omega_0}{\omega} \approx \frac{2\Delta\omega}{\omega}$, $\delta = \frac{r}{\omega L}$, this equation can be transformed in

$$i_1\,(\beta - \varepsilon - j\delta) = i_2\,(\beta + \varepsilon - j\delta)\,. \tag{5}$$

From equations (3) and (5) can be found

$$i_1 = \frac{i}{2}\cdot\frac{\beta + \varepsilon - j\delta}{\beta - j\delta}. \tag{6}$$

$$i_2 = \frac{i}{2}\cdot\frac{\beta - \varepsilon - j\delta}{\beta - j\delta}, \tag{7}$$

As may be expected, for $\varepsilon = 0$ both i_1 and i_2 equal $i/2$. From (6) and (7) the absolute values may be calculated:

$$\left|\frac{i_1}{{}^1\!/_2\, i}\right| = \sqrt{1 + \frac{\varepsilon^2 + 2\varepsilon\beta}{\beta^2 + \delta^2}}, \tag{8}$$

$$\left|\frac{i_2}{{}^1\!/_2\, i}\right| = \sqrt{1 + \frac{\varepsilon^2 - 2\varepsilon\beta}{\beta^2 + \delta^2}}. \tag{9}$$

The voltage across the (diode) capacities is found by multiplying i_1 and i_2 by $1/\omega C$ (disregarding the slight difference). However, to judge the influence of the asymmetry it is sufficient to consider equations (8) and (9).

In fig. 14 the right-hand terms of these equations have been plotted as a function of β/δ. We had to assume a value for ε and chose $\varepsilon = \delta$.

To eliminate the influence of asymmetry it is necessary to choose β high, which means a high intermediate frequency. We may write down as a condition

$$\frac{\varepsilon^2 + 2\varepsilon\beta}{\beta^2 + \delta^2} \ll 1 . \tag{10}$$

A stronger condition is

$$\frac{\varepsilon^2 + 2\varepsilon\beta}{\beta^2} = \frac{\varepsilon^2}{\beta^2} + \frac{2\varepsilon}{\beta} \ll 1, \tag{11}$$

and this is satisfied if

$$\frac{2\varepsilon}{\beta} \ll 1, \tag{12}$$

or

$$\beta = \frac{2\Delta\omega}{\omega} \gg 2\varepsilon . \tag{13}$$

Now it is quite clear that the asymmetry can hardly be made smaller than 1%; so a minimum condition is

$$\frac{\Delta\omega}{\omega} \gg \frac{1}{100}, \tag{14}$$

say

$$\frac{\Delta\omega}{\omega} \geqq \frac{1}{20}. \tag{15}$$

To eliminate the influence of asymmetry in the push-pull circuit, the difference between local-oscillator frequency and signal frequency should at least be one-twentieth of the signal frequency. If the push-pull circuit is very heavily damped a smaller value for β may be tolerable, according to equation (10).

Eindhoven, September 1946

R 81 *Philips Res. Rep. 3, 213-226, 1948*

ON THE THEORY OF COUPLED ANTENNAE

by C. J. BOUWKAMP **621.396.671**

Summary

The purpose of this paper is to provide formulae for the self and mutual impedances of an antenna system consisting of two identical, centre-fed, parallel, cylindrical wires. Tables of auxiliary functions are given facilitating numerical investigation in the range $1 < 2\pi l/\lambda < 2$, $0 < d/l < 2$, $\Omega = 2 \ln(2l/a) > 10$, where $2l$ is the length of each antenna, d their mutual distance, $2a$ the wire diameter, and λ the wavelength. Examples illustrating the general theory are deferred to a subsequent paper.

Résumé

L'objet de cet article est de fournir des formules pour les impédances propre et mutuelle d'un système d'antennes constitué par deux minces brins identiques, parallèles, cylindriques, alimentés au centre. L'article comporte des tableaux de fonctions auxiliaires permettant de faire des investigations numériques dans la gamme $1 < 2\pi l/\lambda < 2$, $0 < d/l < 2$, $\Omega = 2 \ln(2l/a) > 10$, où $2l$ est la longueur de chaque antenne, d leur distance mutuelle, $2a$ le diamètre du fil et λ la longueur d'onde. Les exemples d'application de la théorie générale sont réservés à un article suivant.

1. Introduction

As is obvious from first principles of electromagnetic theory, the radiation properties of a transmitting antenna ultimately depend on and are determined by the distribution of current and charge. Once the currents and charges are known, the electromagnetic field is easily obtained by the classical method of vector and scalar potentials. Therefore, an adequate starting point in the theory of antenna radiation is to *assume* the currents and charges, that is, to consider them as *given* functions of time and position. In fact the older theories are all based upon this method, apart from a very few exceptions. Of course the theoretical results so obtained may be expected to agree fairly well with experiments if, and only if, the *assumed* sources are good approximations of the *actual* ones.

The quasi-stationary theory often leads to useful approximations for the currents and charges. It is then customary to calculate the actual currents and charges approximately, by first neglecting the effect of radiation. As a consequence, in the development to shorter waves there is a general trend to extrapolate such important concepts as capacitance and inductance to the ultra-high-frequency technique of to-day. On the other hand, the electrical engineer is well aware that he has often to return to more fundamental principles, that is, to Maxwell's equations of the electromagnetic field.

In this connection the antenna theory provides a striking example. The distribution of current in an isolated, centre-driven, cylindrical antenna was formerly assumed to be sinusoidal, and this assumption is quite sound, as pointed out by various investigators 1), 2), 3), 4). Though only the refined theory is able to treat satisfactorily such topics as anti-resonance, where the impedance is very large and highly dependent on the thickness of the wire, other corrections are usually small and almost negligible in practice. However, there are other examples which show that the older theories do not suffice at all 5), 6). The calculation of the self and mutual impedances of an antenna system in resonance is usually based on the assumption that the current along any of the conductors, whether driven or parasitic, is the same as that along a free centre-driven antenna of the same dimensions. This assumption is not justifiable. On the contrary, especially for non-resonance, the current distribution in a receiving antenna placed in a homogeneous field is not equal to that of the same antenna when used as transmitter, let alone that a loaded or unloaded parasitic antenna located in the neighbourhood of the driven antenna would show the same current distribution as the driven one. Furthermore, one should be careful in phase reasoning for coupled antennae because, in the neighbourhood of the transmitting antenna, space differences have little to do with phase differences. At any rate, the relationship between phase changes and distances travelled is completely different from that existing in the wave zone.

Since a rigorous theory of the electromagnetic coupling of antennae should be able to provide us with data concerning input resistance at resonance, resonance shortening, etc., there is only one way to choose: one has to return to the fundamentals of electromagnetic theory — it is not so simple as to assume "convenient" currents; rather, the currents must first be *calculated.*

The present paper contains some results of a laboratory report 5) the publication of which has been delayed by the war. That report dealt with the radiation properties of the simplest case of the Yagi antenna, the system consisting of a centre-fed, straight wire in the presence of an unloaded parasitic antenna parallel to and not displaced in length with respect to the driven conductor (both wires being thin cylinders of equal cross-sections and lengths, and of perfectly conducting material).

In passing we remark that following upon Hallén's fundamental contribution to antenna theory 1) numerous investigations were published by Ronold King and collaborators. One of their papers 6) bears a close relation to the present report. However, since some of our results are either given differently or not dealt with by these authors, the present publication may be justified.

The basic ideas and methods developed here are similar to those of a former paper [3]). Characteristic of the Hallén problems is the appearance of the large parameter $\Omega = 2 \ln (2l/a)$, where $2l$ and $2a$ are respectively the length and the diameter of the wires. Whereas in [3]) terms of the order Ω^{-2} were included, here we take into account only terms of the order Ω^{-1}; otherwise the mathematics would become too involved.

Finally, the present paper is devoted to the general outlines of the theory, numerical applications being postponed to a subsequent report.

2. Formulation in terms of the vector potential

Let d denote the distance between two identical, parallel, cylindrical wires, both of length $2l$ and diameter $2a$ ($l \gg a$, $d \gg a$), the line connecting the centres being perpendicular to both wires. The latter are centre-fed by slice generators of driving potential differences V_1 and V_2 *). Furthermore, the two wires are supposed to be perfectly conducting. By virtue of the symmetry in the feeding, the current distribution is symmetrical with respect to z, where z denotes the distance along either antenna measured from the corresponding centre. Let $I_1(z)$ and $I_2(z)$ stand for the currents, which we may suppose to flow at the surfaces of the wires. These currents are subjected to the condition that the resulting tangential electric field shall vanish at the surface of both wires. Alternative formulations of the problem are (*i*) the currents flow at the surfaces of the cylinders supposed to be hollow, while the electric field vanishes on the two axes, and (*ii*) the currents are flowing in the axes, while the axial electric field vanishes at distances a from the axes. These three different interpretations are equivalent when effects of the order a/l are neglected [3]).

Let $\varphi_{11}(z)$ denote the axial component of the vector potential on the axis of the first antenna as due to its own current, $I_1(z)$. Let further $\varphi_{21}(z)$ be the same component due to the current $I_2(z)$ flowing in the second antenna. The functions $\varphi_{12}(z)$ and $\varphi_{22}(z)$ are defined similarly. Then, upon introducing $r^2 = (z-\zeta)^2 + a^2$, $R^2 = (z-\zeta)^2 + d^2$, we have **)

$$\left.\begin{aligned} \varphi_{11}(z) &= \frac{1}{c}\int_{-l}^{l} I_1(\zeta)\,\frac{e^{-jkr}}{r}\,\mathrm{d}\zeta, & \varphi_{21}(z) &= \frac{1}{c}\int_{-l}^{l} I_2(\zeta)\,\frac{e^{-jkR}}{R}\,\mathrm{d}\zeta, \\ \varphi_{12}(z) &= \frac{1}{c}\int_{-l}^{l} I_1(\zeta)\,\frac{e^{-jkR}}{R}\,\mathrm{d}\zeta, & \varphi_{22}(z) &= \frac{1}{c}\int_{-l}^{l} I_2(\zeta)\,\frac{e^{-jkr}}{r}\,\mathrm{d}\zeta. \end{aligned}\right\} \qquad (1)$$

---

*) As usual, the discussion is confined to harmonic vibrations of frequency $\omega/2\pi$; the time dependence is $\exp(j\omega t)$.

**) c is the velocity of light, k the wave number ($k = \omega/c = 2\pi/\lambda$, where λ is the wavelength in free space). Gaussian units are used throughout.

The axial components of the electric field due to the currents $I_1(z)$ and $I_2(z)$, at the axes of the antennae, can be found by differentiation according to

$$jkE(z) = \left(\frac{\mathrm{d}^2}{\mathrm{d}z^2} + k^2\right)\left(\varphi_{11} + \varphi_{21}\right),$$

$$jkE(z) = \left(\frac{\mathrm{d}^2}{\mathrm{d}z^2} + k^2\right)\left(\varphi_{12} + \varphi_{22}\right),$$

for the first and for the second wire respectively. Now $E(z)$ must vanish along the corresponding antenna, except at the centre, where it must cancel the impressed electromotive force. In terms of the delta function we may thus write

$$\left.\begin{aligned}\left(\frac{\mathrm{d}^2}{\mathrm{d}z^2} + k^2\right)\left(\varphi_{11} + \varphi_{21}\right) &= -jkV_1\,\delta(z),\\ \left(\frac{\mathrm{d}^2}{\mathrm{d}z^2} + k^2\right)\left(\varphi_{12} + \varphi_{22}\right) &= -jkV_2\,\delta(z).\end{aligned}\right\}\ |z| \leqslant l$$

Moreover, as the φ-functions are symmetrical in z, we have by integration

$$\left.\begin{aligned}\varphi_{11}(z) + \varphi_{21}(z) &= -\tfrac{1}{2}\,jV_1 \sin k|z| + A_1 \cos kz,\\ \varphi_{12}(z) + \varphi_{22}(z) &= -\tfrac{1}{2}\,jV_2 \sin k|z| + A_2 \cos kz,\end{aligned}\right\}\ |z| \leqslant l \qquad (2)$$

where the constants of integration, A_1 and A_2, will be determined later on.

3. Approximate integral equations for the currents, and their solution

Analogous to the reasoning of paper [3]), the functions $\varphi_{11}(z)$ and $\varphi_{22}(z)$ are approximately proportional to the corresponding current distributions, viz.:

$$\varphi_{11}(z) \approx \frac{1}{c}\,I_1(z)\,\Omega(z) + \frac{1}{c}\int_{-l}^{l} \frac{I_1(\zeta)\,e^{-jk|z-\zeta|} - I_1(z)}{|z-\zeta|}\,\mathrm{d}\zeta, \qquad (3)$$

and its analogue for $\varphi_{22}(z)$ obtained when I_1 is replaced by I_2. As before [3]), $\Omega(z)$ is an abbreviation for

$$\Omega(z) = \int_{-l}^{l} \frac{\mathrm{d}\zeta}{r} \approx \Omega + \ln\left(1 - \frac{z^2}{l^2}\right),\ z \neq l.$$

We thus obtain from (1), (2), (3):

$$\frac{1}{c}\,\Omega\,I_1(z) \approx -\tfrac{1}{2}\,jV_1 \sin k|z| + A_1 \cos kz - \frac{1}{c}\,I_1(z) \ln\left(1 - \frac{z^2}{l^2}\right) -$$

$$-\frac{1}{c}\int_{-l}^{l} \frac{I_1(\zeta)\,e^{-jk|z-\zeta|} - I_1(z)}{|z-\zeta|}\,\mathrm{d}\zeta - \frac{1}{c}\int_{-l}^{l} I_2(\zeta)\,\frac{e^{-jkR}}{R}\,\mathrm{d}\zeta, \qquad (4)$$

together with a similar equation containing the corresponding quantities with suffixes (2,1) instead of (1,2).

These equations are *simultaneous* integral equations for the currents I_1 and I_2, which are approximately solved by a process of iteration, under the boundary conditions $I_1(\pm l) = I_2(\pm l) = 0$. However, this set of simultaneous equations may first be transformed into a set of mutually independent equations. For this purpose we introduce the following combinations:

$$\begin{aligned} I_\pm(z) &= I_1(z) \pm I_2(z)\,, \\ V_\pm &= V_1 \pm V_2\,, \\ A_\pm &= A_1 \pm A_2\,. \end{aligned} \tag{5}$$

While so doing we readily obtain from (4) and its analogue that

$$\frac{1}{c}\,\Omega\, I_\pm(z) \approx -\tfrac{1}{2} jV_\pm \sin k|z| + A_\pm \cos kz - \frac{1}{c}\, I_\pm(z) \ln\left(1-\frac{z^2}{l^2}\right) - \\ -\frac{1}{c}\int_{-l}^{l} \frac{I_\pm(\zeta)\, e^{-jk|z-\zeta|} - I_\pm(z)}{|z-\zeta|}\,\mathrm{d}\zeta \mp \int_{-l}^{l} I_\pm(\zeta)\,\frac{e^{-jkR}}{R}\,\mathrm{d}\zeta\,. \tag{6}$$

Evidently, the equations (6) are two different integral equations, one for I_+ and one for I_-. They, too, have to be solved under certain side conditions, namely $I_\pm(l) = 0$. If $z = l$ is substituted in the right-hand side of (6) and the resulting expression is subtracted from (6), we obtain

$$\frac{1}{c}\,\Omega\, I_\pm(z) \approx -\tfrac{1}{2} jV_\pm \{\sin k|z| - \sin kl\} + A_\pm \{\cos kz - \cos kl\} - \\ -\frac{1}{c}\, I_\pm(z) \ln\left(1-\frac{z^2}{l^2}\right) - \frac{1}{c}\int_{-l}^{l} \frac{I_\pm(\zeta)\, e^{-jk|z-\zeta|} - I_\pm(z)}{|z-\zeta|}\,\mathrm{d}\zeta + \\ +\frac{1}{c}\int_{-l}^{l} I_\pm(\zeta)\,\frac{e^{-jk(l-\zeta)}}{l-\zeta}\,\mathrm{d}\zeta \mp \frac{1}{c}\int_{-l}^{l} I_\pm(\zeta)\,\frac{e^{-jkR}}{R}\,\mathrm{d}\zeta \pm \\ \pm\frac{1}{c}\int_{-l}^{l} I_\pm(\zeta)\,\frac{e^{-jk\sqrt{(l-\zeta)^2+d^2}}}{\sqrt{(l-\zeta)^2+d^2}}\,\mathrm{d}\zeta\,. \tag{7}$$

As a first approximation we ignore the expressions on the right-hand side of (7) as far as they contain $I_\pm$ explicitly; thus

$$I_\pm(z) \approx \frac{c}{\Omega}\left[-\tfrac{1}{2} jV_\pm \{\sin k|z| - \sin kl\} + A_\pm \{\cos kz - \cos kl\}\right]. \tag{8}$$

To get the next approximation let us substitute (8) in the right-hand side of (7). The left-hand side of (7) then becomes equal to

$$\frac{1}{c}\,\Omega I_\pm(z) = -\tfrac{1}{2}\,jV_\pm\left\{f(z)+\frac{F(l)-F(z)}{\Omega}\pm\frac{H(l)-H(z)}{\Omega}\right\}+ \\ + A_\pm\left\{g(z)+\frac{G(l)-G(z)}{\Omega}\pm\frac{K(l)-K(z)}{\Omega}\right\}, \qquad (9)$$

where the following abbreviations are used:

$$f(z) = \sin k|z| - \sin kl,$$
$$g(z) = \cos kz - \cos kl,$$

$$\left.\begin{aligned}
F(z) &= \int_{-l}^{l} \frac{f(\zeta)\,e^{-jk|z-\zeta|}-f(z)}{|z-\zeta|}\,\mathrm{d}\zeta + f(z)\ln\left(1-\frac{z^2}{l^2}\right),\\
G(z) &= \int_{-l}^{l} \frac{g(\zeta)\,e^{-jk|z-\zeta|}-g(z)}{|z-\zeta|}\,\mathrm{d}\zeta + g(z)\ln\left(1-\frac{z^2}{l^2}\right),\\
H(z) &= \int_{-l}^{l} f(\zeta)\,\frac{e^{-jk\sqrt{(z-\zeta)^2+d^2}}}{\sqrt{(z-\zeta)^2+d^2}}\,\mathrm{d}\zeta,\\
K(z) &= \int_{-l}^{l} g(\zeta)\,\frac{e^{-jk\sqrt{(z-\zeta)^2+d^2}}}{\sqrt{(z-\zeta)^2+d^2}}\,\mathrm{d}\zeta.
\end{aligned}\right\} \qquad (10)$$

Explicit expressions for the integrals (10) will be given in section 5.

Except for the constants of integration, $A_\pm$, we have completely determined the currents by (9). These constants can be obtained as follows. First, substitution of $z = l$ in (6) leads to

$$0 = -\tfrac{1}{2}\,jV_\pm \sin kl + A_\pm \cos kl - \\ -\frac{1}{c}\int_{-l}^{l} I_\pm(\zeta)\,\frac{e^{-jk(l-\zeta)}}{l-\zeta}\,\mathrm{d}\zeta \mp \frac{1}{c}\int_{-l}^{l} I_\pm(\zeta)\,\frac{e^{-jk\sqrt{(l-\zeta)^2+d^2}}}{\sqrt{(l-\zeta)^2+d^2}}\,\mathrm{d}\zeta. \qquad (11)$$

Then, under the signs of integration in (11) we substitute for the current $I_\pm$ the first approximation as given by (8). The final equation is linear in $A_\pm$; its solution is readily found to be

$$A_\pm = \tfrac{1}{2}\,jV_\pm\,\frac{\Omega\sin kl - F(l) \mp H(l)}{\Omega\cos kl - G(l) \mp K(l)}. \qquad (12)$$

We shall now return to the actual currents, $I_1(z)$ and $I_2(z)$. By means of (5), (9) and (12) is is thus found that

$$\begin{aligned}
I_1(z) &= V_1\,Y_0(z) + V_2\,Y_m(z),\\
I_2(z) &= V_1\,Y_m(z) + V_2\,Y_0(z),
\end{aligned} \qquad (13)$$

in which the functions $Y_0(z)$ and $Y_m(z)$ are known completely, viz.:

$$\left.\begin{aligned} Y_0(z) &= \frac{c}{2j\Omega}\left[f(z) + \frac{F(l)-F(z)}{\Omega} - \alpha\,\Big\}g(z) + \frac{G(l)-G(z)}{\Omega}\Big\{ - \beta\,\Big\}\frac{K(l)-K(z)}{\Omega}\Big\{\right], \\ Y_m(z) &= \frac{c}{2j\Omega}\left[\frac{H(l)-H(z)}{\Omega} - \beta\,\Big\}g(z) + \frac{G(l)-G(z)}{\Omega}\Big\{ - \alpha\,\Big\}\frac{K(l)-K(z)}{\Omega}\Big\{\right], \end{aligned}\right\} \quad (14)$$

where α, β are independent of z and defined by

$$\left.\begin{aligned} 2\alpha &= \frac{\Omega \sin kl - F(l) - H(l)}{\Omega \cos kl - G(l) - K(l)} + \frac{\Omega \sin kl - F(l) + H(l)}{\Omega \cos kl - G(l) + K(l)}, \\ 2\beta &= \frac{\Omega \sin kl - F(l) - H(l)}{\Omega \cos kl - G(l) - K(l)} - \frac{\Omega \sin kl - F(l) + H(l)}{\Omega \cos kl - G(l) + K(l)}, \end{aligned}\right\} \quad (15)$$

4. Expressions for the input and mutual impedances/admittances

It is important to note that the set of equations (13) is the natural extension of one of the possible forms of the input-current - input-voltage equations of the antenna system considered as a four-terminal network. The latter equations contain the input currents rather than the current distribution, viz.:

$$\begin{aligned} I_1(0) &= Y_0(0)\ V_1 + Y_m(0)\ V_2, \\ I_2(0) &= Y_m(0)\ V_1 + Y_0(0)\ V_2. \end{aligned}$$

The driving-point admittance, $Y_0(0)$, and the transfer admittance, $Y_m(0)$, will now be considered in detail. As already indicated by the notation, they follow from (14) upon substitution of $z = 0$. The resulting expressions, however, can be simplified considerably with the aid of (15). One then obtains

$$\left.\begin{aligned} Y_0(0) &= \frac{cj}{2\Omega^2}\,[F(0) + \alpha\,\}\Omega - G(0)\{ - \beta K(0)], \\ Y_m(0) &= \frac{cj}{2\Omega^2}\,[H(0) + \beta\,\}\Omega - G(0)\{ - \alpha K(0)]. \end{aligned}\right\} \quad (16)$$

Particularly when the two antennae are driven in phase by equal voltages the input admittance of either antenna in the presence of the other is given by

$$Y_s = Y_0(0) + Y_m(0).$$

When they are driven in opposite phases, again at equal voltages, the input admittance is

$$Y_a = Y_0(0) - Y_m(0).$$

The explicit expressions for the symmetrical and anti-symmetrical admittances are readily obtained fom (16); thus

$$\left.\begin{aligned} Y_s &= \frac{cj}{2\Omega^2}[F(0)+H(0)+(\alpha+\beta)\}\Omega - G(0) - K(0)\{], \\ Y_a &= \frac{cj}{2\Omega^2}[F(0)-H(0)+(\alpha-\beta)\}\Omega - G(0) + K(0)\{]. \end{aligned}\right\} \quad (17)$$

In the same way the corresponding impedance functions may be introduced. One then gets

$$\begin{aligned} V_1 &= Z_0\, I_1(0) + Z_m\, I_2(0), \\ V_2 &= Z_m\, I_1(0) + Z_0\, I_2(0), \end{aligned}$$

where the driving-point impedance, Z_0, and the transfer impedance, Z_m, can be combined into the input impedances for the symmetrical and anti-symmetrical cases as follows:

$$Z_s = Z_0 + Z_m, \quad Z_a = Z_0 - Z_m.$$

At the same time, Z_s and Z_a are connected with Y_s and Y_a by the relations

$$Z_a\, Y_a = Z_s\, Y_s = 1.$$

5. Evaluation of the integrals (10)

It is convenient to introduce the following functions:

$$S(x) = \int_0^x \frac{\sin t}{t}\,\mathrm{d}t, \quad C(x) = \int_0^x \frac{1-\cos t}{t}\,\mathrm{d}t.$$

They are related to the well-known sine and cosine integrals by

$$S(x) = Si(x), \quad C(x) = \gamma + \ln x - Ci(x),$$

where γ is Euler's constant. Moreover, we shall introduce functions $E(x)$ and $N(x)$ by

$$\begin{aligned} E(x) &= C(x) + jS(x), \\ N(x) &= Ci(x) - jSi(x) = \gamma + \ln x - E(x), \end{aligned}$$

while $L(x)$ is an abbreviation for

$$L(x) = \int_{-l}^{l} \frac{e^{-jk\sqrt{(x-\xi)^2+d^2}}}{\sqrt{(x-\xi)^2+d^2}}\,\mathrm{d}\xi.$$

After some tedious integrations it is found that

$$F(z) = (\sin k|z| - \sin kl) \ln\left(1 - \frac{z^2}{l^2}\right) - \tfrac{1}{2}j \left\{e^{jkz} E(2kl + 2kz) + e^{-jkz} E(2kl - 2kz)\right\} +$$
$$+ je^{jk|z|} E(2k|z|) - 2 \sin k|z| \ln\left(1 + \frac{l}{|z|}\right) + \sin kl \left\{E(kl + kz) + E(kl - kz)\right\},$$

$$G(z) = (\cos kz - \cos kl) \ln\left(1 - \frac{z^2}{l^2}\right) - \tfrac{1}{2} \left\{e^{jkz} E(2kl + 2kz) + e^{-jkz} E(2kl - 2kz)\right\} +$$
$$+ \cos kl \left\{E(kl + kz) + E(kl - kz)\right\},$$
$$H(z) = \tfrac{1}{2}j\, e^{-jkz} \left\{N(kl_1) + N(kl_2) - 2N(kl_5)\right\} +$$
$$+ \tfrac{1}{2}j\, e^{jkz} \left\{N(kl_3) + N(kl_4) - 2N(kl_6)\right\} - \sin kl\, L(z),$$
$$K(z) = \tfrac{1}{2}\, e^{-jkz} \left\{N(kl_1) - N(kl_2)\right\} + \tfrac{1}{2}\, e^{jkz} \left\{N(kl_3) - N(kl_4)\right\} - \cos kl\, L(z),$$

where

$$l_1 = \sqrt{(l - z)^2 + d^2} + l - z,$$
$$l_2 = \sqrt{(l + z)^2 + d^2} - l - z,$$
$$l_3 = \sqrt{(l + z)^2 + d^2} + l + z,$$
$$l_4 = \sqrt{(l - z)^2 + d^2} - l + z,$$
$$l_5 = \sqrt{z^2 + d^2} - z,$$
$$l_6 = \sqrt{z^2 + d^2} + z.$$

It is to be remarked that $F(z)$ and $G(z)$ are identical with $-F_1(z)$ and $-G_1(z)$, respectively, given before [3]).

In order to calculate the various admittance and impedance functions we have to know the values of the functions above at $z = 0$ and $z = l$. When l and d are expressed in radians ($x = kl = 2\pi l/\lambda$; $y = kd = 2\pi d/\lambda$), then

$$F(0) = -j\, E(2x) + 2 \sin x\, E(x),$$
$$G(0) = - \quad E(2x) + 2 \cos x\, E(x),$$
$$H(0) = j\left[N(\sqrt{x^2 + y^2} + x) + N(\sqrt{x^2 + y^2} - x) - 2N(y)\right] -$$
$$- 2 \sin x \int_0^x \frac{e^{-j\sqrt{y^2+t^2}}}{\sqrt{y^2 + t^2}}\, \mathrm{d}t,$$

$$K(0) = N(\sqrt{x^2 + y^2} + x) - N(\sqrt{x^2 + y^2} - x) - 2 \cos x \int_0^x \frac{e^{-j\sqrt{y^2+t^2}}}{\sqrt{y^2 + t^2}}\, \mathrm{d}t,$$
$$F(l) = -\tfrac{1}{2}je^{jx} E(4x) + j \cos x\, E(2x) - \ln 4 \sin x,$$
$$G(l) = -\tfrac{1}{2}\, e^{jx} E(4x) + \cos x\, E(2x),$$

$$H(l) = \tfrac{1}{2}\, j e^{-jx} \left[N(y) + N(\sqrt{4x^2+y^2} - 2x) - 2\, N(\sqrt{x^2+y^2} - x) + \right.$$
$$+ \tfrac{1}{2}\, j e^{jx} \left[N(y) + N(\sqrt{4x^2+y^2} + 2x) - 2\, N(\sqrt{x^2+y^2} + x) - \right.$$
$$- \sin x \int_0^{2x} \frac{e^{-j\sqrt{y^2+t^2}}}{\sqrt{y^2+t^2}}\, dt,$$

$$K(l) = \tfrac{1}{2}\, e^{-jx} \left[N(y) - N(\sqrt{4x^2+y^2} - 2x)\right] +$$
$$+ \tfrac{1}{2}\, e^{jx} \left[N(\sqrt{4x^2+y^2} + 2x) - N(y)\right] -$$
$$- \cos x \int_0^{2x} \frac{e^{-j\sqrt{y^2+t^2}}}{\sqrt{y^2+t^2}}\, dt.$$

6. Tables

The functions $F(0)$, $G(0)$, $F(l)$, and $G(l)$ are readily tabulated with the aid of existing tables of the sine and cosine integrals [7]). They are given in table I; the functions depend on x, not on y.

The four remaining functions are less tractable because of the definite integral

$$\int_0^{x} \frac{e^{-j\sqrt{y^2+t^2}}}{\sqrt{y^2+t^2}}\, dt. \tag{18}$$

The integral (18) has been evaluated by graphical methods [8]); there is also available an analytical solution [9]) involving double summations, and the present author evaluated (18) by another analytical procedure [10]), further details of which will not be given for the moment. Only recently we developed an expression that, though not investigated on convergence yet, seems very useful because of its remarkable simplicity, the integral (18), when $x > 0$ and $y > 0$, being equal to

$$J_0(y) \ln \left\{ \sqrt{1 + \frac{x^2}{y^2}} + \frac{x}{y} \right\} +$$
$$+ \sum_{n=1}^{\infty} (-j)^n \frac{J_n(y)}{n} \left[\left\{ \sqrt{1 + \frac{x^2}{y^2}} + \frac{x}{y} \right\}^n - \left\{ \sqrt{1 + \frac{x^2}{y^2}} - \frac{x}{y} \right\}^n \right], \tag{19}$$

where J_n denotes the ordinary Bessel function. To prove this formula we introduce a new variable of integration by

$$t = \frac{y}{2} \left(\frac{1}{s} - s \right),$$

which transforms the integral (18) into

$$\int\limits_{\sqrt{1+\frac{x^2}{y^2}}-\frac{x}{y}}^{1} \exp\left\{\tfrac{1}{2}y\left(\frac{s}{j}-\frac{j}{s}\right)\right\} \mathrm{d}s/s\,,$$

and next integrate term-by-term, after having expanded the exponential function according to a well-known theorem of Bessel functions, namely,

$$\exp\left\{\tfrac{1}{2}y\left(\frac{s}{j}-\frac{j}{s}\right)\right\} = J_0(y) + \sum_{n=1}^{\infty} (-j)^n\,(s^n + s^{-n})\,J_n(y)\,.$$

As numerical values of the N-functions are obtainable from the American tables of the sine and cosine integrals, the functions $H(0)$, $K(0)$, $H(l)$ and $K(l)$ can now be determined. The corresponding data are presented in tables II-V. They enable one to calculate the impedances and admittances in the neighbourhood of the first resonance (half-wave antenna, $x \approx \pi/2$) when the distance between the two conductors does not exceed the length of either of them ($d/l \leqslant 2$).

Eindhoven, June 1947

REFERENCES

1) **Erik Hallén**, Theoretical investigations into the transmitting and receiving qualities of antennae, Nova Acta regiae societatis scientiarum upsaliensis, Ser. IV, **11**, 1-44, 1938.

2) **Ronold King** and **F. G. Blake**, The self-impedance of a symmetrical antenna, Proc. Inst. Radio Engrs **30**, 335-349, 1942.

3) **C. J. Bouwkamp**, Hallén's theory for a straight perfectly conducting wire, used as a transmitting or receiving aerial, Physica, 's-Grav. **9**, 609-631, 1942.

4) **Ronold King** and **C. W. Harrison**, Jr, The distribution of current along a symmetrical center-driven antenna, Proc. Inst. Radio Engrs **31**, 548-567 (697), 1943.

5) **C. J. Bouwkamp**, Laboratory report nr 1731, November 1942 (unpublished).

6) **Ronold King** and **C. W. Harrison**, Jr, Mutual and self-impedance for coupled antennas, J. appl. Phys. **15**, 481-495, 1944.

7) Federal Works Agency, Work projects administration for the City of New York, Tables of sine, cosine and exponential integrals, vols I, II, New York, 1940; Tables of sine and cosine integrals, New York, 1942.

8) **C. W. Harrison**, Jr, A note on the mutual impedance of antennas, J. appl. Phys. **14**, 306-309, 1943.

9) **C. Weinbaum**, On the solution of definite integrals occurring in antenna theory, J. appl. Phys. **15**, 840-841, 1944.

10) **C. J. Bouwkamp**, Laboratory report nr 1693, June 1942 (unpublished).

Contents of tables:

$$E(x) = \int_0^x \frac{\sin t}{t}\,\mathrm{d}t + j\int_0^x \frac{1-\cos t}{t}\,\mathrm{d}t,\quad N(x) = \gamma + \ln x - E(x),$$

Table I:
$$F(0) = -j\,E(2x) + 2\sin x\,E(x),$$
$$G(0) = -\,E(2x) + 2\cos x\,E(x),$$
$$F(l) = -\tfrac{1}{2}je^{jx}E(4x) + j\cos x\,E(2x) - \ln 4\,.\,\sin x,$$
$$G(l) = -\tfrac{1}{2}e^{jx}E(4x) + \cos x\,E(2x).$$

Table II:
$$H(0) = j\left[N(\sqrt{x^2+y^2}+x) + N(\sqrt{x^2+y^2}-x) - 2N(y)\right] - 2\sin x\int_0^x \frac{e^{-j\sqrt{y^2+t^2}}}{\sqrt{y^2+t^2}}\,\mathrm{d}t.$$

Table III:
$$K(0) = N(\sqrt{x^2+y^2}+x) - N(\sqrt{x^2+y^2}-x) - 2\cos x\int_0^x \frac{e^{-j\sqrt{y^2+t^2}}}{\sqrt{y^2+t^2}}\,\mathrm{d}t.$$

Table IV:
$$H(l) = \tfrac{1}{2}je^{-jx}\left[N(y) + N(\sqrt{4x^2+y^2}-2x) - 2N(\sqrt{x^2+y^2}-x)\right] + \tfrac{1}{2}je^{jx}\left[N(y) + N(\sqrt{4x^2+y^2}+2x) - 2N(\sqrt{x^2+y^2}+x)\right] - \sin x\int_0^{2x} \frac{e^{-j\sqrt{y^2+t^2}}}{\sqrt{y^2+t^2}}\,\mathrm{d}t.$$

Table V:
$$K(l) = \tfrac{1}{2}e^{-jx}\left[N(y) - N(\sqrt{4x^2+y^2}-2x)\right] + \tfrac{1}{2}e^{jx}\left[-N(y) + N(\sqrt{4x^2+y^2}+2x)\right] - \cos x\int_0^{2x} \frac{e^{-j\sqrt{y^2+t^2}}}{\sqrt{y^2+t^2}}\,\mathrm{d}t.$$

TABLE I

x	$F(0)$	$G(0)$	$F(l)$	$G(l)$
1·0	2·009 + 0·745 *j*	— 0·588 — 0·583 *j*	— 0·674 + 0·629 *j*	0·629 — 0·493 *j*
1·1	2·200 + 0·843 *j*	— 0·730 — 0·754 *j*	— 0·620 + 0·687 *j*	0·687 — 0·616 *j*
1·2	2·385 + 0·930 *j*	— 0·890 — 0·950 *j*	— 0·547 + 0·728 *j*	0·728 — 0·745 *j*
1·3	2·559 + 1·002 *j*	— 1·069 — 1·167 *j*	— 0·458 + 0·750 *j*	0·750 — 0·878 *j*
1·4	2·722 + 1.056 *j*	— 1·267 — 1·405 *j*	— 0·357 + 0·753 *j*	0·753 — 1·009 *j*
1·5	2·871 + 1·087 *j*	— 1·484 — 1·661 *j*	— 0·248 + 0·734 *j*	0·734 — 1·135 *j*
1·6	3·002 + 1·092 *j*	— 1·719 — 1·933 *j*	— 0·134 + 0·696 *j*	0·696 — 1·252 *j*
1·7	3·113 + 1·070 *j*	— 1·971 — 2·215 *j*	— 0·020 + 0·638 *j*	0·638 — 1·355 *j*
1·8	3·201 + 1·017 *j*	— 2·238 — 2·506 *j*	0·092 + 0·562 *j*	0·562 — 1·442 *j*
1·9	3·264 + 0·932 *j*	— 2·663 — 2·801 *j*	0·192 + 0·471 *j*	0·471 — 1·510 *j*
2·0	3·299 + 0·815 *j*	— 2·810 — 3·094 *j*	0·296 + 0·367 *j*	0·367 — 1·556 *j*

TABLE II, *H*(0)

y/*x* \ *x*	1·0	1·2	1·4	1·6	1·8	2·0
0·2	— 2·208 + 0·739 *j*	— 2·303 + 0·921 *j*	— 2·264 + 1·041 *j*	— 2·099 + 1·073 *j*	— 1·834 + 0·994 *j*	— 1·498 + 0·793 *j*
0·4	— 1·312 + 0·729 *j*	— 1·311 + 0·894 *j*	— 1·220 + 1·001 *j*	— 1·066 + 1·018 *j*	— 0·860 + 0·930 *j*	— 0·651 + 0·731 *j*
0·6	— 0·853 + 0·700 *j*	— 0·794 + 0·847 *j*	— 0·675 + 0·934 *j*	— 0·518 + 0·929 *j*	— 0·359 + 0·828 *j*	— 0·234 + 0·634 *j*
0·8	— 0·559 + 0·667 *j*	— 0·458 + 0·792 *j*	— 0·318 + 0·844 *j*	— 0·169 + 0·813 *j*	— 0·044 + 0·696 *j*	0·020 + 0·511 *j*
1·0	— 0·345 + 0·625 *j*	— 0·220 + 0·720 *j*	— 0·072 + 0·739 *j*	0·063 + 0·675 *j*	0·143 + 0·544 *j*	0·177 + 0·372 *j*
1·2	— 0·187 + 0·577 *j*	— 0·044 + 0·637 *j*	0·104 + 0·618 *j*	0·227 + 0·525 *j*	0·281 + 0·383 *j*	0·248 + 0·231 *j*
1·4	— 0·065 + 0·523 *j*	0·090 + 0·545 *j*	0·234 + 0·490 *j*	0·329 + 0·371 *j*	0·342 + 0·226 *j*	0·274 + 0·100 *j*
1·6	0·035 + 0·463 *j*	0·188 + 0·449 *j*	0·316 + 0·360 *j*	0·376 + 0·222 *j*	0·352 + 0·081 *j*	0·254 — 0·012 *j*
1·8	0·110 + 0·400 *j*	0·257 + 0·351 *j*	0·359 + 0·233 *j*	0·380 + 0·084 *j*	0·319 — 0·041 *j*	0·203 — 0·098 *j*
2·0	0·167 + 0·335 *j*	0·301 + 0·253 *j*	0·368 + 0·113 *j*	0·349 — 0·034 *j*	0·256 — 0·135 *j*	0·134 — 0·152 *j*

TABLE III, *K*(0)

y/*x* \ *x*	1·0	1·2	1·4	1·6	1·8	2·0
0·2	1·553 — 0·580 *j*	2·069 — 0·940 *j*	2·570 — 1·387 *j*	3·018 — 1·899 *j*	3·374 — 2·450 *j*	3·647 — 3·009 *j*
0·4	0·955 — 0·568 *j*	1·226 — 0·912 *j*	1·446 — 1·331 *j*	1·590 — 1·799 *j*	1·640 — 2·286 *j*	1·569 — 2·760 *j*
0·6	0·633 — 0·548 *j*	0·753 — 0·868 *j*	0·806 — 1·241 *j*	0·765 — 1·641 *j*	0·624 — 2·029 *j*	0·386 — 2·371 *j*
0·8	0·418 — 0·522 *j*	0·439 — 0·807 *j*	0·372 — 1·222 *j*	0·207 — 1·432 *j*	— 0·055 — 1·696 *j*	— 0·395 — 1·880 *j*
1·0	0·262 — 0·490 *j*	0·207 — 0·734 *j*	0·057 — 0·979 *j*	— 0·186 — 1·185 *j*	— 0·505 — 1·313 *j*	— 0·879 — 1·333 *j*
1·2	0·140 — 0·451 *j*	0·030 — 0·649 *j*	— 0·173 — 0·818 *j*	— 0·454 — 0·916 *j*	— 0·784 — 0·909 *j*	— 1·115 — 0·778 *j*
1·4	0·043 — 0·408 *j*	— 0·103 — 0·555 *j*	— 0·334 — 0·647 *j*	— 0·617 — 0·641 *j*	— 0·910 — 0·514 *j*	— 1·155 — 0·263 *j*
1·6	— 0·031 — 0·361 *j*	— 0·202 — 0·456 *j*	— 0·437 — 0·471 *j*	— 0·693 — 0·373 *j*	— 0·911 — 0·152 *j*	— 1·033 + 0·170 *j*
1·8	— 0·090 — 0·313 *j*	— 0·271 — 0·354 *j*	— 0·490 — 0·301 *j*	— 0·692 — 0·128 *j*	— 0·813 + 0·153 *j*	— 0·798 + 0·493 *j*
2·0	— 0·135 — 0·262 *j*	— 0·313 — 0·270 *j*	— 0·501 — 0·142 *j*	— 0·632 + 0·083 *j*	— 0·643 + 0·383 *j*	— 0·498 + 0·688 *j*

TABLE IV, $H(l)$

y/x \ x	1·0	1·2	1·4	1·6	1·8	2·0
0·2	— 0·551 + 0·624 j	— 0·433 + 0·720 j	— 0·266 + 0·742 j	— 0·084 + 0·681 j	0·086 + 0·546 j	0·219 + 0·354 j
0·4	— 0·426 + 0·609 j	— 0·299 + 0·697 j	— 0·142 + 0·707 j	0·016 + 0·638 j	0·144 + 0·500 j	0·221 + 0·312 j
0·6	— 0·302 + 0·589 j	— 0·167 + 0·660 j	— 0·015 + 0·652 j	0·124 + 0·571 j	0·216 + 0·427 j	0·244 + 0·250 j
0·8	— 0·191 + 0·559 j	— 0·048 + 0·608 j	0·101 + 0·580 j	0·221 + 0·482 j	0·281 + 0·334 j	0·265 + 0·172 j
1·0	— 0·093 + 0·521 j	0·056 + 0·546 j	0·199 + 0·493 j	0·297 + 0·377 j	0·324 + 0·229 j	0·272 + 0·087 j
1·2	— 0·007 + 0·477 j	0·144 + 0·474 j	0·274 + 0·397 j	0·346 + 0·264 j	0·340 + 0·120 j	0·258 + 0·004 j
1·4	0·065 + 0·428 j	0·214 + 0·396 j	0·327 + 0·293 j	0·367 + 0·150 j	0·328 + 0·016 j	0·225 — 0·070 j
1·6	0·127 + 0·375 j	0·266 + 0·314 j	0·358 + 0·189 j	0·360 + 0·042 j	0·291 — 0·077 j	0·172 — 0·127 j
1·8	0·179 + 0·318 j	0·301 + 0·232 j	0·359 + 0·090 j	0·327 — 0·055 j	0·233 — 0·153 j	0·111 — 0·164 j
2·0	0·213 + 0·260 j	0·316 + 0·149 j	0·337 — 0·001 j	0·276 — 0·135 j	0·156 — 0·197 j	0·046 — 0·175 j

TABLE V, $K(l)$

y/x \ x	1·0	1·2	1·4	1·6	1·8	2·0
0·2	0·480 — 0·490 j	0·524 — 0·737 j	0·493 — 0·993 j	0·383 — 1·225 j	0·207 — 1·401 j	— 0·018 — 1·499 j
0·4	0·355 — 0·479 j	0·347 — 0·713 j	0·261 — 0·949 j	0·097 — 1·148 j	— 0·128 — 1·282 j	— 0·387 — 1·330 j
0·6	0·248 — 0·461 j	0·193 — 0·675 j	0·057 — 0·874 j	— 0·150 — 1·025 j	— 0·412 — 1·095 j	— 0·690 — 1·069 j
0·8	0·155 — 0·438 j	0·060 — 0·623 j	— 0·117 — 0·777 j	— 0·354 — 0·864 j	— 0·632 — 0·857 j	— 0·898 — 0·745 j
1·0	0·075 — 0·409 j	— 0·053 — 0·558 j	— 0·258 — 0·659 j	— 0·508 — 0·676 j	— 0·774 — 0·586 j	— 0·997 — 0·391 j
1·2	0·007 — 0·374 j	— 0·147 — 0·485 j	— 0·364 — 0·529 j	— 0·610 — 0·472 j	— 0·833 — 0·305 j	— 0·983 — 0·043 j
1·4	— 0·051 — 0·335 j	— 0·220 — 0·405 j	— 0·436 — 0·390 j	— 0·660 — 0·267 j	— 0·814 — 0·037 j	— 0·864 + 0·265 j
1·6	— 0·098 — 0·294 j	— 0·273 — 0·321 j	— 0·476 — 0·252 j	— 0·650 — 0·071 j	— 0·724 + 0·198 j	— 0·669 + 0·503 j
1·8	— 0·135 — 0·249 j	— 0·308 — 0·235 j	— 0·481 — 0·117 j	— 0·591 + 0·101 j	— 0·578 + 0·388 j	— 0·421 + 0·653 j
2·0	— 0·163 — 0·204 j	— 0·324 — 0·151 j	— 0·458 + 0·006 j	— 0·496 + 0·247 j	— 0·394 + 0·510 j	— 0·152 + 0·707 j

R 82 *Philips Res. Rep. 3, 227-234, 1948*

VALVE CHARACTERISTIC GIVING LINEAR MODULATION WHEN A FEEDBACK RESISTOR IS INSERTED IN THE CATHODE LEAD

by W. W. BOELENS

621.396.619.231:621.396.645.37

Summary

It is well known that a high-frequency voltage can be modulated with a low-frequency signal by applying both voltages to the control grid of a radio valve. If the I_a-V_g characteristic is quadratic, there will be no distortion in the modulation. The available valves, however, generally have a characteristic that is not so much quadratic as exponential. A feedback resistor in the cathode lead was found to improve the linearity of the modulation; there was an optimal value for the resistance.
The theoretical question was put as to what valve characteristic would give linear modulation with a given feedback resistance. This problem is solved in the present article and a simple answer is found. Two figures are drawn for the characteristics with the feedback resistance as a parameter.

Résumé

Il est bien connu qu'une tension de haute fréquence peut être modulée par un signal de basse fréquence en appliquant les deux tensions sur la grille de commande d'un tube radioélectrique. Si la caractéristique I_a-V_g est quadratique il y aura modulation sans distorsion. Toutefois, les tubes disponibles ont généralement une caractéristique plus exponentielle que quadratique. Une résistance de contre-réaction dans la cathode parut améliorer la linéarité de la modulation; il existait une valeur optimum pour la résistance.
Une question théorique se posait. Quelle forme de la caractéristique du tube donnerait une modulation linéaire avec une résistance de contre-réaction donnée. Le problème est résolu dans cet article et apporte une solution simple et élégante à la question. Deux figures sont tirées des caractéristiques, avec la résistance de contre-réaction comme paramètre.

1. Introduction

There are several examples in radio engineering where a high-frequency voltage has to be modulated with a low-frequency signal. This can be done in many ways, one of the simplest being to apply the two voltages to the control grid of a valve. If the I_a-V_g characteristic is not linear, the plate current will contain the desired modulation component, in addition to the components caused by the original voltages. The best results are obtained when the valve characteristic is mainly quadratic, as is well known.

We came across this problem when engaged on an investigation in connection with frequency modulators. One of the first possibilities suggested is that of the reactance valve with a small high-frequency voltage imposed on the control grid, in phase quadrature with the voltage on the oscillator circuit. The low-frequency signal is also fed to this electrode, for changing the working point. Many examples of this circuit may be found in the literature of 1940 and thereabouts.

The characteristic of a reactance valve should be quadratic. However, there are only a few types that satisfy this condition reasonably, and they have other drawbacks. The normal valve, with sharp cut-off, is too straight in the usual working range and can only be used as a modulator near cut-off, where the currents are low. The characteristic of the other type, the variable-mu valve, is more exponential and the approximation by a quadratic holds only over too small a part.

Using a variable-mu valve as a reactance modulator we found that the linearity of the modulation could be much improved by inserting a resistor in the cathode lead, not by-passed for the low frequencies, so that feedback for the modulating voltage was obtained.

It proved that a particular value of the resistance gave the best results, whereas the linearity was less with higher and smaller values, contrary to the behaviour of the normal amplifier with cathode feedback.

In fact this was to be expected, for a curved characteristic is flattened by a feedback resistor in the cathode lead. Consequently, if a valve with a more than quadratic, e.g. an exponential, characteristic is used and a quadratic one is desired, it is evident that by applying a specified measure of feedback the best possible approximation can be obtained and that with more or with less feedback the result will not be so good.

This, of course, is only a qualitative reasoning; in order to obtain a clearer insight the following theoretical problem was set up.

2. Mathematical problem

Let us assume that we have a valve with an extremely high dynamic plate resistance, e.g. a pentode, in the circuit drawn in fig. 1. Both the high-frequency voltage $a \cos \omega t$ and the low-frequency signal $\lambda = \lambda(t)$ are applied to the control grid; ω is assumed to be high compared with all the frequencies and their harmonics, as far as they are of importance, contained in λ.

In the cathode lead there is a resistor by-passed with an inductor and a capacitor, the values of which are such that the total impedance is zero for direct current and all currents with frequencies of the order of ω and its harmonics, whilst the impedance is R for all currents with frequencies contained in λ and their harmonics. In the plate lead an L-C circuit is inserted; it is assumed to have a constant impedance R_p for the frequency ω and all sidebands caused by the modulation with λ, whilst the impedance is zero for the direct current, the frequencies contained in λ and their harmonics as as well for all harmonics of ω, modulated as they are with λ or harmonics thereof.

The valve is limited neither by grid current nor by plate-current cutoff. A.C. voltage should not exist between the cathode and the screen or the suppressor grid.

We want to know the valve characteristic for the case that the voltage on the plate network is the high-frequency signal modulated linearly with the low-frequency intelligence according to $a_p \{1 + m\lambda(t)\} \cos \omega t$.

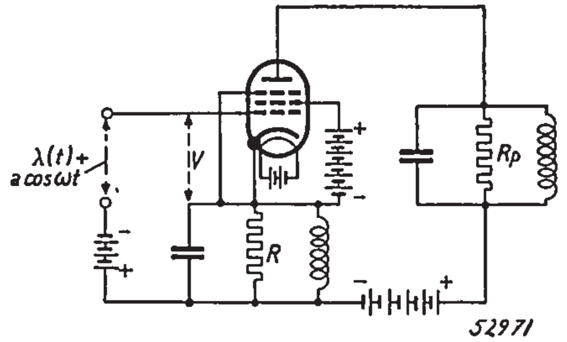

Fig. 1. Circuit in which the valve is used.
Impedance in cathode lead is 0 for direct current,
R for λ and its harmonics,
0 for ω and its harmonics.
Impedance in plate lead is 0 for direct current and λ and its harmonics,
R_p for ω and its sidebands,
0 for all harmonics of ω.

3. Solution

Let i denote the total plate current, i_λ that part of i composed of currents with frequencies contained in λ and their harmonics, as far as they cannot be disregarded, and i_ω that part of i that is composed of the current with the frequency ω and all currents with frequencies consisting of the sum or the difference of ω and frequencies contained in λ or harmonics thereof.

The valve characteristic in the neighbourhood of the working point is represented as a Maclaurin series with the D.C. component ignored:

$$i = \sum_{n=1}^{\infty} S_n \frac{v^n}{n!}.$$

Thus i is the deviation from the normal plate current corresponding to a deviation v from the normal grid voltage. S_n is the value of the nth derivative in the working point of the characteristic, $S_n = \mathrm{d}^n i/\mathrm{d}v^n$. Consequently S_1 is the normal transconductance.

Because of the feedback,

$$v = a \cos \omega t + \lambda - i_\lambda R.$$

Accordingly,

$$i = \sum_{n=1}^{\infty} \frac{S_n}{n!} (a \cos \omega t + \lambda - i_\lambda R)^n.$$

From this i_λ and i_ω can be calculated, considering that $\cos^{2k}\omega t$ has a D.C. part

$$\frac{1}{2\pi} \int_{-\pi}^{\pi} \cos^{2k}\omega t \, \mathrm{d}(\omega t) = \frac{(2k)!}{4^k (k!)^2},$$

and $\cos^{2k+1}\omega t$ a part with frequency ω and amplitude

$$\frac{1}{\pi} \int_{-\pi}^{\pi} \cos^{2k+2}\omega t \, \mathrm{d}(\omega t) = \frac{2(2k+2)!}{4^{k+1}\{(k+1)!\}^2}.$$

Now

$$i_\lambda = \sum_{a=1}^{\infty} \frac{1}{a!} (\lambda - i_\lambda R)^a . \sum_{k=0}^{\infty} A_k S_{a+2k},$$

in which $A_k = \dfrac{a^{2k}}{4^k (k!)^2}$ and consequently $A_0 = 1$.

In fact, according to the definition of i_λ, the powers of $(\lambda - i_\lambda R)$ ought to be developed in harmonics and intermodulation terms of λ, whilst the D.C. term should be ignored. But in the following the coefficients of the various terms of this power series will be made equal to the corresponding coefficients of a second power series, originating from the calculation of i_ω. The conditions resulting from this procedure will be the same either for the two power series or for the developments of both series in harmonics and intermodulation terms, but as these developments would necessitate a complicated calculation the power series will be used.

The first term, $a = 1$, is separated from the summation over a; the part with $i_\lambda R$ is combined with i_λ on the left side of the equation and then i_λ is resolved:

$$i_\lambda = \lambda \frac{\sum\limits_{k=0}^{\infty} A_k S_{2k+1}}{1 + R \sum\limits_{k=0}^{\infty} A_k S_{2k+1}} + \sum_{a=2}^{\infty} \frac{(\lambda - i_\lambda R)^a}{a!} . \frac{\sum\limits_{k=0}^{\infty} A_k S_{a+2k}}{1 + R \sum\limits_{k=0}^{\infty} A_k S_{2k+1}}.$$

If we define $B_l = \dfrac{a^{2l}}{4^l \, l! \, (l+1)!}$,

$$i_\omega = a\cos\omega t \sum_{a=0}^{\infty} \frac{(\lambda - i_\lambda R)^a}{a!} \sum_{l=0}^{\infty} B_l S_{a+2l+1} =$$

$$= a\cos\omega t \left[\sum_{l=0}^{\infty} B_l S_{2l+1} + (\lambda - i_\lambda R)\sum_{l=0}^{\infty} B_l S_{2l+2} + \sum_{a=2}^{\infty} \frac{(\lambda - i_\lambda R)^a}{a!}\sum_{l=0}^{\infty} B_l S_{a+2l+1}\right].$$

In the second term the value of i_λ is substituted:

$$i_\omega = a\cos\omega t \left[\sum_{l=0}^{\infty} B_l S_{2l+1} + \lambda \frac{\sum\limits_{l=0}^{\infty} B_l S_{2l+2}}{1 + R\sum\limits_{k=0}^{\infty} A_k S_{2k+1}} + \right.$$

$$\left. + \sum_{a=2}^{\infty} \frac{(\lambda - i_\lambda R)^a}{a!} \left\{ \sum_{l=0}^{\infty} B_l S_{a+2l+1} - \frac{R\left(\sum\limits_{k=0}^{\infty} A_k S_{a+2k}\right)\left(\sum\limits_{l=0}^{\infty} B_l S_{2l+2}\right)}{1 + R\sum\limits_{k=0}^{\infty} A_k S_{2k+1}} \right\}\right].$$

In the expression between brackets the first term is the amplitude of the carrier, the second one the value of the desired linear modulation, the third term comprising the distortion in the modulation. Consequently, there will be no distortion if this term is zero for all values of λ and i_λ, that is, if

$$\sum_{l=0}^{\infty} B_l S_{a+2l+1} = \frac{R\left(\sum\limits_{k=0}^{\infty} A_k S_{a+2k}\right)\left(\sum\limits_{l=0}^{\infty} B_l S_{2l+2}\right)}{1 + R\sum\limits_{k=0}^{\infty} A_k S_{2k+1}} \qquad \text{for } a = 2,\ 3,\ 4, \ldots.$$

This can also be written

$$\frac{\sum\limits_{l=0}^{\infty} B_l S_{a+2l+1}}{\sum\limits_{l=0}^{\infty} B_l S_{2l+2}} = \frac{R\sum\limits_{k=0}^{\infty} A_k S_{a+2k}}{1 + RS_1 + R\sum\limits_{k=1}^{\infty} A_k S_{2k+1}}.$$

When S_1 and S_2 are chosen arbitrarily and

$$S_n = \left(\frac{RS_2}{1 + RS_1}\right)^{n-2} . S_2 \quad , \quad n = 2, 3, 4, 5, \ldots,$$

this condition is fulfilled, for the quotient on the left side then becomes

$$\left(\frac{RS_2}{1 + RS_1}\right)^{a-1},$$

and the quotient on the right side has the same value if the denominator is reduced thus:

$$1 + RS_1 + R\sum_{k=1}^{\infty} A_k S_{2k+1} = 1 + RS_1 + RS_2 \sum_{k=1}^{\infty} A_k \left(\frac{RS_2}{1 + RS_1}\right)^{2k-1} =$$

$$= \left(\frac{1+RS_1}{RS_2}\right) RS_2 \left\{1 + \sum_{k=1}^{\infty} A_k \left(\frac{RS_2}{1+RS_1}\right)^{2k}\right\} = \left(\frac{1+RS_1}{RS_2}\right) RS_2 \sum_{k=0}^{\infty} A_k \left(\frac{RS_2}{1+RS_1}\right)^{2k}.$$

With this value of S_n the valve characteristic becomes

$$i = S_1 v + S_2 \sum_{n=2}^{\infty} \left(\frac{RS_2}{1+RS_1}\right)^{n-2} \frac{v^n}{n!} = \frac{(1+RS_1)^2}{R^2 S_2}\left(e^{\frac{RS_2}{1+RS_1}v} - 1\right) - \frac{v}{R}.$$

The transconductance S can be found by differentiating this expression with respect to v:

$$S = \frac{\mathrm{d}i}{\mathrm{d}v} = \frac{1 + RS_1}{R} e^{\frac{RS_2}{1+RS_1}v} - \frac{1}{R}.$$

4. Discussion of the characteristic derived

The characteristic derived is a combination of an exponential and a linear function. The extreme cases are (a) no cathode resistor ($R = 0$) and (b) a very large resistance ($R \rightarrow \infty$). When $R = 0$ the first expression for i gives

$$i_{R=0} = S_1 v + \frac{S_2}{2} v^2,$$

the quadratic characteristic that could be expected.
With $R \rightarrow \infty$ the exponential expression becomes

$$i_{R\rightarrow\infty} = \frac{S_1^2}{S_2}\left(e^{\frac{S_2}{S_1}v} - 1\right).$$

To get a clearer insight into these characteristics, curves have been drawn for several values of R, while S_1 and S_2 are kept constant. For the calculation new variables can be introduced according to

$$X = \frac{S_2}{S_1} v,\ \ Y = \frac{S_2}{S_1^2} i,\ \ \varrho = \frac{RS_1}{1 + RS_1};$$

then the equation for the characteristic becomes

$$Y = \frac{1}{\varrho^2}\left(e^{\varrho X} - 1\right) - \frac{1-\varrho}{\varrho} X,$$

and the formula for the transconductance

$$\frac{S}{S_1} = \frac{\mathrm{d}Y}{\mathrm{d}X} = \frac{1}{\varrho}\left(e^{\varrho X} - 1 + \varrho\right).$$

Curves for five values of R, including the extremes, are drawn in figs 2 and 3. By comparing a given valve characteristic with these, the value of the cathode resistance necessary for a linear modulation can be found. It is often possible to use quite a large part of the characteristic.

The same effect can be obtained by inserting a resistor in the screen-grid lead. From the ratio between screen-grid and plate current and the amplification factor between control grid and screen grid the resistance can be calculated that gives the same feedback as that obtained by introducing a suitable cathode resistor. But since these ratios are still somewhat

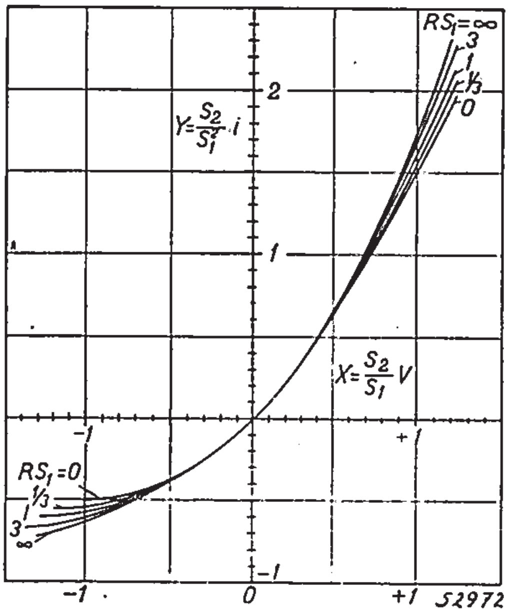

Fig. 2. Valve characteristics that give linear modulation with a specified cathode resistance.

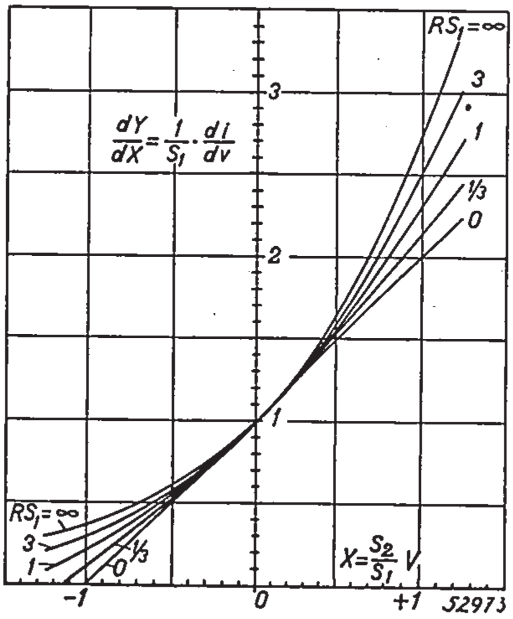

Fig. 3. Transconductance curves giving linear modulation with a specified cathode resistance.

dependent upon the other valve parameters, the value found will only be a fairly good approximation. The optimal resistance has to be determined by measurement.

The trend of the curves in fig. 2 is to flatten with decreasing RS_1, and one would expect them to flatten further when negative values of RS_1 are used. An examination of the exponential expression for the characteristic shows that if RS_1 is chosen just smaller than -1 (or $\varrho = -\infty$),

$$Y = X,$$

the straight line through the origin and the point (1,1). When values of RS_1 are taken between -1 and 0, curves will be found between the linear and the quadratic.

Consequently, valve characteristics that are curved but less than quadratic can be improved with feedback by a negative cathode resistance. This is of course the same as a normal positive feedback. There being no resistors with negative value, the circuit has to be changed, e.g. a transformer can be used that imposes a voltage, derived from the low-frequency plate-current component, in the grid circuit or in any other suitable place.

However, in general a valve will be used that can be improved with a simple resistor. The other solution will only be chosen if great advantages of that special valve outweigh the complications of an extra transformer.

Eindhoven, April 1948

R 83 *Philips Res. Rep.* **3**, *235-238, 1948*

SOME INVESTIGATIONS IN THE SYSTEM Na_2O-PbO-TiO_2-SiO_2

by J. M. STEVELS **666.115:539.213**

Summary

A number of diagrams is given showing the vitreous and the crystalline regions in the systems Na_2O-SiO_2-Pb_2TiO_4, Na_2O-SiO_2-$PbTiO_3$ and Na_2O-SiO_2-$PbTi_2O_5$.

Résumé

Pour les systèmes Na_2O-SiO_2-Pb_2TiO_4, Na_2O-SiO_2-$PbTiO_3$, et Na_2O-SiO_2-$PbTi_2O_5$ l'auteur donne des diagrammes indiquant si à une composition donnée correspond l'état vitreux ou l'état cristalline.

It is well known that Ti^{4+} and Pb^{++} ions may be used for producing a considerable increase in the refractive index of glass. Pb^{++} ions, however, make the glass very sensitive to reduction during the melting process, whereas Ti^{4+} ions tend to produce a coloured glass, especially if more than of the order of 5% TiO_2 is present *).

Colourless glasses may be obtained, if TiO_2 is added simultaneously with ZnO and (or) CdO even if TiO_2 is added in fairly large proportions [1]). Hence it seemed worth trying to prepare lead-titanate glasses that, in comparison with those prepared with Zn_2TiO_4 and Cd_2TiO_4, should have the advantage of a considerably lower melting range, particularly so when Na_2O is used as the fourth component.

These arguments induced us to investigate the system Na_2O-PbO-TiO_2-SiO_2. However, though the vitreous state was found to exist over a wide range of compositions, not a single of these glasses proved to be colourless.

The reason for this behaviour is to-day (1948) much better understood than it was at the time of the investigation (1945). We have elsewhere discussed the colour of glass in extenso [2]) so that we feel justified in only briefly treating the problem here.

The Ti^{4+} ions may occur in glass as network-formers or as network-modifiers; in other words, they may have (for oxygen ions) a coordination number 4 or 6. In the latter case the absorption of the Ti^{4+} ions lies entirely in the near ultraviolet region of the spectrum, whereas in the former case the absorption extends into the violet part of the spectrum, thus giving rise to a yellow colour of the glass. Since both the Zn^{++} and the Cd^{++} ions prefer the tetrahedral places in the glass, a major fraction of the Ti^{4+}

---

*) In keeping with common usage in glass technology, all percentages quoted are weight percentages.

ions is by these ions forced into the octohedral positions. Pb^{++} ions, on the other hand, prefer the octohedral places, so that by them the Ti^{4+} ions are moved into the tetrahedral places, thus causing the yellow colour observed in our experiments.

Since the diagram resulting from our investigations may be of more general utility we shall briefly describe our experiments in the following section.

Finally it should be noted that the boundary lines in the diagrams have been drawn by free hand so as to fit the observations in the most reasonable manner.

Experimental results

Three different mixtures of Pb_3O_4 and TiO_2 were prepared, such as might be expected to act in glass as $PbO + TiO_2$, $PbO + 2TiO_2$ and $2PbO + TiO_2$ respectively *). Without preliminary sintering, these mixtures were then added to suitable amounts of SiO_2 and Na_2CO_3 in order to obtain the batches used in the experiments.

All the melting was carried out in alumina crucibles sintered at 1950 °C.

By analysing a number of samples taken at random we found an average content of 0·3 % Al_2O_3 in our glasses, the maximum observed being 1%. This proves pre-sintered alumina a valuable refractory.

In each experiment about 20 grams of a batch was fired during 2 hours at 1300 °C in an oven as described by Ouweltjes [3]). Then the melt was poured out on an iron plate and, after adequate annealing, it was judged by visual inspection whether the system was (a) purely vitreous, (b) purely crystalline, or (c) a coexistent mixture of these two phases. In this last case the mixture investigated belongs to the critical region intermediate between the crystalline and the vitreous phases. The results obtained have been recorded in figs 1, 2 and 3.

In the three systems investigated we observed a vitreous region (within the solid line), a crystalline region (outside the dashed line) and a comparatively narrow intermediate region (between the solid and the dashed lines). It should be noted that the boundaries as drawn in these figures hold only for a temperature of firing of 1300 °C. For higher temperatures, the vitreous region would undoubtedly be larger, and conversely.

Discussion of results

After firing at 1300 °C the system Na_2O-SiO_2 possesses a vitreous region between 32% SiO_2 - 68% Na_2O and 76% SiO_2 - 24% Na_2O. If we raise the temperature of firing the former of these boundaries will certainly not shift much, but the latter boundary will shift considerably. As expected, the system Na_2O - lead titanate does not show a vitreous region, whereas for the system SiO_2 - Pb_2TiO_4 (fig. 1) there exists a narrow range of glass formation at about 30% SiO_2 - 70% Pb_2TiO_4 corresponding to a composition in mole fractions of about 0·55 SiO_2, 0·30 PbO and 0·15 TiO_2.

---

*) It is well known that Pb_3O_4 added to the batch results in the presence of 3 PbO in the glass.

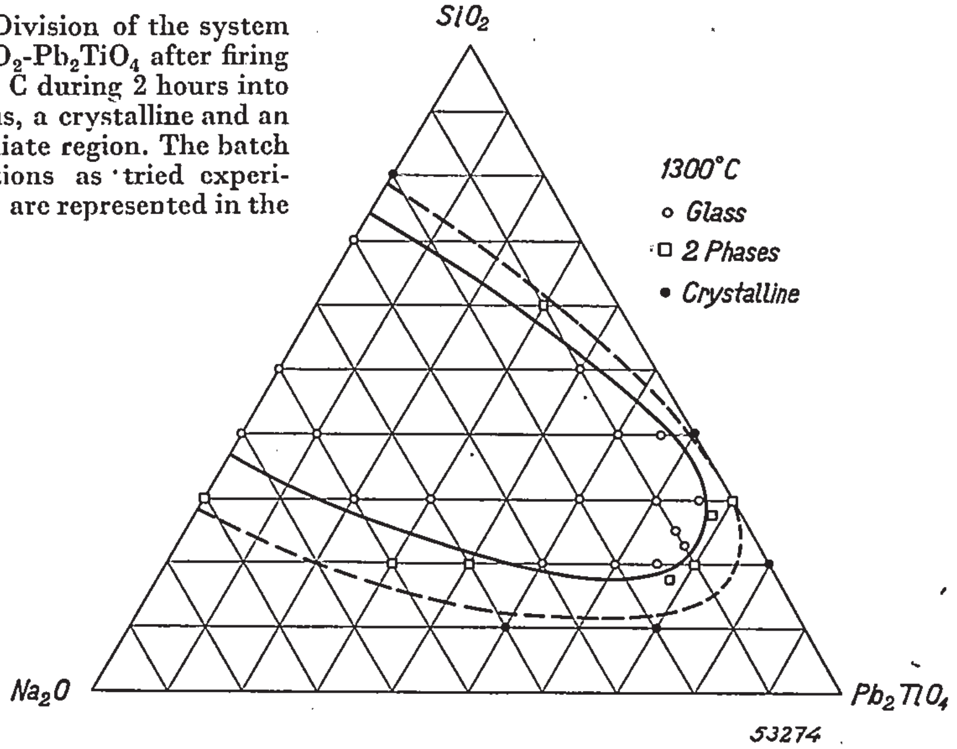

Fig. 1. Division of the system Na_2O-SiO_2-Pb_2TiO_4 after firing at 1300° C during 2 hours into a vitreous, a crystalline and an intermediate region. The batch compositions as tried experimentally are represented in the diagram.

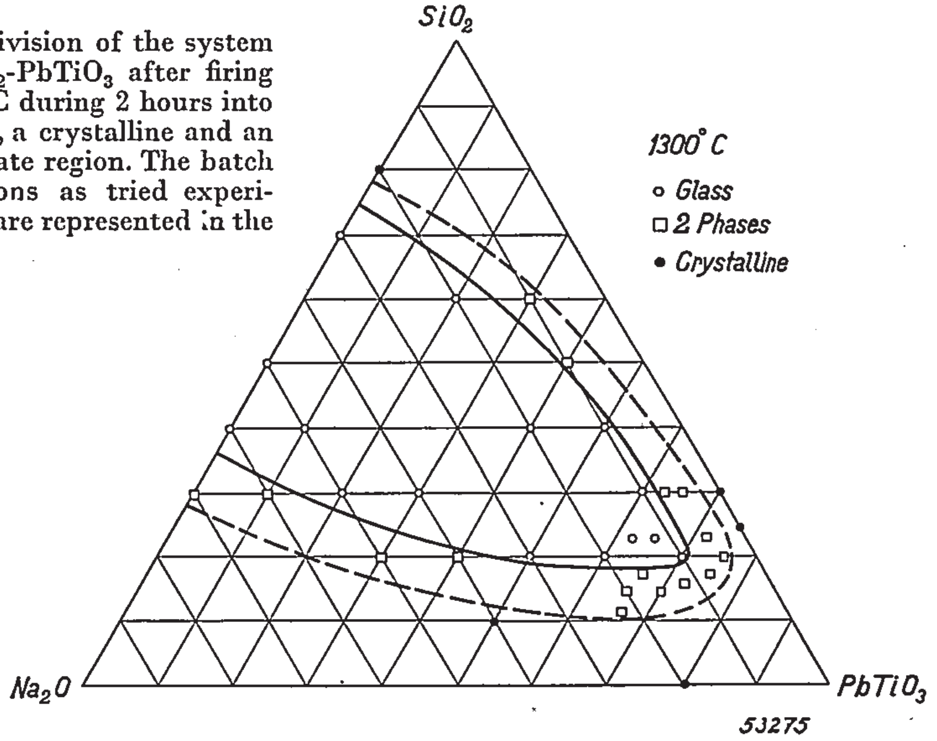

Fig. 2. Division of the system Na_2O-SiO_2-$PbTiO_3$ after firing at 1300 °C during 2 hours into a vitreous, a crystalline and an intermediate region. The batch compositions as tried experimentally are represented in the diagram.

If the content of Ti^{4+} in the lead titanates is increased, the devitrifying influence of this ion, known from so many other facts, gains in importance, which results in the disappearance of the vitreous region in the other systems SiO_2-lead titanate.

Similar properties were observed in the quasi-ternary system where an increase in the amount of Ti^{4+} produces a contraction of the vitreous range in the diagrams shown.

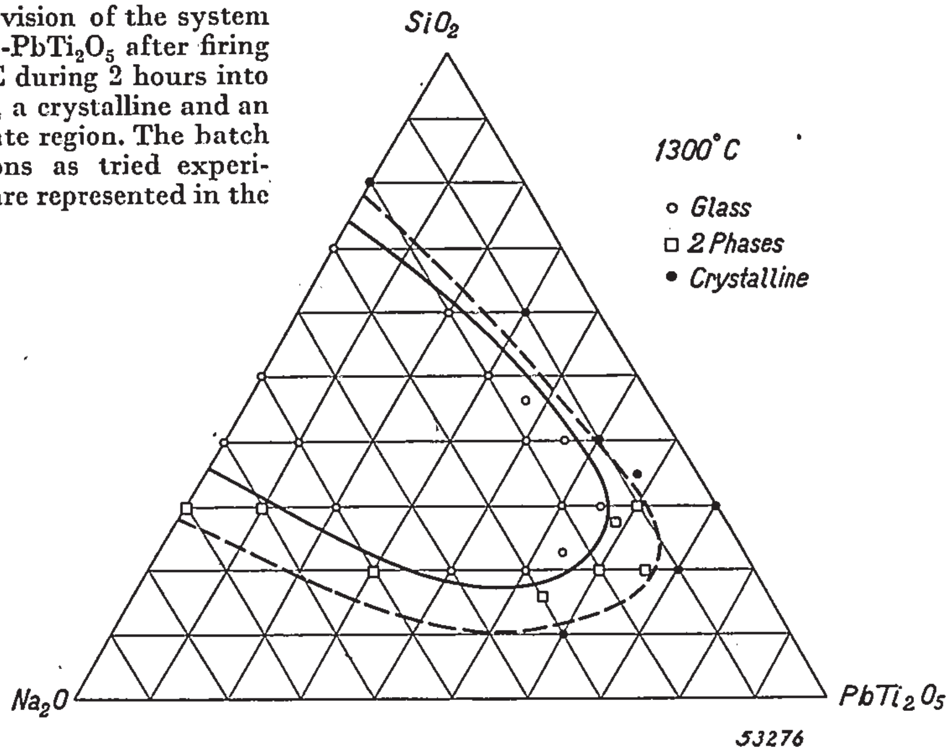

Fig. 3. Division of the system Na_2O-SiO_2-$PbTi_2O_5$ after firing at 1300 °C during 2 hours into a vitreous, a crystalline and an intermediate region. The batch compositions as tried experimentally are represented in the diagram.

The glass with the highest weight percentage of lead titanate (fig. 2; composition 10% Na_2O - 70% $PbTiO_3$ - 20% SiO_2, or in mole fractions: 0·17 Na_2O, 0·35 SiO_2, 0·24 PbO, 0·24 TiO_2) was found to possess a refractive index of 1·83. This glass was slightly yellow, while the colouring could not be removed by the well-known practice of replacing Na_2CO_3 by $NaNO_3$.

Eindhoven, April 1948

REFERENCES

1) D.R.P. 763.797. In this patent the addition of TiO_2 in the form of Zn_2TiO_4 and (or) Cd_2TiO_4 is claimed.

2) J. M. Stevels, Verres et réfractaires 2, 2-12, 1948; Ned. Tijdschr. Natuurkunde, in the press.

3) J. L. Ouweltjes, Chem. Weekblad, Amsterdam, in the press.

ABSTRACTS OF RECENT SCIENTIFIC PUBLICATIONS OF THE N.V. PHILIPS' GLOEILAMPENFABRIEKEN

Reprints of the majority of these papers can be obtained on application to the Administration of the Research Laboratory, N.V. Philips' Gloeilampenfabrieken Eindhoven, Netherlands. Those papers of which no reprints are available are marked with an asterisk (*).

1739: E. J. W. Verwey, P. W. Haayman and F. C. Romeyn: Physical properties and cation arrangement of oxides with spinel structure. II. Electronic conductivity (J. chem. Phys. **15**, 181-187, 1947).

The relations between the electronic conductivity of certain spinels and the arrangement of the cations in the crystal structure are studied. Several arguments favour the assumption that Fe_3O_4 contains both divalent and trivalent iron in the 16-fold position. The transition point in the neighbourhood of liquid-air temperature is probably associated with an increased degree of order at low temperature in the distribution of the 8 electrons between the 16 Fe-lattice points per unit cell. The considerably increased conductivity below the transition points shows tetragonal anistotropy when the crystal is cooled in a magnetic field. The possible distributions of the electrons in the crystal at low temperature are discussed. In more complicated spinels, containing other metal atoms as well as iron in both the divalent and the trivalent state, the electronic interchange is more or less inhibited by the foreign metal atoms. The higher values of their resistance in comparison to that of Fe_3O_4 can be roughly described by an increased activation energy. The investigation of a number of substances with different arrangements of the cations shows that the activation energy (and therefore the electrical resistance) is lowest for those cases in which the electrons can travel, as in Fe_3O_4, along the Fe of the 16-fold position.

For the contents of this paper see also the article by E. J. W. Verwey, P. W. Haayman and F. C. Romeyn, Philips tech. Rev. **9**, 239, 1947.

1740: A. H. W. Aten, Jr: Activation of hafnium with neutrons (Science **105**, 386, 1947).

With slow neutrons acting on Hf a period of 20 sec is found; with fast neutrons periods of 20 sec, 10 min, and 6 hours. As the stable Hf isotopes are 174, 176, 177, 178, 179 and 180, the second period was initially supposed to be due to Hf 175. The results are compared with those of Flammersfeld. An isomeric form of 176, 177, 178 or 179 is now more probable. The periods found are useful for the determination of Hf as a contamination of Zr, whereas the long periods of Zr may be used for the determination of Zr as a contamination of Hf.

1741: **J. A. Keverling Buisman, W. Stevens** and **J. van der Vliet:** Investigations on Sterols. I. A new synthesis of 7-dehydrocholesterol (provitamin D) (Rec. Trav. chim. Pays-Bas **66**, 83-92, 1947).

A new synthesis of 7-dehydrocholesterol (provitamin D_3) from cholesterol is described, which gives a higher yield than the well-known Windaus synthesis. The synthesis is carried out via a 7-bromo cholesteryl ester, from which hydrogen bromide is eliminated to give an ester of 7-dehydrocholesterol.

1742: **A. H. W. Aten, Jr:** High-energy ions in crystal lattices (Phys. Rev. **71**, 641-642, 1947).

The valency is determined of P^{32} ions formed by (n,p) and (n,α) reactions due to recoil in crystals containing S and Cl, respectively. It is an open question whether the phosphate and phosphite ions are formed inside the lattice or whether they adopt their final states at the moment the crystal is dissolved.

1743: **W. P. van den Blink:** Note on the influence of the water content of an electrode coating on the hydrogen content of weld metal (Welding J. Res. Supp. July 1947).

The question is discussed whether an increase in the moisture content of the coating of a welding electrode increases the hydrogen content of the weld metal. It is shown that both an increase and a lowering of the hydrogen content may result, dependent on the partial pressures of H_2O, CO, H_2 and CO_2 in the welding arc.

1744: **K. W. de Langen:** The manifold of physical quantities (Physica, 's-Grav. **13**, 349-352, 1947).

In electrodynamics all operations are carried out in a manifold of quantities, each element of which may be written in the form

$$a\ \mathrm{cm}^k\ \mathrm{g}^l\ \mathrm{sec}^m \mathrm{el}^n$$

(el = electrostatic unit of charge). The numbers k, l, m, n determine the class of the quantity (dimension). The author advocates the use of quantity equations ("Grössengleichungen").

1745: **J. H. F. Custers:** The texture of copper wire drawn with backpull (Physica, 's-Grav. **13**, 366-378, 1947).

The preferred orientations of copper wire drawn either in the normal way or with backpull are investigated. In the outer zones these orientations show definite differences. In wire drawn with backpull the so-called conical fibre texture which predominates particularly in the outer zones has developed less intensively than in wire drawn in the normal way. It is, however, still an open question whether properties like tensile strength are improved in such a degree as to lead one to expect special advantages by the application of backpull.

VOL. 3 NR 4 AUGUST 1948

Philips Research Reports

EDITED BY THE RESEARCH LABORATORY
OF N.V. PHILIPS' GLOEILAMPENFABRIEKEN, EINDHOVEN, NETHERLANDS

R 84 *Philips Res. Rep.* **3**, *241-254, 1948*

NOISE IN A PULSE-FREQUENCY-MODULATION SYSTEM

by F. L. H. M. STUMPERS

621.396.619.16:621.396.822

Summary

The optimum filter for pulse-frequency-modulation is derived for any given pulse form and large signal-to-noise ratio. For some special pulse forms the signal-to-noise ratio is calculated and it is shown that normal frequency modulation gives a better result. A method is given for the calculation of the noise spectrum, which is valid for all signal-to-noise ratios, though the intricacy of the formula restricts the possibilities for application. The noise threshold is estimated and the suppression of the modulation by noise is calculated.

Résumé

L'auteur établit le filtre optimum pour la modulation de fréquence à impulsions (pour un grand rapport du signal au bruit de fond). Le rapport du signal au bruit de fond est calculé pour quelques formes spéciales des impulsions et on montre que la modulation de fréquence normale donne encore un meilleur résultat. L'auteur indique une méthode de calcul du spectre du bruit de fond, méthode valable pour tous les rapports du signal au bruit de fond mais la complexité des formules restreint les possibilités d'application. Dans la dernière partie on considère la suppression de la modulation en présence de bruit de fond.

1. Introduction

Amplitude modulation, phase modulation, and frequency modulation usually start from a sinusoidal signal. Instead any other periodic signal can be used for modulation purposes, and in the last years attention has been drawn to the use of periodic pulses. In this case the unmodulated signal is given by

$$F_1(t) \cos \omega_0 t, \tag{1}$$

where ω_0 is the carrier-wave frequency (in radians per second) and $F_1(t)$ a periodic function of t, which is different from zero only for a small part of its period. We shall choose the period of $F_1(t)$ equal to $T = 2\pi/\omega_1$.

When modulation is applied the carrier-wave frequency ω_0 remains constant and $F_1(t)$ is varied in accordance with the audio input in the same way as is the sinusoidal signal in ordinary modulation systems. In this paper we shall restrict ourselves to pulse-frequency-modulation, of which there are two forms. Firstly, in the periodic function

$$F_1(t) = \sum_0^\infty{}_k \{A_k \cos k\omega_1 t + B_k \sin k\omega_1 t\} = \mathrm{Re} \sum_0^\infty{}_k \{C_k\, e^{ik\omega_1 t}\}, \tag{2}$$

the phase $\omega_1 t$ is changed into

$$\omega_1 t + \int^t v(\tau)\, \mathrm{d}\tau,$$

where $v(\tau)$ is proportional to the audio input. Then the form of the pulse changes in proportion to the length of the period. In the second system the pulses remain identical and only their mutual distance is varied. We choose our fundamental period in such a way that $F_1(t)$ is different from zero in the central part of it, and when modulation is applied the centre of each period coincides with the passing through zero in a positive direction of

$$\cos\{\omega_1 t + \int^t v(\tau)\, \mathrm{d}\tau\}.$$

As a result of the modulation the pulses shift in time. This shift is calculated in the following way. Observe a zero t_0 of $\cos \omega_1 t$. Let the shift of this zero (and of the attached pulse) be Δt_0. Then

$$\cos\{\omega_1 t_0 + \omega_1 \Delta t_0 + \int^{t_0+\Delta t_0} v(\tau)\, \mathrm{d}\tau\} = 0.$$

Thus

$$\omega_1 \Delta t_0 = -\int^{t_0+\Delta t_0} v(\tau)\, \mathrm{d}\tau. \tag{3}$$

Since the effect of the modulation is continuous no extra shift of $k2\pi$ has to be taken into account. Δt is a function of t which so far is defined only at the zeros $t_0 + k2\pi/\omega_1$ of $\cos \omega_1 t$. There are, however, many pulses for each audio-frequency period, and we can link all the ordinates of Δt as a function of t by a smooth curve. Then the modulation is obtained from the shifts Δt of the zeros by

$$v(t) = \frac{\mathrm{d}}{\mathrm{d}t}(\omega_1 \Delta t). \tag{4}$$

In addition to the shift caused by modulation, there is a shift caused by disturbances and noise. In the receiver we cannot distinguish between these two. Therefore the shifts caused by noise, too, are translated into an audio-output, which we shall now investigate.

In the mixer stage of the receiver the high frequency ω_0 is changed into the intermediate frequency ω_2 and, mainly by the intermediate-frequency filters, $F_1(t)$ is changed into $F(t)$. Apart from the signal

$$\mathrm{Re}\{F(t)\, e^{i\omega_2 t}\},$$

we receive noise, which after the filters may be given by

$$\operatorname{Re}\{g(t)\, e^{i\omega_2 t}\}.$$

A linear rectifier followed by a low-pass filter gives a low-frequency output proportional to

$$|F(t) + g(t)|. \tag{5}$$

Let the noise be small compared to the signal. Without noise $F(t_0) = A$. Let Δt_0 be the shift caused by the noise; then

$$F(t_0) + \Delta t_0 F'(t_0) = -g(t) + A\,,$$

$$\Delta t_0 = -\frac{g(t)}{F'(t_0)}. \tag{6}$$

Comparing this result with formula (4) we see that the noise is received as a spurious modulation

$$v_n(t) = -\omega_1 \frac{g'(t)}{F'(t_0)}. \tag{7}$$

2. The optimum filter characteristic for pulse-frequency-modulation

Let the complex filter characteristic be given by $f_1(\omega)$. This means that a signal $\operatorname{Re}\{A\, e^{i(\omega t+\varphi)}\}$ before the filter is changed into $\operatorname{Re}\{f_1(\omega)\, A\, e^{i(\omega t+\varphi)}\}$ after it. At the input of the receiver the noise is given by

$$\operatorname{Re}\Big\{\int_0^\infty r_1(\omega)\, e^{i\omega t}\, \mathrm{d}\omega\Big\}.$$

The mean-square amplitude of all noise frequencies is the same. About the noise spectrum more will be said in section 4. After it has passed the filter the noise is defined by

$$\operatorname{Re}\Big\{\int_0^\infty r_1(\omega)\, f_1(\omega)\, e^{i\omega t}\, \mathrm{d}\omega\Big\} = \operatorname{Re}\Big\{e^{i\omega_2 t}\int_{-\omega_2}^\infty r_1(\omega+\omega_2)\, f_1(\omega+\omega_2)\, e^{i\omega t}\, \mathrm{d}\omega\Big\}.$$

Here ω_2 is the intermediate frequency.

Now we introduce a new function,

$$\begin{aligned} f(\omega) &= f_1(\omega+\omega_2) &\quad (-\omega_2 \leqq \omega < \infty),\\ f(\omega) &= 0 &\quad (-\infty < \omega < -\omega_2), \end{aligned}$$

and in the same way $r(\omega)$ is defined. Then,

$$g(t) = \operatorname{Re}\int_{-\infty}^{\infty} r(\omega)\, f(\omega)\, e^{i\omega t}\, \mathrm{d}\omega = \operatorname{Re}\sum_{-\infty}^{+\infty}{}_k \int_{-\omega_1/2}^{\omega_1/2} r(k\omega_1+s)\, f(k\omega_1+s)\, e^{i(k\omega_1+s)t}\, \mathrm{d}s. \tag{8}$$

The function $g(t)$ defines the time shift at points a distance $k2\pi/\omega_1$ apart, and at all those points $e^{ik\omega_1 t}$ has the same value. Thus for the differentiation it can be regarded as a constant,

$$g'(t) = \operatorname{Re}\sum_{-\infty}^{+\infty}{}_k \int_{-\omega_1/2}^{\omega_1/2} is\, f(k\omega_1+s)\, r(k\omega_1+s)\, e^{ik\omega_1 t_0}\, e^{ist}\, \mathrm{d}s.$$

The energy of the noise for the frequency s is

$$E(s) = \frac{\omega_1^2 \overline{r^2} s^2 \, \Sigma \{ |f(k\omega_1 + s)|^2 + |f(k\omega_1 - s)|^2 \}}{2\,|F'(t_0)|^2}. \tag{9}$$

The original signal is

$$\mathrm{Re}\,\{F_1(t)\, e^{i\omega_0 t}\} = \mathrm{Re}\,\{\Sigma\, C_k e^{ik\omega_1 t}\, e^{i\omega_0 t}\}.$$

After passing the intermediate-frequency filters, this becomes

$$\mathrm{Re}\,\{F(t)\, e^{i\omega_2 t}\} = \mathrm{Re}\,\{\Sigma\, C_k\, f_1(\omega_2 + k\omega_1)\, e^{ik\omega_1 t + i\omega_2 t}\},$$

$$F(t) = \mathrm{Re}\,\{\Sigma\, C_k\, f(k\omega_1)\, e^{ik\omega_1 t}\},$$

and

$$F'(t) = \mathrm{Re}\,\{\Sigma\, C_k\, ik\omega_1 f(k\omega_1)\, e^{ik\omega_1 t}\}. \tag{10}$$

In equation (9) we can approximate

$$|f(k\omega_1 + s)|^2 + |f(k\omega_1 - s)|^2$$

very well by 2 $|f(k\omega_1)|^2$. The energy for the noise frequency s then is

$$E(s) = \frac{\omega_1^2 s^2 \overline{r^2} \sum_{-\infty}^{+\infty}{}_k\, |f(k\omega_1)|^2}{|\Sigma\, C_k\, ik\omega_1 f(k\omega_1)\, e^{ik\omega_1 t_0}|^2}. \tag{11}$$

The best choice for the filter characteristic is now deduced by the use of the "Schwarz's inequality". In our case this inequality yields for the quotient in (11)

$$E(s) \geqq \frac{\omega_1^2 s^2 \overline{r^2}}{\Sigma\, |C_k\, k\omega|^2}, \tag{12}$$

and the equality sign holds only when

$$f^*(k\omega_1) = C_k\, ik\omega_1\, e^{ik\omega_1 t_0} \tag{13}$$

($f^*(k\omega_1)$ is the conjugate-complex of $f_1(k\omega_1)$).

Using a property of Fourier series we can also write

$$E(s) \geqq \frac{2\pi s^2\, \omega_1 \overline{r_1^2}}{\int_{-\pi/\omega_1}^{\pi/\omega_1} |F_1'(t)|^2\, \mathrm{d}t}. \tag{12a}$$

Thus for the best obtainable signal-to-noise ratio the mean square of the derivative of the pulse with regard to time is conclusive. The optimum filter characteristic is — apart from a phase factor — the complex conjugated of the Fourier transform of the time derivative of the pulse.

This result is at variance with that given by Van Vleck and Middleton [1]), where the "simple criterion" of the highest ratio of the signal amplitude to the rms value of the noise amplitude is postulated. For a large signal-to-noise ratio this result is easily derived, as after the filter the signal is given by

$$F(t) = \mathrm{Re}\,\{\Sigma\, C_k f(k\omega_1)\, e^{ik\omega_1 t}\}, \tag{14}$$

and the mean square of the noise amplitude is proportional to

$$\frac{\overline{r^2}}{2} \int_{-\infty}^{+\infty} |f(\omega)|^2\, \mathrm{d}\omega \approx \omega_1 \frac{\overline{r^2}}{2}\, \Sigma_k\, |f(k\omega_1)|^2 . \tag{15}$$

Then, according to the "Schwartz's inequality", the optimum filter characteristic is the complex conjugated of the Fourier transform of the pulse. Van Vleck and Middleton have proved that this result is also true for larger noise values. Are this "matched filter" and the optimum filter for pulse-frequency-modulation realizable? The answer is that they can be approximated as accurately as necessary. For if the periodic pulse is given by $F_1(t) \cos \omega_0 t$ and we define

$$\begin{aligned} h(t) &= F_1(t) \qquad && (-\pi/\omega_1 < t \leqq \pi/\omega_1), \\ h(t) &= 0 && (-\infty < t \leqq -\pi/\omega_1,\ \pi/\omega_1 < t < \infty)\,, \end{aligned} \tag{16}$$

then the optimum filter for pulse-frequency-modulation is the filter with transfer time impedance $h(t_0-t)$. See fig. 1. This means that such a filter gives an output $h(t_0-t)$ for the input unit function $U(t)$. The unit function is defined by

$$\begin{aligned} U(t) &= 0, -\infty < t < 0, \\ U(0) &= \tfrac{1}{2}, \\ U(t) &= 1, 0 < t < \infty. \end{aligned}$$

Choose t_0 in such a way that $h(t_0-t) = 0$ for $t < 0$. Then, for instance, Lee's [2]) method for synthesis of electrical networks by means of the Fourier transforms of Laguerre functions can be applied to approximate the desired filter characteristic. Another method is discussed by Lévy [3]).

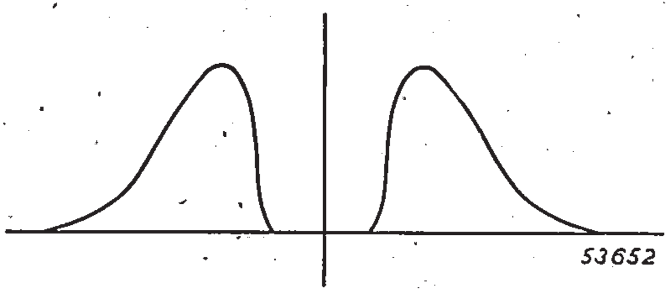

Fig. 1. Left: Pulse form. Right: Time impedance of the "optimum filter" for pulse-frequency-modulation. The filter gives an output voltage proportional to the given form for the input current function $U(t)$.

In the same way the "matched filter" is the filter that gives the response $h(t_0-t)$ to an input δ-function.

The best result for pulse modulation is evidently reached also when the "matched filter" of Van Vleck and Middleton is applied first, and the low-frequency output given by a linear rectifier is differentiated. An objection to this procedure may be made, as the largest value of $F'(t)$ is reached when $F(t)$ is zero. Of course we cannot define the modulation by the number of times $F(t)$ passes through zero. It is, however, possible to count only those zeros coming after a large deviation. We can, for instance, apply pulse renewal. Normally this means that a new ideal pulse is given each time the received signal passes a value A in the positive direction (fig. 2).

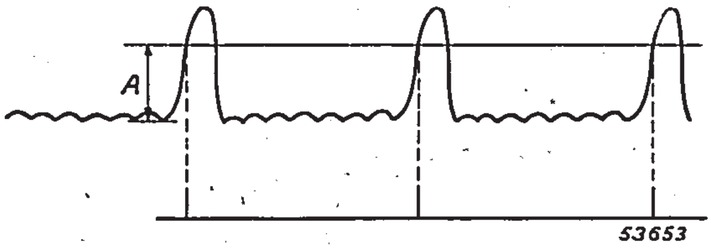

Fig. 2. Above: Output of the linear rectifier in the receiver. Below: A new pulse is given each time this output passes the value A in the positive direction.

In the revised form the passing through D in the positive direction of $F'(t)$ operates a relay circuit and a new pulse is given at the first passing of a zero. This puts the relay circuit out of action until the next passing of D (fig. 3).

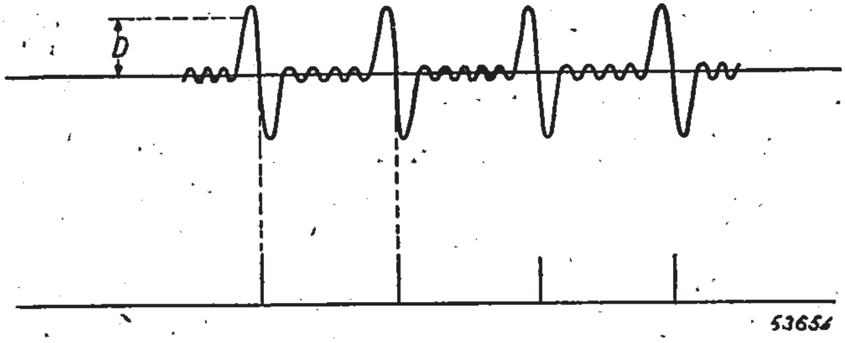

Fig. 3. Above: The differentiated output of fig. 2. Below: The first zero after each passing of the value D in the positive direction coincides with a new pulse.

3. Application of the theory to special pulse forms

As an example we shall apply the theory to the pulse form defined by

$$h(t) = e^{-a^2t^2},$$

where $h(t)$ is defined as in equation (16). The Fourier transform is

$$f(i\omega) = \int_{-\infty}^{+\infty} e^{-a^2t^2} e^{-i\omega t} dt = \frac{\sqrt{\pi}}{a} e^{-\omega^2/4a^2}.$$

(It is assumed here that $e^{-a^2t^2}$ is near enough to zero for $t = \pi/\omega_1$ to permit the use of the limits ± ∞.)
The optimum filter characteristic for pulse-frequency-modulation is proportional to

$$f_3(\omega) = \omega\, e^{-\omega^2/4a^2}.$$

The characteristic of the "matched" filter is proportional to

$$f_4(\omega) = e^{-\omega^2/4a^2}.$$

By application of the equations (11) to (15), we see that the noise energy for the filter f_3 and the frequency s is

$$E_{3,s} = 2^{3/2}\, \pi^{1/2}\, \frac{\omega_1}{a}\, s^2\, \overline{r^2},$$

or for the band from 0 to ω_a:

$$E_3(0, \omega_a) = \frac{2^{3/2}\pi^{1/2}}{3} \frac{\omega_1}{a}\, \omega_a{}^3\, \overline{r^2}.$$

For the second filter f_4 the noise-energy values are

$$E_{4,s} = 2^{3/2}\, \pi^{1/2}\, e\, \frac{\omega_1}{a}\, s^2\, \overline{r^2} \text{ and } E_4(0, \omega_a) = \frac{2^{3/2}}{3}\, \pi^{1/2}\, e\, \frac{\omega_1}{a}\, \omega_a{}^3\, \overline{r^2}$$

respectively.

Here e is the base of natural logarithms. On the other hand the ratio of the noise energy to the squared maximum signal amplitude for the "matched" filter f_4 is

$$A(f_4) = a\, \overline{r^2}\, \sqrt{2\pi},$$

and after differentiation, or for the filter f_3, $A(f_3) = ea\overline{r^2}\, \sqrt{2\pi}$.

Now we shall investigate whether a better result for pulse-modulation noise can be reached when a filter is chosen with a characteristic similar to the one of the matched filter but with a different constant,

$$f_5(\omega) = e^{-\omega^2/4\beta^2}.$$

The ratio of the noise energy to the squared maximum signal amplitude for the filter f_5 is calculated in the same way:

$$A(f_5) = \frac{a\overline{r^2}}{2} \left(\frac{a}{\beta} + \frac{\beta}{a}\right) \sqrt{2\pi}.$$

The noise energy for the frequency s after this filter is

$$E_{5,s} = \frac{(\alpha^2 + \beta^2)^2}{\alpha^2\,\beta^3}\,\omega_1\, s^2\, \overline{r^2}e\, \sqrt{\pi/2}\,,$$

and for the band $(0, \omega_a)$

$$E_5(0, \omega_a) = \frac{(\alpha^2 + \beta^2)^2}{\alpha^2\,\beta^3}\,\omega_1\,\frac{\omega_a{}^3}{3}\,\overline{r^2}e\,\sqrt{\pi/2}\,.$$

The lowest noise energy is obtained for $\beta = \alpha\sqrt{3}$. Then the noise energy is 0·7698 times the value for the matched filter, but still 2·093 times the best attainable value. The value of $A(f_5)$ then is $\frac{2}{3}\sqrt{3} = 1{\cdot}155$ times its minimum value.

We shall now compare the signal-to-noise ratio for pulse modulation with the same ratio for ordinary frequency modulation. For pulse modulation the maximum shift is $\beta\omega_1$, where $\beta > 1$, for instance $\beta = 0{\cdot}8$. The maximum audio-signal energy is proportional to $\beta^2\omega_1{}^2/2$. This has to be compared with the maximum audio-signal energy for ordinary frequency modulation, $\Delta\omega^2/2$. The ratio of the maximum audio-signal energy to the noise energy in the band $(0, \omega_a)$ is for ordinary frequency modulation

$$\frac{\Delta\omega^2}{2}\,\frac{3}{\omega_a{}^3\,\overline{r^2}},$$

and for pulse-frequency-modulation

$$\frac{\beta^2\omega_1{}^2}{2}\,\frac{3}{\omega_a{}^3\,\overline{r^2}}\,\frac{1}{2\sqrt{2\pi}}\,\frac{a}{\omega_1}.$$

The energy per second necessary to produce this signal-to-noise ratio is $\frac{1}{2}$ for frequency modulation and $(\omega_1/2\pi)\int\limits_{-\infty}^{+\infty} e^{-2a^2t^2}\cos^2\omega_0 t\; dt = \omega_1/4a\sqrt{2\pi}$ for pulse modulation.

For the same transmitter energy the signal-to-noise ratio for ordinary frequency modulation is $\Delta\omega^2/a^2\beta^2$ times its value for pulse modulation. The bandwidth of the frequency spectrum is $2\Delta\omega$ for frequency modulation (if the sweep is large compared to the audio frequencies) and $\int\limits_{-\infty}^{+\infty} e^{-\omega^2/2a^2}\, d\omega = a\sqrt{2\pi}$ for pulse modulation. The latter value is flattered. If we ask for the bandwidth containing 95% of the energy we get $3{\cdot}92a$, and for 99% even $5{\cdot}15\,a$. In any case it is quite clear that for the same transmitter energy and the same audio signal-to-noise ratio, pulse modulation needs a wider band of the spectrum. We have proved this only for pulses of the form $e^{-a^2t^2}$.

For a pulse form $F_1(t)$ corresponding to a transmitter signal $F_1(t)\cos\omega_0 t$, the audio signal-to-noise ratio for pulse frequency-modulation is

$$(S/N)_\mathrm{p} = \frac{\beta^2 \int\limits_{-T/2}^{T/2} |F_1{}'(t)|^2 \,\mathrm{d}t}{\Delta\omega^2 \int\limits_{-T/2}^{T/2} |F_1(t)|^2 \,\mathrm{d}t} (S/N)_\mathrm{f.m.}, \tag{17}$$

where $(S/N)_\mathrm{f.m.}$ is the value obtainable with ordinary frequency modulation of the same transmitter energy, and $\omega_1 T = 2\pi$.

As

$$F_1(t) = \mathrm{Re}\left\{\sum_0^\infty C_k\, e^{ik\omega_1 t}\right\}, \tag{2}$$

we can also write

$$(S/N)_\mathrm{p} = \frac{\beta^2 \Sigma |C_k\, k\omega|^2}{\Delta\omega^2\, \Sigma |C_k|^2} (S/N)_\mathrm{f.m.}. \tag{18a}$$

We shall apply formula (14) to triangular and trapezoidal pulse forms (see fig. 4).

(a) Triangular pulse form:

$$(S/N)_\mathrm{p} = \frac{3\beta^2\gamma^2}{\Delta\omega^2} (S/N)_\mathrm{f.m.}. \tag{19a}$$

The bandwidth containing 95% of the transmitter energy is $3{\cdot}14\,\gamma$, and for 99% it is 4γ.

(b) For the trapezoidal pulse form,

$$(S/N)_\mathrm{p} = \frac{3\beta^2\gamma^2}{\Delta\omega^2\,(1 + 3\,\gamma/\delta)} (S/N)_\mathrm{f.m.}. \tag{19b}$$

The bandwidth containing 95% of the transmitter energy is 2γ when $\delta = 2\,\gamma$, and $1{\cdot}48\,\gamma$ when $\delta = \gamma$. For 99% the bandwidths are $3\,\gamma$ and $1{\cdot}6\,\gamma$ respectively.

It is seen that for these examples, too, the signal-to-noise ratio for ordinary frequency modulation is greater. Moreover it may be more difficult to reach the theoretical ratio in actual pulse-modulation systems.

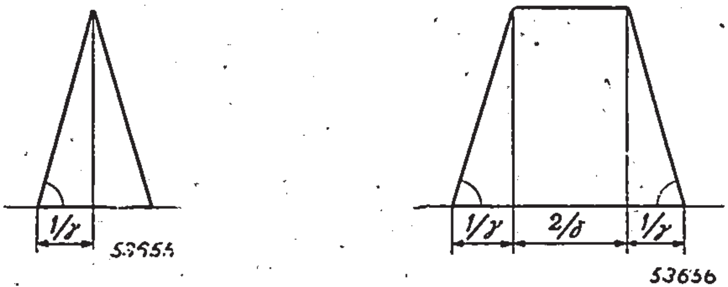

Fig. 4. Left: Idealized triangular pulse form. Right: Idealized trapezoidal pulse form.

4. The calculation of signal-to-noise ratio in general

So far we have assumed that the noise energy is small compared to the signal energy. Elsewhere we have already given a calculation of signal-to-noise energy for frequency modulation that does not depend on this assumption [4]). Now we shall try to outline such a calculation method for pulse modulation, without, however, entering into detailed applications.

The pulse signal is passed through an intermediate-frequency filter and rectified by means of a linear rectifier. Then pulse renewal is applied and a new pulse is given each time the signal obtained from the rectifier passes the value A in the positive direction. The new pulses are congruent. Though it is not necessary to do so, we shall give the new pulses in our calculation the form of a Dirac δ-function. When the new system of pulses passes an audio-frequency filter the output is directly proportional to the desired audio signal. This demodulation system is not the only one possible, but we have chosen it as it is sure to give an undistorted output and to make a calculation of the results readily possible.

Then, let input signal and noise be given by

$$v_0(t) = \mathrm{Re}\,\}F(t) + g(t)\{\, e^{i\omega_0 t}.$$

After passing the filter the voltage is $v_1(t)\cos(\omega_2 t + \varphi)$. New pulses are given when $v_1(t)$ passes $+A$ in the positive direction or $-A$ in the negative direction, viz.

$$v_2(t) = \delta\,\}v_1(t) - A\{\, v_1'\, U(v_1') + \delta\,\}v_1(t) + A\{\, v_1'\, U(-v').$$

Now introduce the Laplace transforms and make a Fourier spectrum

$$v_2(t) = \Sigma f_m\, e^{imt};$$

$$f_m = -\frac{1}{4\pi^2}\int_{-\pi}^{\pi} e^{-imt}\,\mathrm{d}t \int_{-\infty-ic}^{\infty-ic} \mathrm{d}z_1 \int_{-\infty-ic}^{\infty-ic} \mathrm{d}z_2\, z_2^{-2}\,\}e^{iz_1(v_1-A)+iz_2v_1'} + e^{iz_1(v_1+A)-iz_2v_1'}\{\,. \tag{20}$$

The output energy for the frequency m is given by $2 f_m f_m^*$, and for direct current by $f_0 f_0^*$.

The Fourier spectrum of the receiver input-noise is

$$g(t) = \sum_0^\infty (a_n \cos nt - b_n \sin nt)\,.$$

The probability distributions of a_n and b_n are

$$W(a_n)\mathrm{d}a_n = \frac{1}{\sqrt{\pi C}}\, e^{-a_n^2/C}\, \mathrm{d}a_n\,, \tag{21}$$

$$W(b_n)\,\mathrm{d}b_n = \frac{1}{\sqrt{\pi C}}\, e^{-b_n^2/C}\, \mathrm{d}b_n\,. \tag{21a}$$

(For more information about noise see Rice[5])).

Let the frequency characteristic of the intermediate-frequency filter be given by $f(i\omega)$, where, as in section 1, ω is reckoned from the central frequency. After this filter we thus have

$$F(t) = \sum_{-\infty}^{+\infty} C_k f(k\omega_1)\, e^{ik\omega_1 t}, \tag{22a}$$

$$g(t) = \sum_{-\infty}^{\infty} (a_n + ib_n) f(n)\, e^{int}, \tag{22b}$$

$$v_1(t) = F(t) + g(t). \tag{23}$$

Introduce (22) in (23) and then (23) in (20). Write down also $f_m{}^*$ in analogous form. Then $2\, f_m f_m{}^*$ is a function of the coefficients a_n, b_n. We have to take the average of this function for all values of a_n, b_n:

$$\overline{2\, f_m f_m{}^*} = \int_{-\infty}^{+\infty}\int\int\ldots\int \prod_n W(a_n)\, W(b_n)\, 2\, f_m f_m{}^*\, \mathrm{d}a_n\, \mathrm{d}b_n. \tag{24}$$

This integration gives the result

$$\overline{2\, f_m f_m{}^*} = \frac{1}{8\pi^4} \int_{-\pi}^{\pi}\!\!\int e^{-im(t_1-t_2)}\, \mathrm{d}t_1 \mathrm{d}t_2 \int_{-\infty-ic}^{+\infty-ic}\!\!\int\!\!\int\!\!\int e^{-\frac{c}{4}X} \cdot \frac{H(z_1 z_2 t_1)\, H(z_3 z_4 t_2)}{z_2{}^2\, z_4{}^2}\, \mathrm{d}z_1 \mathrm{d}z_2 \mathrm{d}z_3 \mathrm{d}z_4, \tag{25}$$

where $X = \Sigma\, |f(n)|^2\, \}z_1{}^2 + n^2 z_2{}^2 + z_3{}^2 + n^2 z_4{}^2 + 2n(z_1 z_4 - z_2 z_3) \sin n(t_1 - t_2) +$
$+\, 2(z_1 z_3 + n^2 z_2 z_4) \cos n(t_1 - t_2)\{$,

$$H(z_1 z_2 t_1) = e^{iz_1(F-A)+iz_2F'} + e^{iz_1(F+A)-iz_2F'},$$

and

$$F = F(t_1),\ F' = F'(t_1).$$

We take $g(n) = |f(n)|^2$, and of the exponential form we develop

$$\exp\left[-\frac{C}{4}\, \Sigma\, g(n)\, \}2n(z_1 z_4 - z_2 z_3) \sin nu + 2(z_1 z_3 + n^2 z_2 z_4) \cos nu\{\right], \tag{26}$$

where $u = t_1 - t_2$, into a power series and integrate term-by-term. In the linear term we introduce $n = k\omega + s$, where $-\infty < k < \infty$ and $-\omega_1/2 < s < \omega_1/2$.

In this case the result of the integrations with respect to z_1, z_2, z_3, z_4 is:

$$\begin{aligned} \overline{2\, f_s f_s{}^*} = & -\frac{\omega_1 C s^2}{\pi^2} \iint \mathrm{d}t\, \mathrm{d}u\, \varepsilon(t)\, \varepsilon(t+u)\, \frac{u^2}{2}\, a(u) + \\ & + \frac{\omega_1 C s^2}{2\pi^{3/2}} \iint \mathrm{d}t\, \mathrm{d}u\, \}\varepsilon(t)\, \eta(t+u) - \varepsilon(t+u)\, \eta(t)\{\, u\, a(u) + \\ & + \frac{\omega_1 C s^2}{4\pi} \iint \mathrm{d}t\, \mathrm{d}u\, \eta(t)\, \eta(t+u)\, a(u) + \\ & + \frac{\omega_1 C}{\pi^2} \iint \mathrm{d}t\, \mathrm{d}u\, \varepsilon(t)\, \varepsilon(t+u)\, a(u), \end{aligned} \tag{27}$$

where

$$\begin{aligned} g_0^3\, g_2\, \varepsilon(t) = {} & e^{-(F-A)^2/g_0^2-F'^2/g_2^2}\{(F-A)g_2^2+F''\,g_0^2\}+ \\ & + e^{-(F+A)^2/g_0^2-F'^2/g_2^2}\{(F+A)g_2^2-F''\,g_0^2\}- \\ & -2\sqrt{\pi}\,g_2(F+A)F'\,e^{-(F+A)^2/g_0^2}\{1-\Phi\,(F'/g_2)\} \end{aligned}$$

and

$$g_0\,\eta(t)=e^{-(F-A)^2/g_0^2}\{1+\Phi(F'/g^2)\}+e^{-(F+A)^2/g_0^2}\{1-\Phi(F'/g_2)\},$$

$$\rho(u)=\int_{-\infty}^{+\infty} g(n)\,e^{inu}\mathrm{d}n\,.$$

In these forms

$$g_0^2=C\,\Sigma\,g(n)\,,\quad g_2^2=C\,\Sigma\,n^2\,g(n)\,,\quad \Phi(x)=(2/\sqrt{\pi})\int_0^x e^{-y^2}\,\mathrm{d}y\,.$$

The limits of integration in (27) are $-\pi/\omega_1$ and π/ω_1. It is assumed that the bandwidth of the filters is large compared to ω_1.

For small noise energy the third of the four integrals in equation (27) is dominant; it is equivalent to the approximation (11). The first two integrals in (27) give only a small correction of the proportionality factor of the triangular noise spectrum. The fourth integral is more important since it indicates the presence of a noise background independent of frequency.

In addition to the linear term of the power-series development of formula (26) we have also taken into account the quadratic term. This gives again a frequency-independent term and a term proportional to s^2. As the resulting formulae are rather long, we shall omit them here.

We have applied the theory to a pulse form $e^{-\alpha^2t^2}$ and used an intermediate-frequency filter $e^{-\omega^2/12\alpha^2}$ as suggested in section 3. A rough approximation of the first-order term for the noise spectrum, corresponding to the linear term in the development of (22), gives the spectrum

$$\frac{0{\cdot}026\,\omega_1\,e^{-0\cdot23/g_0^2}}{\pi\{23\,g_0^4+1{\cdot}2\,g_0^2+0{\cdot}014\}^{1/2}}+\frac{8\,e\,\omega_1\,g_0^2}{9\,\{1+2{\cdot}67\,eg_0^2\}^{1/2}}\,\frac{s^2}{\alpha^2}.$$

In the same way the second-order term for the noise spectrum is

$$\frac{3\,(g_0^2+0{\cdot}06)^3\,\omega_1\,e^{-0\cdot23/g_0^2}}{4\pi\,g_0^2\{(0{\cdot}46\,g_0^2+0{\cdot}0075)\,(6\,g_0^4+0{\cdot}84\,g_0^2+0{\cdot}0075)\}^{1/2}}+\frac{32\,e^2g_0^4\,\omega_1}{27\,(1+5{\cdot}33\,eg_0^2)^{3/2}}\,\frac{s^2}{\alpha^2}.$$

It is tempting to try these first- and second-order terms as an approximate solution, for the output noise spectrum as a function of the input noise-to-signal ratio. The experience with analogous calculations for ordinary frequency modulation has shown that the convergence of the series, of which we now have only the first and second terms, is rather bad (nth term proportional to $n^{-3/2}$).

If the audio-frequency bandwidth ω_a is of the order of 0·05 to 0·1 a, then, if $g_0^2 = 0{\cdot}025$, the energy of the frequency-independent noise is already of the same order as that of the triangular noise spectrum. This means that for this value of g_0 we are at the other side of the noise threshold. (The noise threshold corresponds to the value of the input-noise-to-signal ratio, where the deviation of the simplified analysis becomes apparent. It is not exactly defined.) It seems that the noise threshold will be nearer to $g_0^2 = 0{\cdot}01$. Since $\frac{1}{2} g_0 \sqrt{2}$ is the rms value of the noise voltage after the filter, and the top value of the pulse is 1 before and $\frac{1}{2}\sqrt{3}$ after the filter, a ratio between the rms value of the noise and the top-value of the pulse of 1 : 8 is insufficient, and 1 : 12 seems permissible, if we desire that the noise energy shall confirm the simplified analysis. The signal energy calculated in section 3 was $\omega_1/4a\sqrt{2\pi}$. Since a is from 10 to 20 ω_a and ω_1 is of the order of 2 to 3 ω_a this makes the input-noise-to-signal-energy ratio at the threshold about 0·4, whereas for ordinary frequency modulation it is about 0·1. This results in a slightly more favourable behaviour of pulse modulation for large noise values.

5. Suppression of the modulation by noise

So far it did not matter whether the first or the second system of pulse-frequency-modulation was chosen since no modulation was present. Now we shall only consider the system with identical pulses. We assume that the modulation is $\Delta\omega \cos pt$ and that the centres of the pulses coincide with the passage through zero in the positive direction of $\cos \}\omega_1 t + (\Delta\omega/p) \sin pt\{$. The formula (25) can be used directly for the calculation of the modulation energy, as only the repetition frequency of the functions F changes. This leads to the result that in the presence of noise the amplitude of the demodulated-signal frequency p is:

$$\begin{aligned} A_p = \Delta\omega \int_{-\pi/\omega}^{\pi/\omega} \Bigg[& \frac{1}{2\, g_0 \sqrt{\pi}} F' e^{-(F-A)^2/g_0^2} \Big\}1 + \Phi\,(F'/g_2)\Big\{ - \\ & - \frac{1}{2\, g_0 \sqrt{\pi}} F' e^{-(F+A)^2/g_2^2} \Big\}1 - \Phi(F'/g_2)\Big\{ + \\ & + \frac{g_2}{2\pi g_0} \Big\}e^{-(F-A)^2/g_0^2 - F'^2/g_2^2} + e^{-(F+A)^2/g_0^2 - F'^2/g_2^2}\Big\{ - \\ & - \frac{g_2}{g_0} e^{-A^2/g_0^2}\, dt \Bigg]. \end{aligned} \qquad (28)$$

It is easily seen that the integral has the limit 1 when no noise is present. The integral can be calculated since the pulse form after the filter $F(t)$ and the filter characteristic (determining g_0 and g_2) are known. We have again applied the formula to the pulse form $e^{-a^2t^2}$ and the filter characteristic $e^{-\omega^2/12a^2}$. The result is shown in fig. 5. The abscissa indicates g_0, the ratio of the rms value of the noise after the filter, multiplied by $\sqrt{2}$, to the top value of the pulse before the filter (to be multiplied by $2/\sqrt{3}$, if the ratio to the top value of the pulse after the filter is required). As the input noise-to-signal ratio is a simple function of g_0, it is easy to calculate the curve for the suppression of the modulation as a function of the input noise-to-signal ratio from fig. 5. In most cases the integral (28) has to be calculated by graphical methods.

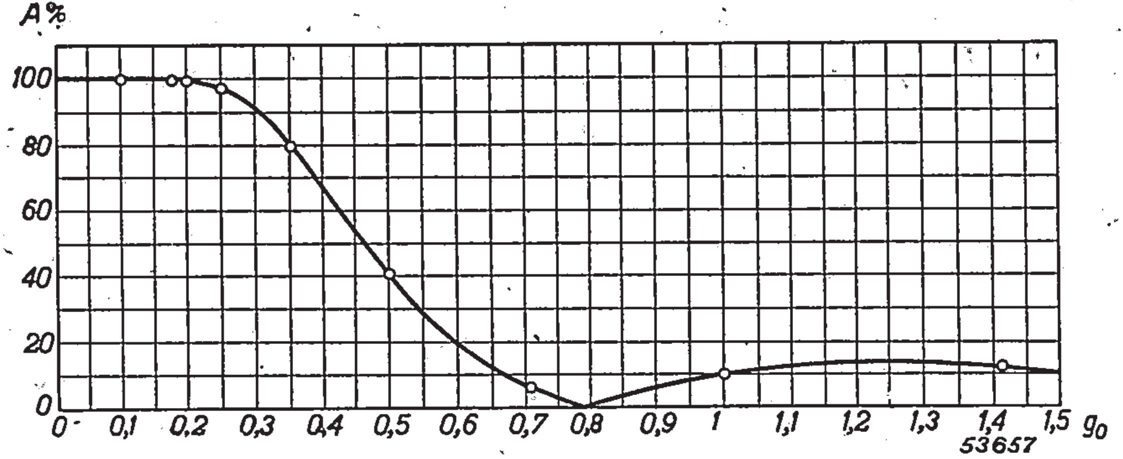

Fig. 5. Suppression of the modulation by noise. The received level of modulation as a function of the ratio between the rms value of the noise after the filter, multiplied bij $\sqrt{2}$, to the top value of the impulse before the filter.

I wish to express my thanks to my colleague Mr Tj. Douma for an advanced copy of his report on "Methods of modulation and noise-signal ratio", in which he tackles similar problems along different lines, and, for instance, reaches results very similar to my formulae (19) in the case of triangular and trapezoidal pulses.

Eindhoven, December 1947

REFERENCES

[1] J. H. van Vleck and D. Middleton, A theoretical comparison of the visual, aural and meter reception of pulsed signals in the presence of noise. J. appl. Phys. **17**, 940-971, 1946.

[2] Y. W. Lee, Synthesis of electric networks by means of the Fourier transforms of Laguerre's functions. J. Math. Phys. **11**, 83-113, 1932.

[3] M. Lévy, Etude des propriétés des quadripôles par la réponse impulsiale. Onde élect. **27**, 261-275, 1947.

[4] F. L. H. M. Stumpers, Theory of frequency modulation noise, Proc. Inst. Radio Engrs **36**, 1948.

[5] S. O. Rice, Mathematical theory of random noise, Bell. Syst. tech. J. **24**, 282-332, 1944; **25**, 46-156, 1945.

R 85 *Philips Res. Rep.* **3**, 255-270, 1948

THE NOISE FACTOR OF GROUNDED-GRID VALVES

by A. van der ZIEL *) and A. VERSNEL

621.385.1:621.396.822

Summary

Measurements are given of the noise factor of grounded-grid valves at 7·25-m wavelength. In such valves part of the output noise currents also flow through the input circuit, thus giving rise to a partial noise suppression.

A general theoretical treatment of the problem is given, dealing with the influence of circuit losses, dielectric losses, transit-time effects, field inhomogeneities, and of an independent noise current in the output circuit which is not present in the input circuit. This theory is applied to grounded-grid triodes and to grounded-grid pentodes and secondary-emission valves.

The experimental results for grounded-grid triodes agree qualitatively with theory. The various effects mentioned above all give rise to the same form of the curves: noise factor versus transformed antenna resistance. Our experiments prove that a loose antenna coupling is favourable for a low noise factor, but that a complete noise suppression is impossible.

It is shown that with a loose antenna coupling the noise suppression is most pronounced in only a relatively small frequency band, so that for very wide frequency bands grounded-grid triodes are less effective.

Measurements were also carried out for grounded-grid secondary-emission valves. These measurements agree quantitatively with the theoretical results on long wavelengths. The noise factor, however, is much larger than with grounded-grid triodes.

Résumé

L'article fait état de mesures du nombre de soufflement de tubes dont la grille est à la terre et effectuées à 7,25 m de longueur d'onde. Dans de tels tubes une part des courants de soufflement de sortie passe dans le circuit d'entrée supprimant ainsi partiellement le soufflement.

Les auteurs donnent une solution théorique générale du problème où entrent l'influence des pertes du circuit, des pertes diélectriques, du temps de transit, des inhomogénéités de champ et d'un courant de soufflement indépendant, présent dans le circuit de sortie mais pas dans le circuit d'entrée. Cette théorie est appliquée à plusieurs types de tubes à grille mise à la terre: triodes, pentodes et tubes à émission secondaire.

Les résultats expérimentaux relatifs aux triodes cadrent qualitativement avec la théorie. Les influences mentionnés ci-dessus donnent lieu à une même forme des courbes du nombre de soufflement en fonction de la résistance transformée d'antenne. Leurs expériences prouvent qu'un couplage d'antenne lâche est favorable à un faible nombre de soufflement mais que la suppression complète du soufflement est impossible.

Les auteurs montrent qu'avec un couplage d'antenne lâche la suppression du soufflement est la plus prononcée dans une bande relativement étroite de fréquences seulement, de sorte que pour de très larges bandes de fréquences les triodes à grille mise à la terre sont moins effectives.

Des mesures ont également été faites sur des tubes à émission secondaire. Elles cadrent quantitativement avec les résultats théoriques aux grandes longueurs d'onde. Le nombre de soufflement est cependant beaucoup plus grand qu'avec les triodes.

---

*) At present, University of British Columbia, Vancouver.

1. Introduction

Some time ago one of the authors of this article published a paper on the theory of noise suppression in grounded-grid triodes [1]. In that paper, in the calculation of the noise factor F, the dielectric losses, circuit losses, and transit-time effects were ignored; $(F-1)$ was shown to be inversely proportional to the transformed antenna resistance R_1', and this was experimentally verified for relatively small values of R_1'.

A more thorough investigation which was extended to large values of R_1' revealed that $(F-1)$ attained a minimum value for a given large value of R_1' and increased for still larger values of R_1'. Moreover, it was found that for very large values of R_1' the noise suppression was most pronounced in only a relatively small frequency band.

The aim of this paper is to show that the measurements may be quantitatively explained by considering the influence of circuit and valve losses and of transit-time effects. In order to do so we shall first deal with these effects theoretically, and then compare the results with our experiments.

A similar theory may be given for grounded-grid tetrodes and pentodes as well as for secondary-emission valves. The theoretical results are quantitatively verified by experiments on grounded-grid secondary-emission valves.

Fig. 1 shows the input circuit of a grounded-grid triode with short-circuited output. The "cold" valve capacities form part of the circuit, whilst C denotes the detuning of the input circuit. R_1' represents the transformed antenna resistance and R the parallel resistance due to circuit losses, dielectric losses inside the valve (glass, emission layer of the cathode), and losses due to the resistance of the electrode leads. The thermal noise of R_1' and R is represented by noise-current generators i' and i_R in parallel to the input circuit, such that

$$\overline{i'^2} = \frac{4kT\Delta\nu}{R_1'}; \quad \overline{i_R^2} = \alpha \cdot \frac{4kT\Delta\nu}{R}. \tag{1}$$

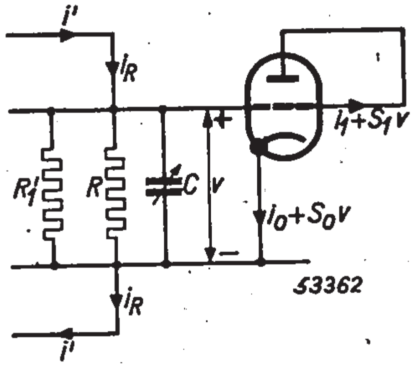

Fig. 1. Input circuit of a grounded-grid triode with short-circuited output. For the meaning of the symbols, see the text.

In these equations k denotes Boltzmann's constant, T the absolute room temperature, $\Delta\nu$ a small frequency interval, and α the noise ratio of R ($\alpha = 1$ if R consists only of circuit losses, $\alpha > 1$ if dielectric losses cannot be ignored).

When a voltage v is applied between grid and cathode, a current $S_0 v$ will flow from cathode to grid and a current $S_1 v$ from grid to anode. Due to electronic transit-time effects $S_0 v$ and $S_1 v$ are delayed in phase with respect to v, such that $S_1 v$ is delayed more than $S_0 v$. According to fig. 1, S_0 forms part of the total input admittance of the input circuit. Putting

$$S_0 = |S_0|\, e^{-j\varphi_0} = \frac{1}{R_e} + j\omega C_e, \tag{2}$$

we have R_e and C_e denoting the input resistance and input capacity due to electronic motion.

According to (2), C_e is a negative quantity. R_e and C_e are independent of ω, except for the highest frequencies where φ_0 is no longer a small quantity.

Hence we have for the total admittance Y_i of the input circuit (cf. fig. 1)

$$Y_i = \frac{1}{R_1'} + \frac{1}{R} + j\omega C + S_0, \tag{3}$$

so that

$$|Y_i|^2 = \left(\frac{1}{R_1'} + \frac{1}{R} + \frac{1}{R_e}\right)^2 + \omega^2 (C + C_e)^2. \tag{3a}$$

The input circuit is tuned to the received signal when $(C + C_e) = 0$.

Due to shot-effect a noise current i_0 flows from cathode to grid and a noise current i_1 from grid to anode. Owing to electronic transit-time effects i_1 is delayed in phase with respect to i_0. In our theory we shall first assume that i_0 and i_1 are completely correlated, but afterwards we shall drop this assumption *). i_0 gives rise to a voltage v across the input circuit, and this voltage v gives rise to a noise current $S_1 v$ flowing into the output circuit. If i_0 and i_1 are completely correlated, i_1 and $S_1 v$ will be completely correlated too. This means that i_1 and $S_1 v$ have to be added, taking due account of their correct phase relation.

In our calculations we have to introduce also the capacity C_0 and the resistance R_0, defined as

$$i_1 S_0 - i_0 S_1 = i_1 \left(\frac{1}{R_0} + j\omega C_0\right). \tag{4}$$

This is allowed if i_0/i_1 is a well-defined complex number, which is the case when i_0 and i_1 are completely correlated.

---

*) Complete correlation means that i_0/i_1 is a complex number independent of the intensity of the fluctuations (but dependent upon the electronic transit times).

2. Calculation of the noise factor

The noise factor F of a receiver stage may be calculated from the following definition [2]):

$$F = \frac{\text{mean-square output current due to noise of the receiver stage}}{\text{mean-square output current due to antenna noise}}.$$

$(F—1)$ denotes the contribution of the stage without antenna to the noise factor.

The mean-square noise current flowing into the output circuit due to i' is (cf. fig. 1)

$$\frac{4kT\Delta\nu}{R_1'} \cdot |Y_i|^{-2} \cdot |S_1|^2, \tag{5}$$

and the mean-square output noise current due to i_R is

$$a \cdot \frac{4kT\Delta\nu}{R} \cdot |Y_i|^{-2} \cdot |S_1|^2. \tag{6}$$

We finally have to calculate the noise current due to emission fluctuations. The noise current $(i_0 + S_0 v)$ flowing through the input circuit gives rise to the noise voltage v:

$$v = -(i_0 + S_0 v)\left[\frac{1}{R_1'} + \frac{1}{R} + j\omega C\right]^{-1}, \text{ or } v = -i_0 Y_i^{-1}, \tag{7}$$

and the noise current through the output circuit becomes

$$\begin{aligned}(i_1 + S_1 v) = i_1 - i_0 S_1 Y_i^{-1} &= \left[i_1\left(\frac{1}{R_1'} + \frac{1}{R} + j\omega C\right) + i_1 S_0 - i_0 S_1\right] Y_i^{-1} = \\ &= i_1\left[\left(\frac{1}{R_1'} + \frac{1}{R_1} + \frac{1}{R_0}\right) + j\omega\left(C + C_0\right)\right] Y_i^{-1}.\end{aligned} \tag{7a}$$

Defining the equivalent noise resistance R_n of the valve by

$$\overline{i_1^2} = 4kTR_n\Delta\nu\,|S_1|^2,$$

we obtain for the mean-square value of (7a):

$$\overline{(i_1 + S_1 v)^2} = 4kTR_n\Delta\nu\,|S_1|^2 . |Y_i|^{-2}\left[\left(\frac{1}{R_1'} + \frac{1}{R} + \frac{1}{R_0}\right)^2 + \omega^2\left(C + C_0\right)^2\right]. \tag{8}$$

Adding (6) and (8), and dividing by (5) yields $(F—1)$:

$$\begin{aligned}(F-1) &= a\frac{R_1'}{R} + \frac{\overline{(i_1 + S_1 v)^2}\,|Y_i|^2 R_1'}{4kT\Delta\nu\,|S_1|^2} = \\ &= a\frac{R_1'}{R} + R_1' R_n\left[\left(\frac{1}{R_1'} + \frac{1}{R} + \frac{1}{R_0}\right)^2 + \omega^2\left(C + C_0\right)^2\right].\end{aligned} \tag{9}$$

Considering $(F-1)$ as a function of the tuning capacity, a minimum value is attained for $C = -C_0$. It may be shown that C_0 is approximately equal to C_e *). Hence the output signal current is practically tuned to its *maximum* value when the output noise current is tuned to its *minimum* value.

Assuming the input circuit to be tuned to minimum noise $(C + C_0 = 0)$, we have according to (9)

$$(F-1) = a\frac{R_1'}{R} + R_1'R_n\left(\frac{1}{R_1'} + \frac{1}{R} + \frac{1}{R_0}\right)^2 =$$
$$= \frac{R_n}{R_1'} + 2\left(\frac{R_n}{R} + \frac{R_n}{R_0}\right) + \frac{R_1'}{R_n}\left\{a\frac{R_n}{R} + \left(\frac{R_n}{R} + \frac{R_n}{R_0}\right)^2\right\}, \tag{10}$$

which is of the general form

$$(F-1) = \frac{R_n}{R_1'} + 2A + B\frac{R_1'}{R_n}; \tag{10a}$$

it has a minimum value

$$(2A + 2\sqrt{B}) \quad \text{for} \quad R_n/R_1' = \sqrt{B}. \tag{10b}$$

The relation between A and B follows from (10).

Equation (10a) may be experimentally checked by measuring $(F-1)$ as a function of the transformed antenna resistance R_1'. The constant B of (10a) may also be obtained from the "noise resonance curve" for $R_1' = \infty$, in which the output noise voltage of the receiver is plotted against the tuning capacity C of the input circuit. If the change in tuning capacity C is so small (e.g. a few pF) that $|Y_i|$ remains practically unaltered, we may learn from equations (6) and (8) that the mean square of the output noise current of the valve is proportional to

$$a\frac{R_n}{R} + \left(\frac{R_n}{R} + \frac{R_n}{R_0}\right)^2 + \omega^2(C + C_0)^2 R_n^2 = B + \omega^2(C + C_0)^2 R_n^2. \tag{10c}$$

As B is only a relatively small quantity, an important increase in output noise current may occur for small values of $(C + C_0)$.

---

*) Theoretically, we have in the first order of approximation 3)4)

$$\begin{aligned} i_1 &= i_0(1-{}^1/_3\, j\omega\tau_{cg} - {}^2/_3\, j\omega\tau_{ga}), \\ S_0 &= S(1-{}^1/_5\, j\omega\tau_{cg}), \\ S_1 &= S(1-{}^{11}/_{30}\, j\omega\tau_{cg} - {}^2/_3\, j\omega\tau_{ga}), \end{aligned}$$

where τ_{cg} and τ_{ga} denote the electronic transit times from cathode to grid and from grid to anode, whilst S is the l.f. transconductance of the valve.

Introducing these relations into the definition of C_e and C_0, we obtain in the first order of approximation

$$C_e = -{}^1/_5\, \tau_{cg}\, S, \quad C_0 = -{}^1/_5\, \tau_{cg}\, S + {}^1/_{30}\, \tau_{cg}\, S,$$

so that C_e and C_0 are practically equal.

At present the theory is insufficiently accurate to calculate R_0.

Determining the values of C for which the mean-square output noise current of the valve is equal to twice its minimum value, we obtain according to (10c) an independent estimate of B, which may be compared to the value obtained from $(F—1)$ as a function of R_1'.

We have now completed the general theoretical treatment of a grounded-grid-triode circuit. The only assumption which had to be made was that i_0 and i_1 were completely correlated. Dropping this assumption, we have the following possibilities.

(a) *i_0 can be split up into two parts, one part i_0' completely correlated to i_1 and another part i_0'' independent of i_1.* This case may occur at u.h.f. due to total-emission noise [9]), which is practically independent of shot noise.

(b) *i_1 can be split up into two parts, one part i_1' completely correlated to i_0 and another part i_1'' independent of i_0.* This case occurs with grounded-grid pentodes or secondary-emission valves. In grounded-grid pentodes partition-current fluctuations flow into the output circuit, these fluctuations being independent of the shot-effect fluctuations flowing through the input circuit. In grounded-grid secondary-emission valves the same holds for the secondary-emission fluctuations flowing through the output circuit.

The cases (a) and (b) might also be treated simultaneously as special forms of the following general case:
i_0 and i_1 consist of a large number of independent parts such that every part of i_0 is completely correlated to some part of i_1. This case may occur due to valve inhomogeneities, e.g. asymmetrical construction, field inhomogeneities, inhomogeneities in transit time. It may be shown that this general case can be treated as a linear combination of the cases (a) and (b), by assuming

$$i_0 = i_0' + i_0'',$$
$$i_1 = i_1'' + i_1''',$$

such that only i_0'' and i_1'' are completely correlated. Hence it is not necessary to discuss this general case.

We shall first discuss case (a). The part i_0' has to be treated in a similar way as i_0 was treated before. The part i_0'' gives rise to an additional independent noise voltage across the input circuit. According to (6) and (7) this may formally be taken into account by suitably choosing the value of the noise ratio a of the resistance R in equation (6), so that this case only affects the quantity B of equation (10a).

In case (b) the part i'_1 has to be treated in a similar way as i_1 was previously treated. The second part i''_1 is an independent noise current flowing through the short-circuited output lead. In order to calculate the noise factor of the stage we have to introduce into our previous calculations i'_1 instead of i_1, and have to add the new term $\overline{i''^2_1}$ to $\overline{(i'_1 + S_1 v)^2}$. Introducing the new equivalent noise resistances R'_n and R''_n by the relations

$$\overline{i'^2_1} = 4kTR'_n \Delta\nu \, |S_1|^2, \quad \overline{i''^2_1} = 4kTR''_n \Delta\nu \, |S_1|^2, \tag{11}$$

we obtain in analogy to our previous calculations

$$(F-1) = a\,\frac{R'_1}{R} + \frac{\overline{[(i'_1 + S_1 v)^2 + \overline{i''^2_1}]} \cdot |Y_i|^2 R'_1}{4kT\Delta\nu \, |S_1|^2} \tag{12}$$

or

$$(F-1) = a\,\frac{R'_1}{R} + R'_1 R'_n \left[\left(\frac{1}{R'_1} + \frac{1}{R} + \frac{1}{R_0}\right)^2 + \omega^2 \left(C + C_0\right)^2\right] + \\ + R'_1 R''_n \left[\left(\frac{1}{R'_1} + \frac{1}{R} + \frac{1}{R_e}\right)^2 + \omega^2 \left(C + C_e\right)^2\right]. \tag{13}$$

The latter term may become important for large values of R'_1, especially if $R_0 \gg R_e$ ($R_e = 100\ \Omega$, R_0 is generally much larger). Usually, the input circuit is tuned to minimum noise. Even if C_0 were slightly different from C_e, it should be advisable to choose $C = -C_0$, because generally $1/R_e{}^2 \gg \omega^2 (C_0 - C_e)^2$.
Hence (12) becomes

$$(F-1) = a\,\frac{R'_1}{R} + R'_1 R'_n \left(\frac{1}{R'_1} + \frac{1}{R} + \frac{1}{R_0}\right)^2 + R'_1 R''_n \left(\frac{1}{R'_1} + \frac{1}{R} + \frac{1}{R_e}\right)^2. \tag{13a}$$

(13a) is of the same form as (10). Without loss of generality we may ignore $1/R$ and $1/R_0$ against $1/R'_1$ and $1/R_e$, as this does not change the form of (13a). Moreover, this is allowed for secondary-emission valves. We obtain

$$(F-1) = \frac{R'_n}{R'_1} + \frac{R''_n}{R'_1} + 2\,\frac{R''_n}{R_e} + \frac{R''_n R'_1}{R_e{}^2} = A\,\frac{R_e}{R'_1} + 2B + B\,\frac{R'_1}{R_e}, \tag{13b}$$

such that

$$A = \left(1 + \frac{R''_n}{R'_n}\right)\frac{R'_n}{R_e}, \quad B = \frac{R''_n}{R'_n} \cdot \frac{R'_n}{R_e}. \tag{13c}$$

Equation (13b) attains a minimum value

$$(F_{\min}-1) = 2\,\frac{R'_n}{R_e}\left[\frac{R''_n}{R'_n} + \sqrt{\frac{R''_n}{R'_n}\left(1 + \frac{R''_n}{R'_n}\right)}\right] \tag{13d}$$

for
$$\frac{R_n'}{R_1'} = \frac{R_n'}{R_e}\sqrt{\frac{R_n''/R_n'}{1+R_n''/R_n'}}. \tag{13e}$$

Fig. 2 shows the right-hand factor of (13d) as a function of R_n''/R_n'. Obviously, a small value of R_n''/R_n' is favourable for a low noise factor.

A comparison of (13b) and (10a) reveals that the two equations are qualitatively the same. This makes it difficult to distinguish between the two equations, and therefore a careful quantitative experimental analysis is needed.

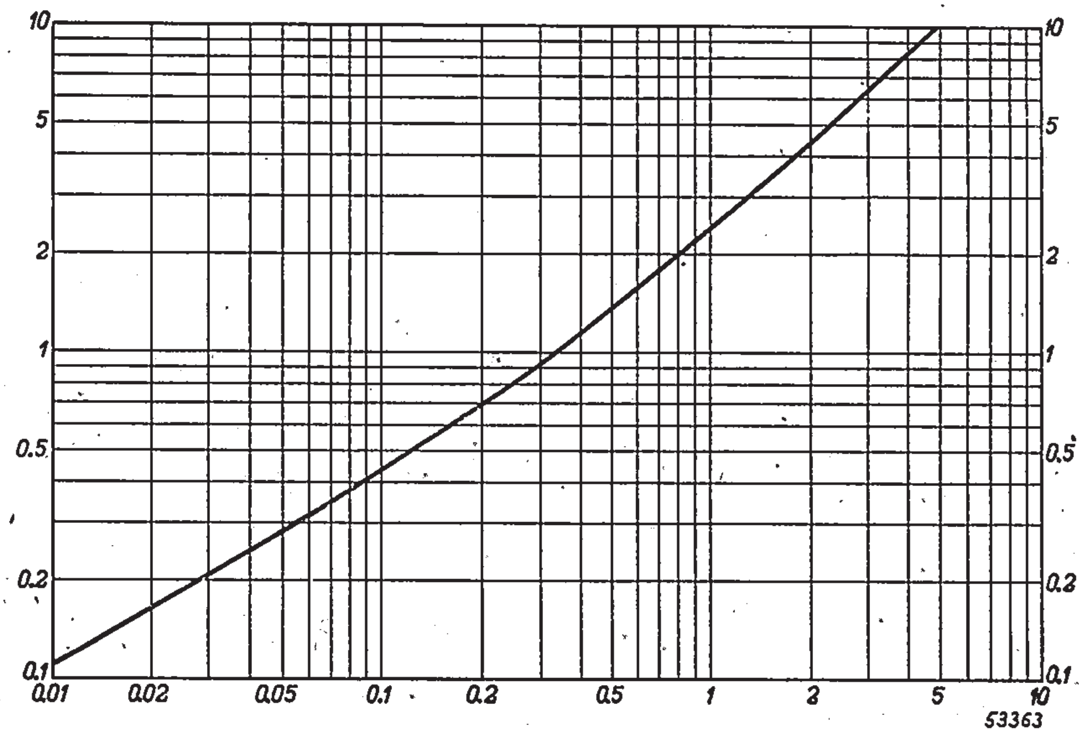

Fig. 2. $\frac{R_n''}{R_n'} + \sqrt{\frac{R_n''}{R_n'}\left(1+\frac{R_n''}{R_n'}\right)}$ as a function of $\frac{R_n''}{R_n'}$.

3. Experimental results for grounded-grid triodes

Measurements of the noise factor F as a function of the transformed antenna resistance R_1' were carried out, using a linear amplifier with thermo-couple detector [5]). Particularly for large values of R_1' accurate measurements of the noise factor of grounded-grid triodes are very difficult to perform. The reason is that for large values of the transformed antenna resistance R_1' the output noise current of the grounded-grid stage due to shot effect is suppressed within a few percent, whilst the output noise current due to antenna noise is small, because a large value of R_1' means a very loose coupling.

Hence only a very small part of the total noise output of the linear amplifier is due to the measured grounded-grid stage. A small error in the determination of the part of the noise output that is due to the subsequent stages of the amplifier may thus give rise to a large error in the noise factor. We finally succeeded in measuring that part (and hence $(F-1)$) with a good accuracy.

At a wavelength of 7·25 m we measured $(F-1)$ as a function of R_1', the "noise resonance curve" of the input circuit for $R_1' = \infty$, and R; for the latter we found a value of 10 000 Ω for valve nr 1.

Fig. 3 shows $(F-1)$ as a function of R_1' for two experimental grounded-grid triodes nr 1 and nr 2 having an amplification factor of about 100 and a transconductance of about 12 mA/V. For valve nr 1 the measured points (circles) were represented by the equation (full-drawn curve)

$$(F-1) = 225/R_1' + 0{\cdot}18 + 0{\cdot}00023\, R_1',$$

and for valve nr 2 (measured points denoted by crosses) by the equation (full-drawn curve)

$$(F-1) \doteq 250/R_1' + 0{\cdot}26 + 0{\cdot}00048\, R_1'.$$

The form of these equations is compatible with equation (10a).

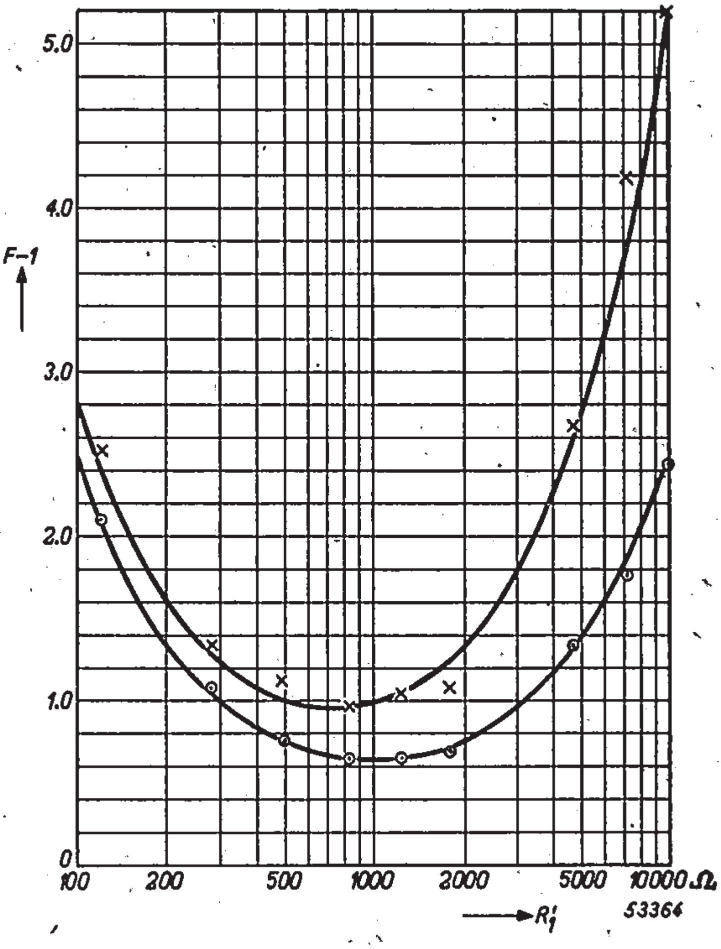

Fig. 3. $(F-1)$ as a function of the transformed antenna resistance R_1' for two experimental grounded-grid triodes (nrs 1 and 2). Full-drawn curves are theoretical ones; the measured values are denoted by circles (nr 1) and by crosses (nr 2).

Fig. 4 shows the noise resonance curve of valve nr 1 for $R_1' = \infty$. Measured points are denoted by circles, the full-drawn line represents the equation

$$\text{Amplifier output} = 1{\cdot}00 + 0{\cdot}12 \left[1 + \left(\frac{C—C_{\min}}{3{\cdot}6}\right)^2\right],$$

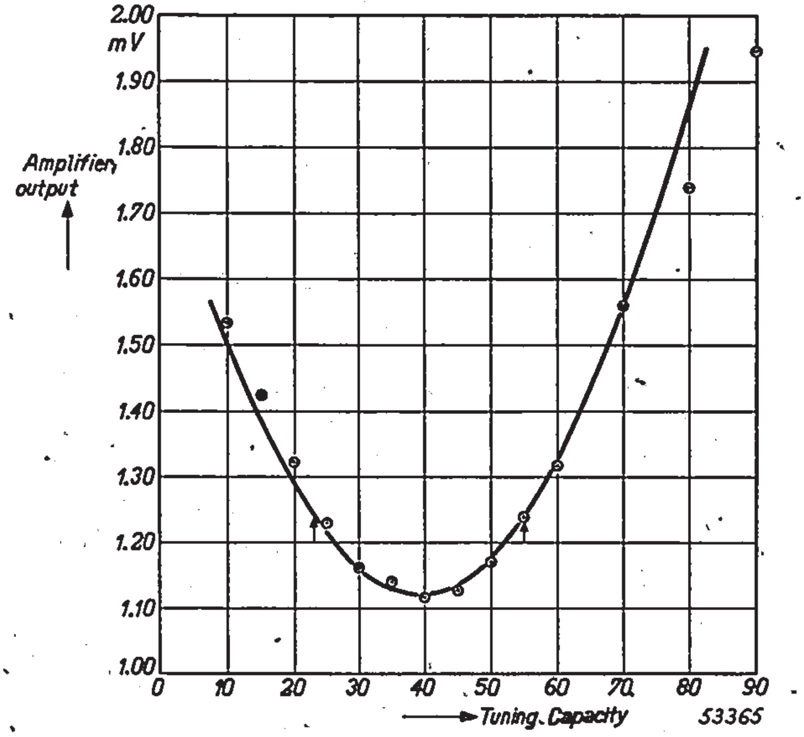

Fig. 4. "Noise resonance curve" of the input circuit of the grounded-grid triode nr 1 of the previous figure, taken for $R_1' = \infty$ (no transformed antenna resistance). This curve gives the output of the amplifier as a function of the tuning capacity; one scale division of the condenser corresponds to 0·225 pF. The full-drawn curve is a theoretical parabola; circles denote measured values. The contribution of the subsequent part of the amplifier to the output noise was 1·00 mV. The arrows denote the value of the tuning condenser for which the mean-square value of the output noise current of the grounded-grid triode is doubled.

in which $(C—C_{\min})$ is in pF. The first term is due to the subsequent part of the linear amplifier. The second term, which has a minimum value for $C = C_{\min}$, represents the noise due to the grounded-grid stage itself. This equation is also compatible with equation (10c) as well as with equation (13).

Assuming the validity of equations (10) and (10c) we have for the noise output of the linear amplifier according to (10c)

$$C_1 + C_2 [1 + \omega^2 (C—C_{\min}{}^2)\, R_n{}^2/B]. \tag{10c}$$

Hence from the measured resonance curve we may calculate B. The result agrees with that obtained from the equation for $(F—1)$ within the limits of experimental error.

Finally, fig. 5 shows $(F-1)$ for another type of experimental valve having an amplification factor of 50 and about the same transconductance. Unfortunately we did not measure $(F-1)$ for $R_1' > 2000\ \Omega$. Fig. 6 shows the noise resonance curve for $R_1' = \infty$ for the same valve.

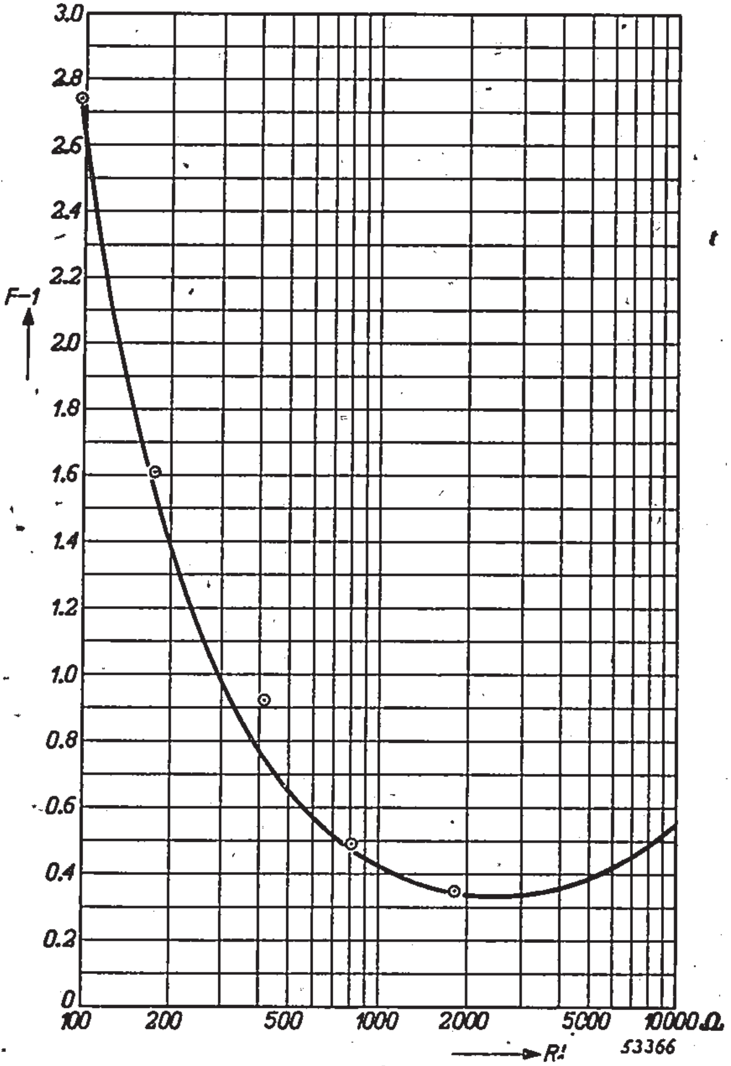

Fig. 5. $(F-1)$ as a function of the transformed antenna resistance R_1' for another type of experimental grounded-grid triode for which $F_{\min}$ is lower than for the valves of fig. 3.

These experiments show that values of $F < 2$ may be obtained for grounded-grid triodes at 7-m wavelength by suitably choosing the transformed antenna resistance R_1'. Experimentally it remains undecided whether electronic transit-time effects, independent noise sources, or inhomogeneities are responsible for the shape of the $(F-1)$-curve. However, from a *theoretical* point of view it is not very probable that in triodes i_1 should contain a noise component that is independent of i_0. It would be more likely to assume that electronic transit-time effects are to a large extent responsible for the measured values of $(F-1)$.

Calculating R_n, a, and R_0 from (10) and from the measured values of $(F-1)$, we find for valve nr 1

$$R_n = 225\ \Omega, \quad 2\left(\frac{R_n}{R}+\frac{R_n}{R_0}\right) = 0{\cdot}18, \quad a\frac{R_n}{R}+\left(\frac{R_n}{R}+\frac{R_n}{R_0}\right)^2 = 0{\cdot}052.$$

(The second result is less accurate than the others, because a change in this term would only result in a relatively small shift of the theoretical curve of fig. 3 in the vertical direction.)

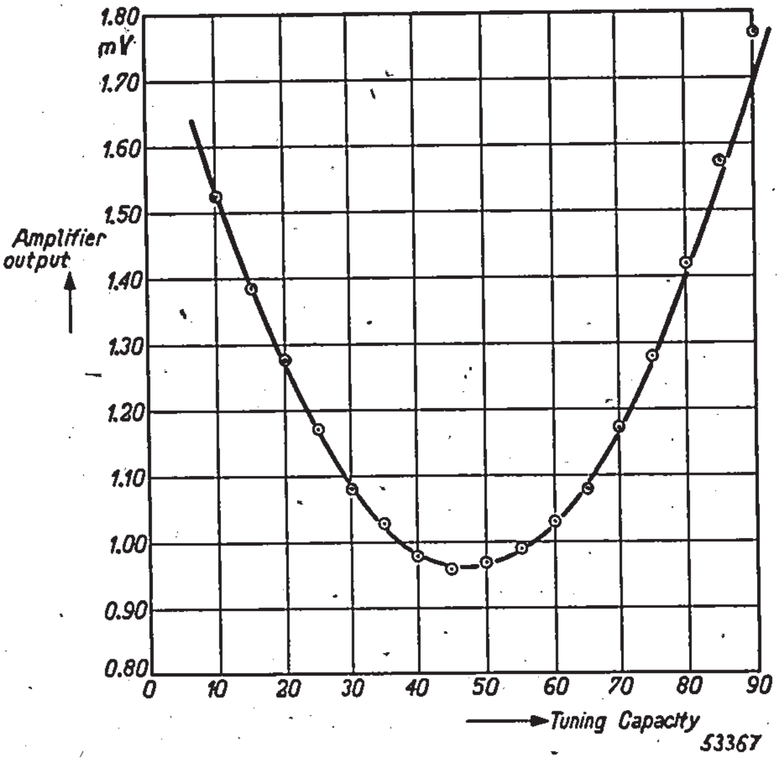

Fig. 6. "Noise resonance curve" of the input circuit of the grounded-grid triode of fig. 5, taken under the same condition as in fig. 4.

Introducing $R = 10\,000\ \Omega$ yields $a = 2{\cdot}0$ and $R_0 = 3000\ \Omega$. The deviation of a from unity may be accounted for by dielectric losses inside the valve, valve inhomogeneities, and total-emission noise. The experimental value of R_0 is not very accurate, but the order of magnitude is reliable.

We also calculated R_0 from the u.h.f. noise theory [3]) [7]) [8]) of triodes. It is beyond the scope of this paper to give a detailed account of this investigation, and we only mention that our final result was $R_0 = \infty$! This shows that the present theory is still in a poor form and has to be substantially improved.

Our measurements show that it would be recommendable to use a grounded-grid triode with loose antenna coupling as a first stage in u.h.f. receivers or i.f. radar amplifiers. For receivers with a very wide band, however, such stages find less application, because the gain of such a receiver stage becomes relatively low, so that the noise of the second receiver stage plays an important part.

Moreover, the measurements of the noise resonance curve show that for very wide bands the noise suppression is most effective in the middle of the received band, so that for very large bandwidths the final noise factor of the stage may be much larger than the measured values given in figs 3 and 5. This is one of the reasons why the noise factor of wide-band grounded-grid stages may sometimes be relatively large.

4. Noise factor of grounded-grid pentodes and secondary-emission valves

A theory of the noise factor of these valves has already been given in section 2. Ignoring the influence of circuit losses and transit-time effects, which is allowed here because the noise factor is much larger than in the case of a triode due to partition-current fluctuations or secondary-emission fluctuations, we have to apply equations (13b) and (13d). In these cases the values of R_n'' are practically independent of frequency at 7-m wavelength.

Applying these results to the valves already mentioned, we have for the noise currents in a slightly different notation [6]):

for a *triode*

$$\overline{i_t^2} = 2eI_cF_c^2\Delta\nu, \qquad F_c^2 = \gamma\frac{S_c}{I_c}, \tag{14a}$$

for a *tetrode* or *pentode*

$$\overline{i_a^2} = \overline{i_t^2}\left(\frac{I_a}{I_c}\right)^2 + 2e\frac{I_aI_2}{I_c}\Delta\nu = 2eI_a\Delta\nu\left[F_c^2\frac{I_a}{I_c}+\frac{I_2}{I_c}\right], \tag{14b}$$

and for a *secondary-emission valve*

$$\overline{i_a^2} = \overline{i_t^2}\,\delta^2 + 2eI_c\,(\varkappa-\delta)\delta\,\Delta\nu = 2eI_a\Delta\nu\,[F_c^2\delta + (\varkappa-\delta)]. \tag{14c}$$

In these equations I_c denotes the cathode current, I_a the anode current, I_2 the screen-grid current of the pentode (obviously $I_c = I_a + I_2$); δ denotes the secondary-emission factor; if all primary electrons arrive at the secondary emitter and all secondary electrons at the anode, we have $I_a = \delta I_c$; S_c denotes the transconductance of the cathode current I_c; i_t denotes the noise current when the valve is used as a triode; F_c^2 is the suppression factor for the emission fluctuations. The constant γ has a value between 0·1 and 0·2 and depends slightly upon valve dimensions. $\varkappa$ is a factor that has to be determined experimentally from noise measurements. The second term in equation (14b) is due to partition noise and the second term in equation (14c) is due to secondary-emission noise. Hence we have:

for a pentode
$$\frac{R_n''}{R_n'}=\frac{I_2}{F_c{}^2 I_a}, \tag{15a}$$

and for a secondary-emission valve
$$\frac{R_n''}{R_n'}=\frac{\varkappa-\delta}{F_c{}^2\delta}. \tag{15b}$$

For both types of valve we have in the grounded-grid circuit, under the assumption $|S_1| = S_c$,
$$R_e=\frac{1}{S_c}, \qquad R_n'=\frac{e}{2kT}\cdot\frac{\gamma}{S_c}, \tag{16a}$$

according to the definition of R_n' and equation (14a), and hence
$$\frac{R_n'}{R_e}=\frac{e}{2kT}\,\gamma=20\,\gamma, \tag{16b}$$

in practical units.

According to the above equations low values of I_2/I_a for a pentode and low values of $(\varkappa-\delta)/\delta$ for a secondary-emission valve are favourable for a low noise factor. Moreover, a large value of $F_c{}^2$ is important (this corresponds to a large value of S_a/I_a); the largest value of $F_c{}^2$ is obtained in the exponential part of the characteristic for which $F_c{}^2 = 1$. $(\varkappa-\delta)/\delta$ depends upon the constitution of the secondary emitter and is practically independent of the applied voltage; for caesium under favourable conditions its value may be 0·25, but in our measurements on secondary-emission valves we found a somewhat larger value. The value of I_2/I_a for normal valves is about 0·3, but smaller values (down to about 0·10) may be obtained by using a large screen-grid pitch and thin screen-grid wires; still smaller values may be obtained by electron-optical methods.

The above theory was verified at 7·25-m wavelength. In this test we used secondary-emission valves that had been developed by Dr G. Diemer of this laboratory. The measured valve had the following data:

$$I_c = 1{\cdot}03\ \text{mA},\ I_a = 4{\cdot}12\ \text{mA};\ \delta = I_a/I_e = 4{\cdot}0,\ R_e = 1/S_c = 330\ \Omega.$$

The above value of δ, which was obtained for a voltage of 160 V at the secondary-emitting electrode, is somewhat smaller than usual, whereas the measured value of $(\varkappa-\delta)/\delta$ was larger. According to Dr Diemer the method of preparation of the secondary-emitter could still be improved.

The measured values of $(F-1)$ are shown in fig. 7 (denoted by crosses), whilst the full-drawn curve is a theoretical one of the type (13b):

$$(F-1) = 6{\cdot}4\,\frac{R_e}{R_1'} + 6{\cdot}4 + 3{\cdot}2\,\frac{R_1'}{R_e}.$$

Hence we have

$$\left(1+\frac{R_n''}{R_n'}\right)\frac{R_n'}{R_e}=6{\cdot}4, \qquad \frac{R_n''}{R_n'}\cdot\frac{R_n'}{R_\epsilon}=3{\cdot}2,$$

or

$$\frac{R_n''}{R_n'}=1, \qquad \frac{R_n'}{R_e}=3{\cdot}2,$$

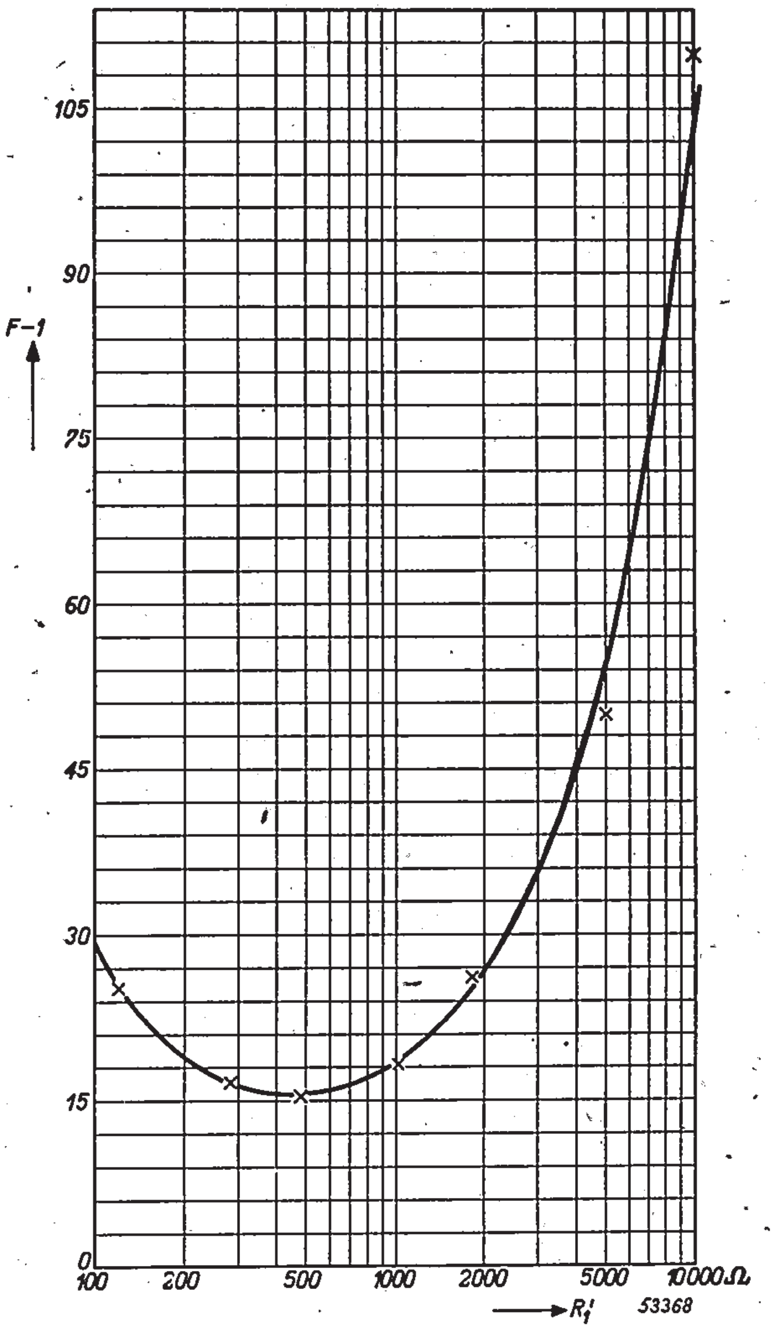

Fig. 7. (F—1) as a function of the transformed resistance R_1' for a grounded-grid secondary-emission valve. Crosses denote measured values; the full-drawn curve is a theoretical one.

and, with the help of (16b) and (15b),

$$\gamma = 0{\cdot}16, \qquad \left(\frac{\varkappa-\delta}{\delta}\right) = 0{\cdot}47, \qquad \varkappa = 5{\cdot}9,$$

which are quite reasonable values.

Eindhoven, July 1947

REFERENCES

1) A. van der Ziel, Philips Res. Rep. **1**, 381-399, 1946.
2) H. P. Friis, Proc. Inst. Radio Engrs **32**, 419-422, 1944.
3) C. J. Bakker, Physica, 's-Grav., **8**, 23-43, 1941.
4) M. J. O. Strutt and A. van der Ziel, Physica, 's-Grav., **8**, 81-108, 1941; **9**, 65-83, 1942.
5) A. van der Ziel, Philips Res. Rep. **2**, 321-330, 1947.
6) C. J. Bakker and Balth. van der Pol, Comptes Rendus des Assemblées Générales de l'Union Radioscientifique Internationale, Venise, 217-227, 1938.
7) A. J. Rack, Bell Syst. tech. J. **17**, 592-619, 1938.
8) W. E. Benham, Proc. Inst. Radio Engrs **26**, 1093-1170, 1938.
9) A. van der Ziel and A. Versnel, Philips Res. Rep. **3**, 13-23, 1948.

R 86 Philips Res. Rep. 3, 271-280, 1948

THE EQUILIBRIUM BETWEEN LIQUID SILICA AND LIQUID IRON

by J. D. FAST

541.127.4:669.15:669.782.018.11

Summary

The equilibrium between liquid SiO_2 and liquid Fe is computed with the aid of experimental data from the literature and thermodynamic considerations (see table III). The possible sources of error are discussed.

Résumé

L'équilibre entre le SiO_2 et le Fe liquides est déterminé à l'aide de données expérimentales prises dans la littérature et de considérations thermodynamiques (voir tableau III). L'article comporte aussi une discussion des sources possibles d'erreurs.

1. Introduction

The coating of a welding rod contains as a rule a large proportion of SiO_2 and, for that reason, the equilibrium between liquid SiO_2 and liquid Fe is of importance in arc-welding technique. In section 2 the reaction constant for the equilibrium between the pure substances will be computed from thermodynamic data taken from the literature, and in subsequent sections the results obtained will be used for a closer study of the actual equilibrium conditions under various circumstances.

2. The reaction between pure liquid SiO_2 and pure liquid Fe

The equilibrium constant of reaction (1) between liquid, or vitreous, SiO_2 and liquid Fe under formation of liquid Si and liquid FeO, may be computed from the corresponding constants of reactions (2) and (3):

$$
\begin{array}{rll}
 & SiO_2(v) + 2\,CO \rightleftarrows Si_l + 2\,CO_2\,, & (2)\\
- & 2\,FeO_l + 2\,CO \rightleftarrows 2\,Fe_l + 2\,CO_2\,, & (3)\\
\hline
 & SiO_2(v) + 2\,Fe_l \rightleftarrows Si_l + 2\,FeO\,. & (1)
\end{array}
$$

The equilibrium constant of (3) has already been computed in a previous paper 1). To calculate the reaction constant of (2) we shall make use of the standard enthalpies of formation and the standard entropies recorded in table I.

The data referring to CO and CO_2 were taken from a report by the U.S. Bureau of Standards 2), and the standard entropy of Si from a publication by the U.S. Bureau of Mines 3). The value of $\Delta H^0_{298\cdot1}$ for $SiO_2(v)$ was computed from the enthalpy of formation of α-quartz, $-208{\cdot}3$ kcal.mole^{-1}

TABLE I

Molar enthalpy of formation, ΔH^0, and molar entropy, s^0, of vitreous SiO_2, Si_s, CO_2 and CO at 25 °C and 1 atm.

	$\Delta H^0_{298\cdot1}$ kcal.mole^{-1}	$s^0_{298\cdot1}$ cal.mole^{-1}.degree^{-1}
$SiO_2(v)$	$-205{\cdot}3$	$11{\cdot}2$
Si_s	0	$4{\cdot}50$
CO_2	$-94{\cdot}05$	$51{\cdot}06$
CO	$-26{\cdot}41^5$	$47{\cdot}30$

according to Roth and Troitzsch [4]), and the enthalpy of the transition quartz glass → α-quartz, which is —3·0 kcal.mole^{-1} according to Troitzsch [5]).

The difference in entropy, $s_{298\cdot1}$—s_0, between vitreous quartz at 298·1 °K and the same substance at 0°K, was determined by a graphical integration using the specific heats as observed from 10 °K upwards by Simon [6]) and by Simon and Lange [7]); this gave a value 10·30 cal.mole^{-1}.degree^{-1}. As a disordered phase, vitreous quartz possesses a zero-point entropy, which according to Simon and Lange [7]) amounts to 0·9 cal.mole^{-1}.degree^{-1}, and this must be added to obtain the value recorded in table I.

From the data of table I we may now compute the reaction enthalpy and the reaction entropy of reaction (2), provided we replace Si_l by Si_s.

$$\Delta H^0_{298\cdot1} = -\,2 \times 94{\cdot}05 + 2 \times 26{\cdot}41^5 + 205{\cdot}3 = +\,70{\cdot}03 \text{ kcal}\,, \qquad (4)$$

$$\Delta S^0_{298\cdot1} = 4{\cdot}50 + 2 \times 51{\cdot}06 - 11{\cdot}2 - 2 \times 47{\cdot}30 = 0{\cdot}82 \text{ cal.degree}^{-1}. \qquad (5)$$

From these values, which only hold at 298·1 °K, we can now deduce the reaction enthalpy and the reaction entropy at higher temperatures, if we know the molar enthalpies and the molar entropies of all the substances that enter into the reaction. For CO_2 and CO the requisite data are accurately known from spectral observations [2]), while for vitreous SiO_2 and Si they can be calculated from the calorimetric determinations of the molar specific heat at constant pressure. These are given by

$$c_p^{SiO_2} = 12{\cdot}8 + 4{\cdot}47 \times 10^{-3}\, T - 3{\cdot}02 \times 10^5\, T^{-2} \text{ cal.mole}^{-1}\text{.degree}^{-1}, \qquad (6)$$

$$c_p^{Si_s} = 5{\cdot}70 + 0{\cdot}82 \times 10^{-3}\, T - 1{\cdot}01 \times 10^5\, T^{-2} \text{ cal.mole}^{-1}\text{.degree}^{-1}, \qquad (7)$$

formulae due to Kelley [3]), though (7) has been slightly altered in connection with later observations by Körber and Oelsen [8]).

Vitreous SiO_2, being in the state of an undercooled liquid, does not undergo a change in modification or aggregation upon heating. Hence its molar enthalpy and its molar entropy relative to 298·1 °K may be computed by the well-known formulae

$$h_T - h_{298\cdot 1} = \int_{298\cdot 1}^{T} c_p \mathrm{d}T, \tag{8}$$

$$s_T - s_{298\cdot 1} = \int_{298\cdot 1}^{T} \frac{c_p}{T} \mathrm{d}T. \tag{9}$$

Si on the other hand melts at 1688 °K with a heat of fusion of 11·1 kcal.mole^{-1}, so that for this substance we have

$$h_T - h_{298\cdot 1} = \int_{298\cdot 1}^{1688} c_p(s)\mathrm{d}T + 11100 + \int_{1688}^{T} c_p(l)\mathrm{d}T \quad \text{cal.mole}^{-1}, \tag{10}$$

$$s_T - s_{298\cdot 1} = \int_{298\cdot 1}^{1688} \frac{c_p(s)}{T}\mathrm{d}T + \frac{11100}{1688} + \int_{1688}^{T} \frac{c_p(l)}{T}\mathrm{d}T \quad \text{cal.mole}^{-1}\text{.degree}^{-1}, \tag{11}$$

where $c_p(l)$, the molar specific heat of liquid Si, is 6·5 cal.degree^{-1}.mole^{-1}.

For a temperature of 1800 °K we thus eventually computed the values given in table II, where the spectroscopic data for CO_2 and CO have also been recorded.

TABLE II

The molar enthalpy in cal and the molar entropy in cal.degree^{-1} of vitreous SiO_2, Si, CO_2 and CO at 1800 °K and 1 atm, taking 298·1 °K as point of reference.

	SiO_2	Si	CO_2	CO
$h_{1800} - h_{298\cdot 1}$	25420	20600	19020	11835
$s_{1800} - s_{298\cdot 1}$	28·08	17·46	21·35	13·69

Using these data we find the enthalpy and the entropy of reaction (2) at 1800 °K and 1 atm to be

$$\Delta H^0_{1800}(2) = 70{\cdot}03 + 20{\cdot}6 + 2\times 19{\cdot}02 - 25{\cdot}42 - 2\times 11{\cdot}835 = +79{\cdot}58 \text{ kcal},$$
$$\Delta S^0_{1800}(2) = 0{\cdot}82 + 17{\cdot}46 + 2\times 21{\cdot}35 - 28{\cdot}08 - 2\times 13{\cdot}69 = +5{\cdot}52 \text{ cal.degree}^{-1}.$$

For reaction (3) we have [1])

$$\Delta H^0_{1800}(3) = -2 \times 4{\cdot}575 \times 1685 = -15{\cdot}42 \text{ kcal},$$
$$\Delta S^0_{1800}(3) = -2 \times 4{\cdot}575 \times 1{\cdot}615 = -14{\cdot}78 \text{ cal.degree}^{-1}.$$

Hence we obtain for reaction (1):

$$\Delta H^0_{1800}\,(1) = \Delta H^0_{1800}\,(2) - \Delta H^0_{1800}\,(3) = +95{\cdot}0 \text{ kcal}, \tag{12}$$

$$\Delta S^0_{1800}\,(1) = \Delta S^0_{1800}\,(2) - \Delta S^0_{1800}\,(3) = +20{\cdot}30 \text{ cal.degree}^{-1}. \tag{13}$$

3. The reaction between the components in solution

In computing the actual equilibrium conditions for reaction (1) we have also to take into account that the silicon formed will be dissolved in the liquid iron, and that the iron oxide will be dissolved partly in the liquid SiO_2 and partly in the liquid metal phase.

The integral heat evolved in mixing x mole liquid Si and $(1-x)$ mole liquid Fe has been determined by Körber and coworkers [9]), whose data are reproduced in fig. 1; as heat is evolved, the enthalpy of mixing, ΔH, is negative. From these figures we may read at once the differential enthalpy of mixing, Δh_{Si}, that is, the heat effect when 1 mole liquid Si is dissolved in such a large amount of the liquid mixture that the change in concentration may be ignored; Δh_{Si} is seen to possess the constant value of $-20{\cdot}5$ kcal.mole^{-1} up to a concentration of about 30 atom % Si.

For very small Si concentrations the differential entropy of mixing can be approximated by $\Delta s_{Si} = -R \ln x_{Si}$, so that in view of the relation

$$\Delta \mu_{Si} = RT \ln a_{Si} = \Delta h_{Si} - T\Delta s_{Si},$$

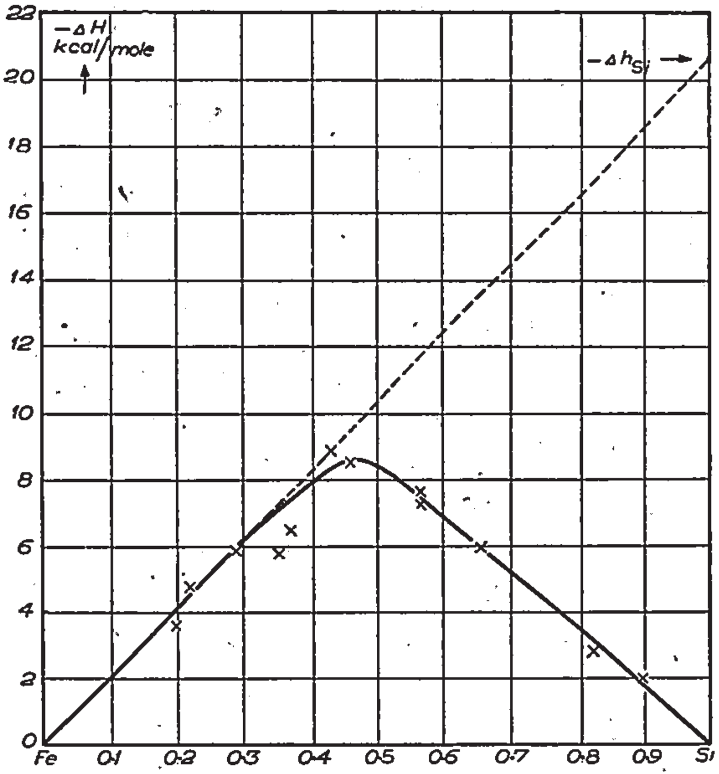

Fig. 1. Integral enthalpies of mixing for liquid Fe and liquid Si at a temperature of 1600 °C as measured by Körber and coworkers [9]).

the activity of Si in liquid mixtures rich in iron can be represented by

$$\log a_{\mathrm{Si}} = -\frac{20500}{4{\cdot}575\ T} + \log x_{\mathrm{Si}}\,. \tag{14}$$

From its derivation it will be clear that (14) expresses the activity relative to pure liquid Si as standard of reference.

The activity of FeO in liquid Fe has been computed in our previous paper [1]), where for small values of x_{FeO} we obtained

$$\log a_{\mathrm{FeO}} = \frac{18300}{4{\cdot}575\ T} + \log x_{\mathrm{FeO}}\,. \tag{15}$$

The reaction constant of (1) is given by

$$K_1 = \frac{[a_{\mathrm{Si}}]\ [a_{\mathrm{FeO}}]^2}{[a_{\mathrm{SiO_2}}]\ [a_{\mathrm{Fe}}]^2}, \tag{16}$$

where brackets indicate the metallic phase, and where $a_{\mathrm{SiO_2}}$ and a_{Fe} may be put equal to unity, because we are only considering very dilute solutions (of FeO in SiO_2, and of Si and FeO in Fe). Using (12), (13) and the relation

$$\log K = -\frac{\Delta H^0}{4{\cdot}575\ T} + \frac{\Delta S^0}{4{\cdot}575} \tag{17}$$

we are thus, for reaction (1), led to

$$\log \{[a_{\mathrm{Si}}]\ [a_{\mathrm{FeO}}]^2\} = -\frac{95000}{4{\cdot}575\ T} + \frac{20{\cdot}30}{4{\cdot}575},$$

or, after substituting from (14) and (15), to

$$\log \{[x_{\mathrm{Si}}]\ [x_{\mathrm{FeO}}]^2\} = -\frac{24300}{T} = 4{\cdot}44\,. \tag{18}$$

It should be noted that these equations essentially assume that the concentrations of Si and FeO in the liquid iron phase are so small that these two components do not influence each other's activities.
Expressing the Si and FeO content in weight % Si and O this equation may further be written as

$$\log \{[\%\ \mathrm{Si}]\ [\%\ \mathrm{O}]^2\} = -\frac{24300}{T} + 9{\cdot}05\,. \tag{19}$$

Though, according to the foregoing section, this holds strictly only for a narrow range of temperatures around 1800 °K, relation (19) can be applied without serious errors up to 2000 °K, a temperature at which

SiO_2 is in the liquid state under conditions of equilibrium and at a pressure of 1 atm.

The product

$$[\% \text{ Si}] [\% \text{ O}]^2$$

has experimentally been determined by Körber and Oelsen [10]). They obtained rather divergent values, fluctuating for instance between 2×10^{-5} and 9×10^{-5} at a temperature of 1873 °K; 3.6×10^{-5} was recorded as the most probable value at this temperature, as compared with $1{\cdot}2 \times 10^{-4}$ computed from (19). It must be borne in mind, however, that these two data are not strictly comparable; for (19) refers to the equilibrium with vitreous SiO_2, whereas Körber and Oelsen's experiments were made with reference to a crystalline SiO_2 phase (crystobalite). They investigated the equilibrium between liquid Fe and a liquid slag consisting of a homogeneous mixture of FeO, MnO and SiO_2, but in the presence of a surplus of crystobalite as a third phase; consequently their slag must have been saturated with respect to this crystalline SiO_2 phase. It may be added that the temperature in these experiments never surpassed the melting point of crystobalite (1980 °K).

By the same methods as used above we have also computed the equilibrium between crystobalite and liquid iron which yielded

$$\log \{[\% \text{ Si}] [\% \text{ O}]^2\} = -\frac{24800}{T} + 9{\cdot}30 \tag{20}$$

instead of (19). For 1873 °K this expression yields

$$[\% \text{ Si}] [\% \text{ O}]^2 = 1{\cdot}15 \times 10^{-4},$$

so that this refinement does not remove the discrepancy between the calculated and the experimental values.

4. The influence of the amount of slag on the equilibrium conditions

Using the various equations deduced above we shall now try to estimate the total amount of silicon and of oxygen taken up in a liquid iron phase when in equilibrium with liquid SiO_2.

To compute what fraction of the FeO will be dissolved in the liquid metal and what fraction will be dissolved in the slag, we have to know the ratio of the amount of metal to the amount of slag, and also the activity of the FeO in the metal and in the slag.

A rough estimate of the activity of FeO in liquid SiO_2 is all that can be achieved. According to the phase diagram FeO-SiO_2, as constructed by Bowen and Schairer [11]) and reproduced in fig. 2, the two liquids are not miscible in all proportions, though the compositions of the two coexisting liquid solutions are not precisely known; at 2000 °K they are lying in the neighbourhood of 4 and 40 mole % FeO. From the analysed oxygen contents of samples of liquid iron in equilibrium with FeO-SiO_2 solutions rich in FeO, it follows that the activity of this component is roughly equal to its mole fraction [12]). And since the activities in two coexisting liquids must be equal we obtain as a crude approximation for the liquid rich in SiO_2 at 2000 °K

$$(a_{\mathrm{FeO}}) = 10\,(x_{\mathrm{FeO}}), \tag{21}$$

the parentheses indicating the slag phase.

The activity in the metallic phase at 2000 °K is by (15)

$$[a_{\mathrm{FeO}}] = 100\,[x_{\mathrm{FeO}}], \tag{22}$$

brackets denoting the metallic phase. In equilibrium the activities in metal and slag must be equal so that from (21) and (22) we deduce

$$(x_{\mathrm{FeO}}) = 10\,[x_{\mathrm{FeO}}]\,. \tag{23}$$

Furthermore we have at 2000 °K from (18)

$$[x_{\mathrm{Si}}]\,[x_{\mathrm{FeO}}]^2 = 1{\cdot}95 \times 10^{-8}. \tag{24}$$

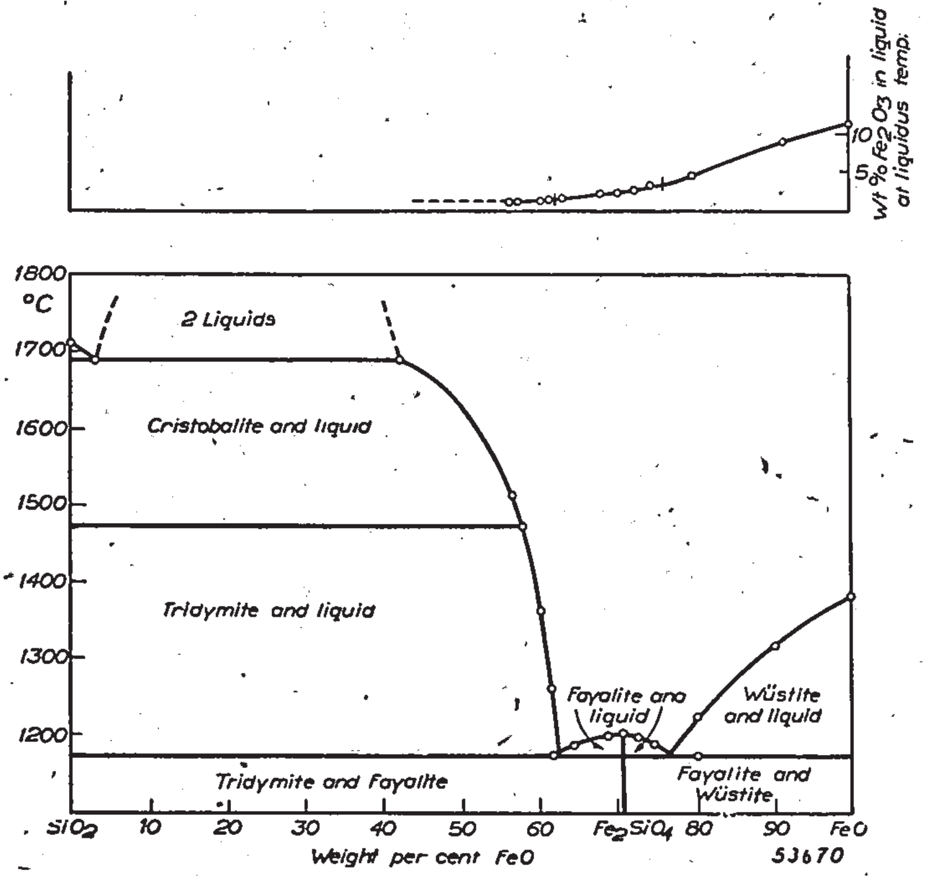

Fig. 2. Equilibrium diagram of the system SiO_2-FeO according to Bowen and Schairer [11]). The temperatures corresponding to the two eutectic points fayalite-tridymite and fayalite-wüstite differ only so slightly (about 1 °C) that the two eutectic horizontals seem to coincide in the figure.

If we start from pure SiO_2 and pure Fe then for each atom Si two molecules FeO are formed; so we must have approximately

$$2\,[x_{Si}] = [x_{FeO}] + (x_{FeO})\,\frac{SiO_2}{Fe}, \tag{25}$$

SiO_2/Fe indicating the mole ratio of these two components. For a set of different values of this ratio the concentrations in the metal and the slag computed from (23), (24) and (25) have been entered in table III, the concentrations of Si and O being expressed as weight % Si and O in the metal and as mole % FeO in the slag.

TABLE III

Computed compositions of the metal and the slag phases, when liquid Fe is in equilibrium with liquid SiO_2 at 2000 °K.

Mole ratio $\frac{SiO_2}{Fe}$	Metal		Slag
	wt % Si	wt % O	Mole % FeO
1/16	0·12	0·083	2·89
1/8	0·15	0·074	2·59
1/4	0·20	0·064	2·24
1/2	0·28	0·054	1·87

5. Discussion of results

Sources of error in the foregoing arguments are the standard heat of formation and the standard entropy of vitreous SiO_2, the heat of solution of Si in liquid Fe, and the compositions of the coexisting liquids in the system FeO-SiO_2.

To arrive at some estimate of the errors possible in table III let us for a moment assume, (a) that the standard heat of formation of vitreous SiO_2 is —206·0 instead of —205·3 kcal.mole^{-1}, (b) that the standard entropy of this substance is 11·4 instead of 11·2 cal.mole^{-1}.degree^{-1}, and (c) that the differential heat of solution of liquid Si in liquid Fe is —19·0 instead of —20·5 kcal.mole^{-1}; these are all changes lying within the range of possible experimental errors, and chosen so that they will influence the value of the product [% Si] [% O]^2 in the same sense.

With these altered values (18) becomes

$$\log \}[x_{Si}]\,[x_{FeO}]^2\{ = -\frac{24800}{T} + 4{\cdot}39, \tag{26}$$

giving at 1873 °K

$$[\%\ \mathrm{Si}]\,[\%\ \mathrm{O}]^2 = 5{\cdot}9 \times 10^{-5},$$

a result in much closer accord with the experimental value $3{\cdot}6 \times 10^{-5}$ of Körber and Oelsen [10]) than the value of $1{\cdot}2 \times 10^{-4}$ computed earlier from (18). With the altered equation (26) the top row of table III is converted into

$\frac{SiO_2}{Fe}$	Metal		Slag
	wt % Si	wt % O	mole % FeO
1/16	0·093	0·066	2·29

A further inaccuracy in our theoretical deductions is that we have disregarded the interaction between the Si and O atoms or ions in solution.

Owing to the great affinity between Si and O, we must expect a mutual lowering of the activity coefficients of these two components which will become more pronounced with increasing concentrations of Si and O.

Hence the product [% Si] $[\% \mathrm{O}]^2$ may be considered as virtually constant only in a very limited range of small concentrations. With increasing concentrations the value of this product will rise as a consequence of the lowering of the activity coefficient of Si with increasing O content and a lowering of the activity coefficient of O with increasing Si content.

The decrease in the activity coefficients has experimentally been demonstrated by Zapffe and Sims [13]). They observed the composition of gaseous mixtures of H_2O and H_2 in equilibrium with a liquid iron phase with some Si dissolved in it and contained in an SiO_2 crucible, and in some of their experiments they also analysed the O content of the liquid iron phase. The ratio p_{H_2O}/p_{H_2} is a direct measure of the *activity* of oxygen in the metal, while from work of Fontana and Chipman [14]) and of Chipman and Samarin [15]) the *concentration* of oxygen in liquid iron corresponding to given values of the ratio p_{H_2O}/p_{H_2} is known. With silicon dissolved in the liquid iron, Zapffe and Sims invariably obtained O concentrations higher than those corresponding to the activity in silicon-free iron, the discrepancy increasing with the concentration of Si. For example, a Si concentration of 1 to 2 weight % was found, after heating to 1600 °C for several hours in an $H_2O + H_2$ atmosphere, to produce an oxygen concentration 3 to 5 times as high as that computed for Si-free iron; but at a Si concentration of 0·03 % the computed and experimental values were in reasonable accord.

In most of their experiments Zapffe and Sims computed the oxygen activity from the ratio p_{H_2O}/p_{H_2} without analysing the corresponding oxygen content of the liquid metal phase. At constant temperature, the product $[a_{FeO}]^2$ [% Si] was found not to be constant, but to increase with a_{FeO}. Since by (16) the product $[a_{\mathrm{FeO}}]^2\,[a_{\mathrm{Si}}]$ is constant, we must infer that the activity coefficient of the dissolved Si,

$$k_{\mathrm{Si}} = \frac{a_{\mathrm{Si}}}{x_{\mathrm{Si}}},$$

diminishes with rising activity of the oxygen.

Zapffe and Sims prefer to interpret their observations on the hypothesis that at high oxygen concentrations silicon is dissolved mainly as monoxide SiO, while at lower concentrations it is dissolved mainly as Si.

From the arguments adduced in this section we must conclude that the concentrations recorded in table III can only be considered as giving the right order of magnitude.

Eindhoven, January 1948

REFERENCES

1) J. D. Fast, Philips Res. Rep. **2**, 205-227, 1947.
2) D. D. Wagman, J. E. Kilpatrick, W. J. Taylor, K. S. Pitzer and F. D. Rossini, J. Res. Nat. Bur. Stand. **34**, 143-161, 1945.
3) K. K. Kelley, Bur. Mines Bull. 394, 1936.
4) W. A. Roth and H. Troitzsch, Landolt-Börnstein, Phys. Chem. Tabellen, Dritter Ergänzungsband **3**, 2749, 1936.
5) H. Troitzsch, Thesis Braunschweig 1936.
6) F. Simon. Ann. Phys., Lpz., **68**, 241-280, 1922.
7) F. Simon and F. Lange, Z. Phys. **38**, 227-236, 1926.
8) F. Körber and W. Oelsen, Mitt. K.W.I. Eisenforsch. **18**, 109-130, 1936; H. Ulich, Kurzes Lehrbuch der phys. Chemie, Dresden und Leipzig, 1941, p. 317.
9) F. Körber, Stahl Eisen **56**, 1401-1411, 1936.
10) F. Körber and W. Oelsen, Mitt. K.W.I. Eisenforsch. **15**, 271-309, 1933.
11) N. L. Bowen and J. F. Schairer, Am. J. Sci. **24**, 177-213, 1932.
12) J. Chipman, Trans. Am. Soc. Metals **30**, 817-854, 1942.
13) C. A. Zapffe and C. E. Sims, Metals Technology, Tech. Publ. Nr 1498, 1-30, 1942.
14) M. G. Fontana and J. Chipman, Trans. Am. Soc. Metals **24**, 313-336, 1936.
15) J. Chipman and A. M. Samarin, Trans. A.I.M.E. **125**, 331-345, 1937.

R 87 Philips Res. Rep. 3, 281-302, 1948

RETROGRADE SOLUBILITY CURVES ESPECIALLY IN ALLOY SOLID SOLUTIONS

by J. L. MEIJERING 541.123.24

Summary

Using Gibbs's entropy of mixing and Richards's rule for the entropy of fusion of metals, a graph is derived thermodynamically, which serves to predict whether a solidus in a binary alloy system is retrograde or not, knowing only e.g. the eutectic concentration of the liquid and the coexisting solid solubility at the eutectic temperature. No disagreement is found with the solidus curves determined experimentally up till now. When the solid solubility is very low, a retrograde solidus is the normal thing to expect.

The graph can be tested in a more quantitative way by using the data at the solubility maxima found experimentally. Then systematic deviations arise, at least when the solid solubility is rather low. An analysis of their possible causes leads to the conclusion that important deviations from the Gibbs entropy of mixing can occur in dilute solid solutions when the solubility is small, owing to a loosening of the lattice by the substitution of solvent atoms by solute atoms.

Some remarks are made on solidus curves in non-metallic systems, transformation curves in iron alloys and retrograde solubility in liquids. It is shown that Grube and Flad's measurements in the Ni-Cr system, and the thermodynamic data calculated therefrom, are incorrect.

Résumé

Utilisant l'entropie de mélange de Gibbs et la règle de Richards pour l'entropie de fusion de métaux, l'auteur établit thermodynamiquement un graphique servant à prédire quand un solidus d'un système d'alliage binaire est rétrograde ou non, en connaissant seulement p.e. la concentration eutectique du liquide et la solubilité solide coexistante à la température eutectique. On n'a pas encore trouvé d'écart aux courbes solidus, relevées expérimentalement jusqu'ici. Lorsque la solubilité solide est très faible, il faut s'attendre normalement à un solidus rétrograde.

Le graphique peut être contrôlé de manière plus quantitative en utilisant les données à la solubilité maximum trouvées expérimentalement. Des écarts systématiques apparaissent tout au moins lorsque la solubilité solide est plutôt faible. Une analyse de leurs causes possibles conduit à la conclusion que des écarts importants à l'entropie de mélange de Gibbs peuvent se produire dans des solutions solides diluées lorsque la solubilité est petite, et dus à un relachement du réseau lors de la substitution d'atomes du solvant par des atomes dissous. Quelques remarques sont faites à propos de courbes solidus dans des systèmes non-métalliques, de courbes de transformation dans des alliages de fer et de la solubilité rétrograde dans des liquides.

L'auteur montre que les mesures de Grube et Flad sur le système Ni-Cr et les données thermodynamiques calculées à partir de ces mesures, sont incorrectes.

1. Introduction

In 1908 Van Laar ¹) calculated several binary phase diagrams, starting from different melting points and enthalpies ("heats") of melting for the components A and B, and different mixing-enthalpy curves for the liquid and solid phases, while for the mixing entropies the Gibbs "paradoxon" expression was used. Among the resulting synthetic diagrams were some of the type in fig. 1. Often a non-stable maximum solubility in the solidus curve occurred also *below* the eutectic temperature in diagrams of normal type, like fig. 2. The possibility of fig. 1 seems to have been practically forgotten for a long time. This will be due partly to the fact that Van Laar did not stress the point of the retrograde solidus particularly besides the other results of his calculations *), but also to the absence of an experimental example for fig. 1 until 1926 (so far as the author is aware). So when in that year Jenkins [3]) found a maximum in the Zn-rich solidus in the system Zn-Cd, which was confirmed by Stockdale [4]), this was considered so abnormal that a tentative interpretation was given, which made the maximum a discontinuous one, requiring an allotropic transformation in Zn.

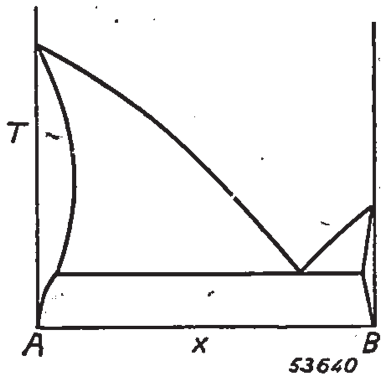

Fig. 1. Eutectic system with a retrograde solidus.

Hansen [5]) discarded this interpretation, and gave a continuous solidus as in fig. 1, stating, however, that this course of the solidus was against

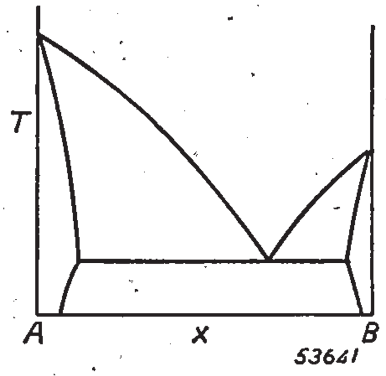

Fig. 2. "Normal" eutectic system.

---

*) In his book [2]) the maxima are shown in some diagrams, but not mentioned at all in the text.

all previous experience and that no adequate explanation for it was available.

Only in 1942 and afterwards were more examples found, especially by Raub and coworkers [6] [7] [8]). The maxima in the silver-rich solidus curves of Ag-Pb, Ag-Bi and Ag-Tl were very pronounced indeed. Meanwhile Scheil, apparently unaware of Van Laar's results, stated in a short paper [9]) that a solidus starting from the melting point of A will mostly end at $x = 0$ again at absolute zero temperature. The lower part of the curve is of course metastable, but when the eutectic temperature is relatively low, there is a good chance that the maximum will lie in the stable part. Scheil expects that the system Al-Ga will be found to have a retrograde solidus. The same prediction is made for Fe-S, as it will explain the fact that sulphur-bearing iron is more succesfully forged at 1200 °C than at lower temperatures (above the eutectic one), where it shows the phenomenon of red-shortness.

We now propose to examine the matter in a more quantitative way, and to derive an approximate relation which — in contrast with Van Laar's results — can be practically applied to experimental phase diagrams, especially of alloys.

2. Enthalpy and entropy relations for the temperature dependence of solubilities

The sign of the temperature coefficient of a solubility is given by the principle of Le Chatelier. In fig. 3a and 3b two different examples of enthalpy ("heat content") curves of two-phase systems at a certain temperature are given. The sign of H is in the usual thermodynamical sense; thus in fig. 3a, on mixing, the system is absorbing heat from the surroundings. When x stands for the atomic (or molecular) fraction of B, H is the enthalpy of one mole of the mixture. The linear central portion gives H for the heterogeneous mixtures.

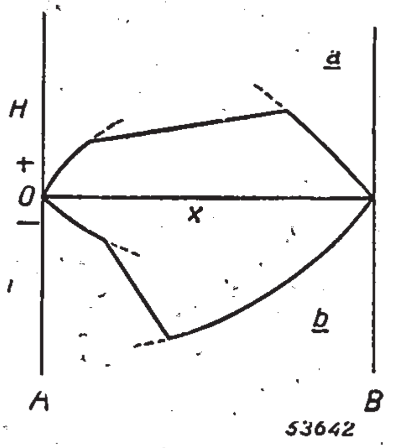

Fig. 3a and b. Two examples of enthalpy-concentration curves for a system with a two-phase region.

If we take a concentration *just* inside this two-phase region, the course of the dashed extension of the one-phase H-curve nearby teaches whether the temperature must be raised or lowered to make our mixture homogeneous. According to Le Chatelier in fig. 3a both mutual solubilities increase on heating; in fig. 3b the right-side solubility must decrease on heating. If we call the difference in concentration of the coexistent phases Δx and the difference in their respective H-values ΔH, it is seen that $\mathrm{d}x/\mathrm{d}T$ in the phase diagram has always the same sign as $(\mathrm{d}H/\mathrm{d}x - \Delta H/\Delta x)$, $\mathrm{d}H/\mathrm{d}x$ pertaining to the same phase boundary as $\mathrm{d}x/\mathrm{d}T$ of course. Writing S for the entropy of mixing for one mole, we can also substitute $(\mathrm{d}S/\mathrm{d}x - \Delta S/\Delta x)$ for the above term in parentheses, since $(\mathrm{d}G/\mathrm{d}x - \Delta G/\Delta x)$ is always zero in equilibrium and G, the free enthalpy, is $H—TS$ (T is absolute temperature).

Also known since a long time are the quantitative versions of these relations:

$$\frac{\mathrm{d}x}{\mathrm{d}T} = \frac{\dfrac{\mathrm{d}H}{\mathrm{d}x} - \dfrac{\Delta H}{\Delta x}}{T\dfrac{\mathrm{d}^2G}{\mathrm{d}x^2}} = \frac{\dfrac{\mathrm{d}S}{\mathrm{d}x} - \dfrac{\Delta S}{\Delta x}}{\dfrac{\mathrm{d}^2G}{\mathrm{d}x^2}}. \tag{1}$$

It is to be noted that $\mathrm{d}^2G/\mathrm{d}x^2$ is always positive for stable and metastable phases.

(1) is identical with Van der Waals's coexistence equation for constant pressure. A short derivation goes as follows: In equilibrium the tie-line (with slope $\Delta G/\Delta x = (G'-G)/(x'-x)$) must coincide with the double-tangent to the free-enthalpy curves of both phases (fig. 4). When T is changed, $\partial G/\partial x$ must remain equal to $\Delta G/\Delta x$, thus $\mathrm{d}\,\partial G/\partial x = \mathrm{d}\,\Delta G/\Delta x$.

$\mathrm{d}\dfrac{\partial G}{\partial x} = \dfrac{\partial\left(\dfrac{\partial G}{\partial x}\right)}{\partial T}\mathrm{d}T + \dfrac{\partial\left(\dfrac{\partial G}{\partial x}\right)}{\partial x}\mathrm{d}x$, and $\mathrm{d}\dfrac{\Delta G}{\Delta x} = \dfrac{\partial\left(\dfrac{\Delta G}{\Delta x}\right)}{\partial T}\mathrm{d}T$, because small changes in x and x' (at constant T) do not affect the slope of the tie-line, owing to its tangency.

As $\dfrac{\partial G}{\partial T} = -S$, we get $-\dfrac{\partial S}{\partial x}\mathrm{d}T + \dfrac{\partial^2 G}{\partial x^2}\mathrm{d}x = -\dfrac{\Delta S}{\Delta x}\mathrm{d}T$, which is identical with (1).

These relations seem to be less universally known than they deserve. Grube and Flad [11])

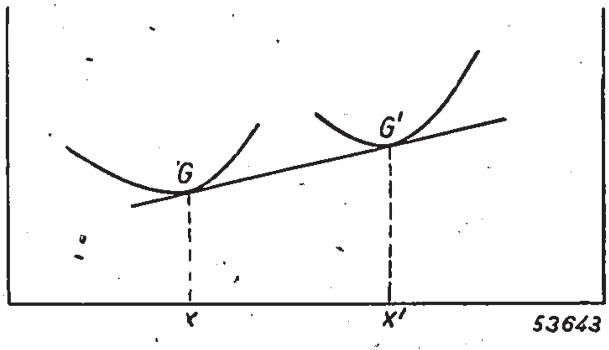

Fig. 4. Free-enthalpy curves (at a certain temperature) of two phases; x and x' are their concentrations in mutual equilibrium.

have measured the equilibrium $3\ H_2 + Cr_2O_3 \rightleftarrows 3\ H_2O + 2\ Cr$ (alloyed with Ni) at 1100° and 1200 °C, and derived the (H, x)-curve for the Ni-Cr system therefrom. It is given in fig. 5, turned upside down, as they take H positive when the surroundings absorb heat from the system. With the help of the above rules for the sign of dx/dT they would have seen immediately that their results are in contradiction with the phase diagram of Ni-Cr (fig. 6), in which the solubilities increase with rising temperature. The trend of the solubilities in it is surely right, and is also confirmed by Grube and Flad's measurements themselves (in the heterogeneous region p_{H_2O}/p_{H_2} is constant for a given temperature).

In a paper on the entropy of mixing in alloys Kubaschewski and Schneider [12]) derive an (S, x)-curve from Grube and Flad's data, which is negative over the whole range of concen-

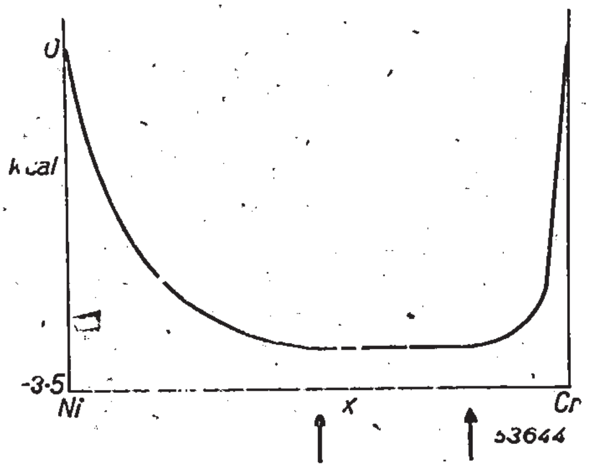

Fig. 5. Enthalpy-concentration curve of Ni-Cr at about 1150 °C, according to Grube and Flad [11]) *).

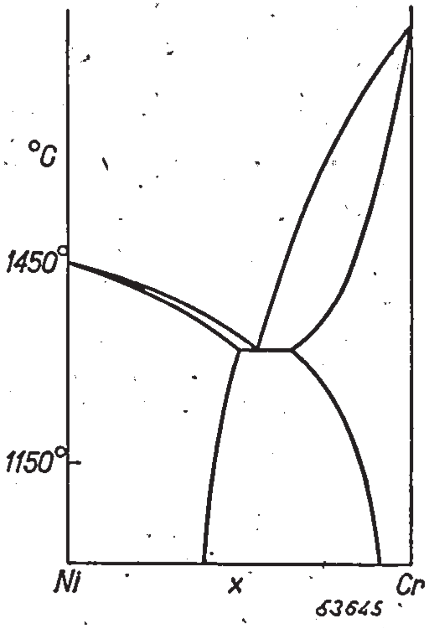

Fig. 6. Phase diagram of Ni-Cr (semi-schematical).

---

*) The calculation of the enthalpy by Grube and Flad was executed for round values of x, including the sequence 40, 50, 80 and 90 at. %. A straight line was drawn between the points at 50 and 80 %. According to their own results, however, this straight part should extend from 43 to 86 %, and the curved parts should be shorter and less curved at the ends. Then the kinks, with their wrong directions, would have been still more striking. This also applies to fig. 7.

trations (fig. 7)! This is termed to be unusual, but in qualitative agreement with a fall in the specific heat of Ni on alloying with Cr. Now the abnormal trend of this curve at $x = 0$ and 1 is practically impossible, as it would imply that e.g. the very first few Cr-atoms substituted in the Ni lattice would take up ordered positions with respect to each other. But surprising is that these authorities on thermochemistry of alloys in spite of the unusual result fail to note that it is contradicted by the phase diagram.

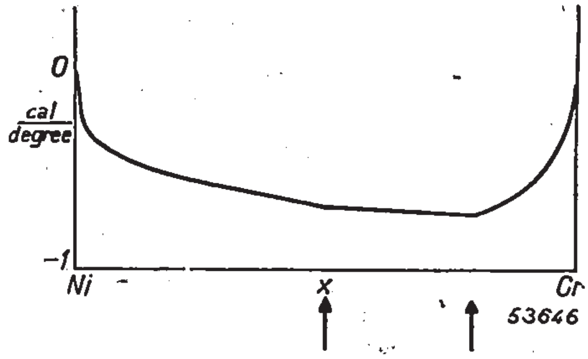

Fig. 7. Entropy-concentration curve of Ni-Cr at ± 1150 °C, according to Kubaschewski and Schneider [12]) (see note on preceding page).

The discrepancy on the Cr-side of the system is not so surprising, as here the values obtained for H and S are extremely sensitive to small temperature deviations. E.g. a difference of only 2° between the experiments at 1200 °C with pure Cr and with alloys (atomic fraction of Cr $= x$) would entail an error in the entropy of not less than $1{\cdot}8\ x$ cal/degree, sufficient to make it positive over the greater part of the system! In the alloys poor in Cr perhaps equilibrium with Cr_2O_3 was not always attained.

3. Derivation of a graph for predicting whether an alloy solidus will be retrograde or not

After this digression, which serves to emphasize the usefulness of the relations for the sign of dx/dT in general, we apply them to the case of the solidus. For a general survey the entropy relation is indicated, because generally the Gibbs expression for the entropy of mixing,

$$-R\,\{x \ln x + (1-x)\ln(1-x)\},$$

constitutes at least a reasonable approximation for both the liquid and the solid phase, while the enthalpies of mixing of course vary widely for different systems. We will restrict ourselves firstly to (binary) alloys, which are the most important systems when we are concerned with solid solutions; all cases of retrograde solidus curves now known experimentally are in fact alloy systems. A further schematization is now possible, as according to Richards's rule the entropy of melting of monatomic solids is approximately 2·1 cal/degree. After a survey of these entropies for metals, calculated from Landolt-Börnstein's tables, we chose the slightly greater value of $1{\cdot}1\ R$ (2·2 cal/degree) as a mean standard value for "normal" metals. The melting entropies of Sb, Bi, Si [13]) and Ga are much greater, about 2·5 R. These elements have in the solid state a structure with low coordination number, while in the liquid state the structure is probably more close-packed; at least Ga and Bi are known to contract on melting. The melting entropy of gray tin, by summation of that of white tin and the transformation entropy, also turns out to be large (2·5 R-3 R). We assume therefore that this will also be the case with Ge, which has diamond structure like Si and gray Sn. We take the melting entropy per mole, S_m, for Si, Ge, Sb, Bi and Ga to be (2·5 ± 0·2) R, for the other metals (1·1 ± 0·1) R *). We ignore the relatively small individual deviations because of the scatter of the values of different authors for one metal, and the temperature dependence of S_m, a consequence of the solid and liquid not having the same specific heat.

Now it is just an obvious step to assume that for metastable (and even unknown) modifications, too, the melting entropy lies between R and 1·2 R or between 2·3 R and 2·7 R, dependent on the kind of structure and not on the individual metal. Thus S_m for e.g. body-centred cubic Ni and face-centred cubic Bi would fall between the lower limits, and that for diamond-structured Al between the higher ones.

We now take the case that solid A and B (where B has the same crystal structure as the stable modification of A, and thus in most cases will be metastable) have precisely the same melting entropy $= \sigma R$. Calling the atomic fractions of B in the solid phase and in the liquid phase x and y respectively, we write for the entropy of the solid phase (which is thus the phase with A-structure):

$$S_{\text{sol}} = -R \, \} x \ln x + (1-x) \ln (1-x) \{$$

and for the entropy of the liquid phase:

$$S_{\text{liq}} = R \, \} \sigma - y \ln y - (1-y) \ln (1-y) \{ .$$

Thus $(\mathrm{d}S/\mathrm{d}x)_{\text{sol}} = R \ln \} (1-x)/x \{$ and

$$\frac{\Delta S}{\Delta x} = R \frac{\sigma - y \ln y - (1-y) \ln (1-y) + x \ln x + (1-x) \ln (1-x)}{y-x} .$$

These two expressions must be equal when the *solidus* (at the A-side) is just *vertical* ($\mathrm{d}T/\mathrm{d}x = \infty$). After a simple transformation, and writing Brigg's logarithms, one gets:

$$\log x = \log y - 0{\cdot}434 \frac{\sigma}{y} + \frac{1-y}{y} \log (1-y) - \frac{1-y}{y} \log (1-x) . \qquad (2)$$

---

*) Se, Te and As are not considered as basis metals here.

In fig. 9 the four curves bordering the two shaded bands give this function for the values of the parameter σ : 1·0, 1·2, 2·3 and 2·7 respectively (from top to bottom). It is to be noted that the scale of x is logarithmic, that of y linear. The calculation of log x for a given value of y is easy, as the last

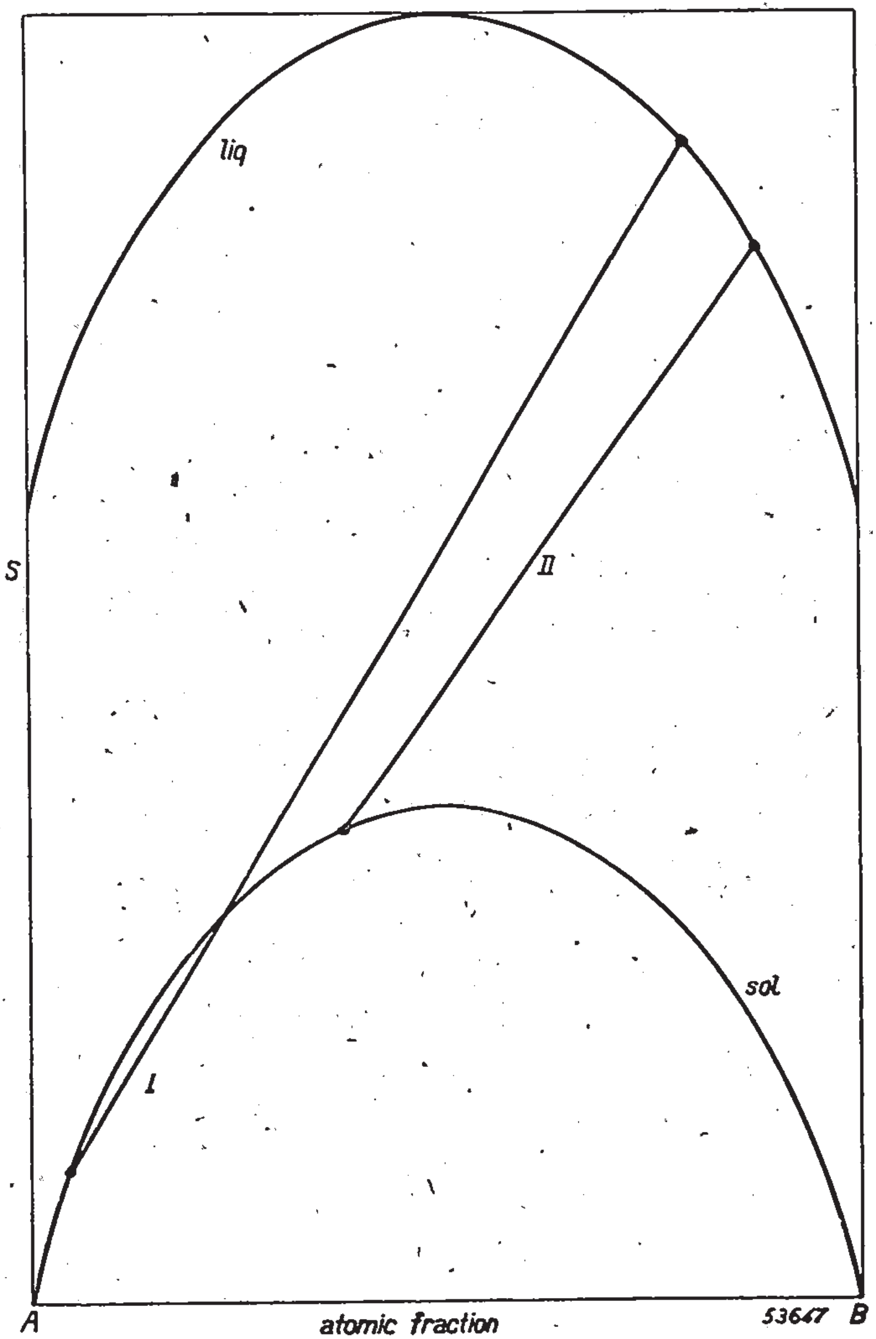

Fig. 8. The curves give the entropies of the solid and the liquid phase, Gibbs's expression for the entropy of mixing being used, and 1·1 R taken as the entropy of melting per mole. The entropies of two-phase mixtures lie on a straight line joining the points representing the coexisting solid and liquid. In example I an alloy consisting of the saturated solid solution plus a small amount of liquid has a smaller entropy than the solid solution of the same overall concentration. Therefore the solid solubility must rise with temperature. In example II the opposite is the case.

term on the right-hand side is 0 both for $x = 0$ and for $y = 1$, and remains small there between. Neglecting it, a provisional value for x is firstly calculated, which is substituted in the term in question. For the upper pair of curves this correction nowhere exceeds 0·02; a second approximation is unnecessary. For the lower pair the correction can be omitted, as it does not exceed 0·003 here.

When σ for A and for B (with A-structure) vary e.g. between 1·0 and 1·2, the curve for A-B lies inside the upper shaded band, also when these two values of σ are not precisely the same.

Fig. 9 can be used for all binary alloy systems; it is not applicable to the solid solubility curves of any intermetallic phases, but only to those of the phases adjoining one of the pure metals. When this is Sb, Bi, Si, Ge or Ga, we are concerned with the lower band, in other cases with the upper band, which is thus by far the more important one. E.g., in the system Al-Si we need the upper band for the Al-rich solidus, and the lower one for the Si-rich solidus. Of course the values of y and x to be plotted are atomic fractions of Si in the first case, and atomic fractions of Al in the second case.

Such a band constitutes a boundary area, wherein the solidus is very steep, and — owing to the uncertainties of the generalizations used — might as well be sloping to the right as to the left. In the area below the band we must expect (with an increasing certainty when the point representing the

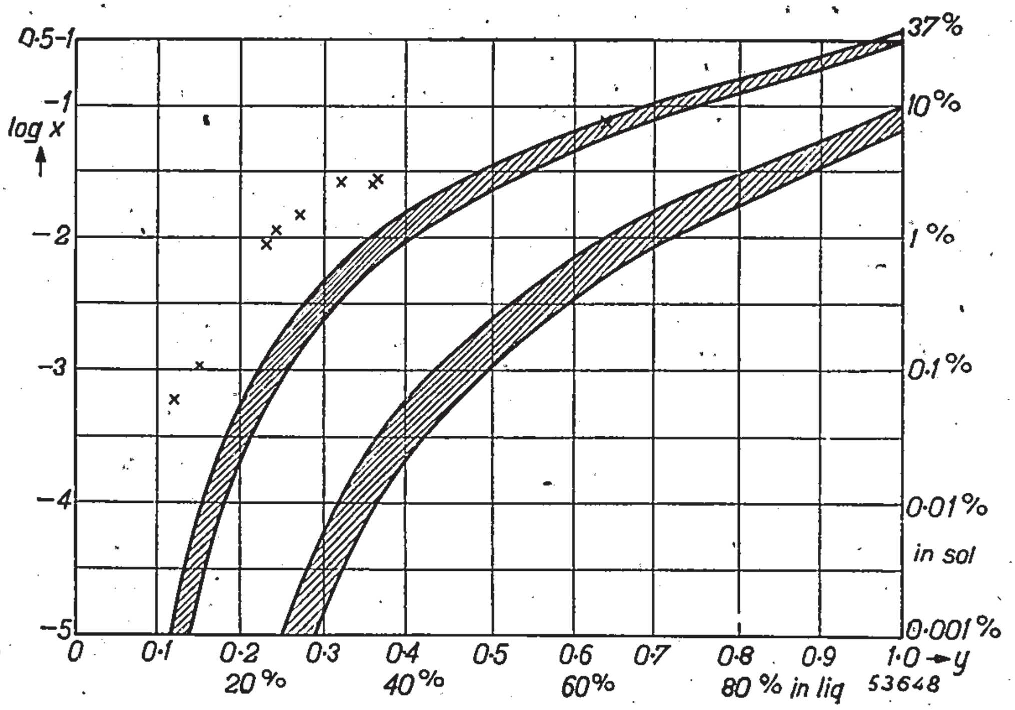

Fig. 9. Graph used to predict wether a solidus is retrograde or not. The four curves bordering the two shaded bands represent equation (2) with $\sigma = 1{\cdot}0, 1{\cdot}2, 2{\cdot}3$ and $2{\cdot}7$ respectively. As for the crosses, see end of section 4 and table III.

coexisting values of x and y is getting further away from the band) $\mathrm{d}T/\mathrm{d}x$ to be positive, which is required for the "retrograde part" of a solidus. On the other hand in the area above and to the left of the band we must expect $\mathrm{d}T/\mathrm{d}x$ to be negative, which is "normal". There is one restriction: when the curve $x = y$ is crossed, $\mathrm{d}T/\mathrm{d}x$ becomes zero and then positive again ($\Delta S/\Delta x$ is negative for $y < x$). When the solid solution is more concentrated than the liquid (as in Cu-Ni) the solidus must rise with concentration. This is trivial and has nothing to do with retrograde lines; so we have omitted the curve $x = y$ from fig. 9, and will *only consider cases where* $x < y$.

In general no precise knowledge of the solid solubility is needed, e.g. when at a certain temperature the concentration of the liquidus is 60 at.% B, the solidus can be predicted to have a positive $\mathrm{d}T/\mathrm{d}x$ (at that temperature), when we only know that (at that temperature) the solid solubility is less than 4·6 at.% B, when A is a normal metal.

The three-phase temperature (eutectic, peritectic) where solidus and liquidus terminate on decreasing temperature, will be often the only one where x is known, e.g. from an extrapolation of the solid solubilities at lower temperatures, where the A-rich phase coexists with another solid phase. Furthermore this temperature is crucial for classifying solidus curves in the retrograde or the normal category. When $\mathrm{d}T/\mathrm{d}x$ is negative here, it will not become infinite at a higher temperature, because a *minimum* of x can be excluded. *)

When on the other hand $\mathrm{d}T/\mathrm{d}x$ is positive at the three-phase temperature, the solidus must have a vertical tangent at some higher temperature, provided it runs right through to the melting point of pure A. There are two cases, however, where a solidus of a phase adjoining pure A terminates

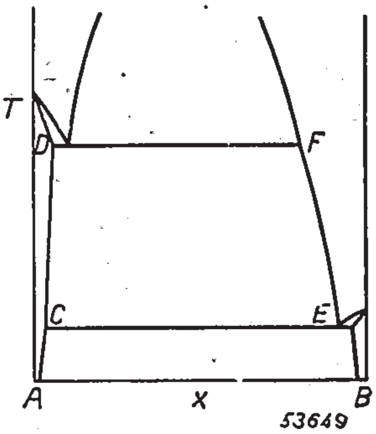

Fig. 10. System with miscibility gap in the liquid phase.

---

*) It would necessitate — with the assumptions made concerning the entropies — an *increase* of y with T; such a retrograde *liquidus* has never been found in alloy systems and is incompatible with the assumed Gibbs mixing entropy of the liquid. See last section.

in a three-phase equilibrium at rising temperatures too, and will only be classified as retrograde when $\mathrm{d}T/\mathrm{d}x$ at this highest temperature is already negative again. The first case is connected with an allotropic transformation in *A*; two examples predicted to be retrograde are the solidus curves of γFe-Cu and γFe-S (table I). The second case is connected with a miscibility gap in the liquid phase, and concerns the solidus *CD* in fig. 10. Practically always in such a case (example: Ni-Ag) x remains small along *CD*, and y relatively large along *EF*, so that as a rule the solid solubility will increase steadily from *C* to *D*, and we will not call *CD* a retrograde solidus. *)

4. Application to experimental phase diagrams

The phase diagrams in Hansen [5]) and, sofar as possible, the subsequent literature were examined on the basis of fig. 9. Table I gives the solidus curves, which are predicted to be retrograde; those in table II are labelled as "possibly retrograde", because here the points representing x and y at the three-phase temperature fall inside the requisite band, the lower one for the right-hand column.

The eight solidus curves in the left-hand column of table I have indeed been found to be retrograde, while the other ones in this table (mostly given as dotted lines) are not known experimentally.

As the two remaining solidus curves known to be retrograde, Cu-Cd and Au-Sb, are contained in table II, no disagreement between theory and experiments is found. The Cu-Tl solidus was found by Raub and Engel [7]) to be just about retrograde when determined microscopically, but definitely not so according to their X-ray measurements. Fig. 9 favours the second possibility.

Systems where no solid solutions are reported have not been included in the tables; the majority of these solidus curves with "zero" solubility will be retrograde. The number of experimentally known retrograde solidus curves will increase enormously with the application of refined techniques of determination of small solid solubilities. The smaller the solubility, the higher temperature (or rather: smaller concentration in the coexisting liquid) at the maximum solubility. Very great *relative* increases in solid solubility above the eutectic temperature must be expected when this temperature is low (in comparison with the melting point of pure *A*) and the solubility in *A* is small. Voce and Hallowes [14]) found a tenfold increase in the solid solubility of Bi in Cu even from 600° (330° above the eutectic temperature) to 800 °C; according to fig. 9 the maximum lies still higher up.

---

*) The typical phenomenon of partial liquefaction on cooling nevertheless exists here of course.

Very qualitatively we can say that it is only natural for a solubility to increase with temperature, so long as the concentration of the coexisting phase (i.e. the liquid) is not coming "too near".

The phenomenon of complete solidification at rising temperatures can have practical consequences not only on hot working, but also on sintering properties.

Of the last eight solidus curves in table II ("possibly retrograde"), the first four have been determined experimentally; they are not found retrograde, but Cu-Ag and Sb-Pb run practically vertical at the eutectic temperature. 5) Also very steep is the solidus of Ag-Hg 26), where log x lies only 0·09 above the upper band in fig. 9. It is to be noted that quantitatively $\mathrm{d}T/\mathrm{d}x$ is also controlled by the value of $\mathrm{d}^2G/\mathrm{d}x^2$ (see equation (1) in section 2), which is normally great at small x. The Sn-In solidus was found by Rhines, Urquhart and Hoge 27) to be so steep at its lower end that they regard it with suspicion. Log x lies about 0·5 above the upper band, but a value of 15 kcal for $\mathrm{d}^2G/\mathrm{d}x^2$ was calculated to make that steep slope (± 50° per at.%) possible. Subtracting $RT/x(1-x) = 7{\cdot}2$ kcal for the contribution of the entropy, there remains 8 kcal for $\mathrm{d}^2H/\mathrm{d}x^2$. This is a normal value; when the enthalpy of mixing (in the Sn-structured phase) is assumed to be parabolic: $H = -ax\ (1-x)$, $\mathrm{d}^2H/\mathrm{d}x^2 \doteq 2a$ and the minimum of H (at $x = \frac{1}{2}$) $= -\frac{1}{4}\ a$, i.c. — 1 kcal/g.atom.

In those nine cases where the solubility maximum has been determined, one can also plot this maximum x against the value of y at the temperature where it occurs, and expect these points to fall in the upper band of fig. 9. The result can be seen from the crosses in fig. 9 and from table III. The fourth column gives the experimental y, derived from $t_{\max}$ and the liquidus curves in Hansen; the fifth column gives the range of y theoretically necessary to make the solidus curve vertical, derived from $x_{\max}$ and the upper band in fig. 9. It is seen that only with Ag-Tl falls y_{exp} inside this range; in the other eight cases the deviations are all to the same side. Owing to the uncertainty in log $x_{\max}$ the range of y_{theor} should be in fact a little bit greater for the lowest systems in table III, while a variation of several atomic per cent in y_{exp} is possible, owing to the uncertainty in $t_{\max}$. But in all eight cases the discrepancies are too great to be explained in this way. Thus our relation does not stand up to this more rigorous test: the increase in solubility with temperature continues longer than expected theoretically. The success of the qualitative test at the three-phase temperature is due to the fact that this temperature lies well below $t_{\max}$ in all experimental cases up till now, which by the way will be more or less required for a pronounced retrograde effect. The chance that the 20 solidus curves in the second and third columns of table I will indeed turn out to be retrograde is more raised than lowered by the deviation from theory.

TABLE I

Systems that theoretically should have a retrograde solidus

Zn-Cd
Ag-Tl 7)5)
Ag-Pb 6)5)
Ag-Bi 7)5)
Au-Tl 7)5)
Au-Pb 7)5)
Au-Bi 7)5)
Cu-Bi 14)5)

Cd-Pb
Cd-Sn
Zn-Sn 15)5)
Zn-In 16)
Zn-Hg
Cu-Hg
Al -Hg
Al -Ga *)
Be-Al
Be-Ag 17)

Co-Au
Cr-Au
Au-As 18)5)
Ni-Bi
γFe-Cu
γFe-S *)
W-Fe
W-Co 19)
W-Ni 20)
Mo-Ni 21)

The solidus curves concerned are those at the side of the first-named element in each system. Where no reference is given, the experimental data are to be found in Hansen 5), When a reference preceeds the reference 5), the first one gives only solid solubility data, and the liquidus from Hansen is used.

TABLE II

Systems with a "possibly retrograde" solidus

Cu-Cd 8)5)
Au-Sb 18)5) **)
Cu-Ag
Pb-Hg
In-Ga 22)

Sb-Pb 23)
Bi-Sn 24)
Ge-Sb 25)
Si-Ag
Si-Al

The subscript of table I also applies to this table.

TABLE III

A-B	x_{max}	t_{max}	y_{exp}	y_{theor}	δS	Δ dS/dx
Ag-Tl	0·075	550°	0·64	0·63-0·69	0·05 *R*	0·1 *R*
Ag-Pb	0·028	650°	0·365	0·47-0·52	0·4 *R*	1·1 *R*
Ag-Bi	0·027	525°	0·32	0·46-0·52	0·55 *R*	1·8 *R*
Cu-Cd	0·0255	650°	0·36	0·46-0·51	0·4 *R*	1·1 *R*
Zn-Cd	0·015	340°	0·27	0·40-0·45	0·55 *R*	2·0 *R*
Au-Sb	0·0115	550°	0·24	0·37-0·42	0·6 *R*	2·4 *R*
Au-Tl	0·009	800°	0·23	0·35-0·40	0·55 *R*	2·4 *R*
Au-Pb	0·0011	850°	0·15	0·22-0·26	0·5 *R*	3·3 *R*
Au-Bi	0·0006	900°	0·12	0·20-0·24	0·55 *R*	4·6 *R*

x and y in atomic fraction of B; t_{max} in °C; R = gas constant.

---

*) Already predicted by Scheil 9)!

**) The solid solubility curve of Owen and Roberts shows a kink at 430 °C. No three-phase temperature has been found here, however, by previous investigators 5). As three-phase temperature we take accordingly the eutectic one at 360 °C.

These deviations will be rather small (perhaps even of opposite sign) in the systems Cu-Ag, Pb-Hg, In-Ga, Sb-Pb (see table II) and Ag-Hg, otherwise they should have been found to have a retrograde solidus.

In all five systems the value of y at the three-phase temperature (and thus even more so that at a lower temperature where the metastable solubility maximum would be) is 0·60 or greater. Sb-Pb belongs to the lower band in fig. 9, but the other four make it probable that it is no coincidence that Ag-Tl (see table III) *does* agree with the upper band. Apparently this band should be raised above the theoretical course, but only to the left of, say, $y = 0{\cdot}6$.

5. Analysis of systematic entropy deviations

Fig. 9, with the crosses included, will be a rather good guide in the field of retrograde solidus curves in binary alloy systems, but the systematic deviations ask for an explanation. This will probably tell us something about the thermodynamics of mixtures, which can be of interest, quite apart from retrograde solidus curves.

From the derivation of equation (2) it can be seen that there are two possibilities: $\Delta S/\Delta x$ may be smaller or $\mathrm{d}S/\mathrm{d}x$ larger than was calculated. The sixth column of table III contains the values δS, which must be subtracted from the entropy of the liquid alloy of concentration y_{exp} (with the mean value of $\sigma = 1{\cdot}1$) to make $\Delta S/\Delta x$ equal to the theoretical value of $\mathrm{d}S/\mathrm{d}x$. If we call the vertical deviations of the crosses in fig. 9 from the middle of the upper band $\Delta \log x$, then $\delta S = 2{\cdot}3\, R\, y_{\mathrm{exp}}\, \Delta \log x$. When on the other hand S_{liq} is maintained on the theoretical value, a positive extra linear term $x\, \Delta \mathrm{d}S/\mathrm{d}x$ must be added to S_{sol} to equalize $\mathrm{d}S/\mathrm{d}x$ and $\Delta S/\Delta x$. This $\Delta \mathrm{d}S/\mathrm{d}x$ equals $\delta S/y_{\mathrm{exp}}$ and not $\delta S/(y_{\mathrm{exp}} - x_{\mathrm{max}})$, because besides the increase in $\mathrm{d}S/\mathrm{d}x$, $\Delta S/\Delta x$ is decreased a little.

The values of δS (except that of Ag-Tl of course) are about as great as the respective Gibbs mixing entropies; in all four gold alloys the total mixing entropy of the liquid would even have to be negative to remove the discrepancy, which is very improbable. The systems Cu-Cd [28]) and Zn-Cd [29]) have been examined by measurements of vapour pressures and electromotive forces respectively. For Cu-Cd the deviation of the entropy from the Gibbs value is somewhat more than 0·1 R; for Zn-Cd we calculate somewhat less than 0·1 R from Taylor's activities. Both deviations apply to the concentrations in the fourth column of table III, and to temperatures about 100° higher than t_{max}.

The chance that the form of the mixing entropy curve of the liquid phase is responsible for a major part of the deviations in the eight cases (below Ag-Tl) in the table thus seems negligible. We now consider the possibility that the melting entropies at t_{max} are much less than at the melting points of the pure metals. Large differences in specific heat between liquid and solid would be required to arrive at the discrepancies in the sixth column. Undercooled liquid Ag and Au should have great specific-heat "humps", and still more so liquid Zn. In the system Zn-Cd matters are relatively simple, because t_{max} is about the same as the melting point of Cd, and the temperature dependence of the melting entropy of this element can thus have no great influence. A simple calculation shows that undercooled liquid Zn, between the melting point and 340 °C, should have a mean specific heat of about $2\frac{1}{2}$ times its value above the melting point, to get rid of the discrepancy δS. The assumption of such a, not directly controllable, specific-heat anomaly would not suffice: the specific heat of the liquid 27%Cd-Zn alloy between 420° and 340 °C (a wholly stable range) should also be much greater than the value averaged between solid Zn and liquid Cd, to convert the normal entropy of the liquid alloy at 420 °C into the abnormal one at 340 °C. It is all very unlikely. Still, an examination of the melting entropies of the right-hand-side (B) elements is needed; not only because their melting points lie well *below* t_{max} (except in Au-Sb and Zn-Cd), and specific heats of superheated solids are still more hypothetical than those of undercooled liquids, but also because face-centred cubic Bi, Sb, Cd and Tl *) are not known, and their melting entropies have been assumed to be 1·1 R (see section 3). (This last difficulty does not apply to Ag-Pb, Au-Pb and Zn-Cd, where both elements have the same structure). It is easy to see that this value 1·1 R must be diminished by the values $\Delta \mathrm{d}S/\mathrm{d}x$ in the seventh column to explain the discrepancies by deviating entropies of B (with A-structure) at t_{max}. Nothing would be left for the melting entropy of B in the case of Ag-Pb and Cu-Cd, while in the other six cases (not Ag-Tl of course) it would have to be negative. This is not acceptable, even for superheated hypothetical modifications.

Perhaps one or few of the eight discrepancies in table III could be thought to be due to a combination of the three factors considered, but to explain all eight of them in this way (and not get one for Ag-Tl) does not look feasible. Fortunately they can be accounted for by a fourth factor: the form of the mixing entropy curve of the solid phase (with A-structure). This means that the Gibbs values of $\mathrm{d}S/\mathrm{d}x$, namely $R \ln \}(1-x)/x\{$, should be raised with the values of $\Delta\ \mathrm{d}S/\mathrm{d}x$ in the seventh column of table III, while the entropy of pure B (with structure of A) is held on the same level as that of pure A. If this is really the case, entropy anomalies must also be apparent from solubility data below the eutectic temperatures, where the liquid phase does not come into the picture.

---

*) The high temperature modification of Tl has been found by Lipson and Stokes [30]) to be body-centred cubic.

When we plot the logarithm of the solid solubility x of B in A (the coexisting phase having an atomic fraction of B that is fairly constant $= x'$) against $1/T$, a straight line is mostly found *when x remains small.* When we write $\log x = -\alpha/T + \beta$, it is well known that $2{\cdot}3\, R\, \alpha = \mathrm{d}H/\mathrm{d}x - H'/x'$, where H is the enthalpy of the A-rich solid solution and H' that of the coexisting phase *). The corresponding relation for the entropies is

$$2{\cdot}3\, R\beta = \left(\frac{\mathrm{d}S}{\mathrm{d}x}\right)_{\mathrm{ex}} - \frac{S'}{x'},$$

where $(\mathrm{d}S/\mathrm{d}x)_{\mathrm{ex}}$ is the difference between the real $\mathrm{d}S/\mathrm{d}x$ and the theoretical Gibbs value for it; in contrast with $\mathrm{d}S/\mathrm{d}x$, $(\mathrm{d}S/\mathrm{d}x)_{\mathrm{ex}}$ can be treated as a constant when x remains small. We now look for which of the nine cases in table III this $(\mathrm{d}S/\mathrm{d}x)_{\mathrm{ex}}$ can be deduced, and compared with $\Delta \mathrm{d}S/\mathrm{d}x$ in the seventh column. In Cu-Cd, Au-Sb, Au-Pb and Au-Bi there is an intermetallic phase coexisting, so that S' is unknown; Ag-Bi is also not very suitable, as S' (i.e. the entropy difference between normal solid Bi and its face-centred cubic modification) can only be guessed to be roughly $1{\cdot}1 - 2{\cdot}5 = -1{\cdot}4$ times R (see section 3). For Tl, S' will be much less, but no solid solubilities below the Au-Tl eutectic are known, and the three determinations in Ag-Tl [31]) lie to both sides of the transformation temperature of Tl (besides: these solubilities of Tl in Ag are already rather large). In the remaining two cases, however, Ag-Pb and Zn-Cd (where S' is virtually zero, as the coexisting phase is nearly pure B, with the same structure as A), $(\mathrm{d}S/\mathrm{d}x)_{\mathrm{ex}}$ can be found, from the X-ray measurements of Chiswik and Hultgren [31]) and Boas [32]) respectively. As with these low solubilities the error range of $\log x$ is rather large, the straight lines can be shifted somewhat without violating the experimental results. A definite positive value for $(\mathrm{d}S/\mathrm{d}x)_{\mathrm{ex}}$ results, however, which is at least some $1{\cdot}8\, R$ and $2{\cdot}0\, R$ for Ag-Pb and Zn-Cd respectively. Such values, mostly of the same sign, occur in several other systems. They (or rather the values of β) are discussed by Scheil [33]), who shows that (positive) deviations should arise when x is not small enough (see especically his fig. 11; it is to be noted that there $\log \}x/(1-x)\{$ is plotted). But in our opinion Scheil goes too far, when he regards the matter as settled herewith, and evidently assumes that the deviations would disappear when the ($\log x$, $1/T$)-lines could be extended experimentally to very low x. When the value of x used are only 1% and less, as is the case in Ag-Pb and Zn-Cd, less than $0{\cdot}5\, R$ can be reasonably accounted for in this way. So there remain in these two systems values for $(\mathrm{d}S/\mathrm{d}x)_{\mathrm{ex}}$ that are of the same magnitude as those of $\Delta \mathrm{d}S/\mathrm{d}x$ in table III. Thus it looks justified to attribute the systematic discrepancies in fig. 9 to deviations of the mixing entropy of the solid solutions from the Gibbs mixing entropy. The physical meaning of these deviations can scarcely be other than this:

---

*) This can also be easily derived from equation (1) in section 2.

When the solid solubility of B in A is small, the substitution of A-atoms by B-atoms will generally loosen the lattice considerably, resulting in an extra rise of the entropy with concentration.

This also explains qualitatively why the deviations $\Delta \mathrm{d}S/\mathrm{d}x$ rise with decreasing $x_{\max}$ in table III, and seem to be small in Ag-Tl, Cu-Ag, Pb-Hg and In-Ga (end of section 4), where the solid solubility is rather large.

When we plot $\log x$ against $1/T$ for several solutes in the same basis metal A we expect the following: the smaller the solubility is (in the experimental range), the greater α will be, but also (according to our point of view) the greater β will be. Thus on extrapolating the straight lines, they must cross each other before $1/T = 0$ is reached. Now this is just what Fink and Freche [34]) found when plotting simultaneously the solubilities of Ni, Cr, Mn, Si, Cu and Mg *) in aluminium. All six lines passed virtually through the point with coordinates $1/T = 0{\cdot}35.10^{-3}$ and $\log x = +\,0{\cdot}26$ (x = atomic fraction). From their values of β we calculate $(\mathrm{d}S/\mathrm{d}x)_{\mathrm{ex}} - S'/x'$ to be $4{\cdot}8\ R$ for Al-Ni and $2{\cdot}3\ R$ for Al-Cu. Admittedly the influence of S'/x' can be somewhat different in the six cases (in five of them the coexisting phase is an intermetallic one, in Al-Si it is the diamond-structured Si-rich phase), but still the results of Fink and Freche give further support to the view that the lattice-loosening effect can give great deviations in $\mathrm{d}S/\mathrm{d}x$. It is only desirable to put this effect on a more quantitative theoretical basis, so that we can see that the deviations must indeed be expected to be so great.

If we call the characteristic (Debije) temperature Θ, the dependence of the entropy on Θ (at temperatures sufficiently larger than Θ) is given by $S = -3R \ln \Theta$. In solid solutions Θ will be a function of x. The values for pure A and pure B (with A-structure!) we call Θ_1 and Θ_2. Putting S for $x = 0$ and $x = 1$ at the same level, we find

$$(\mathrm{d}S/\mathrm{d}x)_{\mathrm{ex}} = 3\,R\,(-\,\mathrm{d}\ln\Theta/\mathrm{d}x - \ln\,\Theta_1 + \ln\,\Theta_2)\,.$$

We now make use of the Lindemann formula

$$\ln\,\Theta = \text{const.} + \tfrac{1}{2}\ln T_m - \tfrac{1}{2}\ln A_w - \tfrac{1}{3}\ln V,$$

where T_m, A_w and V are absolute melting point, atomic weight and atomic volume respectively. This formula gives very satisfactory results for pure metals, and we think for a rough calculation it may be applied for solid solutions too. While A_w and V may be interpolated, e.g. linearly, and are of minor importance in the cases we are interested in, the estimation of a melting *point* for a solid solution presents a difficulty. It is obvious to define it as the temperature where the free enthalpies G of solid and liquid are equal; when diffusion were virtually stopped, the solid solution would melt sharply at that point. In general it cannot be located between the solidus and liquidus, but in dilute solutions we shall show it can.

---

*) in the order of increasing solubility.

In fig. 11 the free-enthalpy curves for the solid and the liquid phase are drawn for a temperature just below the melting point of pure A. The atomic fraction of B we call here u; x and y (given by the common tangent) are the values of u for the solidus and the liquidus at this temperature, and z is that for the melting "point". For the free enthalpies we can always write (for binary alloys, or other systems without a dissociating component B):

$$G_{\mathrm{sol}} = R\,T\,u \ln u + a_1 + b_1\,u\,, \tag{3}$$

$$G_{\mathrm{liq}} = R\,T\,u \ln u + a_2 + b_2\,u\,, \tag{4}$$

when u is small enough, so that terms with u^2 etc. can be ignored. It follows that $z = (a_2 - a_1)/(b_1 - b_2)$. When we take the common tangent horizontal (which we are allowed to do of course), we find by differentiating G_{sol} and G_{liq}:

$$R\,T\,(\ln x + 1) + b_1 = R\,T\,(\ln y + 1) + b_2 = 0. \tag{5}$$

This gives $b_1 - b_2 = RT \ln (y/x)$. After multiplying the first and second members of equation (5) with x and y respectively, and subtracting the results from (3) (with $u = x$) and (4) (with $u = y$), one finds

$$a_2 - a_1 = RT\,(y - x)\,.$$

Thus

$$\frac{z}{y} = \frac{(1 - x/y)}{\ln (y/x)}\,. \tag{6}$$

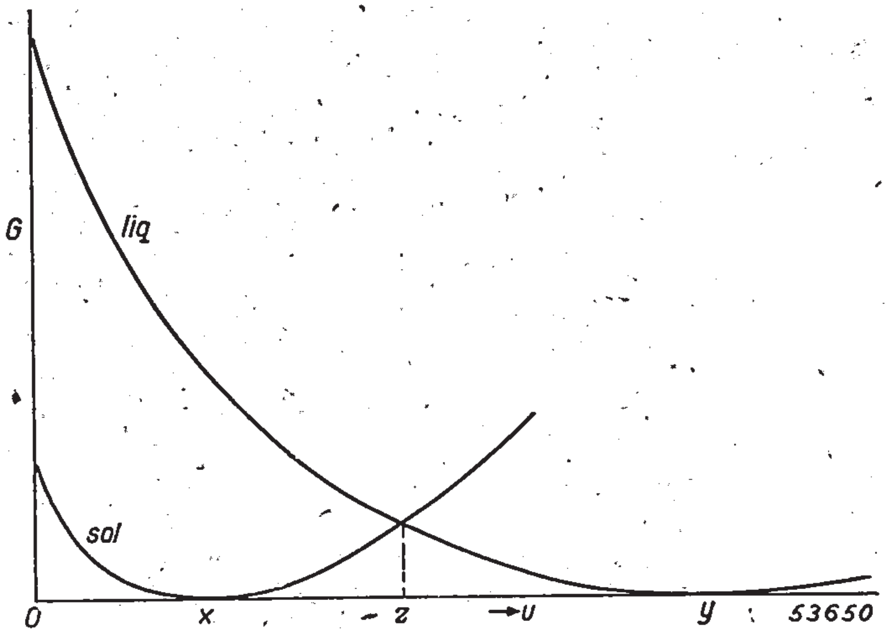

Fig. 11. Free-enthalpy curves of solid and liquid phases, at a temperature close below melting point of pure A. Common tangent chosen as horizontal axis.

Therefore, when the intial slopes of the solidus and liquidus curves, at the melting point of pure A, in the phase diagram are known, the initial slope of the "melting curve" can be calculated, and thus also $\mathrm{d}\ln\Theta/\mathrm{d}x$ and $(\mathrm{d}S/\mathrm{d}x)_{\mathrm{ex}}$ for $x = 0$, provided that the melting point of pure B with A-structure is known.

Appreciable deviations of $\mathrm{d}S/\mathrm{d}x$ must obviously arise when the solid solubility (or rather x/y) is very small *). For the five systems in table IV, where A and B have really the same structure, $(\mathrm{d}S/\mathrm{d}x)_{\mathrm{ex}}$ is given as calculated with the complete Lindemann formula, with linearly interpolated values for the atomic weight and volume. A_w and V give contributions of the same sign as T_m; those of V are small (0·2 R or less), but those of A_w (except in Au-Pb) are quite appreciable, as can be seen by comparing the second column with the third, where only the influence of T_m on Θ is taken into account.

In the last column the values of $\Delta\,\mathrm{d}S/\mathrm{d}x$ (for the three uppermost systems, compare table III) respectively $(\mathrm{d}S/\mathrm{d}x)_{\mathrm{ex}} - S'/x'$ (for the two Al-systems, compare p. 297) are given, which should not differ too much from $(\mathrm{d}S/\mathrm{d}x)_{\mathrm{ex}}$. It seems that the lattice-loosening effect can be indeed largely responsible for the entropy anomalies encountered.

TABLE IV

	$\left(\frac{\mathrm{d}S}{\mathrm{d}x}\right)_{\mathrm{ex}}$ Lindemann		$\Delta\frac{\mathrm{d}S}{\mathrm{d}x}$ or $\left(\frac{\mathrm{d}S}{\mathrm{d}x}\right)_{\mathrm{ex}} - \frac{S'}{x'}$
	complete	only T_m	
Ag-Pb	1·95 R	1·35 R	1·1 R
Zn-Cd	2·5 R	2·15 R	2·0 R
Au-Pb	5·2 R	5·0 R	3·3 R
Al-Cu	4·1 R	3·3 R	2·3 R
Al-Ni	7·4 R	6·7 R	4·8 R

Recently Lawson 10), in a paper on segregation of solid solutions, also calculated approximately Θ as a function of x. The extra entropy can be written as $3RH/(Q_1 + Q_2)$, H being the mixing enthalpy of one mole, and Q_1 and Q_2 the heats of sublimation of both pure components. This formula gives much smaller values; for Ag-Pb and Zn-Cd one gets only about 0·2 R for $(\mathrm{d}S/\mathrm{d}x)_{\mathrm{ex}}$ at $x = 0$. The difference in results is due to the loosening of the lattice being viewed with regard to sublimation, by Lawson, and with regard to melting, in this paper.

---

*) For a rough orientation we add that, according to the interpolation formula (6), z lies between the geometric and the arithmetic means of x and y.

6. Retrograde solidus curves in systems of non-metals

The melting entropy of compounds (per mole) generally increases with the number of atoms in the molecule, although when rotation can occur in the solid state (e.g. in camphor), it may be small. Consequently (see section 3, equation 2) we can say that, generally speaking, retrograde solidus curves in systems of compounds are more confined to cases of low solid solubility than in alloy systems. As the mutual solid solubilities of compounds are often very small, the number of theoretically retrograde solidus curves must be very great. Perhaps in some cases they can manifest themselves in anomalies in the behaviour of slightly impure substances below the melting point.

7. Retrograde allotropic-transformation curves

We can also apply the considerations of section 2 on the two coexisting curves which start from an allotropic-transformation point in A, when B and A form solid solutions. When the transformation is lowered in temperature by the addition of B, and the boundary of the high-temperature phase reaches fairly great concentrations of B, the other boundary may well show a relatively large maximum concentration, because the transformation entropy is generally small. The author knows of no other cases than several iron-alloy systems, where such a retrograde transformation curve has been found. In Fe-Mn [35]), Fe-Co [36]) and Fe-Ni [37]) the α-boundary starting downward from the $\alpha \rightarrow \gamma$ transformation in Fe at 900 °C was found retrograde. A simple quantitative thermodynamical treatment is not feasible, as the differences in specific heat are relatively important and change the transformation entropy considerably. As is known, in iron its sign is even changed above 900 °C, which gives rise to the reversed transformation $\gamma \rightarrow \alpha$ at 1400 °C and (in systems where B stabilizes α with respect to γ, e.g. Fe-Si), to the so-called γ-loops, where both the α- and the γ-boundary are retrograde.

8. Retrograde solubility in liquids

"Retrograde" *) liquidus curves are universally known (e.g. the solubility of several salts in water decreases on heating), but from a theoretical point of view their occurrence is much less natural than that of retrograde solidus curves.

In fig. 12 a short piece of the entropy curve of a liquid is drawn to both sides of the point representing the concentration of the liquid in equilibrium with pure solid A (this is not essential; the solid may just as well be a

---

*) The quotation marks are meant to indicate that here we are not interested in the maximum concentration of the liquidus being continuous or discontinuous (at the three-phase temperature).

solid solution or e.g. a salt-hydrate). The straight line gives the entropies of the two-phase mixtures. It has to be less steep than the curve of the liquid, if the concentration of A in the liquid is to decrease on rising temperature (see section 2). But (metastable) liquid A must have a higher entropy than the solid. Evidently the complete entropy curve of the liquid phase must have a part that is convex to the concentration axis ($\mathrm{d}^2S/\mathrm{d}x^2$ positive).

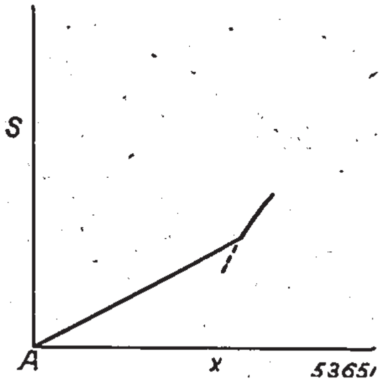

Fig. 12. Part of entropy-concentration curve of liquid phase and its heterogeneous mixtures with solid A, in the case that the solubility of A in the liquid decreases on heating.

This *may* partly fall in the stable portion of the curve (to the right in fig. 12). The positive curvature means that there is a range of liquids that *lose* entropy by mutual (isothermal) mixing. This is of course quite possible (by a stiffening or ordering effect), but still rather curious.

The same considerations can be applied to miscibility gaps in liquids. When the whole entropy curve of the liquid phase has normal curvature, and we draw the tie-line joining the two points representing the coexisting liquids, it is seen that both mutual solubilities must increase on heating. When one or both solubilities decrease, the entropy curve must have a part with abnormal curvature. Again, without further knowledge of the system, we cannot say whether this part is confined to the metastable and unstable regions of the liquid.

When a miscibility gap closes in a lower critical point (e.g. in triethylamine-water), we are sure that there is a region of stable liquids with abnormal $\mathrm{d}^2S/\mathrm{d}x^2$. This follows directly from the fact that $\partial^2G/\partial x^2$ is zero at the critical point, and positive below it. Thus $-\,\partial^3G/\partial x^2\partial T = \partial^2S/\partial x^2$ is positive in the neighbourhood of the critical point.

Eindhoven, December 1947

REFERENCES

1) J. J. van Laar, Z. physik. Chem. **63**, 216-253, 1908; **64**, 257-297, 1908.
2) J. J. van Laar, Die Thermodynamik einheitlicher Stoffe und binärer Gemische, Groningen, 1935.
3) C. H. M. Jenkins, J. Inst. Met., London, **36**, 63-97, 1926.
4) D. Stockdale, J. Inst. Met., London, **44**, 75-80, 1930.
5) M. Hansen, Der Aufbau der Zweistofflegierungen, Berlin, 1936.
6) E. Raub and A. von Polaczek-Wittek, Z. Metallk. **34**, 93-96, 1942.
7) E. Raub and A. Engel, Metallforschung **1**, 76-81, 1946.
8) E. Raub, Metallforschung **2**, 119-120, 1947.
9) E. Scheil, Z. Metallk. **34**, 96, 1942.
10) A. W. Lawson, J. Chem. Phys. **15**, 831-842, 1947.
11) G. Grube and M. Flad, Z. Elektrochem. **48**, 377-389, 1942.
12) O. Kubaschewski and A. Schneider Z. Elektrochem. **49**, 261-269, 1943.
13) F. Körber and W. Oelsen, Mitt. K.W.I. Eisenf. **18**, 109-130, 1936.
14) E. Voce and A. P. C. Hallowes, J. Inst. Met., London, **73**, 323-376, 1947.
15) G. Tammann and H. J. Rocha, Z. Metallk. **25**, 133-134, 1933.
16) F. N. Rhines and A. H. Grobe, Met. Technol. T.P. 1682, 1944.
17) O. Winkler, Z. Metallk. **30**, 162-173, 1938.
18) E. A. Owen and E. A. O'Donnell Roberts, J. Inst. Met., London, **71**, 213-254, 1945.
19) W. P. Sykes, Trans. Am. Soc. Steel Treat. **21**, 385-421, 1933.
20) F. H. Ellinger and W. P. Sykes, Trans. Am. Soc. Metals **28**, 619-643, 1940.
21) F. H. Ellinger, Trans. Am. Soc. Metals **30**, 607-637, 1942.
22) S. J. French, D. J. Saunders and G. W. Ingle; J. Phys. Chem. **42**, 265-274, 1938.
23) H. Seltz and B. J. de Witt, J. Am. Chem. Soc. **61**, 2594-2597, 1939.
24) A. C. Davidson, Tech. Publ. Internat. Tin Res. Dev. Council, A 77, 1938.
25) H. Stöhr and W. Klemm, Z. anorg. Chem. **244**, 205-223, 1940.
26) H. M. Day and C. H. Mathewson, Trans. A.I.M.M.E. **128**, 261-280, 1938.
27) F. N. Rhines, W. M. Urquhart and H. R. Hoge, Trans. Am. Soc. Metals **39**, 694-711, 1947.
28) A. Schneider and H. Schmid, Z. Elektrochem. **48**, 640-646, 1942.
29) N. W. Taylor, J. Am. Chem. Soc. **45**, 2865-2890, 1923.
30) H. Lipson and A. Stokes, Nature, London, **148**, 437, 1941.
31) H. H. Chiswik and R. Hultgren, Trans. A.I.M.M.E. **137**, 442-446, 1940.
32) W. Boas, Metallwirtschaft **11**, 603, 1932.
33) E. Scheil, Z. Elektrochem. **49**, 242-254, 1943.
34) W. L. Fink and H. R. Freche, Trans. A.I.M.M.E. **111**, 304-317, 1934.
35) A. R. Troiano and F. Mc. Guire, Trans. Am. Soc. Metals **31**, 340-357, 1943
36) W. C. Ellis and E. S. Greiner, Trans. Am. Soc. Metals **29**, 415-432, 1941.
37) E. A. Owen and A. H. Sully, Phil. Mag. **27**, 614-636, 1939.

R 88 Philips Res. Rep. 3, 303-317, 1948

THE HEAT DISSIPATION IN THE ANODE OF AN X-RAY TUBE

by W. J. OOSTERKAMP

621.386.1.032.22:536.212.1

III. CONTINUOUS LOADS

Summary

This third and last paper of the series considers the problem of continuous loads. A copper-sheet anode is hit by a beam of electrons on the front side, and cooled by a water current at the back. The equations of heat conduction are solved by considering the heat flow between an infinite arrangement of foci alternately generating and absorbing heat. The rating capacity may be limited (1) by the permissible maximum temperature of the front or (2) by the maximum amount of heat transferable to the cooling fluid. A balance between these two factors can be obtained by a suitable choice of the anode thickness, which now enters as an essential feature into the problem. The line focus and foci finite in all their dimensions are separately treated, while in a final section the gain resulting from a combined use of water cooling and a rotating anode is computed.

Résumé

Le troisième et dernier article de cette série traite du problème de la charge continue. Une anode constituée par une plaque de cuivre est touchée du côté antérieur, au foyer, par un faisceau d'électrons, tandis que la chaleur développée est évacuée par refroidissement par eau du côté postérieur. Le problème de la conduction de la chaleur peut être résolu en considérant un nombre infini de foyers également espacés entreux et produisant et absorbant alternativement de la chaleur. La charge maximum peut être limitée par (1) la température admissible au foyer ou (2) la quantité de chaleur qui peut être transmise au maximum à l'eau de refroidissement. Un équilibre peut être trouvé entre ces deux facteurs limitatifs par un choix judicieux de l'épaisser de l'anode qui apparait ici comme une grandeur essentielle. Les foyers linéaires et les foyers finis dans toutes leurs dimensions sont traités séparément. Le dernier paragraphe est consacré aux avantages, en ce qui concerne la charge admissible, de l'emploi combiné d'une anode tournante et du refroidissement par eau.

5. A line focus and a stationary anode

Fig. 9 depicts a tube with stationary anode as commonly used in crystal structure analyses [1]). The anode *A*, connected to earth, is cooled by a flow of water. The *X*-ray beam leaves the tube through two windows *L* of low absorbing power, which are protected against secondary emission by the screen *S* attached to the cathode. Special care has been devoted to obtaining a homogeneous beam of electrons, and consequently a homogeneous brightness of the focal spot, this being important for an exact interpretation of diffraction patterns obtained with such a tube.

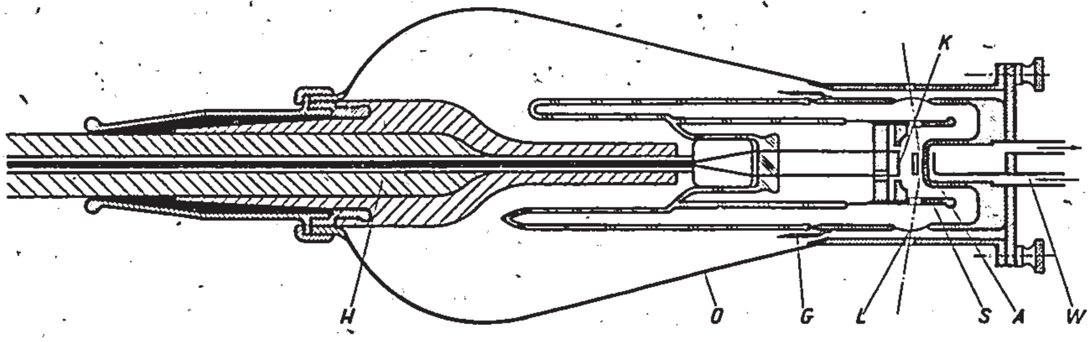

Fig. 9. Diagram of an X-ray tube as used for crystal analysis or stress investigations.

Fig. 10 visualizes the flow of heat through the anode. The corresponding differential equation and boundary conditions are:

$$\frac{\partial^2 T}{\partial x^2} + \frac{\partial^2 T}{\partial z^2} = 0 \tag{35}$$

$$\begin{aligned} z = 0 : \frac{\partial T}{\partial z} &= -\frac{W}{k} && \text{when } |x| < \delta \\ \frac{\partial T}{\partial z} &= 0 && \text{when } |x| > \delta \\ z = d : T &= 0 \end{aligned} \tag{36}$$

where 2δ is the focal width, W the load per cm length, and d the thickness of the anode, the focus being supposed a line focus.

Now consider an infinite number of plane line foci perpendicular to the the plane of drawing, of width 2δ, and distances $2d$ apart, as shown in fig. 11; then, if these line foci are alternately producing and absorbing heat at the rate of $2W$ watts per cm length per second, the temperature distribution in this system between the planes $z = 0$ and $z = d$ will be identical to that prevailing in the anode of fig. 10.

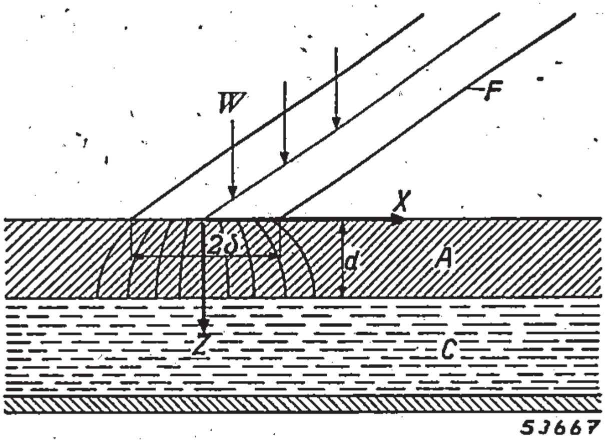

Fig. 10. Schematic representation of the conduction of heat through the anode.

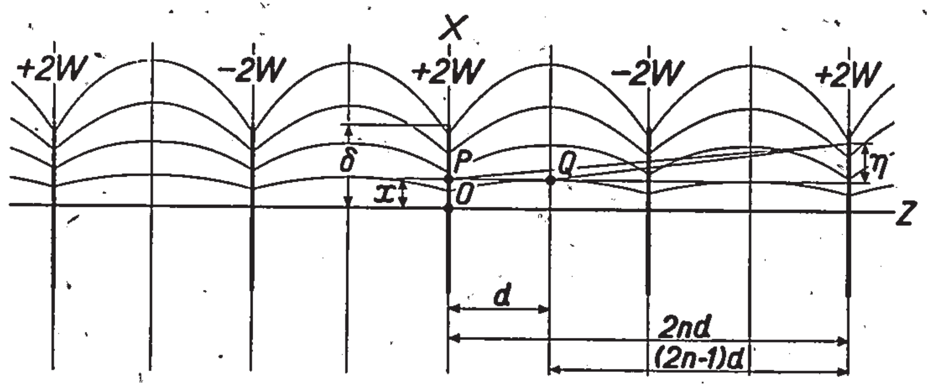

Fig. 11. Arrangement of an infinite number of foci alternately generating and absorbing heat, used as a substitute for solving the problem indicated in fig. 10.

That the boundary conditions are satisfied in the plane $z = 0$ is evident from symmetry. To prove that they are also satisfied for $z = d$, let us first assume that all the sources change their sign; thereby all temperature gradients, $\mathrm{d}T/\mathrm{d}x$ in particular, change sign also. Next we turn the system through 180° about the axis $z = d$ in the xz-plane; this will leave $\mathrm{d}T/\mathrm{d}x$ for $z = d$ unchanged, and will at the same time bring the system back in its original position.

We conclude that, for $z = d$, $\mathrm{d}T/\mathrm{d}x$ must be equal to $-\mathrm{d}T/\mathrm{d}x$, and hence must be zero; thus for $z = d$ the temperature is constant, and this constant value may be put zero without loss of generality.

We can find the temperature distribution for the arrangement of fig. 11 by applying the principle of superposition, equation (35) being linear. A true line source at point O (fig. 12) perpendicular to the plane of drawing, and generating heat at the rate of $\mathrm{d}W$ watts per cm length, produces a temperature difference between points P and Q given by

$$T_P - T_Q = \frac{\mathrm{d}W}{2\pi k} \ln \frac{q}{p}, \tag{37}$$

as it is easy to show.

We are mainly interested in the temperature difference between points in the planes $z = 0$ and $z = d$; let us therefore consider two such points, P and Q; both at a distance x from the plane $x = 0$ (see fig. 11). Let us moreover consider an element of the focus in the plane $z = 2nd$ located between $(x + \eta)$ and $(x + \eta + \mathrm{d}\eta)$, and of heat capacity $(-1)^n\, 2W\, \mathrm{d}\eta$ per unit length; then the temperature difference between the points $P(x, 0)$ and $Q(x, d)$ produced by this focus element is

$$\mathrm{d}T = (-1)^n \frac{W \mathrm{d}\eta}{\pi k} \ln \sqrt{\frac{(2n-1)^2 d^2 + \eta^2}{(2n)^2 d^2 + \eta^2}}, \tag{38}$$

and the actual temperature difference between P and Q is found by integrating over the focus width and by summing over all the sources; this gives

$$\frac{\pi k T}{W} = \sum_{n=-\infty}^{n=+\infty} (-1)^n \int\limits_{-x-\delta}^{\delta-x} \mathrm{d}\eta \ln \sqrt{\frac{(2n-1)^2 d^2 + \eta^2}{(2n)^2 d^2 + \eta^2}}; \tag{39}$$

or

$$\frac{\pi k T}{W} = \sum_{n=-\infty}^{n=+\infty} (-1)^n \int\limits_{-x-\delta}^{\delta-x} \mathrm{d}\eta \ln \sqrt{(2n-1)^2 d^2 + \eta^2} + \sum_{n=-\infty}^{n=+\infty} (-1)^{n+1} \int\limits_{-x-\delta}^{\delta-x} \mathrm{d}\eta \ln \sqrt{(2n)^2 d^2 + \eta^2}. \tag{40}$$

But since

$$(2n-1)^2 = \{2(-n+1)-1\}^2$$

and

$$(-1)^n = -(-1)^{-n+1}, \tag{41}$$

the contributions of the sources at $z = nd$ and $z = -(n-1)d$ will annihilate each other in the first sum, so that we are left with

$$\frac{\pi k T}{W} = \sum_{n=-\infty}^{n=+\infty} (-1)^{n+1} \int\limits_{-x-\delta}^{\delta-x} \mathrm{d}\eta \ln \sqrt{(2n)^2 d^2 + \eta^2}. \tag{42}$$

It may be worth mentioning that nearly the same expression can be used when the distribution of the load is inhomogeneous; we have then only to bring W under the sign of integration. And the method of solving this problem by means of a set of image foci also applies to short or intermediate exposures where the temperature distribution varies with time; for the fundamental differential equation remains linear in these cases.

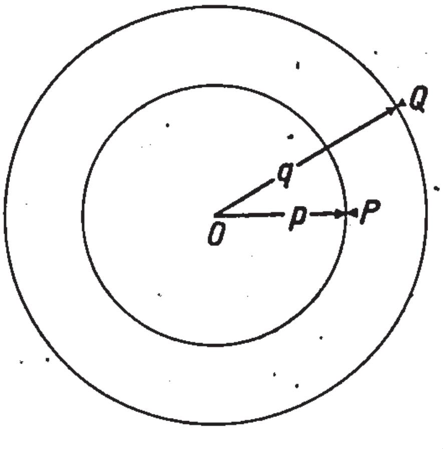

Fig. 12. Illustrating the heat conduction around a single line source of heat.

When d is of the same order of magnitude or larger than δ, δ^2 may be ignored in comparison with $(4d)^2$, and (42) simplifies to

$$\frac{\pi k T}{W} = \int_{-x-\delta}^{\delta-x} d\eta \ln \sqrt{\frac{(2d)^2+\eta^2}{\eta^2}} + \int_{-x-\delta}^{\delta-x} d\eta \ln \sqrt{\frac{(2d)^2+\eta^2}{(4d)^2}} + + 2\delta \ln \frac{6d}{4d} + 2\delta \ln \frac{6d}{8d} + \dots \quad (43)$$

Since

$$\int_{-x-\delta}^{\delta-x} \ln \{(2d)^2+\eta^2\}\, d\eta = (\delta+x) \ln \{(2d)^2+(\delta+x)^2\} + + (\delta-x) \ln \{(2d)^2+(\delta-x)^2\} - 4\delta + 4d \left\{\arctan \frac{\delta+x}{2d} + \arctan \frac{\delta-x}{2d}\right\}$$

and

$$\int_{-x-\delta}^{\delta-x} \ln \sqrt{\eta^2}\, d\eta = (\delta+x) \ln (\delta+x) + (\delta-x) \ln (\delta-x) - 2\delta$$

and [2])

$$\ln \left(\frac{3}{2}\cdot\frac{3}{4}\cdot\frac{5}{4}\cdot\frac{5}{6}\cdots\right) = \ln \frac{4}{\pi},$$

we finally obtain

$$\frac{\pi k T}{W} = (\delta+x) \ln \{4d^2+(\delta+x)^2\} + (\delta-x) \ln \{4d^2+(\delta-x)^2\} + + 4d\left(\arctan \frac{\delta+x}{2d} + \arctan \frac{\delta-x}{2d}\right) - (\delta+x) \ln (\delta+x) - - (\delta-x) \ln (\delta-x) - 2\delta \ln 4d + 2\delta \ln \frac{4}{\pi} - 2\delta . \quad (44)$$

The maximum temperature in the centre of the focus is found by putting $x = 0$, which gives

$$\frac{kT_m}{Wd} = \frac{2}{\pi}\,\frac{\delta}{d} \ln \frac{4d}{\pi e \delta} \left\{1 + \left(\frac{\delta}{2d}\right)^2\right\} + \frac{8}{\pi} \arctan \frac{\delta}{2d}. \quad (45)$$

If we neglect lateral dissipation of heat we should have

$$T_m = \frac{Wd}{k},$$

so that the right-hand side of (45) represents the reduction in the temperature relative to this case. This relative reduction has been plotted as a function of the ratio $2\delta/d$ in fig. 13, curve I.

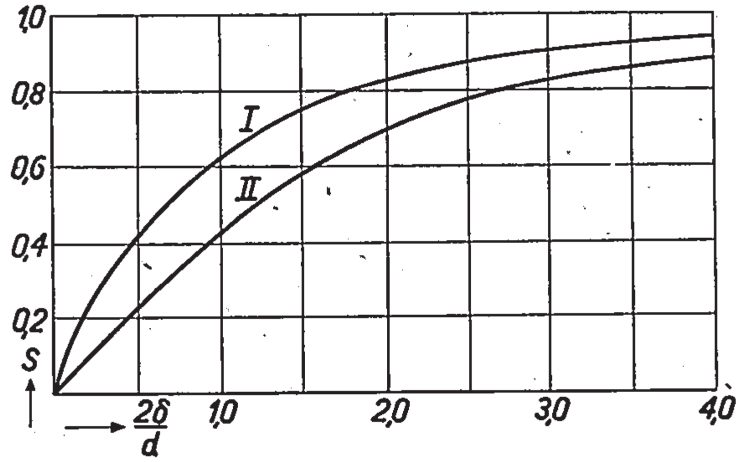

Fig. 13. The quantity $S = kT_m/Wd$, measuring the decrease in the maximum temperature relative to the case where no heat is dissipated in a lateral direction, and plotted as a function of $2\delta/d$ or $2R/d$; the load must be understood to be continuous, and homogeneously distributed over the focal area.
Curve I: infinite line focus. Curve II: circular focus.

The temperature distribution across the focus is given by (44), which for $\delta \ll d$ simplifies to

$$\frac{\pi k T}{W} = 2\delta \ln \frac{4ed}{\pi} - (\delta + x) \ln (\delta + x) - (\delta - x) \ln (\delta - x). \qquad (46)$$

After dividing by (45) we find that the ratio T/T_m can be expressed as a function of x/δ, the ratio $2\delta/d$ serving as parameter; for $2\delta/d = 0{\cdot}5$ this function has been plotted in fig. 14, curve I.

In fig. 15, curve I, we have plotted the specific rating capacity for a copper anode, and a focus 1·2 mm wide, assuming that the temperature of the water-cooled surface is 100 °C (see below), and that the permissible maximum temperature of the target is 300 °C. Because of the small angle under which the X-ray beam is leaving the target and of the high absorption of the soft X-rays emitted by copper, only slight roughening of the surface can be permitted, so that the maximum temperature must be kept at such a low value.

A second limit to the rating capacity is set by the temperature of the water-cooled surface, which should not rise above 100 °C. This cooled surface will not be at a uniform temperature, because the drop in temperature between the copper and the cooling water will be proportional to the heat flux per cm². This heat flux will be greatest at the centre and to this point we shall direct our attention. The permissible maximum heat flux will be that flux for which the surface temperature reaches 100 °C, and will a.o. depend on the speed of the cooling water.

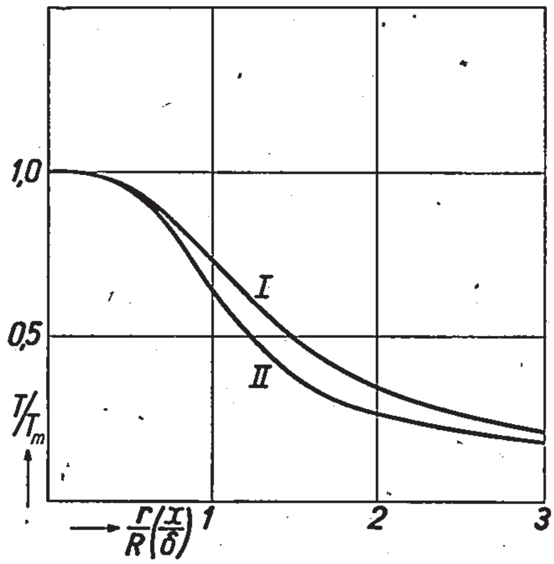

Fig. 14. The temperature distribution in the focus for a continuous and homogeneous load. Curve I: infinite line focus; $2\delta/d = 0{\cdot}5$, Curve II: circular focus of radius R; $2R/d = 0{\cdot}5$.

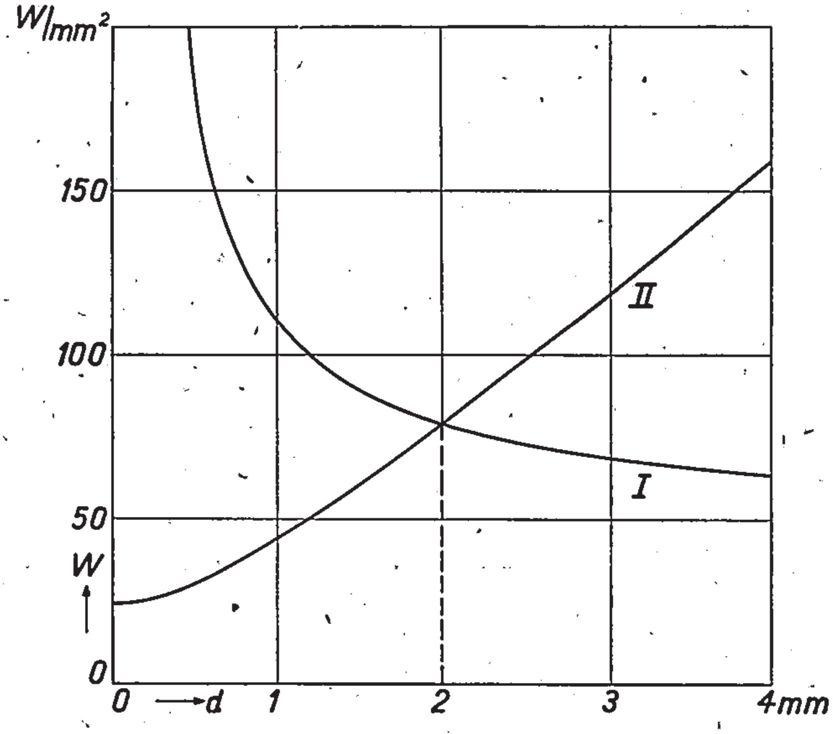

Fig. 15. Specific focal load as a function of anode thickness for a copper anode and a homogeneously loaded infinite line focus of 1·2-mm width.
Curve I: assuming that the permissible maximal temperature of the focus is 300 °C and that the water-cooled surface is at 100 °C. Curve II: assuming that the maximal heat current across the cooling surface is fixed at 24 W/mm².

The heat flux will be proportional to the temperature gradient $\partial T/\partial z$ at the cooled surface, and this gradient may be computed in the same way as the temperature itself. An element $(-1)^n\, 2W\mathrm{d}x$ of the image focus in the plane $z = 2nd$ (fig. 11) and at a distance x from the yz-plane will contribute to the temperature gradient in the z-direction at the point O, d an amount

$$\mathrm{d}\left(\frac{\partial T}{\partial z}\right) = (-1)^n \frac{W}{\pi k} \cdot \frac{(2n-1)\, d}{(2n-1)^2 d^2 + x^2}\, \mathrm{d}x. \tag{47}$$

By integration, and by summation over all sources we find the actual temperature gradient to be

$$\frac{\partial T}{\partial z} = \frac{W}{\pi k} \sum_{n=-\infty}^{n=+\infty} (-1)^n \int_{-\delta}^{+\delta} \frac{(2n-1)\, d}{(2n-1)^2 d^2 + x^2}\, \mathrm{d}x, \tag{48}$$

which after performing the integration becomes

$$\frac{\partial T}{\partial z} = \frac{4W}{\pi k} \sum_{1}^{\infty} (-1)^n \arctan \frac{\delta}{(2n-1)d}. \tag{49}$$

In fig. 16, curve I, we have presented the ratio of the maximum heat flux at the cooled surface to the maximum heat flux in the focus, as a function of the ratio of focus width to anode thickness. If the focus width is large compared with the anode thickness, the temperature gradients at the front and at the back are the same; but if the focus width is of the same order as or less than the anode thickness, the divergence of the heat flux causes a considerable reduction in the

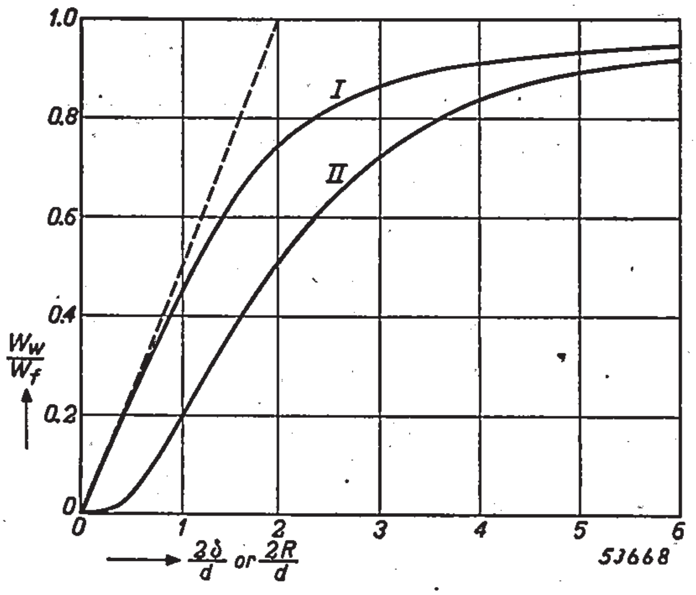

Fig. 16. The ratio of the maximum heat flux across the cooled surface to the heat flux in the focus, plotted as a function of $2\delta/d$.

temperature gradient at the cooled surface. Consequently the thicker the anode the greater will be the maximum possible heat transfer from copper to water. Curve II in fig. 15 shows how the maximum rating capacity in the focus increases with anode thickness, when the maximum specific heat flux across the cooling surface is set at 24 watts/mm^2. It was observed that this heat flux raised the water temperature to just below the boiling point when the water current was flowing at its normal speed of 8m/sec.

The optimum thickness of the anode is that for which the water temperatute remains just below 100 °C while the focus is as its permissible maximum temperature. This condition is satisfied at the point of intersection of curves I and II in fig. 15; a thickness less than that fixed by this point necessitates a reduction in the heat transferred to the cooling water; a greater thickness necessitates a reduction in the load in order to keep the target temperature at its permissible value. For the tube described above, utilizing a line focus 1·2 mm wide and a cooling current of 8m/sec, the optimum thickness of the anode is 2 mm. The maximum specific load of the focus is then 80 watts/mm^2, in good accord with a value of 72 watts/mm^2 determined by experiment.

As mentioned earlier, experiments showed that for a cooling-water current of 8m/sec the maximum amount of heat that can be dissipated is 24 watts per mm^2 of the cooled surface. The highest resistance to the transfer of heat occurs in a thin laminary boundary layer where the conveyance of heat takes place by pure conduction. As the thermal conductivity of water is 0·006 watts/cm°C, it follows that for a wall temperature of 100 °C, a water temperature of 20 °C, and a heat transfer of 24 watts/mm^2, the boundary layer must be of the order of 2×10^{-4} mm thick; this is of the order of magnitude that might hydrodynamically be expected. It may be added that, if the turbulence in the cooling current is artificially increased, the thickness of the boundary layer will decrease and the heat transfer will be improved accordingly.

6. A two-dimensional focus

For a circular focus Müller [3]) has computed the temperature distribution and the conditions of heat flow, under the assumption that the specific load decreases from the centre to the periphery according to a Gauss-function. By following the same line of reasoning as adopted above for the line focus, we shall easily arrive at more general formulae valid for a focus of arbitrary shape and with an arbitrary distribution of the load. These will then be applied to a circular focus with a homogeneous load, where we shall be led to qualitatively the same conclusions as Müller.

We have now to use the three dimensional differential equation

$$\frac{\partial^2 T}{\partial x^2} + \frac{\partial^2 T}{\partial y^2} + \frac{\partial^2 T}{\partial z^2} = 0 \tag{50}$$

with the boundary conditions

$$\begin{aligned} z = 0 &: \frac{\partial T}{\partial z} = -\frac{W}{k} \text{ inside } F, \\ &\frac{\partial T}{\partial z} = 0 \text{ outside } F, \\ z = d &: \ T = 0. \end{aligned} \tag{51}$$

As in fig. 11 we shall again assume a set of image foci located in the planes $z = \pm 2nd$, alternately generating and absorbing heat, and with the same distribution of the load as the true focus at $z = 0$. The actual temperature distribution in the anode will then be the same as the distribution between $z = 0$ and $z = d$ in this system.

Since the foci are now finite in the direction of y also, we must instead of (37) use its three-dimensional analogue. A source element dF with a capacity $(-1)^n\, 2W\mathrm{d}F$ will produce a temperature difference between two points P and Q at a distance r from the z-axis given by

$$\mathrm{d}T = (-1)^n \frac{W\mathrm{dF}}{2\pi k} \left\{ \frac{1}{\sqrt{\varrho^2 + (2n)^2 d^2}} - \frac{1}{\sqrt{(2n-1)^2 d^2 + \varrho^2}} \right\}, \tag{52}$$

where ϱ measures the distance between the projections of P (or Q) on the xy-plane and the element dF (see fig. 17). By summation and integration over all sources we obtain

$$T = \frac{1}{2\pi k} \sum_{n=-\infty}^{n=+\infty} (-1)^n \int_F \frac{W}{\sqrt{(2n)^2 d^2 + \varrho^2}}\, \mathrm{d}F, \tag{53}$$

the terms with $\sqrt{(2n-1)^2 d^2 + \varrho^2}$ cancelling out. In this expression W may be any function of x and y, and is independent of n. We shall now apply this equation to some particular cases.

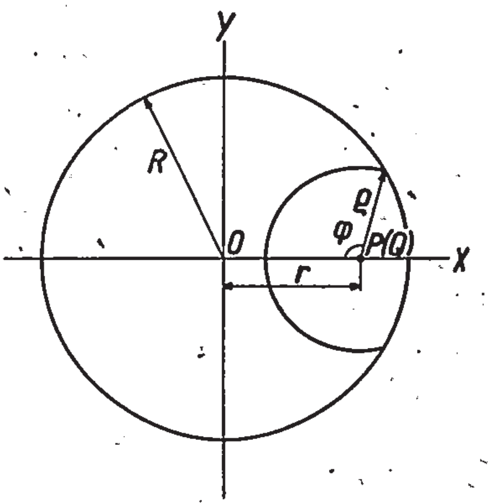

Fig. 17. Illustrating the formulae for computing the temperature distribution in a homogeneously loaded circular focus under a continuous load.

A) *A circular focus with homogeneous load*

If the thickness of the anode is large compared with the radius of the focus we have $R/d \ll 1$, and the terms for $n = 0$ may be ignored; this gives

$$T = \frac{W}{2\pi k}\int_F \frac{1}{\varrho}\,\mathrm{d}F = \frac{W}{2\pi k}\int_F \mathrm{d}\varrho\,\mathrm{d}\varphi. \tag{54}$$

Inside the focus we have

$$r < R \qquad \text{(fig. 17)}$$

and

$$R^2 = r^2 + \varrho^2 - 2\,r\,\varrho\cos\varphi.$$

or

$$\varrho = r\cos\varphi + \sqrt{R^2 - r^2\sin^2\varphi},$$

giving

$$T = \frac{W}{2\pi k}\left\{2\pi\int_0^{R-r}\mathrm{d}\varrho - 2\int_{R-r}^{R+r}\varphi\,\mathrm{d}\varrho\right\}.$$

By partial integration we obtain

$$T = \frac{W}{2\pi k}\left\{2\pi\,(R-r) - 2\varrho(\varphi)\,.\,\varphi\,\Big|_0^{\pi} + 2\int_0^{\pi}\varrho\,\mathrm{d}\varphi\right\}$$

or

$$T = \frac{2}{\pi}\,\frac{WR}{k}\,\mathrm{E}\left(\frac{r}{R}\right), \tag{55}$$

where $\mathrm{E}(r/R)$ is the complete elliptic integral of the second kind and of argument r/R. *)

Outside the focus we have

$$r > R$$

which leads in a similar way to

$$T = \frac{2WR^2}{\pi k r}\left[\mathrm{K}\left(\frac{R}{r}\right) - \frac{r^2}{R^2}\left\{\mathrm{K}\left(\frac{R}{r}\right) - \mathrm{E}\left(\frac{R}{r}\right)\right\}\right], \tag{56}$$

where $\mathrm{K}(R/r)$ and $\mathrm{E}(R/r)$ are the complete elliptic integrals of the first and second kind, now of argument R/r.

---

*)

$$\mathrm{E}(k) = \int_0^{\pi/2}\sqrt{1 - k^2\sin^2\psi}\,\mathrm{d}\psi$$

and

$$\mathrm{K}(k) = \int_0^{\pi/2}\frac{\mathrm{d}\psi}{\sqrt{1 - k^2\sin^2\psi}}.$$

Thus for $R \ll d$ the temperature T_m at the centre of the focal spot is by (55)

$$T_m = WR/k\,. \tag{57}$$

The temperature distribution across the focus under these circumstances is represented by curve II in fig. 14.

When $R \gg d$, we have evidently

$$T_m = Wd/k\,, \tag{58}$$

since in this case no appreciable divergence of heat current will occur.

Whenever the focal diameter is of the same order of magnitude as the thickness d, the terms for $n = 0$ in (53) must be taken into account, which requires more elaborate calculations. The result is reproduced in fig. 13, curve II.

We may infer from these expressions that the specific rating capacity will be inversely proportional to the diameter of the focus, when the focal dimensions are small compared with the thickness of the anode. Hence the permissible total load increases as the square root of the focal area.

When, on the other hand, the focal dimensions are large compared with anode thickness, equation (58) will hold good, and the total load will vary in proportion to the focal area itself.

From the shape of the temperature-distribution curves for a line focus and for a circular focus as shown in fig. 14, it may be concluded that an isothermal focus can be achieved by applying a load heavier at the edge than at the centre. For a given size of the focus the rating capacity will then be somewhat higher than for a homogeneous load.

B) *Elliptic focus with homogeneous load*

If the focus is an ellipse, in all its dimensions small compared with the thickness of the anode, the maximum temperature at the centre can be shown to be

$$T_m = \frac{2}{\pi}\,\frac{Wb}{k}\,\mathrm{K}\left(\sqrt{1-\frac{b^2}{a^2}}\right), \tag{59}$$

where a and b denote half the major and minor axes of the focus, and where K is once more the complete elliptic integral of the first kind. As particular cases we mention

(i) $a = b$ (a circle), which gives $T_m = \dfrac{Wa}{k}$,

and

(ii) $a = 3b$, which gives $T_m = 0{\cdot}51\,\dfrac{Wa}{k}$.

C) *Rectangular focus with homogeneous load*

For this case the maximum temperature at the centre has been computed from (45) as

$$T_m = \frac{2}{\pi}\frac{W}{k}\left\{a \ln\left(\frac{b}{a} + \sqrt{1 + \frac{b^2}{a^2}}\right) + b \ln\left(\frac{a}{b} + \sqrt{1 + \frac{a^2}{b^2}}\right)\right\}, \tag{60}$$

where $2a$ and $2b$ are the length and the width of the focal spot. This yields for $a = b$ (a square)

$$T_m = \frac{1{\cdot}12\ Wa}{k},$$

and for $a = 3b$

$$T_m = \frac{0{\cdot}59\ Wa}{k}.$$

7. Rotating anode

When the time of exposure is indefinitely increased the specific rating capacity for a rotating anode, as computed in section 4, is reduced to zero as a consequence of the assumptions (1) that the anode does not itself dissipate heat and (2) that it possesses a finite heat capacity. With such tubes as depicted in fig. 4 of our second paper, a certain amount of heat can, however, be dissipated by radiation, thus permitting the application of a continuous load of some hundreds of watts, on which instantaneous loads of up to 50 kW can be superimposed. This suffices for medical diagnostics. The temperature requirements under these circumstances have already been discussed in section 4.

For other purposes, such as crystal analysis, much heavier continuous loads are required, and this has led Müller [4]), Astbury and Preston [5]), Du Mond and Youtz [6]), Fournier, Gondet and Mathieu [7]) to constructing tubes with rotating anode and water cooling combined.

A complete though fairly complicated calculation of the temperature in the focus of such a tube was accomplished by Du Mond, Watson and Hicks [8]). We can, however, arrive at reasonably exact results in a much simpler way as follows. During the passage of the beam the temperature in the focus rises by an amount (see eq. (15))

$$T_1 = \frac{2W}{\pi}\sqrt{\frac{2\delta}{D\nu kc}}, \tag{61}$$

where, as before, 2δ measures the width of the focus, D the diameter of the focal path, and ν the number of revolutions per second. This temperature rise is superimposed on the temperature T_2 of the front face of the anode just before the passage of the beam. Roughly we may put T_2 equal to the temperature the front face would assume if the power input W were uniformly distributed over the entire area traversed by the focus, which gives

$$T_2 = \frac{Wd}{k} \frac{2\delta}{\pi D}. \tag{62}$$

The actual temperature of the front face will fluctuate about an average temperature given by (62). The temperature just before the passage of the beam will consequently be lower than this value, but as, owing to the water cooling, the average temperature will be comparatively low, the difference will be of little importance. By adding (61) and (62) we obtain

$$T_m = \frac{2}{\pi} W \sqrt{\frac{2\delta}{D\nu kc}} \left(1 + \frac{d}{a} \sqrt{\frac{\delta\nu}{2D}}\right), \tag{63}$$

in good agreement with the results of Du Mond, Watson and Hicks. From (63) we may compute the rating capacity for a continuous load; the rating capacity for one revolution will be only slightly higher, since the temperature rise T_1 is the same in both cases, while T_2 is low in comparison with T_1. Müller has actually calculated the temperature for a circular focus, entirely neglecting the basic temperature T_2 [9]); for his tube, the anode of which had a relatively large diameter, this makes but little difference.

When $D = 38$ mm, $\nu = 50$, the focal width $2\delta = 1{\cdot}2$ mm, and the anode thickness is 2·0 mm, we obtain for a copper anode

$$T_1 = 4{\cdot}3.10^3\, W \text{ and } T_2 = 0{\cdot}52.10^3\, W.$$

Assuming a permissible maximum temperature difference between front and back of 200 °C, the rating capacity will be 410 watts/mm²; that is five times as much as for a stationary anode. However, as already pointed out in section 4, a rotating anode permits a higher maximum temperature, so that a reasonable lifetime can be realized with even double this load.

The use of a rotating anode has the yet further advantage of a considerably enlarged cooled surface. Since the cooled surface increases with the diameter of the anode, while the rating capacity by (63) only increases as the square root of the anode diameter, the specific heat flow will be reduced. For instance under the conditions specified above the heat flow at the back of the anode will be only 4 watts/mm² so that only a moderate speed of the water current will be required for effective cooling.

Since T_2 is small compared with T_1, the anode thickness will not be a critical factor and will be of much less importance than for a stationary anode. The situation may be compared with that prevailing in a rotating tungsten anode with copper backing, where we also found that the thickness of the tungsten target has relatively little influence.

It will be generally advisable not to reduce the anode thickness below 1 mm, since then the high local temperature in the focal spot will produce high local temperature gradients at the back of the anode, which will necessitate a greater speed of the cooling current.

REFERENCES

[1]) J. E. de Graaf and W. J. Oosterkamp, J. sci. Instr. **15**, 293-303, 1938.
[2]) L. B. W. Jolley, Summation of Series, Chapman and Hall, London, 1925, p. 178.
[3]) A. Müller, Proc. roy. Soc. A **117**, 30-42, 1927.
[4]) A. Müller, Nature, London, **124**, 128, 1929.
[5]) W. T. Astbury and R. D. Preston, Nature, London, **133**, 460-461, 1934.
[6]) J. W. M. Du Mond and J. P. Youtz, Rev. sci. Instr. **8**, 291-307, 1937.
[7]) Fournier, Gondet and Mathieu, J. Physique **7**, 160-164, 1937.
[8]) J. W. M. Du Mond, B. B. Watson and B. Hicks, Rev. sci. Instr. **6**, 183-193, 1935.
[9]) A. Müller, Proc. roy. Soc. A **125**, 507-516, 1929.

ABSTRACTS OF RECENT SCIENTIFIC PUBLICATIONS OF N.V. PHILIPS' GLOEILAMPENFABRIEKEN

Reprints of the majority of these papers can be obtained on application to the Administration of the Research Laboratory of N.V. Philips' Gloeilampenfabrieken, Eindhoven, Netherlands. Those papers of which no reprints are available are marked with an asterisk (*).

1746: J. F. H. Custers: Note on the measurement of specular and diffuse photographic density (Photogr. J. Sect. B **87**, 59-63, 1947).

In measuring the density of photographic films, the smallest value or so-called diffuse density is measured when the measuring instrument catches the whole transmitted flux, and the largest value or so-called specular density is measured when only the flux transmitted normally to the layer is recorded.

The author has made some measurements in order to test a method recommended by Pitt (1938) for separating specular and diffuse densities. He arrives at the conclusion that Pitt's method can be used only for films or layers scattering light according to Lambert's cosine law, whereas it is of little value for all ordinary photographic films or plates because these show a scattering mechanism obeying quite different laws.

1747: P. M. van Alphen and C. J. Dippel: New technical possibilities in the micro-reproduction and multiplication of documents (Rapports de la 17me conférence de la F.I.D. Berne 25-30 août 1947).

An analysis is made of the possibilities and limitations in connection with the resolving power and optical conditions for recording a micro-picture and making it legible.

The contents of this paper partly cover the articles by C. J. Dippel and co-workers in Philips tech. Rev. **9**, 65 and 289, 1947.

1748: J. Hoekstra and C. P. Fritzius: De hechting van verf en vernis (De Verfkroniek, Amsterdam, **20**, 195-198, 1947.) (The adhesion of paints and varnishes; in Dutch).

Paint adhesion may be defined as the energy necessary for lifting a unit surface of paint from its base. As it is practically impossible to measure this energy, a method is looked for in which a paint film is drawn from the base under specified conditions while the applied force is measured. The authors, choosing a shearing force rather than a force perpendicular to the film, describe a method in which the upper surface of two metal blocks with a metal strip between them is painted. After unscrewing, the strip is drawn off in parallel with the paint layer (see also Philips tech. Rev. **8**, 147-148, 1946).

1749: J. F. H. Custers: Diffusion of water into a polymer (J. Polymer Sci. **2**, 301-305, 1947).

In contradistinction with usual methods, the diffusion of water into a polymer is investigated by starting from a disc of the material surrounded by water. In this way actual-service conditions are often closely approached. Since a theoretical basis is desirable, equations are given for this type of diffusion and experiments are described from which values for the permeation constant could be derived.

1750*: C. J. Bouwkamp and N. G. de Bruijn: The electrostatic field of a point charge inside a cylinder, in connection with wave guide theory (J. appl. Phys. **18**, 562-577, 1947).

The field of a point charge inside a hollow infinitely long circular cylinder is studied. The case of an axial point charge is treated in detail. The surface-density function is obtained as the solution of a Fourier type of integral equation. Then the potential caused by these charges is obtained. A second method works in the opposite direction. Here the potential is obtained as solution of a boundary-value problem. A third method is based on the theory of Fourier-Bessel-Dini series. The potential is developed into discrete normal solutions of the potential equation in cylindrical coordinates. It is emphasized that the study of the potential problem can serve as a guide in questions of wave propagation in hollow circular cylinders. In this connection the third method is shown to be extremely useful. This is demonstrated in the case of acoustic waves inside a cylinder, caused by a harmonically vibrating point source.

1751: N. Warmoltz: Variational principles in the theory of the cathode fall of a glow discharge (Physica, 's-Grav., **13**, 479-480, 1947).

One has to demand that a function, taking into account the formation (ionisation) and the transport of the ions as well, attains an extreme value for the real field distribution. Attention is drawn to a recent remark of Seeliger (Phys. Z. **45**, 141, 1944) who criticizes Rogowski's theory of the cathode fall. By following a procedure given by Seeliger it is possible to find an infinite number of these functions, but it seems difficult to select a function permitting a simple physical interpretation.

1752: C. J. Bouwkamp: A new method for computing the energy of interaction between two spheres under a general law of force (Physica, 's-Grav., **13**, 501-507, 1947).

A new method is communicated, based on the theory of Bessel functions, for calculating the energy of interaction of two homogeneous spheres, on the assumption that $V(r)$ is the mutual potential energy of two unit point masses a distance r apart. Particularly, when $V(r)$ is proportional to the nth power of $1/r$, an early result of Bradley is obtained. For integral values of n subject to $1 < n < 8$ a limiting process leads to logarithmic terms.

1753: K. F. Niessen: On a cavity resonator of high quality for the fundamental frequency (Appl. sci. Res., 's-Grav., **B1**, 18-34, 1947).

The quality of a cavity resonator, the cross-section of which is a parallelogram of a very special shape, is evaluated. It is shown that this cavity resonator may be used where a good quality is required, without the possibility of lower frequencies occurring, when the cavity is used as a part of a triode generator.

1754: M. J. Druyvesteyn: Experiments on the effect of low temperature on some plastic properties of metals (Appl. sci. Res., 's-Grav., **A1**, 66-80, 1947).

The yield value, breaking strength, elongation, and hardness of a number of pure polycrystalline metals are measured at room temperature and at —183 °C. The yield value was always higher at —183 °C than at 20 °C, the difference being relatively small (< 75 per cent) for the cubic face-centred and a number of hexagonal metals (e.g., Mg). The same difference is large for the body-centred metals and for Zn, Cd, and Sn. The former metals have a larger elongation at lower temperatures, the latter, however, become more or less brittle at low temperatures. The breaking strength and the hardness generally increase with decreasing temperature.

1755*: J. A. Haringx: Over sterk samendrukbare schroefveren en rubberstaven en over hun toepassing bij trillingsvrije opstellingen (Dissertatie, Delft, 1947) (On highly compressible helical springs and rubber rods, and on their application to vibration-free mountings; in Dutch).

The contents of this thesis will appear in full in Philips Res. Reports. Part of the subject has been treated in Philips tech. Rev. **9**, 16 and 85, 1947.

1756: Balth. van der Pol: Wiskunde en radioproblemen (Simon Stevin, Groningen, **25**, 179-198, 1947) (Mathematics and radio problems; in Dutch).

A lecture read before the Mathematical Centre at Amsterdam. An English translation of this paper was published in Philips Res. Rep. **3**, 174-190, 1948, under number R 79.

VOL. 3 NR 5 OCTOBER 1948

Philips Research Reports

EDITED BY THE RESEARCH LABORATORY
OF N.V. PHILIPS' GLOEILAMPENFABRIEKEN, EINDHOVEN, NETHERLANDS

R 89 *Philips Res. Rep.* **3**, *321-337, 1948*

THE SYNTHESIS OF PASSIVE, RESISTANCELESS FOUR-POLES THAT MAY VIOLATE THE RECIPROCITY RELATION

by B. D. H. TELLEGEN

621.392.5

Summary

The most general, passive, resistanceless four-poles of a certain order that may violate the reciprocity relation are investigated. They can be realized by means of inductances, capacitances, ideal transformers, and ideal gyrators. Of every order there are two types of four-pole, which can be transformed one into the other by connecting an ideal gyrator to any one of their terminal pairs.
The necessary and sufficient conditions of realizability are derived.

Résumé

Les plus généraux quadripôles passifs, sans résistance, d'une certaine ordre, qui peuvent transgresser la relation de réciprocité, sont étudiés. Ils peuvent être réalisés au moyen d'inductances, de capacitances, de transformateurs idéaux et de gyrateurs idéaux. Pour chaque ordre il y a deux types de quadripôles; on peut passer de l'un à l'autre en connectant un gyrateur idéal à quelqu'une des paires de bornes. Les conditions de réalisation, nécessaires et suffisantes, sont établies.

1. Introduction

In a former article [1]) we showed that besides the four known ideal, linear, constant, passive network elements — the capacitor, the resistor, the inductor, and the transformer — a fifth similar network element can be conceived, which we termed the gyrator. The ideal gyrator is a four-pole defined by

$$\left.\begin{aligned} v_1 &= -si_2, \\ v_2 &= si_1, \end{aligned}\right\} \qquad (1)$$

which violates the reciprocity relation. In circuit diagrams we shall represent it by the symbol of fig. 1.

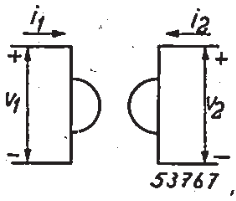

Fig. 1. Symbol for the ideal gyrator.

In this article we shall discuss the synthesis of passive, resistanceless four-poles that may violate the reciprocity relation, and we shall show how this can be achieved with the help of the ideal gyrator.

2. The concept of order of a four-pole

As in a discussion on the synthesis of resistanceless four-poles satisfying the reciprocity relation [2]), we begin by introducing the concept of *order* of a four-pole. For this purpose we connect the four-pole Z, whose equations are

$$\left.\begin{aligned} V_1 &= Z_{11}\, I_1 + Z_{12}\, I_2 , \\ V_2 &= Z_{21}\, I_1 + Z_{22}\, I_2 , \end{aligned}\right\} \tag{2}$$

where the coefficients Z_{ij} are rational functions of the frequency parameter $\lambda = j\omega$, in the way indicated in fig. 2 to a four-pole r containing no capacitors and no inductors, whose equations are

$$\left.\begin{aligned} -V_1 &= r_{11}\, I_1 + r_{12}\, I_2 , \\ -V_2 &= r_{21}\, I_1 + r_{22}\, I_2 . \end{aligned}\right\} \tag{3}$$

The order of the differential equation of the free vibrations of the system so formed we call the order of the four-pole.

By eliminating V_1, V_2, and I_1 or I_2 from (2) and (3) we arrive at

$$(Z_{11} + r_{11})\,(Z_{22} + r_{22}) - (Z_{12} + r_{12})\,(Z_{21} + r_{21}) = 0,$$

or

$$\begin{aligned} Z_{11}Z_{22} - Z_{12}Z_{21} + r_{22}Z_{11} + r_{11}Z_{22} - r_{21}Z_{12} - r_{12}Z_{21} + \\ + r_{11}r_{22} - r_{12}r_{21} = 0 . \end{aligned} \tag{4}$$

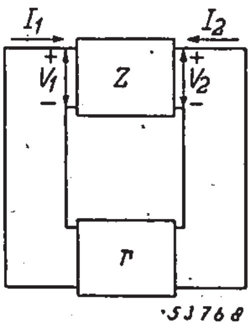

Fig. 2. The four-pole Z connected to a four-pole r containing no capacitors and no inductors.

To obtain from this the differential equation of the free vibrations we bring $Z_{11}Z_{22} - Z_{12}Z_{21}$, Z_{11}, Z_{22}, Z_{12}, and Z_{21} to the same denominator and put

$$Z_{11} = \frac{A}{C},\ Z_{22} = \frac{B}{C},\ Z_{12} = \frac{H_1}{C},\ Z_{21} = \frac{H_2}{C},\ Z_{11}Z_{22} - Z_{12}Z_{21} = \frac{D}{C}. \tag{5}$$

A, B, C, D, H_1, and H_2 are thus polynomials in λ with real coefficients between which there exists the relation

$$AB - H_1H_2 = CD . \tag{6}$$

We may suppose that these six polynomials have no common factor.

By substituting (5) in (4), multiplying by C, and replacing λ by $\mathrm{d}/\mathrm{d}t$, the differential equation of the free vibrations is obtained. The order of the four-pole is thus equal to the highest degree in λ of A, B, C, D, H_1, and H_2.

Four-poles may now be classified by their order.

3. Various forms of the four-pole equations

By introducing the polynomials A, B, C, D, H_1, H_2, the four-pole equations (2) take the form

$$\left.\begin{aligned} V_1 &= \frac{A}{C} I_1 + \frac{H_1}{C} I_2, \\ V_2 &= \frac{H_2}{C} I_1 + \frac{B}{C} I_2. \end{aligned}\right\} \tag{7}$$

Instead of expressing V_1 and V_2 in terms of I_1 and I_2 as is done in (7), we can also express I_1 and I_2 in terms of V_1 and V_2, or I_1 and V_2 in terms of V_1 and I_2, or V_1 and I_2 in terms of I_1 and V_2. From (7) and (6) we can thus derive the following three sets of equations

$$\left.\begin{aligned} I_1 &= \frac{B}{D} V_1 - \frac{H_1}{D} V_2, \\ I_2 &= -\frac{H_2}{D} V_1 + \frac{A}{D} V_2, \end{aligned}\right\} \tag{8}$$

$$\left.\begin{aligned} I_1 &= \frac{C}{A} V_1 - \frac{H_1}{A} I_2, \\ V_2 &= \frac{H_2}{A} V_1 + \frac{D}{A} I_2, \end{aligned}\right\} \tag{9}$$

$$\left.\begin{aligned} V_1 &= \frac{D}{B} I_1 + \frac{H_1}{B} V_2, \\ I_2 &= -\frac{H_2}{B} I_1 + \frac{C}{B} V_2. \end{aligned}\right\} \tag{10}$$

We see that the common denominators of the coefficients in these sets are successively C, D, A, B. *) These equations illustrate the usefulness of the six polynomials connected by (6) in characterizing a four-pole.

4. Resistanceless four-poles

If the equations (2) belong to a resistanceless four-pole, it is shown in the appendix, in section 5, that both Z_{11} and Z_{22} are imaginary, and that of Z_{12} and Z_{21} the imaginary parts are equal and the real parts are oppositely equal. As by (5) $Z_{11} = A/C$ and $Z_{22} = B/C$, both A/C and B/C will be imaginary. As by (5) $Z_{12} = H_1/C$ and $Z_{21} = H_2/C$, we introduce two new polynomials, H and K, defined by

$$H_1 = H - K, \quad H_2 = H + K. \tag{11}$$

---

*) If we express I_2 and V_2 in terms of I_1 and V_1, or I_1 and V_1 in terms of I_2 and V_2, the common denominator of the coefficients becomes H_1 or H_2, respectively.

Then H/C will be imaginary, and K/C will be real. By the introduction of H and K equation (6) changes into

$$AB - H^2 = CD - K^2 . \tag{12}$$

We can now distinguish between two types of resistanceless four-pole, namely either A, B, and H containing only terms of even degree in λ, and C, D, and K containing only terms of odd degree in λ, or vice versa (for the zero order this means: either A, B, and H are constant, and C, D, and K are zero, or vice versa). If we connect an ideal gyrator to any one of the terminal pairs of a four-pole of one of these types, it transforms into a four-pole of the other type. If, for example, we connect a gyrator with gyration resistance s to the primary terminal pair of a four-pole characterized by the six polynomials A, B, H, C, D, K, it transforms into a four-pole characterized by A', B', H', C', D', K', such that $A' = s^2C$, $B' = D$, $H' = sK$, $C' = A$, $D' = s^2B$, $K' = sH$.

We shall now investigate the number of independent parameters characterizing a general resistanceless four-pole of order n. The number of coefficients of an even and an odd four-pole polynomial together is $n + 1$; so the total number of coefficients of all six polynomials amounts to $3(n + 1)$. By (12) there exist relations between these coefficients. As (12) contains only terms of even degree and the highest degree is $2n$, it leads to $n + 1$ relations between the coefficients, so that there are only $2(n + 1)$ independent coefficients. As a four-pole is characterized by the ratio of these coefficients, a general resistanceless four-pole of order n is characterized by $2n + 1$ independent parameters.

4·1. Four-poles of order zero

(a) *A, B, and H constant; C, D, and K zero.*

Substituting this in (9) and (11) we come to

$$\left. \begin{aligned} I_1 &= -\frac{H}{A} I_2 , \\ V_2 &= \frac{H}{A} V_1 , \end{aligned} \right\} \tag{13}$$

which constitute the equations of an ideal transformer.

(b) *C, D, and K constant; A, B, and H zero.*

Substituting this in (7) and (11) we come to

$$\left. \begin{aligned} V_1 &= -\frac{K}{C} I_2 , \\ V_2 &= \frac{K}{C} I_1 , \end{aligned} \right\} \tag{14}$$

which constitute the equations of an ideal gyrator.

4·2. The most general four-poles of order n

By (7) we see that A/C is the impedance between the primary terminals of a four-pole when the secondary terminals are open ($I_2 = 0$). For a four-pole of order n, A/C will therefore in general represent the impedance of a resistanceless two-pole of order n. We shall show that this condition, together with the conditions for A, B, H, C, D, K stated in section 4, is sufficient for the realizability of the four-pole. In special cases A/C may represent an impedance of order less than n. These will be dealt with in section 4·3.

For $n = 0$ the above statement is proved in section 4·1. We shall now prove it for $n \geqq 1$. We must distinguish between two cases: the degree of A, B, and H can exceed that of C, D, and K by one, or vice versa.

(a) *A, B, and H of degree n; C, D, and K of degree n—1.*

We put

$$\left.\begin{aligned} A &= a_0\lambda^n + a_2\lambda^{n-2} + \dots, \\ B &= b_0\lambda^n + b_2\lambda^{n-2} + \dots, \\ H &= h_0\lambda^n + h_2\lambda^{n-2} + \dots, \\ C &= c_1\lambda^{n-1} + c_3\lambda^{n-3} + \dots, \\ D &= d_1\lambda^{n-1} + d_3\lambda^{n-3} + \dots, \\ K &= k_1\lambda^{n-1} + k_3\lambda^{n-3} + \dots. \end{aligned}\right\} \tag{15}$$

From (12) it follows, if we pay attention to the terms with λ^{2n}, that

$$a_0b_0 - h_0^2 = 0. \tag{16}$$

We start from the four-pole equations of the form (7) which by (11) may be written as

$$\left.\begin{aligned} V_1 &= \frac{A}{C}I_1 + \left(\frac{H}{C} - \frac{K}{C}\right)I_2, \\ V_2 &= \left(\frac{H}{C} + \frac{K}{C}\right)I_1 + \frac{B}{C}I_2. \end{aligned}\right\} \tag{17}$$

A/C, B/C, and H/C all have a pole at $\lambda = \infty$. To remove these poles we split these fractions into two partial fractions by putting

$$\left.\begin{aligned} \frac{A}{C} &= \frac{a_0\lambda}{c_1} + \frac{A'}{C}, \\ \frac{B}{C} &= \frac{b_0\lambda}{c_1} + \frac{B'}{C}, \\ \frac{H}{C} &= \frac{h_0\lambda}{c_1} + \frac{H'}{C}. \end{aligned}\right\} \tag{18}$$

The fractions A'/C, B'/C, and H'/C have zeros at $\lambda=\infty$. As A/C represents the impedance of a resistanceless two-pole of order n, it follows from the theory of two-poles [3]) that a_0/c_1 is positive and that A'/C represents the impedance of a resistanceless two-pole of order n—1.

Substituting (18) in (17) we get

$$\left.\begin{aligned} V_1 &= \left(\frac{a_0\lambda}{c_1}+\frac{A'}{C}\right) I_1 + \left(\frac{h_0\lambda}{c_1}+\frac{H'}{C}-\frac{K}{C}\right) I_2 ,\\ V_2 &= \left(\frac{h_0\lambda}{c_1}+\frac{H'}{C}+\frac{K}{C}\right) I_1 + \left(\frac{b_0\lambda}{c_1}+\frac{B'}{C}\right) I_2 .\end{aligned}\right\} \qquad (19)$$

This represents the series connection of a four-pole defined by

$$\left.\begin{aligned} V_1 &= \frac{a_0\lambda}{c_1} I_1 + \frac{h_0\lambda}{c_1} I_2 ,\\ V_2 &= \frac{h_0\lambda}{c_1} I_1 + \frac{b_0\lambda}{c_1} I_2 ,\end{aligned}\right\} \qquad (20)$$

which, by virtue of (16) and the positiveness of a_0/c_1, can be represented by an ideal transformer with an inductance in parallel to one of its terminal pairs, and a four-pole defined by

$$\left.\begin{aligned} V_1 &= \frac{A'}{C} I_1 + \left(\frac{H'}{C}-\frac{K}{C}\right) I_2 ,\\ V_2 &= \left(\frac{H'}{C}+\frac{K}{C}\right) I_1 + \frac{B'}{C} I_2 ,\end{aligned}\right\} \qquad (21)$$

as is illustrated by fig. 3.

To investigate the order of the four-pole (21), we calculate the quantity D' defined by

$$D' = \frac{A'B' - H'^2 + K^2}{C} .$$

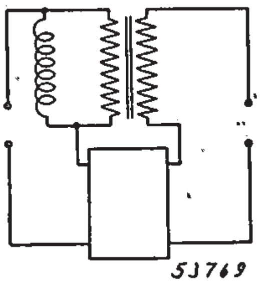

Fig. 3. Reduction of a four-pole if A, B, H are of higher degree than C, D, K.

By substituting the values of A', B', H' from (18) we get

$$D' = \frac{AB - H^2 + K^2 - (Ab_0 + Ba_0 - 2Hh_0)\,\lambda C/c_1}{C} = $$
$$= D - (Ab_0 + Ba_0 - 2Hh_0)\,\lambda/c_1 ,$$

a polynomial of degree n—1. We have thus found six polynomials, A', B', H', C, D', K, satisfying a relation of the type (12), containing only terms of even degree or only terms of odd degree, of which A', B', H' are of degree n—2 and C, D', K are of degree n—1, and of which C/A' represents the admittance of a resistanceless two-pole. The four-pole defined by these quantities has thus properties similar to those of the original four-pole.

with the exception that it has the order $n-1$, and that A', B', H' have a degree one less than the degree of C, D', K.

(b) *A, B and H of degree $n-1$; C, D, and K of degree n.*

This can be treated quite analogously to the former case. We start from the four-pole equations of the form (9) which by (11) may be written as

$$\left.\begin{aligned} I_1 &= \frac{C}{A} V_1 + \left(\frac{K}{A} - \frac{H}{A}\right) I_2 , \\ V_2 &= \left(\frac{K}{A} + \frac{H}{A}\right) V_1 + \frac{D}{A} I_2 . \end{aligned}\right\} \tag{22}$$

Now C/A, D/A, and K/A all have a pole at $\lambda = \infty$, which can be removed by a splitting into partial fractions. The four-pole can correspondingly be represented by the series-parallel connection of a four-pole consisting of an ideal gyrator with a capacitance in series with the primary terminals (or an inductance in parallel to the secondary terminals, which is equivalent to this), and a four-pole of order $n-1$, as is illustrated by fig. 4.

The four-poles of order $n-1$ that enter in figs 3 and 4 can again be represented by a combination as in fig. 4, respectively fig. 3, leading to four-poles of order $n-2$. Thus, by alternately splitting off a series connection of an ideal transformer with an inductance in parallel to one of its terminal pairs, and a series-parallel connection of an ideal gyrator with a capacitance in series with its primary terminals, the order of the four-pole can be successively reduced until we come to a four-pole of order zero which, as shown in section 4·1, can be realized by an ideal transformer or by an ideal gyrator. Thus we have shown that the conditions mentioned in the beginning of this section are sufficient for the realizability of the four-pole.

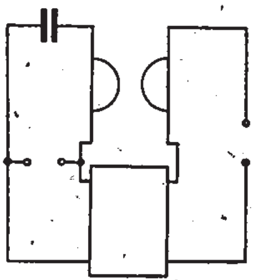

Fig. 4. Reduction of a four-pole if A, B, H are of lower degree than C, D, K.

The reduction of the order of a four-pole discussed above is based on the removal of poles at $\lambda = \infty$. We can also base this reduction in a similar way on the removal of poles at $\lambda = 0$. We must distinguish between two cases: A, B, and H can be of even degree and C, D, and K of odd degree, or vice versa.

(a) *A, B, and H of even degree; C, D, and K of odd degree.*

We put

$$\left.\begin{aligned} A &= a_0 + a_2 \lambda^2 + \dots , \\ B &= b_0 + b_2 \lambda^2 + \dots , \\ H &= h_0 + h_2 \lambda^2 + \dots , \\ C &= c_1\lambda + c_3 \lambda^3 + \dots , \\ D &= d_1\lambda + d_3 \lambda^3 + \dots , \\ K &= k_1\lambda + k_3 \lambda^3 + \dots . \end{aligned}\right\} \tag{23}$$

From (12) it follows, if we pay attention to the terms without λ, that

$$a_0 b_0 - h_0^2 = 0 . \tag{24}$$

We start from the four-pole equations of the form (17), where now A/C, B/C, and H/C all have a pole at $\lambda = 0$. To remove these poles we split these fractions into two partial fractions by putting

$$\left.\begin{aligned} \frac{A}{C} &= \frac{a_0}{c_1\lambda} + \frac{A'}{C'}, \\ \frac{B}{C} &= \frac{b_0}{c_1\lambda} + \frac{B'}{C'}, \\ \frac{H}{C} &= \frac{h_0}{c_1\lambda} + \frac{H'}{C'}, \end{aligned}\right\} \tag{25}$$

where $C' = C/\lambda$.

The four-pole can thus be represented by the series connection of a four-pole defined by

$$\left.\begin{aligned} V_1 &= \frac{a_0}{c_1\lambda} I_1 + \frac{h_0}{c_1\lambda} I_2 , \\ V_2 &= \frac{h_0}{c_1\lambda} I_1 + \frac{b_0}{c_1\lambda} I_2 , \end{aligned}\right\} \tag{26}$$

which can be represented by an ideal transformer with a capacitance in parallel to one of its terminal pairs, and a four-pole defined by

$$\left.\begin{aligned} V_1 &= \frac{A'}{C'} I_1 + \left(\frac{H'}{C'} - \frac{K'}{C'}\right) I_2 , \\ V_2 &= \left(\frac{H'}{C'} + \frac{K'}{C'}\right) I_1 + \frac{B'}{C'} I_2 , \end{aligned}\right\} \tag{27}$$

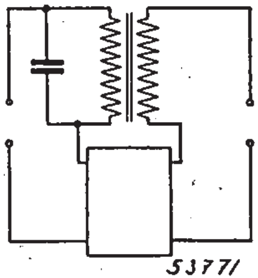

Fig. 5. Reduction of a four-pole if A, B, H are of even degree and C, D, K are of odd degree.

where $K' = K/\lambda$, as is illustrated by fig. 5.

To investigate the order of the four-pole (27) we calculate the quantity D' defined by

$$D' = \frac{A'B' - H'^2 + K'^2}{C'} .$$

By substituting the values of A', B', H' from (25) we get

$$D' = \frac{AB - H^2 + K^2 - (Ab_0 + Ba_0 - 2Hh_0)\, C/c_1\lambda}{C\lambda} =$$

$$= D/\lambda - (Ab_0 + Ba_0 - 2Hh_0)/c_1\lambda^2 ,$$

a polynomial of even degree.

Thus we come to six polynomials of which A', B', H' as well as C', D', K' are of degree one less than that of A, B, H, respectively C, D, K.

(b) *A, B, and H of odd degree; C, D, and K of even degree.*

Starting from the four-pole equations of the form (22) we are led to the series-parallel connection of an ideal gyrator with an inductance in series with the primary terminals (or a capacitance in parallel to the secondary terminals, which is equivalent to this), and a four-pole of order one less than the order of the original four-pole, as is illustrated by fig. 6.

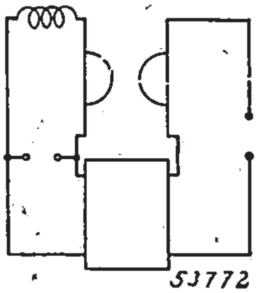

Fig. 6. Reduction of a four-pole if *A*, *B*, *H* are of odd degree and *C*, *D*, *K* are of even degree.

The methods discussed for the reduction of the order of a four-pole of order *n* all started from A/C representing the impedance of a resistanceless two-pole of order *n*. Instead, we may also start from B/C, D/B, or D/A representing the impedance of a resistanceless two-pole of order *n*. We can thus develop four alternative modes of reduction, illustrated by fig. 7 *d*, *e*, *f*, and *g*. Fig. 7 and its caption summarizes all our results on the reduction of general resistanceless four-poles.

By starting from the ideal transformer or the ideal gyrator, and using fig. 7, we come to circuit diagrams for the general four-pole of order *n*

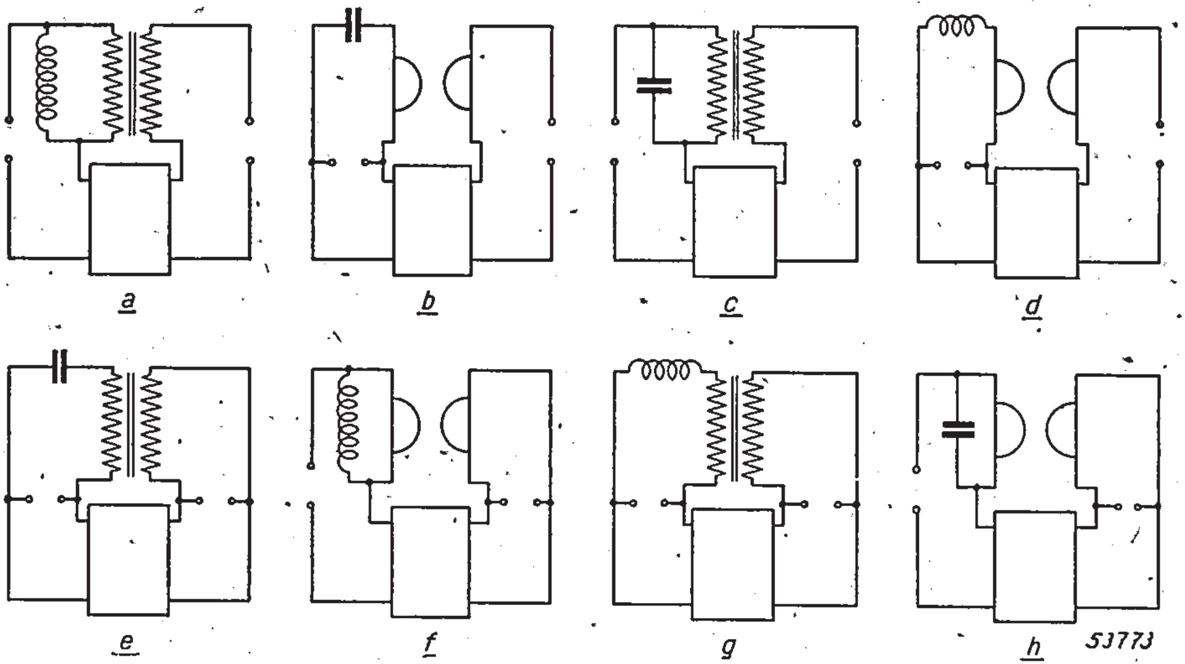

Fig. 7. The reduction of general resistanceless four-poles.
a and *e*: *A*, *B*, *H* of higher degree than *C*, *D*, *K*; degree of *A*, *B*, *H* diminished by 2, degree of *C*, *D*, *K* not diminished.
b and *f*: *A*, *B*, *H* of lower degree than *C*, *D*, *K*; degree of *A*, *B*, *H* not diminished, degree of *C*, *D*, *K* diminished by 2.
c and *g*: *A*, *B*, *H* of even degree, *C*, *D*, *K* of odd degree; degree of *A*, *B*, *H* and of *C*, *D*, *K* diminished by 1.
d and *h*: *A*, *B*, *H* of odd degree, *C*, *D*, *K* of even degree; degree of *A*, *B*, *H* and of *C*, *D*, *K* diminished by 1.

containing $2n+1$ elements. As we saw in section 4, this equals the number of independent parameters, and so all these circuit diagrams contain the minimum number of elements. The number of L's and C's in these diagrams is equal to n, the order of the four-pole; the number of ideal transformers and gyrators is equal to $n+1$.

In fig. 8 circuit diagrams for the two types of general resistanceless four-pole of the zeroth, first, and second orders are thus drawn. Besides these, many equivalent circuits are possible.

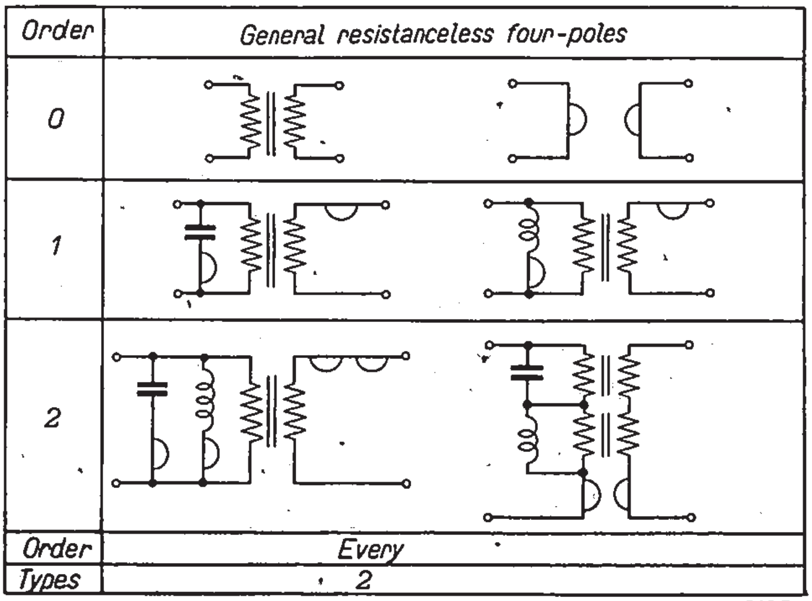

Fig. 8. Synthesis of general resistanceless four-poles.

The circuit diagrams for general resistanceless four-poles without gyrator developed in a former article 2), and which for the zeroth, first, and second orders are reproduced in fig. 9, are special cases of the circuit diagrams of fig. 8. By making the gyration resistance of a gyrator equal to zero the latter turns into two short-circuited terminal pairs; by making the gyration resistance infinite the gyrator turns into two open terminal pairs. By means of this the four-poles of zeroth order of fig. 8 directly turn into the four-poles of zeroth order of fig. 9. By replacing the gyrator in the first-order four-poles of fig. 8 by short-circuited terminal pairs, two of the four first-order four-poles of fig. 9 arise. By replacing in the first-order four-poles of fig. 8 the C or L in series with a gyrator branch by an L, respectively a C, in parallel to the other gyrator branch, and by then replacing the gyrator by two open terminal pairs, the other two first-order four-poles of fig. 9 arise. In an analogous way, from the first second-order four-pole of fig. 8 four second-order four-poles of fig. 9 may be derived, and from the second second-order four-pole of fig. 8 one second-order four-pole of fig. 9 may be derived.

This illustrates that the synthesis of resistanceless four-poles that may violate the reciprocity relation is simpler and more symmetric than the synthesis of resistanceless four-poles that satisfy the reciprocity relation.

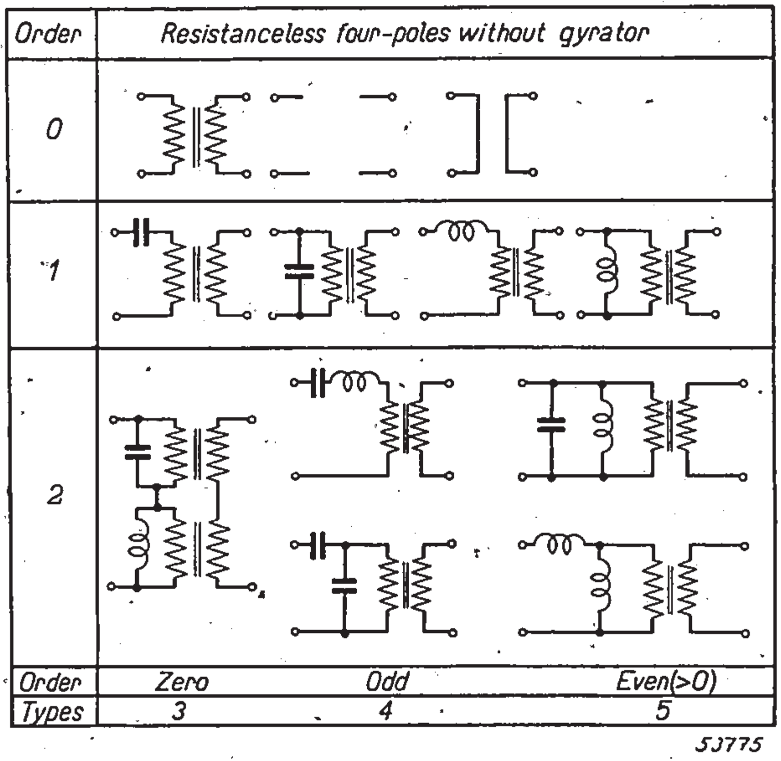

Fig. 9. Synthesis of resistanceless four-poles without gyrator.

4·3. The necessary and sufficient conditions of realizability

In the preceding section we investigated the case where A/C represents an impedance of order n. This is not a necessary condition: A/C may also represent an impedance of order less than n. We shall now investigate what additional conditions are required in this case to come to a set of necessary and sufficient conditions. Here we shall only give the results of these investigations, details of which are given in the appendix, sections 6-8.

In general the polynomials defining a four-pole of order n are of degree n. Any such polynomial has n zeros. When the coefficient of the term of degree n of a polynomial tends to zero, one of its zeros tends to infinity. Therefore we shall conceive every polynomial defining a four-pole of order n to have n zeros, some of which may be infinite.

Keeping this in mind, we can state that if A/C represents an impedance of order less than n, A and C must have common zeros. In the case of resistanceless four-poles these common zeros are always imaginary, zero and infinity included, and in at least A or C these zeros are simple.

For any such common zero, B/C and D/A have corresponding simple poles with positive-real residues. Now, B/C and D/A represent the impedance between the secondary terminals of the four-pole when the primary terminals are open or are short-circuited, respectively. Poles can be removed from an impedance by splitting it up into partial fractions, as demonstrated by Foster [3]). Physically this removal of poles corresponds to splitting up the impedance into several parts in series: a pole at infinity corresponds to an inductance; a pole at the origin corresponds to a capacitance; a pair of conjugate-imaginary poles corresponds to a parallel circuit of an inductance and a capacitance. Thus the removal of common poles from B/C and D/A corresponds to splitting up the four-pole into a two-pole in series with the secondary terminals and a four-pole of lower order.

If a common zero of A and C is simple in both A and C, the corresponding residues in B/C and D/A are equal, so that we can perform this splitting up of the four-pole by splitting up B/C or D/A at will. If a common zero is multiple in C but simple in A, the corresponding residue in D/A will be smaller than the residue in B/C. We can then perform the splitting up of the four-pole only by splitting up D/A. Conversely, if a common zero is multiple in A but simple in C, we can perform this by splitting up B/C only. If by this process all common zeros of A and C have been removed, we are left with a four-pole of lower order which may be realized by the methods of the foregoing section.

We thus come to the following

Theorem

The necessary and sufficient conditions for six polynomials A, B, H, C, D, K in λ, without a common factor, to represent a passive, resistanceless four-pole of order n are that

(a) *the highest degree is n;*
(b) *the coefficients are real;*
(c) $AB - H^2 = CD - K^2$;
(d) *A, B, H contain only terms of even degree and C, D, K contain only terms of odd degree, or vice versa;*
(e) *A/C represents the impedance of a passive, resistanceless two-pole;*
(f) *if A and C have common zeros, these are imaginary, zero and infinity included, and simple in at least A or C;*
(g) *if such a zero is simple in C, B/C has a corresponding simple pole with a positive-real residue;*
(h) *if such a zero is multiple in C, D/A has a corresponding simple pole with a positive-real residue.*

If A/C represents an impedance of order $p < n$, the four-pole may be realized by a four-pole of order p, whose A/C-value is the same as the A/C-value of the original four-pole, with a resistanceless two-pole of order $n—p$ connected in series with its secondary terminals.

The above theorem may be stated in other equivalent forms. In the first place, C and A, and B and D may be interchanged in (g) and (h). In the second place, in (e) A/C may be replaced either by B/C, or by D/B, or by D/A, and corresponding changes in (f), (g), and (h). These three cases lead to a realization by a four-pole with a resistanceless two-pole in series with the primary terminals, or in parallel to the secondary terminals, or in parallel to the primary terminals, respectively.

APPENDIX

5. A property of resistanceless four-poles

The mean dissipated power in a four-pole is equal to the real part of

$$V_1 I_1^* + V_2 I_2^* ,$$

where the asterisk denotes the conjugate-complex value. For a resistanceless four-pole this must be zero. If such a four-pole is characterized by the equations

$$\left.\begin{aligned} V_1 &= Z_{11} I_1 + Z_{12} I_2 , \\ V_2 &= Z_{21} I_1 + Z_{22} I_2 , \end{aligned}\right\}$$

we come to

$$\operatorname{Re} (Z_{11} |I_1|^2 + Z_{12} I_2 I_1^* + Z_{21} I_1 I_2^* + Z_{22} |I_2|^2) = 0 . \tag{28}$$

If $I_2 = 0$, this leads to $\operatorname{Re} (Z_{11}) = 0$; therefore Z_{11} is imaginary. By similar reasoning we may show that also Z_{22} is imaginary. The equation (28) is thereby reduced to

$$\operatorname{Re} (Z_{12} I_2 I_1^* + Z_{21} I_1 I_2^*) = 0 . \tag{29}$$

As $\operatorname{Re} (I_2 I_1^*) = \operatorname{Re} (I_1 I_2^*)$ and $\operatorname{Im} (I_2 I_1^*) = - \operatorname{Im} (I_1 I_2^*)$, we get

$$\operatorname{Re} (Z_{12} + Z_{21}) \operatorname{Re} (I_2 I_1^*) - \operatorname{Im} (Z_{12} - Z_{21}) \operatorname{Im} (I_2 I_1^*) = 0.$$

As this must be true for every value of $I_2 I_1^*$, we finally come to

$$\operatorname{Re} (Z_{12} + Z_{21}) = 0 \quad \text{and} \quad \operatorname{Im} (Z_{12} - Z_{21}) = 0 .$$

Thus of Z_{12} and Z_{21} the imaginary parts are equal and the real parts are oppositely equal.

6. An auxiliary theorem on four-poles

From every four-pole we can deduce a two-pole by connecting the two pairs of four-pole terminals to two pairs of terminals of a six-pole. For the six-pole we choose one consisting of two ideal transformers and an ideal gyrator, as is illustrated by fig. 10. The four-pole equations we write in the form (17)

$$\left.\begin{aligned} V_1 &= \frac{A}{C} I_1 + \frac{H-K}{C} I_2 , \\ V_2 &= \frac{H+K}{C} I_1 + \frac{B}{C} I_2 . \end{aligned}\right\} \qquad (30)$$

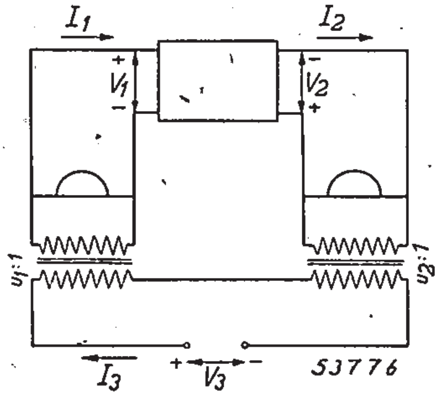

Fig. 10. Two-pole deduced from a four-pole by means of two transformers and a gyrator.

If the transformation ratios are u_1 and u_2 and the gyration conductance is t, we can write the six-pole equations as

$$\left.\begin{aligned} I_1 &= \qquad - tV_2 + u_1 I_3 , \\ I_2 &= tV_1 \qquad + u_2 I_3 , \\ V_3 &= u_1 V_1 + u_2 V_2 \qquad . \end{aligned}\right\} \qquad (31)$$

By eliminating I_1, I_2, V_1, V_2 from (30) and (31) we can calculate the impedance $Z = V_3/I_3$ of the two-pole. If we put

$$u_1 = \frac{\alpha_1}{\beta_1} , u_2 = \frac{\alpha_2}{\beta_1} , t = \frac{\beta_2}{\beta_1} ,$$

and make use of (12), we then come to

$$Z = \frac{\alpha_1^2 A + 2\alpha_1\alpha_2 H + \alpha_2^2 B}{\beta_1^2 C + 2\beta_1\beta_2 K + \beta_2^2 D} . \qquad (32)$$

Thus, if A, B, H, C, D, K are six polynomials representing a passive four-pole, for every value of α_1, α_2, β_1, β_2 (32) represents the impedance of a passive two-pole.

7. The conditions of section 4·3 are necessary

We have already proved the necessity of conditions (a) - (e). To prove the necessity of (f) we suppose A and C to have a common zero that is not imaginary. As the numerator and the denominator of the impedance of a resistanceless two-pole cannot have zeros that are not imaginary, from (32) we conclude, by putting $\beta_2 = 0$, that a non-imaginary zero of C must also be a zero of A, H, and B. Further we conclude from (32), by putting $\alpha_2 = 0$, that a non-imaginary zero of A must also be a zero of C, K, and D. Such a zero is therefore common to all six polynomials, and thus these have a corresponding common factor which may be divided out. So the only common zeros of A and C that have to be considered are imaginary zeros.

Suppose now, A and C have a common multiple zero. As the numerator and the denominator of the impedance of a resistanceless two-pole cannot have multiple zeros, from (32) we conclude, by putting $\beta_2 = 0$, that a multiple zero of C must also be a zero of A, H, and B. Further we conclude from (32), by putting $\alpha_2 = 0$, that a multiple zero of A must also be a zero of C, K, and D. Such a zero is therefore common to all six polynomials, which thus have a corresponding common factor which may be divided out. So the only common zeros of A and C that have to be considered are simple in at least A or C.

To prove the necessity of (g) and (h) we first prove that a common zero of A and C is also a zero of H and K. From (12) it follows that a common zero of A and C is also a zero of $H^2—K^2$. As such a zero is imaginary, and H is an even function and K an odd function, or vice versa, for this zero H is real and K is imaginary, or vice versa, and so $H^2—K^2$ is the sum, or the negative of the sum, of two squares. This can only be zero if both terms are zero, and a common zero of A and C is therefore also a zero of H and K.

If such a zero is simple in C, and it is not a zero of B, B/C has a corresponding simple pole, which, as B/C represents the impedance of a resistanceless two-pole. has a positive-real residue. If such a zero is simple in C, and it is also a zero of B, it follows from (12) that it is a multiple zero of CD, and it is therefore also a zero of D. Thus all six polynomials have a common zero, which may be divided out, so that this need not be considered.

If a common zero of A and C is multiple in C, it is simple in A. In an analogous way we may then prove that D/A has a corresponding simple pole with a positive-real residue.

8. The conditions of section 4·3 are sufficient

As, by condition (b), the coefficients of A and C are real, the conjugate complex of a common zero of A and C is also a common zero. To every common zero of A and C there corresponds a common factor of A and C. If we multiply the factors corresponding to two conjugate-complex zeros, we come to a factor with real coefficients. So, in considering a factor Q corresponding to common zeros of A and C, we can suppose Q to have real coefficients. From condition (f) we know that the zeros of Q are imaginary and simple, and so Q contains only terms of even or of odd degree.

In section 7 we deduced from conditions (b), (c), (d), and (f) that Q is also a factor of H and of K. So we can put

$$A = A_0Q, C = C_0Q, H = H_0Q, K = K_0Q, \tag{33}$$

where A_0, C_0, H_0, and K_0 are polynomials with real coefficients, of which A_0 and H_0 contain only terms of even degree and C_0 and K_0 contain only terms of odd degree, or vice versa.

Let us first suppose that Q corresponds to zeros that are simple in C. By condition (g), B/C has corresponding simple poles. So we can split up B/C uniquely into two partial fractions by putting

$$\frac{B}{C}=\frac{B}{C_0Q}=\frac{B_0}{C_0}+\frac{P}{Q}, \tag{34}$$

where B_0 and P are polynomials with real coefficients. If C_0 contains only terms of odd degree, B_0 will contain only terms of even degree, and vice versa; and the same holds for Q and P. Moreover, we saw that the zeros of Q are imaginary and simple; and, by condition (g), the poles of P/Q have positive-real residues. So P/Q represents the impedance of a realizable resistanceless two-pole.

By substituting (33) and (34) in (17) we get

$$\left.\begin{aligned}V_1&=\frac{A_0}{C_0}I_1+\left(\frac{H_0}{C_0}-\frac{K_0}{C_0}\right)I_2,\\ V_2&=\left(\frac{H_0}{C_0}+\frac{K_0}{C_0}\right)I_1+\left(\frac{B_0}{C_0}+\frac{P}{Q}\right)I_2.\end{aligned}\right\} \tag{35}$$

This represents a four-pole characterized by A_0, B_0, C_0, H_0, K_0 with a two-pole of impedance P/Q connected in series with its secondary terminals.

To investigate the four-pole we consider the function D_0 defined by

$$D_0=\frac{A_0B_0-H_0^2+K_0^2}{C_0}. \tag{36}$$

From (34) we get

$$B=B_0Q+C_0P. \tag{37}$$

Putting (33) and (37) into (12) we get

$$(A_0B_0-H_0^2+K_0^2)\,Q=(D-A_0P)\,C_0\,. \tag{38}$$

As C_0 has no zeros in common with Q, $D-A_0P$ has Q as a factor. Thus

$$\frac{D-A_0P}{Q}=\frac{A_0B_0-H_0^2+K_0^2}{C_0}=D_0$$

is a polynomial with real coefficients. If C_0 contains only terms of odd (or of even) degree, D_0 will also contain only terms of odd (or of even) degree.

If Q corresponds to common zeros of A and C that are multiple in C, from condition (f) we know that these are simple in A, and from condition (h) that D/A has corresponding simple poles with positive-real residues. We then can in a manner analogous to the one above, by splitting D/A into partial fractions and using (22), also come to a representation of the four-pole by a four-pole characterized by six polynomials A_0, B_0, C_0, D_0, H_0, K_0 and a resistanceless two-pole in series with its secondary terminals.

After removing all common zeros of A and C, we are left with a four-pole which is characterized by six polynomials that fulfil the conditions (b)-(e), and which can be realized by the methods of section 4·2.

Eindhoven, December 1947

REFERENCES

1) B. D. H. Tellegen, The gyrator, a new electric network element, Philips Res. Rep. 3, 81-101, 1948.
2) B. D. H. Tellegen, Network synthesis, especially the synthesis of resistanceless four-terminal networks, Philips Res. Rep. 1, 169-184, 1946.
3) R. M. Foster, A reactance theorem, Bell Syst. tech. J. 3, 259-267, 1924.

R 90 Philips Res. Rep. 3, 338-360, 1948

DISSIPATION OF HEAT BY FREE CONVECTION *)

by W. ELENBAAS

536.25

Summary

A body differing in temperature from the surroundings loses energy not only by radiation but also by conduction and convection. The general laws governing the latter dissipation of heat are investigated. The many quantities governing this transfer may be combined into a few dimensionless numbers by means of similarity considerations. This leads to an important simplification and facilitates the survey of experimental and theoretical results. First, the above-mentioned considerations are applied to bodies that may be characterized by one linear dimension only (the vertical plate, the horizontal cylinder, the sphere), and further, to bodies characterized by two such quantities (the vertical cylinder of finite height, cooling ribs, the inner surface of vertical tubes).

Résumé

Un corps qui se trouve à une température plus élevée que celle de son ambiance perd de la chaleur par rayonnement et aussi par conduction et par convection. Le présent article traite des lois et principes généraux qui régissent la perte de chaleur par conduction et convection. Des considérations d'analogie permettent de combiner les différentes grandeurs qui apparaissent dans les équations fondamentales en un petit nombre d'indices numériques sans dimension. Il en résulte des simplifications considérables et cela nous permet de donner un aperçu synthétique de données expérimentales et de considérations théoriques, dans ce domaine.

Avec cette façon de considérer les choses, l'article traite successivement de corps caractérisés par une seule dimension linéaire (la plaque verticale, le cylindre horizontal, et la sphère), et de corps caractérisés par deux dimensions linéaires (le cylindre vertical de longueur finie, les ailettes de refroidissement, et la surface intérieure d'un tuyau vertical).

Symbols and definitions

Suffix w means that the quantity should be taken at the temperature of the wall (ϑ_w).

Suffix ∞ means that the quantity should be taken at the temperature of the medium at a great distance from the body (ϑ_∞).

Suffix m means that the mean should be taken, for instance:

$$\lambda_m = \frac{1}{\vartheta_w - \vartheta_\infty} \int_{\vartheta_\infty}^{\vartheta_w} \lambda(\vartheta)\, \mathrm{d}\vartheta .$$

Suffix s means that the quantity should be taken for the hydrostatic state.

---

*) The paper is essentially identical to that published in De Ingenieur **60**, O 21-O 34, 1948, by the same author, under the same title.

Nu = $\alpha\, l/\lambda$, Nusselt's number.
Gr = $l^3\, g\, \varrho^2\, \beta\, \Theta_w/\eta^2$, Grashof's number.
Re = $\varrho\, V\, l/\eta$, Reynold's number.
Pr = $c_p\, \eta/\lambda$, Prandtl's number.
Pé = $\varrho\, c_p\, V\, l/\lambda$, Péclet's number.
λ = heat conductivity.
c_p = specific heat at constant pressure.
ϱ = density.
η = viscosity.
β = coefficient of cubic expansion; for gaseous media $\beta = 1/T_\infty$.
g = acceleration of gravity.
V = velocity; u, v, and w are velocity components in the x-, y-, and z-directions.
α = coefficient of heat transfer = the dissipation of heat per unit of area per unit of time and per unit of temperature difference.
$\bar{\alpha}$ = mean value of α on the surface.
l = linear dimension.
d = diameter.
h = height.
T = temperature in °K.
ϑ = temperature in °C.
Θ = difference of temperature as compared to remote sections of the medium, $\Theta = T - T_\infty = \vartheta - \vartheta_\infty$.
t = time.
Φ = quantity of heat dissipated per second.
F = heat-dissipating surface.
$[\Psi\,.\,\mathbf{Re}]$ = the so-called Poiseuille coefficient.
b = spacing between the cooling ribs.
δ = plate thickness of the cooling ribs.
S = surface of the cross-section of a cylindrical tube.
U = circumference of the cross-section of a cylindrical tube.
r = hydraulic radius of the cross-section = $2S/U$.
γ = the angle that the plates or cylinders make with the vertical.
p = pressure.
p_s = hydrostatic pressure.
P = $p - p_s$.

1. Introduction

In the anode of an X-ray tube or of a transmitting valve, in electrically heated wires (such as the filament of an incandescent lamp, or a heating element of an electrical furnace), in the windings of a choke coil or a transformer, in the plates of barrier-layer rectifiers, and in many other apparatus, energy is transformed into heat. As a consequence of the heat developed, the temperature of these bodies rises above that of the surroundings. As the temperature difference increases, the amount of heat dissipated rises until a state of equilibrium is reached, where the amount of heat developed is equal to that dissipated.

It is often desirable to calculate the temperature if the amount of heat produced is known. Very often one aims at reducing the dimensions of the apparatus, or parts thereof, as much as possible with a view to saving space or lowering the weight, the load, and with it the temperature, being increased to the highest permissible value. In a number of cases one wants the body, such as a furnace or a filament, to reach a certain temperature. In order to ascertain the connection between the amount of heat Φ dissipated per second, and the temperature difference with respect to the surroundings, we shall first investigate the mechanism of heat transfer.

2. Radiation, conduction, convection

It is usual to divide the dissipation of energy into heat transferred by radiation, by conduction, and by convection. In this paper we shall not consider radiation because the laws governing the radiation of heat are generally well known, and in most cases it is possible to investigate this cause of heat transfer separately, and study the loss of heat by conduction and by convection apart from radiation. This is evident from the following argument: if a body is cooled by a liquid, the difference in temperature from the surroundings is usually so small that the loss of heat by radiation is negligible in comparison to that by conduction and convection. If the cooling is accomplished by a gas, the amount of heat radiated may be considerable (e.g. in the case of the filament of a gasfilled incandescent lamp or of a heating element in an electric heating unit), but in this case the radiation penetrates the surrounding medium without appreciably heating it, and it is only absorbed when impinging upon the wall of the tube or that of the room. Thus radiation has practically no influence upon the conditions of the surrounding medium; hence the loss by conduction and by convection is practically unaffected by the radiation loss, which therefore may be simply added to the former. To measure the contribution of the radiation one may put the body in a vacuum, the radiation losses then equalling the energy input when the equilibrium is reached, or one may measure the radiation by suitable means (thermopile, etc.).

As to the heat transfer by conduction and convection, it may be pointed out that the primary phenomenon is always conduction. For it can be shown experimentally that at the surface of the body the medium is practically at rest with respect to that surface. Whether we have a flowing medium (in the case of convection) or whether the medium is stagnant (in the case of pure conduction), the heat at the surface of the body must always be carried away by conduction only. If the heat conductivity of the medium should be zero, heat transfer by convection would be impossible too.

If n is the distance from a point in the medium to the surface of the body, measured along the normal to the surface, and $-\,\mathrm{d}\vartheta/\mathrm{d}n$ the temperature gradient, the energy $\mathrm{d}\Phi$ transferred from a surface element $\mathrm{d}F$ equals

$$\mathrm{d}\Phi = -\,(\lambda\,\mathrm{d}\vartheta/\mathrm{d}n)_w\,\mathrm{d}F, \tag{1}$$

where λ is the heat conductivity of the medium, while the suffix w means that for λ and $\mathrm{d}\vartheta/\mathrm{d}n$ the values at the surface of the body should be taken.

If the convection currents in the medium increase, the value of $\mathrm{d}\vartheta/\mathrm{d}n$ increases, and with it that of $\mathrm{d}\Phi$. This may be understood by remembering that the stronger the current, the faster the liquid heated by the body is carried away, the medium remaining cool to within a shorter distance from the surface of the body. Hence the temperature gradient is larger. In fig. 1 the behaviour of the temperature as a function of the distance from the surface, is represented in three different cases: (a) without any flow (pure conduction), (b) in the case of natural or free convection; in

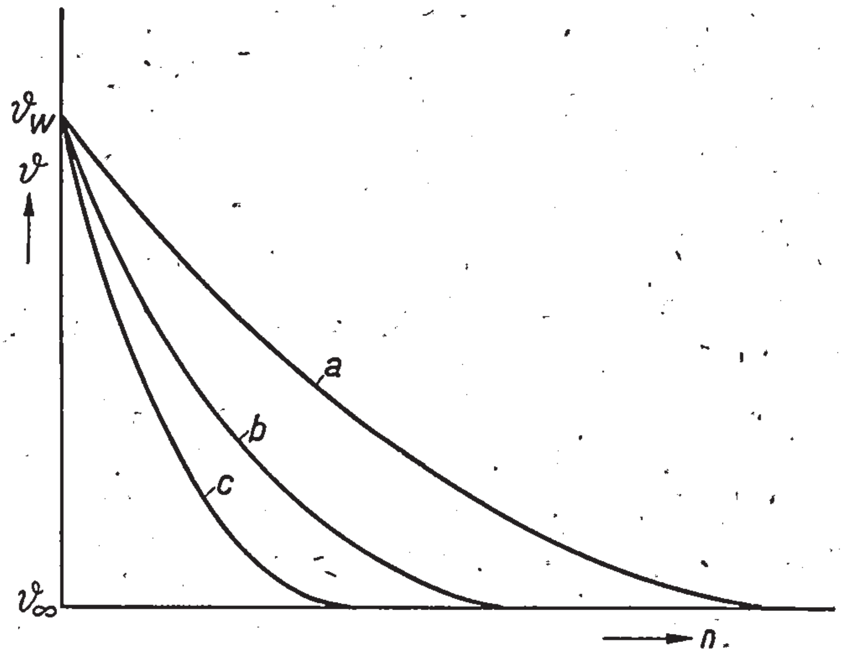

Fig. 1. Temperature ϑ as a function of the distance n to the heat-dissipating surface. The temperature of the body is ϑ_w and that of the surroundings ϑ_∞.
a. pure conduction without convection currents.
b. natural cooling or free convection.
c. forced convection.

this case the motion of the liquid is caused by gravitation in association with the density variations occurring as a result of the temperature variations brought about by the heat-dissipating body, (c) in the case of forced convection, where the motion is determined by external conditions. In this case natural convection occurs at the same time, but generally it may be neglected in comparison to the forced convection.

In the present paper we shall not deal with cooling by forced convection, restricting ourselves further to stationary conditions, the energy transfer Φ not depending on time.

3. The equation of heat dissipation

According to Newton's rule the heat transfer is proportional to the total surface area of the body and to the temperature difference between the body and the surrounding medium. If ϑ_w represents the temperature of the body and ϑ_∞ that of the medium at a great distance from the surface, the flow of heat through an element $\mathrm{d}F$ of the surface is given by

$$\mathrm{d}\Phi = a(\vartheta_w - \vartheta_\infty)\,\mathrm{d}F. \tag{2}$$

According to Newton's law a is a constant. However, in the case of natural convection this simple rule with constant a does not hold. Nevertheless one may retain equation (2), a then simply meaning the quantity required.

If we introduce the quantity $\Theta = \vartheta - \vartheta_\infty$, the heat transfer (2) assumes the form

$$\mathrm{d}\Phi = a\,\Theta_w\,\mathrm{d}F,$$

the total energy transferred becoming

$$\Phi = \int a\,\Theta_w\,\mathrm{d}F.$$

If Θ_w is constant all over the surface, the body having a constant temperature, then

$$\Phi = \Theta_w \int a\,\mathrm{d}F. \tag{3}$$

Introducing the average value $\bar{a} = (\int a\,\mathrm{d}F)/F$, we obtain:

$$\Phi = \Theta_w\,\bar{a}\,F. \tag{4}$$

The above transformation, however, does not yet bring about the solution of the problem, all the difficulties being embodied in the quantity $\bar{a}$.

To find a relation from which $\bar{a}$ may be deduced, we shall submit the state of flow and the temperature distribution of the medium to a closer scrutiny.

The velocities and the temperatures of the medium will appear to depend on a number of quantities, such as the density (ϱ), the viscosity (η), the heat conductivity (λ), the coefficient of cubic expansion (β), the specific heat at constant pressure (c_p) and the acceleration of gravity (g). Further, the conditions in the medium depend on the size and the shape of the heat-dissipating body and on Θ_w. In addition, the differential equations obtained appear to be of such a complicated form that an exact evaluation of $\bar{\alpha}$ is in general not practicable. Calculations have therefore been carried out in the case of bodies of a very simple shape only, whilst moreover use has been made of simplifying suppositions.

Notwithstanding, from consideration of the differential equations one important conclusion may be drawn, namely, that the above-mentioned quantities and parameters only occur in special combinations. Therefore the theoretical and experimental results may be expressed as relations between these special combinations (characteristic numbers).

4. The velocity field, the pressure field and the temperature field

Let us consider a body cooled by natural convection. As observed above, the temperature differences give rise to convection currents in the surrounding medium. At a given point in the medium the temperature and the velocity have definite values not dependent on time. This means that stationary conditions only are considered. Turbulence is not accounted for, it being of secondary importance, at least in the case of natural convection and in the immediate neighbourhood of the heated body.

Therefore we may say that a temperature field and a velocity field exist, to be described by the quantities ϑ (or Θ) and u, v, w, the velocity components in the direction of the coordinate axes OX, OY, OZ, which are functions of x, y and z. The Z-axis will be chosen pointing vertically upwards.

Further, the pressure in the medium may be described by a pressure field. However, the pressures and the velocities of the medium are so closely related that we shall consider them together under the heading "velocity field".

A) Apart from boundary conditions the *velocity field* is determined by two differential equations. The first equation is the fundamental hydrodynamic equation of Navier and Stokes for a liquid with internal friction. This equation is based on Newton's law: force = mass × acceleration, applied to an element of volume dxdydz, ϱ dxdydz being the mass of the liquid in this element. The x-component of the acceleration is

$$\frac{\mathrm{d}u}{\mathrm{d}t} = \frac{\partial u}{\partial t} + \frac{\partial u}{\partial x}\frac{\mathrm{d}x}{\mathrm{d}t} + \frac{\partial u}{\partial y}\frac{\mathrm{d}y}{\mathrm{d}t} + \frac{\partial u}{\partial z}\frac{\mathrm{d}z}{\mathrm{d}t} = \frac{\partial u}{\partial t} + u\frac{\partial u}{\partial x} + v\frac{\partial u}{\partial y} + w\frac{\partial u}{\partial z}.$$

Analogous equations are valid for the y- and z-components dv/dt and dw/dt. The first term of the right-hand member may be omitted because only stationary conditions are considered; the other terms are due to the fact that the volume element is displaced by the motion and then arrives at places where the velocity components have different values. The total force on the volume element, e.g. in the x-direction, consists of the following components:

1) the force due to a pressure gradient

$$-\frac{\partial p}{\partial x}\, dx\, dy\, dz;$$

2) the external force $\varrho K_x\, dxdydz$ where K_x is the total external force for unit mass (for instance, in the case of gravity alone being active, $K_x = K_y = 0$, $K_z = -g$);

3) the frictional force

$$\eta\left(\frac{\partial^2 u}{\partial y^2}+\frac{\partial^2 u}{\partial z^2}\right) dx\, dy\, dz,$$

due to the changes of the velocity gradients;

4) a frictional force

$$\eta\left\{\frac{\partial^2 u}{\partial x^2}+\tfrac{1}{3}\frac{\partial}{\partial x}\left(\frac{\partial u}{\partial x}+\frac{\partial v}{\partial y}+\frac{\partial w}{\partial z}\right)\right\} dx\, dy\, dz,$$

being due to the deformation of the volume element considered [1]). The final form of Navier and Stoke's equation for the x-component is:

$$\varrho\left(u\frac{\partial u}{\partial x}+v\frac{\partial u}{\partial y}+w\frac{\partial u}{\partial z}\right)=-\frac{\partial p}{\partial x}+\varrho K_x+$$
$$+\eta\left\{\tfrac{1}{3}\frac{\partial}{\partial x}\left(\frac{\partial u}{\partial x}+\frac{\partial v}{\partial y}+\frac{\partial w}{\partial z}\right)+\frac{\partial^2 u}{\partial x^2}+\frac{\partial^2 u}{\partial y^2}+\frac{\partial^2 u}{\partial z^2}\right\}, \qquad (5a)$$

with analogous equations (5b) and (5c) for the y- and z-components.

In applying these equations to natural convection a simplification arises as to the terms

$$-\frac{\partial p}{\partial x}+\varrho K_x.$$

To see this we start from the initial state where the temperature of the body is equal to that of the surroundings. In that case ϱ is a function of z only, $\varrho_s(z)$. The index s indicates hydrostatic equilibrium. The pressure in this case is the hydrostatic pressure p_s. The components ϱK_x and ϱK_y are zero, whereas $\varrho K_z = -g\varrho_s(z)$.

Then p_s obeys the equations (Archimedes's law):

$$\frac{\partial p_s}{\partial x}=0,\ \frac{\partial p_s}{\partial y}=0,\ -\frac{\partial p_s}{\partial z}-g\,\varrho_s(z)=0. \qquad (6)$$

The element of volume considered thus floats in the surrounding medium. If, however, an element of volume with a higher temperature and corresponding lower density ϱ is surrounded by a medium of a different density ϱ', the Archimedes force $g\,\varrho'$ and the force of gravity $g\,\varrho$ do not balance and the element is subjected to a force in the vertical direction, which sets the medium in motion. Thus a state of flow is established where the pressure is no more equal to the hydrostatic pressure, but differs from it by a certain amount, say P. Thus $p = p_s + P$.

In equation (5c) we have therefore:

$$-\frac{\partial p}{\partial z} + \varrho K_z = -\frac{\partial p_s}{\partial z} - \frac{\partial P}{\partial z} - g\varrho = -\frac{\partial p_s}{\partial z} - g\varrho_s - \frac{\partial P}{\partial z} + g(\varrho_s - \varrho).$$

As, according to (6), $-\partial p_s/\partial z - g\varrho_s = 0$, we obtain for the combined pressure forces and external forces:

$$-\frac{\partial P}{\partial z} + g(\varrho_s - \varrho).$$

In the same way the corresponding terms in equation (5a, b) are reduced to

$$-\frac{\partial P}{\partial x} \text{ and } -\frac{\partial p}{\partial y},$$

respectively.

Now we shall make the simplifying supposition that ϱ does not appreciably depend on the pressure. In the case of a liquid this is evident, whereas in the case of a gas it implies that the differences in height occurring in our problem in connection with the dimensions of the body and the extent of the temperature field are so small that ϱ_s has a constant value ϱ_∞, ϱ being a function of the temperature only.

Introducing the coefficient of thermal expansion

$$\beta = \frac{\varrho_\infty - \varrho}{\varrho(\vartheta - \vartheta_\infty)},$$

we have:

$$g(\varrho_s - \varrho) = g(\varrho_\infty - \varrho) = g\varrho\beta(\vartheta - \vartheta_\infty) = g\varrho\beta\Theta.$$

For gases we have:

$$\varrho_\infty - \varrho = \varrho(T - T_\infty)/T_\infty = \varrho\Theta/T_\infty \text{ or } \beta = 1/T_\infty.$$

Introducing these simplifications, eqs (5a, b, c) take on the form:

$$\varrho\left(u\frac{\partial u}{\partial x} + v\frac{\partial u}{\partial y} + w\frac{\partial u}{\partial z}\right) = -\frac{\partial P}{\partial x} + \eta\left[\tfrac{1}{3}\frac{\partial}{\partial x}\left(\frac{\partial u}{\partial x} + \frac{\partial v}{\partial y} + \frac{\partial w}{\partial z}\right) + \frac{\partial^2 u}{\partial x^2} + \frac{\partial^2 u}{\partial y^2} + \frac{\partial^2 u}{\partial z^2}\right] \qquad (7a)$$

$$\varrho\left(u\frac{\partial v}{\partial x}+v\frac{\partial v}{\partial y}+w\frac{\partial v}{\partial z}\right)=-\frac{\partial P}{\partial y}+$$
$$+\eta\left[\tfrac{1}{3}\frac{\partial}{\partial y}\left(\frac{\partial u}{\partial x}+\frac{\partial v}{\partial y}+\frac{\partial w}{\partial z}\right)+\frac{\partial^2 v}{\partial x^2}+\frac{\partial^2 v}{\partial y^2}+\frac{\partial^2 v}{\partial z^2}\right] \quad (7b)$$

$$\varrho\left(u\frac{\partial w}{\partial x}+v\frac{\partial w}{\partial y}+w\frac{\partial w}{\partial z}\right)=-\frac{\partial P}{\partial z}+g\,\varrho\beta\,\Theta+$$
$$+\eta\left[\tfrac{1}{3}\frac{\partial}{\partial z}\left(\frac{\partial u}{\partial x}+\frac{\partial v}{\partial y}+\frac{\partial w}{\partial z}\right)+\frac{\partial^2 w}{\partial x^2}+\frac{\partial^2 w}{\partial y^2}+\frac{\partial^2 w}{\partial z^2}\right] \quad (7c)$$

The second differential equation determining the velocity field is the *equation of continuity*:

$$\frac{\partial(\varrho u)}{\partial x}+\frac{\partial(\varrho v)}{\partial y}+\frac{\partial(\varrho w)}{\partial z}=0, \quad (8)$$

expressing the conservation of matter for a fixed element dxdydz in the stationary condition.

The *boundary conditions* for the solutions of (7) and (8) are that the velocity at the surface of the body and at infinity shall be zero.

B) The *temperature field* is governed by a differential equation expressing the equality of energy input and output of a fixed element of volume dxdydz.

The heat developed by internal friction, being relatively small, is neglected.

The energy transport through a surface element dydz being $\varrho c_p\Theta\, u$ dydz, one obtains for the total energy input, taking into account eq. (8):

$$-\varrho\, c_p\left(u\frac{\partial\Theta}{\partial x}+v\frac{\partial\Theta}{\partial y}+w\frac{\partial\Theta}{\partial z}\right)\mathrm{d}x\mathrm{d}y\mathrm{d}z\,.$$

This energy is carried away by heat conduction.

$-\lambda(\partial\Theta/\partial x)$ dydz being the conduction loss through the surface dydz, we obtain for the total loss by conduction:

$$-\lambda\left(\frac{\partial^2\Theta}{\partial x^2}+\frac{\partial^2\Theta}{\partial y^2}+\frac{\partial^2\Theta}{\partial z^2}\right)\mathrm{d}x\,\mathrm{d}y\,\mathrm{d}z\,.$$

Equalling the two expressions one obtains the equation for the temperature field in the form:

$$\varrho c_p\left(u\frac{\partial\Theta}{\partial x}+v\frac{\partial\Theta}{\partial y}+w\frac{\partial\Theta}{\partial z}\right)=\lambda\left(\frac{\partial^2\Theta}{\partial x^2}+\frac{\partial^2\Theta}{\partial y^2}+\frac{\partial^2\Theta}{\partial z^2}\right). \quad (9)$$

The boundary conditions are: $\Theta=\Theta_w$ at the surface of the heated body and $\Theta=0$ at infinity.

As stated above, no general solutions of eqs (7), (8) and (9) have been found. However, without writing down the solution, important simplifications and a reduction of the number of variables and parameters may be obtained by comparing "corresponding" or "similar" states. Supposing the heat transfer by natural convection to be known in one case, the transfer in the corresponding "similar" cases may be computed. In the case of natural convection this principle was first applied by Nusselt [2]).

5. Heat dissipation of similar bodies

Let us consider a number of similar bodies $L_1, L_2, \ldots$, placed in the media $M_1, M_2, \ldots$, the outer boundaries of which are assumed either to be similar or to lie at such distances as to have no influence. The shape of the bodies being given, they may be characterized by one linear dimension (e.g. the diameter of a cylinder, the edge of a cube). These dimensions we call $l_1, l_2, \ldots$. Now the velocity fields in M_1 and M_2 will be compared. We shall call these fields similar if in every set of corresponding points $(x_1/x_2 = y_1/y_2 = z_1/z_2 = l_1/l_2)$ the corresponding velocities have the same ratio $(u_1/u_2 = v_1/v_2 = w_1/w_2 = V_1/V_2 = a$, where V_1 is the total velocity in M_1, etc.). Similar velocity fields are only possible if eqs (7) and (8) are the same in either case and if the boundary conditions are equal. The latter condition is always fulfilled, as $V = 0$ on the surface of the body and at the outer boundary of the medium. The remaining necessary and sufficient condition is that the various corresponding terms in eqs (7) and (8) have the same ratio. In this case the equations may be made identical by multiplying them by an appropriate number and hence have identical solutions (the boundary conditions being equal). The similarity conditions for the velocity fields of cases 1 and 2 are thus, for instance:

$$\frac{(\varrho u \partial w/\partial x)_1}{(\varrho u \partial w/\partial x)_2} = \frac{(\partial P/\partial z)_1}{(\partial P/\partial z)_2} = \frac{(g\varrho\beta\Theta)_1}{(g\varrho\beta\Theta)_2} = \frac{(\eta \partial^2 w/\partial y^2)_1}{(\eta \partial^2 w/\partial y^2)_2}. \tag{10}$$

The equation (10) is valid for all terms, provided

$$\frac{(\varrho V^2/l)_1}{(\varrho V^2/l)_2} = \frac{(P/l)_1}{(P/l)_2} = \frac{(g\varrho\beta\Theta)_1}{(g\varrho\beta\Theta)_2} = \frac{(\eta V/l^2)_1}{(\eta V/l^2)_2}, \tag{10a}$$

or, in symbols, $A = B = C = D$.

Combining A and D, we obtain:

$$\left(\frac{\varrho\ V^2/l}{\eta\ V/l^2}\right)_1 = \left(\frac{\varrho V^2/l}{\eta V/l^2}\right)_2 \quad \text{or} \quad \left(\frac{\varrho V l}{\eta}\right)_1 = \left(\frac{\varrho V l}{\eta}\right)_2. \tag{11}$$

The quantity $\varrho Vl/\eta$ is called Reynold's number; it will be denoted by **Re**. It has zero dimension, being obtained by dividing a "force of inertia" by a frictional force. Equality of **Re** thus means that the ratio of the inertia force to the frictional force is the same in either case. It is immaterial for which pair of points the condition is written down, provided the points are corresponding points.

Combination of C and D gives a second condition for similar velocity fields:

$$\left(\frac{g\varrho\beta\Theta l^2}{\eta V}\right)_1 = \left(\frac{g\varrho\beta\Theta l^2}{\eta V}\right)_2, \tag{12}$$

i.e., the frictional forces must be in the same ratio as the buoyancy forces.

Equalling A and B, we obtain as a third condition

$$(P/\varrho V^2)_1 = (P/\varrho V^2)_2. \tag{13}$$

$P/\varrho V^2$ is called Euler's number (**Eu**).

Eqs (11), (12) and (13) are equivalent to (10a). Hence, the velocity fields are similar, provided the latter three equations are satisfied. (Eq. (8) does not provide us with new conditions as the terms are all of the same kind.)

In the case of free convection eqs (11), (12), (13) demand more than is necessary, P and V not being given independently (as in the case of forced convection). As a matter of fact, V is determined by the given quantities l, g, ϱ, β, Θ, λ and c. Therefore V may be eliminated from (11) and (12) in the case of natural convection, giving:

$$(l^3\, g\, \varrho^2\, \beta\, \Theta/\eta^2)_1 = (l^3\, g\, \varrho^2\, \beta\, \Theta/\eta^2)_2. \tag{14}$$

The dimensionless quantity $l^3 g\, \varrho^2 \beta\, \Theta/\eta^2$ is called Grashof's number (**Gr**). Eq. (14) being satisfied, (11) and (12) are fulfilled automatically. P not being independently prescribed either, (13) is also fulfilled. Hence in the case of natural convection the numbers **Re** and **Eu** are of no importance.

We thus arrive at the conclusion that *in the case of natural cooling of similar bodies equality of* **Gr** *at corresponding points is a sufficient condition to ensure similarity of the corresponding velocity fields.* Which pair of corresponding points is chosen is immaterial, the temperature fields being supposed similar at the same time. Usually Θ_w, the value of Θ at the surface of the body, is inserted in (14).

The next step is to investigate the conditions ensuring the similarity of the temperature fields.

From (9) we obtain for the necessary condition:

$$\left(\frac{\varrho\, c_p\, u\, \partial\Theta/\partial x}{\lambda\, \partial^2\Theta/\partial x^2}\right)_1 = \left(\frac{\varrho\, c_p\, u\, \partial\Theta/\partial x}{\lambda\, \partial^2\Theta/\partial x^2}\right)_2.$$

This leads to:

$$(\varrho\, c_p\, V\, l/\lambda)_1 = (\varrho\, c_p\, V\, l/\lambda)_2\,. \tag{15}$$

This quantity is called Péclet's number (**Pé**). On the same grounds as given above, V may be eliminated (dividing by **Re**), giving:

$$(c_p\, \eta/\lambda)_1 = (c_p\, \eta/\lambda)_2\,. \tag{16}$$

The quantity $c_p\, \eta/\lambda$ is called Prandtl's number (**Pr**). In the case of natural convection and the velocity fields being similar, the fulfilment of (16) suffices to ensure similar temperatur fields.

Therefore, *when considering similar bodies cooled by natural convection, the velocity and the temperature fields are similar provided* **Gr** *and* **Pr** *are equal at corresponding points.*

Supposing these conditions to be satisfied, one may determine the ratio of the amounts of heat dissipated in either case. In similar temperature fields the energies transferred in unit time by equal surface elements are according to (1) in the proportion $(\lambda\, \Theta_w/l)_1$ to $(\lambda\, \Theta_w/l)_2$, and hence the energies dissipated by the whole surface per second have the ratio:

$$\Phi_1 : \Phi_2 = (\lambda\, \Theta_w l)_1 : (\lambda\, \Theta_w l)_2\,. \tag{17}$$

This follows also from (9), bearing in mind that corresponding volume elements are in the ratio $l_1^3 : l_2^3$.

According to (4),

$$\Phi_1 : \Phi_2 = (\bar{\alpha}\, \Theta_w l^2)_1 : (\bar{\alpha}\, \Theta_w l^2)_2. \tag{18}$$

Combining (17) and (18), we have

$$(\bar{\alpha}\, l/\lambda)_1 = (\bar{\alpha}\, l/\lambda)_2\,. \tag{19}$$

From this the ratio $\bar{\alpha}_1 : \bar{\alpha}_2$ and, by (4), that of $\Phi_1 : \Phi_2$ may be calculated. The quantity $\bar{\alpha}\, l/\lambda$ is called Nusselt's number (**Nu**).

We thus arrive at the conclusion: *If, with natural cooling of two similar bodies the numbers* **Gr** *and* **Pr** *at corresponding points are the same, the velocity and temperature fields are similar and hence the* **Nu**-*numbers are likewise the same; thus* **Nu** *is a function of* **Gr** *and* **Pr** *only.* Therefore the solution of our problem takes the form:

$$\frac{\bar{\alpha} l}{\lambda} = f_1\left(\frac{l^3 g \varrho^2 \beta \Theta}{\eta^2}, \frac{c_p \eta}{\lambda}\right), \tag{20}$$

or

$$\mathbf{Nu} = f_1(\mathbf{Gr}, \mathbf{Pr})\,. \tag{20a}$$

This important simplification makes the survey of results much easier. A further simplification is obtained in the case where corresponding media are gases having the same number of atoms in the molecule, for **Pr** is a quantity containing only properties of the medium and is moreover independent of the temperature, being dependent only on the number of atoms in the molecule.

For molecules with n degrees of freedom, we have:

$$\mathbf{Pr} = (n + 2)/(n + \tfrac{9}{2}).$$

When restricting ourselves to gases having the same number of atoms per molecule, eq. (20a) may thus be reduced to

$$\mathbf{Nu} = f_2(\mathbf{Gr}). \tag{21}$$

For bodies of a given shape the heat transfer is then represented by one single curve.

When comparing the heat transfer in arbitrary media eq. (20) should be used. This equation may be represented by a number of curves, $\mathbf{Nu} = f(\mathbf{Gr})$, having **Pr** as a parameter. In the first approximation a much simpler representation of facts may also be obtained in this case. Remembering that with natural cooling the velocities are generally small, the inertia forces may generally be neglected in comparison to the frictional forces and the buoyancy forces. Therefore, in order to ensure similarity, only (12) has to be satisfied. V not being independently given, the heat transfer is a function of a combination of (12) and (15) that does not contain V. Such a combination being

$$\frac{g\,\varrho\,\beta\,\Theta l^2}{\eta V} \cdot \frac{\varrho\,c_p\,Vl}{\lambda} = \mathbf{Gr} \cdot \mathbf{Pr},$$

we have:

$$\mathbf{Nu} = f_3(\mathbf{Gr} \cdot \mathbf{Pr}). \tag{22}$$

Thus neglecting inertia forces in the case of natural convection, **Nu** *is a function of one variable only, viz.* **Gr · Pr**.

It is necessary now to consider the following complications. Until now the quantities β, η, λ and c_p were treated as constants. In reality they depend more or less on the temperature and hence assume different values at different points of the temperature field. In addition ϱ was considered constant, whereas in the problem of natural convection the dependence of ϱ on the temperature is essential. If β does not depend on the temperature, the density fields are similar, and in this case it is immaterial which density is substituted in (11), provided the values are taken at corresponding points. In the case of gases β is independent of the temperature Θ and even equal for different gases ($\beta = 1/T_\infty$), whereas the temperature dependence of η, λ and c_p is almost the same for different gases. However, when comparing a gas with a liquid, this no longer holds, η and λ increasing with increasing temperature in the case of a gas, whereas in the case of liquids the reverse is true.

This is the reason why (22) must not be used when comparing gases and liquids. Therefore it is not permissible to apply the data with a liquid model to the problem of cooling by a gaseous medium.

Nusselt proposed to use mean values ϱ_m, η_m, etc., for the temperature-dependent quantities occurring in the characteristic numbers or, if this should result in too large a scattering of measuring points, to introduce a new parameter (Θ_w/T_∞) (cf. Hermann [3]). Eq. (22) is then to be replaced by

$$\mathbf{Nu} = f_4'(\mathbf{Gr} \cdot \mathbf{Pr}, \Theta_w/T_\infty), \qquad (23)$$

where some arrangement still has to be made as to the temperature (be it T_w or T_∞ or an intermediate temperture) at which the values of ϱ, η, etc., occurring in **Gr**, **Pr** and **Nu** shall be taken. Although (23) is more accurate than (22), it is generally permissible to use (22), provided ϱ, η, etc., are taken at adequately chosen tempertures.

6. The dissipation of heat by bodies characterized by one linear dimension only

We shall begin by considering the form of the function f_3 (eq. (22)) for a number of bodies having simple shapes that may be characterized by one linear dimension only. These considerations will be based partly on results of measurements, partly on theoretical foundations as laid down in the formulae (4) to (9). Calculations are only possible in the simplest cases and with the aid of simplifying assumptions. It is always supposed that the outer boundaries of the medium have no influence on the problem.

The quantities **Nu**, **Gr**, and **Pr** will be provided with two suffixes, the first indicating the characteristic dimension chosen (h = height, d = diameter, etc.) and the second whether λ, ϱ, etc., are taken at the surface temperature (suffix w) or whether an intermediate value (suffix m) is used. For instance, $\mathbf{Nu}_{d,m}$ means $\bar{\alpha}\, d/\lambda_m$, where

$$\lambda_m = \frac{1}{\Theta_w} \int_{\vartheta_\infty}^{\vartheta_w} \lambda(\vartheta)\, \mathrm{d}\vartheta . \qquad (24)$$

In **Gr** we always substitute Θ_w for Θ. **Nu**, **Gr** and **Pr** being dimensionless, it is immaterial which units are used, provided they are consistent *).

---

*) In the figures showing the coefficient $\bar{\alpha}$, this quantity is always expressed in watts/m^2 per degree. The heat transfer in kcal/m^2 per degree per hour is obtained from this by multiplication by 0·86.

a) *The flat vertical plate*

The heat transfer by flat vertical plates in air was measured by Schmidt and Beckmann [4]) and King [5]), that in oil by Lorentz [6]). Plotting $\mathbf{Nu}_{h,w}$ as a function of $(\mathbf{Gr}\cdot\mathbf{Pr})_{h,w}$ (h = height of the plate) on a doubly logarithmic scale, the measuring points are approximately on a straight line with an inclination of $\frac{1}{4}$. The proportionality factor lies between 0·52 and 0·65. The experimental results are thus approximately represented by

$$\mathbf{Nu}_{h,w} = 0{\cdot}6\,(\mathbf{Gr}\cdot\mathbf{Pr})_{h,w}^{1/4}. \qquad (25)$$

This formula is valid for a limited range only, namely for $10^4 < \mathbf{Gr}\cdot\mathbf{Pr} < 10^9$. This means that in air of 1 atm and $\Theta_w = 10$ and 100 °C, the corresponding limits for h are $1\frac{1}{2} < h < 70$ cm and $\frac{3}{4} < h < 35$ cm, respectively. When using a height equal to twice the upper limit, the error made in using (25) is small, so that formula (25) may be said to cover an important range of practical applications.

A formula of the form (25) may also be obtained by calculation. For a vertical plate in air this calculation was carried out by Schmidt, Pohlhausen and Beckmann [4]) making use of the following simplifying suppositions:
(1) the flow is laminar;
(2) where the temperature difference and the velocity are appreciable, the thickness of the layer is small with respect to the height;
(3) the dimension of the plate in horizontal direction (y-direction in fig. 2) is so large that edge effects may be neglected, all derivatives with respect to y being zero.

Under these suppositions it follows from (7), (8) and (9) that Θ/Θ_w is a function of

$$x\left(\frac{g\varrho^2{}_w\beta\Theta_w}{\eta_w{}^2 z}\right)^{1/4}.$$

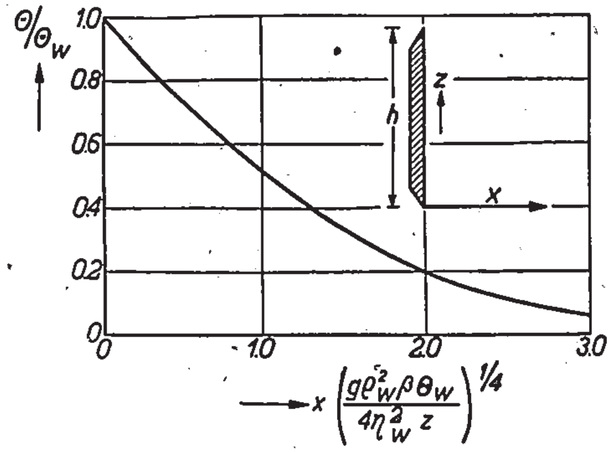

Fig. 2. Temperature field in front of a warm vertical plate, as calculated with formulae (7) to (9). At given circumstances Θ/Θ_w is only a function of $x/z^{1/4}$. Equi-temperature planes thus bend away from the plate with increasing height. (Taken from Schmidt and Beckmann [4]).)

In fig. 2 this function is represented. It appears that at a fixed distance x from the surface of the plate, the temperature increases with increasing z. According to (1)

$$d\Phi = -\lambda_w(\partial\Theta/\partial x)_w\, dF = C\,\lambda_w\,\Theta_w\left(\frac{g\varrho^2_w\beta\Theta_w}{\eta_w{}^2 z}\right)^{1/4} dz, \tag{26}$$

where $d\Phi$ is the energy transferred per cm width between z and $z + dz$, and C is a constant. The heat losses per unit of surface area thus appear to decrease with increasing z. This is a consequence of the fact that the air, when moving upwards, is warmed already by lower zones of the plate, which results in a decrease of $-(\partial\Theta/\partial x)_w$ with increasing z. According to eq. (26) the energy transfer is infinite for $z = 0$. This, however, is of no consequence, the total energy transfer being formed by integration, with the result:

$$\Phi = C_1\,\lambda_w\,\Theta_w\left(\frac{h^3 g\varrho^2_w\beta\Theta_w}{\eta^2_w}\right)^{1/4} = C_1\,\lambda_w\,\Theta_w\,\mathrm{Gr}^{1/4}_{h,w}. \tag{27}$$

As, by definition, $\Phi = \bar{a}\,h\,\Theta_w$, it follows from (27) that

$$\mathrm{Nu}_{h,w} \equiv \frac{\bar{a}h}{\lambda_w} = C_1\,\mathrm{Gr}^{1/4}_{h,w}. \tag{28}$$

For air Schmidt and Beckmann found the value 0·48 for C_1. Extending eq. (28) to other media in accordance with eq. (22), one obtains

$$\mathrm{Nu}_{h,w} = 0{\cdot}525\,(\mathrm{Gr}\cdot\mathrm{Pr})^{1/4}_{h,w}. \tag{29}$$

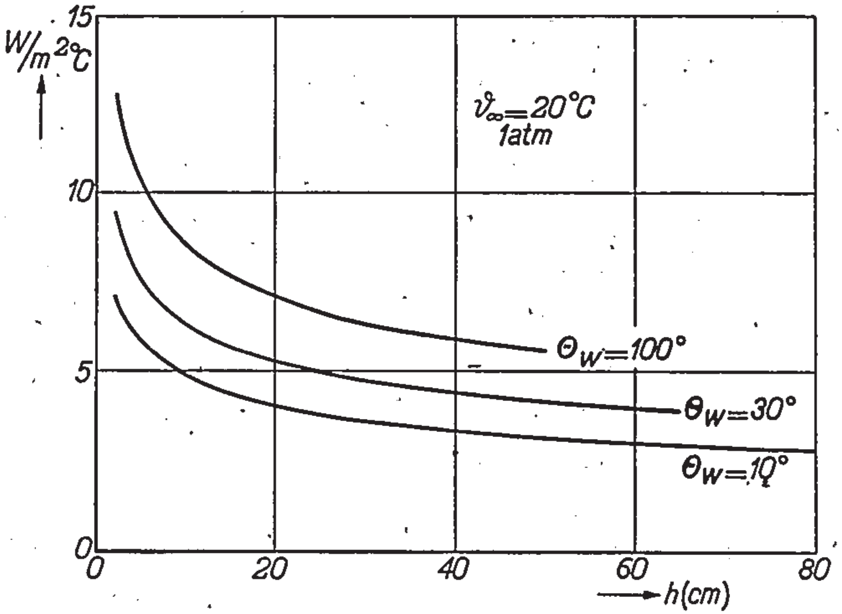

Fig. 3. Heat dissipation in watts per m² and per degree of temperature difference of vertical plates in air of 1 atm and room temperature for different excess temperatures calculated with (25). The dimension of the plate in a horizontal direction is supposed to be large compared to the height.

The factor 0·525 arises from division of 0·48 by $(0{\cdot}73)^{1/4}$, 0·73 being the value of **Pr** for air. The calculations of Schmidt, Pohlhausen and Beckmann are thus in fair agreement with the experimental result (eq. (25)). The limited validity of (29) is caused by the fact that outside the region of values indicated above the first and the second suppositions are no longer fulfilled. At the upper limit the flow ceases to be laminar and becomes turbulent, whereas at the lower limit the second supposition does no longer hold. If the third supposition is not fulfilled, the cooling is increased by the edge effects. In the experiments this may be avoided by applying transverse plates to the edges or by making the dimensions in the y-direction very large.

In fig. 3 the heat transfer $\overline{\alpha}$ by vertical plates in air at 1 atm and 20 °C is plotted for a number of Θ_w-values as a function of h, according to (25).

b) *The horizontal cylinder*

The heat dissipation of horizontal cylinders in diatomic gases has been investigated experimentally several times. In these experiments the length of the cylinder is so chosen that edge effects may be neglected, the transfer being proportional to the length. Nusselt was the first to arrange the experimental results by plotting $\mathbf{Nu}_{d,m}$ vs $\mathbf{Gr}_{d,m}$. Afterwards Hermann [7]) classified the whole material taking into account the dependence on Θ_w/T_∞ (cf. eq. (23)).

In fig. 4, being valid for diatomic gases, the most probable course of the

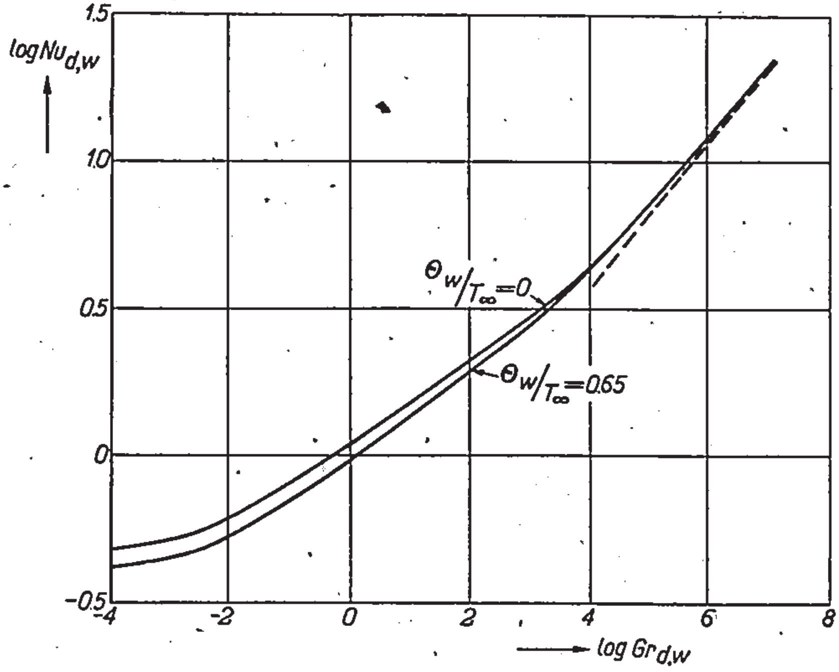

Fig. 4. Log $\mathbf{Nu}_{d,w}$ as a function of log $\mathbf{Gr}_{d,w}$ for two values of Θ_w/T_∞ for horizontal cylinders in air, after Hermann [7]); —— experimental, - - - calculated with (31).

function is shown for two values of Θ_w/T_∞ in terms of $\mathbf{Gr}_{d,w}$ and $\mathbf{Nu}_{d,w}$. It is seen that for $\mathbf{Gr}_{d,w} > 10^4$ the values of $\mathbf{Nu}_{d,w}$ are practically independent of Θ_w/T_∞. In this region the results may be summarized in a formula that does not contain Θ_w/T_∞, viz.

$$\mathbf{Nu}_{d,w} = 0{\cdot}43\ \mathbf{Gr}_{d,w}^{1/4}. \tag{30}$$

The suffix *w* may also be replaced by *m*.

Also in this case a calculation of the heat transfer has proved to be possible. For an infinitely long horizontal cylinder Hermann [7]) computed, in the case of diatomic gases (in a manner analogous to that of Schmidt, Pohlhausen and Beckmann in the case of a vertical plate):

$$\mathbf{Nu}_{d,w} = 0{\cdot}37\ \mathbf{Gr}_{d,w}^{1/4}. \tag{31}$$

In deriving (31), the same simplifying assumptions were made as were used in the derivations of (26) to (29). Therefore eq. (31) is also valid in a limited region only (namely for $10^4 < \mathbf{Gr}_{d,w} < 5{\cdot}10^8$), which forms part of the region where, according to fig. 4, $\mathbf{Nu}_{d,w}$ does not depend on Θ_w/T_∞ and where the empirical formula (30) holds.

Whereas in the case of the vertical plate the existence of a lower limit to the validity of (29) does not imply a serious restriction on most of the practical applications, it does in the case of a cylinder, the cooling of a cylinder with a diameter <1 cm in air of atmospheric pressure not being adequately described by (30) and (31). Horizontal wires are quite beyond the region of validity of these equations.

Langmuir [8]), who carried out measurements on wires having diameters from 40 μ to 510 μ, was able to interpret his results by assuming the wire to be surrounded by a thin layer of finite thickness through which the heat is solely transferred by conduction, whereas outside this layer the gas has the temperature T_∞. The thickness of the layer was assumed to be determined by the condition that the temperature gradient at the boundary (the angle δ in fig. 5) has a value independent of the diameter of the wire.

Combining Langmuir's results with those of Nusselt, one obtains a formula with a much larger range of applicability [9]), namely:

$$\mathbf{Nu}^3_{d,m}\, e^{-6/\mathbf{Nu}_{d,m}} = \mathbf{Gr}_{d,m}/500. \tag{32}$$

The factor 1/500 was found by experiment; it is valid in the case of diatomic gases.

For large values of $\mathbf{Gr}_{d,m}$, $\mathbf{Nu}_{d,m}$ is large too; hence the exponential function approaches 1, $\mathbf{Nu}_{d,m}$ being proportional to $\mathbf{Gr}_{d,m}^{1/3}$ in this region. The diameter *d* occurring in the first power in $\mathbf{Nu}_{d,m}$ $(= \bar{\alpha} d/\lambda_m)$ and in the third power in $\mathbf{Gr}_{d,m}$ $(= d^3 g\, \varrho^2{}_m \beta\ \Theta_w/\eta^2{}_m)$, we find that for large values of $\mathbf{Gr}_{d,m}$, $\bar{\alpha}$ is independent of the diameter.

For small values of $\mathbf{Gr}_{d,m}$, owing to the large influence of the exponential function, $\mathbf{Nu}_{d,m}$ decreases slowly with decreasing $\mathbf{Gr}_{d,m}$. In this region, therefore, $\bar{\alpha}\, d/\lambda_m$ almost has a constant value. As $\bar{\alpha}$ means the heat transfer per cm² and as the circumference of the cylinder is proportional to d, the total heat transfer per cm of length is proportional to $\bar{\alpha}d$. For small values of $\mathbf{Gr}_{d,m}$ the dissipation of heat per cm of length, as it occurs in the case of thin wires, is thus almost independent of the diameter. Langmuir's invention of coiled filaments in gasfilled incandescent lamps is an application of this property. The effective length of a coil being much smaller than that of a straight filament, the energy loss by convection is much less in the former case. Although (32) fairly checks the experimental results, there are deviations to an amount of about 20 per cent. Moreover (32) only holds for diatomic gases. A slightly more complicated formula, which is at the same time valid for different media, runs [10]):

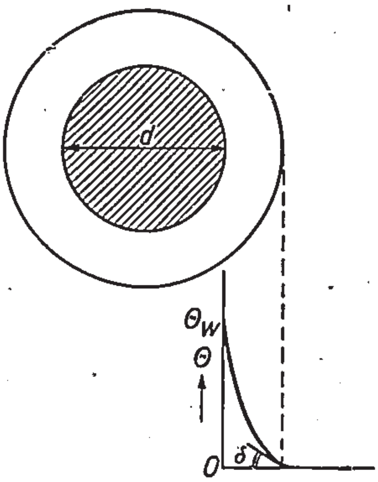

Fig. 5. Radial temperature course in the medium surrounding a wire. According to the supposition of Langmuir the temperature gradient at the boundary of the film in which only pure conduction plays a part (the angle δ) does not depend on the diameter of the wire.

$$\mathbf{Nu}^3_{d,w}\, e^{-6/\mathbf{Nu}_{d,m}} = \frac{(\mathbf{Gr}\cdot\mathbf{Pr})_{d,w}}{235\, f(\mathbf{Gr}\cdot\mathbf{Pr})_{d,w}}. \tag{33}$$

The function $f(\mathbf{Gr}\cdot\mathbf{Pr})_{d,w}$ occurring in (33) has been determined experimentally. Fig. 6 is a graphical representation of it. For $(\mathbf{Gr}\cdot\mathbf{Pr})_{d,w} < 10^4$, f is a constant ($= 1$). With increasing value of $(\mathbf{Gr}\cdot\mathbf{Pr})_{d,w}$, f increases. This makes the increase of $\mathbf{Nu}$ less than it would be if f were constant. We may interpret the occurrence of the function f by imagining that in the case of a relatively thin layer (large value of d) the medium in the layer is appreciably heated on flowing past the cylinder. As a result, the value of α in the higher parts of the cylinder is smaller than that in the lower parts, resulting in a smaller value of $\overline{\alpha}$ (this effect is to be compared with that occurring in the case of the vertical plate (eq. (26)). As, with a thin layer, Hermann's theory is applicable, one should expect the influence of f to be discernable likewise for $\mathbf{Gr} > 10^4$; this is confirmed by experiment, as may be seen from fig. 6.

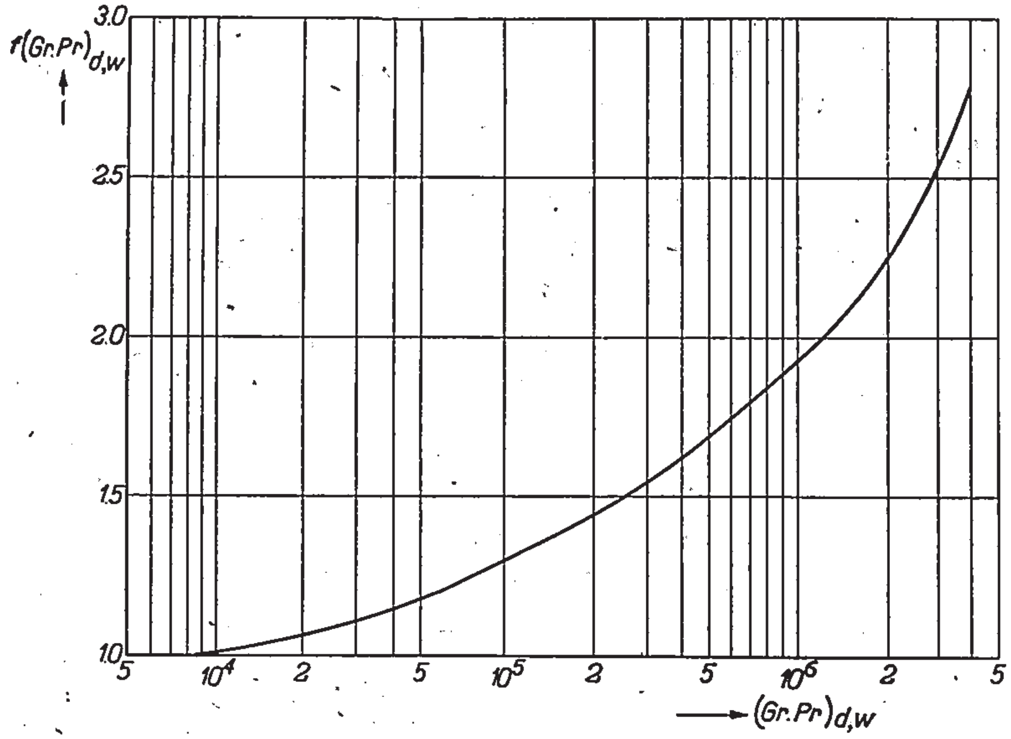

Fig. 6. The function $f\,(\mathbf{Gr}\cdot\mathbf{Pr})_{d,w}$ occurring in the formulae (33) and (34), as determined experimentally. For $(\mathbf{Gr}\cdot\mathbf{Pr})_{d,w} < 10^4$, $f = 1$.

In (33) $\mathbf{Nu}_{d,w}$ as well as $\mathbf{Nu}_{d,m}$ occurs. This makes the parameter Θ_w/T_∞ superfluous. In order to determine $\overline{\alpha}$, $\mathbf{Gr}_{d,w}$ being known, one may write $\mathbf{Nu}_{d,w}$ as $\mathbf{Nu}_{d,m}\ (\lambda_m/\lambda_w)$. Bringing the factor $(\lambda_m/\lambda_w)^3$ on the right side of (33), $\mathbf{Nu}^3_{d,m}\ \exp\ (-6/\mathbf{Nu}_{d,m})$ is known, hence $\mathbf{Nu}_{d,m}$ and $\overline{\alpha}$ may be calculated. The value of λ_m may be computed from (24). In the table at the end of the paper λ_m is given for air and water. In fig. 7 $\mathbf{Nu}_{d,w}$ is plotted against $(\mathbf{Gr}\cdot\mathbf{Pr})_{d,w}$, according to the measurements (see fig. 4) and according to eq. (33). The agreement is good. The theoretical curves meet at large values of $(\mathbf{Gr}\cdot\mathbf{Pr})_{d,w}$, the influence of the function exp $(-6/\mathbf{Nu}_{d,m})$ being negligible for large values of $\mathbf{Nu}_{d,m}$. The dependence on Θ_w/T_∞ is thus rightly described by (33). The agreement for $(\mathbf{Gr}\cdot\mathbf{Pr})_{d,w} > 10^4$ is trivial, because the function f in fig. 6 is chosen in such a way that (33) describes the experiments.

Fig. 8 shows the dissipation of heat of horizontal cylinders in air (at

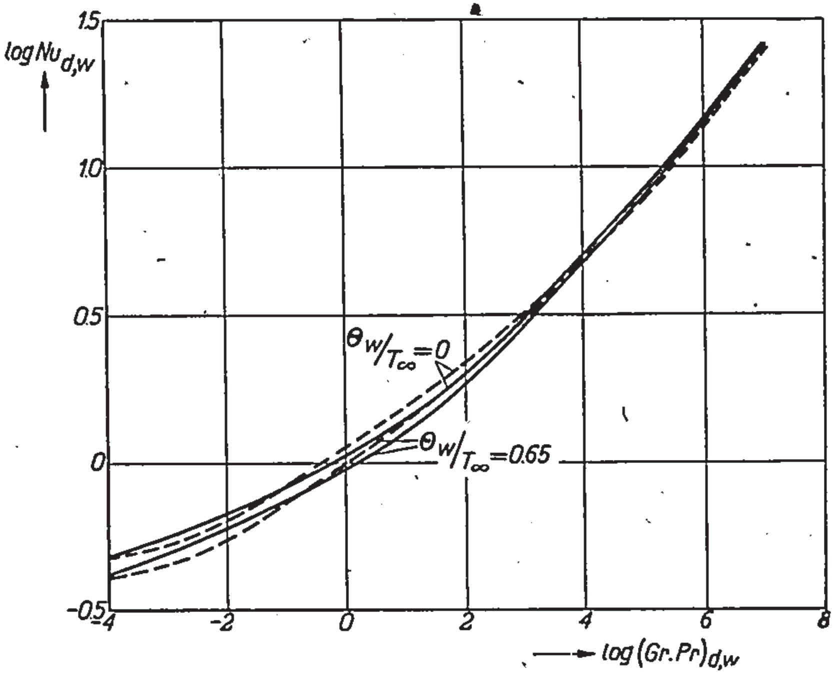

Fig. 7. —— log $\mathrm{Nu}_{d,w}$ as a function of log $(\mathrm{Gr}\cdot\mathrm{Pr})_{d,w}$ for horizontal cylinders according to (33). - - - The experimental curves of fig. 4 now plotted as a function of $(\mathrm{Gr}\cdot\mathrm{Pr})_{d,w}$.

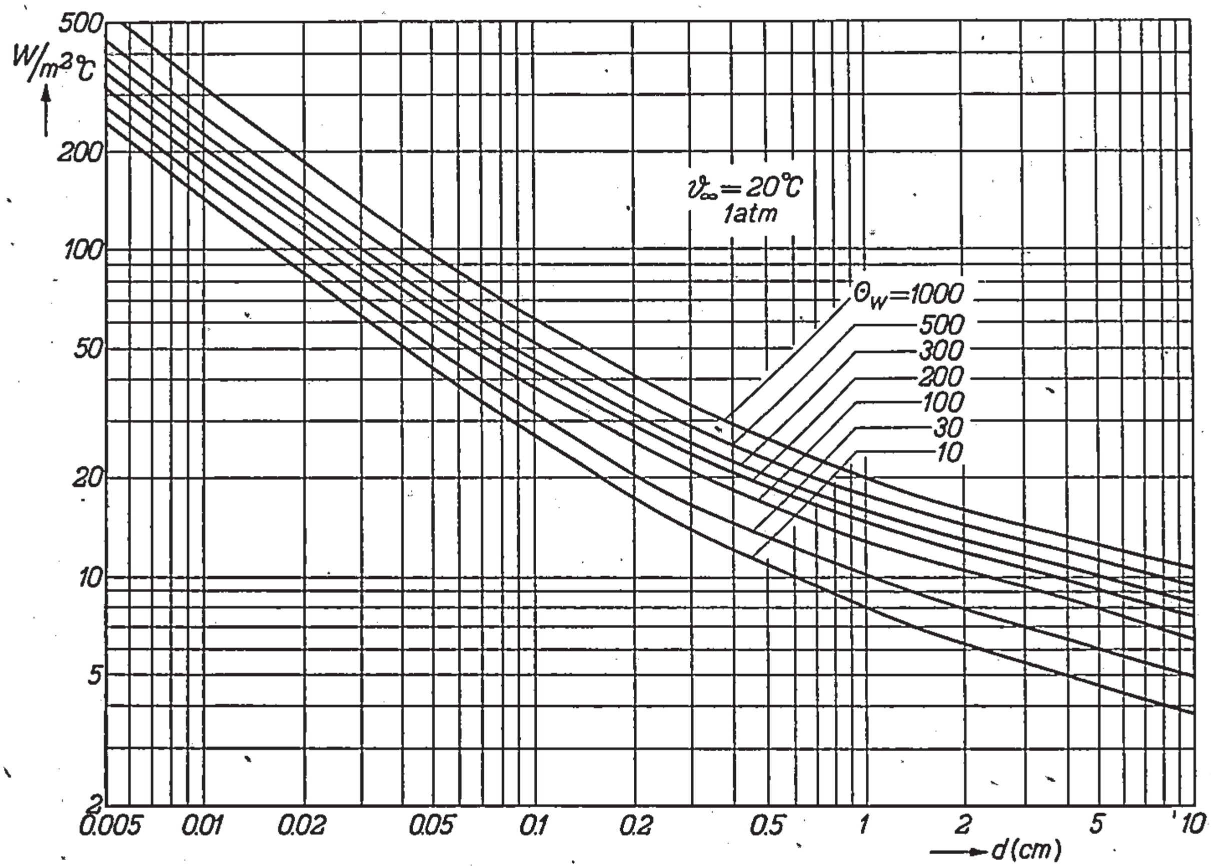

Fig. 8. The heat dissipation in watts per m² and per degree of temperature difference for horizontal cylinders in air of 1 atm and room temperature as a function of the diameter, for different excess temperatures, calculated with (33). The length of the cylinders is large as compared to the diameter.

20° C) as a function of d, calculated with the aid of (33), use having been made of the curve of fig. 6.

c) *The sphere*

In a way analogous to the derivation of (33) one finds for the heat dissipation of a sphere [10]):

$$\mathrm{Nu}^3{}_{d,w}(1-2/\mathrm{Nu}_{d,m})^6 = \frac{(\mathrm{Gr}\cdot\mathrm{Pr})_{d,w}}{235\,f(\mathrm{Gr}\cdot\mathrm{Pr})_{d,w}}. \tag{34}$$

For small values of $(\mathrm{Gr}\cdot\mathrm{Pr})_{d,w}$, $\mathrm{Nu}_{d,m}$ according to (34) approaches the value 2. This means that the situation approaches that of pure conduction, the thickness of the Langmuir layer becoming large as compared to the radius. In this case we may compute the heat dissipation Φ as follows: Through each concentric sphere with a radius $R > \frac{1}{2}d$ the heat Φ flows through the spherical section $4\pi\,R^2$. Thus we have:

$$\Phi = -4\,\pi\,R^2\,\lambda(\vartheta)\,\mathrm{d}\vartheta/\mathrm{d}R \tag{35}$$

with the boundary conditions $\Theta = \Theta_w$ for $R = \frac{1}{2}d$ and $\Theta = 0$ for $R = \infty$.

From (35), we obtain:

$$\lambda(\vartheta)\,\mathrm{d}\vartheta = -\frac{\Phi}{4\pi}\frac{\mathrm{d}R}{R^2},$$

and integrating:

$$\int_{\vartheta_w}^{\vartheta_\infty} \lambda(\vartheta)\,\mathrm{d}\,\vartheta = -\frac{\Phi}{2\pi d}. \tag{36}$$

As, according to (24),

$$\int_{\vartheta_w}^{\vartheta_\infty} \lambda(\vartheta)\,\mathrm{d}\,\vartheta = -\,\Theta_w\,\lambda_m,$$

we obtain from (36):

$$\Phi = 2\pi\,d\,\Theta_w\,\lambda_m.$$

As by definition of $\bar{\alpha}$ we have $\Phi = \pi d^2\bar{\alpha}\Theta_w$, we obtain $\bar{\alpha}d/\lambda_m = 2$.

It is well known that in the case of the heat-dissipating cylinder this reasoning leads to a constant temperature field all around the cylinder with zero dissipation.

A comparison of (33) and (34) shows that for small values of $(\mathrm{Gr}\cdot\mathrm{Pr})_{d,w}$ the heat transfer per cm² of a sphere exceeds that of a horizontal cylinder of the same diameter, if the conditions are the same, whereas the two values meet at large values of $(\mathrm{Gr}\cdot\mathrm{Pr})_{d,w}$.

Actually in the case of a small sphere the experiment gives a heat transfer superior to that of a cylinder of the same diameter at the same excess temperature Θ_w. In fig. 9 we show the heat transfer of spheres in air (1 atm, 20 °C) according to (34), making use of fig. 6.

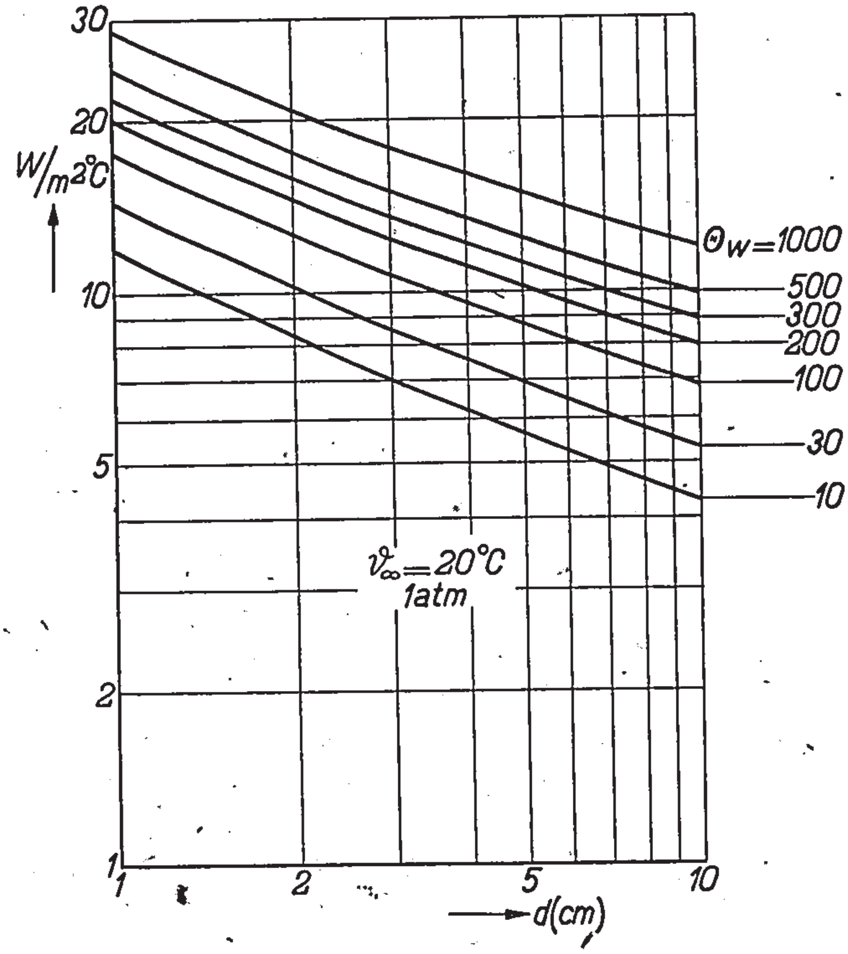

Fig. 9. The heat dissipation in watts per m² and per degree of temperature difference for spheres in air of 1 atm and room temperature as a function of the diameter, for different excess temperatures, calculated with (34).

(to be continued)

Eindhoven, April 1948

REFERENCES

1) L. Prandtl & O. Tietjens, Hydro und Aeromechanik, Bd II, p. 60; Handbuch exp. Phys. IV^{I} p. 47-71; H. Lamb. Hydrodynamics, Cambridge.
2) W. Nusselt, Gesundheits Ing. **38**, 477, 1915.
3) R. Hermann, Phys. Z. **33**, 425, 1932.
4) E. Schmidt & W. Beckmann, Tech. Mech. Thermodyn. **1**, 341, 391, 1930.
5) W. J. King, Mech. Eng. **54**, 347, 1932.
6) H. A. Lorentz, Z. tech. Phys. **15**, 362, 1934.
7) R. Hermann, Forschungsheft 379; Beilage Forsch. auf dem Geb. des Ingw. 1936.
8) I. Langmuir, Phys. Rev. **34**, 40, 1912.
9) W. Elenbaas, Physica **6**, 380, 1939.
10) W. Elenbaas, Physica **9**, 665, 1942.

R 91 Philips Res. Rep. 3, 361-370, 1948

A NEW PRINCIPLE FOR TRANSCEIVERS

by A. van WEEL 621.396.5:621.396.611.4

Summary

It is shown that the self-oscillating triode mixing stages described in a former article offer distinct advantages for transceiver circuits, the most important of which is that the switching from transmitting to receiving, and vice versa, can be accomplished fully electrically, without any mechanical switching in the antenna circuit. As a consequence, switching in an ultra-sonor frequency can be used, making it possible to establish a two-way communication. A system is described for stabilizing the frequency of both the transmitting oscillator and the local oscillator for reception with the aid of one cavity resonator.

Résumé

L'auteur montre que les étages changeurs de fréquence à triode auto-oscillante décrits dans un article précédent offrent des avantages particuliers pour des circuits d'émetteurs-récepteurs, le plus important consistant à pouvoir passer tout à fait électriquement de la transmission à la réception et vice versa, sans la moindre commutation mécanique dans le circuit d'antenne. On peut en conséquence utiliser une commutation à une fréquence ultra-sonore rendant possible d'établir une communication à double voie. L'auteur décrit un système pour stabiliser la fréquence de l'oscillateur d'émission et celle de l'oscillateur local du récepteur à l'aide d'une seule résonateur à cavité.

1. Introduction

In a former article ¹) we described a principle by which it was possible to design self-oscillating triode mixing stages. As this is the basic principle of the transceiver circuits with which we shall now deal, it is well worth recapitulating its properties here.

In fig. 1 a push-pull circuit of two triodes is drawn. The input electrodes are connected to two different circuits with different resonance frequencies: a push-pull or symmetric circuit consisting of the impedance Z_1, and an asymmetric circuit consisting of both halves of Z_1 connected in parallel, in series with Z_2. For the symmetric circuit the internal grid-cathode impedances are connected in series, while for the asymmetric circuit these impedances are connected in parallel.

In fig. 1 means are provided for a feedback for both circuits. As these push-pull mixing stages are of special importance for ultra-high frequencies, we shall consider only the feedback caused by the so-called three-point diagrams, which means that no inductive feedback is used. However, it should be stated here that these transceivers may be built up on the same principle on much lower frequencies, in which case the possible application of inductive feedback should be taken into account as well.

Returning to fig. 1, it can be seen that the feedback for the push-pull circuit is brought about by the impedance Z_4 (together with the internal grid-anode capacitances), while the feedback for the asymmetric circuit depends on the value of the impedance of Z_3 in series with the two halves of Z_4 in parallel.

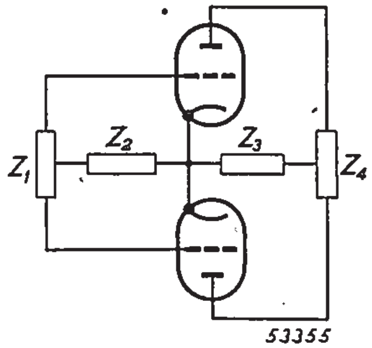

Fig. 1. Triodes that belong to both a push-pull and an asymmetric oscillator circuit.

By increasing sufficiently the positive feedback for the asymmetric circuit, this circuit will start generating oscillations. If the push-pull circuit is coupled to an antenna, the triodes will act as converter valves and a component of the intermediate frequency will be found in the anode current; it is on this principle that the self-oscillating triode mixing stage is based.

It is quite clear that, instead of making the asymmetric feedback very strong, the push-pull circuit may be undamped to such an extent that oscillation will start in the push-pull circuit. An interesting question arises as to what will happen if both circuits are undamped, so that they both can generate oscillations.

In most cases it appears that only one frequency is generated. This can be easily understood. With the usual system of grid-leak resistance the generated voltage is limited by the fact that increasing voltage means decreasing average slope of the valve. Stable conditions are reached when the average slope is just sufficient to maintain the oscillation. This minimum average slope depends on the damping of the circuit and the amount of feedback.

If there are two circuits connected to the valves, in general the minimum average slope required to maintain oscillation in each of them will differ according to different damping and feedback. Therefore, the circuit generating the highest voltage will in the end be the only oscillator, since with the average slope corresponding to this voltage no oscillation can exist in the other circuit.

From this it could be expected that the possibility of simultaneous generation of two frequencies in these circuits would be only a theoretical possibility, as only two tuned circuits generating exactly the same voltage could oscillate simultaneously. However, practice has shown that the two circuits can be brought to simultaneous oscillation without much difficulty. Even when the filament of one of the valves was disconnected, so that only one valve was functioning, both frequencies were measured. There are reasons to expect that these oscillations were not stable, but that the frequency jumped from one value to the other and back again, probably with rather a high repeating frequency. However, this point has not yet been fully investigated.

It is important to stress the fact that the occurrence of two frequencies simultaneously in these circuits is a phenomenon quite different from the generation of parasites in transmitter circuits. In these circuits the two generated frequencies are usually very different, so that it may be assumed that the parasitic oscillation is built up during the part of the period of the oscillator frequency desired, when the oscillating valve is carrying current, but that it is absent during the part of the period that the valve is cut off. However, in the circuits described above the two frequencies may show only a very small difference.

To end this section we would point out that although in this article we are considering circuits with push-pull antenna signal and, therefore, asymmetric local-oscillator voltage, the reversed circuit (asymmetric antenna signal and symmetric local-oscillator voltage) may, under certain conditions, be just as useful.

2. Principle of the transceiver circuit

To use the self-oscillating triode mixing circuit as a transceiver circuit, the feedback for both the push-pull and the asymmetric circuit must be sufficient to start oscillations in either of the two circuits. Let us consider for a moment only the push-pull circuit. The antenna is coupled to this circuit and will therefore radiate. Suppose that the circuit is so designed that maximum power is radiated. As this involves a heavy damping of the input circuit it is not difficult to arrange for a feedback for the asymmetric circuit (which is not damped by the antenna) that causes the generated asymmetric voltage to be larger than the symmetric voltage. According to section 1, this means that only the asymmetric voltage will be generated.

Since the antenna remains coupled to the balanced input circuit, the whole stage now acts as a receiver converter stage; a push-pull circuit, tuned to the intermediate frequency, should be connected to the anodes. The whole circuit is now "receiving".

To switch the apparatus to "transmitting", the asymmetric circuit should, in some way or other, be so heavily damped that asymmetric oscillation can no longer be maintained. The circuit will then start generating push-pull oscillations. This damping of the asymmetric circuit can be accomplished without influencing the balanced circuit, for instance in fig. 1 by damping the impedance Z_2 or Z_3, or both.

The advantage of these transceivers lies in the fact that the switch-over from receiving to transmitting, or vice versa, can be accomplished fully electrically, since the damping of the asymmetric circuit can be obtained by means of a diode or a triode. No mechanical switching of the antenna connections is necessary; the transmitting and receiving frequencies are equal or almost equal, and the input circuit need not be retuned when switching from one position to the other. The matching of the antenna to the valves needs no correction either, as this matching is independent of the direction in which the power has to be transmitted, and the input impedances of the valves will not show large differences when the A.C. voltages on the grids do not differ very much in the two positions.

The modulation of these oscillators may be brought about by conventional means.

3. Consequences of the electrical switching

The possibility of electrical switching makes remote control quite easy. Another advantage is the possibility to use the modulation signal for switching the apparatus from receiving to transmitting: when nobody is speaking into the telephone, the apparatus is "receiving"; speaking into the telephone causes the apparatus to switch over to "transmitting". This can easily be accomplished by detecting the modulation signal and using this detected signal to switch on the damping of the asymmetric circuit.

The most important property of the electrical switching lies in its small inertia, so that it can be accomplished in an ultra-sonor frequency. This makes it possible to carry on a two-way conversation without any external switching. We shall now go more closely into the details of this system.

To make a two-way conversation possible the apparatus is switched over from receiving to transmitting, and vice versa, in an ultra-sonor frequency. During the receiving periods the incoming signal is received, amplified, and detected, while during the transmitting periods the outgoing signal is given. The two switching frequencies used at the two ends should be either exactly equal or their frequency difference should be ultra-sonor itself, as will be clear from the following considerations.

Let us assume that the two switching frequencies are synchronized. This is not sufficient, for their phase relations must answer certain requirements, as is clear from the fact that it might be possible for the signal of post A to arrive at post B just during the periods that the latter post is transmitting. Under these circumstances no signal whatsoever would be received by B.

Should the switching frequencies show a small difference, interference will occur and a tone of the difference frequency would be heard. This is the reason why, if different switching frequencies are chosen, their difference should be ultra-sonor itself.

4. Synchronized switching frequencies

We shall go more closely into the details of the system of synchronized switching frequencies and shall first consider what demands on the phase relations have to be satisfied.

In fig. 2 the transmitting and receiving periods of two posts with arbitrary phase relations are drawn diagrammatically. For one period of each post it is indicated how the transmitted signal will arrive at the other post after a certain time τ. Only if the second post is in the receiving position will the incoming signal be used. In fig. 2 the parts of the periods during which the signal is effective are hatched, and these parts we shall call the effective receiving periods.

From fig. 2 it can be seen that with arbitrary phase relations these effective receiving periods will generally be different for the two posts. For a properly functioning communication system the following conditions must be fulfilled:

(1) the effective receiving period should be the same for both posts;

(2) the effective receiving period should be maximal.

The first demand can be answered by adjusting the phase relations between the two posts, while, to fulfil the second condition, the switching frequency has to be adapted to the distance between the posts. To bring about the same effective receiving period it is necessary that the switching frequencies in the two posts should be either in phase or shifted 180°. This can be seen from fig. 3, where the two frequencies are supposed to be in phase.

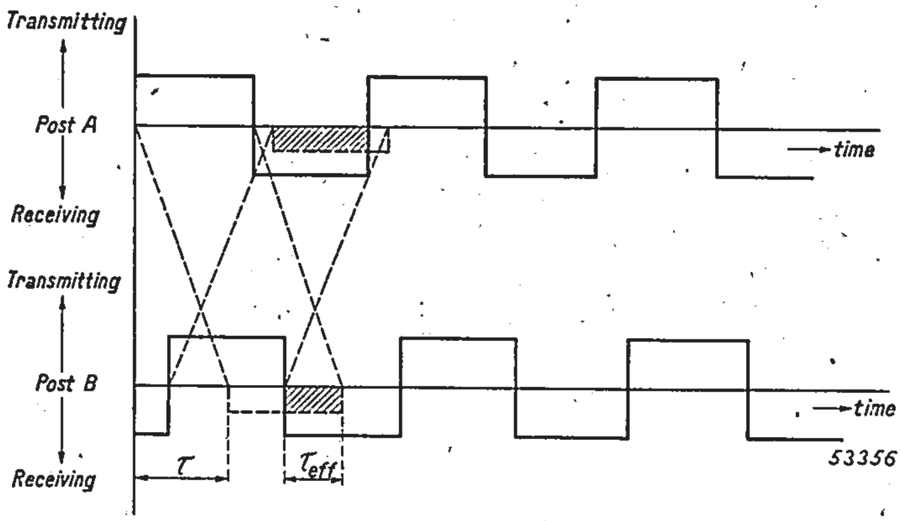

Fig. 2. Transmitting and receiving periods of two posts with arbitrary phase relations.

The effective receiving periods are the same for the two posts, independently of τ.

The optimum value for the effective receiving period is given by

$$t_{eff} = \tfrac{1}{2}\,T.$$

From fig. 3 it can be seen that if the two switching frequencies are in phase this optimum value is obtained if

$$\tau = (2n + 1)\,\frac{T}{2},$$

where $n = 0,\ 1,\ 2, \ldots .$

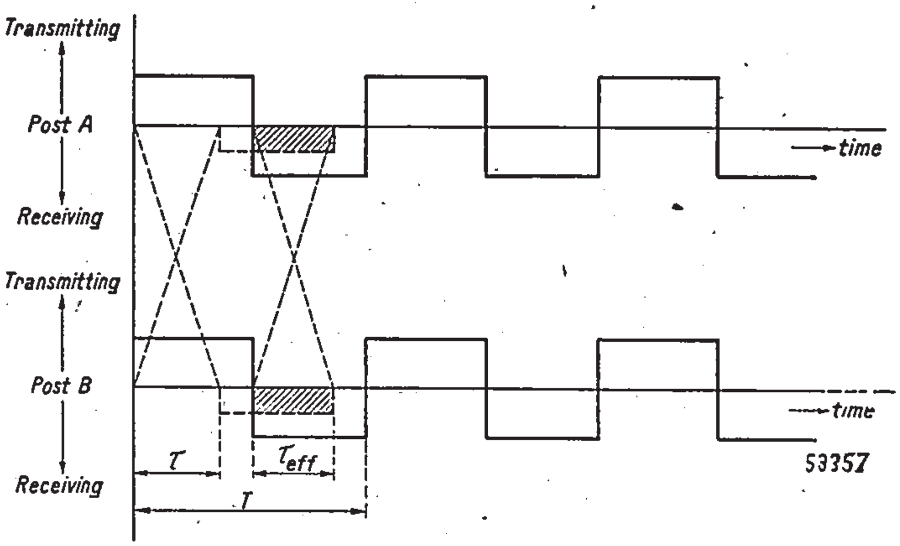

Fig. 3. Transmitting and receiving periods of two posts with equal phase.

If there is a 180° phase shift between the two switching frequencies the condition is

$$\tau = 2n\,\frac{T}{2},$$

for $n = 0,\ 1,\ 2, \ldots .$

From the foregoing it can be gathered what demands have to be satisfied by a communication system constructed on this principle. They are:

(1) the switching frequencies of the two posts should be synchronized;
(2) these frequencies should be adapted to special phase conditions;
(3) the switching frequency should be adapted to the distance between the posts.

An elaborate apparatus is necessary to answer these demands if the switching frequencies are to be generated separately in the two posts, synchronized, etc. However, there is a much simpler method of attaining these optimum conditions. It consists in using a generator for the switching frequency only in one of the posts, while in the other post the switching frequency is detected from the signal received. The first condition is thus automatically fulfilled. How the other two demands can be answered, will be shown in what follows.

In this system, when there is no communication with another post, each transceiver is continually in the receiving position. Now let us assume that post *A* wants to make communication with post *B*. Post *A* switches on its switching-frequency oscillator in an arbitrary frequency and therefore transmits intermittently. Post *B* receives a signal consisting of blocks (indicated by hatched blocks in fig. 4). Post *B* is constructed in such a way that when a "block signal" is received, the transmitter is switched to intermittent receiving and transmitting in such a phase that on the second flank of each block, the receiver is switched over to transmitting. Under these circumstances the effective receiving period in post *B* is always optimal.

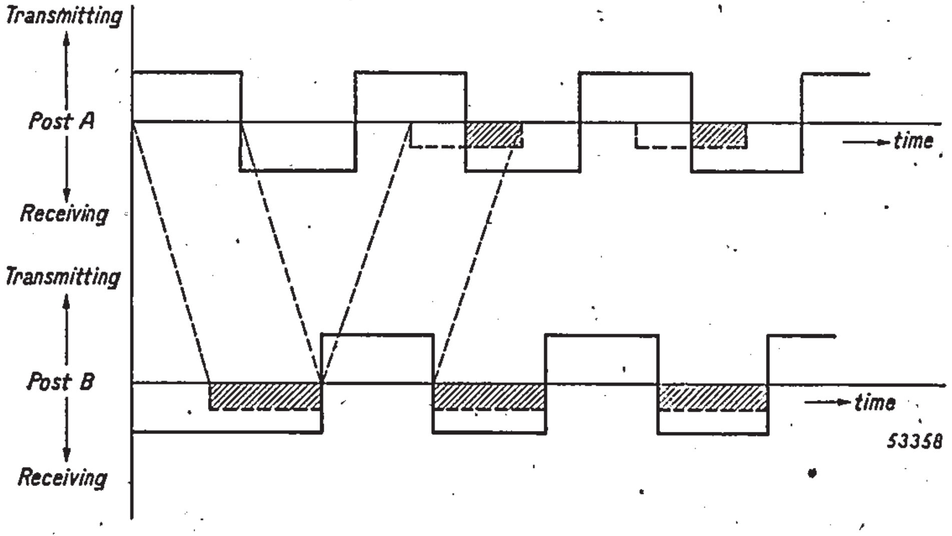

Fig. 4. Phase relation between transmitting and receiving periods of the two posts giving optimum receiving period in post *B*.

In general this will not be the case with post *A*, as may be seen from fig. 4, but post *A* can then adjust its switching frequency (which is automatically followed by post *B*), so that post *A* has an optimum effective receiving period as well. To achieve this, post *A* only needs to vary its switching frequency until the signal received from post *B* is strongest.

5. Stabilizing the transmitting and the local-oscillator frequencies

The practical applications of these principles have not yet been so fully examined that results can be published at the moment. However, there is one interesting detail that can be described here.

If the transceiver is designed to function on very high frequencies, stability of the generated frequencies may prove to be insufficient. This stability can be improved by using cavity resonators as circuit elements. Both the transmitting and the local-oscillator frequency should be stabilized, and in principle one could design the circuit in such a way that the cavity resonator for the local-oscillator frequency is connected in a branch carrying only the asymmetric current, while in the same way the cavity resonator for the push-pull frequency carries only current of this frequency.

However, the second demand is not so easily met, as a cavity resonator has appreciable dimensions and therefore an appreciable capacitance with respect to the chassis. As a consequence asymmetric current will flow through this cavity resonator and the whole resonator becomes "live".

We have therefore designed a cavity resonator that stabilizes both frequencies simultaneously. The principle underlying this cavity resonator is shown in fig. 5. There are two resonances in this resonator, one for symmetric oscillations and the other for asymmetric oscillations. The symmetrically tuned circuit consists of the inductances of the two internal conductors in series and a capacitance consisting of C_3 in parallel to the series connection of C_2' and C_2''. The condenser C_1 does not carry current of the symmetric frequency.

The asymmetric circuit consists of the inductance of the two internal conductors in parallel and the capacitance formed by the condenser C_1 in series with the parallel connection of C_2' and C_2''. Condenser C_3 does not carry current of the asymmetric frequency.

The two circuits can be independently tuned by C_1 and C_3.

The degree of frequency stabilization depends on the degree of coupling between oscillator and cavity resonator. As the balanced circuit shows a damping that differs considerably from that of the asymmetric circuit, it would be an advantage if the amount of coupling between oscillator and cavity resonator could be adjusted separately for the two frequencies. In fig. 5 two leads are drawn that are to a certain degree coupled to the internal circuits, and it is not simple to vary this coupling. However, there

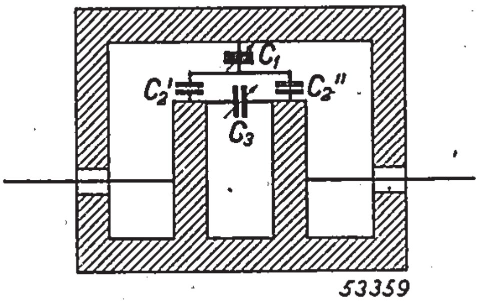

Fig. 5. Cavity resonator with a symmetric and an asymmetric mode of oscillation.

is a better method, not based on inductive coupling but on capacitive coupling. The principle of this method is shown in fig. 6 for a conventional asymmetric circuit, in which figure a tuned-grid tuned-anode oscillator circuit is drawn. The anode tuned circuit, which may be formed by a cavity resonator, is coupled to the anode via the impedance Z.

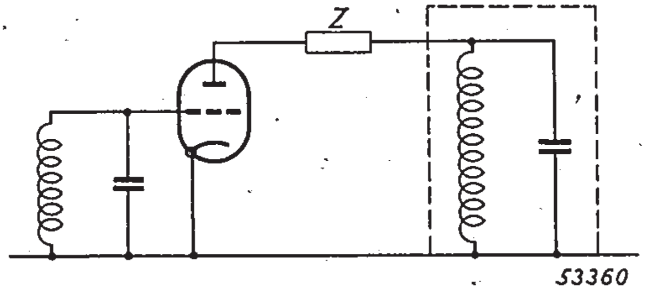

Fig. 6. Tuned-grid tuned-anode oscillator with the valve tapped on the anode circuit by means of a series impedance Z.

If Z is capacitive the anode is tapped on the tuned circuit (the impedance of which must show an inductive parallel component to make oscillations possible), and the frequency is more stabilized. On the other hand, if Z is made inductive, part of the inductive impedance needed between anode and earth is formed by this inductance, and therefore the tuned circuit must show a smaller parallel inductive component, what means that the oscillator frequency must differ more from the resonance frequency of the circuit. As a consequence the frequency stability is decreased.

Fig. 7 shows a transceiver circuit in which this principle is used to enable a separate adjustment to be made for the amount of coupling for the two frequencies. A grounded-grid kind of oscillator valve is used. For the sake of simplicity we have omitted all elements and leads not carrying the symmetric or the asymmetric oscillator frequency.

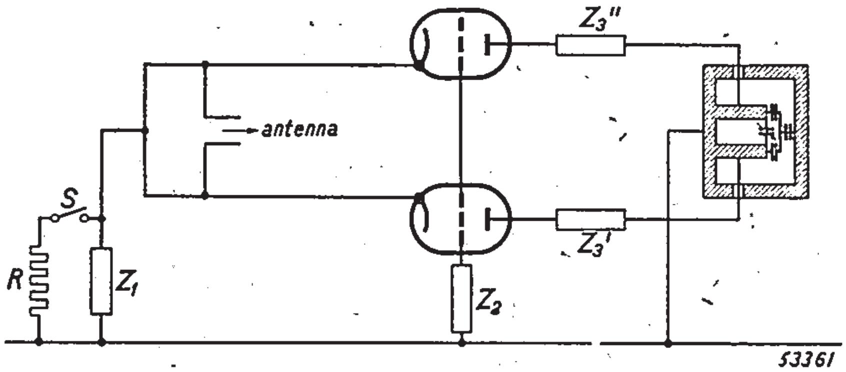

Fig. 7. Transceiver circuit stabilized by a cavity resonator with two modes of oscillation.

To the input electrodes a parallel-wire system is connected, on which the antenna is conveniently tapped. The short-circuited end of the parallel-wire system is connected to an impedance Z_1, which tunes the asymmetric input circuit. Z_1 can be damped with the aid of resistance R and switch S, which switch commands the transmitting or receiving position.

The anode circuit consists of the two equal impedances Z_3' and Z_3'' and the cavity resonator. The anode-grid circuit is closed by Z_2, which impedance is common to the input and the output circuit.

The amount of coupling between oscillator and cavity resonator depends, for the symmetric frequency, only on Z_3' and Z_3'', whereas for the asymmetric frequency it is controlled by Z_3', Z_3'', and Z_2. From this it can be seen that the coupling can be made different for the two frequencies.

A transceiver designed on the principles of fig. 7 has been built for a wavelength of 100 cm (local-oscillator wavelength 106 cm) and has proved that these principles are fully workable.

Eindhoven, September 1946

REFERENCE

[1] A. van Weel, Philips Res. Rep. 3, 191-212, 1948.

R 92 Philips Res. Rep. 3, 371-377, 1948

THE TEMPERATURE DEPENDENCY OF THE INDEX OF REFRACTION OF HETEROPOLAR SOLIDS

by J. H. van SANTEN and G. H. JONKER

535.327:539.13

Summary

While the electronic polarizability of molecules does not vary much with temperature it is found that the electronic polarizability of heteropolar lattices shows a pronounced dependency on temperature. A tentative explanation is suggested based upon the assumption that the electronic polarizability of heteropolar lattices is mainly of an electron-transfer type.

Résumé

Alors que la polarisabilité des électrons de molécules varie peu avec la température, on trouve que celle de réseaux hétéropolaires dépend de la température. L'explication que les auteurs donnent de cette dépendance se base sur l'hypothèse d'un transfert d'électrons au cours des processus qui contribuent à la polarisabilité des électrons.

1. Introduction

It is well known that the Lorentz-Lorenz formula,

$$\frac{n^2-1}{n^2+2}=\frac{4\pi}{3}N\alpha\,, \tag{1}$$

where n = index of refraction,
N = number of atoms (ions) per unit of volume,
α = electronic polarizability of an atom (ion),

theoretically holds only for an assembly of spherical atoms (ions) with a polarizability concentrated at the centres, the atoms being situated at positions with purely cubic symmetry ("purely cubic crystals").

Since we believe that in a large number of cases the Lorentz-Lorenz formula is a fair first approximation, and since, moreover, the phenomena we shall discuss are found to be essentially similar for purely cubic crystals and for other crystals, we shall apply the Lorentz-Lorenz formula.

From equation (1) the following expression for the change of the index of refraction with temperature can be derived:

$$\frac{\mathrm{d}n}{\mathrm{d}T}=\frac{(n^2-1)\,(n^2+2)}{6n}\left\{\frac{1}{N}\frac{\partial N}{\partial T}+\frac{1}{\alpha}\frac{\partial \alpha}{\partial T}\right\}. \tag{2}$$

For isotropic or cubic substances

$$\frac{1}{N}\frac{\partial N}{\partial T} = -3\beta_{\text{lin}}, \tag{3}$$

where β_{lin} denotes the coefficient of linear expansion.

Writing

$$\beta_a = \frac{1}{a}\frac{\partial a}{\partial T}, \tag{4}$$

equation (2) becomes:

$$\frac{\mathrm{d}n}{\mathrm{d}T} = \frac{(n^2-1)\,(n^2+2)}{2n}\left\{-\beta_{\text{lin}} + \tfrac{1}{3}\,\beta_a\right\}. \tag{5}$$

For a large number of substances the temperature dependency of n has been found to be caused by the variation with temperature of N alone, from which it may be concluded that the polarizability does not depend on temperature.

As we shall show, with the aid of data from the literature, for some *heteropolar* solids of different structures, the term $\frac{1}{3}\,\beta_a$ cannot be neglected.

In section 3 we shall give a tentative explanation of this fact essentially based on the assumption that in these lattices the most important atomic processes with which the electronic polarizability is connected, are not confined within the separate atoms, but consist in an electron transfer from one ion to some other.

2. Experimental data

a) *Sodium chloride* [1])

In figs 1a and 1b, respectively n and $\mathrm{d}n/\mathrm{d}T$, measured at room temperature, are plotted against wavelength λ. The graph for n is found to be the well-known curve for an index of refraction at the long-wave side of an absorption peak. The dependency of $\mathrm{d}n/\mathrm{d}T$ on the wavelength shows a positive contribution which becomes the more important, the more we proceed towards shorter wavelengths.

Extrapolation to $\lambda \rightarrow \infty$ yields

$$\frac{\mathrm{d}n_\infty}{\mathrm{d}T} = -3{\cdot}8 \times 10^{-5}.\,^{*)}$$

From this value and from the coefficient of linear expansion, $4{\cdot}04 \times 10^{-5}$, we calculate with the aid of eq. (5)

$$\beta_{a,\infty} = +\,6{\cdot}1 \times 10^{-5} = +\,1{\cdot}5\;\beta_{\text{lin}}\,. \tag{6}$$

---

*) For brevity we have omitted the dimension "degree^{-1}" throughout.

b) *Calcium fluoride* 1)

In a completely analogous way one obtains

$$\frac{\mathrm{d}n_\infty}{\mathrm{d}T} = -2{\cdot}1 \times 10^{-5}; \quad \beta_{\text{lin}} = +1{\cdot}9 \times 10^{-5},$$

$$\beta_{a,\infty} = +3{\cdot}2 \times 10^{-5} = +1{\cdot}7\,\beta_{\text{lin}}.$$

In the case of the next two optically anisotropic crystals we must distinguish between n_ω and n_ε, the indices of refraction for light with the electric vector perpendicular respectively parallel to the optical axis. It is certainly not allowed to use here the Lorentz-Lorenz formula; nevertheless we may try to make an estimation of $\beta_{a,\infty}/\beta_{\text{lin}}$ by averaging over all directions.

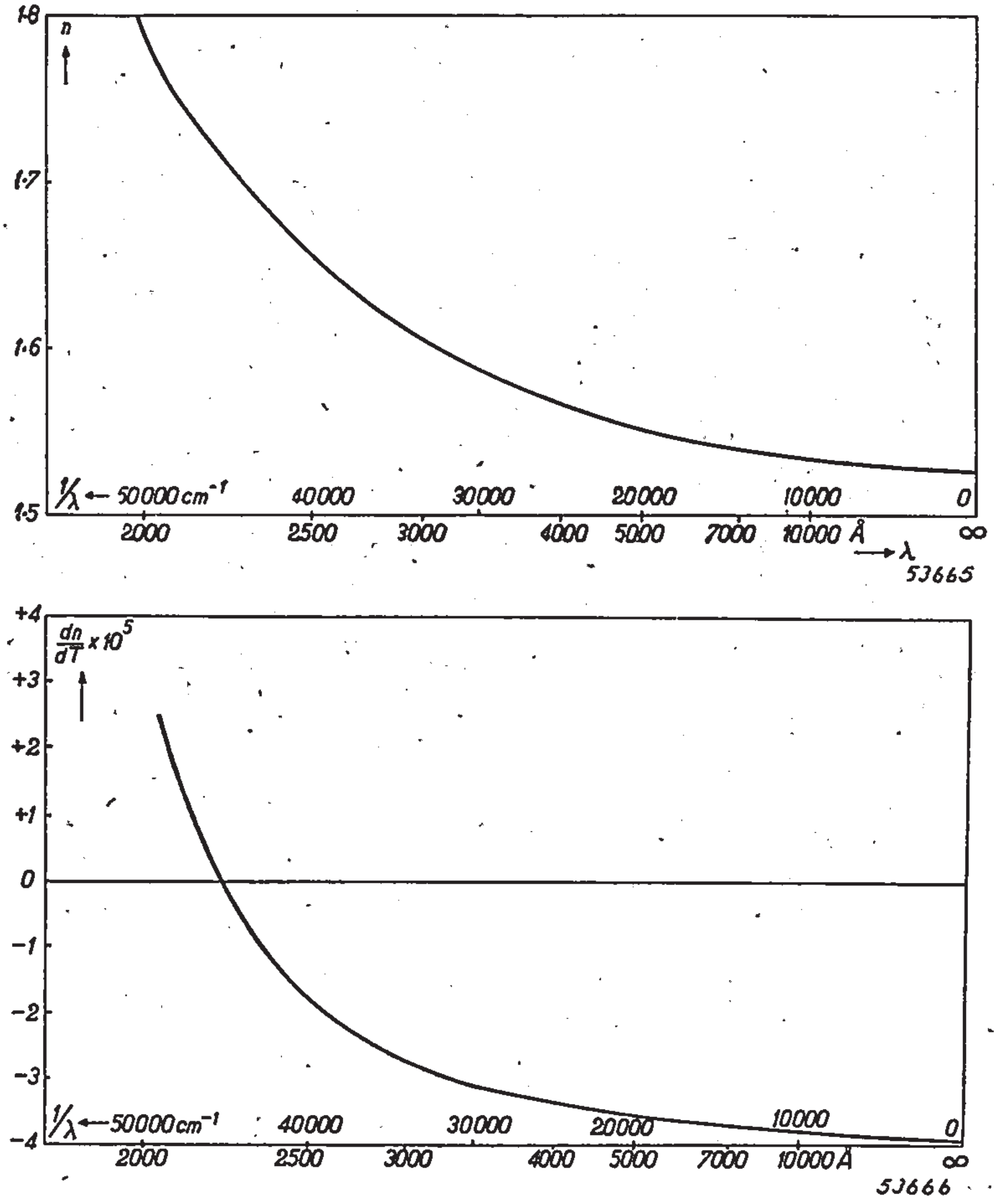

Dependency of the index of refraction, n, and the temperature derivative of the index of refraction, $\mathrm{d}n/\mathrm{d}T$, on the wavelength λ for sodium chloride.

c) *Quartz* [1])

$$\frac{\mathrm{d}n_{\omega,\infty}}{\mathrm{d}T} = -0{\cdot}72 \times 10^{-5};\ \beta_{a\omega,\infty} = 3{\cdot}14 \times 10^{-5};\ \beta_{\mathrm{lin}}(\perp) = 1{\cdot}42 \times 10^{-5}.$$

$$\frac{\mathrm{d}n_{\varepsilon,\infty}}{\mathrm{d}T} = -0{\cdot}83 \times 10^{-5};\ \beta_{a\varepsilon,\infty} = 1{\cdot}33 \times 10^{-5};\ \beta_{\mathrm{lin}}(\parallel) = 0{\cdot}87 \times 10^{-5}.$$

From this it follows

$$\frac{\beta_{a,\infty}\,(\text{average})}{\beta_{\mathrm{lin}}(\text{average})} = +2{\cdot}0\,.^{*})$$

d) *Calcite* [1])

Here we find a pronounced anisotropy caused by the presence of layers composed of planar CO_3 groups.

$$\frac{\mathrm{d}n_{\omega,\infty}}{\mathrm{d}T} = -0{\cdot}1 \times 10^{-5};\ \beta_{a\omega,\infty} = -1{\cdot}7 \times 10^{-5};\ \beta_{\mathrm{lin}}(\perp) = -0{\cdot}52 \times 10^{-5},$$

$$\frac{\mathrm{d}n_{\varepsilon,\infty}}{\mathrm{d}T} = +0{\cdot}96 \times 10^{-5};\ \beta_{a\varepsilon,\infty} = +9{\cdot}3 \times 10^{-5};\ \beta_{\mathrm{lin}}(\parallel) = +2{\cdot}53 \times 10^{-5},$$

$$\frac{\beta_{a,\infty}\,(\text{average})}{\beta_{\mathrm{lin}}(\text{average})} = +4{\cdot}0\,.^{*})$$

e) *Vitreous silica* [1])

$$\frac{\mathrm{d}n_{\infty}}{dT} = +0{\cdot}93 \times 10^{-5};\ \beta_{a,\infty} = 1{\cdot}92 \times 10^{-5};\ \beta_{\mathrm{lin}} = 0{\cdot}037 \times 10^{-5},$$

$$\beta_{a,\infty} = +52\ \beta_{\mathrm{lin}}.$$

This abnormally high value of $\beta_{a,\infty}/\beta_{\mathrm{lin}}$ might be caused by the very low coefficient of thermal expansion of vitreous SiO_2. Measurements on various crown and flint glasses showed, however, that the vitreous state is not necessarily connected with a high value of $\beta_{a,\infty}/\beta_{\mathrm{lin}}$.

f) *Silicate glasses* [2])

For flint glasses we have

$$\frac{\beta_{a,\infty}}{\beta_{\mathrm{lin}}} = 2{\cdot}8 - 3{\cdot}8,\ \text{average}\ 3{\cdot}5\,;$$

for crown glasses

$$\frac{\beta_{a,\infty}}{\beta_{\mathrm{lin}}} = 2{\cdot}3 - 2{\cdot}7,\ \text{average}\ 2{\cdot}5^{5}\,.$$

---

*) It may be seen that the ratios $\beta_{a\omega,\infty}/\beta_{\mathrm{lin}}(\perp)$ and $\beta_{a\varepsilon,\infty}/\beta_{\mathrm{lin}}(\parallel)$, though being without physical meaning, are of the same order of magnitude.

Not taking into account vitreous silica and the highly anisotropic calcite, we may conclude from these measurements that the ratio $\beta_{\alpha,\infty}/\beta_{\text{lin}}$ varies between 1·5 and 3·5.

In section 3 we shall discuss how to understand the order of magnitude of this ratio.

3. Discussion

In order to discuss the dependency of the polarizability on the temperature we have to consider α more closely.

According to dispersion theory we can write for an assembly of isolated atoms

$$\frac{n^2-1}{n^2+2}=\frac{4\pi}{3}N\alpha=\sum_i \frac{C_{0,i}}{\nu_{0i}^2-\nu^2}, \tag{7}$$

where

$$C_{0,i}=\frac{8\pi N}{9h}\nu_{0i}\,M_{0i}\,M_{i0},$$

$h\nu_{0i}$ = energy difference between the ground state and the excited state i,

M_{ij} = matrix component of the electric moment between the states i and j (the index 0 refers to the ground state),

ν = frequency of the light used for the determination of n.

We shall consider the case where most important contributions to ν_{0i} result from a rather narrow band of energy levels situated at a distance $h\nu_e$ above the ground level. So we can then replace the sum in (7) by a single term

$$\frac{n^2-1}{n^2+2}=\frac{4\pi}{3}N\alpha=\frac{C}{\nu_e^2-\nu^2}, \tag{8}$$

or

$$n^2-1=\frac{C'}{\nu_e'^2-\nu^2}, \tag{9}$$

where

$$C'=3C \tag{10}$$

and

$$\nu_e'^2=\nu_e^2-C. \tag{11}$$

The corresponding absorption of the lattice should be found at the frequency ν_e', shifted towards longer wavelengths with respect to ν_e.

In the right-hand side of equation (8) both C and ν_e may vary with temperature.

According to quantum mechanics C/N should be a constant for an assembly consisting of isolated atomic systems under different conditions since this ratio should be proportional to the number of dispersion electrons contributing to ν_e *).

From equation (8) and from the constancy of C/N it follows that *)

$$\beta_a = -\frac{2\nu_e}{\nu_e^2 - \nu^2}\frac{\partial \nu_e}{\partial T} \tag{12}$$

and

$$\beta_{a,\infty} = -\frac{2}{\nu_e}\frac{\partial \nu_e}{\partial T}. \tag{13}$$

In the case of sodium chloride, a substance that is a rather good example of a heteropolar crystal, we estimated $\beta_{a,\infty}$, in the following way. From dispersion data we calculated ν_e' and C' (or C); by means of a rather crude picture adopted for the electronic transition process we could estimate $\partial\nu_e'/\partial T$; from these data $\beta_{a,\infty}$ could be derived.

Evaluation of ν_e' and C from the dispersion data [1]) with the aid of equation (9) yielded $\nu_e' = 2{\cdot}48 \times 10^{15}$ sec^{-1} and $C = 2{\cdot}71 \times 10^{30}$ sec^{-2}. The value of ν_e' is in agreement with results of Herzfeld and Wolff [3]) and also Mayer [4]) who have found that for sodium chloride the most important process with which the electronic polarizability can be connected causes an absorption at about 1200 Å.

According to theories developed by De Boer [5]) and Mott [6]) one should assume that in these processes an electron is transferred from a halogen ion to an alkali-metal ion, the latter being situated at such a distance that the interaction between the electron and the empty place left behind at the chlorine, may be neglected. This is in agreement with experiments by Ferguson [7]) who found that on passing towards shorter wavelengths photoconductivity starts only at about 1270 Å (second absorption peak).

So we may write

$$h\nu_e' = 2\,A_M\frac{e^2}{r} - J_{\mathrm{Na}} + E_{\mathrm{Cl}} - P, \tag{14}$$

---

*) We found, however, that for a rather large number of such heteropolar oxides (e.g. MgO, A_2lO_3, TiO_2) where the electronic polarizability must be attributed to the oxygen ions alone, the ratio $C/N\nu_e$ rather than C/N is approximately constant. The cause of this discrepancy is probably that for these heteropolar crystals the model of isolated atoms is rather inadequate.
Since for these oxides $C/N\nu_e$ varies only slightly for different lattices at one and the same temperature one might assume that also in the case of temperature variations of a single lattice this quantity remains to some extent a constant.
From equation (8) and from this assumption one calculates

$$\beta_a = -\frac{\nu^3 + \nu_e^2}{\nu_e(\nu_e^2 - \nu^2)}\frac{\partial \nu_e}{\partial T} \tag{12'}$$

and

$$\beta_{a,\infty} = -\frac{1}{\nu_e}\frac{\partial \nu_e}{\partial T}, \tag{13'}$$

a result differing from equation (13) by a factor 2.

where A_M = Madelung's constant,
J = ionization energy,
E = electron affinity,
r = shortest distance between two ions carrying opposite charges, and
P = polarization term due to the electron transfer giving rise to a polarization of the lattice.

Tentatively we shall assume that the polarizability is affected by temperature variations only by the average interionic distances being changed (thermal expansion) and, particularly we shall suppose that mainly the first term of the right-hand side is influenced.

From these assumptions and from the values $A_M = 1{\cdot}75$, $r = 2{\cdot}79$ Å, one calculates with the aid of (10), (11) and (13)

$$\frac{1}{\nu_e'}\frac{\partial \nu_e'}{\partial T} \approx -1{\cdot}7\ \beta_{\text{lin}}$$

and
$$\beta_{a,\infty} = -\frac{2}{\nu_e}\frac{\partial \nu_e}{\partial T} = -\frac{2\nu_e'\dfrac{\partial \nu_e'}{\partial T} - 3C\beta_{\text{lin}}}{\nu_e^2} \approx 3{\cdot}3\ \beta_{\text{lin}},$$

a result of the right order of magnitude *). By taking into account the dependency of the polarization term P on the interionic distance r a smaller value of $\beta_{a,\infty}$ will be found.

It seems not unreasonable to assume that also for other heteropolar substances the dependency of the electronic polarizability on temperature is caused by the electron-transfer character of the underlying electronic processes **).

---

*) With the assumptions underlying equation (13′) one obtains $\beta_{a,\infty} = 1{\cdot}6\ \beta_{\text{lin}}$. So our estimation is not very sensitive to whether $C/N\nu_e$ or C/N is independent of temperature.

**) In order to explain the abnormally high value of $\beta_{a,\infty}/\beta_{\text{lin}}$ for vitreous silica one might suppose that owing to some folded structure, the Si-O distances, seen microscopically, do expand with temperature, while the macroscopic crystals do not show a large thermal dilatation.

Eindhoven, January 1948

REFERENCES

1) Landolt-Bornstein, Physik. Chem. Tabellen, Berlin, 1923, table 168.
2) C. Pulfrich, Ann. Phys., Lpz., **45**, 609-665, 1892.
H. Rubens, Ann. Phys., Lpz., **45**, 238-261, 1892.
3) K. F. Herzfeld and K. L. Wolff, Ann. Phys., Lpz., **78**, 35-56, 1925.
4) J. E. Mayer, J. Chem. Phys. **1**, 270-279, 1933.
5) J. H. de Boer, Electronic emission and adsorption phenomena, Cambridge, 1935, section 73.
6) N. F. Mott, Trans. Faraday Soc. **34**, 500-506, 1938.
7) J. N. Ferguson, Phys. Rev. **66**, 220-223, 1944.

R 93 *Philips Res. Rep.* **3**, *378-400, 1948*

EMPIRICAL DETERMINATION OF WAVE-FILTER TRANSFER FUNCTIONS WITH SPECIFIED PROPERTIES

by J. F. KLINKHAMER

621.392.52:621.317.729.1

PART II *)

Summary: see Part I.

CONTENTS OF PART II

3. Second method of defining the poles and zeros of h, g, f

3·1. Analytic continuation of the auxiliary function ln F to form the auxiliary function H
3·2. Representation of a part of the λ-plane on the H-plane
3·3. Singularities of h/f in the H-plane
3·4. Approximation of the value of h/f in the H-plane
3·5. A configuration of electrodes producing the conjugate H-field
3·6. Simple proportionalities between the currents in the various band electrodes of the original configuration
3·7. Determination of the poles and zeros of h/f by means of the conjugate electrode configuration
3·8. Finding the zeros of $g(\lambda)\,g(-\lambda)$
3·9. A function g/f with poles not on the ω-axis

4. Analytic characteristics of the H-function

4·1. Behaviour of H in the λ-plane
4·2. Analytic definition of H
4·3. Calculation of the differences in value between the horizontal parts of the H-curve when the analytic expression of H is given.
4·4. Definition of the analytic expression of H when the differences in value of the horizontal parts of H, as well as the branch points ω_1, ω_2, . . . are given.
4·5. Saddle points
4·6. Representation of the λ-plane on the H-surface
4·7. The function h/f, found in sections 2 and 3, is the one that gives the best attenuation characteristic with a given number of poles and zeros
4·8. On Darlington's method

5. Manupulations

---

*) For Part I, see Philips Res. Rep. 3, 60-80, 1948.

3. Second method of defining the poles and zeros of h, g, f

We shall now describe a method of finding the positions of the singularities of $\ln|h/f|$ that is more efficient than that discussed in section 2·6. At the same time this method gives the positions of the zeros of g/f.

As will be shown in section 3·3, all singularities of $\ln|h/f|$ and $\ln|g/f|$ are situated on a definite set of gradient curves of the potential field $\ln|F|$ the electrode configuration of which has been defined in section 2·4 — F having been defined at the end of section 2·5.

Now, according to section 3·5, we are able to construct a "conjugate electrode configuration" which gives equipotentials coinciding with the gradient curves of $\ln|F|$, and vice versa. With this second electrode configuration we may therefore trace without difficulty the required gradient curves of $\ln|F|$ (3·7). The points where these curves meet the ω-axis then give the singularities of $\ln|h/f|$, whilst the zeros of g are the points where the curves meet an equipotential of the $\ln|F|$-field which may be traced in the original electrode configuration (3·8).

In order to ascertain on which of the gradient curves of $\ln|F|$ the roots of h, g, f are lying, we use a transformation in which the λ-plane is represented on the H-plane, H being a function derived directly from $\ln F$ by inclusion of all the analytic continuations of $\ln F$ (3·1, 3·2). In this H-plane the roots of h (or f) are now found to lie on a series of equidistant points (3·3), corresponding to the fact that the number of needles, representing the roots of h (or f), should be proportional to the current per cm on the band electrodes (2·6). This means that, when the conjugate electrode configuration is used, the roots of h (and f) lie on a set of equipotentials, the voltage difference between any two successive equipotentials of the set being the same (3·7). The roots of g lie on the same equipotentials (3·8).

3·1. Analytic continuation of the auxiliary function $\ln F$ to form the auxiliary function H

The function $\ln F$ is analytic in every part of the λ-plane except along the band electrodes. The real part of the analytic continuation along one of the electrodes may be found by the Laplace differential equation. Its analogue in the electrolytic tank is the electric image of the potential field in both faces of the band electrode that is considered, the left face of the band electrode giving on the right side the image of the left part of the potential field, and vice versa. The function $\ln F$ and its image therefore form a function with at least two branches, two branch points being represented by the edges of the electrode. Now at each of the band electrodes a continuation may be constructed, corresponding to an electric image. The complete function, therefore, consists in general of an infinite set of branches, each branch corresponding to an image of the electric field that represents $\ln|F|$. (The expression "image" is to be understood in this respect as either a direct image or an image of an image, or an image of multiple degree.)

3.2. Representation of a part of the λ-plane on the H-plane

The function $\ln F$, completed with all its images in the various electrodes, will from now on be called H.

The part of the λ-plane adjoining one of the electrodes (for instance D) and bounded by an equipotential β (fig. 8) can be represented in the H-plane. By introducing an additive constant we make the potential of the electrode equal to zero. The image of the electrode on the H-plane will then fall along the imaginary axis. The equipotentials will appear as straight lines parallel to the imaginary axis and the gradient curves as straight lines perpendicular to it (fig. 9).

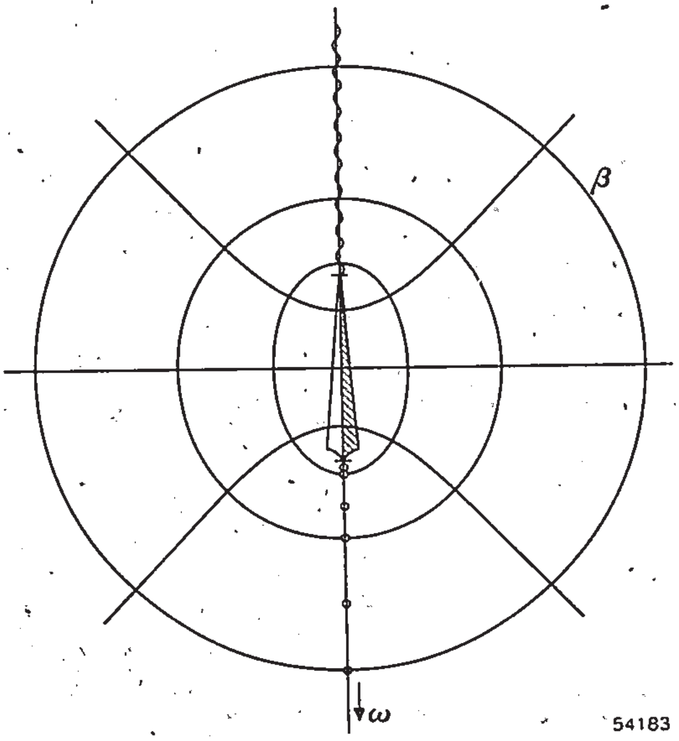

Fig. 8. Electrode and equipotentials representing the function H in the part of the λ-plane close to a transmission band.

In fig. 8 a black and a white triangle are drawn in the λ-plane, on opposite sides of the transmission area D along the ω-axis. The attenuation area at the upper side of D is marked by a wave line; the attenuation at the lower side by a series of small circles. The images of these figures in the H-plane are represented in fig. 9 by similar figures.

How the representation of the λ-plane continues outside the lines β is of no interest for the moment. A representation of the whole λ-plane upon an H-surface is discussed in section 4·6; this surface consists of two finite plane areas of a definite shape, joined discontinuously.

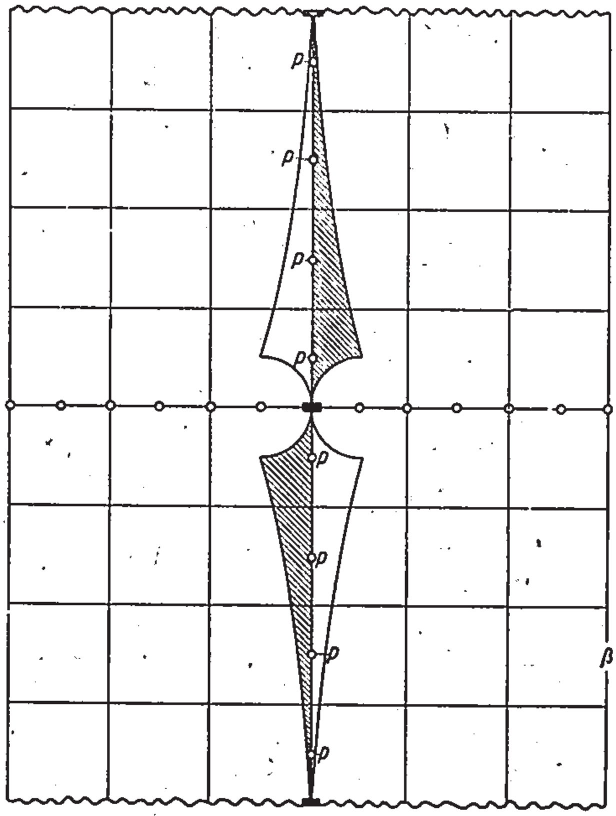

Fig. 9. Representation of the H-function of fig. 8 in the H-plane.

3·3 Singularities of h/f in the H-plane

In section 2·6 we found the positions of the needle electrodes by dividing the band electrodes into a series of intervals carrying equal currents, and putting a needle electrode into each of these intervals so as to divide it again into two sub-intervals both carrying half of its current. As equal currents on the band electrode are represented in the H-plane by equal distances on the imaginary axis, the needle electrodes needed for the function h/f are represented in the H-plane by a series of equidistant points on the imaginary axis, as indicated in fig. 9 by the points p. In fact, we may now become independent of physical auxiliaries and define the function h/f as having its poles or zeros on a series of equidistant points in the H-plane along the straight lines representing the attenuation and transmission bands, respectively.

3·4. Approximation of the value of h/f in the H-plane

With the aid of the H-plane we may calculate to a close approximation the values of h/f for all points in the λ-plane, including those that are close to the zeros of h.

This is important, as the value of h/f in the transmission bands determines the variation of attenuation. As is shown in this section a difference $\ln 2$ exists in the transmission bands between the minimal value of $\ln|h/f|$ and the value of $\ln|F_1|$ from which it is derived by formulae (19) and (20). Correcting this difference we get formulae (23) and (24).

A function in the H-plane that is to a close approximation constant along the lines β and has an equidistant series of logarithmic poles along the imaginary axis (at intermediate distances π) may be described as $C \ln |\cosh H| + D$ if the distance between the lines β and the axis is greater than π. The extreme value of the function along the axis is $C \ln|\cosh 0| + D = D$.

The values of C and D are found in the following way. At the point $H = x + jy$ we find, if x is not too small, for instance $x > \pi$,

$$C \ln|\cosh H| + D = C \ln\left|\frac{\varepsilon^{x+jy} + \varepsilon^{-x-jy}}{2}\right| + D \approx$$
$$\approx C \ln\left|\frac{\varepsilon^{x+jy}}{2}\right| + D = C(x - \ln 2) + D.$$

In the proximity of β this field and its derivative must be approximately equal to the field representing the real part of H and its derivative. Therefore,

$$C\,(x - \ln 2) + D \equiv x;$$

thus $$C = 1 \quad \text{and} \quad D = \ln 2.$$

Along the axis, therefore, the function $\ln|\cosh H| + D$ will vary between $-\infty$ and $+\ln 2$. This may be interpreted by saying that, when the band electrode is replaced by needles in the manner indicated, the maximal potential in the transmission band will increase, and the minimal potential in the attenuation band will decrease by an amount $\ln 2$ (see fig. 10).

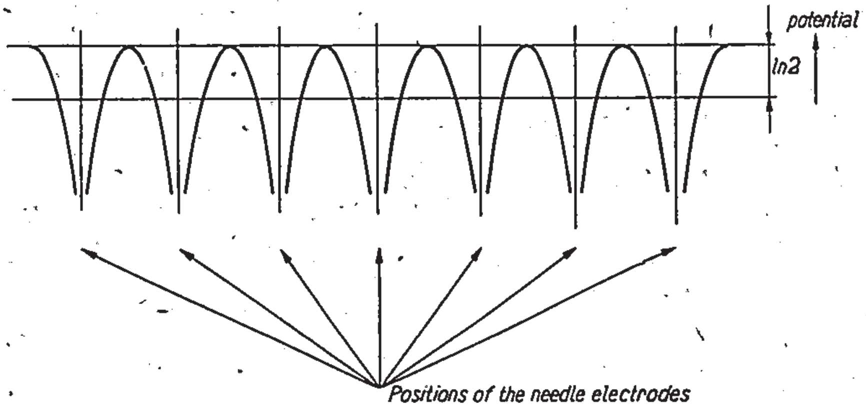

Fig. 10. When the band electrode in a transmission band is substituted by a set of needle-electrodes (represented by equidistant points in the H-plane) the maximal potential differs an amount $\ln 2$ from the mean potential.

Therefore, in actual experiment we should use a function $\ln|F|$ that is given by

$$\ln|F| = \ln|F_1| - \ln 2 \text{ in the transmission bands,}$$

and by

$$\ln|F| = \ln|F_1| + \ln 2 \text{ in the attenuation bands.}$$

The formulae (19) and (20) then give rise to the following two:

$$\text{in the transmission band } D_\nu, \quad \ln|F| - \alpha_0 \text{ must be} \leqq \tfrac{1}{2}\ln \Delta\alpha_\nu, \tag{23}$$

$$\text{in the attenuation band } G_\mu, \quad \ln|F| - \alpha_0 \text{ must be} \geqq \alpha_\mu + \ln 2. \tag{24}$$

3·5. A configuration of electrodes producing the conjugate *H*-field

To define experimentally the positions of the needle electrodes we can use an other configuration of band electrodes in the tank. As mentioned in section 3·1, the only singularities of the *H*-function are branch points on the edges of the band electrodes.

Furthermore, we saw that the current defined in section 1·6 is a measure for the imaginary part of *H*. For that part the same Laplace differential equation is valid as for the real part, and therefore it should be possible to find a configuration of electrodes in the tank producing a field that represents the imaginary part of *H*. This field, in accordance with common usage, we shall call the conjugate of the field representing the real part of *H*, and the new electrode configuration will be said to be conjugate to the old one.

The branch points must be the same for both parts of *H*. The equipotentials of the old field must coincide with the gradient curves of the new one, and vice versa. The new field, therefore, is symmetrical to the ω-axis and has equipotentials on that axis between every pair of the old band electrodes. So, when we put along the ω-axis new band electrodes in all the open spaces between the old ones and then remove the old ones, we can produce a field having singularities at the right places and equipotentials coinciding with the ω-axis at the right places. Now, when we put the electrodes on the right potentials, we have the field representing the imaginary part of *H*.

To find the potentials of the electrodes we move from one of the new electrodes to the next along the ω-axis. The increase of the potential along that path must be proportional to the increase of the imaginary part of *H* and, therefore, in accordance with sections 1·6 and 2·6, to the current taken by the intermediate old electrode.

3·6. Simple proportionalities between the currents in the various band electrodes of the original configuration

The imaginary part of H is an approximation of the imaginary part of ln h/f, i.e., the argument of h/f. All poles and zeros of h/f lie on the ω-axis. Plotting arg h/f against ω, one therefore finds a horizontal straight line making a jump π at every pole or zero.

As only an integral number of poles or zeros is possible in a band, the increase in arg h/f will always have to be an integral multiple of π. This means that the difference in potential between any two neighbouring electrodes in the second configuration must be an integral multiple of π and therefore the current taken by any band electrode in the original configuration must be an integral multiple of the unit current.

As a small number of poles and zeros is desirable for an inexpensive and simple filter network, the proportionality between the currents of the different electrodes must be one of simple integers. When this conditions is not fulfilled, the requirements of section 2·1 must be modified until it is.

3·7. Determination of the poles and zeros of h/f by means of the conjugate electrode configuration

Fig. 11 gives the imaginary part of H along the ω-axis (continuous curve) and that of ln (h/f) (step curve).

From section 3·5 it follows that the potential differences between the places of any two successive needle electrodes must be equal. In fig. 11 we can therefore find these places by constructing the points where the curve Im (H) intersects a set of equidistant horizontal lines.

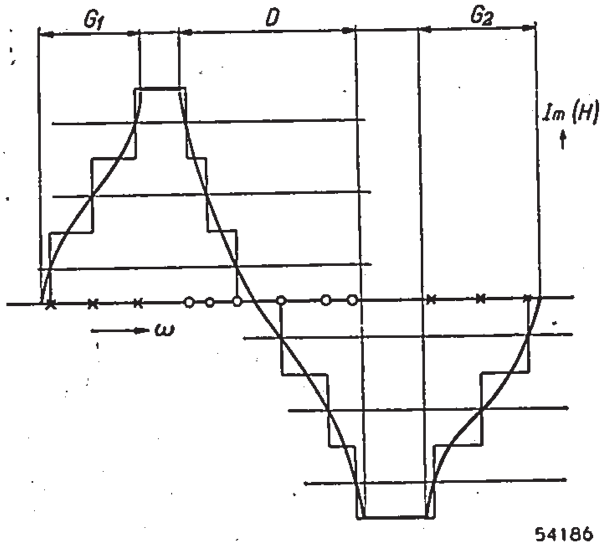

Fig. 11. Imaginary part of H (continuous curve) and of ln (h/f) (step curve) along the ω-axis. The poles × and zeros o of h/f are the projections on the ω-axis of the points of intersection of the curve Im (H) with a set of equidistant horizontal lines.

The number of these lines must be taken equal to the total number n of current units carried by the set of band electrodes in the old electrode configuration that represented the transmission bands *). (This number is equal, of course, to the total number of current units carried by the attenuation-band electrodes in the old electrode configuration.)

From section 3·5 it follows that n is equal to the maximal number of units of potential difference between two of the band electrodes in the conjugate electrode configuration, and therefore to the height of fig. 11 if the vertical distance representing a potential unit is used as length unit.

The vertical distances from the horizontal lines to the lowest point of fig. 11 must be $(2\nu-1)/2n$, ν being an integral number increasing from 1 to n.

In the tank we can find the place of the needles directly by dividing the potential difference between the two band electrodes having the maximal potential difference into a number n of equal parts Δ, and determining the places along the axis where the potential is $\frac{1}{2}\Delta$, $\frac{3}{2}\Delta$, . . ., $(2n-1)\Delta/2$.

3·8. Finding the zeros of $g(\lambda)\,g(-\lambda)$

The zeros of $g(\lambda)\;g(-\lambda)$ lie at the places where

$$\frac{h(\lambda)\,h(-\lambda)}{f(\lambda)\,f(-\lambda)} = -\varepsilon^{2\alpha_0} \quad \text{(see (18))},$$

i.e., according to section 3·3, on the equipotential of Re(H) where the potential is $2\alpha_0$. As $-\varepsilon^{2\alpha_0}$ is negative real, the argument of

$$\frac{h(\lambda)\,h(-\lambda)}{f(\lambda)\,f(-\lambda)}$$

must be $\pi \pm 2n\pi$ at these points.

The gradient curves of Re (H) on which the zeros of g lie are found, as will be discussed below, by considering fig. 9, in which the λ-plane is represented on the H-plane. The zeros of h are marked p. It is immaterial whether band electrodes or needle electrodes are used in the other bands, as these bands are too far away to influence the field around the band D seriously.

As the poles and zeros of h/f all lie on the ω-axis, and as h/f must be symmetrical to the $\varkappa$-axis, we find $h(\lambda)/f(\lambda) = +\,h(-\lambda)/f(-\lambda)$ or $-h(-\lambda)/f(-\lambda)$. The plus sign is valid if neither h nor f have a zero at $\lambda = 0$: the minus sign in the opposite case. Therefore the argument of $h(\lambda)/f(\lambda)$ at the zeros of g/f must be

$$\tfrac{1}{2}\,(\pi \pm 2n\pi) \text{ or } \tfrac{1}{2}\,(\pm\, 2n\pi), \text{ respectively.}$$

---

*) The number has to be integral as is discussed in section 3·6.

The zeros of g must therefore lie on the gradient curves of h/f in the λ-plane with the argument $\pi/2 \pm n\pi$, or $\pm n\pi$ respectively. The same applies for the H-plane. In the H-plane the imaginary axis is a gradient curve of h/f with argument $\pm n\pi$ or $\pi/2 \pm n\pi$, respectively.

Around a zero h_1 of h the increase of the argument equals the increase of the angle of the radius to that zero. Therefore at the zero there starts a gradient curve with the argument $\pi/2 \pm n\pi$ or $\pm n\pi$, respectively, perpendicular to the imaginary axis. For reasons of symmetry this line will continue to run perpendicular to the imaginary axis, and it therefore corresponds to the image in the H-plane of a gradient curve of the H-function running through the zero of h. This gradient curve corresponds to an equipotential in the conjugate configuration.

Thus the zeros of $g(\lambda)\, g(-\lambda)$ are the points where $\mathrm{Re}(H) = 0$ and where $\mathrm{Im}(H)$ is equal to $\mathrm{Im}(H)$ at a zero point of h. For the zeros of g we may take the zeros of $g(\lambda)\, g(-\lambda)$ lying in the negative half-plane.

3·9. A function g/f with poles not on the ω-axis

As is known from section 2·3, the relative error, resulting from the substitution of h/f by g/f, is very small if $\ln|g/f| - a_0 > 15$ db, that is to say, at points lying outside the closed curve $\ln|h/f| - a_0 = 0$ at a not too small distance from that curve. Confining ourselves to that range, we therefore put $h/f = g/f$ and examine f/h.

From this function we can deduce a function $\overline{f}/h$ in the same way as we deduced g/f from h/f, i.e., by an equation

$$\frac{f}{h}(\lambda)\,\frac{f}{h}(-\lambda) + a^2 = \frac{\overline{f}}{h}(\lambda)\,\frac{\overline{f}}{h}(-\lambda).$$

This will lead, in accordance with formula (18), to a function $\overline{f}/h$ or $\overline{f}/g$ of which the attenuation in the attenuation band is an amount $\ln a$ less than that of f/h, whereas the attenuation variation in that band is $\overline{\varDelta} a_\mu = (a/2)^2$ and the poles lie as indicated in fig. 12. The same procedure may be followed for every attenuation band separately, thus leading to an attenuation function as mentioned in section 2·1.

The requirements for h/f must now be changed into the following:

in the transmission band D_ν, $\ln|h/f| - a_0$ must be $\leqq \ln 2 + \frac{1}{2} \ln \varDelta a_\nu$, (25)
in the attenuation band G_μ, $\ln|h/f| - a_0$ must be $\geqq a_\mu - \ln 2 - \frac{1}{2} \ln \overline{\varDelta} a_\mu$. (26)

Those for F become:

in the transmission band D_ν, $\ln|F| - a_0 \leqq \frac{1}{2} \ln \varDelta a_\nu$, (27)
in the attenuation band G_μ, $\ln|F| - a_0 \geqq a_\mu - \frac{1}{2} \ln \overline{\varDelta} a_\mu$. (28)

It should be remembered that, according to section 2·3, the equations (26) and (28) are valid to a good approximation only if $\overline{\Delta a}_\mu < 0{\cdot}1$ neper. When $\overline{\Delta a}_\mu > 0{\cdot}1$ neper, we must, if necessary, replace the term $-\frac{1}{2}\ln \overline{\Delta a}_\mu$ by $-\frac{1}{2}\ln(\varepsilon^{4\overline{\Delta a}_\mu}-1)+\ln 2+2\,\overline{\Delta a}_\mu$.

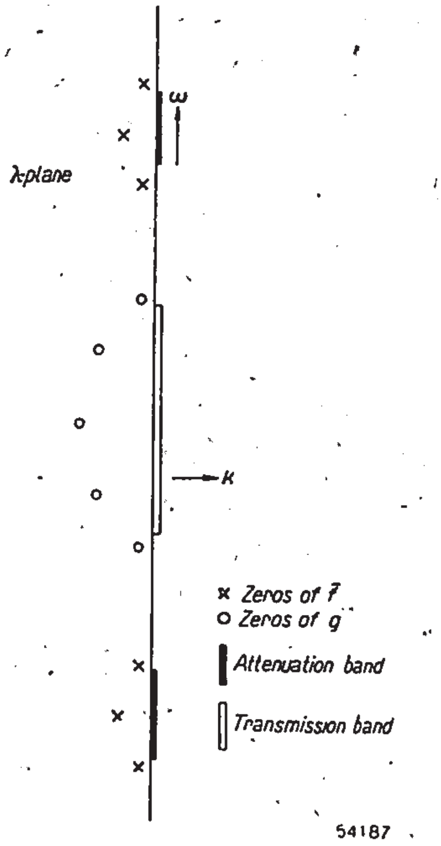

Fig. 12. Poles and zeros of a function $g/\bar{f}$.

4. Analytic characteristics of the H-function

4·1. Behaviour of H in the λ-plane

In the foregoing we have found a method for the determination of transfer functions by using the H-function, which we determined by defining the potential field representing that function. We shall now, for the sake of completeness, define the H-functions analytically. They will prove to be a special kind of hyper-elliptic integrals, which could in principle be computed as outlined in sections 4·2 and 4·4.

In section 4 no new conclusions as to the experimental determination are found; therefore the reader that is not interested may turn directly to section 5.

By the definition given in section 3·1, at every band electrode the field H passes over into its own electrical image; so when one plots vertically the value of Re(H) over the λ-plane, the plotted surface must be symmetrical to every horizontal plane representing the potential of one of the band electrodes. So when there are more than one band electrode, the surface will have an endless chain of branches. In fig. 13 we have reproduced a part of an H-function along the ω-axis (the $\ln|F|$-function from which it is derived is drawn more heavily). The imaginary part of H will form an analogous chain of curves.

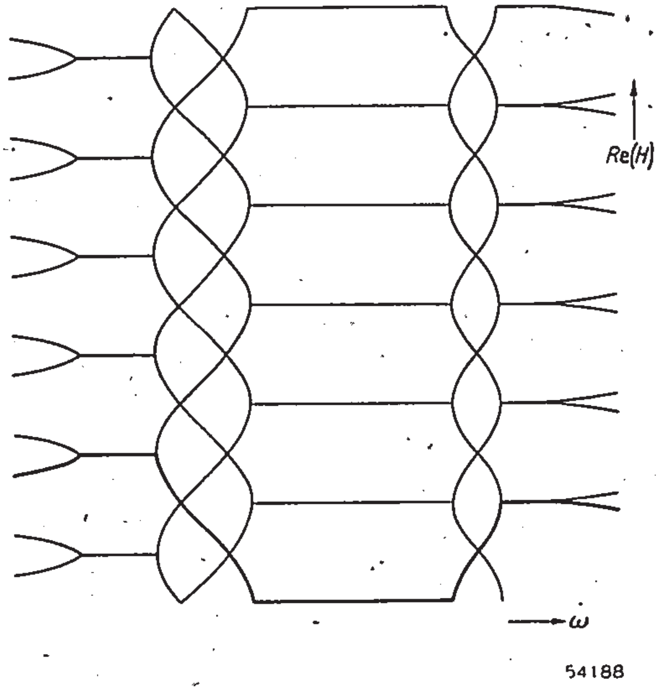

Fig. 13. An H-function mostly has an endless chain of branches. In this figure the real part of an H-function is drawn for real values of ω.

4·2. Analytic definition of H

We shall derive an analytic expression for H, starting from a consideration of the complex function

$$\frac{1}{\sqrt{q}} = \frac{1}{\sqrt{(\lambda^2+\omega_1^2)\,(\lambda^2+\omega_2^2)\,\ldots\,(\lambda^2+\omega_n^2)}},$$

all ω_ν being real. Along the imaginary λ-axis $1/\sqrt{q}$ will be double-valued and alternately purely real and purely imaginary. The same holds for functions $p/\sqrt{q}$ in which p and q are polynomials that are real at the imaginary λ-axis (see, for example, fig. 14) *).

---

*) There is very little similarity between the functions $1/\sqrt{q}$ or $p/\sqrt{q}$ and Cauer's Q-functions, which are also given as square-root expressions; e.g., the Q-functions, if they are real in the transmission band, are imaginary in the attenuation band, whereas $1/\sqrt{q}$ or $p/\sqrt{q}$ is real in both kinds of bands and imaginary in the intermediate bands.

When we now integrate the real part of $p/\sqrt{q}$ along the ω-axis, the integral will be a constant along the bands where $p/\sqrt{q}$ is imaginary. Starting the integration from an ω^{ν} on a band where $p/\sqrt{q}$ is real, we can always find two branches of the integral according to the two branches of $p/\sqrt{q}$, and by integrating forwards and backwards again we can find an endless chain of branches. So $\int \frac{p}{\sqrt{q}}\,\mathrm{d}\lambda$ is an *H*-function (fig. 15). This holds for every integral

$$\int \frac{p(\lambda)}{\sqrt{q(\lambda)}}\,\mathrm{d}\lambda$$

with the following properties:

(1) p and q are polynomials in $j\lambda$;

(2) the roots of q all lie on the ω-axis, and q is real along that axis;

(3) p is purely real or purely imaginary along the ω-axis: this implies that its roots form a pattern symmetrical to the ω-axis;

(4) in order to keep the integral finite at the point ∞ the integrand must there tend to zero more quickly than $\omega^{-3/2}$ or ω^{-2}, according to the degree of q being odd or even, respectively.

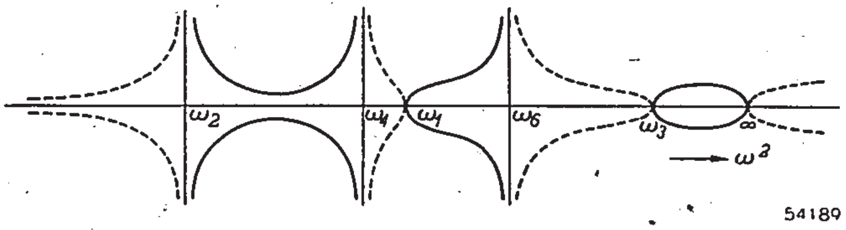

Fig. 14. The function $\dfrac{(\lambda^2 + \omega_1^2)\,(\lambda^2 + \omega_3^2)}{\sqrt{(\lambda^2 + \omega_2^2)\,(\lambda^2 + \omega_4^2)\,(\lambda^2 + \omega_6^2)\,(\lambda^2 + \omega_1^2)\,(\lambda^2 + \omega_3^2)}}$ for $\lambda^2 = -\omega^2$. The function is two-valued and either purely real (dashed lines) or purely imaginary (full-drawn lines).

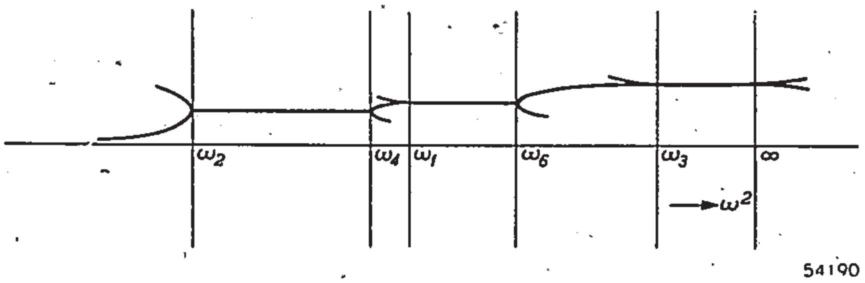

Fig. 15. Integral of the real part of the function of fig. 14.

4·3. Calculation of the differences in value between the horizontal parts of the H-curve when the analytic expression of H is given

$\bar{a}_1$, the difference in value *) of H between two successive branch points ω_1 and ω_2, can be found by evaluating the definite integral

$$\int_{\omega_1}^{\omega_2} \frac{p(\lambda)}{\sqrt{q(\lambda)}} \, \mathrm{d}\lambda \, .$$

If we substitute $x = -j\lambda - (\omega_1 + \omega_2)/2$ and $\omega_1 - \omega_2 = 2a$, we can split the integral into three parts, viz.

$$\int_{\omega_1}^{\omega_2} (\lambda) = \int_{-a}^{+a} (x) = \int_{-a}^{-a+\varepsilon} (x) + \int_{-a+\varepsilon}^{a-\varepsilon} (x) + \int_{a-\varepsilon}^{a} (x) \, ,$$

provided ε is a small number that tends to zero. In the region $-a + \varepsilon < x < a - \varepsilon$ the function is analytic and can be integrated by expansion into a power series. The other two integrals tend to zero when ε tends to zero. Therefore, the original integral too can be integrated by series expansion.

4·4. Definition of the analytic expression of H when the differences in value of the horizontal parts of H, as well as the branch points $\omega_1, \omega_2, \ldots$ are given

$q(\lambda)$ is directly given by the branch points $\omega_1, \omega_2, \ldots$:
$q(\lambda) = (\lambda - j\omega_1)(\lambda - j\omega_2) \ldots (\lambda - j\omega_n)$.
To find p we split the integral into a series of terms

$$\int \frac{p(\lambda)}{\sqrt{q(\lambda)}} \, \mathrm{d}\lambda = \sum_{\mu=1}^{n} p_\mu \int \frac{\lambda^\mu}{\sqrt{q(\lambda)}} \, \mathrm{d}\lambda \, .$$

The real part of $\displaystyle\int \frac{\lambda^\mu}{\sqrt{q(\lambda)}} \, \mathrm{d}\lambda$ is constant in the same band as that of $\displaystyle\int \frac{p}{\sqrt{q}} \, \mathrm{d}\lambda$. We designate the real part of $\displaystyle\int \frac{\lambda^\mu}{\sqrt{q(\lambda)}} \, \mathrm{d}\lambda$ in the band ν by $\bar{a}_\nu{}^{(\mu)}$.

We can calculate the values of the integrals on the right side in accordance with section 4·3. Then we can calculate the coefficients p_μ by evaluating the system of linear equations

---

*) If the H-function is derived from the requirements of a filter transmission function, $\bar{a}_1$ is the sum of a discrimination a_μ and terms depending on the attenuation variations Δa_ν and $\overline{\Delta} a_\mu$. To stress this relationship the difference in value under consideration has been denoted by an a.

$$\begin{aligned} \bar{a}_1 &= p_n\, a_1^{(n)} + p_{n-1}\, a_1^{(n-1)} + \ldots + p_0\, a_1^{(0)}, \\ \bar{a}_2 &= p_n\, a_2^{(n)} + p_{n-1}\, a_1^{(n-1)} + \ldots + p_0\, a_2^{(0)}, \\ &\vdots \end{aligned}$$

There are $n/2-1$ or $(n+1)/2-1$ different $\bar{a}$'s according to whether n is even or odd, and therefore the number of equations is $n/2-1$ or $(n+1)/2-1$.

The highest power of λ in $p(\lambda)$ is $(n-4)/2$ or $(n-3)/2$ (see section 4·2). Therefore, including p_0, the number of unknown quantities is $n/2-1$ and $(n-1)/2$, respectively.

We conclude that the number of unknowns equals the number of equations, and the expression $\int \frac{p(\lambda)}{\sqrt{q(\lambda)}}\,\mathrm{d}\lambda$ is completely defined. This expression is a special case of a hyper-elliptic integral. When the number of branch points is four it degenerates into an elliptic integral.

4·5. Saddle points

The saddle points of H are the zeros of p. In fig. 16 the approximate places of saddle points Z are given for various cases. The places may be estimated by considering rubber-membrane models.

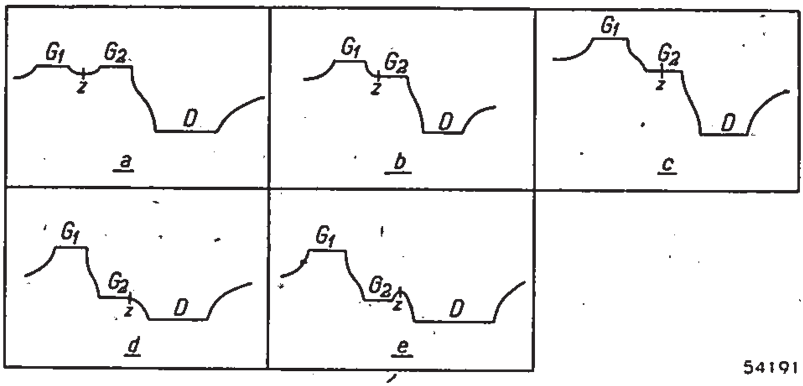

Fig. 16. Saddle points of several H-functions are indicated by z.

4·6. Representation of the λ-plane on the H-surface

In section 3·2 we represented a part of the λ-plane on the H-plane. Here we shall represent the λ-plane on a surface that may be visualized as the total outer surface of a sheet of material of infinitesimal thickness and of a shape that is defined by the H-function. The equipotentials and the gradient curves of H likewise form two sets of mutually perpendicular straight lines on this surface, which we shall call an H-surface.

Let us consider the H-function in fig. 17. The drawing represents the

λ-plane. The heavily-drawn intervals are the transmission and attenuation bands. The curved line represents the gradient curve passing through the saddle point.

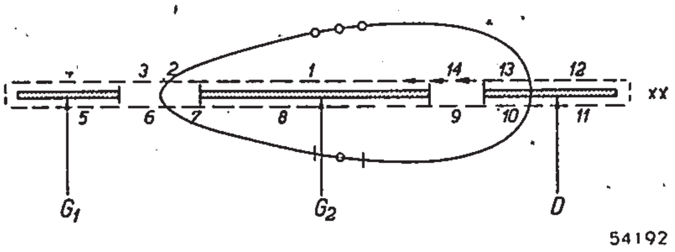

Fig. 17. *H*-function in λ-plane. The curved line is the gradient curve passing through the saddle point. The dashed line 1-14 is represented in the *H*-plane in fig. 18. The representations of the lines marked × ×, ooo, |o| are marked in fig. 18 by the same characteristics.

We shall follow the dashed line in the direction 1-14 (the area on the inside is supposed to be infinitely narrow). After having passed from 1 to 14 we have alternately followed equipotentials and gradient lines and ultimately reached the starting point again. The representation of this line in the *H*-plane is therefore a closed contour (fig. 18) consisting of straight intervals in two mutually perpendicular directions.

The whole of the λ-plane is represented on the inside of this contour. This representation, however, is not yet perfect as the points on the intervals 1, 2, 3, 4, 12, 13, 14 must coincide with those on the intervals 8, 7, 6, 5, 11, 10, 9 respectively. We can attain our object by extending this representation of the λ-plane by a set of other representations in such a fashion as to make the resulting figure symmetrical with respect to any of the

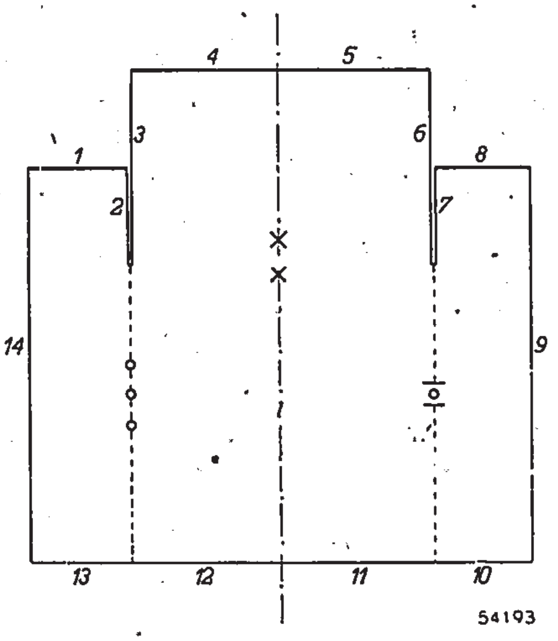

Fig. 18. Representation in the *H*-plane of the *H*-function fig. 17.

straight intervals of the circumference. Then, however, we come to a complicated set of Riemann surfaces.

Another possibility is to fold the figure about the line l and mould together the then coinciding parts of the surroundings. The whole surface then consists of two flat pieces of the shape of fig. 19.

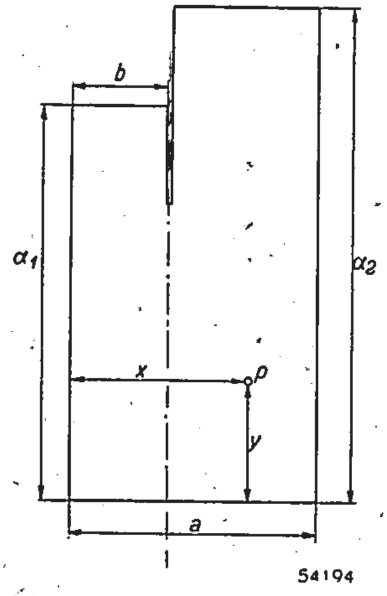

Fig. 19. H-surface for the H-function of fig. 17.

A physical model makes the shape of this surface clear. Take a blade of mica of the shape of fig. 19 and cover it on both sides and on the rims with a homogeneous layer of silver. The layer of silver then has the shape of the H-surface and forms a representation of the λ-plane. The figures 20

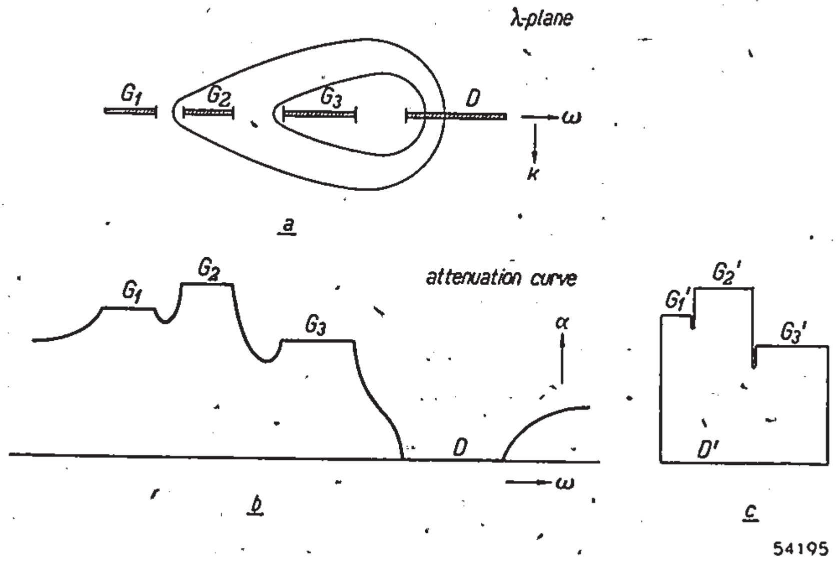

Fig. 20. *a*. H-function in λ-plane. The curves are the gradient curves passing through the saddle points.
b. Real part of the H-function of fig. 20*a* along the ω-axis.
c. H-surface for the H-function of fig. 20*a*.

and 21 give analogous surfaces for other H-functions. In fig. 21 two different views are given of the surface. In fig. 22 the situation of the poles and zeros of the function $g/\overline{f}$ is given on the H-surface. By putting, in a mental experiment, electrodes at the positions of these poles and zeros, and feeding each of the poles with a positive current unit and each of the zeros with a negative one, we find that the shaded areas will form two-dimensional analogies of the inside of a Faraday cage and therefore will have no perceptible potential gradient, whereas in the blank area the potential will have a constant slope surmounted by a small ripple having the period p.

The approximations become perceptible when the horizontal lines carrying the poles descend below the image of the saddle point, i.e., below the slit in the H-surface. These cases seem to be of little practical importance.

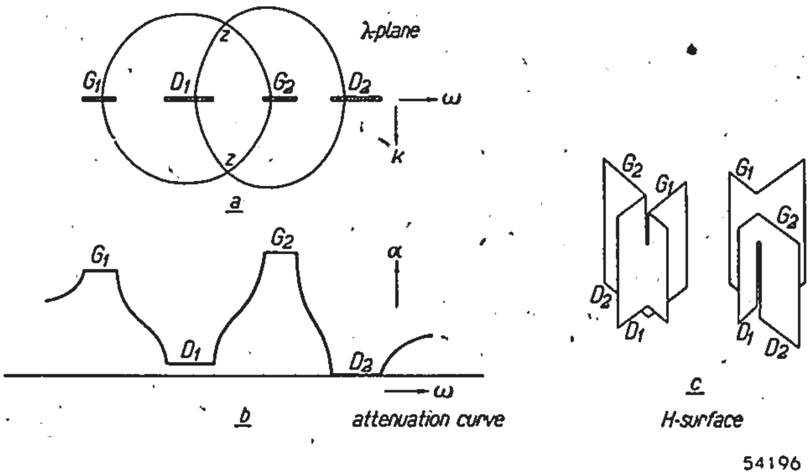

Fig. 21. *a*. H-function in the λ-plane. The saddle points are marked z. The curves are the gradient curves through the saddle points.
b. Real part of the H-function of fig. 21a along the ω-axis.
c. Two different views of the H-surface for the H-function of fig. 21a.

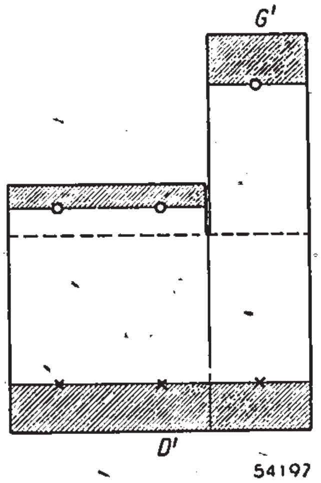

Fig. 22. Poles and zeros of a function $\overline{f}/g$ on the H-surface.

4·7. The function h/f, found in sections 2 and 3, is the one that gives the best attenuation characteristic with a given number of poles and zeros

From fig. 23 we can conclude that the function h/f we have defined in sections 2 and 3 is the best one that is possible with a given number of poles and zeros.

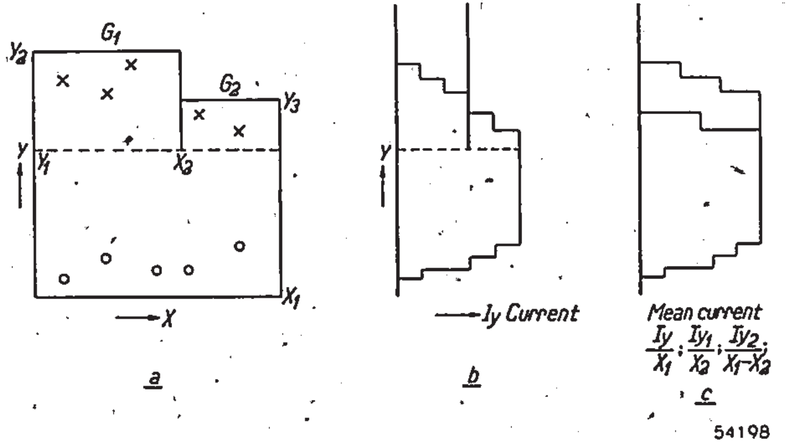

Fig. 23. The H-surface is shown in fig. 23a, with an arbitrary function h/f (except that all poles are close to G_1, G_2, and all zeros close to D).
In fig. 23b the vertical current through a horizontal cross-section is plotted horizontally against the vertical coordinate of the cross-section. It takes a jump each time the cross-section passes a zero or a pole. For $y > y_1$, the graph is split into two parts, the left part corresponding to the part of the H-surface ending in G_1 and the right part to that ending in G_2. In 23c the mean currents are plotted against y.

Consider the case that the minimal attenuations allowed in the bands G_1 and G_2 be a_1 and a_2, the maximal attenuations ∞, and the maximal variation of attenuation in the transmission band Δa. The difference between the minimal value of $\ln|h/f|$ in the attenuation band G_1 (or G_2) and the maximal value in the transmission band then is a_1 (resp. a_2) $+ \ln 2 - \frac{1}{2}\ln \Delta a$ (a generalization to other cases gives no complications to the proofs, only to the notations). The best function h/f gives rise to the minimal Δa when a_1 and a_2 are given, and vice versa. Therefore it is the one with the maximal difference between its minimal value in the attenuation bands and its maximal value in the transmission band:

$$\text{for } \ln(h/f)_{\text{opt}} \text{ the difference } \ln(h/f)_{G\,\min} - \ln(h/f)_{D\,\max}$$

is minimal.

We can write the minimal value $\ln(h/f)_{G\,\min}$ as the difference of the mean value $\overline{\ln(h/f)_G}$ and the maximal deviation in negative direction $\Delta_G \ln(h/f)$.

The condition for an optimal h/f then is that

$$\left\{\overline{\ln\left|\frac{h}{f}\right|_G} - \overline{\ln\left|\frac{h}{f}\right|_D}\right\} - \Delta_G \ln\left|\frac{h}{f}\right| - \Delta_D \ln\left|\frac{h}{f}\right| \tag{29}$$

is maximal.

The term between braces will prove to be maximal if all poles are on the upper edges and all zeros on the lower edge of the H-surface. In this case we shall call this term $B_G - B_D$.

The deviations from B_D, if indeed all poles and zeros are on the edges, will prove to be minimal if they are arranged in equidistant series.

When the zeros are moved away from the edge D, the difference between the maximal value in the transmission band and B_D will be seen to increase. The same goes for a vertical displacement of the poles. Therefore the expression (29) is maximal if the poles and zeros are on equidistant series along the edges of the H-surface, that is, if h/f is derived as in section 2 and 3.

Proof.

The mean value $\overline{\ln (h/f)}_D$ along the lower edge of the H-surface (fig. 23*a*) is represented in the physical model by the mean potential on that edge $\dfrac{\int_0^{x_1} V \mathrm{d}x}{\int_0^{x_1} \mathrm{d}x}$, if x denotes the horizontal distance from the point $(0, x)$ to the left edge of the H-surface (x represents the imaginary part of the H-function, and V the potential at the point $(0, x)$).

To find the term between braces in (29) we shall also express the mean potential in a horizontal straight line, passing through the end of the slit in the H-surface (fig. 23*a*), on the vertical distance y_1 from the lower edge. This mean potential can be expressed as $\displaystyle\int_0^{x_1} \frac{V(x, y_1)\mathrm{d}x}{x_1}$.

The difference is

$$\int_0^{x_1} \frac{V(x,y_1) - V(x,0)}{x_1}\,\mathrm{d}x = \frac{\int_0^{x_1} \mathrm{d}x \int_0^{y_1} \frac{\partial V(x,y)}{\partial y}\,\mathrm{d}y}{x_1} = \frac{\int_0^{y_1} \mathrm{d}y \int_0^{x_1} \frac{\partial V(x,y)}{\partial y}\,\mathrm{d}x}{x_1} =$$

$$= \frac{\int_0^{y_1} \mathrm{d}y \int_0^{x_1} - F_y\,\mathrm{d}x}{x_1} = \frac{\int_0^{y_1} \mathrm{d}y \int_0^{x_1} - \varrho\, i_y\,\mathrm{d}x}{x_1} = \frac{\int_0^{y_1} - \varrho\, I_y\,\mathrm{d}y}{x_1},$$

if F_y denotes the vertical field strength, ϱ the specific resistance of the conducting surface, i_y the vertical current density, and I_y the total vertical current passing the horizontal cross-section of the H-surface, with vertical coordinate y. This current is determined by the number of zeros situated below the cross-section. Therefore I_y as a function of y will be constant except for a jump each time the cross-section passes a pole or a zero.

In the same way we can determine values of I_{y1} and I_{y2} above the cross-section y_1, I_{y1} and I_{y2}, respectively, being the vertical currents that pass through the parts of the H-surface ending in G_1 and G_2. The mean current densities in these separate parts may be expressed as I_{y1}/x_2 and $I_{y2}/(x_1-x_2)$. The mean potential difference

$$\int_0^{x_2} \frac{V(x,y_2)}{x_2}\,\mathrm{d}x - \int_0^{x_1} \frac{V(x,0)}{x_1}\,\mathrm{d}x$$

now can be calculated as

$$\int_0^{y_1} \frac{I_y}{x_1}\,\mathrm{d}y + \int_{y_1}^{y_2} \frac{I_{y1}}{x_2}\,\mathrm{d}y. \tag{30}$$

From fig. 23 it is clear that this integral is maximal if all zeros of h/f are on the lower edge and all poles on the edges G_1 and G_2. Also from (30) we see that if we take the mean potential of D to be $B_D = 0$ the ratio of the mean potentials at G_1 and G_2 is y_2/y_3 (as is required by the attenuation conditions) if the numbers of poles at G_1 and G_2 bear the proportion $x_2/(x_1-x_2)$.

Now by varying the positions of the zeros at D we can get different potential distributions at D leading to different maximal deviations of the actual potential from the mean potential. (The influence of the electrodes at the edges G_1 and G_2 is small in D as these electrodes must be arranged in a way to give small deviations from the mean potential in G_1 and G_2, and therefore much smaller deviations in D.)

The edge D is represented in the H-plane periodically at the imaginary axis. We can represent it again on another complex plane by the substitution of $P = + \cosh (\pi H/x_1)$.

The edge D then is represented in the P-plane by the area $-1 < P < +1$ and the zeros on D by as many zeros in $-1 < P < +1$ (we have made an approximation by disregarding the other representations of the zeros h/f in the P-plane).

The function with $2n$, or $2n-1$, zeros in the P-plane (approximating to P^{2n}, resp. P^{2n-1} for $P \rightarrow \infty$) with the minimal deviations from 0 at $-1 < P < +1$ is the Chebyshev function $\cos \}2n \arcsin P\{$, resp. $\sin \}(2n-1) \arcsin P\{$. This function is represented in the H-plane by a hyperbolic cosine or sine function, and in the H-surface by an equidistant series of zeros.

If it is conditioned that the zeros of h should be on the edge D; therefore they must be equidistant to give an optimal h/f. A similar reasoning shows that if the poles are on G_1 and G_2 they should be equidistant too.

It might yet be possible to improve the function h/f by moving the zeros away from the edge D (or the poles from G_1 and G_2). The mean potential at D then increases, but if the maximal deviation would decrease faster, an improvement would be achieved.

We can show, however, that, if a zero is moved away from D, the maximum potential at D increases, meaning that the expression (29) decreases, which amounts to a worse filter characteristic. If the poles remain on G_1 and G_2 they continue to have a small influence in D. The H-surface near D then can also be represented in the P-plane if the zeros are not all in D.

The removing of the zeros from D is represented in the P-plane by the removing of the zeros from $-1 < P < +1$. The absolute value $|a|$ of the extreme of the rational function in $-1 < P < +1$ then increases, as is stated by Chebyshev's theorem; therefore its logarithm also increases. A similar reasoning shows that the function h/f also is made worse by removing poles from G_1 and G_2.

4·8. On Darlington's method

At this point mention should be made of the method of calculation given by Darlington [7]) who derived transmission functions with Chebyshev properties in the transmission band from a transmission function of a reference filter consisting of constant k and m-derived sections between matched impedances.

This reference-filter transmission function is in our terminology a special case of an H-function. In the electrolytic tank it would be represented by a band electrode in the transmission band and separate needle electrodes for the frequencies of infinite attenuation of the m-derived sections.

The approximation used by Darlington to calculate the zeros of g consists in replacing each m by the mean m, which amounts to gathering all needle electrodes in one point. The approximate positions of the g zeros then are improved by root-improving methods.

5. Manipulations

In conclusion we shall recapitulate the manipulations necessary to determine a transfer function that gives the desired filter curve.

I. To find the proportionality constant C of the tank: Put two needle-shaped electrodes into the tank at the points, say, $\lambda = \pm 10$ cm. One of them carries a positive and the other a negative unit current I. The potential difference V_0 between, e.g., the points $\lambda = \pm 5$ cm is then

$$C \ln \left| \frac{5-10}{5+10} \cdot \frac{-5+10}{-5-10} \right| = -C \ln 9.$$

Therefore

$$C = -\frac{V_0}{\ln 9}.$$

II. Put into the tank band-shaped electrodes covering the transmission and attenuation bands required. Feed each transmission-band electrode with an integral number of negative current units I, and each attenuation-band electrode with an integral number of positive current units, such that the potential of a transmission band D_ν, where an attenuation variation Δa_ν is wanted, becomes $V_{D\nu} \leqq C\,[\frac{1}{2}\ln \Delta a_\nu]$, and that of an attenuation band G_μ, where a minimal attenuation a_μ and an attenuation variation $\bar{\Delta} a_\mu$ is wanted, becomes

$$V_{G\mu} \geqq C\,[a_\mu - \tfrac{1}{2}\ln(\varepsilon^{4\bar{\Delta} a_\mu} - 1) + \ln 2 + 2\bar{\Delta} a_\mu].$$

The latter condition may be simplified to

$$V_{G\mu} \geqq C\,[a_\mu + \ln 2] \quad \text{if } \bar{\Delta} a_\mu = \infty,$$
$$V_{G\mu} \geqq C\,[a_\mu - \tfrac{1}{2}\ln \bar{\Delta} a_\mu] \text{ if } \bar{\Delta} a_\mu < 0{\cdot}1 \text{ neper}.$$

III. Check whether there are parts of the attenuation-band electrode that have a lower potential than the surrounding electrolyte in the nearest vicinity (which means that those parts are taking current from the electrolyte). If so, shorten the electrodes until all transmission-band electrodes are giving current over their entire length.

In the same way shorten, if necessary, the transmission-band electrodes until they are all taking current over the whole of their length.

IV. Measure the potentials of the modified electrode configuration. Check whether the modified configuration makes it possible to reach the conditions mentioned in II with a smaller number of current units.

V. Trace the equipotentials $V = 0$ (*A*)

and, in the case $\bar{\Delta} a_\mu \neq \infty$, $V_\mu = a_\mu$. (*B*)

VI. Put into the tank the conjugate electrode configuration by placing band-shaped electrodes along the ω-axis, filling the gaps between the original ones, and then removing the original band electrodes.

Make the potential difference between any two adjoining electrodes of this conjugate configuration equal to N times the current taken by the intermediate electrode of the original configuration (N being an arbitrary proportionality constant).

VII. Trace the equipotentials $V = V_0 + N\,(\frac{1}{2} + m)$; V_0 being the lowest potential occurring at the electrodes (in the conjugate configuration) and m running through the positive integers from zero onward, until $N(\frac{1}{2} + m)$ becomes higher than the highest potential in the tank.

The points g_m where these equipotentials intersect the equipotentials (A) from V are the poles of the transfer function wanted (zeros of g); the points of intersection f_m with (B) are the zeros (zeros of $\bar{f}$), the intersection points h_m with the ω-axis in the transmission bands are the zeros of h, and those in the attenuation bands are the zeros of f (for definitions of g, $\bar{f}$, h, f, see section 2·2 and 3·9).

The transfer function

$$\frac{\bar{f}}{g} = \frac{(\lambda-\bar{f}_1)\,(\lambda-\bar{f}_2)\ldots}{(\lambda-g_1)\,(\lambda-g_2)\ldots}$$

and the auxiliary function

$$\frac{h}{f} = \frac{(\lambda-h_1)\,(\lambda-h_2)\ldots}{(\lambda-f_1)\,(\lambda-f_2)\ldots}$$

may now be written down numerically.

I should like to conclude by expressing my gratitude to all with whom I had the opportunity to discuss this and related subjects. In particular I would mention J.F. Schouten who initiated this manner of approach by using soap-film models in the discussion of filter losses, B. D. H. Tellegen and W. Nijenhuis, to whom I am indebted for their introduction into several parts of the network theory, and who gave valuable suggestions for the manuscript of this paper.

Eindhoven, July 1947

REFERENCE

⁷) S. Darlington, Synthesis of reactance 4-poles which produce prescribed insertion-loss characteristics, J. Math. Phys. **18**, 257-352, 1939.

VOL. 3 NR 6 DECEMBER 1948

Philips Research Reports

EDITED BY THE RESEARCH LABORATORY
OF N.V. PHILIPS' GLOEILAMPENFABRIEKEN, EINDHOVEN, NETHERLANDS

R 94 *Philips Res. Rep. 3, 401-449, 1948*

ON HIGHLY COMPRESSIBLE HELICAL SPRINGS AND RUBBER RODS, AND THEIR APPLICATION FOR VIBRATION-FREE MOUNTINGS, I*)

by J. A. HARINGX

531.2:621-272.2:621-272.6

Summary

A survey of the contents of a series of six papers, of which this is the first, is given in the introduction. The remainder of the first paper is devoted to a study of the elastic stability of helical springs under compression, or under combined compression and twist. It is shown that, if the problem is simplified by replacing the helical spring by an elastic prismatic rod, its rigidity with respect to shearing must be referred to the transverse force acting in that plane which in the unloaded state is normal to the central line of the rod, but is no longer so in the deflected state. From this interpretation of the simplified model a new relation is deduced between the relative compression at which buckling occurs and the ratio of the length to the diameter of the spring. For this ratio there exists a limiting value below which no buckling occurs, not even under complete compression, and which is dependent only on the method of fixing the spring ends. A more accurate calculation, which takes the helical structure of the spring into account, confirms that the wire diameter and the number of coils are of secondary importance provided that the pitch of the helix is less than, say, half its diameter.

Résumé

L'introduction donne un aperçu sur le contenu d'une série de six articles dont celui-ci est le premier. Le reste du premier exposé est consacré à l'étude de la stabilité élastique de ressorts hélicoidaux soumis à compression ou à compression et torsion combinées. L'auteur montre que le problème peut être simplifié en remplaçant le ressort hélicoidal par une barre élastique et prismatique, à condition que la rigidité de cisaillement se réfère à la force transversale agissant dans le plan qui, en l'absence des flexions, est normal à l'axe de la barre, mais qui ne l'est plus dans l'état fléchi. Cette interprétation de la rigidité de cisaillement a conduit à une nouvelle relation entre la compression relative à laquelle apparaît le flambage et le rapport de la longueur au diamètre du ressort. Pour ce rapport, il existe une valeur limite sous laquelle ne se produit pas de flambage même sous compression complête; cette valeur dépend seulement du mode de fixation des extrémités du ressort. Une calculation plus précise tenant compte de la structure hélicoidale du ressort confirme que le diamètre du fil et le nombre de spires sont d'importance secondaire, pourvu que le pas de l'hélice soit inférieure à la moitié de son diamètre.

---

*) This is the first of a series of six papers to be published in these Reports and comprising an unabridged translation of the author's thesis (Delft, December 1947), which was approved by Prof. Dr Ir C. B. Biezeno, professor of applied mechanics at the Technical University of Delft, Netherlands.

INTRODUCTION

When a body is subject to troublesome effects of vibrations an attempt is usually made to counteract this by mounting the body resiliently. Helical springs or rods and sheets of a more or less elastic material, such as rubber, cork and felt, are used, depending on the nature of the problem. Of course a quantitative investigation of a vibration-isolating effect of such a resilient mounting is only possible when all spring rigidities to be considered are accurately known. In this treatise, therefore, the technical subject proper — the design of vibration-free mountings with their appropriate resilient and damping elements — is preceded by a study of the elastic properties of helical springs and rubber rods.

Whereas the axial rigidity of helical springs is to be found in any elementary text-book and we also have some knowledge of the axial rigidity of well-vulcanized rubber rods [1])*), so far the lateral rigidity of helical springs has been known only in cases where these springs are not at the same time compressed by an axial force [2]). When, however, the resilient element serves simultaneously as a supporting element — as is generally the case — an axial force is always present. Bearing in mind that springs, just as well as straight rods, are apt to buckle under a certain compressive load and that their lateral rigidity under this load becomes nil, it is obvious that the lateral rigidity depends to a very great extent upon the axial load. A rough approximation of this dependency can be obtained by means of a correction factor given by Röver [3]). Another, in many respects better, formula for the lateral rigidity of a compression-loaded spring is to be found in Gross and Lehr [4]). But, as recently demonstrated by the author [5]), also this formula leaves room for an important improvement, since the differential equation on which the formula is based [6]) needs some correction.

When this correction is applied, the differential equation in question leads to results that are in excellent agreement with those obtained from experiments concerning both the elastic stability and the lateral rigidity. As a matter of fact these results are also confirmed theoretically by a more accurate method of dealing with the problem, where the spring is not regarded as an elastic prismatic rod — as usual hitherto — but actually as a helically wound wire stucture.

All this is discussed in parts A and B of chapter I, whereas part C of chapter I is devoted to the natural frequencies of helical springs under compression when vibrating longitudinally or transversely. Knowledge of these frequencies is necessary in connection with the low internal damping of metal springs, causing the tendency of these springs to resonate at their natural frequencies, such in contrast with resilient elements of other materials.

---

*) The numbers refer to the notes at the end of the introduction.

In chapter II similar problems are discussed with regard to rubber rods, though here the calculation of the natural frequencies is omitted, because the internal damping of this material generally prevents any resonance. As regards the elastic stability of rubber rods, some experimental data of Kosten [7]) are at our disposal. The theoretical derivation given in this chapter appears to lead to reasonable agreement with empirical results, particularly for circular rubber rods. With very short rubber rods, however, a fundamental deviation occurs, the cause of which is to be sought on the one hand in incomplete knowledge of the elastic properties of highly compressed rubber and on the other hand in the disturbing influence of both rod ends being in contact with the compression surfaces. According to Kosten [8]) this disturbing influence can be eliminated by assuming the presence of a thin, incompressible layer at each end of the rod. It must be borne in mind, however, that when shearing occurs this layer retains its original elasticity.

Now that we have rules at our disposal for calculating any desired rigidity of helical springs and rubber rods, it is possible to make space constructions meet certain pre-determined demands with respect to their resilience. Although the original intention was to design vibration-free mountings for instruments like balances, microscopes and galvanometers (so-called passive damping), the resilient constructions discussed in chapter III are also suitable as supporting elements for vibration-exciting mechanisms, when the transmission of these vibrations to the surroundings has to be prevented (so-called active damping).

When applying a resilient construction in order to eliminate the interfering vibrations as far as possible, we must remember that certain natural frequencies are introduced which may also prove troublesome. Therefore, in order to minimize the effect of possible resonances of this construction it is necessary to employ damping elements in addition to the resilient elements. Whereas the behaviour of the elementary resilient mounting with one single mass and so-called relative damping in the one-dimensional case is fully known, the favourable results attainable by applying simultaneously an extra auxiliary mass are not so well known [9]). Usually the application of such a damped, dynamic vibration absorber is limited by the demand that the auxiliary mass shall be small in relation to the main mass; with vibration-free mounting of instruments, however, there is usually no objection to these auxiliary masses being so large as to be able to take full advantage of the damping properties of this system in the region of the resonances. As a matter of fact the results obtained when using such auxiliary masses are surprisingly good. For one-dimensional freedom of movement this is discussed in part A of chapter III.

As regards vibrations in several dimensions, little has so far been known [10]) of the elementary mounting with one single mass, and — to the best of our knowledge — nothing at all of the mounting with an extra auxiliary mass. For this reason, in part B of chapter III the space problem is treated more fully.

In chapter IV special attention is paid to the practical construction of some vibration-free mountings with and without auxiliary mass, whilst also the resilient and damping elements are subject to a closer study.

As to the numbering in the text of the sections and the equations it is to be noted that the numbering begins anew from 1 in every chapter. Where a section or equation is quoted in another chapter its number is preceded by a Roman figure corresponding to the number of the chapter to which it belongs.

REFERENCES

[1]) **C. W. Kosten**, Over de elastische eigenschappen van gevulcaniseerde rubber (On the elastic properties of vulcanized rubber), thesis, Delft (1942), p. 47.

[2]) **E. Rausch**, Die Steifigkeit von Schraubenfedern senkrecht zur Federachse, Z. Ver. Dtsch. Ing. 78, 388-389, 1934; **W. E. Burdick**, **F. S. Chaplin** and **W. L. Sheppard**, Deflection of helical springs under transverse loadings, Trans. Amer. Soc. mech. Engrs 61, 623-632, 1939.

[3]) See **E. Rausch**, Die Steifigkeit von Schraubenfedern senkrecht zur Federachse (Nachtrag), Z. Ver. Dtsch. Ing. 78, 964, 1934.

[4]) **S. Gross** and **E. Lehr**, Die Federn, ihre Gestaltung und Berechnung, VDI-Verlag Berlin (1938), p. 94; **S. Gross**, Berechnung und Gestaltung der Federn, Springer Berlin (1939), p. 77; a graph is given in **K. de Gruben**, Knicksicherheit und Querfederung von Druckfedern, Z. Ver. Dtsch. Ing. 86, 316, 1942.

[5]) **J. A. Haringx**, On the buckling and the lateral rigidity of helical compression springs I, Proc. Kon. Ned. Akad. Wetenschappen Amsterdam 45, 533-539, 1942.

[6]) The differential equation of the helical spring deflected under compression, and imagined as an elastic prismatic rod, was first given in **R. Grammel**, Die Knickung von Schraubenfedern, Proc. first int. Congr. appl. Mech. Delft (1924); pp. 276-278 or Z. angew. Math. Mech. 4, 384-389, 1924. In these articles the shear elasticity of the rod (replacing the spring) is ignored. The differential equation referred to here, which aims at taking the shear elasticity into account, is to be found in **C. B. Biezeno** and **J. J. Koch**, Knickung von Schraubenfedern, Z. angew. Math. Mech. 5, 279-280, 1925, or in **C. B. Biezeno** and **R. Grammel**, Technische Dynamik, Springer, Berlin (1939), pp. 548-553.

[7]) **C. W. Kosten**, loc. cit., p. 66.

[8]) **C. W. Kosten**, loc. cit., pp. 47, 48.

[9]) See, i.a., **J. P. den Hartog**, Mechanical Vibrations, McGraw Hill, New York, (1934), p. 103; **E. Hahnkamm**, Das reibungs- und trägheitsgekoppelte Schwingungssystem Schiff und Schlingertank, Ing. Arch. 3, 251-276, 1932; **E. Hahnkamm**, Die Dämpfung von Fundamentschwingungen bei veränderlicher Erregerfrequenz, Ing. Arch. 4, 192-202, 1933; **L. Geislinger**, Theorie des Resonanzschwingungsdämpfers, Ing. Arch. 5, 146-155, 1934.

[10]) See, i.a., **E. Rausch**, Federnde Lagerung von Maschinen, Z. Ver. Dtsch. Ing. 82, 495-501, 1938.

CHAPTER I. ELASTIC STABILITY, LATERAL RIGIDITY AND NATURAL FREQUENCIES OF HIGHLY COMPRESSIBLE HELICAL SPRINGS

PART A. ELASTIC STABILITY OF HELICAL SPRINGS

1. Introduction

The elastic stability of helical springs was first dealt with by Hurlbrink *) in 1910. Later on the same results were obtained by Grammel **) in a much clearer way by treating the spring as an elastic prismatic rod, as shown in a paper read before the first international Congress of applied Mechanics at Delft in 1924. Shortly thereafter Biezeno and Koch **) pointed out that the results given were not confirmed experimentally and that the discrepancy had to be sought in the fact that the shear elasticity of the spring had been ignored. In deducing the differential equation, however, the last-mentioned authors over-estimated the effect of the shear elasticity, implying as a consequence that any spring, however short, would be liable to buckling. The fact that this was not borne out by their experiments was accounted for by stating that the simplifications employed were no longer permissible for short springs. When, however, due allowance is made for this shear elasticity, the results lie between those obtained by Grammel (Hurlbrink) and those of Biezeno and Koch, and it is found that, entirely in accordance with the experiment, short springs are indeed not liable to buckling (section 3).

The new insight into the manner in which allowance has to be made for the shear elasticity not only applies for calculating the buckling force and the corresponding critical compression of a helical spring but is also useful for solving all problems where the lateral deflection of the spring plays a part (sections 10, 13 and 15).

In addition to the calculations mentioned, all of which are based on the simplifying supposition that the spring can be replaced by an elastic prismatic rod of suitable coefficients of rigidity, also the more accurate calculation is given of a compression-loaded, helically wound, wire structure (sections 4-7). This more accurate calculation teaches that in cases of buckling the simplifications introduced are permissible so long as the slope of the helix is not too steep, a condition that is usually satisfied.

The more accurate method of calculation lends itself equally well for dealing with a helical spring under combined compression and twist

---

*) E. Hurlbrink, Berechnung zylindrischer Druckfedern auf Sicherheit gegen seitliches Ausknicken, Z. Ver. Dtsch. Ing. 54, 133-137 and 181-184, 1910.

**) See the references in note ^{6}) at the end of the preceding introduction.

(sections 8 and 9). In this paper it is chosen in preference to the method of calculation followed in an earlier publication *).

2. Some simplifying suppositions

If the helical spring (which we shall once for all take as being a right-handed one) has a sufficiently small pitch when compressed, the deformation of one single coil under a certain load will differ little from that of an unclosed circular ring lying in a flat plane. Consequently we may imagine the compressed helical spring as being replaced by a number of similar rings *a* connected by perfectly rigid elements *b*, as represented in fig. 1.

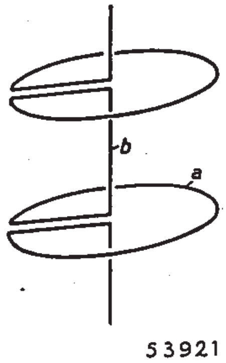

Fig. 1. Diagrammatic representation of a spring consisting of a number of unclosed circular rings *a* connected by perfectly rigid elements *b*.

The influence of the axial force having been discounted, since the successive coils are imagined as being flat after compression of the spring, we now have to see what distortions occur as a result of the bending moments and transverse forces to be transmitted by these flat coils.

With respect to the bending moments each ring will act as a flexible hinge, so that the corresponding distortion will appear, diagrammatically, as given in fig. 2. The plane *a* in which the ring is (approximately) situated bisects the angle between two successive rigid connections *b*, and is thus perpendicular to the central line *c* of the spring, running through the "hinge" points. The transverse force, on the other hand, causes deflection of the ring in its plane only, so that the ends of the rigid connections are displaced with respect to each other in the direction of the transverse force, with the result illustrated in fig. 3. The planes *a* of the rings have not altered their positions from those in fig. 2, only the rigid connections *b* having been displaced parallel to themselves. We now see that the planes *a* are no longer at right angles to the central line *c* of the spring which is found by drawing a smooth curve through the midpoints of the connections.

---

*) J. A. Haringx, On the buckling and the lateral rigidity of helical compression springs II, Proc. Kon. Ned. Akad. Wetenschappen Amsterdam 45, 650-654, 1942.

We should therefore bear in mind that we must not take as transverse force the force acting in the direction perpendicular to the central line of the deflected spring, but the force lying in the "plane" of the ring itself, which plane was *originally* perpendicular to the central line.

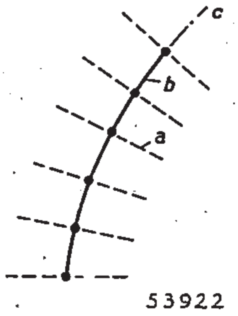

Fig. 2. The spring distorted by bending moments.

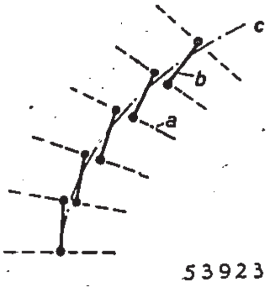

Fig. 3. The spring distorted by bending moments and transverse forces.

a. "plane" of the unclosed ring,
b. perfectly rigid connection,
c. central line of the spring.

In order to avoid the discontinuity of the elasticity of the imaginary construction we distribute this elasticity uniformly over the whole length and now imagine the original helical spring as being replaced by an elastic prismatic rod. This rod has to be made of such a material that the various rigidities with respect to bending, shearing and compression correspond exactly to those of the helical spring, on the understanding that the rigidity with respect to shearing relates to the transverse force acting in the plane that in the unloaded state is normal to the central line of the rod, but is no longer so in the deflected state.

The rigidities with respect to bending, shearing and compression, defined per unit of instantaneous length of spring, are denoted by α, β and γ. If further ψ denotes the angle through which the originally normal section has turned and φ the shear angle due to the transverse force, the extra deformation of an element dz of the compressed spring due respectively to a bending moment M and a shear force Q consists of

$$\left.\begin{aligned} &\text{a relative rotation of the end planes, } d\psi = \frac{M}{\alpha}\,dz,\\ &\text{a relative translation of the end planes, } \varphi dz = \frac{Q}{\beta}\,dz. \end{aligned}\right\} \qquad (1)$$

Further, let

n_0 = number of free coils,
$D_0 = 2R_0$ = diameter of the coils,
l_0 = length of the unloaded spring,
l = length of the loaded spring,

I_0 = the polar moment of inertia of the wire section around the axis through the centre of gravity,

I_1 = the linear moment of inertia of the wire section around the first principal axis, which in the unloaded state is understood to be at right angles to the central line of the spring,

I_2 = the linear moment of inertia of the wire section around the second principal axis,

$\varkappa$ = a factor related to the twisting of the wire and depending on the shape of its cross-section,

E = Young's modulus of elasticity,

G = shear modulus,

m = Poisson's ratio;

then the reciprocal values of the various rigidities per unit of length of the unloaded spring are *)

$$\frac{1}{\alpha_0} = \frac{n_0}{l_0}\frac{\pi D_0}{2EI_1}\left(1 + 2\varkappa\frac{m+1}{m}\frac{I_1}{I_0}\right), \quad \frac{1}{\beta_0} = \frac{n_0}{l_0}\frac{\pi D_0^3}{8EI_2}, \quad \frac{1}{\gamma_0} = \varkappa\frac{m+1}{m}\frac{n_0}{l_0}\frac{\pi D_0^3}{2EI_0}. \qquad (2)$$

The rigidities, defined per unit of length of the loaded spring, follow from the relations

$$\alpha = \frac{l}{l_0}\alpha_0, \quad \beta = \frac{l}{l_0}\beta_0, \quad \gamma = \frac{l}{l_0}\gamma_0. \qquad (3)$$

3. Buckling of the helical spring under compression, regarded as a rod

When the rod (replacing the spring) is loaded at the ends by two equal and opposite compressive forces P, causing a deflection $y = f(z)$ (fig. 4), a section of the rod that in the unloaded state is a normal cross-section (but no longer so in the loaded state) is subjected to a normal force N, a bending moment M and a shear force Q. The angle through which this section is turned has already been denoted by ψ, so that we have

$$M = Py, \quad Q = P\sin\psi \approx P\psi, \quad N = P\cos\psi \approx P. \qquad (4)$$

Substitution of these expressions in (1) gives

$$\mathrm{d}\psi = \frac{M}{\alpha}\mathrm{d}z = \frac{Py}{\alpha}\mathrm{d}z, \quad \varphi = \frac{Q}{\beta} = \frac{P\psi}{\beta}. \qquad (5)$$

As shown in fig. 5 and in accordance with eq. (5), the slope of the central line of the deflected rod is equal to

$$-\frac{\mathrm{d}y}{\mathrm{d}z} = \psi + \varphi = \left(1 + \frac{P}{\beta}\right)\psi. \qquad (6)$$

---

*) See C. B. Biezeno and R. Grammel, Technische Dynamik, Springer, Berlin (1939), p. 549.

Differentiation of this equation gives

$$-\frac{d^2y}{dz^2} = \left(1 + \frac{P}{\beta}\right)\frac{d\psi}{dz},$$

or in connection with (5)

$$\frac{d^2y}{dz^2} + \frac{P}{\alpha}\left(1 + \frac{P}{\beta}\right)y = 0. \tag{7}$$

Given

$$q^2 = \frac{P}{\alpha}\left(1 + \frac{P}{\beta}\right), \tag{8}$$

the solution of eq. (7) is:

$$y = A \sin qz + B \cos qz.$$

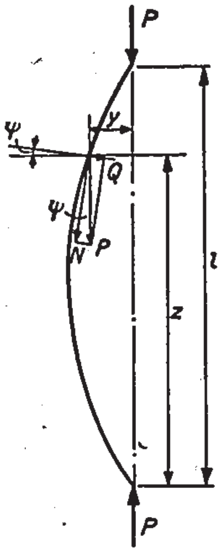

Fig. 4. The deflected central line of the elastic prismatic rod replacing a helical spring, the rod being hinged at both ends and loaded with a compressive force.

In the simple case of hinged ends the boundary conditions ($y = 0$, at $z = 0$ and $z = l$) lead to the following equation for the smallest critical load

$$\frac{P}{\alpha}\left(1 + \frac{P}{\beta}\right)l^2 = \pi^2. \tag{9}$$

Taking the relative compression of the spring equal to ξ we get

$$\Delta l = l_0 - l = \xi l_0 \quad \text{or} \quad l = (1 - \xi)\, l_0, \tag{10}$$

and, in agreement with the definition of the rigidity γ_0,

$$P = \frac{\gamma_0}{l_0}\Delta l = \gamma_0 \xi. \tag{11}$$

Having regard to eqs (3), (9), (10) and (11), we find that the relative compression ξ at which the spring buckles satisfies the equation

$$\xi\left\{1-\xi\left(1-\frac{\gamma_0}{\beta_0}\right)\right\}\frac{\gamma_0}{\alpha_0}\,l_0^2=\pi^2. \tag{12}$$

The corresponding buckling force P can then be calculated with the aid of eq. (11).

For the ratios of the rigidities occurring in eq. (12) we can write, on account of (2),

$$\frac{\gamma_0}{\beta_0}=\frac{m}{m+1}\,\frac{I_0}{4\varkappa I_2},\qquad \frac{\gamma_0}{\alpha_0}=\left(2+\frac{m}{m+1}\,\frac{I_0}{\varkappa I_1}\right)\frac{1}{D_0^2}. \tag{13}$$

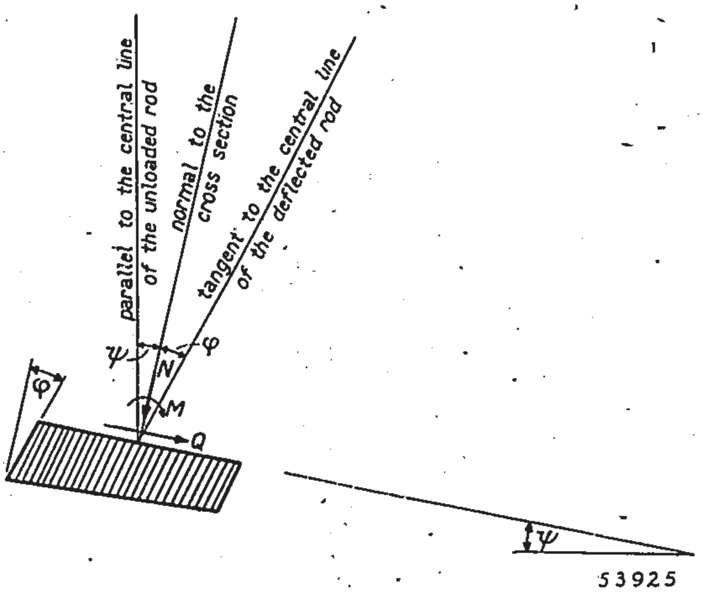
parallel to the central line of the unloaded rod
normal to the cross section
tangent to the central line of the deflected rod
ψ
φ
N
M
Q
φ
ψ
53925

Fig. 5. An element of the elastic prismatic rod replacing the spring, in the deformed state.

If for the spring other boundary conditions are specified the calculation has to be repeated, and for the smallest critical load one usually finds a much more complicated equation than that given in (9). Nevertheless, in certain cases to be mentioned presently it appears that eq. (12) still holds if we only replace the length l_0 by the so-called reduced buckling length of the spring. In the case that both ends are constrained parallel (i.e., only free to move in a lateral direction without any rotation) this reduced buckling length is equal to the length l_0 of the spring itself, whilst with both ends clamped it is $\frac{1}{2}\,l_0$, and with one end clamped and the other free it is $2l_0$.

(a) *Helical spring with circular wire section*

When the wire section is circular (diameter d)

$$I_1=I_2=\tfrac{1}{2}\,I_0=\tfrac{1}{64}\,\pi d^4 \tag{14}$$

and $\varkappa = 1$, so that for the various rigidities according to (2) we may now write

$$\frac{1}{\alpha_0} = \frac{n_0}{l_0}\frac{\pi D_0}{EI_0}\frac{2m+1}{m}, \quad \frac{1}{\beta_0} = \frac{n_0}{l_0}\frac{\pi D_0^3}{4EI_0}, \quad \frac{1}{\gamma_0} = \frac{n_0}{l_0}\frac{\pi D_0^3}{EI_0}\frac{m+1}{2m}. \tag{15}$$

The condition of instability (12) thus becomes

$$\pi^2\left(\frac{D_0}{l_0}\right)^2 = \frac{2\,(2m+1)}{m+1}\,\xi\left\{1 - \frac{m+2}{2\,(m+1)}\,\xi\right\}. \tag{16}$$

With $m = 10/3$ we obtain

$$\left.\begin{aligned} \left(\frac{D_0}{l_0}\right)^2 &= 0{\cdot}3585\,\xi\,(1 - 0{\cdot}615\,\xi), \\ \text{or} \quad \xi &= 0{\cdot}8125\left\{1 \pm \sqrt{1 - 6{\cdot}87\,(D_0/l_0)^2}\right\}. \end{aligned}\right\} \tag{17}$$

The corresponding buckling force P is determined by eq. (11), from which γ_0 can be eliminated with the aid of (15).

In fig. 6 the relative compression ξ at which the spring with hinged ends buckles is plotted as a function of the so-called slenderness l_0/D_0 (curve 3). Only that part of the curve which corresponds to $\xi < 1$ is of practical importance *). The curves 1 and 2 represent the results arrived at respec-

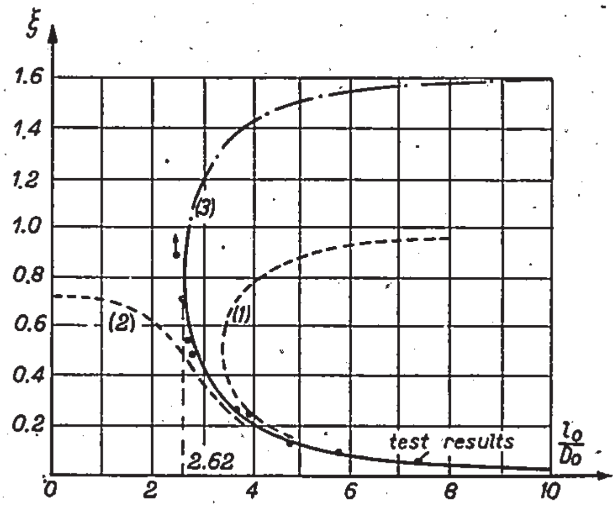

Fig. 6. The critical relative compression ξ of a helical spring with circular wire section and ends hinged or constrained parallel, plotted as function of the slenderness l_0/D_0. A comparison with the results 1 and 2 of other authors and with some test results.

---

*) Since the completion of this treatise it has been found that a helical spring with a relative compression $\xi > 1$ can also be realized. There markable phenomena arising with such a spring will be treated in the author's paper entitled "Elastic stability of helical springs at a compression larger than original length", to be published in Applied Scientific Research.

tively by Grammel (Hurlbrink) and by Biezeno and Koch *). Further, the separate points represent the test results obtained with helical springs of different lengths ($D_0 = 18$ mm, wire diameter = 0·5 or 2 mm, pitch = 5 mm); the vertical arrow at one of the test points indicates that the spring in the fully compressed state did not buckle. As is to be seen, there is a very satisfactory agreement between the theory and the experiment. The graph shows that a certain critical slenderness ($l_0/D_0 = 2{\cdot}62$) exists above which the spring will buckle and below which it will not buckle. Owing to the steep slope of the curve at that point a small variation in the slenderness round about 2·62 leads to very great differences in the behaviour of the spring. If the slenderness exceeds this value ever so slightly ($l_0/D_0 = 2{\cdot}75$) the spring buckles when compressed to about half its original length, whereas in the case of a spring of slightly less slenderness ($l_0/D_0 = 2{\cdot}5$) there is no question of instability at all **).

As already remarked, the same curve is directly applicable in the case where the two ends of the spring are constrained parallel. For a spring with clamped ends the abscissa has to be multiplied by a factor 2, and in the case of a spring with one end clamped and the other free it has to be halved, the critical values of the slenderness being 5·24 and 1·31 respectively.

Although fig. 6 shows a satisfactory agreement between the calculated and the practical results, under certain conditions there may be quite considerable deviations. In the first place we must not lose sight of the fact that in practice the "clamping" of the spring ends is usually no fixture at all but only a pressing of the flat-wound end coils against a fixed surface. Since under these conditions the elasticity of the end coils also plays a part, the spring is apt to buckle at what would appear to be a too small compression.

In the second place we have to bear in mind that the length of the spring is to be understood as the "free" length, i.e., the length of the portion of the spring taking part in the deflection. It may happen, especially in the case of a spring having a pitch relatively small with respect to the thickness of the wire, that in the compressed state the last free coils make contact with the end coils. If we were to take no account of the fact that this limits the free length of the spring, the buckling would occur at an apparently too large compression.

The conditions referred to may also occur simultaneously, in which case the two effects will wholly or partly compensate each other.

---

*) See the references in note 6) at the end of the introduction preceding chapter I. Here it may be added that Grammel's results can be derived from ours by taking $\beta = \infty$, whereas the deviation from the results given by Biezeno and Koch is to be explained by the fact that they put $Q = P\,dy/dz$ instead of $Q = P\psi$.

**) See for a clear demonstration of this remarkable behaviour the photographs in a forthcoming paper, to be published in De Ingenieur (in Dutch).

(b) *Helical spring with rectangular wire section*

In the case of a rectangular wire section with the sides a at right angles to the central line of the spring and the sides b in the other direction, the moments of inertia are

$$I_0 = \tfrac{1}{12}\, ab(a^2 + b^2), \quad I_1 = \tfrac{1}{12}\, ab^3, \quad I_2 = \tfrac{1}{12}\, a^3 b, \tag{18}$$

whilst the factor $\varkappa$ *) is given in table I as function of the ratio a/b or b/a. Here it is to be noted that for large values of a/b or b/a we get $\varkappa \approx a^2/4b^2$ and $\varkappa \approx b^2/4a^2$ respectively.

TABLE I

a/b	$\varkappa$	A	B	b/a	$\varkappa$	A	B
1·0	1·183	0·741	8·08	1·0	1·183	0·741	8·08
1·2	1·22	0·681	8·21	1·2	1·22	0·811	7·93
1·5	1·38	0·626	8·27	1·5	1·38	0·914	7·72
2·0	1·82	0·576	8·34	2·0	1·82	1·060	7·36
2·5	2·43	0·551	8·34	2·5	2·43	1·177	7·08
3	3·17	0·536	8·31	3	3·17	1·275	6·82
4	5·04	0·521	8·24	4	5·04	1·421	6·42
5	7·45	0·514	8·19	5	7·45	1·538	6·08
10	27·0	0·504	8·03	10	27·0	1·786	5·45
∞	∞	0·5	7·77	∞	∞	2·165	4·56

For the ratios of the rigidities we now find according to (13) and (18)

$$\frac{\gamma_0}{\beta_0} = \frac{m}{m+1}\,\frac{1}{4\varkappa}\left\{1 + \left(\frac{b}{a}\right)^2\right\}, \quad \frac{\gamma_0}{\alpha_0} = \left[2 + \frac{m}{m+1}\,\frac{1}{\varkappa}\left\{1 + \left(\frac{a}{b}\right)^2\right\}\right]\frac{1}{D_0^2}.$$

These values can be calculated for $m = 10/3$ and are to be substituted in the condition of instability (12). The results appear in the general form

$$\xi = A\left\{1 \pm \sqrt{1 - B(D_0/l_0)^2}\right\}, \tag{19}$$

with the quantities A and B listed in table I for various ratios a/b and b/a respectively.

In fig. 7 the relative compression ξ at which the spring with hinged ends buckles is plotted as a function of the slenderness l_0/D_0, for springs with a square wire section and for springs with rectangular wire sections where

---

*) This factor $\varkappa$ can be determined by conversion from a table given by Timoshenko; see S. Timoshenko, Strength of Materials, Van Nostrand, New York (1941), vol. I, p. 270, table 3. With the notations b, c and β introduced there,

$$\varkappa = (1 + b^2/c^2)/12\beta = f\,(b/c).$$

the sides a and b are as 1 : 2 or 1 : 0·5. Comparing these curves with curve 3 of fig. 6, we see no great differences. Here, too, with the other end conditions of the spring (i.e., those which were previously mentioned) the curves remain the same if l_0 is only regarded as the reduced buckling length. Further, as is self-explanatory, also the remarks made in regard to the "clamping" of the ends of the spring and the free spring length are applicable here.

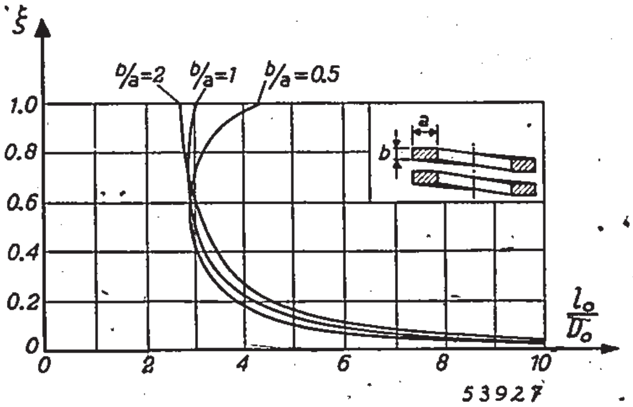

Fig. 7. The critical relative compression ξ of a helical spring with rectangular wire section and ends hinged or constrained parallel, plotted as function of the slenderness l_0/D_0.

4. The helical spring regarded as a wire structure

Whereas in the foregoing sections we assumed the helical spring to be replaced by an elastic prismatic rod, we shall now, in accordance with reality, regard it as a helically wound wire structure. We can then investigate in how far this replacement can be allowed. The basis for this more accurate method of calculation is to be found in a paper by Göhner *).

In addition to the Cartesian coordinates x, y and z, also the cylindrical coordinates r, Θ and z can be employed to indicate a certain point on the central line of the spring wire, so that we have the relations (fig. 8)

$$x = r \cos \Theta, \quad y = r \sin \Theta. \tag{20}$$

At the point in question we further introduce two right-handed orthogonal systems of axes. One of these is completely determined by the space curve indicating the shape of the spring wire; it has the following axes **)

axis I directed along the principal normal towards the centre of curvature,

---

*) O. Göhner, Beanspruchung eines durch Druck und einfache Massenkraft belasteten, beiderseitig eingespannten Schraubenkörpers, Ing. Arch. 7, 237-256, 1936.

**) The numbering of the axes is according to Göhner's system — though it is not commonly used — with the advantage that later on the formulae (99) can be copied at once (section 7).

axis II directed along the binormal, i.e., perpendicular to the plane through the tangent and the principal normal,
axis III directed along the tangent in the sense of increasing Θ.

The other system of axes is fixed to the wire section and has the axes 1, 2 and 3, of which

axis 1 is directed along the first principal axis of inertia of the wire section,
axis 2 is directed along the second principal axis of inertia of the wire section,
axis 3 is directed along the normal to the wire section.

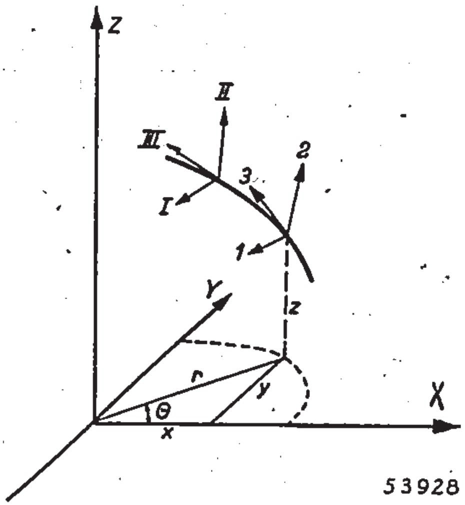

Fig. 8. An element of the helically wound spring wire with the systems of axes introduced.

It is assumed that in the unloaded state the systems of axes I, II, III and 1, 2, 3 are coincident, so that we confine our considerations to those wire sections where in the unloaded state the first principal axis of inertia is perpendicular to the z-axis. This is the case for a circular and generally also for a rectangular cross-section of the wire. If, as is usual with problems of this nature, we ignore the distortion of the spring wire due to the normal and transverse forces as opposed to the distortion due to the bending and twisting moments, the normal to the wire section always falls along the tangent to the curve indicating the shape of the wire; in other words, in the loaded state the directions III and 3 always coincide. The axes I, II and 1, 2 then lie in the same plane and are turned through an angle ϑ with respect to each other (fig. 9).

On the central line of the loaded spring wire we imagine two adjacent points P (Θ) and P' ($\Theta + \mathrm{d}\Theta$), each with the corresponding systems of axes I, II, III and 1, 2, 3; the length of the intermediate element is ds.

In order to match the directions I, II, III at point P with those at point P' a certain rotation is required. This rotation is entirely governed by the shape of the curved central line of the spring wire and depends therefore on the curvature k which is represented by a vector along the binormal II,

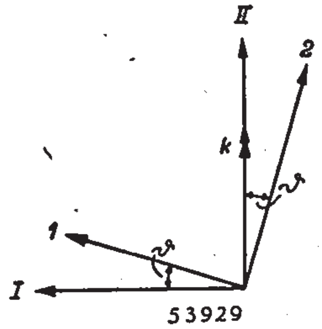

Fig. 9. The axes I, II and 1, 2 in the plane of the cross-section of the wire. The axes III and 3 coincide and are directed backwards.

and the torsion w *) represented by a vector along the tangent III. Now, in order to match also the directions 1, 2, 3 at point P with those at P' a further rotation is necessary, corresponding to the change in the position of the system of axes 1, 2, 3 with respect to the system I, II, III. This position is determined by the angle ϑ, and the corresponding rotation per unit of arc length s is therefore represented by a vector along the coincident axes III and 3 of the order of $\mathrm{d}\vartheta/\mathrm{d}s$. Denoting the components of the final rotation vector with respect to the axes 1, 2, 3 successively by ω_1, ω_2 and ω_3 we obtain

$$\omega_1 = k \sin \vartheta, \quad \omega_2 = k \cos \vartheta, \quad \omega_3 = w + \frac{\mathrm{d}\vartheta}{\mathrm{d}s}. \tag{21}$$

Let us represent the moments with respect to the axes 1, 2, 3 at the point P by M_1, M_2 and M_3, and let us call

A the rigidity with respect to bending around the first principal axis of inertia (axis 1),

B the rigidity with respect to bending around the second principal axis of inertia (axis 2),

C the rigidity with respect to twisting (around axis 3);

then according to the theory of elasticity the following relations hold

$$\omega_1 - (\omega_1)_0 = \frac{M_1}{A}, \quad \omega_2 - (\omega_2)_0 = \frac{M_2}{B}, \quad \omega_3 - (\omega_3)_0 = \frac{M_3}{C}, \tag{22}$$

---

*) By torsion w is here understood the degree of tortuosity of the space curve indicating the shape of the spring wire; it has nothing to do with any elastic twist.

where the subscript 0 signifies that the quantity in question relates to the unloaded state of the spring. Bearing in mind that the angle ϑ in the absence of load is equal to zero, we get in connection with (21)

$$(\omega_1)_0 = 0, \quad (\omega_2)_0 = k_0, \quad (\omega_3)_0 = w_0. \tag{23}$$

The spring wire in the unloaded state changes according to a helix lying with the slope α_0 on a cylinder of radius R_0. The curvature k_0 and the torsion w_0 of such a curve amount to

$$k_0 = \frac{\cos^2\alpha_0}{R_0}, \quad w_0 = \frac{\sin\alpha_0\cos\alpha_0}{R_0}. \tag{24}$$

With the aid of (21), (23) and (24) we now write the relations (22) in the following form

$$k\sin\vartheta = \frac{M_1}{A}, \quad k\cos\vartheta - \frac{\cos^2\alpha_0}{R_0} = \frac{M_2}{B}, \quad w - \frac{\sin\alpha_0\cos\alpha_0}{R_0} = \frac{M_3}{C} - \frac{\mathrm{d}\vartheta}{\mathrm{d}s}. \tag{25}$$

The curvature k and the torsion w can be expressed in the coordinates of the space curve indicating the shape of the spring wire in the loaded state only when that curve deviates but slightly from a helix. Now in the case of the highly compressed helical spring, large displacements take place with respect to the helix in the unloaded state, i.e., the helix of radius R_0 and slope α_0 (state I). But fortunately these displacements are mostly of such a nature that another auxiliary helix of radius R and slope α can be indicated (state II), with respect to which the displacements accompanying the buckling (state III) may as a rule be considered small. What values are to be given to R and α, and how the auxiliary helix lies with respect to the original one, will be considered from case to case in the following sections. Here we need only point out that such an auxiliary helix is indeed present and that, together with the displacements of the helical spring with respect to the auxiliary helix, also the angle ϑ may be regarded as a small quantity. The curvature k then differs but little from that of the helix of radius R and slope α ($k \approx \cos^2\alpha/R$), so that from the first equation (25) it follows that to a first approximation ϑ is equal to

$$\vartheta = \frac{M_1}{Ak} = \frac{M_1 R}{A\cos^2\alpha}. \tag{26}$$

Therefore, with $\mathrm{d}s = R\mathrm{d}\Theta/\cos\alpha$ the two other equations (25) are written as

$$\left.\begin{aligned} k - \frac{\cos^2\alpha_0}{R_0} &= \frac{M_2}{B}, \\ w - \frac{\sin\alpha_0\cos\alpha_0}{R_0} &= -\frac{1}{A\cos\alpha}\cdot\frac{\mathrm{d}M_1}{\mathrm{d}\Theta} + \frac{M_3}{C}. \end{aligned}\right\} \tag{27}$$

If the z-axis is made to coincide with the central line of the auxiliary helix of radius R and slope α (state II) this helix will intersect the plane of $\Theta =$ constant at a point having the coordinates $R \cos \Theta$, $R \sin \Theta$ and $R\Theta \tan \alpha$. The space curve indicating the shape of the spring wire in the final state (state III) will intersect the same plane at another point which in the radial and axial senses may lie ϱ and ζ farther away, so that its coordinates will be

$$x = (R + \varrho) \cos \Theta, \quad y = (R + \varrho) \sin \Theta, \quad z = R\Theta \tan \alpha + \zeta. \tag{28}$$

Using a prime to denote differentiation with respect to Θ we get, from (28),

$$\left.\begin{aligned} x' &= -(R + \varrho) \sin \Theta + \varrho' \cos \Theta , \\ y' &= (R + \varrho) \cos \Theta + \varrho' \sin \Theta , \\ z' &= R \tan \alpha + \zeta' , \end{aligned}\right\} \tag{29}$$

and this enables us to find for the differential quotient of the arc length with respect to Θ, by ignoring terms of higher order,

$$s' = \frac{ds}{d\Theta} = \sqrt{x'^2 + y'^2 + z'^2} = \frac{R}{\cos\alpha}\left(1 + \frac{\varrho}{R} \cos^2\alpha + \frac{\zeta'}{R} \sin \alpha \cos \alpha\right). \tag{30}$$

The direction cosines of the tangent (axis III) with respect to the system of coordinates x, y, z are determined by the equations

$$\lambda_{\mathrm{III}} = \frac{dx}{ds} = \frac{x'}{s'}, \quad \mu_{\mathrm{III}} = \frac{y'}{s'}, \quad \nu_{\mathrm{III}} = \frac{z'}{s'}.$$

Confining our calculations again to terms of the first degree in ϱ and ζ, we therefore find, in connection with (29) and (30),

$$\left.\begin{aligned} \lambda_{\mathrm{III}} &= -\sin\Theta\cos\alpha - \frac{\varrho}{R} \sin\Theta\sin^2\alpha\cos\alpha + \frac{\varrho'}{R} \cos\Theta\cos\alpha + \frac{\zeta'}{R} \sin\Theta\sin\alpha\cos^2\alpha, \\ \mu_{\mathrm{III}} &= \cos\Theta\cos\alpha + \frac{\varrho}{R} \cos\Theta\sin^2\alpha\cos\alpha + \frac{\varrho'}{R} \sin\Theta\cos\alpha - \frac{\zeta'}{R} \cos\Theta\sin\alpha\cos^2\alpha, \\ \nu_{\mathrm{III}} &= \sin \alpha - \frac{\varrho}{R} \sin \alpha \cos^2 \alpha + \frac{\zeta'}{R} \cos^3 \alpha . \end{aligned}\right\} \tag{31}$$

Hence, again ignoring terms of higher order,

$$\lambda'^2_{\mathrm{III}} + \mu'^2_{\mathrm{III}} + \nu'^2_{\mathrm{III}} = \cos^2 \alpha\left(1 - 2 \frac{\varrho''}{R} + 2 \frac{\varrho}{R} \sin^2\alpha - 2 \frac{\zeta'}{R} \sin \alpha \cos \alpha\right),$$

so that by using eq. (30) we obtain for the curvature *)

$$k = \frac{1}{s'} \sqrt{\lambda_{\mathrm{III}}'^2 + \mu_{\mathrm{III}}'^2 + \nu_{\mathrm{III}}'^2}$$

the following expression

$$k = \frac{\cos^2 \alpha}{R}\left(1 - \frac{\varrho''}{R} - \frac{\varrho}{R}\cos 2\alpha - \frac{\zeta'}{R}\sin 2\alpha\right). \tag{32}$$

To determine the direction cosines of the binormal (axis II) we use the formulae

$$\lambda_{\mathrm{II}} = \frac{y'z'' - z'y''}{ks'^3}, \quad \mu_{\mathrm{II}} = \frac{z'x'' - x'z''}{ks'^3}, \quad \nu_{\mathrm{II}} = \frac{x'y'' - y'x''}{ks'^3}.$$

Differentiation of (29) gives

$$\left.\begin{aligned} x'' &= -(R+\varrho)\cos\Theta - 2\varrho'\sin\Theta + \varrho''\cos\Theta\,,\\ y'' &= -(R+\varrho)\sin\Theta + 2\varrho'\cos\Theta + \varrho''\sin\Theta\,,\\ z'' &= \zeta''\,. \end{aligned}\right\} \tag{33}$$

Thus by employing eqs (29), (30), (32) and (33) we find that

$$\left.\begin{aligned} \lambda_{\mathrm{II}} &= \sin\Theta\sin\alpha - \frac{\varrho}{R}\sin\Theta\sin\alpha\cos^2\alpha - 2\frac{\varrho'}{R}\cos\Theta\sin\alpha + \\ &\qquad + \frac{\zeta'}{R}\sin\Theta\cos^3\alpha + \frac{\zeta''}{R}\cos\Theta\cos\alpha\,,\\ \mu_{\mathrm{II}} &= -\cos\Theta\sin\alpha + \frac{\varrho}{R}\cos\Theta\sin\alpha\cos^2\alpha - 2\frac{\varrho'}{R}\sin\Theta\sin\alpha - \\ &\qquad - \frac{\zeta'}{R}\cos\Theta\cos^3\alpha + \frac{\zeta''}{R}\sin\Theta\cos\alpha\,,\\ \nu_{\mathrm{II}} &= \cos\alpha + \frac{\varrho}{R}\sin^2\alpha\cos\alpha - \frac{\zeta'}{R}\sin\alpha\cos^2\alpha\,. \end{aligned}\right\} \tag{34}$$

The direction cosines of the principal normal (axis I) are equal to

$$\lambda_{\mathrm{I}} = \frac{1}{k}\frac{\mathrm{d}^2x}{\mathrm{d}s^2} = \frac{s'x'' - x's''}{ks'^3}, \quad \mu_{\mathrm{I}} = \frac{s'y'' - y's''}{ks'^3}, \quad \nu_{\mathrm{I}} = \frac{s'z'' - z's''}{ks'^3},$$

---

*) The formulae used here for the curvature k, the torsion w and the direction cosines of the axes I and II can be derived in a simple manner from a set of formulae given in Hk de Vries, Leerboek der differentiaal- en integraalrekening, Noordhoff, Groningen (1924), Vol. I, p. 646 et seq. See also F. Schuh and J. G. Rutgers, Compendium der hoogere wiskunde, Noordhoff, Groningen (1928), Vol. IV, p. 278 et seq., or V. and K. Kommerell, Algemeine Theorie der Raumkurven und Flächen, Göschen, Leipzig (1911), Vol. I, p. 4 et seq.

and thus on account of (29), (30), (32) and (33),

$$\left.\begin{aligned}\lambda_{\mathrm{I}} &= -\cos\Theta - \frac{\varrho'}{R}\sin\Theta\,(1+\sin^2\alpha) + \frac{\zeta''}{R}\sin\Theta\sin\alpha\cos\alpha,\\ \mu_{\mathrm{I}} &= -\sin\Theta + \frac{\varrho'}{R}\cos\Theta\,(1+\sin^2\alpha) - \frac{\zeta''}{R}\cos\Theta\sin\alpha\cos\alpha,\\ \nu_{\mathrm{I}} &= -\frac{\varrho'}{R}\sin\alpha\cos\alpha + \frac{\zeta''}{R}\cos^2\alpha.\end{aligned}\right\}\qquad(35)$$

We then calculate the torsion w by means of the formula

$$w = \frac{1}{s'}\sqrt{\lambda'^2_{\mathrm{II}} + \mu'^2_{\mathrm{II}} + \nu'^2_{\mathrm{II}}}.$$

Now [see eq. (34)]

$$\lambda'^2_{\mathrm{II}} + \mu'^2_{\mathrm{II}} + \nu'^2_{\mathrm{II}} = \sin^2\alpha\left(1 - 4\frac{\varrho''}{R} - 2\frac{\varrho}{R}\cos^2\alpha + 2\frac{\zeta'''}{R}\cot\alpha + 2\frac{\zeta'}{R}\cos^2\alpha\cot\alpha\right),$$

and thus, by using eq. (30), we obtain

$$w = \frac{\sin\alpha\cos\alpha}{R}\left(1 - 2\frac{\varrho''}{R} - 2\frac{\varrho}{R}\cos^2\alpha + \frac{\zeta'''}{R}\cot\alpha + \frac{\zeta'}{R}\cos 2\alpha\cot\alpha\right). \qquad (36)$$

Further, the position of the system of axes 1, 2 and 3 with respect to the system I, II, III is determined by the angle ϑ (fig. 9), so that the direction cosines of the axes 1, 2 and 3 are given by

$$\left.\begin{aligned}\lambda_1 &= \lambda_{\mathrm{I}}\cos\vartheta + \lambda_{\mathrm{II}}\sin\vartheta, & \lambda_2 &= \lambda_{\mathrm{II}}\cos\vartheta - \lambda_{\mathrm{I}}\sin\vartheta, & \lambda_3 &= \lambda_{\mathrm{III}},\\ \mu_1 &= \mu_{\mathrm{I}}\cos\vartheta + \mu_{\mathrm{II}}\sin\vartheta, & \mu_2 &= \mu_{\mathrm{II}}\cos\vartheta - \mu_{\mathrm{I}}\sin\vartheta, & \mu_3 &= \mu_{\mathrm{III}},\\ \nu_1 &= \nu_{\mathrm{I}}\cos\vartheta + \nu_{\mathrm{II}}\sin\vartheta, & \nu_2 &= \nu_{\mathrm{II}}\cos\vartheta - \nu_{\mathrm{I}}\sin\vartheta, & \nu_3 &= \nu_{\mathrm{III}}.\end{aligned}\right\}\qquad(37)$$

The expressions found for the curvature k and the torsion w [eqs (32) and (36)] now have to be substituted in eq. (27). These take the form of

$$\cos^2\alpha - \frac{R}{R_0}\cos^2\alpha_0 - \cos^2\alpha\left(\frac{\varrho''}{R} + \frac{\varrho}{R}\cos 2\alpha + \frac{\zeta'}{R}\sin 2\alpha\right) = \frac{M_2 R}{B}, \qquad (38)$$

$$\begin{aligned}\sin\alpha\cos\alpha - \frac{R}{R_0}\sin\alpha_0\cos\alpha_0 &-\\ -\sin\alpha\cos\alpha\left(2\frac{\varrho}{R} + 2\frac{\varrho}{R}\cos^2\alpha - \frac{\zeta'''}{R}\cot\alpha - \frac{\zeta'}{R}\cos 2\alpha\cot\alpha\right) &=\\ = -\frac{M'_1 R}{A\cos\alpha} + \frac{M_3 R}{C}.&\qquad(39)\end{aligned}$$

Among the components of the moment occurring in a certain wire section generally the components M_x, M_y, M_z with respect to the axes of x, y, z are the easiest to determine. With the aid of the direction cosines λ_i, μ_i, ν_i ($i =$ I, II, III) we then calculate the moments about the axes I, II, III according to

$$\left.\begin{aligned} M_{\mathrm{I}} &= \lambda_{\mathrm{I}}\, M_x + \mu_{\mathrm{I}}\, M_y + \nu_{\mathrm{I}}\, M_z, \\ M_{\mathrm{II}} &= \lambda_{\mathrm{II}}\, M_x + \mu_{\mathrm{II}}\, M_y + \nu_{\mathrm{II}}\, M_z, \\ M_{\mathrm{III}} &= \lambda_{\mathrm{III}}\, M_x + \mu_{\mathrm{III}}\, M_y + \nu_{\mathrm{III}}\, M_z, \end{aligned}\right\} \qquad (40)$$

and thence the moments about the axes 1, 2, 3 according to

$$\left.\begin{aligned} M_1 &= M_{\mathrm{I}}\ \cos\vartheta + M_{\mathrm{II}}\sin\vartheta, \\ M_2 &= M_{\mathrm{II}}\ \cos\vartheta - M_{\mathrm{I}}\ \sin\vartheta, \\ M_3 &= M_{\mathrm{III}}. \end{aligned}\right\} \qquad (41)$$

If the loading forces and moments are so small as to cause only slight distortions of the spring, there is no longer any purpose in introducing an auxiliary helix of radius R and slope α, because the distortions can then be described straight away by the two (small) quantities ϱ and ζ. In that case the z-axis naturally coincides with the central line of the helical spring in the unloaded state, and eqs (38) and (39) are reduced by $R = R_0$ and $\alpha = \alpha_0$ to the differential equations

$$-\cos^2\alpha_0\,(\varrho'' + \varrho\cos 2\alpha_0 + \zeta'\sin 2\alpha_0) = \frac{M_2 R_0^2}{B}, \qquad (42)$$

$$-\sin\alpha_0\cos\alpha_0\,(2\varrho'' + 2\varrho\cos^2\alpha_0 - \zeta'''\cot\alpha_0 - \zeta'\cos 2\alpha_0\cot\alpha_0) = \\ = -\frac{M_1' R_0^2}{A\cos\alpha_0} + \frac{M_3 R_0^2}{C}, \qquad (43)$$

where the moments M_1, M_2 and M_3 are functions of Θ only. If, for instance, we now eliminate ζ we find the differential equation

$$\varrho'''' + 2\varrho'' + \varrho = \frac{R_0^2}{\cos^2\alpha_0}\left\{2\frac{M_1'}{A}\sin\alpha_0 - \frac{M_2'' + M_2\cos 2\alpha_0}{B} - \frac{M_3}{C}\sin 2\alpha_0\right\}, \qquad (44)$$

whilst

$$\zeta'\sin 2\alpha_0 = -\varrho'' - \varrho\cos 2\alpha_0 - \frac{R_0^2}{\cos^2\alpha_0}\frac{M_2}{B}. \qquad (45)$$

Thus the problem of the slightly loaded helical spring is to be considered as being solved.

5. Buckling of the helical spring under compression, regarded as a wire structure

In the case of a highly compressed helical spring we must employ the general eqs (38) and (39), and account has to be taken of the fact that the moments M_1, M_2 and M_3 are dependent not only upon the external load but also upon the deflections.

In this section we shall confine the load of the spring to two equal and opposite compressive forces P acting along the z-axis (fig. 10). In a certain section of the deflected wire the following moments then exist

$$M_x = P(R + \varrho)\sin\Theta, \quad M_y = -P(R+\varrho)\cos\Theta, \quad M_z = 0. \tag{46}$$

With the aid of (31), (34), (35), (40) and (46) we now calculate the moments about the axes I, II, III and find to a first approximation

$$\left.\begin{aligned} M_{\mathrm{I}} &= -PR\left\{\frac{\varrho'}{R}(1+\sin^2\alpha) - \frac{\zeta''}{R}\sin\alpha\cos\alpha\right\}, \\ M_{\mathrm{II}} &= PR\sin\alpha\left\{1 + \frac{\varrho}{R}\sin^2\alpha + \frac{\zeta'}{R}\cos^2\alpha\cot\alpha\right\}, \\ M_{\mathrm{III}} &= -PR\cos\alpha\left\{1 + \frac{\varrho}{R}(1+\sin^2\alpha) - \frac{\zeta'}{R}\sin\alpha\cos\alpha\right\}. \end{aligned}\right\} \tag{47}$$

Regarding the angle ϑ as a small quantity, then owing to (41) and (47) we get

$$\left.\begin{aligned} M_1 &= -PR\left\{\frac{\varrho'}{R}(1+\sin^2\alpha) - \frac{\zeta''}{R}\sin\alpha\cos\alpha\right\} + PR\vartheta\sin\alpha, \\ M_2 &= M_{\mathrm{II}} - M_{\mathrm{I}}\vartheta \approx M_{\mathrm{II}}, \\ M_3 &= M_{\mathrm{III}}. \end{aligned}\right\} \tag{48}$$

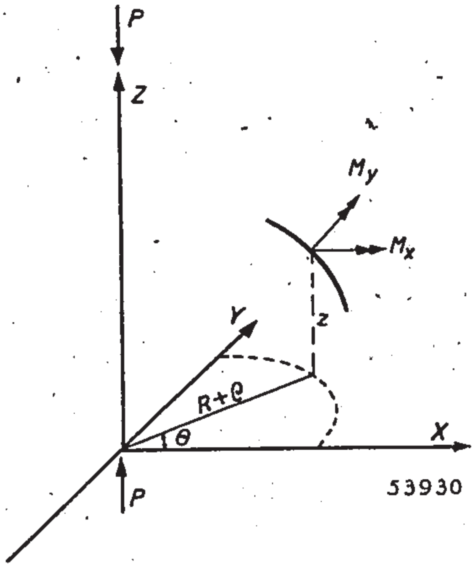

Fig. 10. An element of the helical spring compressed by two equal and opposite forces.

Bearing in mind that the angle ϑ occurring in eq. (48) is related to M_1 according to (26), we find by using (47)

$$\left.\begin{aligned} M_1 &= -\frac{A\cos^2\alpha}{A\cos^2\alpha - PR^2\sin\alpha}\,PR\left\{\frac{\varrho'}{R}(1+\sin^2\alpha) - \frac{\zeta''}{R}\sin\alpha\cos\alpha\right\},\\ M_2 &= PR\sin\alpha\left\{1 + \frac{\varrho}{R}\sin^2\alpha + \frac{\zeta'}{R}\cos^2\alpha\cot\alpha\right\},\\ M_3 &= -PR\cos\alpha\left\{1 + \frac{\varrho}{R}(1+\sin^2\alpha) - \frac{\zeta'}{R}\sin\alpha\cos\alpha\right\}. \end{aligned}\right\} \tag{49}$$

These values now have to be substituted in eqs (38) and (39). In those equations we have, in addition to the terms with the small quantities ϱ and ζ, terms in which the radius R and slope α of the auxiliary helix occur only. This auxiliary helix was introduced in the preceding section to avoid having to account for large displacements, without going further into the size of R and α. Among the many helicis that could serve as auxiliary helix there is one that at the given load might be realized by the spring wire. It will be obvious that preference is to be given to this particular helix. This means that $\varrho = 0$ and $\zeta = 0$ must become a solution of the eqs (38), (39) and (49). When taking ϱ and α in these equations equal to zero we obtain

$$\cos^2\alpha - \frac{R}{R_0}\cos^2\alpha_0 = \frac{PR^2}{B}\sin\alpha, \tag{50}$$

$$\sin\alpha\cos\alpha - \frac{R}{R_0}\sin\alpha_0\cos\alpha_0 = -\frac{PR^2}{C}\cos\alpha. \tag{51}$$

Starting from the given spring dimensions in the unloaded state (state I), these equations enable us to calculate the unknown radius R and the slope α of the auxiliary helix in the state II as functions of the load P. In this state II we have the special feature that the systems of axes I, II, III and 1, 2, 3 coincide in every cross-section just as in the initial state I, since from equations (25) and (49) it follows that with the solution $\varrho = 0$ and $\zeta = 0$ the angle ϑ is zero. The first principal axis of inertia of the wire section (axis 1) thus coincides with the principal normal (axis I) and therefore appears to be radially directed, in the state II as well as in the initial state I. This does not suffice, however, to know completely the shape of the spring in state II, for we also have to know what change has taken place in the number of coils. Since in the distortion of the helical spring the length of the wire remains constant, the actual number of coils n can be deduced from the original number n_0 according to the equation

$$\frac{n}{n_0} = \frac{R_0}{R}\,\frac{\cos\alpha}{\cos\alpha_0}. \tag{52}$$

Substituting (49), (50) and (51) in eqs (38) and (39) and taking

$$a = \frac{PR^2}{A\sin\alpha - PR^2\tan^2\alpha},\quad b = \frac{PR^2}{B\sin\alpha},\quad c = \frac{PR^2}{C\sin\alpha}, \tag{53}$$

we find that the quantities ϱ and ζ must satisfy

$$-\cos^2\alpha\,(\varrho'' + \varrho\cos 2\alpha + \zeta'\sin 2\alpha) = b\sin^2\alpha\,(\varrho\sin^2\alpha + \zeta'\cos^2\alpha\cot\alpha), \tag{54}$$

$$\begin{aligned} -\sin\alpha\cos\alpha\,(2\varrho'' + 2\varrho\cos^2\alpha - \zeta'''\cot\alpha - \zeta'\cos 2\alpha\cot\alpha) &= \\ = a\tan\alpha\,\}\varrho''(1+\sin^2\alpha) - \zeta'''\sin\alpha\cos\alpha\{ &- \\ - c\sin\alpha\cos\alpha\,\}\varrho(1+\sin^2\alpha) - \zeta'\sin\alpha\cos\alpha\{. \end{aligned} \tag{55}$$

After dividing by $\cos^4\alpha$ these equations may be written as

$$\varrho''(1+\tan^2\alpha) + \varrho(1-\tan^2\alpha + b\tan^4\alpha) + \zeta'\tan\alpha\,(2+b) = 0, \tag{56}$$

$$\begin{aligned} \varrho''\tan\alpha\,(1+\tan^2\alpha)\,(2+a+2a\tan\alpha) + \varrho\tan\alpha\,(2-c-2c\tan^2\alpha) &- \\ -\zeta'''\,(1+\tan^2\alpha)\,(1+a\tan^2\alpha) - \zeta'\,\}1-(1+c)\tan^2\alpha\{ &= 0. \end{aligned} \tag{57}$$

Now, by eliminating ζ from eqs (56) and (57) and dividing by $(1+\tan^2\alpha)$ we obtain the following differential equation for ϱ

$$e_0\,\varrho'''' + e_2\varrho'' + e_4\varrho = 0, \tag{58}$$

in which the coefficients e_0, e_2 and e_4 have the meaning

$$\left.\begin{aligned} e_0 &= 1 + (1+a)\tan^2\alpha + a\tan^4\alpha, \\ e_2 &= 2 + (2+3a+2b-c+ab)\tan^2\alpha + (3a+b+2ab)\tan^4\alpha + ab\tan^6\alpha, \\ e_4 &= 1 + (1+2b-3c-bc)\tan^2\alpha - (b+bc)\tan^4\alpha. \end{aligned}\right\} \tag{59}$$

The solution is

$$\varrho = A_1\sin p_1\Theta + B_1\cos p_1\Theta + A_2\sin p_2\Theta + B_2\cos p_2\Theta, \tag{60}$$

in which p_1 and p_2 are determined by

$$p_1^2 + p_2^2 = e_2/e_0,\quad p_1^2\,p_2^2 = e_4/e_0. \tag{61}$$

The general solution (60) must now be adapted to the boundary conditions, which are determined by the method of fixing of the two ends of the spring wire. There can only be a pure buckling problem, as occurs for instance with centrally loaded straight rods, if the boundary conditions lead to the general solution $A_1 = B_1 = A_2 = B_2 = 0$ (thus $\varrho = 0$) and at the same time to a special non-zero solution corresponding to a certain critical value of the compressive force. As we know, the displacements ϱ

and ζ are measured with respect to the auxiliary helix, differing in radius and slope from the original helix in a manner governed by the compressive force [see eqs (50) and (51)]. Since, for constructional reasons, the ends of the spring wire will in general be forced to keep to the cylinder of the original helix, at both ends ϱ usually differs from zero. Thus the boundary conditions lead to certain constants of integration which are dependent upon the size of the compressive force. This means that under any load there is a lateral deflection of the helical spring. This deflection will as a rule be small, but — considering the result of the similar bending-buckling problem of sligthly eccentrically loaded rods — it will increase rapidly as the compressive force approaches the critial value already mentioned.

As we shall find confirmed later on, the case of pure buckling occurs when the point of application of each of the two compressive forces lies on the axis 1 of the respective end section of the spring wire (fig. 11) at a distance from the centre of that section equal to the radius R. Since, otherwise, the end of the wire must be free to adjust itself, for the sake of brevity we shall speak of a helical spring with freely adjustable wire ends.

The axis 1 is fixed to the end of the spring wire (in the initial state it intersects the central line of the helical spring at right angles), so that we can transmit the load on the end of the spring by means of a perfectly rigid connection provided with a centre-punch mark in the said point on the axis 1. The radius R, as we know, is dependent upon the load and therefore, in the experiment with increasing load, the said distance would have to be adapted continually to that load. This, of course, is not practically feasible, so that with the pure buckling problem we apparently have to do

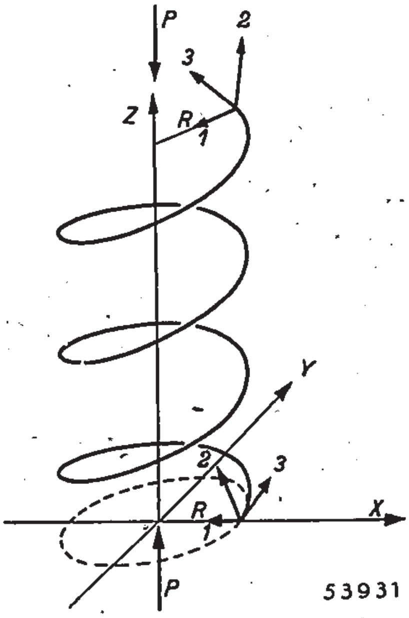

Fig. 11. The helical spring with freely adjustable wire ends compressed by two equal and opposite forces (imaginary experiment).

with an imaginary experiment. Nevertheless, we shall occupy ourselves further with this case, because other boundary conditions lead to the less comprehensible bending-buckling problem and because we are, after all, concerned only with an example enabling as to ascertain in how far the size of the slope a_0 may influence the buckling load.

The fact that the point of application of the compressive force P acting along the z-axis lies on axis 1 implies that at both ends ($\Theta = 0$, and $\Theta = 2\pi n$, where n need not be a whole number) the moment M_1 is equal to zero. According to eq. (49) this leads to the condition

$$\varrho'(1 + 2\tan^2 a) - \zeta'' \tan a = 0 \quad \text{at} \begin{cases} \Theta = 0, \\ \Theta = 2\pi n, \end{cases}$$

or, in connection with (56), to

$$\varrho''' + e\varrho' = 0 \quad (e = 3 + b + b\tan^2 a) \quad \text{at} \begin{cases} \Theta = 0, \\ \Theta = 2\pi n. \end{cases} \tag{62}$$

Further, at both ends we take the distance $R + \varrho$ from the z-axis to the centre of the spring wire as being equal to R, so that

$$\varrho = 0 \quad \text{at} \begin{cases} \Theta = 0, \\ \Theta = 2\pi n. \end{cases} \tag{63}$$

In connection with (60), (62) and (63), the constants of integration must satisfy the equations

$$\left.\begin{aligned} & p_1(p_1^2-e)A_1 + p_2(p_2^2-e)A_2 = 0, \\ & p_1(p_1^2-e)\,(A_1 \cos 2\pi n p_1 - B_1 \sin 2\pi n p_1) + \\ & \qquad\qquad + p_2(p_2^2-e)\,(A_2 \cos 2\pi n p_2 - B_2 \sin 2\pi n p_2) = 0, \\ & B_1 + B_2 = 0, \\ & A_1 \sin 2\pi n p_1 + B_1 \cos 2\pi n p_1 + A_2 \sin 2\pi n p_2 + B_2 \cos 2\pi n p_2 = 0. \end{aligned}\right\} \tag{64}$$

We see that these equations do indeed lead to the solution $A_1 = B_1 = A_2 = B_2 = 0$. According to (56) and (60) both ϱ and ζ then no longer occur and the helical spring does not show a lateral deflection; in other words, the helical spring is in the state II. From this it follows, inter alia, that n in eq. (64) is given by (52).

Under very specific circumstances, however, eqs (64) allow of a solution differing from zero. This is the case if the determinant of the system is equal to zero, i.e., if

$$\left\{\sin 2\pi n p_1 - \frac{p_1(p_1^2-e)}{p_2(p_2^2-e)} \sin 2\pi n p_2\right\} \left\{\sin 2\pi n p_1 - \frac{p_2(p_2^2-e)}{p_1(p_1^2-e)} \sin 2\pi n p_2\right\} + \\ + (\cos 2\pi n p_1 - \cos 2\pi n p_2)^2 = 0$$

or, what comes to the same thing, if

$$\sin[\pi n(p_1 - p_2)] = \pm \frac{p_1(p_1^2-e) - p_2(p_2^2-e)}{p_1(p_1^2-e) + p_2(p_2^2-e)} \sin[\pi n(p_1 + p_2)]. \tag{65}$$

In this case the corresponding values of the constants of integration are indefinite and thus the lateral deflection of the helical spring is unlimited; in other words, the spring buckles.

With given dimensions of the unloaded spring p_1, p_2, n and e are functions of the load P only [eqs (50), (51), (52), (53), (59), (61) and (62)]. Thus with (65) we have found an equation by means of which — at least in principle — we can calculate the load causing a helical spring with freely adjustable wire ends to buckle (in the imaginary experiment).

Mostly, however, it is not the buckling load which is desired to be known but rather the corresponding critical compression. The length of the spring is here understood to be the distance between the points of application of the compressive forces. If, as in the present case, the helical spring is in the state II, the axes 1 are always radially directed and the length l of the spring in the loaded state is therefore determined by the projection of the helix of radius R and slope α on the z-axis. That is to say,

$$l = 2\pi R\, n \tan\alpha\,. \tag{66}$$

Similarly, the length l_0 in the unloaded state is found to be

$$l_0 = 2\pi\, R_0\, n_0 \tan \alpha_0. \tag{67}$$

Using (52), (66) and (67) we get

$$\frac{l}{l_0} = \frac{\sin\alpha}{\sin\alpha_0}\,. \tag{68}$$

With given dimensions of the helical spring in the initial state and with the aid of (50), (51) and (68) we can calculate the length l as function of the load P, so that it is actually possible to determine the critical compression, $\Delta l = l_0 - l$, corresponding to the buckling force.

6. The effect of the number of coils on the buckling of a helical spring under compression with freely adjustable wire ends

We have seen that the formula (65) derived in section 5 has to be taken as a relation from which, with given dimensions of the spring in the initial state, it is possible to calculate the compressive force causing the helical spring with freely adjustable wire ends to buckle (in the imaginary experiment). The various quantities, however, are so complicated in their mutual relations that the result is not directly comprehensible. We therefore take advantage of the fact that, even with helical springs having a pitch equal to their diameter, $\tan^2\alpha_0$ has such a small value $(1/\pi^2)$ that we may ignore its higher powers.

As regards the dimensions of the helical spring in the state II (auxiliary helix of radius R and slope α), eqs (50), (51) and (52) apply. With the notations (52) we derive from (50) and (51), omitting the negligible terms,

$$\frac{R}{R_0} = 1 + \tan^2\alpha_0 - (1 + b)\tan^2\alpha + \ldots, \tag{69}$$

$$\frac{\tan\alpha}{\tan\alpha_0} = \frac{1 - b\tan^2\alpha}{1 + c}. \tag{70}$$

Introducing the relative compression ξ, as before, we have, owing to (10) and (68),

$$\frac{\sin\alpha}{\sin\alpha_0} = 1 - \xi, \tag{71}$$

which relation can be resolved into

$$\frac{\tan\alpha}{\tan\alpha_0} = \frac{1-\xi}{\sqrt{1+\xi(2-\xi)\tan^2\alpha_0}} = (1-\xi)\left\{1 - \tfrac{1}{2}\xi(2-\xi)\tan^2\alpha_0 + \ldots\right\}. \tag{72}$$

With the aid of (72) and with $b = Cc/B$ [eq. (53)] we derive from (70)

$$c = \frac{\dfrac{\tan\alpha_0}{\tan\alpha} - 1}{1 + \dfrac{C}{B}\dfrac{\tan\alpha}{\tan\alpha_0}\tan^2\alpha_0} = \frac{\xi}{1-\xi}\left[1 + \left\{1 - \tfrac{1}{2}\xi - \frac{C}{B}(1-\xi)\right\}\tan^2\alpha_0 + \ldots\right] \tag{73}$$

and hence

$$b = \frac{C}{B}c = \frac{C}{B}\frac{\xi}{1-\xi}\left[1 + \left\{1 - \tfrac{1}{2}\xi - \frac{C}{B}(1-\xi)\right\}\tan^2\alpha_0 + \ldots\right]. \tag{74}$$

From eq. (53) it follows that for a we may write

$$a = \frac{Cc}{A - Cc\tan^2\alpha} = \frac{C}{A}c\left\{1 + \frac{C}{A}c\frac{\tan^2\alpha}{\tan^2\alpha_0}\tan^2\alpha_0 + \ldots\right\}, \tag{75}$$

so that, by using (72) and (73),

$$a = \frac{C}{A}\frac{\xi}{1-\xi}\left[1 + \left\{1 - \tfrac{1}{2}\xi - \frac{C}{B}\left(1-\xi\right)\left(1 - \frac{B}{A}\xi\right)\right\}\tan^2\alpha_0 + \ldots\right]. \tag{76}$$

Further, on account of (69), (72) and (74) the ratio of the radii R and R_0 is equal to

$$\frac{R}{R_0} = 1 + \xi\left\{2 - \xi - \frac{C}{B}(1-\xi)\right\}\tan^2\alpha_0 + \ldots, \tag{77}$$

and on account of (52), (71), (72) and (77) the number of coils changes according to

$$\frac{n}{n_0} = 1 - \xi\left\{1 - \tfrac{1}{2}\xi - \frac{C}{B}(1-\xi)\right\}\tan^2\alpha_0 + \ldots. \tag{78}$$

Owing to the small difference between p_1 and p_2 it appears to be necessary when working out (61) to retain also the terms $\tan^4\alpha$, and we therefore write

$$\left.\begin{aligned} p_1^2+p_2^2 &= 2+(a+2b-c+ab)\tan^2\alpha-(b-c+a^2+ab-ac+a^2b)\tan^4\alpha+\dots,\\ p_1^2\cdot p_2^2 &= 1-(a-2b+3c+bc)\tan^2\alpha-(3b-3c-a^2+2ab-3ac-abc)\tan^4\alpha+\dots \end{aligned}\right\} \quad (79)$$

Here it has to be remembered that a, b and c are functions of α, which may have all possible values from 0 to ∞ [see eqs (73), (74) and (76), where $0<\xi<1$], it being understood, however, that a, b and c multiplied by $\tan\alpha$ are always to be considered small, since from (72), (73), (74) and (76) it follows that to a first approximation

$$a\tan\alpha\approx\frac{C}{A}\xi\tan\alpha_0,\qquad b\tan\alpha\approx\frac{C}{B}\xi\tan\alpha_0,\qquad c\tan\alpha\approx\xi\tan\alpha_0. \quad (80)$$

Any possible large values of a, b and c thus prove to be of minor importance with respect to the permissibility of the expansions in series occurring in (79).

We derive from (79)

$$\left.\begin{aligned} (p_1-p_2)^2 &= (a+c)(2+b)\tan^2\alpha\,(1+f_1\tan^2\alpha+\dots),\\ (p_1+p_2)^2 &= 4+(4b-4c+ab-bc)\tan^2\alpha+\dots, \end{aligned}\right\} \quad (81)$$

where f_1 is equal to

$$f_1=-a+\frac{2b-2c+ab+\frac{1}{4}(a-2b+3c+bc)^2}{(a+c)(2+b)}. \quad (82)$$

In view of the small difference between p_1 and p_2 [see eq. (81)] the coefficient of $\sin[\pi n(p_1+p_2)]$ in eq. (65) cannot be large. If we always take $p_1>p_2$, the value of $\pi n(p_1-p_2)$ will apparently never differ much from $m\pi$ ($m=1, 2, 3, \dots$). It is therefore only a matter of correction with respect to this value, so that in the calculation of the coefficient in question terms with higher powers of $\tan^2\alpha$ or $\tan^2\alpha_0$ may be omitted. Now

$$\frac{p_1(p_1^2-e)-p_2(p_2^2-e)}{p_1(p_1^2-e)+p_2(p_2^2-e)}=\frac{p_1-p_2}{p_1+p_2}\cdot\frac{p_1^2+p_1p_2+p_2^2-e}{p_1^2-p_1p_2+p_2^2-e}$$

or, on account of (63), (74) and (79), to a first approximation

$$\frac{p_1(p_1^2-e)-p_2(p_2^2-e)}{p_1(p_1^2-e)+p_2(p_2^2-e)}\approx\frac{p_1-p_2}{p_1+p_2}\,\frac{b}{2+b}=\frac{p_1-p_2}{p_1+p_2}\,g(\xi), \quad (83)$$

where

$$g(\xi)=\frac{b}{2+b}\approx\frac{\xi\,C/B}{2-(2-C/B)\xi}. \quad (84)$$

Having (83) we write eq. (65) in the form

$$m\pi - \pi n\,(p_1 - p_2) \approx \pm \arcsin\left\{\frac{p_1 - p_2}{p_1 + p_2}\, g(\xi) \sin\left[\pi n\,(p_1 + p_2)\right]\right\}. \qquad (85)$$

Since both for a positive and for an equally large negative value of the right-hand member of eq. (85) a root is found for $p_1 - p_2$, as a rule always two roots are found to lie close together. This means that near to each other two unstable states of the spring are to be indicated, each with its own deflection.

In our problem, however, we are most interested in the least compressive force P or — what amounts to the same thing — the smallest compression ξ causing the spring to buckle. In connection with (72), (73), (74), (76) and (81), this corresponds to the smallest value of $p_1 - p_2$ satisfying eq. (85). This smallest value occurs with $m = 1$ and a positive value of the right-hand member of the equation, so that instability first arises when

$$\pi - \pi n\,(p_1 - p_2) \approx \frac{p_1 - p_2}{p_1 + p_2}\, g(\xi)\, \left|\sin\left[\pi n\,(p_1 + p_2)\right]\right|. \qquad (86)$$

Availing ourselves of the approximation $n(p_1 + p_2) \approx 2n_0$ [see eqs (78) and (81)], the solution for $p_1 - p_2$ is determined by

$$n(p_1 - p_2)\left\{1 + g(\xi)\,\frac{|\sin 2\pi n_0|}{2\pi n_0}\right\} \approx 1. \qquad (87)$$

According to (66)

$$n = \frac{l}{2\pi R}\cdot\frac{1}{\tan\alpha},$$

so that for (87) we can write

$$\left(\frac{2\pi R}{l}\right)^2 \approx \frac{(p_1 - p_2)^2}{\tan^2\alpha}\left\{1 + g(\xi)\,\frac{|\sin 2\pi n_0|}{2\pi n_0}\right\}^2,$$

or, considering (81) and omitting the negligible terms,

$$\left(\frac{2\pi R}{l}\right)^2 = (a + c)\,(2 + b)\left\{1 + g(\xi)\,\frac{|\sin 2\pi n_0|}{\pi n_0} + f_1 \tan^2\alpha + \ldots\right\}. \qquad (88)$$

Using (73), (74) and (76) we now write for $(a + c)\,(2 + b)$

$$(a + c)\,(2 + b) = \left(1 + \frac{C}{A}\right)\frac{\xi}{1 - \xi}\left(2 + \frac{C}{B}\,\frac{\xi}{1 - \xi}\right)\left(1 + f_2 \tan^2\alpha_0 + \ldots\right), \qquad (89)$$

where

$$f_2 = \frac{2\left(1 + \dfrac{C}{B}\,\dfrac{\xi}{1 - \xi}\right)\left\{1 - \tfrac{1}{2}\xi - \dfrac{C}{B}\,(1 - \xi)\right\}}{2 + \dfrac{C}{B}\,\dfrac{\xi}{1 - \xi}} + \frac{C^2}{A^2}\,\frac{\xi(1 - \xi)}{1 + C/A}, \qquad (90)$$

and for f_1 [see eq. (82)]

$$f_1 = -\frac{C}{A}\frac{\xi}{1-\xi} - \frac{2\left(1-\frac{C}{B}\right) - \frac{C}{A}\cdot\frac{C}{B}\cdot\frac{\xi}{1-\xi} - \frac{1}{4}\left(\frac{C}{A} - 2\frac{C}{B} + 3 + \frac{C}{B}\frac{\xi}{1-\xi}\right)^2 \frac{\xi}{1-\xi}}{\left(1+\frac{C}{A}\right)\left(2+\frac{C}{B}\frac{\xi}{1-\xi}\right)}. \tag{91}$$

Instead of (88) we then obtain as the condition of instability, having regard to (10), (72) and (77),

$$\left(\frac{2\pi R_0}{l_0}\right)^2 = \left(1+\frac{C}{A}\right)\xi\left[2-\left(2-\frac{C}{B}\right)\xi\right]\left[1+g(\xi)\frac{|\sin 2\pi n_0|}{\pi n_0} + \right.$$
$$\left. + \left\{f_1(1-\xi)^2 + f_2 - 2\xi\left(2-\xi-\frac{C}{B}(1-\xi)\right)\right\}\tan^2\alpha_0 + \dots\right]. \tag{92}$$

If it is desired to know also the value of the corresponding buckling force P we have to make use of (53), (71), (73) and (77), from which we derive

$$PR_0^2 = C\,\xi\tan\alpha_0\left[1+\frac{1}{2}\left\{1-9\xi+4\xi^2-2\frac{C}{B}(1-\xi)(1-2\xi)\right\}\tan^2\alpha_0 + \dots\right]; \tag{93}$$

We know [see eq. (67)] that the length l_0 of the helical spring in the unloaded state is equal to $2\pi n R_0 n_0 \tan\alpha_0$, so that for $\tan^2\alpha_0$ — having regard to (92) — we can write

$$\tan^2\alpha_0 = \frac{1}{n_0^2}\left(\frac{l_0}{2\pi R_0}\right)^2 \approx \frac{1}{n_0^2}\frac{1}{\left(1+\frac{C}{A}\right)\xi\left\{2-\left(2-\frac{C}{B}\right)\xi\right\}}. \tag{94}$$

Substitution of (94) in eq. (92), and replacement of $2R_0$ by D_0 leads to a result showing that the helical spring with freely adjustable wire ends will buckle (in the imaginary experiment) when

$$\pi^2\left(\frac{D_0}{l_0}\right)^2 = \left(1+\frac{C}{A}\right)\xi\left\{2-\left(2-\frac{C}{B}\right)\xi\right\}\left\{1+g(\xi)\frac{|\sin 2\pi n_0|}{\pi n_0} + f(\xi)\frac{1}{n_0^2} + \dots\right\}, \tag{95}$$

where

$$f(\xi) = \frac{f_1(1-\xi)^2 + f_2 - 2\xi\left\{2-\xi-\frac{C}{B}(1-\xi)\right\}}{\left(1+\frac{C}{A}\right)\xi\left\{2-\left(2-\frac{C}{B}\right)\xi\right\}}. \tag{96}$$

If the spring wire has a circular cross-section and the diameter of the wire is small in relation to the diameter of the spring *) the two rigidities against bending A and B are equal, and their ratio with respect to the rigidity against twisting C is as

$$\frac{C}{A}=\frac{C}{B}=\frac{2G}{E}=\frac{m}{m+1}. \tag{97}$$

Substituting this in (95) we find as the condition of instability

$$\pi^2\left(\frac{D_0}{l_0}\right)^2=\frac{2(2m+1)}{m+1}\,\xi\left\{1-\frac{m+2}{2(m+1)}\,\xi\right\}\left\{1+g(\xi)\,\frac{|\sin 2\pi n_0|}{\pi n_0}+f(\xi)\,\frac{1}{n_0^2}+\ldots\right\}. \tag{98}$$

For the calculation of the corresponding buckling force P we refer to eq. (93).

If n_0 is large the two correction terms in eq. (98) disappear and thus we arrive again at the previously deduced relation between the slenderness and the relative compression [see eq. (16)]. The functions $f(\xi)$ and $g(\xi)$ occurring in the correction terms are plotted in figs 12 and 13 ($m = 10/3$). For $\xi = 0, f(\xi)$ does, it is true, become infinitely large, but by using (90), (91), (94), (96) and (97) it can be proved that the correction term itself is then equal to

$$\lim_{\xi=0} f(\xi)\,\frac{1}{n_0^2}=\frac{m}{(m+1)\,(2m+1)}\tan^2\alpha_0\approx 0{\cdot}10\tan^2\alpha_0,$$

so that even then, when there is a sufficiently large number of coils (small α_0), the correction term may be ignored. The term with $g(\xi)$ in eq. (98)

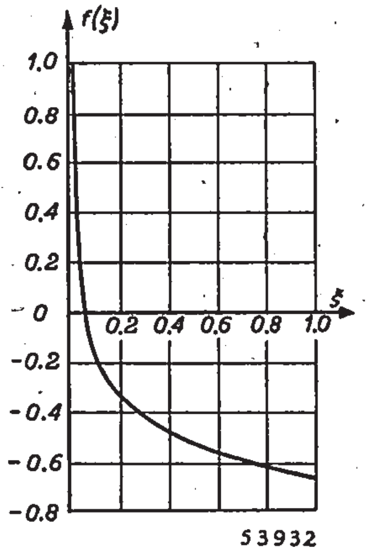

Fig. 12. Curve of $f(\xi)$ in the case of a circular wire section and $m = 10/3$.

---

*) The case where the diameter of the wire is not small in relation to the spring diameter is dealt with separately in section 7.

disappears not only when n_0 is large but also when $2n_0$ is a whole number, and this term therefore indicates in particular what correction has to be applied for a helical spring not possessing a whole number of half-coils.

In order to get an idea of the size of the corrections we shall take as an example a helical spring with a slenderness l_0/D_0 equal to 3 and a pitch equal to the spring diameter, so that the number of coils amounts to 3.

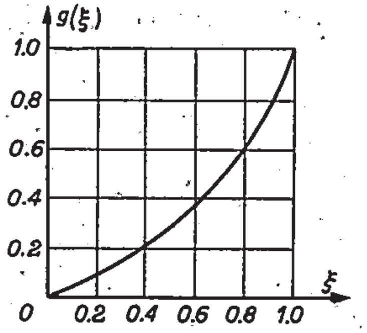

53933

Fig. 13. Curve of $g(\xi)$ in the case of a circular wire section and $m = 10/3$.

According to (98) this spring buckles under a relative compression $\xi = 0{\cdot}455$, whilst the elementary calculation gives $\xi = 0{\cdot}415$, thus showing a deviation of approximately 10%. If the spring has 6 coils (the pitch then being equal to half the spring diameter) it will buckle at $\xi = 0{\cdot}425$ and the difference will be only a few per cent. We therefore arrive at the conclusion that the elementary calculation yields results sufficiently accurate for practical purposes, and certainly so when the helical spring has a pitch smaller than half its diameter.

7. The influence of the ratio of the wire diameter to the spring diameter upon the buckling of the helical spring under compression

If the thickness of the wire is not small in relation to the diameter of the spring we must regard the spring wire as an initially curved rod and the rigidities of the wire against bending and twisting are dependent not only upon the shape of the wire section but also upon the ratio of the thickness of the wire (d) to the diameter of the spring (D_0).

When an asterisk indicates the quantities relating to a straight rod, Göhner *) found the various rigidities of the strongly curved rod with circular cross-section to be as follows:

---

*) O. Göhner, Zur Berechnung des gebogenen oder gedrillten Ringstabs mit Kreisquerschnitt und der zylindrischen Schraubenfeder, Ing. Arch. 9, 355-371, 1938. In regard to k_B and k_C it is to be noted that these do not relate to pure bending and twisting of the ring-shaped rod, so that one has to use the eqs (13) and (33) in the paper referred to here.

$$\left.\begin{aligned}
&\text{with respect to bending around the first principal axis of inertia (axis 1)}\\
&A = A^*\left\{1 + k_A\left(\frac{d}{D_0}\right)^2 + \ldots\right\}, \quad k_A = -\frac{m^3+5m^2+4m+2}{24m^2\,(m+1)} = -0{\cdot}09,\\
&\text{with respect to bending around the second principal axis of inertia (axis 2)}\\
&B = B^*\left\{1 + k_B\left(\frac{d}{D_0}\right)^2 + \ldots\right\}, \quad k_B = -\frac{19m^3+17m^2-16m-8}{48\,m^2\,(m+1)} = -0{\cdot}36,\\
&\text{with respect to twisting (around axis 3)}\\
&C = C^*\left\{1 + k_C\left(\frac{d}{D_0}\right)^2 + \ldots\right\}, \quad k_C = \frac{23m+13}{48\,(m+1)} = 0{\cdot}43\;.\;(m = 10/3)
\end{aligned}\right\}\quad (99$$

Applying the same corrections to the helically wound wire *), we obtain

$$\left(1+\frac{C}{A}\right)\xi\left\{2-\left(2-\frac{C}{B}\right)\xi\right\} = \left(1+\frac{C^*}{A^*}\right)\xi\left\{2-\left(2-\frac{C^*}{B^*}\right)\xi\right\}\left\{1+h(\xi)\left(\frac{d}{D_0}\right)^2+\ldots\right\},$$

where

$$h(\xi) = (k_C - k_A)\,\frac{C^*/A^*}{1+C^*/A^*} + (k_C - k_B)\,\frac{\xi\,C^*/B^*}{2-(2-C^*/B^*)\,\xi}\,. \quad (100)$$

Bearing in mind that in the case of a circular wire section $C^*/A^* = C^*/B^* = m/(m+1)$ [see eq. (97)], we write eq. (95) as

$$\pi^2\left(\frac{D_0}{l_0}\right)^2 = \frac{2\,(2m+1)}{m+1}\,\xi\left\{1-\frac{m+2}{2\,(m+1)}\,\xi\right\}$$
$$\left\{1+g(\xi)\,\frac{|\sin 2\pi n_0|}{\pi n_0} + f(\xi)\,\frac{1}{n_0^2} + h(\xi)\left(\frac{d}{D_0}\right)^2+\ldots\right\}. \quad (101)$$

The function $h(\xi)$ is plotted in fig. 14 ($m = 10/3$). We see that even with a large ratio of the wire diameter to the spring diameter the correction is as

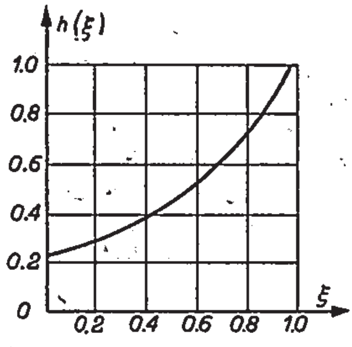

53934

Fig. 14. Curve of $h(\xi)$ in the case of a circular wire section and $m = 10/3$.

---

*) It is to be doubted whether this is admissible (see O. **Göhner**, loc. cit., p. 370), but we follow this course so as to obtain some idea of the magnitude of the corrections to be expected with regard to buckling.

a rule only small, amounting at most to a few per cent. From the foregoing calculations we therefore arrive at the conclusion that neither a small number of coils nor a large wire diameter seriously affects the results of the elementary method of calculation, so that in general this may be considered quite adequate for practical purposes.

8. Buckling of a helical spring with freely adjustable wire ends under combined compression and twist

In an earlier publication *) the problem of a helical spring simultaneously loaded with a compressive force and a torque was solved by assuming the helical spring to be replaced by an elastic prismatic rod. Here we give a direct deduction of the same problem, at least insofar as helical springs with a small slope are concerned. It is therefore emphasized that putting the torque equal to zero leads to the same results for the compression-loaded helical spring as those found by the elementary method of calculation (section 3).

To the two equal and opposite compressive forces P acting along the z-axis we add two equal and opposite torques W exercising a twist about the z-axis (fig. 15). Now in order to distinguish the moments present in a certain cross-section of the spring wire from the corresponding moments occurring when only two compressive forces are in action (see section 5), we employ symbols provided with a bar. These moments are

$$\bar{M}_x = P(R+\varrho)\sin\Theta, \quad \bar{M}_y = -P(R+\varrho)\cos\Theta, \quad \bar{M}_z = W. \tag{102}$$

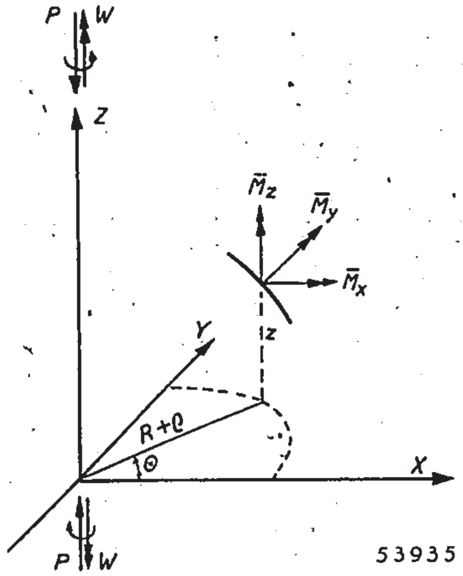

Fig. 15. An element of the helical spring under combined compression and twist.

---

*) J. A. Haringx, On the buckling and the lateral rigidity of helical compression springs II, Proc. Kon. Ned. Akad. Wetenschappen Amsterdam **45**, 650-654, 1942.

Using (31), (34), (35) and (40), in which equations all M-quantities are to be imagined as having a bar, we can write, when ignoring terms of higher order and referring to (47),

$$\left.\begin{aligned}\overline{M}_{\rm I} &= M_{\rm I} - W\cos\alpha\left(\frac{\varrho'}{R}\sin\alpha - \frac{\zeta''}{R}\cos\alpha\right),\\ \overline{M}_{\rm II} &= M_{\rm II} + W\cos\alpha\left(1+\frac{\varrho}{R}\sin^2\alpha - \frac{\zeta'}{R}\sin\alpha\cos\alpha\right),\\ \overline{M}_{\rm III} &= M_{\rm III} + W\sin\alpha\left(1-\frac{\varrho}{R}\cos^2\alpha + \frac{\zeta'}{R}\cot\alpha\cos^2\alpha\right).\end{aligned}\right\}\qquad(103)$$

According to (41), where all M-quantities are likewise to be imagined as being barred, and owing to (47) and (30) in the case of a small angle ϑ

$$\left.\begin{aligned}\overline{M}_1 &= \overline{M}_{\rm I} + \overline{M}_{\rm II}\,\vartheta,\\ \overline{M}_2 &= \overline{M}_{\rm II} - \overline{M}_{\rm I}\,\vartheta \approx \overline{M}_{\rm II},\\ \overline{M}_3 &= \overline{M}_{\rm III}.\end{aligned}\right\}\qquad(104)$$

Substituting in this equation for the angle ϑ [see eq. (26)]

$$\vartheta = \frac{\overline{M}_1 R}{A\cos^2\alpha},\qquad(105)$$

we obtain, when using (47) and (103) and referring to (49),

$$\left.\begin{aligned}\overline{M}_1 &= -\frac{A\cos^2\alpha}{A\cos^2\alpha - PR^2\sin\alpha - WR\cos\alpha}\times\\ &\times\left[PR\left\{\frac{\varrho'}{R}(1+\sin^2\alpha) - \frac{\zeta''}{R}\sin\alpha\cos\alpha\right\} + W\cos\alpha\left(\frac{\varrho'}{R}\sin\alpha - \frac{\zeta''}{R}\cos\alpha\right)\right],\\ \overline{M}_2 &= M_2 + W\cos\alpha\left(1+\frac{\varrho}{R}\sin^2\alpha - \frac{\zeta'}{R}\sin\alpha\cos\alpha\right),\\ \overline{M}_3 &= M_3 + W\sin\alpha\left(1-\frac{\varrho}{R}\cos^2\alpha + \frac{\zeta'}{R}\cot\alpha\cos^2\alpha\right).\end{aligned}\right\}\qquad(106)$$

In eqs (38) and (39) we must now replace M_1, M_2, and M_3 by $\overline{M}_1$, $\overline{M}_2$ and $\overline{M}_3$, which are given by the expressions (106), where M_2 and M_3 have the values of (49). Here again we see that, besides the terms with the small quantitites ϱ and ζ, there are terms in which only the radius R and the slope α of the auxiliary helix occur. This auxiliary helix (state II) is again chosen such that $\varrho = 0$ and $\zeta = 0$ gives a possible solution of eqs (38), (39), (49) and (106). Taking in these equations ϱ and ζ equal to zero, it appears that the following equations must be satisfied

$$\cos^2\alpha - \frac{R}{R_0}\cos^2\alpha_0 = \frac{PR^2}{B}\sin\alpha + \frac{WR}{B}\cos\alpha, \qquad (107)$$

$$\sin\alpha\cos\alpha - \frac{R}{R_0}\sin\alpha_0\cos\alpha_0 = -\frac{PR^2}{C}\cos\alpha + \frac{WR}{C}\sin\alpha. \qquad (108)$$

Eqs (107) and (108) enable us, starting from the given spring dimensions in the initial state (state I), to calculate the unknown radius R and the slope α of the auxiliary helix in the state II as functions of the loads P and W. According to (105) and (106), with $\varrho = 0$ and $\zeta = 0$ we again find that the angle ϑ is equal to zero. Thus in the state II the two systems of axes I, II, III and 1, 2, 3 again coincide. Consequently, also with a combined compression and twist the axis 1 in the state II proves to be radially directed. Further, the number of coils n is once more determined by eq. (52) and the length l is given by eq. (66). It has to be remembered, however, that in these equations R and α now satisfy (107) and (108).

When substituting the expression (106) in eqs (38) and (39) — where the quantities M are to be taken as being barred — we employ in addition to (49), the eqs (107) and (108). The terms in which only R and α occur then cancel out and the terms with ϱ and ζ remain. Whereas the notations (53) apply only for the special case where $W = 0$, here — with a torque — we use the more general notations

$$a = \frac{PR^2}{A\sin\alpha - PR^2\tan^2\alpha - WR\tan\alpha},\quad b = \frac{PR^2}{B\sin\alpha},\quad c = \frac{PR^2}{C\sin\alpha},\quad w = \frac{W}{PR}. \qquad (109)$$

Hence, the equations in question become

$$-\cos^2\alpha(\varrho'' + \varrho\cos2\alpha + \zeta'\sin2\alpha) = b\sin^2\alpha(\varrho\sin^2\alpha + \zeta'\cos^2\alpha\cot\alpha) + \\ + wb\sin\alpha\cos\alpha(\varrho\sin^2\alpha - \zeta'\sin\alpha\cos\alpha), \qquad (110)$$

$$\left.\begin{aligned} &-\sin\alpha\cos\alpha(2\varrho'' + 2\varrho\cos^2\alpha - \zeta'''\cot\alpha - \zeta'\cos2\alpha\cot\alpha) = \\ &a\tan\alpha\{\varrho''(1+\sin^2\alpha) - \zeta'''\sin\alpha\cos\alpha\} + wa\sin\alpha(\varrho''\sin\alpha - \zeta'''\cos\alpha) - \\ &-c\sin\alpha\cos\alpha\{\varrho(1+\sin^2\alpha) - \zeta'\sin\alpha\cos\alpha\} - wc\sin^2\alpha(\varrho\cos^2\alpha - \zeta'\cos^2\alpha\cot\alpha). \end{aligned}\right\} \qquad (111)$$

As agreed, we confine ourselves to helical springs with a small slope α, so that we can greatly simplify the calculation by expanding the various functions into series. It now appears to be necessary to maintain for the time being the powers of α up to and including α^2. After dividing by $\cos^4\alpha$, eq. (110) is then reduced to

$$\varrho''(1+\alpha^2) + \varrho(1-\alpha^2) + \zeta'\alpha(2 + b - wb\alpha) = 0, \qquad (112)$$

whilst, likewise after dividing by $\cos^4\alpha$, eq. (111) becomes

$$\varrho''\alpha(2 + a + wa\alpha) + \varrho\alpha(2 - c - wc\alpha) - \zeta'''\{1 + wa\alpha + (1+a)\alpha^2\} - \\ - \zeta'\{1 - wc\alpha - (1+c)\alpha^2\} = 0. \qquad (113)$$

Eliminating ζ from (112) and (113) and dividing by $(1 + \alpha^2)$ we again obtain the differential equation [see also eq. (58)]

$$e_0\varrho'''' + e_2\varrho'' + e_4\varrho = 0\,, \tag{114}$$

where the coefficients e_0, e_2 and e_4 (written in powers of α), in connection with the presence of a torque, are now equal to

$$\left.\begin{aligned} e_0 &= 1 + wa\alpha + (1 + a)\,\alpha^2 + \dots, \\ e_2 &= 2 + w\,(a - c)\,\alpha + (2 + 3a + 2b - c + ab)\,\alpha^2 + \dots, \\ e_4 &= 1 - wc\alpha + (1 + 2b - 3c - bc)\,\alpha^2 + \dots. \end{aligned}\right\} \tag{115}$$

The general solution of the differential equation (114) is [see also eq. (60)]

$$\varrho = A_1 \sin p_1\Theta + B_1 \cos p_1\Theta + A_2 \sin p_2\Theta + B_2 \cos p_2\Theta\,. \tag{116}$$

On account of (115) p_1 and p_2 are now determined by

$$\left.\begin{aligned} p_1^2 + p_2^2 &= 2 - w(a + c)\,\alpha + \{a + 2b - c + ab + w^2a\,(a + c)\}\,\alpha^2 + \dots, \\ p_1^2 \cdot p_2^2 &= 1 - w(a + c)\,\alpha - \{a - 2b + 3c + bc - w^2a\,(a + c)\}\,\alpha^2 + \dots \end{aligned}\right\} \tag{117}$$

From the second equation (117) it follows that

$$p_1p_2 = 1 - \tfrac{1}{2}w(a + c)\,\alpha - \tfrac{1}{2}\{a - 2b + 3c + bc - \tfrac{1}{4}w^2(a + c)\,(3a - c)\}\alpha^2 + \dots, \tag{118}$$

so that with the aid of the first eq. (117) it can be deduced that instead of (81) we now have

$$\left.\begin{aligned} (p_1 - p_2)^2 &= \{(a + c)\,(2 + b) + \tfrac{1}{4}w^2\,(a + c)^2\}\,\alpha^2 + \dots, \\ (p_1 + p_2)^2 &= 4 - 2w\,(a + c)\alpha + \dots. \end{aligned}\right\} \tag{119}$$

From eq. (119), omitting the terms of higher order, we obtain

$$\left.\begin{aligned} \frac{p_1 - p_2}{2} &\approx \tfrac{1}{2}\alpha\sqrt{(a + c)\,(2 + b) + \tfrac{1}{4}w^2(a + c)^2}\,, \\ \frac{p_1 + p_2}{2} &\approx 1 - \tfrac{1}{4}w(a + c)\,\alpha\,, \end{aligned}\right\} \tag{120}$$

so that with the notations

$$\left.\begin{aligned} 2\gamma_1 &= \left\{\tfrac{1}{2}w(a + c) - \sqrt{(a + c)\,(2 + b) + \tfrac{1}{4}w^2(a + c)^2}\right\}\frac{l}{2R}\,, \\ 2\gamma_2 &= \left\{\tfrac{1}{2}w(a + c) + \sqrt{(a + c)\,(2 + b) + \tfrac{1}{4}w^2(a + c)^2}\right\}\frac{l}{2R}\,, \end{aligned}\right\} \tag{121}$$

we may write for p_1 and p_2 to a first approximation

$$p_1 = 1 - 2\gamma_1\frac{R}{l}\,\alpha\,, \quad p_2 = 1 - 2\gamma_2\frac{R}{l}\,\alpha\,. \tag{122}$$

Substitution of (122) in eq. (116) then leads, with the coordinate $z \approx R\,\Theta\alpha$ [eq. (28)], to the solution

$$\varrho = F_1(z)\sin\Theta + F_2(z)\cos\Theta, \tag{123}$$

where

$$\left.\begin{aligned} F_1(z) &= A_1\cos\frac{2\gamma_1 z}{l} + B_1\sin\frac{2\gamma_1 z}{l} + A_2\cos\frac{2\gamma_2 z}{l} + B_2\sin\frac{2\gamma_2 z}{l},\\ F_2(z) &= -A_1\sin\frac{2\gamma_1 z}{l} + B_1\cos\frac{2\gamma_1 z}{l} - A_2\sin\frac{2\gamma_2 z}{l} + B_2\cos\frac{2\gamma_2 z}{l}. \end{aligned}\right\} \tag{124}$$

If we assume that when Θ is increased by 2π the coordinate z undergoes such a small change that a coil of the spring is practically a flat ring, formula (123) shows that in its entirety this ring undergoes a displacement $F_2(z)$ in the direction of the x-axis and one of $F_1(z)$ in the direction of the y-axis (fig. 16). Since the centre of the ring is to be regarded as a point of the central line of the helical spring, the curves $y = F_1(z)$ and $x = F_2(z)$ in the yz-plane and the xz-plane respectively represent apparently nothing else than the projections of that central line of the spring on these coordinate planes. In the case we are dealing with here (the spring with freely adjustable wire ends) the force acts in the centre of the two end coils of the helical spring, and therefore the central line must intersect the z-axis at the two spring ends. This leads to the boundary conditions

$$F_1(z) = 0, \quad F_2(z) = 0 \quad \text{at} \quad \begin{cases} z = 0,\\ z = l. \end{cases} \tag{125}$$

From this it follows, in connection with (124), that

$$\left.\begin{aligned} A_1 + A_2 &= 0,\\ B_1 + B_2 &= 0,\\ A_1\cos 2\gamma_1 + B_1\sin 2\gamma_1 + A_2\cos 2\gamma_2 + B_2\sin 2\gamma_2 &= 0,\\ -A_1\sin 2\gamma_1 + B_1\cos 2\gamma_1 - A_2\sin 2\gamma_2 + B_2\cos 2\gamma_2 &= 0. \end{aligned}\right\} \tag{126}$$

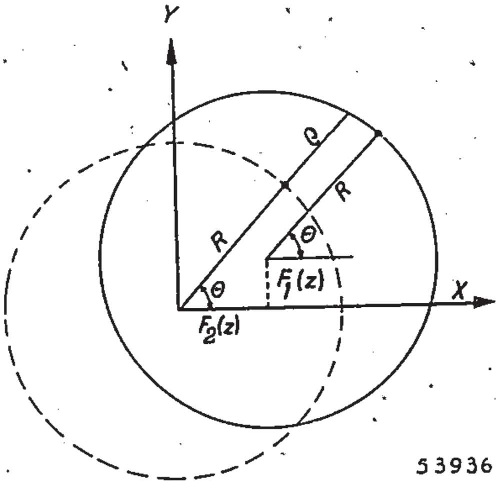

Fig. 16. Displacement of a "flat" coil of the helical spring in the directions of x and y.

These equations allow of a solution differing from zero only when the determinant of the system equals zero. This leads to the condition

$$\cos 2(\gamma_1 - \gamma_2) = 1 \quad \text{or} \quad |\gamma_1 - \gamma_2| = m\pi \ (m = 1, 2, 3, \ldots). \tag{127}$$

In connection with (121) and (127), with increasing load, instability arises for the first time when $m = 1$, thus when

$$\frac{l}{2R}\sqrt{(a+c)\,(2+b) + \tfrac{1}{4}w^2\,(a+c)^2} = \pi. \tag{128}$$

In order to work out this condition of instability we must first ascertain the magnitudes of a, b, c and w. Ignoring the higher powers, we obtain from eqs (107) and (108) with the notations (109) that

$$\frac{R}{R_0} = 1 - wba + \ldots, \tag{129}$$

$$\frac{a}{a_0} = \frac{1 - wba + \ldots}{1 + c - wca + \ldots}. \tag{130}$$

Since here again the length l is given by (66) and l_0 by (67), equation (68) still holds. Therefore, introduction of the relative compression ξ leads in connection with (10) again to eq. (71), which to a first approximation may also be written as

$$\frac{a}{a_0} \approx 1 - \xi. \tag{131}$$

With $b = \frac{C}{B}c$ [eq. (109)] we deduce from (130) and (131)

$$c = \frac{\xi}{1-\xi}\left\{1 + \left(1 - \frac{C}{B}\frac{1}{1-\xi}\right) wa + \ldots\right\}, \tag{132}$$

and thus

$$b = \frac{C}{B}\frac{\xi}{1-\xi}\left\{1 + \left(1 - \frac{C}{B}\frac{1}{1-\xi}\right) wa + \ldots\right\}. \tag{133}$$

Further, from eqs (109) and (132) it follows that

$$a = \frac{Cc}{A - Cc\tan^2\alpha - Cwc\tan\alpha} = \\ = \frac{C}{A}\frac{\xi}{1-\xi}\left\{1 + \left(1 - \frac{C}{B}\frac{1}{1-\xi} + \frac{C}{A}\frac{\xi}{1-\xi}\right) wa + \ldots)\right\}. \tag{134}$$

As regards the magnitude of w it may be said that according to eq. (129)

w is related to a first approximation to the variation of the radius or, in in connection with (52), to the variation in the number of coils, for

$$\frac{n}{n_0} \approx \frac{R_0}{R} = 1 + wba + \ldots . \tag{135}$$

The angle of twist χ of the spring about the z-axis, as caused by the torque, is equal to

$$\chi = 2\pi\,(n-n_0)\,. \tag{136}$$

Thus, on account of (135) and the fact that the length l of the spring is to a first approximation equal to $2\pi\, Rna$, we find for w the relation

$$wb \approx \frac{R}{l}\,\chi\,. \tag{137}$$

The substitution of the given expressions for a, b and c [eqs (132), (133) and (134)] in eq. (119) leads to powers of α that were ignored in the derivation of these equations. From this it is to be concluded that we have apparently confined ourselves in advance to cases with such a small torque that the terms $w\alpha$ occurring in eqs (132), (133), (134) and (135) can be ignored with respect to unity. This involves the condition $wba \ll 1$ and we may therefore write

$$a \approx \frac{C}{A}\,\frac{\xi}{1-\xi}, \qquad b \approx \frac{C}{B}\,\frac{\xi}{1-\xi}, \qquad c \approx \frac{\xi}{1-\xi}, \qquad \frac{n}{n_0} \approx \frac{R_0}{R} \approx 1\,. \tag{138}$$

Since the relative compression ξ lies between 0 and 1, according to (138) a, b and c may apparently have any values between 0 and ∞ and thus, just as in section 6, here again we may expect difficulties in regard to the permissibility of the applied expansions. In connection with (131) and (138), however, the quantities a, b and c multiplied by α are equal to

$$a\alpha \approx \frac{C}{A}\,\alpha_0\xi\,, \qquad b\alpha \approx \frac{C}{B}\,\alpha_0\xi\,, \qquad c\alpha \approx \alpha_0\xi\,, \tag{139}$$

so that any large values of a, b and c prove once more to be of minor importance with respect to the permissibility of the expansion in question.

According to eq. (138), just as in section 6 [see eq. (89)], $(a+c)\,(2+b)$ will again be equal, to a first approximation, to

$$(a+c)\,(2+b) \approx \left(1+\frac{C}{A}\right)\frac{\xi}{1-\xi}\left(2+\frac{C}{B}\,\frac{\xi}{1-\xi}\right), \tag{140}$$

whilst with (137) and (138) we find for $w\,(a+c)$

$$w\,(a+c) \approx \left(\frac{B}{A}+\frac{B}{C}\right)\frac{R}{l}\,\chi\,. \tag{141}$$

In the case of a spring wire with circular cross-section $A = B = (1 + 1/m)\,C$ [see eq. (97)], and so, employing eqs (10), (140), (141) and the identity $D_0 \approx 2R$, we find

$$\left.\begin{aligned} (a+c)\,(2+b)\left(\frac{l}{2R}\right)^2 &= \frac{2(2m+1)}{m+1}\left(\frac{l_0}{D_0}\right)^2 \xi \left\{1 - \frac{m+2}{2(m+1)}\,\xi\right\}, \\ w(a+c)\,\frac{l}{2R} &= \frac{2m+1}{2m}\,\chi . \end{aligned}\right\} \tag{142}$$

Hence, the condition of instability (128) for combined compression and twist becomes

$$\frac{2(2m+1)}{m+1}\left(\frac{l_0}{D_0}\right)^2 \xi \left\{1 - \frac{m+2}{2(m+1)}\,\xi\right\} + \tfrac{1}{4}\left(\frac{2m+1}{2m}\right)^2 \chi^2 = \pi^2 . \tag{143}$$

Thus with $m = 10/3$,

$$\left.\begin{aligned} 0{\cdot}3585\,\xi\,(1 - 0{\cdot}615\,\xi)\left(\frac{l_0}{D_0}\right)^2 + 0{\cdot}0338\,\chi^2 = 1, \\ \text{or} \qquad \xi = 0{\cdot}8125\,\left\{1 \pm \sqrt{1 - (6{\cdot}87 - 0{\cdot}23\,\chi^2)\,(D_0/l_0)^2}\right\}. \end{aligned}\right\} \tag{144}$$

As regards the corresponding loads P and W it may be said that in connection with (109), (138) and (139) the compressive force P is related to the relative compression ξ according to *)

$$PR_0^2 \approx C a_0 \xi , \tag{145}$$

and that, in connection with (66), (109) and (137), the torque W is related to the angle of twist χ according to

$$WR_0 \approx B\,\frac{\chi}{2\pi n_0} . \tag{146}$$

The relation given in eq. (144) between the three quantities ξ, χ and l_0/D_0 is graphically represented in fig. 17. As was to be expected, the curve for $\chi = 0$ (no torque) is identical to curve 3 of fig. 6, which is given by eq. (19). Further, it is to be noted that in the absence of a compression ξ any spring with freely adjustable wire ends will have to buckle if twisted through an angle of 313° **).

The final result of the calculation in the form of (143) or (144) is independent of the slope a_0 and of the number of coils n_0. In section 6 we have seen that the slope α_0 has little effect and that even a pitch equal to the spring diameter involves a deviation of only 10%. Deriving the formulae here, however, we found that we must confine ourselves not only to a small slope, but also to cases where the torque is small ($wba \ll 1$). On account of eq. (146) this torque decreases with increasing number of coils $n \approx n_0$. In order to ascertain the effect of a small number of coils, the approximative calculation would have to be repeated with a larger number of terms.

---

*) Of course, eqs (145) and (146) can also be deduced directly.

**) See also C. B. Biezeno and R. Grammel, Technische Dynamik, Springer, Berlin (1939), p. 553.

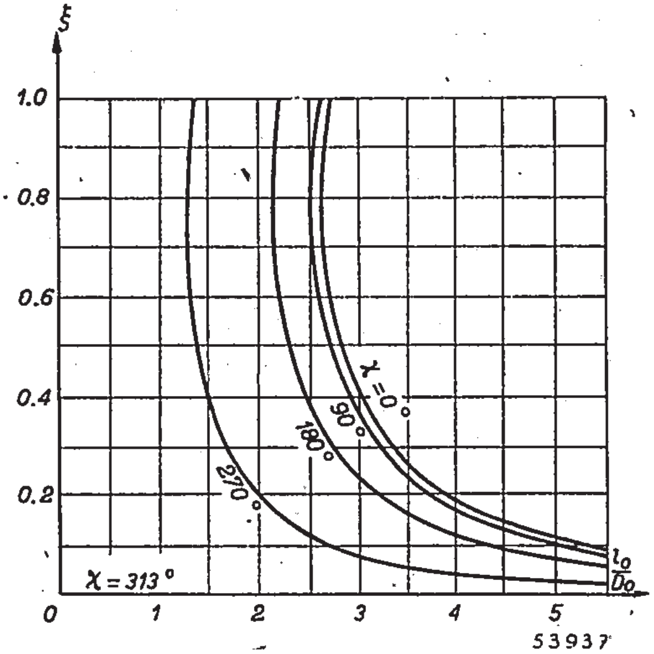

Fig. 17. The critical relative compression ξ of a helical spring with freely adjustable wire ends as function of the slenderness l_0/D_0 at various values of the angle of twist χ.

Instead of doing this, however, we shall merely make an estimate. Since from (144) it follows that buckling will always take place at an angle of twist $\chi \leqq 5{\cdot}46$ ($\xi > 0$), in the case of a helical spring with, say, more than 10 coils we have, according to eqs (135) and (136),

$$wba \approx \frac{\chi}{2\pi n_0} < 0{\cdot}087.$$

In the case of buckling under combined compression and twist the maximum deviation for the spring in question may be expected to be of the same order of magnitude.

9. Buckling of the helical spring with fixed wire ends under combined compression and twist

In the previous section the ends of the spring wire were freely adjustable, on the understanding, however, that a torque could be transmitted to these ends. Since this requires a construction difficult of realization and in practice the ends of a helical spring under twist will mostly be clamped, attention has to be given also to the case of a helical spring with fixed wire ends.

As is known, any load can always be composed to a resulting force and a resulting moment the axis of which coincides with the line of action of the force. Consequently also in the case of a helical spring with fixed wire ends the load may be regarded as consisting of two equal and opposite compressive forces P and two equal and opposite torques W all acting along the z-axis, provided account is taken of the possibility that this axis may assume an oblique position with respect to the "direction of compression".

This direction of compression is to be understood as the direction in which the compression of the spring takes place, thus coinciding with the direction of the central line of the helical spring in the initial state (state I). Therefore we introduce a new system of axes of x', y', z', with the z'-axis coinciding with the central line of the spring in the initial state and the x'-axis passing through the bottom end A of the spring wire. The system of axes of x, y, z then assumes an oblique position with respect to the system of axes of x', y'; z' (fig. 18). Since the end of the spring wire at point A is clamped, the system of axes 1, 2 and 3 at this point is fixed with respect to the system of axes of x', y', z' in a manner as indicated in fig. 18.

Considering the problem in this way we have the advantage that the general solution (123) derived in the preceding section is valid also for this case. It only needs adaption to new boundary conditions. We have seen that the functions $F_1(z)$ and $F_2(z)$ given in eq. (124) determine the projections of the central line of the helical spring in the deflected state

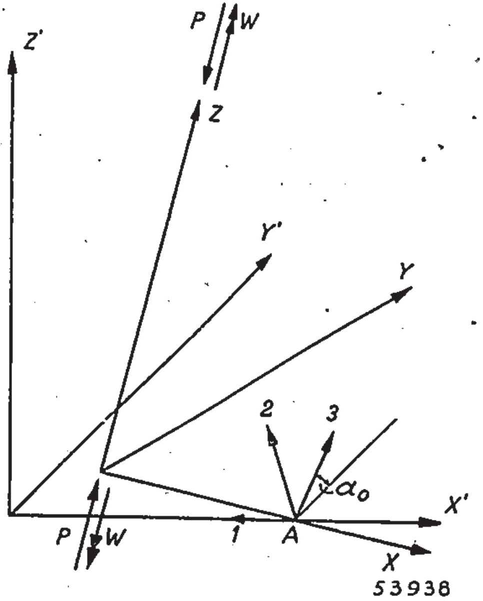

Fig. 18. Position of the central line of the auxiliary helix (z-axis) with respect to the central line of the helical spring in the original state (z'-axis). The bottom end of the spring wire is fixed at A.

(state III) on the yz-plane and the xz-plane respectively. Since we have to do with clamped ends that can only undergo a displacement in the direction of compression (z'-axis), the central line of the deflected helical spring must always intersect the z'-axis at the spring ends. Fig. 19 shows the projection of the central line (indicated by a dot-dash line) on the xz-plane and fig. 20 that on the yz-plane. We have to bear in mind that the positions of the axes of x, y, z differ only very little from those of the axes of x', y', z', so that in the further calculations all effects of the second order can be ignored. In fig. 19 we see that the direction of axis 1 at point A determines the slope of the projection of the z'-axis on the xz-plane, so that to a first approximation — having regard to the signs — we get

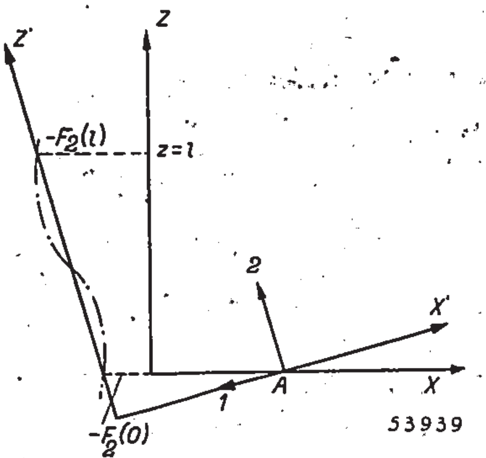

Fig. 19. Projection of the deflected central line of the helical spring under combined compression and twist on the xz-plane of the auxiliary helix.

$$\nu_1 = \frac{F_2(l) - F_2(0)}{l} \quad \text{at} \quad \Theta = 0\,(z = 0)\,. \tag{147}$$

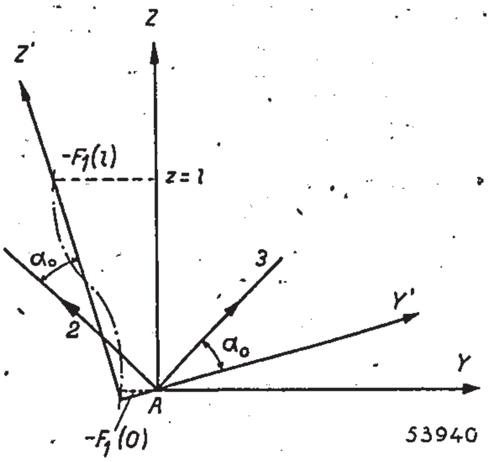

Fig. 20. Projection of the deflected central line of the helical spring under combined compression and twist on the yz-plane of the auxiliary helix.

Likewise, taking into account the angle α_0 (which as a matter of fact proves to play no part in the solution of the problem), the direction of the axis 3 determines the slope of the projection of the z'-axis on the yz-plane (fig. 20); thus, again to a first approximation and having regard to the signs, we get

$$\nu_3 - \alpha_0 = -\frac{F_1(l) - F_1(0)}{l} \quad \text{at} \quad \Theta = 0\,(z = 0). \tag{148}$$

Similar arguments apply to the other clamped end ($\Theta = 2\pi n$ and $z = l$ respectively), except that the projections must be made upon the planes of $\Theta = 2\pi n$ and of $\Theta = 2\pi n + \pi/2$ instead of upon the xz-plane and the yz-plane. Thus we have

$$\left.\begin{aligned} \nu_1 &= \frac{F_1(l) - F_1(0)}{l}\sin\Theta + \frac{F_2(l) - F_2(0)}{l}\cos\Theta, \\ \nu_3 - \alpha_0 &= \frac{F_2(l) - F_2(0)}{l}\sin\Theta - \frac{F_1(l) - F_1(0)}{l}\cos\Theta, \end{aligned}\right\} \text{ at } \quad \Theta = 2\pi n (z = l). \tag{149}$$

On account of eqs (31), (34), (35), (37) and the negligibility of ϑ proved by eqs (105), (106), (145), we find for ν_1 and ν_3, ignoring terms of higher order in α and α_0,

$$\nu_1 = \frac{\zeta''}{R}, \quad \nu_3 = \frac{\zeta'}{R}, \tag{150}$$

whilst according to (112) we have to a first approximation the relation

$$\zeta'\alpha\,(2 + b) = -(\varrho'' + \varrho). \tag{151}$$

Bearing in mind that the coordinate z is to be taken equal to $R\Theta\alpha$, then on account of eq. (123) and omitting the terms of higher order we obtain

$$\varrho'' + \varrho = 2R\alpha\left\{\frac{\mathrm{d}F_1(z)}{\mathrm{d}z}\cos\Theta - \frac{\mathrm{d}F_2(z)}{\mathrm{d}z}\sin\Theta\right\},$$

and thus in connection with eqs (150) and (151)

$$\nu_3 = \frac{\zeta'}{R} = -\frac{2}{2+b}\left\{\frac{\mathrm{d}F_1(z)}{\mathrm{d}z}\cos\Theta - \frac{\mathrm{d}F_2(z)}{\mathrm{d}z}\sin\Theta\right\}. \tag{152}$$

From (151) and (152), likewise omitting the terms of higher order, we find

$$\nu_1 = \frac{\zeta''}{R} = \frac{2}{2+b}\left\{\frac{\mathrm{d}F_1(z)}{\mathrm{d}z}\sin\Theta + \frac{\mathrm{d}F_2(z)}{\mathrm{d}z}\cos\Theta\right\}. \tag{153}$$

Together with (152) and (153) the boundary conditions (147), (148) and (149) now lead, to a first approximation, to

$$\left.\begin{aligned}\left\{\frac{\mathrm{d}F_1(z)}{\mathrm{d}z}\right\}_{z=0} &= \left\{\frac{\mathrm{d}F_1(z)}{\mathrm{d}z}\right\}_{z=l} = (1+\tfrac{1}{2}b)\,\frac{F_1(l)-F_1(0)}{l},\\ \left\{\frac{\mathrm{d}F_2(z)}{\mathrm{d}z}\right\}_{z=0} &= \left\{\frac{\mathrm{d}F_2(z)}{\mathrm{d}z}\right\}_{z=l} = (1+\tfrac{1}{2}b)\,\frac{F_2(l)-F_2(0)}{l}.\end{aligned}\right\} \tag{154}$$

The functions $F_1(z)$ and $F_2(z)$ occurring in these equations are already given in eq. (124), so that the following conditions must be satisfied

$$\left.\begin{aligned}2\gamma_1B_1+2\gamma_2B_2 &= -2\gamma_1A_1\sin2\gamma_1+2\gamma_1B_1\cos2\gamma_1-2\gamma_2A_2\sin2\gamma_2+\\ &\qquad +2\gamma_2B_2\cos2\gamma_2,\\ 2\gamma_1B_1+2\gamma_2B_2 &= (1+\tfrac{1}{2}b)\{A_1(\cos2\gamma_1-1)+B_1\sin2\gamma_1+A_2(\cos2\gamma_2-1)+\\ &\qquad +B_2\sin2\gamma_2\},\\ 2\gamma_1A_1+2\gamma_2A_2 &= 2\gamma_1A_1\cos2\gamma_1+2\gamma_1B_1\sin2\gamma_1+2\gamma_2A_2\cos2\gamma_2+\\ &\qquad +2\gamma_2B_2\sin2\gamma_2,\\ 2\gamma_1A_1+2\gamma_2A_2 &= (1+\tfrac{1}{2}b)\{A_1\sin2\gamma_1-B_1(\cos2\gamma_1-1)+A_2\sin2\gamma_2-\\ &\qquad -B_2(\cos2\gamma_2-1)\}.\end{aligned}\right\} \tag{155}$$

Eliminating B_2 from the first and the last equations (155) and A_2 from the second and the third we find for A_2 and B_2 expressions that when substituted respectively in the first and the third equations (155) lead to

$$\lambda_2A_1+\lambda_1B_1=0,\ \lambda_1A_1-\lambda_2B_1=0, \tag{156}$$

where

$$\left.\begin{aligned}\lambda_1 &= \sin(\gamma_1+\gamma_2)\left\{\sin(\gamma_1-\gamma_2)-(1+\tfrac{1}{2}b)\,\frac{\gamma_1-\gamma_2}{\gamma_1\gamma_2}\sin\gamma_1\sin\gamma_2\right\},\\ \lambda_2 &= \cos(\gamma_1+\gamma_2)\left\{\sin(\gamma_1-\gamma_2)-(1+\tfrac{1}{2}b)\,\frac{\gamma_1-\gamma_2}{\gamma_1\gamma_2}\sin\gamma_1\sin\gamma_2\right\}.\end{aligned}\right\} \tag{157}$$

Therefore, a solution differing from zero is possible only when

$$\lambda_1^2+\lambda_2^2=0, \tag{158}$$

which will be the case when the condition

$$\frac{\sin(\gamma_1-\gamma_2)}{\gamma_1-\gamma_2}=(1+\tfrac{1}{2}b)\,\frac{\sin\gamma_1\sin\gamma_2}{\gamma_1\gamma_2} \tag{159}$$

is satisfied.

Just as was the case in the preceding section, so for a circular wire section we have [see eqs (97), (138) and (142)]

$$\left.\begin{aligned} 1+\tfrac{1}{2}b &= \frac{1}{1-\xi}\left\{1-\frac{m+2}{2(m+1)}\,\xi\right\},\\ (a+c)\,(2+b)\left(\frac{l}{2R}\right)^2 &= \frac{2(2m+1)}{m+1}\left(\frac{l_0}{D_0}\right)^2\xi\left\{1-\frac{m+2}{2(m+1)}\,\xi\right\},\\ w(a+c)\,\frac{l}{2R} &= \frac{2m+1}{2m}\,\chi, \end{aligned}\right\} \quad (160)$$

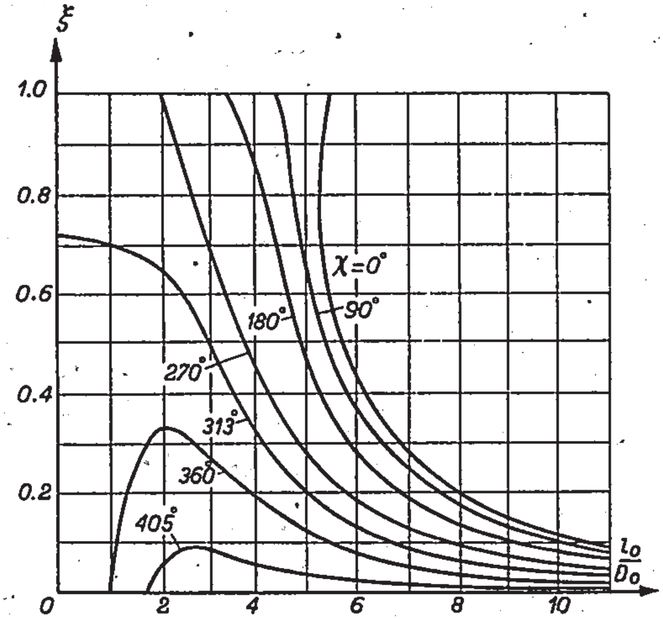

Fig. 21. The critical relative compression ξ of a helical spring with fixed wire ends as function of the slenderness l_0/D_0 at various angles of twist χ.

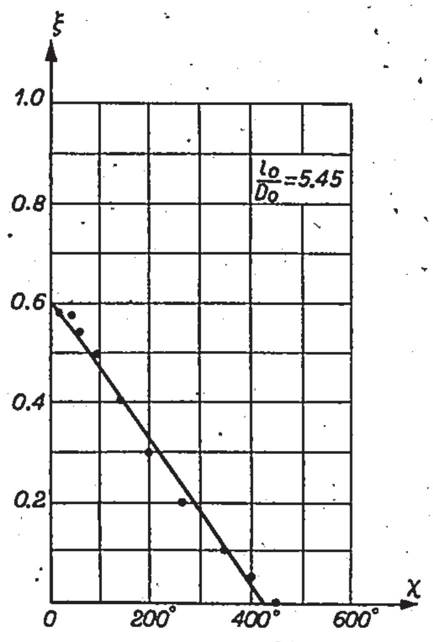

Fig. 22. The critical relative compression ξ of a helical spring with fixed wire ends as function of the angle of twist χ at a slenderness l_0/D_0 of 5·45. Comparison with test results.

so that $(1 + \frac{1}{2}b)$, γ_1 and γ_2 [eq. (121)] can be expressed in ξ, χ and l_0/D_0. Thus eq. (159) gives the relation between the critical relative compression ξ and the angle of twist χ for a spring with the slenderness l_0/D_0. This is graphically represented in fig. 21 ($m = 10/3$). The trend of the curve for $\chi = 0°$ is of course identical with that of curve 3 of fig. 6, taking a factor 2 into account with respect to the abscissa, since the reduced buckling length of the helical spring fixed at both wire ends is only half its full length. Further, attention is drawn to the fact that in the non-compressed state ($\xi = 0$) the helical spring will buckle if it is twisted through an angle varying from 313° ($l_0/D_0 = 0$) to 447° ($l_0/D_0 = \infty$).

Tests have been taken with a helical spring having a slenderness $l_0/D_0 = 5{\cdot}45$ ($D_0 = 18$ mm, d $= 0{\cdot}5$ mm and pitch $= 5$ mm). The results are plotted in fig. 22 side by side with the theoretical curve; this clearly shows the agreement between theory and practice, at least for a spring having a sufficiently large number of coils (here $n_0 \approx 20$).

Eindhoven, June 1948

(To be continued)

R 95 Philips Res. Rep. 3, 450-465, 1948

DISSIPATION OF HEAT BY FREE CONVECTION *)

by W. ELENBAAS

536.25

PART II **)

7. Dissipation of heat by bodies characterized by two linear dimensions

Bodies defined by *two* linear dimensions l_1 and l_2 (for instance, a vertical cylinder of finite length by the diameter $d = l_1$ and the height $h = l_2$) are of the same shape if the ratio of l_1 to l_2 is the same. An equation of the form (22) holds for each definite value of l_1/l_2, so that we can describe the dissipation of heat for arbitrary values of l_1/l_2 by adding the parameter l_1/l_2 to the equation (22):

$$\mathrm{Nu} = f_5(\mathrm{Gr} \cdot \mathrm{Pr}, l_1/l_2)\,. \tag{37}$$

It has been found possible to indicate the form of the function f_5 for some shapes of body.

Two of the cases described above should really be treated with (37) instead of (22). The width of the vertical plate (dimension in the direction of the y-axis, see fig. 2), and the length of the horizontal cylinder affect the dissipation of heat as well. We considered plates of such widths and cylinders of such lengths that the dissipation of heat might be assumed to be proportional to the widths and lengths respectively. If the vertical plate is widened, or the horizontal cylinder extended in length, $\bar{a}$ approaches a limiting value, and it was this limiting value which was considered. However, a formula of the form (37) must be employed for a *vertical* plate of a small width and for a short horizontal cylinder. But no measurements or calculations are known for these cases. With the vertical cylinder things are quite different. A lengthening of the cylinder invariably produces a decrease of $\bar{a}$ and, as long as the flow remains laminar, $\bar{a}$ does not reach a limiting value. This is due to the fact that, whereas with the horizontal cylinder we can indicate equivalent laminae which are cooled by flows running *parallel*, the corresponding laminae of the *vertical* cylinder are cooled *in series*. The higher zones are then cooled by the medium, after this has already been heated by the lower zones. Owing to this the dissipation of heat of the higher zones is smaller.

The function f_5 for some shapes of body

a) *The vertical cylinder*

The defining quantities l_1 and l_2 are the diameter d and the height h. By combining Langmuir's theory with Nusselt's considerations and by the requirement that the formula for the dissipation of heat by a vertical

---

*) The paper is essentially identical to that published in De Ingenieur **60**, O 21-O 34, 1948, by the same author, under the same title.

) For Part I, see Philips Res. Rep. **3, 338-360, 1948.

cylinder for $d \to \infty$ must change into the formula for the *flat vertical plate*, which runs (see formula 25):

$$\mathbf{Nu}_{h,w} = 0{\cdot}6(\mathbf{Gr} \cdot \mathbf{Pr})_{h,w}^{1/4},$$

we obtain the formula for the vertical cylinder [10]):

$$\mathbf{Nu}_{d,w}\, e^{-2/\mathbf{Nu}_{d,m}} = 0{\cdot}6\, \{(\mathbf{Gr} \cdot \mathbf{Pr})\, d/h\}_{d,w}^{1/4}. \tag{38}$$

The equation (38) for the vertical cylinder follows from the equation (33) for the horizontal cylinder:

$$\mathbf{Nu}^3_{d,w}\, e^{-6/\mathbf{Nu}_{d,m}} = (\mathbf{Gr} \cdot \mathbf{Pr})_{d,w}/235\, f(\mathbf{Gr} \cdot \mathbf{Pr})_{d,w}$$

by substituting the function $f\,(\mathbf{Gr} \cdot \mathbf{Pr})_{d,w}$ by $0{\cdot}02\ (\mathbf{Gr} \cdot \mathbf{Pr})_{h,w}^{1/4}$. The function $f\,(\mathbf{Gr} \cdot \mathbf{Pr})_{d,w}$ in (33) serves to include the effect of the heating of the medium when the latter flows upwards along the circumference. In the case of the vertical cylinder the medium flows upwards along generating lines. So in the present case the effect of the heating of the medium is not a function of d, but of h, perfectly analogous to the case of the vertical plate, where the higher zones likewise dissipate a smaller amount of heat than the lower ones (see equation (26)).

We can also compare equation (38) with equation (25) for the vertical plate: $\mathbf{Nu}_{h,w} = 0{\cdot}6\ (\mathbf{Gr} \cdot \mathbf{Pr})_{h,w}^{1/4}$. It is easy to verify that with $d \to \infty$ the equation (38) is converted into equation (25).

Another point deserving attention is the following: equation (38) exclusively describes the dissipation of heat by the cylindrical outer surface. For a hollow cylinder we refer to c). If the cylinder is closed on top and at bottom, we can use equation (38), taking for h the value of the height of the cylindrical portion increased by the surfaces of the bottom and top planes divided by πd. So we assume the entire surface of the body to be situated on the cylinder wall. It is apparent that this does not hold for very short and stout cylinders. Just as (25), equation (38) no longer holds for very small and very large values of h.

Fig. 10 shows the dissipation of heat by vertical cylinders in air of one atmosphere and 20° C as a function of the diameter calculated with (38) for $\Theta_w = 100$ °C and for various values of h. In the same figure the dash line, calculated with the formula (38), represents, under the very same conditions, the dissipation of heat by a horizontal cylinder so long that the end effects are negligible.

b) *Cooling ribs*

For the purpose of promoting the dissipation of heat by a body, it is often provided with a number of plates fitted parallel to one another.

For natural cooling the plates are preferably placed vertically (central heating radiators). The surface thus extended can dissipate the same amount of energy at a smaller value of Θ_w, or, at the same value of Θ_w the dissipation of heat is larger.

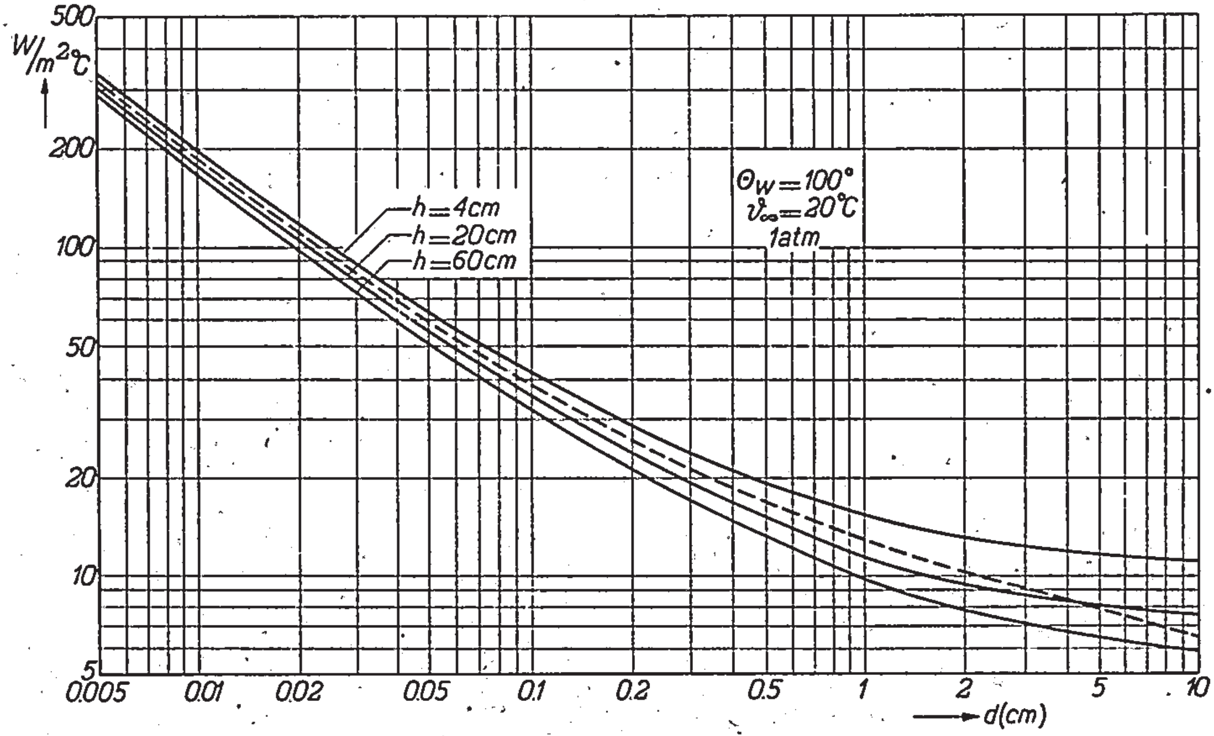

Fig. 10. The dissipation of heat in watts per m^2 and per °C as a function of the diameter for vertical cylinders in air of one atmosphere and room temperature at an excess temperature of 100 °C, calculated with formula (38). For comparison the dash line represents the dissipation of heat of the infinitely long horizontal cylinder (see fig. 8) under the same conditions.

We shall deal with the case of parallel vertical plates having a height h and a spacing b between every two plates. The outsides of the first and of the last plate dissipate heat in accordance with the formula (25), the remaining sides of the plates being mutually in the same position. So we need only consider two mutually parallel plates with a spacing b and an excess temperature Θ_w over the surroundings, and determine the amount of heat given off by the two opposite walls to the surroundings. See fig. 11 for this case. If we assume the plates to be very extensive in the horizontal direction (y-direction in fig. 11), then practically all the vertical laminae of a width of 1 cm are mutually equivalent. It is only the laminae close to the ends which are a bit more cooled, because cold air can flow on from the sides. If we leave this effect out of account for the time being (so, practically speaking, we consider vertical plates extending infinitely in horizontal direction), we have bodies that are characterized by the two magnitudes b and h. So the dissipation of heat is given by a formula of the form (37). For the parallel plates it runs [11]), [12]):

$$\mathrm{Nu}_{b,w} = \frac{1}{24}\frac{b}{h}(\mathrm{Gr}\cdot\mathrm{Pr})_{b,w}\left[1 - e^{-24\left(\frac{0{\cdot}5\,h}{b\,\mathrm{Gr}\cdot\mathrm{Pr}}\right)_{b,w}^{3/4}}\right]. \tag{39}$$

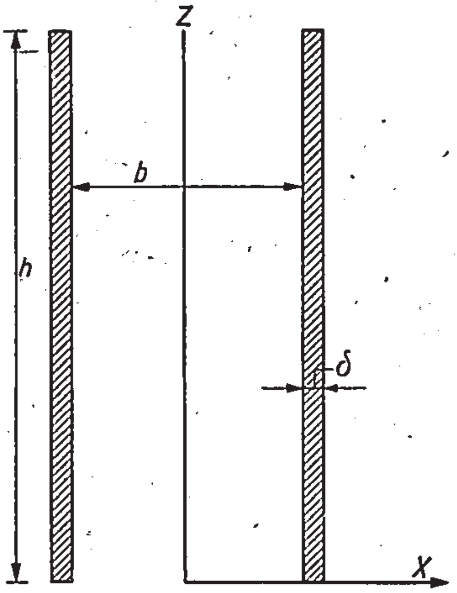

Fig. 11. Cross-section in the xz-plane of two vertical plates with a spacing of b cm. The y-direction is normal to the xz-plane. The plates are assumed to be infinitely long in the y-direction.

So here $\mathrm{Nu}_{b,w}$ is a function of $(\mathrm{Gr}\cdot\mathrm{Pr})_{b,w}b/h$. In fig. 12 this function is drawn on a double-logarithmic scale.

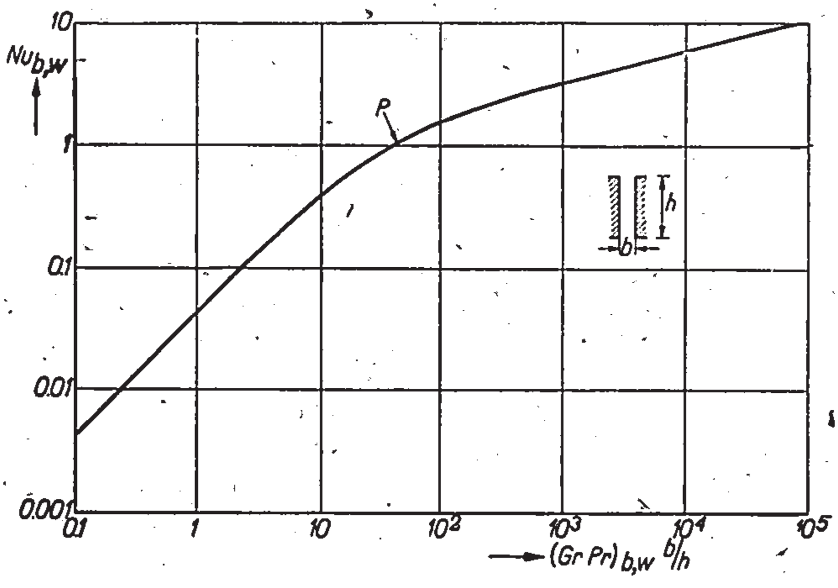

Fig. 12. With vertical parallel plates $\mathrm{Nu}_{b,w}$ is a function of $(\mathrm{Gr}\cdot\mathrm{Pr})_{b,w}\,b/h$ (b = the plate spacing; h = the plate height). The curve is drawn in accordance with formula (39). At P the cooling per cm² of the horizontal cross-section has the maximum value (formula (42)). Inset: vertical cross-section of the cooling body.

For small values of b, $\mathrm{Gr}_{b,w}$ is small, so that the e-power in equation (39) may be neglected. Equation (39) is then simplified to:

$$\overline{\alpha} = \frac{\lambda}{24h} (\mathbf{Gr} \cdot \mathbf{Pr})_{b,w} \, . \tag{40}$$

With a small plate spacing the mean dissipation of heat per cm² of the plate surface thus increases by the third power of the mutual distance, b being in the third power in $\mathrm{Gr}_{b,w}$. The total amount of dissipated energy $\overline{\alpha}\, h\, \Theta_w$ is, according to (40), independent of h. This is because with a small plate spacing the temperature of the outflowing air is the same as that of the plates. So the amount of dissipated heat cannot increase by an increase of h, as in this case the velocity of the air is independent of h. The increase by the third power of b is due to the fact that at this narrow spacing the velocity is proportional to b^3.

With large values of b we develop the e-power of (39) and obtain:

$$\frac{\overline{\alpha} b}{\lambda_w} = \frac{b}{h} (\mathbf{Gr} \cdot \mathbf{Pr})_{b,w} \left(\frac{0{\cdot}5\ h}{b\mathbf{Gr} \cdot \mathbf{Pr}}\right)^{3/4}_{b,w} = 0{\cdot}6 \left(\frac{b}{h}\, \mathbf{Gr} \cdot \mathbf{Pr}\right)^{1/4}_{b,w} . \tag{41}$$

As $\mathbf{Gr}_{b,w} = \mathbf{Gr}_{h,w} b^3/h^3$, we obtain from (41) : $\overline{\alpha} h/\lambda_w = 0{\cdot}6\, (\mathbf{Gr} \cdot \mathbf{Pr})^{1/4}_{h,w}$, which equation is identical with the equation (25), which holds for the free vertical plate. So equation (39) gives, as it should do, for a large plate spacing (where the one plate no longer affects the dissipation of heat by the other), the dissipation of heat by the free vertical plate.

In fig. 13 the dissipation of heat in watts per m² and per °C of vertical plates in air at one atmosphere and 20° C is drawn for different values of h and Θ_w as a function of b, calculated with (39). This figure therefore applies to plates that are infinite in the y-direction. If the dimension in the y-direction is not large with respect to the height, we may approximately assume that on the sides of the plates, sections having a width of $\frac{1}{2}b$ dissipate heat in accordance with the formula (25), the dissipation of heat by the remainder of the surface being described by (39). For small plate spacings this correction becomes appreciable so that the result will be uncertain. In the field in which we preferably operate (in the neighbourhood of the arrows in fig. 13), the correction is already of little importance for square plates.

If we have a certain length L at our disposal wherein we can fit a number of cooling plates having a height h and a width y_0, we may have to face the practical question as to how many plates are to be fitted in order to obtain as large a dissipation of heat as possible with a given value of Θ_w. So we have at our disposal a base of $L \cdot y_0$. Let us assume that the thickness of the plates is δ and that $(n + 1)$ plates (including the end plates) are placed on the length L. Of the $2n + 2$ sides of the plates, two (the outsides of the first and of the last plate) dissipate heat in accordance with formula (25). This dissipation of heat Φ_0 is independent of the situation in the space between the plates, so that it does not depend on n. Let us now consider the dissipation of heat of the $2n$ plate sides. It is easy to see that the dissipation of heat passes through a maximum if n rises from 0 to very great values. If only one plate is fitted ($n = 0$), the dissipation of heat is equal to Φ_0.

With $n = 1$ the dissipation of heat is Φ_0 plus the dissipation of heat of the insides of the two plates, the spacing between which is $L—2\delta$. So the dissipation of heat has increased. If the spacing $L—2\delta$ is so large that the two plates have little or no influence on each other, the application of a plate half-way between the first two plates will cause the dissipation of heat to increase. On the other hand, at very high values of n the plate spacing will become so small that (40) holds. If the thickness δ is neglected, the plate spacing decreases in proportion to $1/n$. According to (40) the dissipation of heat per plate decreases in proportion to b^3, that is, to $1/n^3$. So with high values of n the total dissipation of heat is equal to Φ_0 plus

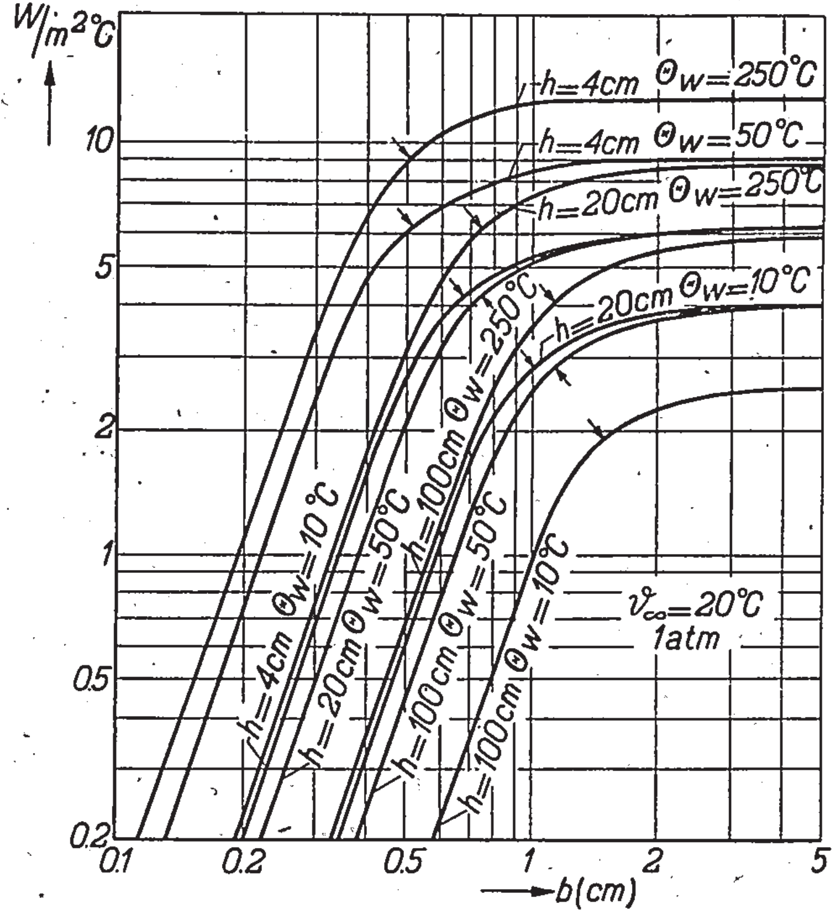

Fig. 13. The dissipation of heat per m² per °C as a function of the mutual spacing b for vertical cooling plates in air of one atmosphere and room temperature, calculated with equation (39). The dimension of the plates in horizontal direction is large as compared with the height. The arrows indicate the values of b where the cooling per cm² of the horizontal cross-section is maximum. The slope of the tangents at the arrows is equal to 1.

an amount that is proportional to $n \cdot n^{-3} = n^{-2}$. Consequently the total dissipation of heat decreases ultimately with an increasing number of plates. If we do not neglect the thickness δ, this will even occur sooner. Therefore it is possible to indicate an optimum spacing b_{opt} at which the dissipation of heat has its maximum value. This spacing can be calculated in the following way. The heat dissipated amounts to $\Phi_0 + 2\,\Theta_w\,\bar{a} y_0\,hn$ in which the second term must be maximum. If we neglect δ, we obtain $n = L/b$; so we have to find the maximum of $\bar{a}/b$.

According to (39), $\bar{a}b/\lambda = \mathbf{Nu}_{b,w}$ is given as a function of

$$q = \frac{b}{h}\,(\mathbf{Gr}\cdot\mathbf{Pr})_{b,w} = \frac{b^4\,g\varrho^2\,\beta\,\Theta_w\,c_p}{h\,\eta_w\,\lambda_w},$$

so that we may just as well say that we want to determine the maximum of

$$\frac{\bar{a}}{b} \sim \frac{\mathbf{Nu}_{b,w}}{b^2} \sim \frac{\mathbf{Nu}_{h,w}}{q^{1/2}} \sim q^{1/2}\left[1 - e^{-24\left(\frac{0\cdot5}{q}\right)^{3/4}}\right]$$

as a function of b, so also as a function of q. This maximum is obtained for the value $q \approx 50$. So this means that the spacing b_{opt} having the optimum dissipation of heat, is defined by

$$\frac{b_{\text{opt}}}{h}\,(\mathbf{Gr}\cdot\mathbf{Pr})_{b_{\text{opt}},w} \approx 50. \tag{42}$$

The relevant point is indicated by the symbol P at the curve of fig. 12. So b_{opt} does not depend on λ. It is easy to see that the tangent at P is equal to $\frac{1}{2}$. For in P the quantity $\mathbf{Nu}/q^{1/2}$ is maximum, so that $\mathrm{d}\,(\log \mathbf{Nu} - \frac{1}{2}\log q) = 0$, or:

$$\frac{\mathrm{d}\log \mathbf{Nu}}{\mathrm{d}\log q} = \tfrac{1}{2}.$$

For air ($\mathbf{Pr} = 0\cdot73$ and $\beta = 1/T_\infty$) it follows from (42) that

$$b_{\text{opt}} = 2\cdot9\,\frac{h^{1/4}\,\eta_w^{\;1/2}\,T_\infty^{1/4}}{g^{1/4}\,\varrho_w^{\;1/2}\,\Theta_w^{\;1/4}}. \tag{43}$$

The figs 14 and 15 show b_{opt} as a function of h and of Θ_w respectively, for air of one atmosphere and room temperature, calculated with (43). Taking also the plate thickness δ into account [11]), we obtain as a first approximation the optimum spacing by increasing b_{opt} by $0\cdot3\,\delta$.

In fig. 13 the spacings at which b has the optimum value for the different values of h and Θ_w, are indicated by arrows. At these points the slope of the tangent is invariably equal to 1, because there $\bar{a}/b$ is maximum, or $\mathrm{d}(\log \bar{a}) - \mathrm{d}(\log b) = 0$ from which follows $\mathrm{d}(\log \bar{a})/\mathrm{d}(\log b) = 1$.

Strictly speaking, the above calculation only holds for plates of infinite length in the y-direction. However, (42) can be applied adequately to square plates, seeing that (39) can be used for square plates in the zone round about P (fig. 12) with practically no correction.

At the spacing b_{opt} the dissipation of heat by conduction and convection is maximum. The loss of heat by radiation increasing with the number of plates, the total loss of energy will be maximum at a value of b that is a little smaller than b_{opt}. However, since the share of the radiation in the total loss of energy at low temperatures is small and the variation of the radiation loss as a function of the plate spacing is slight, we can, in practice, use (42) without objection, the more so as a larger plate spacing means a saving of material. In many cases b will therefore intentionally be chosen larger than b_{opt}. With a plate spacing 30% larger than b_{opt}, the energy

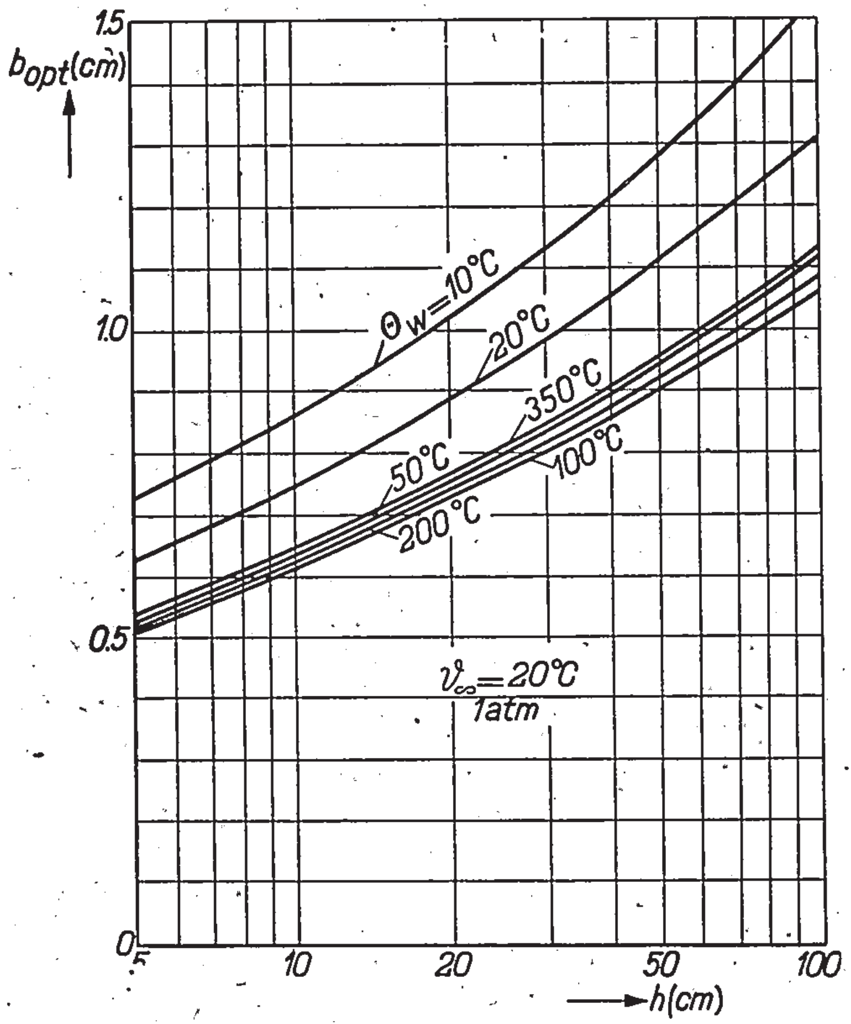

Fig. 14. The optimum distance b_{opt} between infinite thin vertical plates that are very extensive in horizontal direction, as a function of the plate height h, for different values of the excess temperature Θ_w, for air of 1 atm, and room temperature, calculated with (43). With finite plate thickness the optimum spacing is obtained as a first approximation by adding 0·3 δ to b_{opt}. If the plates are under an angle of γ to the vertical, then, if γ is smaller than $\approx$ 70°, the value of b_{opt} is to be divided by $(\cos\gamma)^{1/4}$.

carried away by conduction and convection decreases by about 10% only. If the question of space is of no account, but if weight is, b will even be taken as approximately 2 b_{opt} according to fig. 13. With a further increasing plate spacing the dissipation of heat practically ceases to increase.

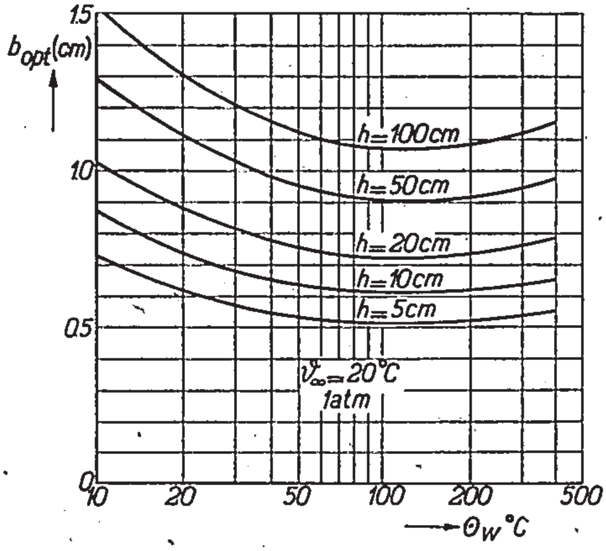

Fig. 15. As fig. 14, but now as a function of Θ_w with h as a parameter.

If we vary the plate height and neglect the plate thickness δ, selecting for each height the optimum plate spacing according to (42), the dissipation of energy increases by the square-root of the height only (see case c)).

c) *The inner surface of vertical tubes*

Under b) we determined the spacing of parallel plates in order to obtain the largest dissipation of heat if the total cross-section is given. We may now ask whether the parallel plates yield the largest possible amount of cooling at a certain size of the base, even if the plates are fitted with the optimum spacing. For instance, we might fit a second set of vertical cooling plates perpendicularly to the first set, so that the cooling would be done by vertical tubes of a rectangular cross-section. In addition to rectangles of varying shapes, we might split up the base into triangles or hexagons.

We may now ask: If we choose the optimum size for each of these shapes, which shape will yield the largest dissipation of heat?

The *forced* laminar flow through tubes or cylinders differing in the shapes of their cross-sections can be calculated; this calculation is easiest in the case of a circular cross-section (Poiseuille's formula). The average velocity through a cross-section then is $\overline{V} = r^2/8\eta \; \mathrm{d}p/\mathrm{d}l$ if p is the pressure and r the radius of the tube. This is often written in the form:

$$\frac{2r}{(\overline{V})^2\varrho}\frac{\mathrm{d}p}{\mathrm{d}l}\cdot\frac{\overline{V}r\varrho}{\eta}=16,$$

or

$$\Psi\cdot\mathbf{Re}=16\,. \tag{44}$$

The flow through cylinders with other shapes of cross-section may be described with an analogous formula. To this end we substitute r in Ψ and **Re** by the so-called hydraulic radius, which we define by

$$r=\frac{2S}{U}, \tag{45}$$

in which S represents the area and U the circumference of the cross-section. In the case of a circle the hydraulic radius is then equal to the actual radius (therefore it is allowed to use the same symbol r); with a square it is half the length of the side, and with a rectangle so extensive that two sides may be looked upon as infinite, r is equal to the distance b of the two infinitely long sides of the rectangle (so in the case of parallel plates r is equal to b). The quantity r is defined by (45) for each shape of cross-section. It appears that the forced flow in every cylinder can be described by the formula:

$$\Psi\cdot\mathbf{Re}=\text{constant},$$

in which the constant depends exclusively on the *shape* of the cross-section, but *not on its absolute size.* We shall denote the value of this constant by $[\Psi\cdot\mathbf{Re}]$. For an equilateral triangle $[\Psi\cdot\mathbf{Re}]=13\tfrac{1}{3}$, [12]) and, as already pointed out, $[\Psi\cdot\mathbf{Re}]=16$ for a circular cylinder. Boussinesq [13]) calculated $[\Psi\cdot\mathbf{Re}]$ for rectangular cross-sections with varying ratios of the sides. The results of these calculations are shown in the graph of fig. 16.

It appears that the dissipation of heat by the *natural* cooling of the inner surface of vertical cylinders having cross-sections of arbitrary shape, can be described by the equation [12]):

$$\mathbf{Nu}_{r,w}\doteq\frac{1}{[\Psi\cdot\mathbf{Re}]}\frac{r}{h}\Big(\mathbf{Gr}\cdot\mathbf{Pr}\Big)_{r,w}\left[1-e^{-[\Psi\cdot\mathbf{Re}]\left(\frac{0{\cdot}5\,h}{r\mathbf{Gr}\cdot\mathbf{Pr}}\right)_{r,w}^{3/4}}\right]. \tag{46}$$

This equation must also include two cases previously dealt with, viz. the free vertical plate $[r=\infty]$ and the parallel plate $[\Psi\cdot\mathbf{Re}]=24$; see fig. 16). With $r\to\infty$, (46) is in fact converted into the equation (25), and with $[\Psi\cdot\mathbf{Re}]=24$, (46) is converted into (39), as in this case $r=b$. So these two special cases are satisfactorily described by (46).

According to (46) $\mathbf{Nu}_{r,w}$ is a function of $(\mathbf{Gr}\cdot\mathbf{Pr})_{r,w}\,r/h$ with $[\Psi\cdot\mathbf{Re}]$ as a parameter. This function is drawn for different values of $[\Psi\cdot\mathbf{Re}]$ in fig. 17. With high values of $(\mathbf{Gr}\cdot\mathbf{Pr})_{r,w}\,r/h$ the curves all come together in the curve applying to the free vertical plate.

With the aid of (46) it can be calculated at what value of r the dissipation of heat for a given cross-section is largest. This appears to be so for the value $r = r_{\text{opt}}$ satisfying the equation

$$\left[\frac{r}{h}\,(\mathbf{Gr}\cdot\mathbf{Pr})_{r,w}\right]_{\text{opt}} = 0{\cdot}72\;[\Psi\cdot\mathbf{Re}]^{4/3}. \tag{47}$$

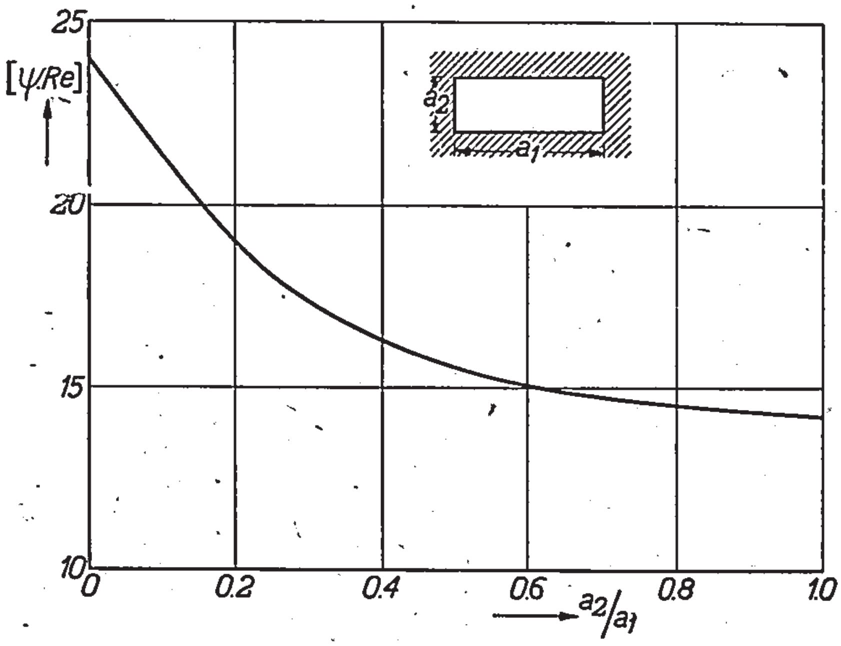

Fig. 16. The value of [$\Psi\cdot$ Re] according to Boussinesq [13]) as a function of a_2/a_1, for the laminar flow in tubes having a rectangular cross-section with the sides a_1 and a_2.

With this value of r_{opt}, we obtain from (46)

$$(\mathbf{Nu}_{r,w})_{\text{opt}} = 0{\cdot}39\;[\Psi\cdot\mathbf{Re}]^{1/3}. \tag{48}$$

For the relation between $(\mathbf{Nu}_{r,w})_{\text{opt}}$ and $[(\mathbf{Gr}\cdot\mathbf{Pr})_{r,w}r/h]_{\text{opt}}$, we deduce from (47) and (48):

$$(\mathbf{Nu}_{r,w})_{\text{opt}} = 0{\cdot}42\left[\frac{r}{h}\,(\mathbf{Gr}\cdot\mathbf{Pr})_{r,w}\right]_{\text{opt}}^{1/4}. \tag{49}$$

In fig. 17 the straight dash line represents the relation

$$\mathbf{Nu}_{r,w} = 0{\cdot}42\;[(\mathbf{Gr}\cdot\mathbf{Pr})_{r,w}\,r/h]^{1/4}.$$

The points of intersection of this line and the six curves which are drawn in accordance with the relation (46), for the different values of $[\Psi\cdot\mathbf{Re}]$, give the values of $(\mathbf{Nu}_{r,w})_{\text{opt}}$ and $[(\mathbf{Gr}\cdot\mathbf{Pr})_{r,w}r/h]_{\text{opt}}$. At these points the cooling is consequently largest for each of the cross-sectional shapes.

Since according to (47) r_{opt} is proportional to $[\Psi\cdot\mathbf{Re}]^{1/3}$ (r figures in $\mathbf{Gr}_{r,w}$ to the third power) and $[\Psi\cdot\mathbf{Re}] = 24$ for the parallel plates, the optimum value of r follows from the value of b_{opt}, as given in figs 14 and 15, by multiplying it by $\{[\Psi\cdot\mathbf{Re}]/24\}^{1/3}$. For square cross-sections the optimum length $2r$ of a side is therefore $2\,(14{\cdot}22/24)^{1/3} = 1{\cdot}68$ as large as the optimum spacing of parallel plates of the same height and excess temperature.

To find out which form yields the most efficient cooling, we calculate for each form the dissipation of energy per cm² of the cross-section for the dimension at which the optimum cooling occurs. This gives:

$$\left(\frac{\Phi}{S}\right)_{\mathrm{opt}} = \left(\frac{\bar{\alpha}\,F\,\Theta_w}{S}\right)_{\mathrm{opt}} = \left(\frac{\bar{\alpha}\,h\,U\,\Theta_w}{S}\right)_{\mathrm{opt}} = 2\,h\,\Theta_w\left(\frac{\bar{\alpha}}{r}\right)_{\mathrm{opt}},$$

in which we availed ourselves of (45) for the last conversion. If we now substitute in this equation α_{opt} from (48) and r_{opt} from (47), we obtain:

$$\left(\frac{\Theta}{S}\right)_{\mathrm{opt}} = 0{\cdot}9\,\frac{h^{1/2}\,\lambda_w\,\Theta_w^{3/2}\,g^{1/2}\,\varrho_w\,\beta^{1/2}\,\mathbf{Pr}^{1/2}}{\eta_w[\Psi\cdot\mathbf{Re}]^{1/2}}. \qquad (50)$$

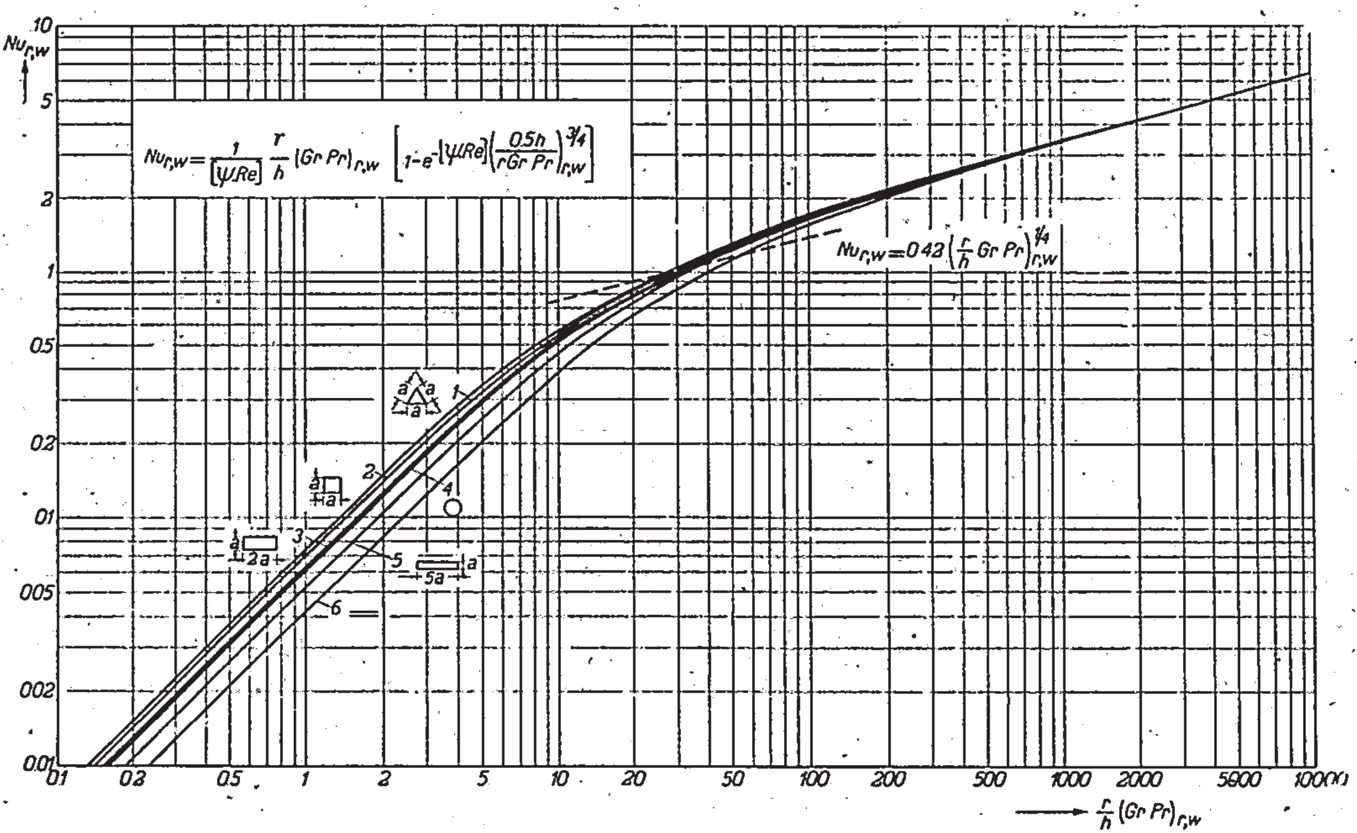

Fig. 17. $\mathbf{Nu}_{r,w}$ as a function of $(\mathbf{Gr}\cdot\mathbf{Pr})_{r,w}\,r/h$ for the cooling of the inner surface of vertical tubes according to (46) for different values of $[\Psi\cdot\mathbf{Re}]$. For infinitely long parallel plates (case b) $[\Psi\cdot\mathbf{Re}] = 24$ (curve 6). For rectangular cross-sections with the following proportions of the sides of the rectangles 1 : 5, 1 : 2 and 1 : 1, $[\Psi\cdot\mathbf{Re}]$ is 19·05, 15·55 and 14·22 respectively (curves 2, 3 and 5). For circular cross-sections $[\Psi\cdot\mathbf{Re}]$ is 16 (curve 4), and for cross-sections in the shape of an equilateral triangle $[\Psi\cdot\mathbf{Re}] = 13^1/_3$ (curve 1). The points of intersection with the dash line drawn in accordance with (49) indicate the points where the cooling per cm³ of the horizontal cross-section is a maximum.

Consequently that shape of the cross-section which has the smallest value of $[\Psi \cdot \mathbf{Re}]$ yields the largest optimum cooling. Of the shapes figuring in fig. 17 this is the equilateral triangle. The proportion to the cooling with square cross-sections amounts to $(14{\cdot}22/13{\cdot}33)^{1/3} = 1{\cdot}02$, so that the triangular cross-section has practically no advantage over the square cross-section. Both shapes of cross-section yield an approximately 20% larger cooling as compared with the parallel plates, provided the optimum dimension is chosen for all cases.

The optimum dissipation of heat per cm² of the base is, according to (50), proportional to the square-root of the height and to the (3/2)th power of the excess temperature.

With the aid of the formulae (50), (47), and (45) we find for the value of $\bar{\alpha}$ at the optimum point:

$$\bar{\alpha}_{\mathrm{opt}} = \left(\frac{\Phi}{U\,h\,\Theta_w}\right)_{\mathrm{opt}} = 0{\cdot}42\,\frac{\lambda_w\,\Theta_w^{1/4}\,g^{1/4}\,\varrho_w^{1/2}\,\beta_w^{1/4}\,\mathbf{Pr}^{1/4}}{\eta_w^{1/2}\,h^{1/4}}, \tag{51}$$

which equation can be more conveniently deduced directly from (49).

Thus $\bar{\alpha}_{\mathrm{opt}}$ does not depend on $[\Psi \cdot \mathbf{Re}]$. *Consequently the mean dissipation of heat per cm² of the heat-dissipating surface at the dimension yielding the optimum of heat dissipation does not depend on the shape of the cross-section.*

If in the cases b) and c) the plates or the cylinders are not in a vertical position, but under an angle of γ to the vertical, the preceding formulae can be used up to a value of γ of about 70°, if g is substituted by $g \cos \gamma$. This is because in the present case the component $g(\varrho_\infty - \varrho) \cos \gamma$ causes the flow of the medium, if ϱ is the density of the latter. Grashof's number decreases owing to this and consequently the Nusselt's number and the cooling. This no longer holds for parallel plates the spacings of which are so ample that the plates practically do not affect one another; neither does it apply to short, wide cylinders.

If $\gamma \neq 0$, the values of b_{opt} in figs 14 and 15 must be divided by $(\cos \gamma)^{1/4}$.

d) *The horizontal flat plate*

Considering exclusively square or circular plates, we are inclined to look upon them as bodies characterized by one linear dimension only. However the dissipation of heat appears to be affected by the thickness of the plate, so that we have to use equation (37). The shape of the function f_5 is not known for this case, however.

Hencky [14]) found with thin square plates in a horizontal position a 20% larger dissipation of heat than with plates of the same size in a vertical position. Weise [15]), on the other hand, found with thick plates ($16{\cdot}16{\cdot}1$ cm³ and $24{\cdot}24{\cdot}1\frac{1}{2}$ cm³) in a horizontal position an approximately 20 % smaller dissipation. Measurements by Weise [15]) and Kraus [16]) of the temperature field and the velocity field, showed that this discrepancy may probably be due to the vertical flow prevailing at the edge of the thick horizontal plates. This impedes the lateral onflow of cold air, owing to which the border sections are cooled on a smaller scale than the central part. This vertical flow does not present itself with the thin plates, so that cold air can flow on from all sides. Hence the cooling is more efficient here than with the vertical plate, where cold air flows in from the bottom only.

8. Concluding remarks

In the foregoing we have given a number of formulae that renders possible to calculate the dissipation of heat at natural cooling. From the deduction it appears that none of them is exact. In air, deviations up to about 10% present themselves. Few measurements have been made in other media. In addition, it should always be borne in mind that these formulae only hold if the medium is *exclusively* set moving by the heat-dissipating body. If the medium is set moving by other agents as well, for instance, by draught, the dissipation of heat is larger. An increase of 10% is soon reached.

In the case of cooling in atmospheric air the height of the barometer plays a part, because ϱ figures in Gr. Owing to this the dissipation of heat is smaller at great heights over the surface of the earth.

We have only considered bodies of simple shapes and found the formulae to be of a pretty complicated nature. It is clear that calculations are well-nigh impracticable for all sorts of different shapes occuring in practice. In such cases we have to resort to measurements made at the body itself or at a reduced model, choosing the same value of **Gr** · **Pr** (for instane, by ncreasing the density of the gas). With the aid of the laws of similarity it is possible to calculate the dissipation of heat of the original from the measurements made at the model. In general, a reduced model will only be used if the manufacture of the body of the actual size is expensive.

If a body is composed of parts the heat-dissipation coefficients of which are known, we can calculate the total dissipation of heat by addition, if the component parts are cooled by *parallel* flows which do not affect one another. For instance, the cooling of a vertical hollow cylinder that is open on top and at bottom, is the sum of the cooling of the outer surface (equation (38)) and the inner surface (equation (46)). However, in case several parts are cooled in *series* the total dissipation of heat is smaller than the sum of the losses of the component parts if the latter were separated. This is because the medium has already been heated by the lower parts before passing along the higher parts.

Up to now we have invariably spoken of dissipation of heat, occurring if the temperature of the body is higher than that of the medium at a great distance. If we exchange the temperature of the body for that of the medium, we may ask whether the body will now absorb as large a quantity of heat as was dissipated in the former case. In general this is not so. Also the formulae deduced give other values because the wall temperature is different now. It is only the values of quantities at the average temperature which remain the same. However, the wall temperature figures in all the formulae. Seeing that in the case of *gaseous media* both λ and η increase with the temperature, the difference between the *dissipation and the absorption of heat* is not very great. With liquids, on the other hand, η decreases with increasing temperature, so that $\mathbf{Gr} \cdot \mathbf{Pr}$ increases. So with dissipation of heat by the body $(\mathbf{Gr} \cdot \mathbf{Pr})_{l,w}$ is larger and consequently $\mathbf{Nu}_{l,w}$ too, and as λ_w is also larger, $\bar{\alpha}$ is larger in the case of dissipation of heat by the body than of absorption of heat in case the temperatures have been exchanged.

Thus this effect is due to the fact that the constants of the materials are dependent on the temperature. If this was not so, an exchange of the temperatures of wall and medium would only result in an inversion of the direction of the heat flow, the amount of the latter remaining the same. Even without the above consideration it is perfectly clear that if a body is cooled in a thick oil, the dissipation of heat will be larger than in the case of heating, because in the former case the high temperature causes the oil to flow more readily close to the body than in the latter case. In the latter case the flow is easier farther away, it is true, but this does not increase the dissipation of heat appreciably.

The following table specifies some properties of air and water expressed in C.G.S. units. When calculating $\mathbf{Gr}$, g must be expressed in cm/sec^2. The value of $\bar{\alpha}$ will then be expressed in calories per cm^2 per sec.

Eindhoven, April 1948

REFERENCES

[11]) W. Elenbaas, Physica **9**, 1, 1942.
[12]) W. Elenbaas, Physica **9**, 865, 1942.
[13]) J. Boussinesq, J. Math. pure appl. (2) **13**, 377, 1868.
[14]) K. Hencky, Die Wärmeverluste durch ebene Wande, Oldenburg, 1921.
[15]) R. Weise, Forschung auf dem Geb. des Ingw. **6**, 281, 1935.
[16]) W. Kraus, Phys. Z. **41**, 126, 1940.

TABLE

Properties of air and water as functions of the temperature in C.G.S. units *)

Air (Pr = 0·73, independent of temperature and pressure; $\beta = 1/T_\infty$; ϱ at 1 atm; λ and η are independent of the pressure).					*Water*						
ϑ (°C)	$10^6\lambda$	$\frac{10^6}{\vartheta-20}\times\int_{20}^{\vartheta}\lambda(\vartheta)d\vartheta = 10^6\lambda_m$	$10^6\varrho$	$10^6\eta$	ϑ (°C)	Pr	$10^5\lambda$	$\frac{10^5}{\vartheta-10}\times\int_{10}^{\vartheta}\lambda(\vartheta)d\vartheta = 10^5\lambda_m$	ϱ	$10^4\eta$	$10^5\beta$
20	60·0	60·0	1205	182	10	9·42	138	138	1·000	129·5	9
30	61·7	60·85	1165	186·5	15	8·10	140·5	139	0·999	113·5	15·4
40	63·4	61·7	1130	191	20	6·97	142·5	140·5	0·998	99·4	20·8
50	65·0	62·5	1090	195	25	6·08	145	141·5	0·997	88·0	25·6
60	66·8	63·4	1060	199	30	5·38	147	142·5	0·996	79·2	30·2
70	68·4	64·2	1030	204	35	4·81	149	143·5	0·994	72·0	34·4
80	70·0	65·0	1000	208	40	4·34	151	144·5	0·992	65·8	38·6
90	72·0	65·9	974	212	45	3·94	153	145·5	0·990	60·5	42·2
100	73·4	66·8	947	216·5	50	3·58	154·5	146·5	0·988	55·4	45·7
120	75·5	68·3	900	225	55	3·27	156	147·5	0·986	51·0	49·0
140	79·5	69·8	855	233	60	2·99	157·5	148·5	0·983	47·1	52·2
160	82·3	71·4	816	241	65	2·74	158·5	149·5	0·981	43·5	55·4
180	85·4	73·0	781	249	70	2·53	159·5	150	0·978	40·4	58·4
200	88·4	74·5	748	257	75	2·35	160·5	151	0·975	37·6	61·4
250	95·7	78·3	675	275	80	2·19	161	151·5	0·972	35·2	64·2
300	102·5	82·1	616	293	85	2·04	161·5	152·5	0·969	32·8	67·0
350	109	85·6	568	310	90	1·91	162	153	0·965	30·9	69·7
400	116	89·2	525	327	95	1·80	162·5	153·5	0·962	29·2	72·3
500	129	96·1	457	358	100	1·72	163	154	0·958	27·7	74·9
600	139	102·5	404	386							
800	160	115	329	436							
1000	182	126	277	484							
1200	202	137	240	526							
1400	222	148	211	567							
1600	242	159	188	604							
1800	261	169	170·5	638							

---

*) Partly taken from: M. ten Bosch, Die Wärmeübertragung, Berlin, Springer, 1936.

R 96 *Philips Res. Rep. 3, 466-473, 1948*

ANTICAUSTICS — A CORD CONSTRUCTION AND A GENERAL FORMULA

by C. ZWIKKER

513.61:535.31

Summary

The author describes a method for constructing anticaustics — if the caustic is given — by generalizing the well-known cord construction for the ellipse. An analytical method of calculation of the anticaustics is developed by means of the geometry of the complex plane.

Résumé

L'auteur décrit une méthode de construction d'anticaustiques — si la caustique est donnée — en généralisant la construction bien connue de l'ellipse au moyen de la corde. Une méthode analytique de calcul des anticaustiques est développée au moyen de la géométrie du plan complexe.

1. From a constructional and geometrical point of view the design of reflecting surfaces producing a certain desired caustic pattern seems to present considerable difficulties. The aim of this article is to offer a simple drawing-board method that will help in many cases, and to give a general formula that will be of use for more accurate constructions. As this problem in mathematical analysis is known as the problem of the anticaustic we will denote the reflecting surface that we are looking for by this name.

2. Suppose a cord is wrapped round part of a polygon *c* (fig. 1) and the cord kept stretched by a pencil. Now move the pencil in such a way that the cord is permanently kept straight. The line *a* that is described by the pencil will consist of parts of ellipses, two vertices of the polygon acting temporarily as the foci of the ellipse. The curve *a* therefore shows the property that its tangent always makes equal angles with the two parts

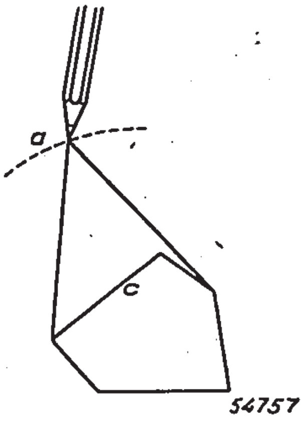

Fig. 1

of the cord leading to the pencil. When we let the number of sides of the polygon *c* increase this equal-angle property of the pencil curve *a* will remain, and in the limit we find that, if we wrap the cord round a closed contour *c* of arbitrary form, the pencil curve *a* will be such that the tangent at any point will make equal angles with the two tangents drawn from this point of *a* to the contour *c*; the curve *a* may in this case be considered as the envelope of a set of ellipses. Now place the cord round a closed contour *c* and a point *S* lying outside this contour, and execute the same construction, again leading to a curve *a* (fig. 2). Again the equal-angle property will occur. Any light ray coming from the source *S* will be reflected by the curve *a* (anticaustic) in such a way that the reflected ray will be tangent to the contour *c*, *c* therefore acting as the caustic. The length of the cord may be varied leading to different anticaustics for a single choice of source *S* and caustic *c*.

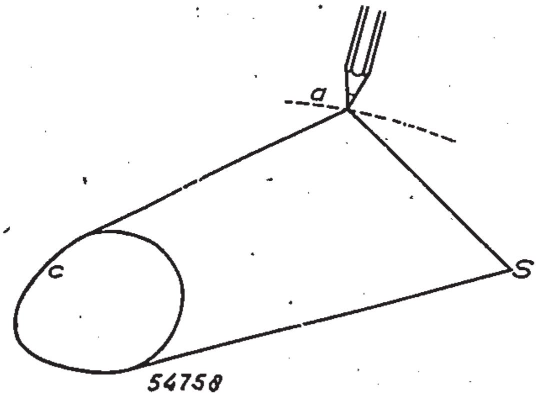

Fig. 2

In practice a light source is never a mathematical point. In fig. 3 we represent the light source by a contour *s*. If we wish to prevent reflected light from entering the contour *c* the cord is now bent round *c* and *s* with a twist. Cases like this occur during the design of incandescent lamps and

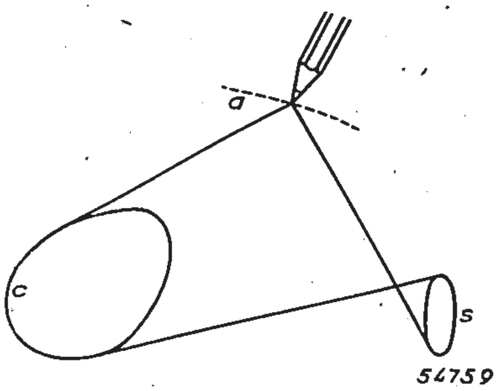

Fig. 3

fittings where one is anxious to keep light from certain lamp parts that are not allowed to reach high tempertures.

Other variations of the cord construction may be imagined dependent on the problem at hand.

3. In order to find an analytical formula for the curve a we shall treat the plane as a complex plane, fixing the place of a point with respect to a certain origin by a vector z:

$$z = x + jy;\ (j^2 = -1).$$

The contour c is given by the dependence of x and y on a parameter ω, written as $z = f(\omega)$. We choose the arc length, s, measured along the curve, as parameter; s contains an arbitrary constant and we shall fix this constant so that s is the length of the cord CAS (fig. 4). Now reflect the point S with respect to the tangent applied to the point A of the anticaustic. The image is E. CAE is straight and of length s; E obviously describes an involute of the contour c if A is moved with the pencil as described.

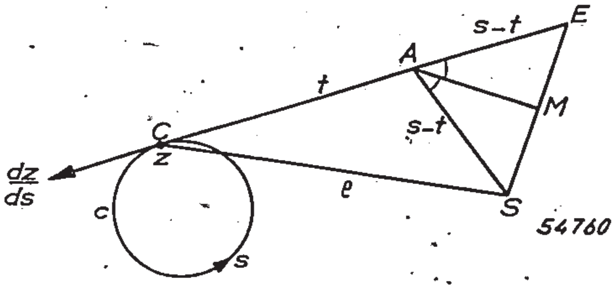

Fig. 4

The "velocity" of point C along the contour c is the vector dz/ds; it has unit value and is directed along the tangent. The place of point E is therefore represented by the vector (fig. 4)

$$z_E = z - s\,\frac{dz}{ds},$$

and for point A, situated somewhere on the tangent, we have

$$z_A = z - t\,\frac{dz}{ds}, \tag{1}$$

where t is a real factor still to be determined.

On the other hand A is situated on the bisector of the line SE. For S as the origin of coordinates, the vector SE is z_E. Point M is represented by $z_M = z_E/2$. The bisector is orthogonal to z_E, and point A on it may be represented by the formula

$$z_A = (\tfrac{1}{2} + j\lambda)\, z_E, \tag{2}$$

where λ is a parameter, j indicating the orthogonal direction of MA with respect to SE. Now t and λ follow from equating (1) and (2):

$$z_A = z - t\frac{\mathrm{d}z}{\mathrm{d}s} = (\tfrac{1}{2} + j\lambda)\, z_E; \quad z_E = z - s\frac{\mathrm{d}z}{\mathrm{d}s}.$$

Thus:

$$\tfrac{1}{2} + j\lambda = \frac{z - t\dfrac{\mathrm{d}z}{\mathrm{d}s}}{z - s\dfrac{\mathrm{d}z}{\mathrm{d}s}}.$$

For the conjugate values, denoting these by asterisks, we obtain

$$\tfrac{1}{2} - j\lambda = \frac{z^* - t\dfrac{\mathrm{d}z^*}{\mathrm{d}s}}{z^* - s\dfrac{\mathrm{d}z^*}{\mathrm{d}s}}.$$

Addition of these two equations eliminates λ and gives an equation for t, the solution of which is:

$$t = \frac{s^2 - zz^*}{2s - \dfrac{\mathrm{d}z}{\mathrm{d}s}z^* - \dfrac{\mathrm{d}z^*}{\mathrm{d}s}z} \quad \text{since} \left|\frac{\mathrm{d}s}{\mathrm{d}z}\right| = 1.$$

Now zz^* is the square of the absolute value of the vector z (CS in fig. 4); we denote it by ϱ^2. As furthermore the denominator of t is the derivative of the numerator, one has

$$t = \frac{s^2 - \varrho^2}{\dfrac{\mathrm{d}}{\mathrm{d}s}(s^2 - \varrho^2)}. \tag{3}$$

Plotting the distance t on the tangent of the caustic c will give us the anticaustic, and thus the geometrical problem has been solved.

Example: Let c be the unit circle and S on the circle. If we let s start at the point S (fig. 5), s is the arc length SC; the straight distance $SC = \varrho = 2\sin(s/2)$; hence

$$t = \frac{s^2 - 4\sin^2(s/2)}{2s - 2\sin s},$$

and this has to be plotted on the tangent at C for all values of s (fig. 6, curve a).

We may make s longer, for example starting the s-scale at the bottom point of the circle (fig. 5b); in this case

$$\varrho^2 = 2\,(1 - \sin s)\,,$$

$$t = \frac{s^2 - 2\,(1 - \sin s)}{2\,s + 2\,\cos\,s}\,.$$

The corresponding curve is shown in fig. 6, curve b.

The anticaustics have a spiral character; by mirroring an arc of the spiral with respect to the horizontal axis of the circle we may obtain symmetrical shapes.

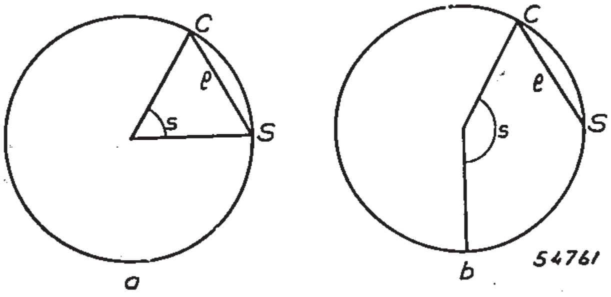

Fig. 5

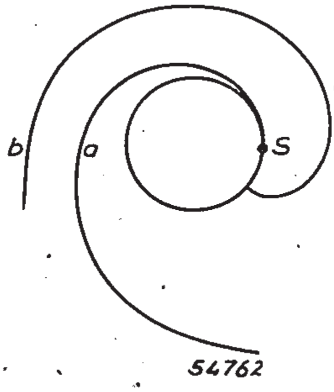

Fig. 6

4. The formula (3) for t is simplified if the light source S moves towards the right to infinity. For this purpose we write:

$$1/t = \frac{d}{ds} \ln\,(s^2 - \varrho^2) = \frac{d}{ds} \ln\,(s + \varrho) + \frac{d}{ds} \ln\,(s - \varrho).$$

Now s and ϱ become infinitely large together and as the derivative of a logarithm tends to zero for infinite value of its argument, $d/ds\,\}\ln\,(s + \varrho)\{$ goes to zero. In the second term we may in the limit substitute $-x$ for ϱ, so that t becomes:

$$t = \frac{s + x}{\dfrac{d}{ds}\,(s + x)}\,,$$

and this introduced into (1) will give anticaustics for parallel rays. We may shift back the origin from infinity, leaving $(s + x)$ constant, and as there is an arbitrary constant in s the choice of the origin does not even interfere; it is only the differences in x for the various points of the caustic that influence the shape of the anticaustic.

Example: Let again c be the unit circle and let us again take the two choices of s that we made in the last section. We take the origin at the centre of the circle. For s starting in the horizontal axis, $x = \cos s$. Thus

$$t = \frac{s + \cos s}{1 - \sin s}. \quad \text{(fig. 7, curve a)}$$

For s starting at the bottom of the circle,

$$x = \sin s,$$

$$t = \frac{s + \sin s}{1 + \cos s}. \quad \text{(fig. 7, curve b)}$$

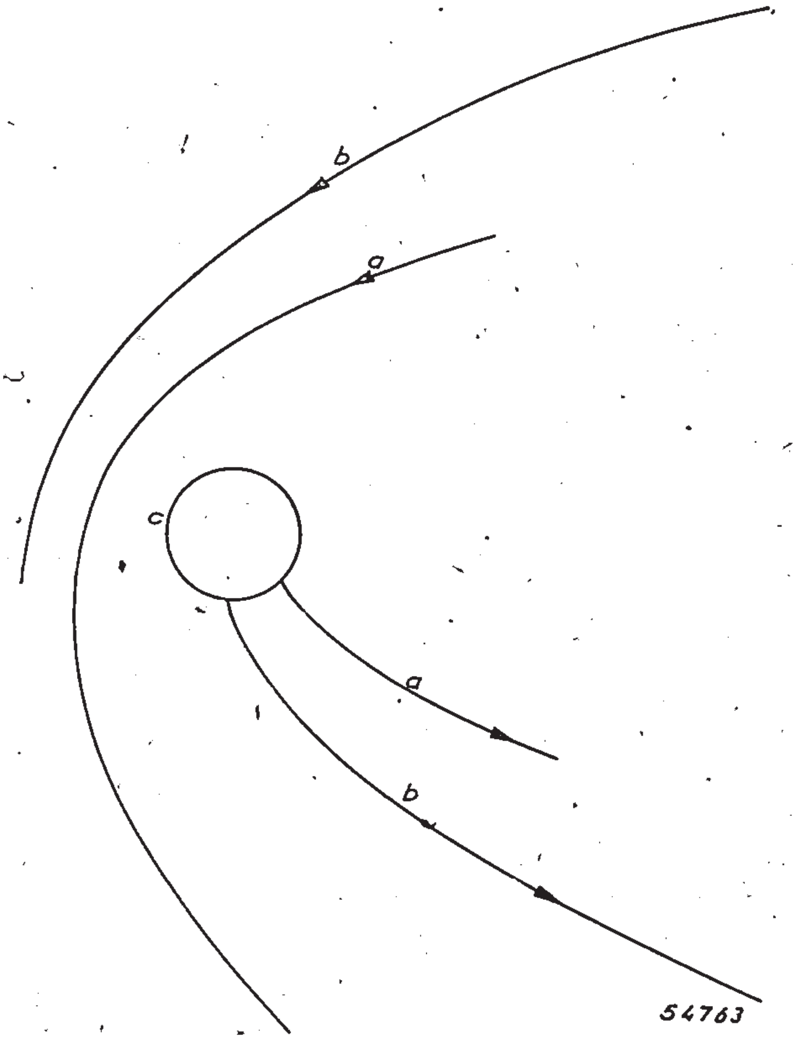

Fig. 7

The anticaustics are spirals that run through the point at infinity of the horizontal axis. Again symmetrical curves may be obtained by mirroring of a branch of the anticaustic with respect to the horizontal axis.

5. The general case is that the caustic is known as $z = f(\omega)$, where ω is different from s. Take for instance the classical case of caustics: the cardioid. This is the trajectory of a point of a circle (say, of unit radius) rolling over an equally big stationary circle. Taking the centre of the stationary circle as origin (fig. 8) the centre M of the rolling circle may be represented by $z_M = 2 \exp(j\omega)$ and the point C of the cardioid by

$$z = 2 \exp(j\omega) + \exp(2\,j\omega);$$

this formula would be much less simple if we tried to transform ω into the arc length s.

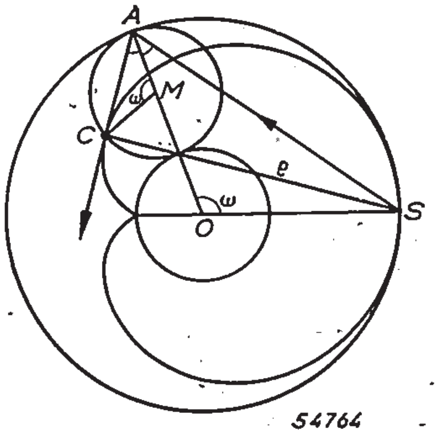

Fig. 8

In this case it is adequate to rewrite (1) as follows:

$$z_A = z - t \frac{\mathrm{d}z}{\mathrm{d}\omega} \frac{\mathrm{d}\omega}{\mathrm{d}s} \tag{4}$$

with

$$t \frac{\mathrm{d}\omega}{\mathrm{d}s} = \frac{s^2 - \varrho^2}{\dfrac{\mathrm{d}}{\mathrm{d}\omega}(s^2 - \varrho^2)},$$

and the difficulties encountered are not greater than before.

Let us work out the case of the cardioid; we take the light source S on the cardioid where it cuts the horizontal axis ($z_s = 3$). The cord ϱ is found by

$$\varrho^2 = (z - 3)(z^* - 3) = 20 - 8 \cos\omega - 12 \cos^2\omega.$$

The arc-length element is:

$$\mathrm{d}s = \sqrt{\frac{\mathrm{d}z}{\mathrm{d}\omega} \frac{\mathrm{d}z^*}{\mathrm{d}\omega}}\, \mathrm{d}\omega = 4 \cos\frac{\omega}{2} \cdot \mathrm{d}\omega\,,$$

and the total arc length:

$$s = \int \mathrm{d}s = 8 \sin (\omega/2)$$

Thus,

$$s^2 = 32\,(1 - \cos \omega)\,,$$
$$s^2 - \varrho^2 = 12\,(1 - \cos \omega)^2\,;$$

and hence:

$$t\,\frac{\mathrm{d}\omega}{\mathrm{d}s} = \frac{1 - \cos \omega}{2 \sin \omega}\,.$$

This introduced into (4) gives $z_A = 3\,e^{j\omega}$, and this is the circle of radius 3 (point A in fig. 8).

Eindhoven, March 1948

ABSTRACTS OF RECENT SCIENTIFIC PUBLICATIONS OF THE N.V. PHILIPS' GLOELAMPENFABRIEKEN

Reprints of the majority of these papers can be obtained on application to the Administration of the Research Laboratory of N.V. Philips' Gloeilampenfabrieken, Eindhoven, Netherlands. Those papers of which no reprints are available are marked with an asterisk (*).

1719a: M. Gevers en F. K. du Pré: Power factor and temperature coefficient of solid (amorphous) dielectrics (Trans. Farady Soc. **42A**, 47-53, 1946).

For the contents of this paper, see Philips tech. Rev. **9**, 91-96, 1947, and these abstracts, Nr **1726.**

The subject treated in this paper has been dealt with extensively in Philips Res. Rep. **1**, 197-224, 279-313, 361-379, 447-463, 1946.

1719b: E. J. W. Verwey and J. Th. G. Overbeek: Long distance forces acting between colloidal particles (Trans. Faraday Soc. **42B**, 117-123, 1946).

The writers have made an extensive investigation on the theory of the long-distance forces acting between the particles in a colloidal solution, in the case where the particles are surrounded by an electrical double layer. The paper gives a summary of these investigations preceded by a critical discussion of the work of previous authors.

For more information, see these abstracts, Nr **1769***.

1757: C. J. Bouwkamp: On spheroidal wave functions of order zero (J. Math. Phys. **26**, 79-92, 1947).

A survey is given of some of the results arrived at by the author in his dissertation (Groningen 1941; dealing with the diffraction of sound by a circular aperture and related problems): calculation of characteristic values and characteristic functions occurring in the separation of the wave equation in spheroidal coordinates; tables of numerical values.

1758: D. Polder: Nature of the hydrogen bond in potassium hydrogen fluoride (Nature, London, **160**, 870, 1947).

The doublet 1450, 1222 cm^{-1} in the infrared absorption of KHF_2 is ascribed by Ketelaar to a doubling of the fundamental asymmetric frequency ν_3, belonging to the vibration of a proton between two F-ions, due to a double minimum of the potential energy (analogous to what happens in the NH_3 molecule). The validity of this conjecture is checked by measuring the temperature coefficient of the dielectric constant ($\varepsilon^{-1}\,d\varepsilon/dT$). A value 2.10^{-4} is found between $T = 80$ °K and $T = 300$ °K, whereas Ketelaar's data would yield a negative temperature coefficient between 0·01 and 0·001.

1759: C. J. Bouwkamp: A study of Bessel functions in connection with the problem of two mutually attracting circular discs (Proc. Kon. Ned. Akad. Wetenschappen, Amsterdam, **50**, 1071-1083, 1947).

Calculation of the potential energy of two coplanar, circular, homogeneous discs for an arbitrary law of force, in terms of integrals containing Bessel functions.

Special attention is paid to the case where the potential energy between two point masses varies with the distance r as r^{-n}. The integrals so obtained are evaluated in terms of elementary functions, complete elliptic integrals of the first and second kinds, and hypergeometric functions.

1760: C. J. Bouwkamp: On the construction of simple perfect squares (Proc. Kon. Ned. Akad. Wetenschappen, Amsterdam, **50**, 1296-1299, 1947).

Correction to a previous paper (these abstracts **1719-1721**). Construction of a simple, perfect square of 55 elements.

1761: Balth. van der Pol: An electro-mechanical investigation of the Riemann zeta function in the critical strip (Bull. Am. Math. Soc. **53**, 976-981, 1947).

A known representation of Riemann's zeta function $\zeta(s)$, valid for Re $s > 1$, is analytically continued in the strip $0 < \text{Re}\ s < 1$. For $s = {}^1/_2 + it$ this representation may be written as the Fourier integral of a certain saw-tooth function. The zeros and maxima of this integral are obtained by an electro-optical method, the Fourier integral being approximated by a Fourier series. A disc carrying the saw-tooth function on its circumference rotates in front of a photo-electric cell. The amplitudes of the harmonics of the resulting periodic time function are plotted as a function of their number.

1762: A. Cramwinckel: The sensitivity of various phototubes as a function of the color temperature of the light source (J. Soc. Mot. Pict. Engrs **49**, 523-529, 1947).

A method is described for measuring the sensitivity of various types of phototube (Cs_2O vacuum and gas-filled, Cs-Sb vacuum, Se) as a function of the temperature of the light source (tungsten ribbon lamp). The results are compared with the function giving the brightness of a complete radiator as a function of temperature. For light sources with high colour temperature (3000 °K) the Cs-Sb cell is at least two times as sensitive as the Cs_2O vacuum cell.

SUBJECT INDEX

Page

Abstracts of papers 156, 239, 318, 474

Aerials
  Theory of coupled antennae 213

Applied mechanics
  Helical springs, rubber rods and vibration-free mountings 401

Chemistry
  Equilibrium between liquid silica and liquid iron 271
  Investigations in the system Na_2O-PbO-TiO_2-SiO_2 235
  Retrograde solubility curves in alloy solid solutions 281
  Temperature dependency of refraction of solids 371

Electrical measuring apparatus
  Empirical determination of wave-filter transfer functions 60, 378
  Non-conducting ferromagnetic material at h.f. 37
  Universal adjustable transformer for u.h.f. work 140

Electronics
  Induced grid noise and total-emission noise 13
  Noise factor of grounded-grid valves 255
  Measurements of noise factors of penthodes at 7·25-m wavelength . . . 121
  Valve characteristic giving linear modulation 227

Ferromagnetic materials
  Non-conducting ferromagnetic material at h.f. 37

Fluorescence
  Fluorescence of hexavalent uranium in glass 46

Glass, ceramics
  Equilibrium between liquid silica and liquid iron 271
  Fluorescence of hexavalent uranium in glass 46
  Investigations in the system Na_2O-PbO-TiO_2-SiO_2 235

Heat
  Dissipation of heat by free convection 338, 450
  Heat dissipation in the anode of an X-ray tube 49, 161, 303

Mathematics
  Anticaustics — A cord construction and a general formula 466
  Determination of integration constants in transient phenomena 24
  Mathematics and radio problems 174

Measurements
  Measurement of permeability and magnetic losses of non-conducting ferromagnetic material at high frequencies 37
  Measurements of noise factors of penthodes at 7·25-m wavelength . . . 121

Metallurgy — Page

Equilibrium between liquid silica and liquid iron 271
Retrograde solubility curves in alloy solid solutions 281

Modulation

Noise in a pulse-frequency-modulation system 241
Valve characteristic giving linear modulation 227

Networks

Determination of integration constants in transient phenomena. 24
Empirical determination of wave-filter transfer functions 60, 378
Gyrator, a new electric network element 81
Synthesis of passive, resistanceless four-poles 321

Noise

Induced grid noise and total-emission noise 13
Measurements of noise factors of penthodes at 7·25-m wavelength . . . 121
Noise factor of grounded-grid valves 255
Noise in a pulse-frequency-modulation system 241

Optics

Anticaustics — A cord construction and a general formula 466
Temperature dependency of refraction of solids. 371

Radio applications

Landing courses independent of weather conditions 1, 130

Radio communication

Mathematics and radio problems 174

Receivers

New principle for transceivers 361
Radio-receiver circuits for the ultra-short-wave range 191

Ultra-short waves

Radio-receiver circuits for the ultra-short-wave range 191
Universal adjustable transformer for u.h.f. work 140

Wave propagation

Spherically symmetric inhomogeneous wave guides 102

Welding

Equilibrium between liquid silica and liquid iron 271

X-ray apparatus

Heat dissipation in the anode of an X-ray tube 49, 161, 303

AUTHOR INDEX

Page

Boelens, W. W. . . . . 227, Valve characteristic giving linear modulation

Botden, Th. P. J. , see Kröger, F. A.

Bouwkamp, C. J. . . . . 213, Theory of coupled antennae

Breggen, J. C. van der, see Lindenhovius, H. J.

Bremmer, H. . . . . 102, Spherically symmetric inhomogeneous wave guides

Elenbaas, W. . . . . 338, 450 Dissipation of heat by free convection I, II

Fast, J. D. . . . . 271, Equilibrium between liquid silica and liquid iron

Haringx, J. A. . . . . 401, Helical springs, rubber rods and vibration-free mountings

Hofweegen, J. M. van, and K. S. Knol 140, Universal adjustable transformer for u.h.f. work

Jonker, G. H., see Santen, J. H. van

Klinkhamer, J. F. . . . . 60, 378 Empirical determination of wave-filter transfer functions I, II

Knol, K. S., see Hofweegen, J. M. van

Kröger, F. A., J. M. Stevels and Th. P. J. Botden . . . . 46, Fluorescence of hexavalent uranium in glass

Lindenhovius, H. J., and J. C. van der Breggen . . . . 37, Non-conducting ferromagnetic material at h.f.

Meijering, J. L. . . . . 281, Retrograde solubility curves in alloy solid solutions

	Page	
Niessen, K. F.	1, 130,	Landing courses independent of weather conditions I, II
Oosterkamp, W. J.	49, 161, 303,	Heat dissipation in the anode of an X-ray tube I, II, III
Pol, Balth. van der	174,	Mathematics and radio problems
Santen, J. H. van, and G. H. Jonker	371,	Temperature dependency of refraction of solids
Stevels, J. M.	235	Investigations in the system Na_2O-PbO-TiO_2-SiO_2
Stevels, J. M., see Kröger, F. A.		
Stumpers, F. L. H. M.	241,	Noise in a pulse-frequency-modulation system
Tellegen, B. D. H.	24,	Determination of integration constants in transient phenomena
Tellegen, B. D. H.	81,	The gyrator, a new electric network element
Tellegen, B. D. H.	321,	Synthesis of passive, resistanceless four-poles
Versnel, A., see Ziel, A. van der		
Weel, A. van	191,	Radio-receiver circuits for the ultra-short-wave range
Weel, A. van	361,	New principle for transceivers
Ziel, A. van der, and A. Versnel	13,	Induced grid noise and total-emission noise
Ziel, A. van der, and A. Versnel	121,	Measurements of noise factors of penthodes at 7·25-m wavelength.
Ziel, A. van der, and A. Versnel	255,	Noise factor of grounded-grid valves
Zwikker, C.	466,	Anticaustics — A cord construction and a general formula

INDEX ACCORDING TO THE UNIVERSAL DECIMAL CLASSIFICATION SYSTEM

UDC-number	Report
51	*R 79*
513.61	*R 96*
517.941	*R 68*
531.2	*R 94*
534.221.1	*R 74*
535.31	*R 96*
.327	*R 92*
.371	*R 70*
536.212.1	*R 71, 78, 88*
.25	*R 90, 95*
537.311.5	*R 68*
538.221	*R 69*
.55	*R 73*
.566.5	*R 74*
539.13	*R 92*
.213	*R 83*
541.123.24	*R 87*
.127.4	*R 86*
546.791.6	*R 70*
621-272.2	*R 94*
621-272.6	*R 94*
621.317.41	*R 69*
.317.43	*R 69*
.317.729.1	*R 72, 93*
.385.1	*R 85*
.385.3	*R 67*
.385.5	*R 75*
.386.1.032.22	*R 71, 78, 88*
.392	*R 73, 74*
.392.1	*R 68*
.392.43.029.6	*R 77*
.392.5	*R 89*
.392.52	*R 72, 93*
.396	*R 79*
.396.5	*R 91*
.396.611.4	*R 91*
.396.619.16	*R 84*
.396.619.231	*R 82*
.396.621.54.029.6	*R 80*
.396.645.37	*R 82*
.396.671	*R 81*
.396.822	*R 67, 75, 84, 85*
.396.933.23	*R 66, 76*
666.113.791.6	*R 70*
.115	*R 83*
669.15	*R 86*
.782.018.11	*R 86*